EFFECT OF SECOND ORDER FORCES ON STEADY TILT BEHAVIOURS AND SOME APPLICATIONS IN DYNAMIC POSITIONING ASPECTS OF TWIN HULLED MARINE VEHICLES

(Volume I)

by

Tong-Ming WU, B.Sc., M.Sc.

This thesis is submitted for the degree of Doctor of Philosophy
in the Department of Naval Architecture and Ocean Engineering
University of Glasgow

June 1993

Great Britain

ProQuest LLC.
789 East Eisenhower Parkway
P.O. Box 1346
Ann Arbor, MI 48106 – 1346

DEDICATION

To my parents and my wife.

DECLARATION

Except where reference is made to the work of others, this thesis is believed to be original.

ACKNOWLEDGEMENTS

The author would like to express his gratitude to all those people who have contributed to the research work presented in this thesis. The following are sincerely acknowledged :

Professor D. Faulkner, Head of Department, for his help in making this research possible, especially with regard to obtaining financial support for the author through the Overseas Research Student Awards and the Postgraduate Scholarship of Glasgow University,

Dr. K.S. Varyani, the Deputy Superintendent of the Hydrodynamics Laboratory and Supervisor of this research work, for his patient guidance, valuable advice and endless encouragement. The discussions which they had are instrumental to the success of the work undertaken for this thesis,

Dr. A. Incecik, the Superintendent of the Hydrodynamics Laboratory, for his kind assistance and valuable discussions,

Mr. R.B. Christison and Mr. D.J. Sinclair, the Chief and Deputy Technician, and all the Mechanical Workshop Technicians, Mr. J.M. Aitken, Mr. F. Sweeney, Mr. D. Nicolson and Mr. G. Dunning, for making the tank testing facilities available, constructing the models and their continuous help during the tedious experiments,

Mr. D. Percival, the Senior Technical Programmer, for his helpful assistance to overcome several numerical difficulties during theoretical computations and experimental analyses,

Dr. H.S. Chan, Mr. B. Hamoudi and Mr. O.S. Williams et al, the Researchers and Staff of the Department, for their warm friendships.

Finally the author would like to thank to his lovely wife Ching-Jung for her endless encouragement and mental support during his study at Glasgow University, to his daughter Yphaye who could not see her papa as much as she wanted and to his loving parents for their continuous interest and encouragement throughout his achievement.

SUMMARY

This thesis is in two volumes and the second one contains the Figures.

Dynamic motion responses of twin hulled offshore structures, such as semi-submersible drilling rigs, are of more concern to designers of offshore structures than those of ships, since it is not easy for such offshore structures to move away from stormy weather. These structures should operate stably around their fixed positions and, from the viewpoint of practical design and construction, they should be well designed to withstand severe wave excitation forces in general.

A lot of the twin hulled offshore structures designed for developing the ocean resources are of two submerged long body configuration. Their behaviour in waves with crests parallel to the long body axis are studied by considering the motion dynamics of two rigidly connected submerged cylinders in waves and the two dimensional radiation and diffraction problems are investigated with the forward speed effect (equivalent current effect). Under a linear assumption of the boundary value problem, the numerical solution is obtained exactly by solving the integral equation for the velocity potential on the body surface.

Chapter One surveys the history of this research work on motion dynamics of floating offshore structures in waves. The new developing theories for predicting radiation forces and wave excitation forces to improve numerical accuracy and computational efficiency are reviewed and a preliminary study on the hydrodynamic behaviour of floating offshore structures in waves is performed. The practical prediction of the Froude Krylov forces acting on floating buoys and twin hulled vehicles in waves is also carried out. The engineering application of the hydrodynamic behaviour of the floating buoys with the mooring systems in waves is reviewed and extended to twin hulled offshore vehicles.

In Chapter Two the complete boundary value problem is theoretically formulated for the velocity potential , which describes the unsteady flow around a submerged long cylinder advancing with a constant forward speed and with wave crests parallel to the long body axis. The theoretical terms due to the forward speed effect are included in the body boundary conditions. The effect of non-uniformity of the steady flow induced by the forward speed in the neighbourhood of the submerged structure is especially considered.

In Chapter Three the mathematical formulation of the Green function for this hydrodynamic problem is described theoretically and its derivatives are worked out for the solutions of the velocity potential over the body boundary contours in the integral equations. The mathematical manipulation of the Green function which makes the numerical computations more convenient is achieved.

In Chapter Four comprehensive derivation of analytical expressions for the radiation and wave excitation forces acting on the submerged structure is described in detail. These forces are of first order with respect to the motion responses and wave amplitudes. Due to forward speed effect there is a contribution from the hydrodynamic restoring force terms proportion to the body displacement. The theoretical relation between the work done by the damping force and the energy transportation of the generated waves by the body motions is mathematically derived and is applied to confirm the accuracy of numerical computations. Based on such radiation forces and wave excitation forces, the motion equations of the dynamic responses of the submerged structure translating at a constant forward speed (equivalent current speed) in waves, but left to oscillate freely, are systematically formulated.

In Chapter Five the theoretical formulation of the m-vector contribution due to the effects of the forward speed and the interaction between two submerged hulls is derived by the image method. The mathematical expression of the m-vector contribution for the single submerged circular or elliptical cylinder is also described. The predicted results in the hydrodynamic aspects with the m-vector

contribution are compared with and without taking the m-vector contributions into consideration. The parametric studies are performed on the hydrodynamic characteristics such as the added mass and damping coefficients and the real and imaginary part of the Kochin functions, with and without the m-vector contributions for different submerged depths, Froude number, separation distance and inclinations.

In Chapter Six the mathematical formulation of the restoring forces due to the forward speed effect for the submerged single and twin circular cylinder cases is derived in detail and the numerical results of the submerged two circular cylinder case is confirmed by the analytical solution of the submerged single circular cylinder case. The dynamic motion responses of an inclined offshore twin hulled structure with and without restoring forces due to the forward speed effect in head and following waves are extensively investigated. The results of a parametric study of the dynamic motion responses of a twin hulled offshore structure for different submerged depths, Froude numbers (equivalent current effect), separation distances and inclinations in head and following waves are studied and discussed. Moreover, the dynamic motion behaviour of twin hulled marine vehicles in the low frequency region at resonance is also investigated.

In Chapter Seven the second order horizontal forces, based on the far field approach, in head and following waves are theoretically formulated and the second order horizontal and vertical forces, based on the near field approach, are also mathematically derived to take into account the effects of the forward speed and interactions between the two hulls. The steady tilt moments due to the effects of the second order forces on an inclined twin hulled structure are predicted to investigate the steady tilt behaviour in head and following waves. The analysis is based on the near field approach and takes into consideration the second order forces in both the horizontal and vertical directions. The numerical result of the near field approach is compared with that of the far field approach and good agreement is confirmed in both second order horizontal and vertical forces. A parametric study of the steady tilt moment acting on the twin hulled vehicle for different submerged depths, current speeds, separation distances and inclinations in head and following waves

is completely investigated. The predicted results of the steady tilt moments due to second order forces are compared with experimental results.

In Chapter Eight both numerical methods, i.e. the discrete source distribution method and the direct Green function method, are reviewed and modified to predict the hydrodynamic interaction of submerged two rigidly connected cylinders advancing in waves. The velocity potential in both methods is calculated by the discrete source distribution technique and the direct solution by the classical integral equation method. The numerical results based on both approaches are comprehensively investigated and it is confirmed that the direct Green function method can deal effectively with such kinds of hydrodynamic problems as far as computational efficiency and numerical accuracy are concerned. It is obvious that as the number of discrete elements on the body surface increases, the numerical accuracy improves. However, a major concern of researchers in marine hydrodynamics is computational efficiency. The direct Green function method with the optimum numbers of discrete elements and images of dipoles are proposed for numerical computations.

In Chapter Nine a mathematical approach using the linear optimal control concept to study the dynamic positioning behaviour of twin hulled marine vehicles is briefly introduced. Experimental work on dynamic positioning aspects of a twin hulled structure is described. A series of experiments were carried out in the Hydrodynamics Laboratory for different submerged depths and trim and drift angles and the sway force and yaw moment acting were measured. Mathematical equations are then fitted so that researchers can make use of these results in simulation analyses for the manoeuvring performance and dynamic positioning of twin hulled marine vehicles.

In Chapter Ten calculated results of the hydrodynamic coefficients between both Tasai's practical and present fundamental approaches are compared and discussed. The results of the steady tilt moments by direct pressure integration are compared with those of experimental work performed in Japan and a parametric

study for different inclinations in varying current speeds is carried out. The predictions of steady tilt moments acting on twin hulled vehicles from previous theoretical approaches are compared and discussed. The calculated results from the present approach is then compared with those from this previous theoretical and experimental work. In particular the work performed by Martin et al (1978) is reviewed and the concept of Martin's model is discussed. The results of both approaches are investigated. The effects due to forward speed and interactions between two hulls using the Martin-type model are extensively investigated and the numerical results are discussed in detail. The effects of the viscous and waterline forces acting on the vertical surface piercing columns on steady tilt behaviour of an inclined offshore structure are studied and discussed. The predicted results for a typical offshore twin hulled structure model, based on the present theoretical approach, are presented to demonstrate the overall value of this research work for engineering applications to twin hulled marine vehicles under the combined actions of wave and current.

Chapter Eleven reviews the original achievements of the work, it draws some conclusions and discusses recommendations for future work.

CONTENTS

NOMENCLATURE

Notations commonly used in the thesis are described here. However in certain cases where certain notations are not frequently used, they are described as and where they appear in respective chapters.

A	Amplitude of incident waves
$A_{1,2,3,4}$	Amplitude of the waves at infinity
A_{k_j}	Added mass coefficient in the k-th direction due to the j-th mode of motion
A_{ij}^{L}	Added mass coefficient of the left cylinder associated with the force in the i-th direction due to the j-th mode of motion.
$\frac{A_{ij}}{\rho\pi a^2}$	Non-dimensionalized added mass coefficients for single cylinder system
$\frac{A_{ij}}{2\rho\pi a^2}$	Non-dimensionalized added mass coefficients for two cylinder system
B_{k_j}	Damping coefficient in the k-th direction due to the j-th mode of motion
B_{ij}^{L}	Damping coefficient of the left cylinder associated with the force in the i-the direction due to the j-th mode of motion.
$\frac{B_{ij}}{\rho\pi a^2\omega}$	Non-dimensionalized damping coefficients for single cylinder system
$\frac{B_{ij}}{2\rho\pi a^2\omega}$	Non-dimensionalized damping coefficients for two cylinder system
$\left\|\frac{B_{jj}(P)-B_{jj}(E)}{B_{jj}(P)+B_{jj}(E)}\right\|\times 100\%$	- Relative error of damping coefficients
C	Phase speed of the waves

C_{k_j}	Restoring coefficient in the k-th direction due to the j-th mode of motion
$E_1(z)$	Exponential integral
E_j	Wave exciting force in the j-th direction
$\frac{E_j}{\rho g A a}$	Non-dimensionalized wave excitation forces for single cylinder system
$\frac{E_j}{2\rho g A a}$	Non-dimensionalized wave excitation forces for two cylinder system
$\bar{F}_j$	Second order steady force in the j-th direction
$\frac{\bar{F}_j}{0.5\rho g A^2}$	Non-dimensionalized second order forces for two cylinder system
Fn	Froude number ($= U/\sqrt{ga}$)
$F_y(F.K.)_1$	Froude Krylov force per wave amplitude acting on vertical columns in sway motion (FYFK1)
$F_y(F.K.)_2$	Froude Krylov force per wave amplitude acting on submerged pontoon in sway motion (FYFK2)
$F_y(F.K.)$	Total Froude Krylov force per wave amplitude acting on twin hulled model in sway motion (TFYFK)
$F_y(\ddot{\eta}_\omega)_1$	Wave excitation force per wave amplitude acting on vertical columns in sway motion (FYYAW1)
$F_y(\ddot{\eta}_\omega)_2$	Wave excitation force per wave amplitude acting on submerged pontoon in sway motion (FYYAW2)
$F_y(\ddot{\eta}_\omega)$	Total wave excitation force per wave amplitude acting on twin hulled model in sway motion (TFYYAW)
F_y	Total sway force per wave amplitude acting on twin hulled model (TSWAY)
F_{z11}	Froude Krylov force per wave amplitude on twin hulled model in heave motion (FZ11)
F_{z12}	Wave excitation force per wave amplitude on twin hulled model in heave motion (FZ12)
F_{z1}	Total heave force per wave amplitude on twin hulled model (TFZ)
G(P,Q)	Green function

$H^+(k), H^-(k)$	Kochin functions of upstream and downstream waves
$H_D^+(k), H_D^-(k)$	Kochin functions of diffraction waves
$H_F^+(k), H_F^-(k)$	Kochin functions of waves due to free oscillation of the body
$H_j^+(k), H_j^-(k)$	Kochin functions of the j-th mode radiation waves
$\tilde{H}_j^+(k), \tilde{H}_j^-(k)$	Kochin functions of the reverse flow radiation waves
I_x	Average momentum flux at x
Ka	Encounter wave number $(=\frac{\omega_e^2 a}{g})$
K_0	Wave number of the steady waves $(=g/U^2)$
$\frac{M}{0.5\rho g A^2 l}$	Non-dimensionalized steady tilt moments for two cylinder system
M	Mass of the cylinder of unit length
$M_\theta(F.K.)_{11}$	Pitch moment due to Froude Krylov force per wave amplitude acting on submerged pontoons (PMFK11)
$-M_\theta(F.K.)_{12}$	Pitch moment due to Froude Krylov force per wave amplitude acting on submerged pontoons with column correction (PMFK1M)
$M_\theta(\ddot{\zeta}_\omega)$	Wave excitation moment per wave amplitude acting on submerged pontoons in pitch motion (PMZAW)
$M_\theta(F.K.)_1 + M_\theta(\ddot{\zeta}_\omega)$	(TPMFKZ)
$M_\theta(F.K.)_2$	Pitch moment due to Froude Krylov force per wave amplitude acting on vertical columns (PMFK2)
$M_\theta(\ddot{\xi}_\omega)$	Pitch moment due to wave excitation force per wave amplitude acting on vertical columns (PMXAW)
M_θ	Total pitch moment acting on twin hulled model (TPM)
$M_\varphi(F.K.)_1$	Roll moment due to to horizontal Froude Krylov force per wave amplitude acting on vertical columns (AMRFK1)
$M_\varphi(F.K.)_2$	Roll moment due to to horizontal Froude Krylov force per wave amplitude acting on submerged pontoons (AMRFK2)
$M_\varphi(F.K.)_3$	Roll moment due to to vertical Froude Krylov force per wave amplitude acting on submerged pontoons (AMRFK3)
$M_\varphi(F.K.)$	Total roll moment due to Froude Krylov forces per wave amplitude acting on twin hulled model (TAMRFK)

$M_\varphi(\ddot{\eta}_\omega)_1$	Roll moment due to wave excitation force per wave amplitude acting on vertical columns (AMRYW1)
$M_\varphi(\ddot{\eta}_\omega)_2$	Roll moment due to wave excitation force per wave amplitude acting on submerged pontoons (AMRYW2)
$M_\varphi(\ddot{\eta}_\omega)$	Total roll moment due to wave excitation force per wave amplitude acting on twin hulled model (TAMRYW)
$M_\varphi(\ddot{\zeta}_\omega)$	Roll moment due to wave excitation force per wave amplitude acting on submerged pontoons (AMRZW)
M_φ	Total roll moment acting on twin hulled model (TMROLL)
N	Element number of the cylinder's contour
N_E	Number of discretized elements
N_I	Number of selected images
N_L	Number of discretized elements on the left cylinder
N_R	Number of discretized elements on the right cylinder
$\bar{P}(x,y,t)$	Dynamic pressure acting on the surface of the body
S_B	Water bottom
S_F	Free surface
S_H	Body surface of the cylinder
$S_{\pm\infty}$	Vertical surfaces at $x = +\infty$ and $x = -\infty$
T	Wave period (seconds)
T_{ij}	Transfer function
U	Forward speed of the body
$\bar{V}$	Steady flow vector
$\frac{\lvert X\rvert}{\rho g \pi r_0^2 \zeta}$	Non-dimensionalized Froude Krylov forces in surge direction
$\frac{\lvert Y\rvert}{\rho g \pi r_0^2 \zeta}$	Non-dimensionalized Froude Krylov forces in heave direction
a	Radius of a circular cylinder, length of semi major axis of ellipse
b	Radius of a circular cylinder, length of semi minor axis of ellipse
c	Separation distance between two cylinders (= 2l)
d	Depth of the cylinder's center
$k_{1,2,3,4}$	Wave numbers
ka	Non-dimensionalized wave number $(= \frac{\omega^2 a}{g})$

$\vec{m}$	Vector m describing the forward speed effect of the body boundary condition
m_i	The mass (for i = 1,2) or the moment of inertia (for i = 3) of the two rigidly held apart cylinders
$\vec{n}$	Unit vector normal to the body surface
n_1, n_2	The x and y components of $\vec{n}$
n_3	$= xn_2 - (y-d)n_1$
$\vec{r}(x,y)$	Coordinate of a point in the reference frame fixed in space
$\vec{r}(x',y')$	Coordinate of a point in the body fixed reference frame
$u(x)$	Heaviside's unit function
$\frac{y_a}{\varsigma_a}$	Non-dimensionalized sway amplitude
$\frac{z_a}{\varsigma_a}$	Non-dimensionalized heave amplitude
α	Inclining angle which the line joining the centres of two cylinders makes with the x-axis
$\tilde{\alpha}$	Motion response of two cylinder model with inclinations
ε	thinness ratio of ellipse
ε_Y	Sway phase angle (in degree)
ε_Z	Heave phase angle (in degree)
ε_θ	Roll phase angle (in degree)
ε_φ	Pitch phase angle (in degree)
θ	Inclining angle
$\frac{\theta_a}{k\varsigma_a}$	Non-dimensionalized pitch amplitude
$\frac{\varphi_a}{k\varsigma_a}$	Non-dimensionalized roll amplitude
$\Phi(x,y,t)$	Velocity potential of total flow
$\phi(x,y)e^{i\omega t}$	Velocity potential of unsteady flow
$\varphi_S(x,y)$	Velocity potential of steady flow
$\varphi_I(x,y)e^{i\omega t}$	Velocity potential of incident waves
$\varphi_D(x,y)e^{i\omega t}$	Velocity potential of diffraction waves
μ	Rayleigh's fictitious friction coefficient

$\psi_j(x,y)e^{i\omega t}$	Velocity potential of radiation waves with the j-th mode of unit velocity potential
$\tilde{\psi}_j(x,y)e^{i\omega t}$	Reverse flow radiation potential
τ	$= U\omega/g$
ω_0	Circular frequency of incident waves in the reference frame fixed in space
ω	Circular frequency of encounter with incident waves or circular frequency of oscillation
δ_{ij}	Kroenecker delta function
ξ_j	Complex amplitudes of oscillatory motions (j=1 : surge, j=2 : heave, j=3 : pitch, clockwise rotation about the centre of cross section of the body)
ξ_ω	Motion displacement of wave particle in x direction
$\frac{\lvert\xi_1\rvert}{A}$	Non-dimensionalized surge amplitude for two cylinder system
$\frac{\lvert\xi_2\rvert}{A}$	Non-dimensionalized heave amplitude for two cylinder system
$\frac{\lvert\xi_3\rvert}{A}$	Non-dimensionalized pitch amplitude for two cylinder system
η_ω	Motion displacement of wave particle in y direction
ς_ω	Motion displacement of wave particle in z direction
$\zeta_\omega(x,t)$	Wave depression

LIST OF FIGURES

CHAPTER 2

CHAPTER 3

CHAPTER 4

CHAPTER 5

CHAPTER 6

CHAPTER 7

CHAPTER 8

CHAPTER 9

CHAPTER 10

LIST OF TABLES

CHAPTER 8

CHAPTER 1
INTRODUCTION AND PRELIMINARY STUDIES

1.1 Historical review on hydrodynamic problems due to forward speed effects

With the linear assumption of the fluid flow, the hydrodynamic forces acting on a structure advancing in waves are categorized into radiation forces and wave excitation forces. The former term is the added mass and damping forces due to the body oscillatory motions in a calm water. The latter one is the hydrodynamic pressure forces acting on the structure in the incident wave train and the body is restrained at its mean position with its motions suppressed. In compliance with the linear approximation of the fluid flow which is valid when the amplitudes of body motions are relatively small in terms of the other length scales, for instance, wave length and body dimensions, the total hydrodynamic forces acting on the translating structure in incident waves can be directly superposed by the terms mentioned above.

In principal, the history of researches on the motion dynamics of floating ships and offshore structures in waves is that of adventure to discover new developing theories for calculating radiation forces and wave exciting forces with improving engineering accuracy. The historical review of previous research work is briefly surveyed as follows.

The strip theory is often used to predict the hydrodynamic forces acting on ships in waves. Several basic assumptions are emphasized to make the numerical solution effective. Ship hull form is considered as a slender geometry and the frequency of the body motion must be high, in other words the length of the waves generated by the ship motions is relatively shorter than the principal dimensions of

the ships. The fundamental concept of the strip theory is to calculate hydrodynamic forces acting on the hull surface of ships as the sum of the hydrodynamic forces acting on each cross section of the ship in the longitudinal direction without considering ship lengthwise fluid flow, in other words, assuming two dimensional flow around each cross section. The two dimensional flow can be simulated to study the hydrodynamic problem of a long cylinder in the direction of the cross section.

A reasonable solution of two dimensional flow around a circular cylinder oscillating on the free surface of the water was given by Ursell (1949) for the first time in the history of marine hydrodynamics. A solution for the more ship-like sectional form was followed by Tasai (1959). However those results gave the radiation and wave excitation forces on a limited family of ship hull forms. More numerical methods were developed to predict hydrodynamic forces on the arbitrary sectional hull form on the free water surface (Frank 1967, Maeda 1969). Perhaps the improvement of the numerical computations in theoretical approaches was due to the effective development of high speed computer systems. The first and second order forces acting on a circular cylinder was analysed by Ogilvie (1963).

All solutions stated above were based on a single cylinder. However the solution of two dimensional flow around two circular cylinders oscillating on the surface of the water was developed by Ohkusu (1969,1970) and several interesting phenomena due to the effects of interactions between two hulls, for instance the negative added mass and zero damping forces at certain particular frequencies were observed.

Obviously the ship has a forward speed, so the effect of the forward speed on the ship motions should be taken into account. But, to account for the forward speed effect together with the existence of the free surface, the hydrodynamic behaviour of the ship motion becomes more complicated. Hence, the forward speed effect is not considered in the fundamental formulation of the strip theory, so it cannot predict accurate solution for the ship motions at high speed.

Frequencies of ship motions are high in head waves and lower in following waves. On account of the effects of the ship forward speed, low encounter frequencies with the following waves lead to low frequencies of the ship motions. In fact the strip theory is not reliable for the low frequency motions (Ogilvie and Tuck 1969) and gives less accurate predictions (Takezawa et al. 1981, 1982).

New reasonable approaches for ship motion theories which do not depend on two dimensional treatment of the fluid flow and does consider the forward speed effect correctly in the theoretical formulation are required for more accurate predictions of the hydrodynamics in various wave conditions especially in following waves. Hence the three dimensional integral equation method was proposed and developed by several researchers (Inglis and Price 1981, Ohkusu and Iwashita 1986). This theoretical approach is to solve numerically the distribution of singularities around the ship hull such that the flow field must satisfy the free surface and ship surface boundary conditions properly. For zero forward speed, this method predicts reasonable solutions (Michelsen and Faltinsen 1974, Standing and Hogben 1974). For finite forward speed, some analytical ambiguity in the theoretical formulation has not yet been overcome so far and the available predicted results are few and not reliable within acceptable engineering accuracy. Therefore further research work needs to be done in this field but with a simpler geometry and more tractable conditions.

The forward speed effect is also recognized in the other aspects of ship motion theories. One is the added resistance of a ship, similar to second order horizontal forces on an offshore structure, in waves (Ohkusu 1984, Naito et al. 1985). The other is the damping moment with rolling motion caused by the viscosity of the fluid (Himeno 1977).

So far the ship motion theory keeping the motions in the frequency domain in mind has been overviewed briefly. The time domain analysis of the ship motions is not described because it might not be directly related to the contents of this research work. The calculated results in the frequency domain analysis are applied to predict the dynamic motion responses of the surface vessels and offshore structures in

irregular waves with the introduction of the superposition principle (St. Denis and Pierson 1953).

The floating offshore structures for developing petroleum under the deep sea bottom are often called mobile drilling units. This kind of offshore structures must be a stable platform which is able to keep station. Their seakeeping performance to withstand the severe environment is quite crucial. Hence the dynamic motion responses in waves is one major concern of designers and engineers in the offshore industries. The interesting characteristics in the geometry of the offshore structures are a small water plane area compared with their displacement which originates from the form of large buoyancy bodies submerged under the water surface and the slender columns piercing the free surface to support the upper platform. This obviously leads to lower natural frequencies of heaving, pitching and rolling; generally speaking the oscillatory motions of the offshore structures in waves are limited within the small magnitude (Tasai 1983) due to their geometries.

The other characteristics of the hydrodynamic forces due to the geometries of the offshore structures are that of drag forces induced from the fluid viscosity which are dominant on the slender parts of the structure, if the wave height is larger than the cross sectional dimensions of the offshore structures (Sarpkaya and Isaacson 1981).

In general offshore structures are moored with several mooring lines. Mooring lines are principally soft springs to resist the steady forces from various sources, for example current and waves, such that the offshore structures do not displace so much from their mean positions. In this aspect the accurate prediction of the steady wave forces which are usually of second order is required exactly. The steady wave forces in the vertical direction induce the steady tilt moments which affect the stability of the offshore structures in waves is presented by Numata et al (1976).

One reason for this rather large inclination by the second order forces is due

to the relatively small water plane area of the offshore structure. Moreover the reaction of mooring lines in this situation might increase their inclination. Thus the steady forces due to waves as well as current and winds are certainly important factors which affect the safety of the offshore structures with mooring lines (Takarada et al. 1984a, 1984b, 1985).

Combined effects of current and waves or wind and waves on the stability of the offshore structures have been investigated experimentally (Takarada et al. 1984a, 1984b, 1985) ; the theoretical methods to predict environmental forces under the influence of combined effects have not yet been proposed.

The reaction of the mooring lines to restore the displacement of the offshore structures to their mean positions is generally very small in terms of the mass of the structure; natural periods of the dynamic motions in the horizontal plane, such as surging, swaying and yawing, are basically longer than 100 seconds. In fact there are no waves of such long periods at sea; no wave excitation forces of the first order of magnitude act on the offshore structure at such a long period. However the second order forces due to sea waves, which are composed of various frequency components, include wave excitation forces with the different frequency of two component waves. In principal the sea wave always has a continuous power spectrum and the difference frequency of two components can be small enough to generate wave excitation forces of such long periods. Although this wave excitation force is of second order, it may cause low frequency motions of large magnitude at resonance because of the low damping force at such a specifically low frequency (the first order motions with the same frequency as waves are hereafter referred to as fast frequency motions as contrasted with low frequency motions). The strength of mooring lines has to be determined such that they can withstand this large displacement of the low frequency motion in the resonant condition (Hsu and Blenkarn 1970, Arai et al. 1976).

The combined motion of low and fast frequencies was analysed by Triantafyllow (1980, 1982). The velocities of the low and fast frequency motions

were assumed to be of identical order of magnitude. Nevertheless the effect of the velocity of the low frequency motion on the fast frequency motion was not considered at that moment. Hence the amplitude of the low frequency motion is supposed to be very large compared with that of the fast frequency motion, the former could be appropriately considered as a quasi-steady motion. With such an approximation the interaction between both motions can be treated as the constant speed effect on the fast frequency motion.

The low frequency motion occurs at resonance ; so its amplitude is certainly determined only by the value of the damping force. Recently it was found that damping forces of the body moving with long stroke in short waves is larger than that of the body moving in calm water (Wichers 1979). Discussions on the origin of the increase of damping forces in waves have not been concluded. To attribute this damping force to added resistance, a second order horizontal force acting on the structure translating in waves was proposed by Saito (1984). The dependence of the velocity on the added resistance (the second order forces) is quite complicated but the tendency is of linear dependence, i.e. the damping force proportional to velocity, can be obtained by assuming moderate variation of the velocity from the mean value.

As mentioned above, theoretical analysis and practical prediction of the hydrodynamic loadings acting on ocean going ships and offshore vehicles which account for forward speed effect in waves is rather important for the solutions of major research topics in ship motion marine hydrodynamics. Here the topics of present work is summarized as follows.

(1) To formulate theoretically and solve numerically a boundary value problem for the velocity potential describing the flow field around a twin hulled offshore structure oscillating in waves and simultaneously translating at a constant forward speed.

(2) For correct evaluation of the hydrodynamic loadings acting on offshore structures, it is necessary to understand the forward speed effect in the case of a

single cylinder as most lower hull structures are circular cylinders.

(3) To predict the hydrodynamic forces acting on a two cylinders rigidly held apart with no further modelling. This represents a simplified model of an offshore structure in the beam sea condition.

(4) To discuss several interesting topics in the offshore engineering field associated with the interaction of wave and current and that of the low and fast frequency motions with the forward speed effect on the hydrodynamic forces acting on such twin hulled marine structure configurations.

(5) To investigate the steady tilt moment due to the steady second order forces and dynamic motion responses with the hydrodynamic restoring forces due to the effects of forward speed and interactions between two hulls of the inclined twin hulled offshore structures in head and following waves.

1.2 Preliminary studies in the ocean engineering field

Preliminary studies of the hydrodynamic behaviour of floating buoys and twin hulled vehicles in waves were performed. The practical engineering applications to the dynamic motion responses of floating buoys with mooring systems in waves and their extension to twin hulled offshore structures is also performed. The spectral analysis of the motion dynamics of floating buoys and twin hulled marine structures in waves is carried out for ocean engineers and designers from the point of view of practical engineering applications.

In fact, these theoretical approaches to predict the hydrodynamic loadings and motion responses of floating buoys and twin hulled structures in the incident wave condition are simplified so that practical computations are easily performed on desktop computer systems and it is also confirmed that the computer programs developed here are rather convenient and effective from the practical point of view

of engineering design considerations of offshore structures in general. From an analysis of the computation time taken for these calculations, it is found that the CPU time is only a few seconds on the VAX 3600 micro computer system. Hence this is an efficient and economical tool for engineers and designers.

The predicted results are also compared with those from previous theoretical and experimental research work and they show reasonable accuracy for practical engineering applications.

1.2.1 Practical approach to Froude Krylov forces on floating buoys and semi-submersibles in heeled conditions

In the offshore engineering field, one of the most attractive and important technical themes is the prediction of hydrodynamic loadings acting on floating buoys and twin hulled marine structures in waves. In general, the conventional offshore structures consist of several structural members, such as bracings, brackets, columns and caissons (lower hulls). The simplest representation of wave excitation forces and moments is based on the assumption that the pressure field is not affected by the presence of the structure and can be approximately determined from the incident wave potential itself. This approach was utilized in the earliest theories for ship motions in waves and is also known as the Froude Krylov hypothesis.

The hydrodynamic forces acting on floating buoys are obtained by direct pressure integration over the body boundary contours. The theoretical approach adopted here is worked out for the case of hydrodynamic forces acting on the left body of the twin hulled structure. The forces acting on the right body of the twin hulled offshore structure can also be written by a slight manipulation of the mathematical equations. Summing up hydrodynamic forces described above, the hydrodynamic forces on the twin hulled offshore structure are obtained, for instance the caisson (hereinafter referred to as " D - buoy ") is considered. A

system can then be composed to be considered as a twin hulled marine structure in general.

The exact solution obtained here is in the framework of the linear theory and interaction effects between the two bodies is neglected. These computed results are compared very well with those from previous approximate research work (Tasai 1983) and are sufficiently accurate for engineering practice, i.e. for large values of the ratio of the wave length to the column diameter, the exact and approximate solutions match very well.

The theoretical calculations are performed on the DEC VAX 3600 micro computer system to obtain hydrodynamic forces on the cylindrical buoy (hereinafter referred to as " C - buoy "), D - buoy and the modified box shape base buoy, which is referred to as " P - buoy " and the details of the coordinate system and of the three different buoy configurations are also indicated in Figs. 1.1, 1.2 and 1.3 respectively. A comparison study of the hydrodynamic forces for three different configurations of twin hulled structures is performed and a parametric study of the floating buoys and twin hulled structures for different separation distances and inclinations is also investigated. Series of experiments to measure the Froude Krylov forces acting on three such different kinds of floating buoys in restricted conditions were performed at the Hydrodynamics Laboratory of Glasgow University, which is 77 m long x 4.6 m wide x 2.7 m deep (maximum water depth 2.4 m).

The wave signals detected by three wave probes are picked up by the Wave Monitoring System (including amplifiers and filters) and the hydrodynamic loads in both horizontal and vertical directions are measured by a straight strain gauge bar and are passed to the FYLDE amplifier and filter system. All the signals are then collected by the Data Collecting System (32 channel analogue to digital converter) and recorded in the Macintosh-2CLA micro computer system as shown in Fig. 1.4. The experimental data are sampled at a rate of one hundred (100) samples per second per channel for twenty (20) seconds.

In the experiments, each buoy model is mounted below the straight bar, which can measure both horizontal and vertical strains simultaneously, and tested in regular incident waves with several different frequencies. The calibration of the straight bar facility, as shown in Fig. 1.5, is individually performed before each experiment is started. All relations of these calibration data, which are converted from induced voltages to actual loads, are linear in general.

All experimental data acquired by the Macintosh-2CLA computer is analysed in the frequency domain with the Fast Fourier Transform technique on the VAX-3100 workstation computer system and in time domain on the VAX/VMS computer system. A comparison study of the predictions between direct pressure integration and experiments is carried out on the Macintosh Plus micro computer system systematically. Basically the experimental data acquisition and analysis system at the Hydrodynamics Laboratory is well set up to deal with hydrodynamic research.

Figs. 1.6 and 1.7 show that the predicted results are in excellent agreement with that of previous researchers (Tasai 1983). The theoretical predictions are also compared with experimental results. In general the theoretical results show reasonable agreement with the experimental ones as Figs. 1.8 to 1.13. Nevertheless some discrepancies induced by several effects, for instance wave diffraction, fluid viscosity and experimental error etc do occur from these experiments and these buoy models in experiments are as in Figs. 1.14 (see pp312), 1.15 and 1.16.

Through a validity test of the computer program, the effectiveness is confirmed for the prediction of the Froude Krylov forces on floating buoys and twin hulled offshore structures in regular waves. Based on specific parameters, such as inclinations and separation distances between two bodies of the twin hulled structure, the force prediction of twin hulled offshore structures is calculated in order to have an extensive knowledge in the field of Froude Krylov forces on floating buoys and offshore structures in regular progressive waves. As for the inclination effect of floating buoys shown in Figs. 1.17 and 1.18, no significant

changes in force prediction is shown in the heave direction. But in the surge mode, the results with no inclination are always larger than that with inclination (5 or 10 degrees) in the range of wave periods. Moreover calculated results with these inclinations show not much variation in general.

In order to extend this study further, the forces acting on the left and right bodies of a twin hulled offshore structure are calculated. The results of both surge and heave forces on each body are as Figs. 1.19 and 1.21 and the phase angles are also presented in Figs. 1.20 and 1.22. The investigation of Froude Krylov forces on three twin hulled structures with different configurations is performed for comparison with previous researches (Tasai 1982 and Wu 1991) and all basic configurations of three different twin hulled models (hereinafter referred to as SSCH models) are shown in Figs. 1.23 to 1.25. In general the calculated results of the SSCH-1 model, shown as Figs. 1.26 and 1.27, show very good agreement with approximate results of other researchers. Similar results for the SSCH-2 and SSCH-3 models are shown in Figs. 1.28 to 1.31. In spite of the range of rather short wave periods, the trends of the calculated results also show reasonable agreement with approximate results (Tasai 1970 and Wu 1991). The pressure integration predicted values of surge forces are generally a little smaller than that of the approximate approach and the calculated results of heave forces are slightly larger. These discrepancies could be mainly due to the form approximations of twin hulled structures.

In practical computations, the exact solution can be reduced to the approximate one when the wave length tends to infinity (i.e. $k \rightarrow 0$). It can be shown that at least for the range of $\lambda/2r_0$ more than 20, the approximate formula of Tasai is in fairly good agreement with the exact solution. For large value of $\lambda/2r_0$, there is hardly any variation in heave force for different inclinations. However it is also noticed that there is an appreciable variation in the surge force and this is confirmed by experimental results.

1.2.2 Dynamic motion responses of floating buoys in waves

A wide variety of storage buoys and their anchoring arrangements in waves have been proposed and constructed in recent decades. A majority of these offshore structures are composed of combinations of circular cylinders with a common longitudinal axis in general.

The approach to predict the highest expected wave excitation forces on offshore structures in waves is based on single regular wave concept. For a particular wave theory, with a certain wave height and wave period chosen to the location of the structure, the corresponding pressure field and horizontal components of the wave particle velocity and acceleration are then determined. The wave kinematics can be written as an appropriate form of the Morrison equation to calculate hydrodynamic loadings acting on structural components of floating offshore buoys in regular waves.

Here a ***strip*** approach is applied in conjunction with linear wave theory and the drag effect is reasonably designed for structural components of floating offshore structures. In general, this simplified approach cannot predict well when the wave length is five (5) times less than the maximum diameter of the cylinder. The approximate approach is derived to predict dynamic motion behaviours of floating buoys in regular progressive waves and the computer program is also developed in order to investigate effects for different geometrical combinations of floating buoy structures in waves.

In principal the wave induced forces on offshore structures in waves are due to Froude Krylov effect (dynamic pressure forces), inertial effect (acceleration forces) and drag effect. The summation of these forces in both horizontal and vertical directions obtains non-zero resultant and it induces surge, heave and pitch motions of offshore structures in waves. The forces due to Froude Krylov and inertial effects can be calculated by linear wave theory as long as the cylinder diameter is less than one fifth (1/5) of the wave length. Otherwise the diffraction effect should be properly considered. The drag forces due to the velocity effect are

not linear, since they depend on the square of the velocity. Compared with the pressure and inertial forces acting on large diameter cylinders, such forces are insignificant but they are important when either the resultant of the former two drops to zero values or at extreme wave lengths. Here based on the Morrison approach, an approximate approach to predict dynamic motion behaviours of floating buoys and offshore structures in regular waves is derived and the computer program is also developed for engineering design applications.

The coordinate system of the floating buoy structures in regular waves is as in Fig. 1.32 and the buoy models are the same as shown in Figs. 1.2 and 1.3. The approximate predictions based on the theory of body motions in regular waves show good agreement with that of previous researches (Tasai 1983). The forces due to inertial and drag effects on both upper and lower portions of the floating buoy structure in regular waves are calculated and the predicted results for the " P - buoy " model in surge, heave and pitch modes are presented in Figs. 1.33 to 1.38 respectively. As noticed in these figures, the force due to inertial effect is dominant and that due to drag effect is not significant for the chosen wave periods.

A series of experiments on dynamic motion responses of floating buoys in regular incident waves were carried out for three different kinds of buoy configurations at the Hydrodynamics Laboratory. A regular wave signal is generated by a plunger type wave maker driven by an electrically controlled hydraulic pump handled by a DELL-200 micro computer system as in Fig. 1.39 and the wave amplitude is measured by three resistance type wave probes. The model is equipped with two inclinometers to measure roll and pitch angles. The surge and heave motions are also measured by the SELSPOT system. This system enables rigid body measurements to be carried out by a pair of light emitting diodes mounted on the model which transmits signals as the model oscillates in waves. The signals generated by the diodes are picked up by a set of cameras located beside tank bank around the model. The data acquisition by the computer system is started when the model behaviour in waves reaches the most steady and consistent pattern.

Here a complete description of hydrodynamic experiments for data acquisition is described systematically and the detail of such system is also shown in Fig. 1.40. The wave signals detected by three wave probes are picked up into the Wave Monitoring System (including amplifiers and filters). Then these signals are passed through the Data Collecting System (32 channels analogue to digital converter) and recorded into the Macintosh-2CLA computer system. The horizontal and vertical displacements of floating model in waves are detected by the SELSPOT system. The displacement signals of the model in motions are picked up by opto-coupled cameras. Then these signals through the Movement Monitoring Instrument System (SELSPOT processing unit) and Data Collecting System are recorded into the micro computer system. The horizontal and vertical forces of floating models in motions are measured by two pairs of load cells and the rotating angles are also picked up by two inclinometers. Then through both FYLDE Amplifier and Filter System and Data Collecting System, such signals are recorded into the micro computer system. The experimental data analysis procedure is similar to the previous one mentioned above. In fact a comprehensive procedure of specific experimental data acquisition and analysis system at Hydrodynamics Laboratory is described and the flowing diagram of such a experimental system is also presented as shown in Fig. 1.41.

The results of experimental work for such three different kinds of buoy models are compared with that of theoretical predictions (Wu 1991) with reasonable accuracy. The surge, heave and pitch motion responses of the " C - buoy " model in regular progressive waves are presented in Figs. 1.42 to 1.44 respectively. In surge motion as shown in Fig. 1.42, the discrepancies between experimental and theoretical results could be due to difficult predictions of damping and restoring coefficients and mooring system etc. The motion response in heave mode, as presented in Fig. 1.43, show good agreement. As for pitch motion, as shown in Fig. 1.44, the large differences may be due to the buoy model rotating in the motion experiment.

Surge, heave and pitch motion responses of the " D - buoy " model in regular

progressive waves are shown in Figs. 1.45 to 1.47 respectively. In surge motion as shown in Fig. 1.45, large discrepancies are due to difficult predictions of damping, restoring coefficients and mooring system etc. As for the heave motion, as presented in Fig. 1.46, large differences also appear. In fact from the inclining and natural frequency experiments, certain information of the buoy model characteristics such as damping coefficients and metacentric GM heights can be used for more accurate predictions of dynamic motions for practical design applications. The pitch motion response, as presented in Fig. 1.47, matches fairly well for the range of wave periods.

Surge, heave and pitch motion responses of the " P - buoy " model in regular progressive waves are presented in Figs. 1.48 to 1.50 respectively. In heave and pitch motions as shown in Figs. 1.49 and 1.50, the agreement between theories and experiments for the range of wave periods is fair.

A comparison study on motion dynamics for the three different kinds of buoy model configurations is as shown in Figs. 1.51 to 1.59. The motion experiments of three different kinds of floating buoy models are also presented as shown in Figs. 1.60, 1.61 and 1.62 respectively.

This preliminary study indicates that a fairly reliable prediction can be made of the motion responses of buoy models, with very little CPU time.

1.2.3 Motion response prediction of a twin hulled offshore structure in waves

Various offshore drilling structures are constructed for the exploration and mining of oil, gas and all kinds of mineral resources in the sea bed and substratum. These marine structures should be stably operated around their fixed position. As these offshore drilling structures are often exposed to severe environmental conditions and forced to keep their operation in good condition, from the point of view of design and construction, they should be well designed to withstand severe

wave excitation forces in general.

Dynamic motions of such offshore structures in waves are of more concern to designers of offshore structures than that of ships, since it is not easy for offshore structures to move away from the stormy weather. Hence the operation safety of these marine structures is a principal factor which should be taken into consideration at the preliminary design stage.

The deep water wave theory with small wave height assumption is applied and submerged parts of twin hulled offshore structures are assumed to be reasonably slender. Moreover it is assumed that the free surface effect is assumed to be negligible and interference effects between columns and caissons are neglected in practical computations. It is also found that damping forces, as obtained from experiments of the offshore structure model, for the conditions of small motion amplitudes in heave, pitch and roll modes can be sufficiently described in linear terms. The computer program has been developed to predict dynamic motion responses of semi-submersible catamaran hull structures in beam and longitudinal waves for practical design applications.

Based on the theory of body motions in waves, approximate predictions of twin hulled marine structures in regular progressive waves show good agreement with that of previous researches (Tasai 1970). Several experimental results in dynamic motion responses of such twin hulled marine vehicles in waves are analysed here for two different kinds of twin hulled models, which have eight cylindrical columns and two caissons with different configurations, in other words, one twin hulled model with nearly rectangular cross sections and sharp end sections (Model-1) and the other one, as shown in Fig. 1.25, with circular cross sections and flat end sections (Model-3). Analysis results of the experimental work are compared with that of preliminary theoretical predictions (Wu 1991) with reasonable accuracy.

In order to confirm the effectiveness of this theoretical approach, validity tests

are performed for two different kinds of twin hulled marine vehicles mentioned above. The basic configuration of the structure model (SSCH-1) has two caissons, eight columns and an operation deck surmounted on the upper part of these columns and the principal particulars are also indicated as shown in Fig. 1.23. The motion experiments of this SSCH-1 model were carried out at Tsuyazaki Sea Safety Research Laboratory, Japan and experimental results are compared to confirm theoretical predictions.

In heave motion, the non-dimensionalized motion amplitudes of experimental and theoretical results match well as shown in Fig. 1.65 and the phase angle by theoretical prediction is also presented in Fig. 1.66. The calculated results of Froude Krylov, wave diffraction and total wave excitation forces per unit wave amplitude are compared and presented in Fig. 1.67.

In pitch motion, the non-dimensionalized motion amplitudes of experimental and theoretical results are in good agreement as shown in Fig. 1.68 and the phase angle by theoretical prediction is also presented in Fig. 1.69. The predicted results of Froude Krylov, wave diffraction and total wave excitation moments per unit wave amplitude are compared and presented in Figs. 1.70 and 1.71 respectively.

In roll motion, the non-dimensionalized motion amplitudes of experimental and theoretical results match well as shown in Fig. 1.72 and the phase angle by theoretical prediction is also presented in Fig. 1.73. The calculated results of Froude Krylov, wave diffraction and total wave excitation moments per unit wave amplitude are compared and presented in Figs. 1.74 to 1.76.

In sway motion, the non-dimensionalized motion amplitudes of experimental and theoretical results have good agreement as shown in Fig. 1.77 and the phase angle by theoretical prediction is also presented in Fig. 1.78. The predicted results of Froude Krylov, wave diffraction and total wave excitation forces per unit wave amplitude are compared and presented in Figs. 1.79 to 1.81.

The basic configuration of SSCH-3 model has two circular cylindrical caissons, eight circular columns and principal particulars are as shown in Figs. 1.25 and 1.82. The motion experiments of this SSCH-3 model were carried out at the Hydrodynamics Laboratory of Glasgow University (Atlar 1986) and the comparison of experimental and theoretical results is also performed. The non-dimensionalized amplitudes in heave and pitch motions match well in short wave period range as in Figs. 1.83 and 1.84 respectively and the SSCH-3 model in motion experiments is also presented in Fig. 1.85 (see pp343). The large discrepancies between experimental and theoretical results at several specific wave periods could be due to several factors, such as linear damping terms, modelling effects of structure models and inevitable experimental errors etc.

In brief, this approximate approach, to predict dynamic motion characteristics on a preliminary basis, is rather convenient and easily performed on desktop calculators.

1.3 The principal objectives of present research work

The main objective of this study is to investigate the effect of second order steady tilt behaviour and to achieve the goal the following sub-objectives have to be carried out.

(1) A preliminary study in ocean engineering field should be extensively performed at the early stage as a learning process. The prediction of the Froude Krylov forces acting on floating buoys and twin hulled marine vehicles in waves is to be studied. The hydrodynamic behaviours of floating buoys with mooring systems in waves are to be reviewed and extended to offshore twin hulled vehicles. A spectral analysis on the motion responses of the floating buoys and twin hulled structures in waves is also carried out(Wu 1992).

(2) Both numerical techniques, discrete source distribution and direct Green function methods (hereinafter referred to as D.S. Method and Direct Method respectively), are to be investigated to solve the boundary value problem, taking into account effects of forward speed and interactions between two hulls, for the

solutions of velocity potentials on the surface of body boundaries directly. The logarithmic part of the Green function will be analytically derived to improve the accuracy of the computation when checking the results of the damping forces by pressure integration and by energy flux consideration and the horizontal second order forces by pressure integration and momentum flux consideration.

(3) In the field of the computational fluid dynamics, the computational efficiency and numerical accuracy are two major concerns of researchers, so both numerical methods will be modified to predict the hydrodynamic loadings acting on offshore structures advancing in waves. The velocity potentials in these methods are calculated by the discrete source distribution technique and the direct solution by the classical integral equation method. These modifications, accomplished by analytically solving the logarithmic part of the Green's function, will help to improve the computational efficiency, in other words, it will cut down the CPU time considerably, for the prediction of the hydrodynamic forces acting on the offshore structures.

(4) The numerical accuracy checked by these newly modified approaches is to be extensively investigated. The numerical results based on both approaches are to be compared as regards computational efficiency and numerical accuracy. The numerical accuracy check is to be performed by varying the number of the elements and for different depths of immersion. It is obvious that as the number of the discrete source elements on the body boundary surface is increased, the numerical accuracy is improved. However a major concern is the computational efficiency. Hence there is a need to carry out the numerical computations which can help researchers to select the optimum numbers of discrete elements and images of dipoles. For the case of twin cylinders the accuracy is to be checked by varying the number of dipole images.

(5) The theoretical formulation of restoring forces acting on two submerged circular cylinders in waves due to forward speed effect is to be derived and the results of numerical computations are to be compared with analytical solutions of a

single submerged cylinder. The dynamic motion responses of an inclined offshore structure in waves taking into consideration the restoring forces due to forward speed effects are to be investigated. The results of motion responses including restoring forces due to specific forward speed effect are to be compared with previous researches (Kashiwagi and Varyani 1987).

(6) The predictions of second order forces due to the effects of forward speed (equivalent current effect) and interactions between two submerged hulls are to be taken into consideration. The theoretical approaches, based on the wave momentum flux consideration in the fluid domain (the far-field concept) and the direct pressure integration over the body boundary contours (the near-field concept), are to be developed and checked for predicting the second order horizontal and vertical forces and steady tilt moments due to the effects of second order forces of twin hulled marine vehicles in head and following waves.

(7) The numerical results of the second order forces on twin hulled marine vehicles will be compared with that of previous work. It may be concluded that the outer solution of the near field approach and the inner solution of the far field approach in the present computations of the second order forces match well. The steady tilt moments on an inclined offshore structure in waves due to the second order horizontal and vertical forces with forward speed effect are to be calculated and numerical results will be compared with that of the three dimensional experimental work (Maeda 1984 et al).

(8) A valuable procedure for the theoretical confirmation of numerical computations is to be newly developed and comprehensively described. The numerical accuracy check of the damping coefficients is calculated by consideration of the energy flux in the fluid domain and by direct pressure integration over the body boundary contours. The results of the wave excitation forces in terms of the Kochin function form is checked by the Haskind-Newman relation. The accuracy check of the second order horizontal forces with forward speed effect on twin hulled structure is investigated by direct pressure integration

(the near field concept) and by momentum flux consideration (the far field concept). The numerical accuracy of the second order vertical forces with forward speed effects is also checked by the Lee-Newman far field approach (1971) for the single submerged body without forward speed effects.

(9) Comparison studies of the steady tilt moments due to second order vertical forces on twin hulled marine vehicles in waves with those previous research work on both theoretical, such as Ogilvie (1963), Lee-Newman (1971), Morrall (1978), Numata (1978), Martin (1978) and Atlar (1986), and experimental, for instance, Japan SR-192 model (1988), sides will be investigated for technical confirmation of engineering applications.

(10) The effects of forward speed and interactions between two submerged hulls of an inclined offshore structure in head and following waves are to be extensively investigated and calculated results in all aspects of added mass and damping coefficients, wave excitation forces, motion responses, second order forces and steady tilt moments will be discussed.

(11) The effects of viscous and waterline forces on vertical surface piercing columns of twin hulled marine vehicles to investigate the steady tilt behaviour of an inclined offshore structure are to be studied and discussed. A comparison study on the steady tilt moments due to the effects of different GM heights of twin hulled vehicles will be also investigated.

(12) The computed results of a twin hulled structure model, based on the present theoretical approach, are to be presented to show the overall functions of present research work for practical applications on offshore twin hulled vehicles in waves.

(13) A mathematical approach with linear optimal control theory to study the dynamic positioning behaviour of twin hulled marine structures will be briefly introduced. In fact a detail description of the data acquisition and analysis system here is to be described systematically. A series of experiments are to be carried out at the Hydrodynamics Laboratory for different submergence depths and trim and

drift angles in the manoeuvring aspects of twin hulled marine vehicles. The experimental results will be based on the technique of curve fitting to obtain several newly developed formulae for predicting the manoeuvring (dynamic positioning) performance of twin hulled marine vehicles under the combined action of wave and current.

CHAPTER 2
BOUNDARY VALUE PROBLEM

2.1 General description

In this section, the formulation of the fluid flow which forms the basis for practical computation of a boundary value problem for a rigid body translating at a constant velocity in incident waves under a free surface. The velocity field of such an irrotational flow is always expressed in terms of the gradient of some scalar function $\Phi(x,y,t)$ (i.e. velocity potential) which must satisfy not only the equation of continuity (i.e. Laplace's equation) but also the prescribed boundary conditions of the given problem.

A submerged body advancing at finite forward speed U into the direction perpendicular to its axis and in incident waves is described as shown in Fig. 2.1. The structure is performing sinusoidal oscillations of small amplitude in surge, heave and pitch modes at a specific frequency ω about its mean position. The centre of the cylinder with its radius a is submerged at a depth d under the free surface. The Cartesian coordinate system Oxy moving at the same speed as that is defined to be fixed relative to the mean position of the structure.

The Laplace's equation which describes the flow field is applied to describe a boundary value problem. The degree of complexity of these equations depends on the mathematical description of fluid properties and flow field. Such differential equations are almost difficult to solve as the exact mathematical description of the fluid properties and the flow field is involved, so it is necessary to introduce certain simplifying assumptions in order to make the formulation of the problem easier. The submerged body of a twin hulled offshore structure is assumed to be long enough and the flow field around it is considered to be two dimensional. In order

to formulate the potential flow, the velocity potential has to satisfy the equation of continuity at every point in the field. If such a velocity potential of this boundary value problem exists, then several following basic assumptions must be satisfied, i.e.

(1) The fluid is homogeneous.
(2) The fluid is incompressible and the flow field is irrotational so that the velocity potential can be introduced to deal with such hydrodynamic problems.
(3) The viscous effect is small enough to be reasonably negligible.

Based on the above assumptions, the velocity potential of the flow field $\Phi(x,y,t)$ which must satisfy the Laplace equation in the fluid domain is written as

$$\nabla^2\Phi(x,y,t) = 0 \qquad (2.1)$$

In general, the velocity potential $\Phi(x,y,t)$ can be decomposed into two parts. One is the time independent steady contribution due to forward motion of the structure in a calm water and the other is the time dependent term associated with incident waves and unsteady body motions. The total velocity potential can then be written as

$$\Phi(x,y,t) = U\{-x + \varphi_s(x,y)\} + Re\{\phi(x,y)e^{i\omega t}\} \qquad (2.2)$$

where :

$U\{-x + \varphi_s(x,y)\}$ is the steady state potential.
$\phi(x,y)$ is the complex amplitude of the unsteady potential with time dependence factored out.
'Re' denotes the real part of the complex variable.
' i ' is $\sqrt{-1}$.
' ω' is the circular frequency of encounter with incident waves or the frequency of

oscillatory motions of the structure.

This boundary value problem has to be further simplified by linearizing as follows :

(1) The amplitude of incident waves is small compared with the wave length and the dimensions of the body's cross sections.
(2) The amplitude of oscillatory motions is also small.

In compliance with the above assumptions mentioned, the second order terms associated with the amplitudes of incident waves and oscillatory motions can be disregarded. The unsteady term of velocity potential $\phi(x,y)$ is then written as

$$\phi(x,y)=\frac{gA}{i\omega_0}\{\varphi_I(x,y)+\varphi_D(x,y)\}+\sum_{j=1}^{3}i\omega\xi_j\psi_j(x,y) \qquad (2.3)$$

where :

$\left(\frac{gA}{i\omega_0}\right)\varphi_I$ is the velocity potential of incident waves and the mathematical expression is given as

$$\frac{gA}{i\omega_0}\varphi_I(x,y)=\frac{gA}{i\omega_0}e^{-ky\pm ikx} \qquad (2.4)$$

where :

ω_0 is the circular frequency in the reference frame fixed in the fluid domain far ahead of the structure.
A is the amplitude of incident waves.
The wave number k is $\frac{\omega_0^{\,2}}{g}$ and g is the gravitational acceleration.
$\pm k$ corresponds to the incident waves propagating into the negative x (head waves) and the positive x directions (following waves).

$\left(\frac{gA}{i\omega_0}\right)\varphi_D$ is the velocity potential (diffraction potential) of the disturbed flow field generated when the body is advancing in incident waves with its oscillatory motions suppressed.

The second term of Eq. (2.3) is the velocity potential (radiation potential) of the flow induced by oscillatory motions $\xi_j e^{i\omega t}$ in the j-th mode of the body advancing at a finite forward velocity under calm water.

where :

ξ_j denotes the complex amplitude of the j-th mode motion.
Mode indices j = 1, 2 and 3 correspond to the surge, heave and pitch motions of the body respectively.

2.2 Body boundary conditions

All the velocity potentials φ_S and ϕ in Eq. (2.2) have to satisfy body boundary conditions on the structure. The theoretical formulation of the body boundary condition for the steady term φ_S is straightforward and it is described by

$$\frac{\partial \varphi_S}{\partial n} = n_1 \quad \text{on the body at mean position} \qquad (2.5)$$

where :
n is the direction of outward normal to the body surface.
n_1 denotes its x-component.

The theoretical derivation of the body boundary condition for the unsteady potential of ϕ, as described in Eq. (2.2) has been worked out by Timman and Newman (1962). In order to formulate such a body boundary condition, an oscillatory coordinate system O'x'y' fixed on the body is defined. Based on the

coordinate system Oxy moving with a finite forward speed U in the positive x direction, the coordinate $\vec{r}(x,y)$ of a point on the body surface is described. If the term $0(\vec{\alpha}^2)$ is neglected, with its coordinate $\vec{r}'(x',y')$ in the oscillatory system fixed to the body, the following relation is obtained as

$$\vec{r}' = \vec{r} - \vec{\alpha}e^{i\omega t} \qquad (2.6)$$

where :

$\vec{\alpha}$ is expressed in terms of surge, heave and pitch motions of the structure as

$$\vec{\alpha} = \left[(\xi_1 - \xi_3(y-d)),(\xi_2 + \xi_3 x)\right] \qquad (2.7)$$

The surface of body contours can be theoretically described in terms of the body fixed coordinate as

$$F(x',y') = 0 \qquad (2.8)$$

In principal, the body boundary condition implies that the normal component of the fluid velocity on the body surface is equal to the normal velocity of the body itself. In other words, no particles of the fluid can penetrate the body boundary surface. Theoretically the substantial derivative of the body surface, Eq. (2.8), is set equal to zero. The mathematical expression can be given as

$$0 = \frac{D}{Dt}F(x',y') = \frac{\partial F}{\partial t} + \left(\vec{V} + \nabla\phi e^{i\omega t}\right)\cdot\nabla F \quad \text{on} \quad F(x',y') = 0 \qquad (2.9)$$

where :

$\vec{V}$ is the steady velocity field equal to $U\cdot\nabla\{-x+\varphi_s\}$

The detail manipulation of each term of the condition, as in Eq.(2.9), are given as follows.

$$\frac{\partial F}{\partial t} = \frac{\partial F}{\partial x'}\frac{\partial x'}{\partial t} + \frac{\partial F}{\partial y'}\frac{\partial y'}{\partial t} \tag{2.10}$$

$$\nabla F = \left[\left\{\frac{\partial F}{\partial x'}\frac{\partial x'}{\partial x} + \frac{\partial F}{\partial y'}\frac{\partial y'}{\partial x}\right\}, \left\{\frac{\partial F}{\partial x'}\frac{\partial x'}{\partial y} + \frac{\partial F}{\partial y'}\frac{\partial y'}{\partial y}\right\}\right] \tag{2.11}$$

By substituting Eq. (2.10) and Eq. (2.11) into Eq. (2.9), the following expression can be obtained

$$0 = -i\omega e^{i\omega t}\vec{\alpha}\cdot\nabla' F + \left(\vec{V} + \nabla\phi e^{i\omega t}\right)\cdot\left\{\nabla' F - e^{i\omega t}\left(\frac{\partial\vec{\alpha}}{\partial x}\cdot\nabla' F, \frac{\partial\vec{\alpha}}{\partial y}\cdot\nabla' F\right)\right\}$$
$$\text{on} \quad F(x',y') = 0 \tag{2.12}$$

where :

∇' denotes $\left(\frac{\partial}{\partial x'}, \frac{\partial}{\partial y'}\right)$

This relation, Eq. (2.12), must be satisfied on the instantaneous position of the body surface which is always displaced from the mean position. A Taylor's expansion of the steady flow field about the mean position of the body is described as

$$\vec{V}(\vec{r}) = \left[\vec{V}(\vec{r}')\right]_{mean} + e^{i\omega t}\left[(\vec{\alpha}\cdot\nabla)\vec{V}(\vec{r}')\right]_{mean} + 0(\alpha^2) \tag{2.13}$$

where :

Subscript " mean " denotes particular values at the mean position of the body.

Considering the body condition for the steady flow, the following expression is valid as

$$\vec{V}(\vec{r}')\cdot\nabla' F = 0 \qquad \text{on} \quad F(x',y') = 0 \tag{2.14}$$

Substituting Eq. (2.13) into Eq. (2.12) and neglecting $0(\alpha^2)$, the following equation for the terms with $e^{i\omega t}$ factor is derived as

$$\nabla\phi\cdot\nabla'F = i\omega\alpha\cdot\nabla'F - \left[(\vec{\alpha}\cdot\nabla')\vec{V}(\vec{r}')\right]_{mean}\cdot\nabla'F + \left[\vec{V}(\vec{r}')\right]_{mean}\cdot\left\{\left(\frac{\partial\vec{\alpha}}{\partial x}\cdot\nabla'F\right),\left(\frac{\partial\vec{\alpha}}{\partial y}\cdot\nabla'F\right)\right\} \quad \text{on} \quad F(x',y')=0 \qquad (2.15)$$

All the terms of the condition, Eq. (2.15), are of first order of magnitude associated with the oscillatory motions of the structure. Meanwhile as the difference between $\vec{r}(x,y)$ and $\vec{r}'(x',y')$ in Eq. (2.15) induces the error of second or higher order only, the manipulation of mathematical differentiation is not necessary.

In compliance with the vector identities, the following expression is described as

$$\nabla\times\left(\vec{A}\times\vec{V}\right) = \left(\vec{V}\cdot\nabla\right)\vec{A} + \vec{A}\left(\nabla\cdot\vec{V}\right) - \vec{V}\left(\nabla\cdot\vec{A}\right) - \left(\vec{A}\cdot\nabla\right)\vec{V} \qquad (2.16)$$

$$\left[\left(\vec{V}\cdot\nabla\right)\vec{\alpha} - \left(\vec{\alpha}\cdot\nabla\right)\vec{V}\right]\cdot\nabla F = \left[\nabla\times\left(\vec{\alpha}\times\vec{V}\right)\right]\cdot\nabla F - \left(\nabla\cdot\vec{V}\right)\vec{\alpha}\cdot\nabla F + \left(\nabla\cdot\vec{\alpha}\right)\vec{V}\cdot\nabla F = \left[\nabla\times\left(\vec{\alpha}\times\vec{V}\right)\right]\cdot\nabla F \qquad (2.17)$$

From Eq. (2.15), the body boundary condition at its mean position is derived as

$$\nabla\phi\cdot\nabla F = \left[i\omega\vec{\alpha} + \nabla\times\left(\vec{\alpha}\times\vec{V}\right)\right]\cdot\nabla F \quad \text{on} \quad F(x,y)=0 \qquad (2.18)$$

Since the outward normal $\vec{n}$ of the body surface is written as

$$\vec{n} = \frac{\nabla F}{(\nabla F\cdot\nabla F)^{1/2}} \qquad (2.19)$$

Hence the body boundary condition, Eq. (2.18), can be written as

$$\frac{\partial \phi}{\partial n} = \left[i\omega\vec{\alpha} + \nabla \times \left(\vec{\alpha} \times \vec{V} \right) \right] \cdot \vec{n} \qquad \text{on} \quad F(x,y) = 0 \qquad (2.20)$$

With the mathematical proof described in Appendix A, Eq. (2.20) can be rewritten as

$$\frac{\partial \phi}{\partial n} = \sum_{j=1}^{3} i\omega\xi_j \left(n_j + \frac{U}{i\omega} m_j \right) \qquad (2.21)$$

where :

$$\vec{n} = (n_1, n_2) \quad , \quad \vec{n}_3 = (\vec{r}_0 \times \vec{n})_3$$
$$\vec{m} = (m_1, m_2) = -(\vec{n} \cdot \nabla)\vec{V} \quad , \quad \vec{m}_3 = -\left[(\vec{n} \cdot \nabla)(\vec{r}_0 \times \vec{V}) \right]_3 \qquad (2.22)$$

where :

' n ' is the unit normal vector of the body surface into the fluid.
' m ' is a vector in order to consider the effect of the perturbation velocity on the body surface induced by the oscillatory motions of the body in the steady flow field.
$\vec{r}_0(x, y-d)$ is the coordinate with its origin at the centre of the body.
Suffixes 1,2 and 3 denote the x, y and z components of the vectors respectively (the z axis is perpendicular to the x-y plane and directed into Fig. 2.1).
The normalized steady flow $\vec{V}$ is written as

$$\vec{V} = \nabla[-x + \varphi_s(x,y)] \qquad (2.23)$$

Basically the theoretical prediction of the m vector contribution is quite complicated especially when the free surface condition for the steady potential φ_s is to be satisfied properly. However the steady potential φ_s can be appropriately assumed by the velocity potential of the steady flow in the unbound fluid domain and the mathematical derivation of such m vector contribution is worked out easily. According to the assumption mentioned above, the detail mathematics of the m

vector contribution for the case of a submerged single cylinder and a set of two rigidly connected circular cylinders will be described later in Chapter Five.

The body boundary conditions of the radiation and diffraction potentials which have to satisfy are summarized as

$$\frac{\partial \psi_j}{\partial n} = n_j + \frac{U}{i\omega} m_j \qquad \text{on} \quad F(x,y) = 0 \tag{2.24}$$

$$\frac{\partial \varphi_D}{\partial n} = -\frac{\partial \varphi_I}{\partial n} \qquad \text{on} \quad F(x,y) = 0 \tag{2.25}$$

2.3 Free surface and bottom conditions

In general, the radiation potentials ψ_j and the diffraction potential φ_D must satisfy the free surface condition. A dynamic free surface condition is expressed by setting the substantial derivative of the hydrodynamic pressure on the free surface equal to zero (Newman 1977). It implies that water particles on the free surface always stay on the free surface and the hydrodynamic pressure at the location of these particles is kept constant and equal to the atmospheric pressure, i.e. it is really a combination of both dynamic and kinematic conditions.

The free surface condition for the unsteady part $\phi_u = \mathrm{Re}\left(\phi e^{i\omega t}\right)$ in Eq. (2.2) is written as

$$\left(\frac{\partial}{\partial t} - U\frac{\partial}{\partial x} + \nabla\phi_u\nabla\right)\left[\frac{\partial \phi_u}{\partial t} - U\frac{\partial \phi_u}{\partial x} + \frac{1}{2}\nabla\phi_u\nabla\phi_u - gy + \mu\phi_u\right] = 0$$
$$\text{on} \qquad y = \xi_\omega(x,t) \tag{2.26}$$

where :

$\xi_\omega(x,t)$ is the unsteady wave depression.

In this theoretical formulation, the interaction of the steady and unsteady flow is assumed to be of higher order of magnitude. By neglecting the second or higher order terms in ϕ, the above equation can be appropriately linearized as

$$\left[\left(i\omega - U\frac{\partial}{\partial x}\right)^2 - g\frac{\partial}{\partial y} + \mu\left(i\omega - U\frac{\partial}{\partial x}\right)\right]\phi(x,y) = 0 \quad \text{on} \quad y = 0 \quad (2.27)$$

Here μ is Rayleigh's fictitious coefficient which is introduced so that the radiation condition of outgoing waves at infinity can be satisfied properly.

In compliance with one more boundary condition for a constant pressure on the free surface, required on $y = 0$, the theoretical expression of the wave depression from the velocity potential ϕ is derived as

$$\zeta_\omega(x,t) = \frac{1}{g}\left(i\omega - U\frac{\partial}{\partial x}\right)\phi(x,y)e^{i\omega t} \qquad \text{on} \quad y = 0 \qquad (2.28)$$

Since the infinite depth of the water is assumed, the velocity potential ϕ must satisfy the following bottom boundary condition as

$$\nabla\phi(x,y) \to 0 \qquad \text{as} \quad y \to \infty \qquad (2.29)$$

2.4 Solution of unsteady potential

Here a general image of solutions of the unsteady potential ϕ in Eq. (2.2) is described systematically.

The velocity potential ϕ indicates the unsteady velocity potential excluding the potential of incident waves $\left(\frac{gA}{i\omega_0}\right)\varphi_I$. In order to obtain the solutions of such velocity potentials, a classical integral equation method is applied.

Making use of the Green's theorem in the fluid domain bounded by the control surfaces S_F, $S_{-\infty}$, S_B, $S_{+\infty}$ and S_H as shown in Fig. 2.1, the mathematical formulation can be defined as

$$\phi(P) = -\int_S \left[\frac{\partial \phi(Q)}{\partial n} - \phi(Q) \frac{\partial}{\partial n} \right] G(P,Q) ds \qquad (2.30)$$

where :

The total control surface S is $S_{-\infty} + S_F + S_H + S_{+\infty} + S_B$.
$P(x,y)$ and $Q(\xi,\eta)$ represent a field point and a source point respectively.
$G(P,Q)$ denotes the Green function which must satisfy the Laplace condition, Eq. (2.1), the free surface condition, Eq. (2.27), the bottom condition, Eq. (2.29) and the body boundary conditions of radiation and diffraction problems.

On account of the radiation, the free surface and the bottom conditions, the contribution from the control surfaces $S_{\pm\infty}$, S_F and S_B are zero, the direct integration in Eq. (2.30) over the body boundary contour S can be reduced to S_H.

In case the field point $P(x,y)$ is located on the body surface, Eq. (2.30) can be written (Newman 1977) as

$$\frac{1}{2}\phi(P) - \int_{S_H} \phi(Q) \frac{\partial}{\partial n} G(P,Q) ds = -\int_{S_H} \frac{\partial \phi(Q)}{\partial n} G(P,Q) ds \qquad (2.31)$$

The theoretical derivation of the Green function $G(P,Q)$ for this problem is discussed in detail in Chapter Three and the final expression is described as

$$G(x,y;\xi,\eta) = -\frac{1}{2\pi}\left[\log \frac{r}{r_1} + \hat{G}(x-\xi, y+\eta) \right] \qquad (2.32)$$

where :

$$\hat{G}(x,y) = -\lim_{\mu\to 0}\int_{-\infty}^{\infty} \frac{e^{-|k|y-ikx}}{|k|-\frac{1}{g}(kU+\omega-i\mu)^2}dk$$

$$= \frac{K_0}{k_1-k_2}\{S_1(x,y)-S_2(x,y)\}+\frac{K_0}{k_3-k_4}\{S_3(x,y)-S_4(x,y)\} \qquad (2.33)$$

and

$$S_j(x,y) = \lim_{\mu\to 0}\int_0^{\infty} \frac{e^{-ky-ikx}}{k-k_j\mp i\mu}dk \qquad \text{for } j=\begin{pmatrix}1\\2\end{pmatrix} \qquad (2.34)$$

$$S_j(x,y) = \lim_{\mu\to 0}\int_0^{\infty} \frac{e^{-ky+ikx}}{k-k_j+i\mu}dk \qquad \text{for } j=3,4 \qquad (2.35)$$

where :

$$K_0 = \frac{g}{U^2} \quad , \quad \tau = \frac{U\omega}{g} \qquad (2.36a)$$

$$P=(x,y) \quad , \quad Q=(\xi,\eta) \quad , \quad \left.\begin{matrix} r \\ r_1 \end{matrix}\right\} = \sqrt{(x-\xi)^2+(y\mp\eta)^2} \qquad (2.36b)$$

Constants k_j (j = 1, 2, 3, 4) are defined as

$$\left.\begin{matrix} k_1 \\ k_2 \end{matrix}\right\} = \frac{K_0}{2}\left[1-2\tau\pm\sqrt{1-4\tau}\right] \qquad (2.37a)$$

$$\left.\begin{matrix} k_3 \\ k_4 \end{matrix}\right\} = \frac{K_0}{2}\left[1+2\tau\pm\sqrt{1+4\tau}\right] \qquad (2.37b)$$

The integrals S_j are described in terms of exponential integrals as

$$S_j(x,y) = e^{-k_j z}\left\{E_1(-k_j z)\pm 2\pi i u\left(\mp I_m(k_j z)\right)u(1-2\tau)\right\}$$

$$j=\begin{pmatrix}1\\2\end{pmatrix} \qquad (2.38)$$

$$S_j(x,y) = e^{-k_j\bar{z}}\left\{E_1\left(-k_j\bar{z}\right) - 2\pi i u(-x)\right\} \quad j = 3,4 \qquad (2.39)$$

where :

$\left.\begin{matrix} z \\ \bar{z} \end{matrix}\right\} = y \pm ix$ and 'I_m' denotes the imaginary part of the complex variable.

u(x) is Heaviside's unit function.

$E_1(z)$ is the exponential integral of complex argument and can be defined as

$$E_1(z) = \int_z^{\infty} \frac{e^{-t}}{t} dt \quad \text{for} \quad |\arg(z)| < \pi \qquad (2.40)$$

2.5 Radiation and diffraction waves at infinity

Because the amplitude and phase angle of the wave induced by total velocity potential ϕ at a distance far upstream and far downstream, hereafter the ambient flow -U is assumed instead of the body translating at a forward velocity U, are obtained, the asymptotical expression of the Green function at $x = \pm\infty$ can be written by substituting into Eq. (2.30) as

$$G(x,y;\xi,\eta) \approx \frac{-iu(1-4\tau)}{\sqrt{1-4\tau}}\left[e^{-k_1\zeta}u(\xi - x) + e^{-k_2\zeta}u(x-\xi)\right] + \frac{i}{\sqrt{1+4\tau}}\left[e^{-k_3\bar{\zeta}}u(\xi - x) - e^{-k_4\bar{\zeta}}u(\xi - x)\right] \qquad (2.41)$$

where :

$$\zeta = (y+\eta) + i(x-\xi) \qquad (2.41a)$$

$$\bar{\zeta} = (y+\eta) - i(x-\xi) \qquad (2.41b)$$

Moreover velocity potentials ϕ at far upstream and far downstream can be described as

$$\phi(x,y) \approx \frac{iu(1-4\tau)}{\sqrt{1-4\tau}} H^{+}(k_2) e^{-k_2 y - ik_2 x} \quad \text{as} \quad x \to +\infty \qquad (2.42a)$$

$$\phi(x,y) \approx \frac{iu(1-4\tau)}{\sqrt{1-4\tau}} H^{+}(k_1) e^{-k_1 y - ik_1 x} + \frac{i}{\sqrt{1+4\tau}} \left[-H^{-}(k_3) e^{-k_3 y + ik_3 x} + H^{-}(k_4) e^{-k_4 y + ik_4 x} \right] \quad \text{as} \quad x \to -\infty \qquad (2.42b)$$

It should be noted that in case τ is larger than 0.25, k_1 and k_2 are complex; it means that the velocity potential $\phi(x,y)$ approaches zero for the far upstream case and the first term of Eq. (2.42b) disappears for the far downstream case. Here $H^{\pm}(k_j)$, associated with the amplitudes of the far upstream and far downstream waves in general, are referred to as the Kochin function (Takagi and Ohkusu 1977) and can be expressed as

$$H^{+}(k_j) = \int_{S_H} \left[\frac{\partial \phi}{\partial n} - \phi \frac{\partial}{\partial n} \right] e^{-k_j \eta + ik_j \xi} ds \quad \text{for} \quad j = (1,2) \qquad (2.43a)$$

$$H^{-}(k_j) = \int_{S_H} \left[\frac{\partial \phi}{\partial n} - \phi \frac{\partial}{\partial n} \right] e^{-k_j \eta - ik_j \xi} ds \quad \text{for} \quad j = (3,4) \qquad (2.43b)$$

According as the velocity potential ϕ can be decomposed into the radiation and diffraction potentials, the Kochin function can be expressed as

$$H^{\pm}(k) = \frac{gA}{i\omega_0} H_D^{\pm}(k) + \sum_{j=1}^{3} i\omega \xi_j H_j^{\pm}(k) \qquad (2.44a)$$

$$= \frac{gA}{i\omega_0} H_F^{\pm}(k) \qquad (2.44b)$$

where :

$$H_F^{\pm}(k) = H_D^{\pm}(k) - \sum_{j=1}^{3} \frac{\omega \omega_0}{g} \frac{\xi_j}{A} H_j^{\pm}(k) \qquad (2.45)$$

Here $H_j^{\pm}(k)$ and $H_D^{\pm}(k)$ are of the same form as $H^{\pm}(k_j)$ of Eq. (2.43) by

substituting the radiation potential ψ_j or the diffraction potential φ_D into the velocity potential ϕ. Moreover the potentials of ψ_j and φ_D at far upstream and far downstream are described by substituting $H_j^{\pm}(k)$ and $H_D^{\pm}(k)$ into $H^{\pm}(k_j)$ in Eq. (2.42).

If the parameter τ is less than or equal to 0.25, all the k_j values in Eq. (2.37) are real. This means that the waves induced by radiation and diffraction potentials generate one wave system of the wave number k_2 at far upstream propagating into positive x direction and three wave systems of wave numbers k_1, k_3 and k_4 at far downstream. Meanwhile the k_1-wave propagates into positive x direction but the other two wave systems propagate into negative x direction.

If τ is larger than 0.25, the k_3 and k_4 wave systems remain, but the other two vanish.

These multiple wave systems associated with translating and oscillating (equivalently in incident waves or current) body are illustrated in Fig. 2.2. Parabola indicates the dispersion relation $C^2 = \frac{g}{k}$ between phase speed C and wave number k at infinitely deep water. Ahead of the body, the phase speed, relative to the fluid flowing at a velocity -U, of the wave system propagating into the positive x direction must be $\frac{\omega}{k} + U$ which describes a straight line as shown in Fig. 2.2. The phase speeds $\mp\left(\frac{\omega}{k} - U\right)$ relative to the flowing fluid of any wave system propagating in the negative or positive x direction behind the body represent straight lines. In general four wave numbers are indicated as intersections of the parabola and the straight lines. Obviously the condition that the first straight line tangent to the parabola is $\tau = 0.25$.

By substituting Eq. (2.42) into Eq. (2.28), the expression of the wave depression $\zeta_\omega(x,t)$ at far upstream and far downstream can be described as

$$\zeta_\omega(x,t) \approx A_2 e^{-ik_2 x} e^{i\omega t} \quad \text{as} \quad x \to +\infty \qquad (2.46a)$$

$$\zeta_\omega(x,t) \approx \left(A_1 e^{-ik_1 x} + A_3 e^{ik_3 x} + A_4 e^{ik_4 x}\right) e^{i\omega t} \quad \text{as} \quad x \to -\infty \quad (2.46b)$$

where :

$$A_j = -\sqrt{\frac{k_j}{g}} \frac{H^+(k_j)}{\sqrt{1-4\tau}} u(1-4\tau) \quad \text{for} \quad j = \begin{pmatrix} 1 \\ 2 \end{pmatrix} \qquad (2.47a)$$

$$A_j = -\sqrt{\frac{k_j}{g}} \frac{H^-(k_j)}{\sqrt{1+4\tau}} \qquad \text{for} \quad j = \begin{pmatrix} 3 \\ 4 \end{pmatrix} \qquad (2.47b)$$

Similarly in case of τ greater than 0.25, the k_2-wave system for $x \to +\infty$ and the k_1-wave system for $x \to -\infty$ vanish in Eq. (2.46).

2.6 Conclusions

The theoretical formulation of the steady and unsteady hydrodynamic problem with the forward speed effect is detailedly described in the context of the potential theory. It is noted that not only the non-linear effect on body boundary and free surface conditions make such problems mathematically intractable but also the instantaneous surface of such boundaries are difficult to determine exactly. These boundary conditions have to be linearized to a certain extent that practical solutions can be obtained by numerical computations.

The mathematical formulation of the boundary value problem to deal with this hydrodynamic problem with the forward speed effect is derived in detail. Under the linear assumption, the numerical solutions can be exactly obtained by solving the integral equation for the velocity potential on the body surface. Moreover the mathematical expression of radiation and diffraction wave depression at the far upstream and far downstream is also described by velocity potentials at infinity in terms of the Kochin functions.

CHAPTER 3
MATHEMATICAL FORMULATION OF THE GREEN FUNCTIONS

3.1 General description

A fundamental formulation of the most generalized form of the Green function to predict hydrodynamic forces is well derived for the two dimensional problem of a single submerged cylinder moving with a constant forward speed and oscillating in incident waves (Kashiwagi and Varyani 1987).

In principal, the cylinder may be simulated as a simplified model of the lower hull of a twin hulled marine vehicle. A practical advantage of this Green function is that it can efficiently predict hydrodynamic forces on twin hulled marine vehicles under combined actions of wave and current in numerical computations.

3.2 Theoretical formulation of the Green functions

Here the theoretical expression of the generalized Green function for a two dimensional hydrodynamic problem taking into consideration the forward speed effect in incident waves is derived. Several fundamental assumptions should be carefully specified before this problem is reasonably studied. The coordinate system of the fluid flow is assumed to be in the negative x-direction and the y-axis is taken positive vertically downwards. The singularity is located at a point $(0,\eta)$ below the free surface as shown in Fig. 3.1. The Green function which satisfies the linear free surface condition, the radiation condition and the bottom boundary condition is derived as

$$\nabla^2 G = -\delta(x)\delta(y-\eta) \qquad (3.1)$$

$$\left(i\omega - U\frac{\partial}{\partial x}\right)^2 G + \mu\left(i\omega - U\frac{\partial}{\partial x}\right)G - g\frac{\partial G}{\partial y} = 0 \quad \text{as} \quad y = 0 \qquad (3.2)$$

$$\frac{\partial G}{\partial y} = 0 \quad \text{as} \quad y \to \infty \qquad (3.3)$$

Here μ is Rayleigh's fictitious friction coefficient and it has been introduced in the free surface condition so that the radiation condition at infinity is completely satisfied. The Fourier transforms of the above equations with respect to x are

$$-k^2 G^* + \frac{\partial^2 G^*}{\partial y^2} = -\delta(y - \eta) \qquad (3.4)$$

$$(-kU + \omega - i\mu)^2 G^* + g\frac{\partial G^*}{\partial y} = 0 \quad \text{as} \quad y = 0 \qquad (3.5)$$

$$\frac{\partial G^*}{\partial y} = 0 \quad \text{as} \quad y \to \infty \qquad (3.6)$$

where G^* denotes the Fourier transform of the Green function G, with the definition as

$$G^*(k,y) = \int_{-\infty}^{\infty} G(x,y)e^{-ikx}dx \qquad (3.7)$$

In order to obtain the solution of G^*, the fluid domain is divided into two regions, i.e. $y \le \eta$ represents the region between free surface and the singularity (hereafter referred to as Region-I) and $y \ge \eta$ for the region between the water bottom and the singularity (hereafter referred to as Region-II). The general solution of Eq. (3.4) is obtained by setting the right hand side equal to zero and thus it is written as

$$G^*(k,y) = c_1 e^{|k|y} + c_2 e^{-|k|y} \qquad (3.8)$$

The solution in the Region-I which is denoted by G_I^* must satisfy the free

surface condition as expressed in Eq. (3.5) and in the same manner the solution in the Region-II which is denoted by G_{II}^* must satisfy the bottom condition as described in Eq. (3.6). After imposing these two conditions, the solution of the respective region with the indetermined coefficients C and D can be described as

$$G_I^* = C * \left[e^{y\lambda} + e^{-y\lambda} + \frac{2m}{g\lambda - m} e^{-y\lambda} \right] \tag{3.9}$$

$$G_{II}^* = D * e^{-y\lambda} \tag{3.10}$$

where :

$$\lambda = |k| \tag{3.10a}$$

$$m = (-kU + \omega - i\mu)^2 \tag{3.10b}$$

The coefficients C and D can be determined by the continuity condition of the Green function and by the condition of discontinuity in its derivatives into the y direction at the $y = \eta$ location which are as follows.

$$G_I^* = G_{II}^* \tag{3.11a}$$

$$\frac{\partial G_I^*}{\partial y} - \frac{\partial G_{II}^*}{\partial y} = -1 \quad \text{at} \quad y = \eta \tag{3.11b}$$

In compliance with these conditions introduced above, such coefficients can be determined as

$$C = \frac{1}{2\lambda} e^{-\eta\lambda} \tag{3.12a}$$

$$D = \frac{1}{2\lambda} \left[\left(1 + \frac{2m}{g\lambda - m} \right) e^{-\eta\lambda} + e^{\eta\lambda} \right] \tag{3.12b}$$

By substituting Eqs. (3.12a) and (3.12b) into Eqs. (3.9) and (3.10), the expression of the Green function, which is valid not only in the Region-I but also in the Region-II, can be written in the following form

$$G^*(k,y)=\frac{1}{2\lambda}\left[e^{-|y-\eta|\lambda}+\left(-1+\frac{2g\lambda}{g\lambda-m}\right)e^{-(y+\eta)\lambda}\right] \qquad (3.13)$$

In order to obtain the expression in the physical plane, the inverse Fourier transform with respect to k should be performed. The expression of the Green function can then be written as follows.

$$G(x,y)=\frac{1}{2\pi}\int_{-\infty}^{\infty}G^*(k,y)e^{ikx}dk \qquad (3.14)$$

Regarding the inverse Fourier transform, the relation is used as

$$\frac{1}{4\pi}\int_{-\infty}^{\infty}\frac{1}{k}\left\{e^{-|y-\eta|k}-e^{-(y+\eta)|k|}\right\}e^{ikx}dk=-\frac{1}{2\pi}\log\frac{r}{r_1} \qquad (3.15)$$

where :

$$\left.\begin{matrix} r \\ r_1 \end{matrix}\right\}=\sqrt{x^2+(y\mp\eta)^2} \qquad (3.15a)$$

With this relation, the expression of the Green function can be rewritten as

$$G=-\frac{1}{2\pi}\log\frac{r}{r_1}+\frac{1}{2\pi}\lim_{\mu\to 0}\int_{-\infty}^{\infty}\frac{e^{-(y+\eta)|k|+ikx}}{\left\{|k|-\frac{1}{g}(-kU+\omega-i\mu)^2\right\}}dk \qquad (3.16)$$

By transforming the variable from k to -k, another expression for the Green function can be written as

$$G = -\frac{1}{2\pi}\log\frac{r}{r_1} + \frac{1}{2\pi}\lim_{\mu\to 0}\int_{-\infty}^{\infty}\frac{e^{-(y+\eta)|k|-ikx}}{\left\{|k| - \frac{1}{g}(kU+\omega-i\mu)^2\right\}}dk \qquad (3.17)$$

As for mathematical simplification of the above integral, they are detailedly described in the following sections.

3.3 Mathematical simplification of the Green functions

For practical computations, the expression of the Green function should be simplified further as

$$G = -\frac{1}{2\pi}\log\frac{r}{r_1} - \frac{K_0}{2\pi}\lim_{\mu\to 0}\int_{0}^{\infty} e^{-(y+\eta)k}\left\{\frac{e^{-ikx}}{f(k)} + \frac{e^{ikx}}{g(k)}\right\}dk \qquad (3.18)$$

where :

$$f(k) = (k+\omega_0 - i\mu')^2 - K_0 k \qquad (3.19a)$$

$$g(k) = (k-\omega_0 + i\mu')^2 - K_0 k \qquad (3.19b)$$

$$K_0 = \frac{g}{U^2} \qquad (3.19c)$$

$$\omega_0 = \frac{\omega}{U} \qquad (3.19d)$$

In order to find the poles, the mathematical expressions of equations $f(k) = 0$ and $g(k) = 0$ must be satisfied. The detail manipulation then is carried out as follows.

At first the poles at $f(k) = 0$ should be investigated as

$$(k+\omega_0-i\mu')^2-kK_0 \equiv k^2+\omega_0{}^2+2k\omega_0-i2\mu'(k+\omega_0)-kK_0$$
$$=k^2+\omega_0{}^2-2k\left(\frac{K_0}{2}-\omega_0+i\mu'\right)-i2\mu'\omega_0 \qquad (3.20)$$

Therefore

$$k=\frac{K_0}{2}-\omega_0+i\mu'\pm\sqrt{\left(\frac{K_0}{2}-\omega_0+i\mu'\right)^2-\omega_0^2+i2\mu'\omega_0} \qquad (3.21)$$

$$=\frac{K_0}{2}\left[1-2\tau+i\frac{2\mu'}{K_0}\pm\sqrt{1-4\tau}\left(1+\frac{i\frac{4\mu'}{K_0}}{1-4\tau}\right)^{\frac{1}{2}}\right] \qquad (3.22)$$

$$=\frac{K_0}{2}\left[1-2\tau\pm\sqrt{1-4\tau}+i\mu\left\{1\pm\frac{1}{\sqrt{1-4\tau}}\right\}\right]$$

$$\left(\text{for } \tau\le\frac{1}{4}\right) \qquad (3.23)$$

where :

$$\tau=\frac{U\omega}{g} \qquad (3.23a)$$

Here Eq. (3.23) is satisfied only for $\tau\le\frac{1}{4}$, but for $\tau\ge\frac{1}{4}$ there will be an imaginary term coming out and which is also clear from Eq. (3.21) as

$$k=\frac{K_0}{2}\left[1-2\tau\pm i\sqrt{4\tau-1}\right] \quad \left(\text{for } \tau\ge\frac{1}{4}\right) \qquad (3.24)$$

and by using Eq. (3.23), the expression of f(k) can be written as

$$f(k)=(k-k_1-i\mu_1)(k-k_2-i\mu_2) \qquad (3.25)$$

$$\left.\begin{matrix}k_1\\k_2\end{matrix}\right\}=\frac{K_0}{2}\left[1-2\tau\pm\sqrt{1-4\tau}\right] \qquad (3.26a)$$

$$\left.\begin{matrix}\mu_1\\ \mu_2\end{matrix}\right\} = \frac{K_0}{2}\mu\left\{1 \pm \frac{1}{\sqrt{1-4\tau}}\right\} \qquad (3.26b)$$

Next the poles in the case of $g(k) = 0$ are also found out. Just as in the case of $f(k) = 0$ and from Eq. (3.19) if the signs of ω_0 and μ' are reversed, the equation, substituting from Eqs. (3.25) and (3.26), can be described as

$$g(k) = (k - k_3 - i\mu_3)(k - k_4 - i\mu_4) \qquad (3.27)$$

$$\left.\begin{matrix}k_3\\ k_4\end{matrix}\right\} = \frac{K_0}{2}\left[1 + 2\tau \pm \sqrt{1+4\tau}\right] \qquad (3.28a)$$

$$\left.\begin{matrix}\mu_3\\ \mu_4\end{matrix}\right\} = \frac{K_0}{2}\mu\left\{1 \pm \frac{1}{\sqrt{1+4\tau}}\right\} \qquad (3.28b)$$

The position of the poles for the various domain of the τ values can then be shown in Fig. 3.2.

For the integration in the complex plane for Eq. (3.18), the following contour of integration will be taken into account.

$$\vartheta_1 = \lim_{\mu\to 0}\int_0^\infty \frac{e^{-(y+\eta)k - ikx}}{f(k)}dk = \lim_{\mu\to 0}\int_0^\infty \frac{e^{-(y+\eta)k - ikx}}{(k - k_1 - i\mu_1)(k - k_2 - i\mu_2)}dk \qquad (3.29)$$

$$\vartheta_2 = \lim_{\mu\to 0}\int_0^\infty \frac{e^{-(y+\eta)k + ikx}}{g(k)}dk = \lim_{\mu\to 0}\int_0^\infty \frac{e^{-(y+\eta)k + ikx}}{(k - k_3 - i\mu_3)(k - k_4 - i\mu_4)}dk \qquad (3.30)$$

1) For the case of $x \geq 0$:

The path of integration for ϑ_1 is C_2 and for ϑ_2 is C_1. The detail is shown in Fig. 3.3.

2) For the case of $x \le 0$:

The path of integration for ϑ_1 is C_1 and for ϑ_2 is C_2.

Hence if the above path of integration taken at infinity is proven, then the following equations can be obtained as

1) For the case of $x \ge 0$:

$$\vartheta_1 + \int_{-\infty}^{0} \frac{e^{-ik(y+\eta)+kx}}{f(ik)} idk = -2\pi i \frac{1}{k_2 - k_1} e^{-k_2(y+\eta)-ik_2 x} \tag{3.31}$$

$$\vartheta_2 + \int_{-\infty}^{0} \frac{e^{-ik(y+\eta)-kx}}{g(ik)} idk = 0 \tag{3.32}$$

Thus from Eq. (3.19), these expressions can be derived as

$$f(ik) = (ik + \omega_0)^2 - ikK_0 = -\{k^2 - \omega_0^2 + ik(K_0 - 2\omega_0)\} \tag{3.33}$$

$$g(ik) = (ik - \omega_0)^2 - ikK_0 = -\{k^2 - \omega_0^2 + ik(K_0 + 2\omega_0)\} \tag{3.34}$$

$$\vartheta_1 + \vartheta_2 = -i\int_0^{\infty} \frac{e^{-ik(y+\eta)-kx} dk}{k^2 - \omega_0^2 + ik(K_0 + 2\omega_0)} + i\int_{-\infty}^{0} \frac{e^{-ik(y+\eta)+kx} dk}{k^2 - \omega_0^2 + ik(K_0 - 2\omega_0)} + \frac{2\pi i}{k_1 - k_2} e^{-k_2(y+\eta)-ik_2 x} \tag{3.35}$$

$$= -i\int_{-\infty}^{\infty} \frac{\mathrm{sgn}(k) e^{-ik(y+\eta)-|k|x} dk}{k^2 - \omega_0^2 + i(kK_0 + 2|k|\omega_0)} + \frac{2\pi i}{k_1 - k_2} e^{-k_2(y+\eta)-ik_2 x} \tag{3.36}$$

$$= i\int_{-\infty}^{\infty} \frac{\mathrm{sgn}(k) e^{ik(y+\eta)-|k|x} dk}{k^2 - \omega_0^2 - i(kK_0 - 2|k|\omega_0)} + \frac{2\pi i}{k_1 - k_2} e^{-k_2(y+\eta)-ik_2 x} \tag{3.37}$$

2) For the case of $x \le 0$:

$$\vartheta_1 + \int_{-\infty}^{0} \frac{e^{-ik(y+\eta)+kx}}{f(ik)} idk = 2\pi i \frac{1}{k_1 - k_2} e^{-k_1(y+\eta)-ik_1 x} \tag{3.38}$$

$$\vartheta_2 + \int_{-\infty}^{0} \frac{e^{-ik(y+\eta)-kx}}{g(ik)} idk = -2\pi i \frac{1}{k_3 - k_4} e^{-k_3(y+\eta)+ik_3 x} - 2\pi i \frac{1}{k_4 - k_3} e^{-k_4(y+\eta)+ik_4 x} \tag{3.39}$$

Therefore

$$\vartheta_1 + \vartheta_2 = -i\int_0^{\infty} \frac{e^{-ik(y+\eta)+kx} dk}{k^2 - \omega_0^2 + ik(K_0 - 2\omega_0)} + i\int_{-\infty}^{0} \frac{e^{-ik(y+\eta)-kx} dk}{k^2 - \omega_0^2 + ik(K_0 + 2\omega_0)} + 2\pi i \frac{1}{k_1 - k_2} e^{-k_1(y+\eta)-ik_1 x} - 2\pi i \frac{1}{k_3 - k_4} \left\{ e^{-k_3(y+\eta)+ik_3 x} - e^{-k_4(y+\eta)+ik_4 x} \right\} \tag{3.40}$$

$$\vartheta_1 + \vartheta_2 = -i\int_{-\infty}^{\infty} \frac{\mathrm{sgn}(k) e^{-ik(y+\eta)+|k|x} dk}{k^2 - \omega_0^2 + i(kK_0 - 2|k|\omega_0)} + 2\pi i \frac{1}{k_1 - k_2} e^{-k_1(y+\eta)-ik_1 x} - 2\pi i \frac{1}{k_3 - k_4} \left\{ e^{-k_3(y+\eta)+ik_3 x} - e^{-k_4(y+\eta)+ik_4 x} \right\} \tag{3.41}$$

As shown above, Both Eq. (3.37) for $x \geq 0$ and Eq. (3.41) for $x \leq 0$ are derived.

By more mathematical manipulation, the expression is written as

$$\vartheta_1 + \vartheta_2 = -\int_{-\infty}^{\infty} \frac{(kK_0 - 2|k|\omega_0) - i\,\mathrm{sgn}(x)(k^2 - \omega_0^2) e^{\mathrm{sgn}(x)\{ik(y+\eta)-|k|x\}} \mathrm{sgn}(k) dk}{(kK_0 - 2|k|\omega_0)^2 + (k^2 - \omega_0^2)^2} + H(x)\left[\frac{2\pi i}{k_1 - k_2} e^{-k_2(y+\eta)-ik_2 x} \right] + H(-x)\left[\frac{2\pi i}{k_1 - k_2} e^{-k_1(y+\eta)-ik_1 x} - \frac{2\pi i}{k_3 - k_4} \left\{ e^{-k_3(y+\eta)+ik_3 x} - e^{-k_4(y+\eta)+ik_4 x} \right\} \right] \tag{3.42}$$

where :

$$k_1 - k_2 = \begin{cases} K_0\sqrt{1-4\tau} & \left(\tau \le \frac{1}{4}\right) \\ iK_0\sqrt{4\tau-1} & \left(\tau \ge \frac{1}{4}\right) \end{cases} \qquad (3.43a)$$

$$k_3 - k_4 = K_0\sqrt{1+4\tau} \qquad (3.43b)$$

For the case of $\tau \le \frac{1}{4}$, Eq.(3.18) and Eq. (3.42) can then be rewritten as

$$G = -\frac{1}{2\pi}\log\frac{r}{r_1} - \frac{K_0}{2\pi}(\vartheta_1 + \vartheta_2) \qquad (3.44a)$$

$$= -\frac{1}{2\pi}\log\frac{r}{r_1} - \frac{K_0}{2\pi}\int_{-\infty}^{\infty} \frac{e^{\mathrm{sgn}(x)\{ik(y+\eta)-i\varepsilon-|k|x\}}\mathrm{sgn}(k)dk}{\sqrt{\left(kK_0 - 2|k|\omega_0\right)^2 + \left(k^2-\omega_0^2\right)^2}}$$
$$-H(x)\frac{i}{\sqrt{1-4\tau}}e^{-k_2(y+\eta)-ik_2x}$$
$$-H(-x)\left[\frac{i}{\sqrt{1-4\tau}}e^{-k_1(y+\eta)-ik_1x} - \frac{i}{\sqrt{1+4\tau}}\left\{e^{-k_3(y+\eta)+ik_3x} - e^{-k_4(y+\eta)+ik_4x}\right\}\right]$$
$$\left(\text{for } \tau \le \frac{1}{4}\right) \qquad (3.44b)$$

where :

$$\varepsilon = \tan^{-1}\frac{k^2-\omega_0^2}{kK_0 - 2|k|\omega_0} \qquad (3.45)$$

For the case of $\frac{1}{4} \le \tau \le \frac{1}{2}$, from Eq. (3.24) as

$$k \equiv \tilde{k} \pm i\nu \qquad (3.46a)$$

where :

$$\tilde{k} = \frac{K_0}{2}(1-2\tau) \qquad (3.46b)$$

$$\nu = \frac{K_0}{2}\sqrt{4\tau-1} \qquad (3.46c)$$

Using the above equations, the Green function is similarly described as

$$G = -\frac{1}{2\pi}\log\frac{r}{r_1} + \frac{K_0}{2\pi}\int_{-\infty}^{\infty}\frac{e^{\mathrm{sgn}(x)\{ik(y+\eta)-i\varepsilon-|k|x\}}\mathrm{sgn}(k)dk}{\sqrt{\left(kK_0-2|k|\omega_0\right)^2+\left(k^2-\omega_0^2\right)^2}}$$
$$-H(x)\frac{1}{\sqrt{4\tau-1}}e^{-(\tilde{k}-iv)(y+\eta)-(v+i\tilde{k})x}$$
$$-H(-x)\left[\frac{1}{\sqrt{4\tau-1}}e^{-(\tilde{k}+iv)(y+\eta)-(-v+i\tilde{k})x}-\frac{i}{\sqrt{4\tau+1}}\left\{e^{-k_3(y+\eta)+ik_3x}-e^{-k_4(y+\eta)+ik_4x}\right\}\right]$$
$$\left(\text{for } \frac{1}{4}\le\tau\le\frac{1}{2}\right) \qquad (3.47)$$

For the case of $\tau \ge \frac{1}{2}$, k_1 and k_2 do not exist. the Green function can then be obtained as

$$G = -\frac{1}{2\pi}\log\frac{r}{r_1} + \frac{K_0}{2\pi}\int_{-\infty}^{\infty}\frac{e^{\mathrm{sgn}(x)\{ik(y+\eta)-i\varepsilon-|k|x\}}\mathrm{sgn}(k)dk}{\sqrt{\left(kK_0-2|k|\omega_0\right)^2+\left(k^2-\omega_0^2\right)^2}}$$
$$+H(-x)\left[\frac{i}{\sqrt{4\tau+1}}\left\{e^{-k_3(y+\eta)+ik_3x}-e^{-k_4(y+\eta)+ik_4x}\right\}\right]$$
$$\left(\text{for } \tau\ge\frac{1}{2}\right) \qquad (3.48)$$

Next the Green function, Eq. (3.44), is simplified further for the critical cases of $U \to 0$ and $\omega \to 0$ and the conventional Green function can be introduced as follows.

1) For the case of $U \to 0$:

From Eqs.(3.26) and (3.28), the formula of k_1, k_2, k_3 and k_4 can be written as

$$\left.\begin{matrix}k_1\\k_2\end{matrix}\right\} = 2K\frac{1}{1-2\tau\mp\sqrt{1-4\tau}} \qquad (3.49a)$$

$$\left.\begin{matrix}k_3\\k_4\end{matrix}\right\} = 2K\frac{1}{1+2\tau\mp\sqrt{1+4\tau}} \qquad (3.49b)$$

Therefore for the case of $U \to 0$, the conditions for these wave numbers indicated below are satisfied.

$$k_1 = \infty,\ k_2 = K,\ k_3 = \infty \text{ and } k_4 = K \tag{3.50}$$

where :

$$K = \frac{\omega^2}{g} \tag{3.50a}$$

$$\text{Here } \frac{\omega_0^2}{K_0} = \frac{\omega^2}{U^2}\frac{U^2}{g} = K \tag{3.50b}$$

and from Eq. (3.45), the following expression can be written as

$$\varepsilon = \tan^{-1}\left(\frac{-K}{k}\right) = -\frac{\pi}{2} + \tan^{-1}\left(\frac{k}{K}\right) \tag{3.51a}$$

or

$$\cos\varepsilon = \frac{k}{\sqrt{k^2 + K^2}} \tag{3.51b}$$

$$\sin\varepsilon = \frac{-K}{\sqrt{k^2 + K^2}} \tag{3.51c}$$

then

$$\begin{aligned}
&\frac{K_0}{2\pi}\int_{-\infty}^{\infty} \frac{e^{\operatorname{sgn}(x)\{ik(y+\eta)-i\varepsilon-|k|x\}}\operatorname{sgn}(k)dk}{\sqrt{\left(kK_0 - 2|k|\omega_0\right)^2 + \left(k^2 - \omega_0^2\right)^2}} \\
&\quad = \frac{1}{2\pi}\int_0^{\infty} \frac{2\left\{k\cos k(y+\eta) - K\sin k(y+\eta)\right\}}{k^2 + K^2} e^{-k|x|}dk \\
&\quad = \frac{1}{\pi}\int_0^{\infty} \frac{\left\{k\cos k(y+\eta) - K\sin k(y+\eta)\right\}}{k^2 + K^2} e^{-k|x|}dk
\end{aligned} \tag{3.52}$$

From Eqs. (3.50) and (3.52), the mathematical expression of this Green function, Eq. (3.44), is derived as

$$G = -\frac{1}{2\pi}\log\frac{r}{r_1} + \frac{1}{\pi}\int_0^\infty \frac{\{k\cos k(y+\eta) - K\sin k(y+\eta)\}}{k^2+K^2} e^{-k|x|}dk - ie^{-K(y+\eta)-iK|x|}$$

$$(\text{for } U \to 0) \qquad (3.53)$$

2) For the case of $\omega \to 0$:

From Eq. (3.26) and Eq. (3.28), the conditions of the specific wave numbers $k_1 = K_0$, $k_2 = 0$, $k_3 = K_0$ and $k_4 = 0$ are satisfied. Then from Eq. (3.45), the mathematical expression can be obtained as

$$\varepsilon = \tan^{-1}\frac{k}{K_0} \qquad (3.54a)$$

or

$$\cos\varepsilon = \frac{K_0}{\sqrt{k^2+K_0^2}} \qquad (3.54b)$$

$$\sin\varepsilon = \frac{k}{\sqrt{k^2+K_0^2}} \qquad (3.54c)$$

Hence

$$\frac{K_0}{2\pi}\int_{-\infty}^{\infty} \frac{e^{sgn(x)\{ik(y+\eta)-i\varepsilon-|k|x\}}sgn(k)dk}{\sqrt{(kK_0-2|k|\omega_0)^2+(k^2-\omega_0^2)^2}}$$

$$= \frac{K_0}{2\pi}\int_0^\infty \frac{2\{K_0\cos k(y+\eta)+k\sin k(y+\eta)\}}{k(k^2+K_0^{\,2})} e^{-k|x|}dk$$

$$= \frac{K_0}{\pi}\int_0^\infty \frac{\{K_0\cos k(y+\eta)+k\sin k(y+\eta)\}}{k(k^2+K_0^{\,2})} e^{-k|x|}dk \qquad (3.55)$$

Thus the above relations and Eq. (3.55) are substituted into Eq. (3.44) to obtain

$$G = -\frac{1}{2\pi}\log\frac{r}{r_1} + \frac{K_0}{\pi}\int_0^{\infty}\frac{\{K_0\cos k(y+\eta)+k\sin k(y+\eta)\}}{k(k^2+K_0{}^2)}e^{-k|x|}dk$$
$$+\{\mathrm{sgn}(x)-1\}e^{-K_0(y+\eta)}\sin K_0 x$$
$$(\text{for } \omega \to 0) \qquad (3.56)$$

In conclusions, the above convergent type of integral equation can be presented, i.e.

1). For the case of $\tau \le \frac{1}{4}$, Eq. (3.44) is represented.

2). For the case of $\frac{1}{4} \le \tau \le \frac{1}{2}$, Eq. (3.47) is described.

3). For the case of $\tau \ge \frac{1}{2}$, Eq. (3.48) is also indicated.

However the integral which contains the Rayleigh's fictitious friction coefficient is described as shown in Eq. (3.44). Hence from now on it should be taken out from the convergent form, but it can be reduced in the form of principal value integral.

Corresponding to Eq. (3.29) and Eq. (3.30), these integrals can be described as

$$\tilde{\vartheta}_1 = \int_0^{\infty}\frac{e^{-k(y+\eta)-ikx}}{(k-k_1)(k-k_2)}dk \qquad (3.57a)$$

$$\tilde{\vartheta}_2 = \int_0^{\infty}\frac{e^{-k(y+\eta)+ikx}}{(k-k_3)(k-k_4)}dk \qquad (3.57b)$$

Here

$$\frac{1}{(k-k_1)(k-k_2)}=\frac{1}{f(k)}=\frac{1}{(k+\omega_0)^2-kK_0}=\frac{1}{(k_1-k_2)}\left\{\frac{1}{(k-k_1)}-\frac{1}{(k-k_2)}\right\} \tag{3.58}$$

$$\frac{1}{(k-k_3)(k-k_4)}=\frac{1}{g(k)}=\frac{1}{(k-\omega_0)^2-kK_0}=\frac{1}{(k_3-k_4)}\left\{\frac{1}{(k-k_3)}-\frac{1}{(k-k_4)}\right\} \tag{3.59}$$

By taking precautions of the poles of Eq. (3.57) for the various range of the τ value, the path of integration over the complex plane, as shown in Fig. 3.4, is conducted as

1) For the case of $x \geq 0$ $(\tau \leq \frac{1}{4})$:

$$\tilde{\vartheta}_1+\frac{\pi i}{k_1-k_2}\left[e^{-k_1(y+\eta)-ik_1x}-e^{-k_2(y+\eta)-ik_2x}\right]+\int_{-\infty}^{0}\frac{e^{-ik(y+\eta)+kx}}{f(ik)}idk=0 \tag{3.60}$$

$$\tilde{\vartheta}_2-\frac{\pi i}{k_3-k_4}\left[e^{-k_3(y+\eta)+ik_3x}-e^{-k_4(y+\eta)+ik_4x}\right]+\int_{-\infty}^{0}\frac{e^{-ik(y+\eta)-kx}}{g(ik)}idk=0 \tag{3.61}$$

Hence

$$\begin{aligned}\tilde{\vartheta}_1+\tilde{\vartheta}_2=&\int_{-\infty}^{\infty}\frac{\mathrm{sgn}(k)e^{ik(y+\eta)-|k|x}}{k^2-\omega_0^2-i(kK_0-2|k|\omega_0)}dk\\&-\frac{\pi i}{k_1-k_2}\left[e^{-k_1(y+\eta)-ik_1x}-e^{-k_2(y+\eta)-ik_2x}\right]\\&+\frac{\pi i}{k_3-k_4}\left[e^{-k_3(y+\eta)+ik_3x}-e^{-k_4(y+\eta)+ik_4x}\right]\end{aligned} \tag{3.62}$$

By comparing Eq. (3.37) and Eq. (3.62), the expression can then be written as

$$\vartheta_1 + \vartheta_2 = \tilde{\vartheta}_1 + \tilde{\vartheta}_2 + \frac{\pi i}{k_1 - k_2}\left[e^{-k_1(y+\eta)-ik_1x} - e^{-k_2(y+\eta)-ik_2x}\right] - \frac{\pi i}{k_3 - k_4}\left[e^{-k_3(y+\eta)+ik_3x} - e^{-k_4(y+\eta)+ik_4x}\right] \quad (3.63)$$

From Eq. (3.57), Eq. (3.58) and Eq. (3.59), the following expression can be derived as

$$\tilde{\vartheta}_1 + \tilde{\vartheta}_2 = \int_{-\infty}^{\infty} \frac{e^{-|k|(y+\eta)-ikx}}{(k+\omega_0)^2 - |k|K_0}\,dk \quad (3.64)$$

$$= \frac{1}{k_1 - k_2}\int_0^{\infty}\left\{\frac{1}{k-k_1} - \frac{1}{k-k_2}\right\}e^{-k(y+\eta)-ikx}\,dk + \frac{1}{k_3 - k_4}\int_0^{\infty}\left\{\frac{1}{k-k_3} - \frac{1}{k-k_4}\right\}e^{-k(y+\eta)+ikx}\,dk \quad (3.65)$$

2) For the case of $x \le 0$:

In a similar way, the reverse contour of integration is taken. Thus the following equation can be written as

$$\tilde{\vartheta}_1 + \tilde{\vartheta}_2 = -i\int_{-\infty}^{\infty} \frac{\mathrm{sgn}(k)e^{-ik(y+\eta)+|k|x}}{k^2 - \omega_0^2 + i(kK_0 - 2|k|\omega_0)}\,dk + \frac{\pi i}{k_1 - k_2}\left[e^{-k_1(y+\eta)-ik_1x} - e^{-k_2(y+\eta)-ik_2x}\right] - \frac{\pi i}{k_3 - k_4}\left[e^{-k_3(y+\eta)+ik_3x} - e^{-k_4(y+\eta)+ik_4x}\right] \quad (3.66)$$

If the above equation is compared with Eq. (3.41), then the following expression can be written as

$$\vartheta_1 + \vartheta_2 = \tilde{\vartheta}_1 + \tilde{\vartheta}_2 + \frac{\pi i}{k_1 - k_2}\left[e^{-k_1(y+\eta)-ik_1x} - e^{-k_2(y+\eta)-ik_2x}\right] - \frac{\pi i}{k_3 - k_4}\left[e^{-k_3(y+\eta)+ik_3x} - e^{-k_4(y+\eta)+ik_4x}\right] \quad (3.67)$$

The $\tilde{\vartheta}_1 + \tilde{\vartheta}_2$ for the above equation is the same as Eq. (3.65). Then Eq.

(3.63) and Eq. (3.67) are also identical, i.e. irrespective whether it is positive or negative, the Green function can be described as

$$
\begin{aligned}
G &= -\frac{1}{2\pi}\log\frac{r}{r_1} - \frac{K_0}{2\pi}(\vartheta_1 + \vartheta_2) \\
&= -\frac{1}{2\pi}\log\frac{r}{r_1} - \frac{K_0}{2\pi}\int_{-\infty}^{\infty}\frac{e^{-|k|(y+\eta)-ikx}}{(k+\omega_0)^2 - |k|K_0}dk \\
&\quad -\frac{i}{2\sqrt{1-4\tau}}\left[e^{-k_1(y+\eta)-ik_1x} + e^{-k_2(y+\eta)-ik_2x}\right] \\
&\quad +\frac{i}{2\sqrt{1+4\tau}}\left[e^{-k_3(y+\eta)+ik_3x} - e^{-k_4(y+\eta)+ik_4x}\right] \\
&\qquad\qquad (\text{for } \tau \le \frac{1}{4}) \qquad\qquad (3.68)
\end{aligned}
$$

or replacing $\tilde{\vartheta}_1 + \tilde{\vartheta}_2$ by Eq. (3.65), the expression can be written as

$$
\begin{aligned}
G &= -\frac{1}{2\pi}\left[\log\frac{r}{r_1} + \frac{1}{\sqrt{1-4\tau}}\left\{\int_0^{\infty}\frac{e^{-k(y+\eta)-ikx}}{k-k_1}dk - \int_0^{\infty}\frac{e^{-k(y+\eta)-ikx}}{k-k_2}dk\right\}\right. \\
&\quad +\frac{1}{\sqrt{1+4\tau}}\left\{\int_0^{\infty}\frac{e^{-k(y+\eta)+ikx}}{k-k_3}dk - \int_0^{\infty}\frac{e^{-k(y+\eta)+ikx}}{k-k_4}dk\right\} \\
&\quad +\frac{\pi i}{\sqrt{1-4\tau}}\left[e^{-k_1(y+\eta)-ik_1x} + e^{-k_2(y+\eta)-ik_2x}\right] \\
&\quad \left.-\frac{\pi i}{\sqrt{1+4\tau}}\left[e^{-k_3(y+\eta)+ik_3x} - e^{-k_4(y+\eta)+ik_4x}\right]\right] \\
&\qquad\qquad (\text{for } \tau \le \frac{1}{4}) \qquad\qquad (3.69)
\end{aligned}
$$

For the range of $\frac{1}{4} \le \tau \le \frac{1}{2}$ and $\tau \ge \frac{1}{2}$, the expression of $\tilde{\vartheta}_1 + \tilde{\vartheta}_2$ should be performed and then compared with that of $\vartheta_1 + \vartheta_2$. The Green function can be described in the following form

$$
\begin{aligned}
\vartheta_1 + \vartheta_2 &= \tilde{\vartheta}_1 + \tilde{\vartheta}_2 - \frac{\pi i}{k_3 - k_4}\left[e^{-k_3(y+\eta)+ik_3x} - e^{-k_4(y+\eta)-ik_4x}\right] \\
&\qquad\qquad (\text{for } \tau \ge \frac{1}{4}) \qquad\qquad (3.70)
\end{aligned}
$$

For the case of $\tau \geq \frac{1}{4}$, the Green function corresponding to Eq. (3.68) and Eq. (3.69) can be written as

$$G = -\frac{1}{2\pi}\log\frac{r}{r_1} - \frac{K_0}{2\pi}\int_{-\infty}^{\infty}\frac{e^{-|k|(y+\eta)-ikx}}{(k+\omega_0)^2 - |k|K_0}dk + \frac{i}{2\sqrt{1+4\tau}}\left[e^{-k_3(y+\eta)+ik_3x} - e^{-k_4(y+\eta)+ik_4x}\right] \quad (\text{for } \tau \geq \frac{1}{4}) \qquad (3.71)$$

The expression can be also written as

$$G = -\frac{1}{2\pi}\left[\log\frac{r}{r_1} - \frac{i}{\sqrt{4\tau-1}}\left\{\int_0^{\infty}\frac{e^{-k(y+\eta)-ikx}}{k-k_1}dk - \int_0^{\infty}\frac{e^{-k(y+\eta)-ikx}}{k-k_2}dk\right\} + \frac{1}{\sqrt{1+4\tau}}\left\{\int_0^{\infty}\frac{e^{-k(y+\eta)+ikx}}{k-k_3}dk - \int_0^{\infty}\frac{e^{-k(y+\eta)+ikx}}{k-k_4}dk\right\} - \frac{\pi i}{\sqrt{1+4\tau}}\left[e^{-k_3(y+\eta)+ik_3x} - e^{-k_4(y+\eta)+ik_4x}\right]\right] \quad (\text{for } \tau \geq \frac{1}{4}) \qquad (3.72)$$

3.4 Mathematical manipulation for numerical computations

For the purpose of numerical computations, the Green function should be simplified further in the form of the exponential integral. If the calculation is performed in the form on Eq. (3.44), the accuracy is easily realised not to be good enough. Thus the Eq. (3.69) should be simplified further, i.e. the principal value integral term of Eq. (3.69) is described as

$$I_1 = \int_0^{\infty}\frac{e^{-k(y+\eta)-ikx}}{k-k_1}dk \qquad (3.73a)$$

$$I_2 = \int_0^{\infty}\frac{e^{-k(y+\eta)-ikx}}{k-k_2}dk \qquad (3.73b)$$

$$I_3 = \int_0^{\infty} \frac{e^{-k(y+\eta)+ikx}}{k-k_3} dk \qquad (3.73c)$$

$$I_4 = \int_0^{\infty} \frac{e^{-k(y+\eta)+ikx}}{k-k_4} dk \qquad (3.73d)$$

Here the effort is concentrated on the local wave term and the expressions of L_j $(j=1,2,3,4)$ corresponding to that of I_j $(j=1,2,3,4)$ are represented as follows.

1) For the case of $x \geq 0$:

$$L_1 = -\int_{-\infty}^{0} \frac{e^{-ik(y+\eta)+kx}}{ik-k_1} idk = \int_0^{\infty} \frac{e^{ik(y+\eta)-kx}}{k-ik_1} dk \qquad (3.74)$$

Here setting

$$(k-k_1)\{x-i(y+\eta)\} = m \qquad (3.75a)$$

and

$$Z = (y+\eta)+ix \qquad (3.75b)$$

then

$$\int_0^{\infty} \frac{e^{-k\{x-i(y+\eta)\}}}{k-ik_1} dk = -\int_{-k_1 Z}^{\infty} \frac{e^{-(m+k_1 Z)}}{m} dm = e^{-k_1 Z} E_1(-k_1 Z) \qquad (3.76)$$

where :

$$E_1(Z) = \int_Z^{\infty} \frac{e^{-m}}{m} dm \quad , \quad |\arg Z| < \pi \qquad (3.77)$$

Therefore

$$L_1 = e^{-k_1 Z} E_1(-k_1 Z) \tag{3.78}$$

where :

$$Z = (y+\eta) + ix \tag{3.78a}$$

The calculation for L_2 is also similar as Eq. (3.78), thus

$$L_2 = e^{-k_2 Z} E_1(-k_2 Z) \tag{3.79}$$

Next the calculations of L_3 and L_4 are performed as

$$L_3 = -\int_{-\infty}^{0} \frac{e^{-ik(y+\eta)-kx}}{ik-k_3} idk = \int_{0}^{\infty} \frac{e^{-ik(y+\eta)-kx}}{k+ik_3} dk \tag{3.80}$$

By setting

$$m = (k+ik_3)\{x+i(y+\eta)\} \tag{3.80a}$$

then

$$L_3 = e^{-k_3 \bar{Z}} E_1(-k_3 \bar{Z}) \tag{3.81}$$

where :

$$\bar{Z} = (y+\eta) - ix \tag{3.81a}$$

Similarly

$$L_4 = e^{-k_4 \bar{Z}} E_1(-k_4 \bar{Z}) \tag{3.82}$$

2) For the case of $x \le 0$:

Nevertheless the mathematical procedure is similar to the above, thus

$$L_1 = \int_0^{\infty} \frac{e^{-k\{|x|+i(y+\eta)\}}}{k+ik_1} dk = e^{-k_1\overline{Y}} E_1(-k_1\overline{Y}) \qquad (3.83)$$

where :

$$\overline{Y} = (y+\eta) - i|x| = (y+\eta) - ix = Z \qquad (3.84)$$

In other words, it is exactly the same as Eq. (3.78) and similarly

$$L_2 = e^{-k_2\overline{Y}} E_1(-k_2\overline{Y}) \qquad (3.85)$$

Moreover the expressions of L_3 and L_4 areexpressed as

$$L_3 = e^{-k_3 Y} E_1(-k_3 Y) \qquad (3.86)$$

$$L_4 = e^{-k_4 Y} E_1(-k_4 Y) \qquad (3.87)$$

where :

$$Y = (y+\eta) + i|x| = (y+\eta) - ix = \overline{Z} \qquad (3.88)$$

From the above mathematical simplification, despite the value of x is positive or negative, the expressions of L_j ($j = 1,2,3,4$) can be represented as Eqs. (3.78), (3.79), (3.81) and (3.82) respectively. Practically, to calculate the exponential integral for $x \leq 0$ is inconvenient. Hence these expression can be written as follows.

$$F(k_j Z) \equiv e^{-k_j Z} E_1(-k_j Z) \qquad (3.89)$$

where :

$$Z = (y + \eta) + i|x| \tag{3.90}$$

By using the above definitions, the following equations can be described as

1) For the case of $x \geq 0$:

$$L_1 - L_2 = F(k_1 Z) - F(k_2 Z) \tag{3.91}$$

$$L_3 - L_4 = \overline{F}(k_3 Z) - \overline{F}(k_4 Z) \tag{3.92}$$

where :

$$Z = (y + \eta) + i|x| \tag{3.93}$$

Here $\overline{F}$ is the complex conjugate of F, subject to the condition that k_j is real, the relation can be described as

$$\overline{F}(k_j Z) = -F(k_j \overline{Z}) \tag{3.94}$$

2) For the case of $x \leq 0$:

$$L_1 - L_2 = \overline{F}(k_1 Z) - \overline{F}(k_2 Z) \tag{3.95}$$

$$L_3 - L_4 = F(k_3 Z) - F(k_4 Z) \tag{3.96}$$

where :

$$Z = (y + \eta) + i|x| \tag{3.97}$$

By substituting the above relations into Eq. (3.69) and rearranging it, the final expression of the Green function can then be described as

$$-2\pi G = \log\frac{r}{r_1} + \frac{1}{\sqrt{1-4\tau}}\left\{F(k_1X) - F(k_2X)\right\} + \frac{1}{\sqrt{1+4\tau}}\left\{\bar{F}(k_3X) - \bar{F}(k_4X)\right\}$$
$$+H(x)\frac{2\pi i}{\sqrt{1-4\tau}}e^{-k_2(y+\eta)-ik_2x}$$
$$+H(-x)\left[\begin{array}{l}\dfrac{2\pi i}{\sqrt{1-4\tau}}e^{-k_1(y+\eta)-ik_1x} \\ -\dfrac{2\pi i}{\sqrt{1+4\tau}}\left\{e^{-k_3(y+\eta)+ik_3x} - e^{-k_4(y+\eta)+ik_4x}\right\}\end{array}\right]$$
$$\left(\text{for } \tau \le \frac{1}{4}\right) \qquad (3.98)$$

where :

$$F(k_jX) = e^{-k_jX}E_1(-k_jX) \qquad (3.99)$$

$$X = (y+\eta) + ix \qquad (3.100)$$

and $E_1(Z)$ is the exponential integral with the complex variable.

Similarly for the different ranges of the τ values, the Green functions are respectively described as follows.

$$-2\pi G = \log\frac{r}{r_1} - \frac{i}{\sqrt{4\tau-1}}\left\{F(k_1X) - F(k_2X)\right\} + \frac{1}{\sqrt{1+4\tau}}\left\{\bar{F}(k_3X) - \bar{F}(k_4X)\right\}$$
$$+H(x)\frac{2\pi}{\sqrt{4\tau-1}}e^{-k_2(y+\eta)-ik_2x}$$
$$+H(-x)\left[\begin{array}{l}\dfrac{2\pi}{\sqrt{4\tau-1}}e^{-k_1(y+\eta)-ik_1x} \\ -\dfrac{2\pi i}{\sqrt{1+4\tau}}\left\{e^{-k_3(y+\eta)+ik_3x} - e^{-k_4(y+\eta)+ik_4x}\right\}\end{array}\right]$$
$$\left(\text{for } \frac{1}{4} \le \tau \le \frac{1}{2}\right) \qquad (3.101)$$

and

$$-2\pi G = \log\frac{r}{r_1} - \frac{i}{\sqrt{4\tau-1}}\left\{F(k_1X) - F(k_2X)\right\} + \frac{1}{\sqrt{1+4\tau}}\left\{\bar{F}(k_3X) - \bar{F}(k_4X)\right\}$$
$$-H(-x)\frac{2\pi i}{\sqrt{1+4\tau}}\left\{e^{-k_3(y+\eta)+ik_3x} - e^{-k_4(y+\eta)+ik_4x}\right\}$$
$$\left(\text{for } \tau \geq \frac{1}{4}\right) \qquad (3.102)$$

where :

$$\left.\begin{matrix} k_1 \\ k_2 \end{matrix}\right\} = \frac{K_0}{2}\left[1 - 2\tau \pm i\sqrt{4\tau-1}\right] \qquad (3.103)$$

$$\left.\begin{matrix} k_3 \\ k_4 \end{matrix}\right\} = \frac{K_0}{2}\left[1 + 2\tau \pm \sqrt{4\tau+1}\right] \qquad (3.104)$$

$$K_0 = \frac{g}{U^2} \quad , \quad \tau = \frac{U\omega}{g} \qquad (3.105)$$

$$\left.\begin{matrix} r \\ r_1 \end{matrix}\right\} = \sqrt{(x-\xi)^2 + (y \mp \eta)^2} \qquad (3.106)$$

3.5 Conclusion

The fundamental formulation of the most generalized form of Green function to predict hydrodynamic forces is theoretically derived for the two dimensional boundary value problem of a single submerged body advancing at constant forward speed and oscillating in incident waves and its derivatives can be derived for the solution of velocity potential over body boundary contours in the integral equations.

CHAPTER 4
FIRST ORDER HYDRODYNAMIC FORCES

4.1 General description

Here the theoretical formulation of the first order hydrodynamic forces acting on a submerged structure oscillating and translating in waves under a free surface is derived in detail. Hydrodynamic forces are described in terms of radiation and diffraction potentials as mentioned in the solutions of the boundary value problems discussed in Chapter Two (Kashiwagi and Varyani 1987).

By neglecting the second and higher order terms associated with the unsteady part ϕ of velocity potentials in the Bernoulli's equation, hydrodynamic pressure forces $\bar{P}(x,y,t)$ can be written as

$$\bar{P}(x,y,t) = -\rho\left\{\left(i\omega + U\vec{V}\cdot\nabla\right)\phi e^{i\omega t} + \frac{U^2}{2}\vec{V}^2\right\} \qquad (4.1)$$

where :

$\vec{V}$ is the velocity of the steady flow equal to $\nabla(-x+\varphi_s)$

On calculating hydrodynamic pressure forces on the oscillating and translating body, the hydrodynamic pressure should be integrated over the instantaneous body boundary contour directly. In the same way, the second and higher order terms associated with the oscillatory motion of the body are neglected, so hydrodynamic pressure forces can be obtained by direct integration of the hydrodynamic pressure $P(x,y)e^{i\omega t}$ on the body surface at the mean position. The mathematical expression of the hydrodynamic pressure $P(x,y)e^{i\omega t}$ is expressed as

$$P(x,y)e^{i\omega t} = -\rho\left\{\left(i\omega + U\bar{V}\cdot\nabla\right)\phi e^{i\omega t} + \frac{U^2}{2}(\bar{\alpha}\cdot\nabla)\bar{V}^2 e^{i\omega t}\right\} \qquad (4.2)$$

where :

$\bar{\alpha}$ is the dynamic amplitude of the body oscillatory motion defined in Eq. (2.7) previously. The last term describes a linear approximation of this additional pressure due to the oscillatory displacement of the body in the steady but non-uniform flow field $\bar{V}$ and the mathematical derivation of these terms will be discussed in Chapter Six in detail.

4.2 Formulation of added mass and damping coefficients

By substituting the velocity potential ϕ in Eq. (4.2) from the radiation potentials ψ_j indicated in the last terms on the right hand side of Eq. (2.3) and integrating the hydrodynamic pressure $P(x,y)e^{i\omega t}$ on the surface S_H at the mean position of the body, hydrodynamic forces on a structure translating and oscillating in surge, heave and pitch modes under calm water are then expressed as

$$f_k e^{i\omega t} = -e^{i\omega t}\int_{S_H} P(x,y)n_k\,ds = \sum_{j=1}^{3}\left(F_{k_j} - C_{k_j}\right)\xi_j e^{i\omega t} \qquad (k=1,2,3) \qquad (4.3)$$

where :

Subscript 1 denotes the surge mode in the x direction, 2 the heave mode in the y direction and 3 the pitch mode with the clockwise moment around a point in the cross section. n_1 is the x component of unit outward normal to the surface S_H, n_2 is for the y component and n_3 is $xn_2 - (y-d)n_1$ for the z component.

The mathematical terms of F_{k_j} and C_{k_j} in Eq. (4.3) represent the contributions of the first and second terms in the right hand side of Eq. (4.2)

respectively and all the expressions are expressed as

$$F_{k_j} = \rho \int_{S_H} \left\{ \left(i\omega + U\bar{V} \cdot \nabla \right) i\omega \psi_j \right\} n_k \, ds \qquad (4.4a)$$

$$\equiv \omega^2 A_{k_j} - i\omega B_{k_j} \qquad (4.4b)$$

and

$$C_{k_1} = -\rho \frac{U^2}{2} \int_{S_H} \frac{\partial}{\partial x} \bar{V}^2 \, n_k \, ds \qquad (4.5a)$$

$$C_{k_2} = -\rho \frac{U^2}{2} \int_{S_H} \frac{\partial}{\partial y} \bar{V}^2 \, n_k \, ds \qquad (4.5b)$$

$$C_{k_3} = -\rho \frac{U^2}{2} \int_{S_H} \left\{ -(y-d) \frac{\partial}{\partial x} + x \frac{\partial}{\partial y} \right\} \bar{V}^2 \, n_k \, ds \qquad (4.5c)$$

where :

Coefficients A_{k_j} are added mass coefficients which represent the forces proportional to the acceleration of body oscillatory motions and induce the same contribution as increase the mass of the body in motions.
Coefficients B_{k_j} are damping coefficients which denote the forces proportional to the velocity of the body motions and have the effect to attenuate the motions if the wave excitation does not exist.
Coefficients C_{k_j} are restoring coefficients which represent the forces proportional to the body displacement due to the oscillatory motions in the steady but non-uniform flow.

The numerical computation is rather complicated for such terms associated with the steady flow field $\bar{V}$ in Eq. (4.4), because it includes the spatial derivatives of radiation potentials ψ_j. This term can be transformed by Tuck's theorem (Ogilvie and Tuck 1969) as

$$\int_{S_H}(\bar{V}\cdot\nabla)\psi_j n_k ds = -\int_{S_H}\psi_j m_k ds \qquad (4.6)$$

This transformation makes direct pressure integration over the body boundary contour much more easier. As for the m_k vector contribution, introduced in Eq. (2.22), it will be detailedly discussed in Chapter Five.

Compared with those terms on the right hand side of the body boundary condition in Eq. (2.24), the radiation potential ψ_j can be divided into two parts as

$$\psi_j(x,y) = \varphi_j(x,y) + \frac{U}{i\omega}\hat{\varphi}_j(x,y) \qquad (4.7)$$

where :

The radiation potentials φ_j and $\hat{\varphi}_j$ must satisfy following conditions on the body surface as

$$\frac{\partial\varphi_j}{\partial n} = n_j \quad , \quad \frac{\partial\hat{\varphi}_j}{\partial n} = m_j \qquad (4.8)$$

By substituting Eqs. (4.6) and (4.7) into Eq. (4.4), the detail expressions for added mass and damping coefficients are systematically written as follows.

$$A_{kj} = -\rho\int_{S_H}\varphi_{jc} n_k\, ds - \rho\frac{U}{\omega}\int_{S_H}\left[\hat{\varphi}_{js} n_k - \varphi_{js} m_k\right]ds$$
$$-\rho\left(\frac{U}{\omega}\right)^2\int_{S_H}\hat{\varphi}_{jc}\, m_k\, ds \qquad (4.9)$$

and

$$B_{kj} = \rho\omega\int_{S_H}\varphi_{js}\, n_k\, ds - \rho\omega\frac{U}{\omega}\int_{S_H}\left[\hat{\varphi}_{jc} n_k - \varphi_{jc} m_k\right]ds$$
$$+\rho\omega\left(\frac{U}{\omega}\right)^2\int_{S_H}\hat{\varphi}_{js}\, m_k\, ds \qquad (4.10)$$

where :

Subscript 'c' and 's' denote the real and imaginary parts and

$$\varphi_j = \varphi_{jc} + i\varphi_{js} \quad , \quad \hat{\varphi}_j = \hat{\varphi}_{jc} + i\hat{\varphi}_{js} \tag{4.11}$$

Although there is no explicit forward speed effect in the first term of both Eqs. (4.9) and (4.10), they satisfy the free surface condition in Eq. (2.27) which includes the forward speed effect. On the other hand the forward speed effect associated with the m vector contribution is taken into consideration in the second and third terms.

Moreover damping coefficients B_{k_j} can also be calculated from the energy transported by the generated waves due to oscillatory motions of the body, because damping forces are relevant to the work done by the body motions to the fluid. The numerical check of damping coefficients can be performed by direct pressure integration on the body boundary contour and by consideration of the energy flux in the fluid domain to confirm the computational accuracy. The theoretical formulation of damping coefficients from the viewpoint of the energy transportation with propagating waves at far distance from the body will be detailedly derived in the following section.

4.3 Formulation of wave excitation forces

In the same way as hydrodynamic forces acting on the body moving into incident waves with its oscillatory motions suppressed, wave excitation forces are derived from the hydrodynamic pressure due to incident and diffraction wave potentials. The hydrodynamic pressure in Eq. (4.2) with the velocity potential ϕ replaced by incident and diffraction wave potentials $\varphi_I + \varphi_D$ is integrated over the body boundary contour directly. In this case the oscillatory motions of the body are suppressed and the second term in Eq. (4.2) due to the body displacement in the steady and non-uniform flow is not to be taken into account. These wave excitation forces acting on the body surface in j-direction are then written as

$$E_j e^{i\omega t} = \frac{\rho g A}{i\omega_0} e^{i\omega t} \int_{S_H} (i\omega + U\bar{V}\cdot\nabla)\{\varphi_I(x,y)+\varphi_D(x,y)\} n_j \, ds$$
$$= \rho g A \left(\frac{\omega}{\omega_0}\right) e^{i\omega t} \int_{S_H} \left[n_j - \frac{U}{i\omega} m_j\right] \{\varphi_I(x,y)+\varphi_D(x,y)\} ds \qquad (4.12)$$

where :

Based on Tuck's theorem (1969), the second line of Eq. (4.12) is written.

The diffraction problem can be obtained from the radiation problem once the Kochin function of the radiation problem can be obtained. This is possible with the well known Haskind-Newman relation.

The reverse flow radiation problem is considered when the body is translating into the negative x direction with identical magnitude of forward speed U and oscillating in a calm water simultaneously. The velocity potentials $\tilde{\psi}_j$ in the reverse flow radiation problem must satisfy the following body boundary condition as

$$\frac{\partial \tilde{\psi}_j}{\partial n} = n_j - \frac{U}{i\omega} m_j \qquad (4.13)$$

where :

Subscript j denotes the mode of motions in the same way as in original radiation potentials.

In compliance with the relation which is valid on the body surface, the following expression can be written by modified Eq. (4.12) as

$$E_j = \rho g A \left(\frac{\omega}{\omega_0}\right) \int_{S_H} (\varphi_I + \varphi_D) \frac{\partial \tilde{\psi}_j}{\partial n} ds \qquad (4.14)$$

According to the Green's theorem for the diffraction potential φ_D and the

reverse flow radiation potential $\tilde{\psi}_j$ in the fluid domain bounded by S_F, $S_{\pm\infty}$, S_H and S_B, and for the unique contribution from body control surface S_H, the mathematical relation is obtained as

$$\int_{S_H} \varphi_D \frac{\partial \tilde{\psi}_j}{\partial n} ds = \int_{S_H} \tilde{\psi}_j \frac{\partial \varphi_D}{\partial n} ds = -\int_{S_H} \tilde{\psi}_j \frac{\partial \varphi_I}{\partial n} ds \qquad (4.15)$$

The last expression of Eq. (4.15) is derived from the body boundary condition of Eq. (2.25).

By substituting Eq. (4.15) into Eq. (4.14), an alternative expression for wave excitation forces can be described as

$$\begin{aligned} E_j &= \rho g A \left(\frac{\omega}{\omega_0}\right) \int_{S_H} \left(\frac{\partial \tilde{\psi}_j}{\partial n} - \tilde{\psi}_j \frac{\partial}{\partial n}\right) \varphi_I \, ds \\ &= \rho g A \left(\frac{\omega}{\omega_0}\right) \tilde{H}_j^{\pm}(k) \end{aligned} \qquad (4.16)$$

where :

$\tilde{H}_j^{\pm}(k)$ denotes the Kochin function for reverse flow radiation waves mentioned in Eq. (2.43) before. It should be noted that wave excitation forces are only in terms of the solutions of the reverse flow radiation problem and the incident waves as written above. This is a theoretical extension of the Haskind-Newman relation (Newman 1965) for the non-zero forward speed case. The check of such wave excitation forces by direct pressure integration over the body boundary contour and by Haskind-Newman relation is certainly another way to investigate the accuracy of numerical computations.

If the body form is symmetrical with respect to the y axis, the Kochin function of the reverse flow radiation problem can be derived from that of the original radiation problem by the relation

$$\tilde{H}_j^{\pm}(k) = (-1)^j H_j^{\pm}(k) \qquad (4.17)$$

4.4 Formulation of free oscillatory motion of the body in waves

In general when the body is translating under the free surface in incident waves with a constant forward speed or is constrained so that it keeps the mean position in waves and current, it should oscillate freely under the effects of wave excitation forces and other hydrodynamic forces associated with its motions. Based on such basic assumptions of small magnitude of body motions and incident waves, all these effects can be superposed linearly.

Assuming that the density is the same as that of the fluid, the following simultaneous linear equations are applied to describe the coupled motions of surge, heave and pitch modes with restoring forces induced by the forward speed effect. Here the dynamic equation of motions for the k modes is briefly indicated as

$$\sum_{j=1}^{3}\left[-\omega^2\left(M\delta_{k_j} + A_{k_j}\right) + i\omega B_{k_j} + C_{k_j}\right]\xi_j = E_k$$
$$(k = 1, 2, 3) \qquad (4.18)$$

where :

$$A_{kj} = 2\pi\rho a^2 A'_{kj} \qquad (4.19a)$$

$$B_{kj} = 2\pi\rho a^2 \omega B'_{kj} \qquad (4.19b)$$

$$C_{kj} = \rho U^2 C'_{kj} = 2\pi\rho a^2\omega^2\left[\left(\frac{1}{2\pi}\right)\left(\frac{U}{\omega a}\right)^2\right]C'_{kj} \qquad (4.19c)$$

$$E_k = 2\rho g A a E'_k = 2\pi\rho a^2\omega^2\left[\left(\frac{A}{\pi}\right)\left(\frac{g}{\omega^2 a}\right)\right]E'_k$$
$$\equiv 2\pi\rho a^2\omega^2\left(\frac{A}{\pi k}\right)E'_k \qquad (4.19d)$$

where :

M denotes the mass per unit length of the body.
δ_{k_j} is Kronecker's delta.

The dynamic equation of motions is then written as

$$\sum_{j=1}^{3}\left\{\left[-\left(\delta_{kj}+A'_{kj}\right)+C'_{kj}\left(\frac{1}{2\pi}\right)\left(\frac{U}{\omega a}\right)^2\right]+iB'_{kj}\right\}\left(\frac{\xi_j}{A}\right)=\left(\frac{E'_k}{\pi k}\right) \qquad (4.20)$$

Here the problem is considered for the case when the body is submerged completely. This means that the hydrostatic restoring force induced by buoyancy variations of the submerged body does not exist. However the coefficients C_{k_j} generated from the oscillatory motion of the body in the non-uniform flow induce the same effect as restoring forces in general. This effect induces natural frequencies of the motions even for the submerged body when the sum of these terms associated with mass, added mass and restoring forces of motion equations becomes zero and it might be classified as the eigen value problem. Therefore in case the frequency of the wave excitation force approaches the natural frequency of the body motion, it will induce the large magnitude of the motion due to resonance.

4.5 Formulation of damping forces in term of the radiation potential at infinity

The waves are generated by oscillatory motions of the body and transport energy outward. The damping coefficient for each mode of body motion predicted by direct pressure integration over body boundary contours can be also evaluated from the energy flux consideration.

If the flow field is described by the velocity potential Φ associated with the steady flow as mentioned in Eq. (2.2), the average energy flux over a period across a vertical plane at x location can then be described as

$$R_x = -\rho\overline{\int_{\eta_\omega}^{\infty} \frac{\partial \Phi}{\partial t}\frac{\partial \Phi}{\partial x}dy} \qquad (4.21)$$

where :

The overbar notation implies the integral to be averaged over a period.

η_ω is the wave depression associated with the steady as well as the unsteady parts.

If the effect of the steady flow φ_s in Eq. (2.2) is assumed to be of the same order of magnitude as the unsteady part ϕ and the second order terms including ϕ in Eq. (4.21) are also retained, the mean value of the energy flux R_x is written as

$$\begin{aligned} R_x &= \rho U\overline{\int_{\zeta_\omega}^{0} \frac{\partial \phi_u}{\partial t}dy} - \rho\overline{\int_0^{\infty} \frac{\partial \phi_u}{\partial t}\frac{\partial \phi_u}{\partial x}dy} \\ &= -\rho\frac{U}{g}\overline{\frac{\partial \phi_u}{\partial t}\left(\frac{\partial \phi_u}{\partial t} - U\frac{\partial \phi_u}{\partial x}\right)_{y=0}} - \rho\overline{\int_0^{\infty} \frac{\partial \phi_u}{\partial t}\frac{\partial \phi_u}{\partial x}dy} \end{aligned} \qquad (4.22)$$

where :

ϕ_u denotes the unsteady part of the velocity potential $\mathrm{Re}\left(\phi e^{i\omega t}\right)$ in Eq. (2.2).

The following expression for the unsteady part of the wave depression ζ_ω is applied to transform the first line of Eq. (4.22) as

$$\zeta_\omega = \frac{1}{g}\left(\frac{\partial \phi_u}{\partial t} - U\frac{\partial \phi_u}{\partial x}\right)_{y=0} \qquad (4.23)$$

If A and B are two complex quantities, the following relation can be written as

$$\overline{\mathrm{Re}\left[Ae^{i\omega t}\right]\mathrm{Re}\left[Be^{i\omega t}\right]} = \frac{1}{2}\mathrm{Re}\left(AB^*\right) \qquad (4.24)$$

where :

The asterisk '*' denotes the complex conjugate.

With the contribution of this mathematical relation, the energy flux of Eq. (4.22) can be written in terms of ϕ as

$$R_x = \frac{\rho}{2}(\vartheta_1 + \vartheta_2) \tag{4.25}$$

where :

$$\vartheta_1 = \frac{U}{g}\mathrm{Re}\left\{\omega^2 \phi\phi^* - i\omega U\phi\frac{\partial\phi^*}{\partial x}\right\}_{y=0} \tag{4.26}$$

$$\vartheta_2 = \mathrm{Re}\left\{i\omega\int_0^{\infty}\phi\frac{\partial\phi^*}{\partial x}dy\right\} \tag{4.27}$$

Since damping coefficients will be discussed further, the velocity potential ϕ is restricted to the radiation potential ψ_j of the j-mode motion. The four wave systems of the radiation potential ψ_j corresponding to wave numbers k_1, k_2, k_3 and k_4 described in Chapter Two are expressed as

$$\psi_j \approx \mathrm{Re}\left\{\frac{-ga_2 e^{-i\delta_2}}{(\omega + k_2 U)}e^{-k_2 y - ik_2 x}e^{i\omega t}\right\} \quad \text{as} \quad x \to +\infty \tag{4.28}$$

$$\begin{aligned}\psi_j \approx\ & \mathrm{Re}\left\{\frac{-ga_1 e^{-i\delta_1}}{(\omega + k_1 U)}e^{-k_1 y - ik_1 x}e^{i\omega t}\right\} + \mathrm{Re}\left\{\frac{ga_3 e^{-i\delta_3}}{(\omega - k_3 U)}e^{-k_3 y + ik_3 x}e^{i\omega t}\right\} \\ & + \mathrm{Re}\left\{\frac{-ga_4 e^{i\delta_4}}{(\omega - k_4 U)}e^{-k_4 y + ik_4 x}e^{i\omega t}\right\} \quad \text{as} \quad x \to -\infty\end{aligned} \tag{4.29}$$

where :

Coefficients a_j and δ_j (j = 1, 2, 3, 4) are the amplitude and the phase angle difference.

All the equations for instance Eqs. (4.28) and (4.29) are for τ smaller than 0.25. Nevertheless by setting a_1 and a_2 equal to zero, the results can be obtained even when τ is larger than 0.25 and the k_1- and k_2- wave systems do not exist.

For the far upstream case, the k_2-wave described in Eq. (4.28) is substituted into the velocity potential ϕ of Eqs. (4.26) and (4.27) and the energy flux is expressed as

$$R_\infty = \left(\frac{\rho g a_2^2 \omega}{4k_2} \frac{\omega - k_2 U}{\omega + k_2 U} \right) \tag{4.30}$$

where :

$$(\omega + k_2 U) = \sqrt{g k_2} \tag{4.30a}$$

For the far downstream case, the velocity potential ϕ of Eqs. (4.26) and (4.27) can be also replaced with the summation of the k_1, k_3 and k_4 wave systems. By mathematical manipulation, the expression of ϑ_1 and ϑ_2 for the energy flux in Eq. (4.25) can be derived as follows.

$$\begin{aligned}
\vartheta_1 = \frac{U}{g}\omega^2 \Bigg[& \frac{g^2 a_1^2}{(\omega + k_1 U)^2} + \frac{g^2 a_3^2}{(\omega - k_3 U)^2} + \frac{g^2 a_4^2}{(\omega - k_4 U)^2} \\
& -2 \frac{g^2 a_1 a_3}{(\omega + k_1 U)(\omega - k_3 U)} \cos\{(k_1 + k_3)x + \delta_1 + \delta_3\} \\
& +2 \frac{g^2 a_1 a_4}{(\omega + k_1 U)(\omega - k_4 U)} \cos\{(k_1 + k_4)x + \delta_1 + \delta_4\} \\
& -2 \frac{g^2 a_3 a_4}{(\omega - k_3 U)(\omega - k_4 U)} \cos\{(k_3 - k_4)x + \delta_3 - \delta_4\} \Bigg] \\
& + \frac{U}{g}\omega U \Bigg[k_1 \frac{g^2 a_1^2}{(\omega + k_1 U)^2} - k_3 \frac{g^2 a_3^2}{(\omega - k_3 U)^2} - k_4 \frac{g^2 a_4^2}{(\omega - k_4 U)^2} \\
& -(k_1 - k_3) \frac{g^2 a_1 a_3}{(\omega + k_1 U)(\omega - k_3 U)} \cos\{(k_1 + k_3)x + \delta_1 + \delta_3\} \\
& +(k_1 - k_4) \frac{g^2 a_1 a_4}{(\omega + k_1 U)(\omega - k_4 U)} \cos\{(k_1 + k_4)x + \delta_1 + \delta_4\}
\end{aligned}$$

$$+(k_3+k_4)\frac{g^2a_3a_4}{(\omega-k_3U)(\omega-k_4U)}\cos\{(k_3-k_4)x+\delta_3-\delta_4\}\Bigg] \tag{4.31}$$

and

$$\begin{aligned}\vartheta_2=-\omega\Bigg[&\frac{1}{2}\frac{g^2a_1^2}{(\omega+k_1U)^2}-\frac{1}{2}\frac{g^2a_3^2}{(\omega-k_3U)^2}-\frac{1}{2}\frac{g^2a_4^2}{(\omega-k_4U)^2}\\&-\frac{k_1-k_3}{k_1+k_3}\frac{g^2a_1a_3}{(\omega+k_1U)(\omega-k_3U)}\cos\{(k_1+k_3)x+\delta_1+\delta_3\}\\&+\frac{k_1-k_4}{k_1+k_4}\frac{g^2a_1a_4}{(\omega+k_1U)(\omega-k_4U)}\cos\{(k_1+k_4)x+\delta_1+\delta_4\}\\&+\frac{g^2a_3a_4}{(\omega-k_3U)(\omega-k_4U)}\cos\{(k_3-k_4)x+\delta_3-\delta_4\}\Bigg]\end{aligned} \tag{4.32}$$

Although these expressions look rather complicated, the mathematical simplification can be achieved in compliance with such relations that the summation of cross terms of two different wave systems in Eqs. (4.31) and (4.32) should be zero. The detail expressions are as follows.

Firstly some coefficients A, B and C are defined systematically as

$$A=\frac{U}{g}\{-2\omega-U(k_1-k_3)\}+\frac{k_1-k_3}{k_1+k_3} \tag{4.33}$$

$$B=\frac{U}{g}\{+2\omega+U(k_1-k_4)\}+\frac{k_1-k_4}{k_1+k_4} \tag{4.34}$$

$$C=\frac{U}{g}\{-2\omega+U(k_3+k_4)\}-1 \tag{4.35}$$

For example the coefficient A in Eq. (4.33) can be extended further into

$$A=\frac{1}{g(k_1+k_3)}\{k_1(g-2U\omega-k_1U^2)-k_3(g+2U\omega-k_3U^2)\} \tag{4.36}$$

According to the definition described in Eq. (2.37), following relations can be obtained as

$$k^2 + \frac{2k\omega}{U} - \frac{kg}{U^2} = -\frac{\omega^2}{U^2} \quad \text{for} \quad (k_1, k_2) \tag{4.37}$$

$$k^2 - \frac{2k\omega}{U} - \frac{kg}{U^2} = -\frac{\omega^2}{U^2} \quad \text{for} \quad (k_3, k_4) \tag{4.38}$$

Therefore the wave number-frequency relations can be easily obtained as follows.

$$k_1\{g - 2U\omega - k_1U^2\} = \omega^2 \tag{4.39}$$

$$k_3\{g + 2U\omega - k_3U^2\} = \omega^2 \tag{4.40}$$

Based on the relations described above, the coefficient A becomes zero and the coefficient B is also zero in the same manner.

For the case of the coefficient C, the relations can be derived by using the definitions of k_3 and k_4 as

$$k_3 + k_4 = K_0(1 + 2\tau) = \frac{g}{U^2} + \frac{2\omega}{U} \tag{4.41}$$

Thus coefficient C becomes zero too.

Finally the energy flux in Eq. (4.25) for the far downstream case can be much simplified as

$$\begin{aligned} R_{--} &= \frac{\rho g a_1^2 \omega}{4k_1} \frac{\omega - k_1U}{\omega + k_1U} - \frac{\rho g a_3^2 \omega}{4k_3} \frac{\omega + k_3U}{\omega - k_3U} - \frac{\rho g a_4^2 \omega}{4k_4} \frac{\omega + k_4U}{\omega - k_4U} \\ &= -\frac{\rho g a_1^2 \omega}{4k_1}\sqrt{1 - 4\tau} + \frac{\rho g a_3^2 \omega}{4k_3}\sqrt{1 + 4\tau} - \frac{\rho g a_4^2 \omega}{4k_4}\sqrt{1 + 4\tau} \end{aligned} \tag{4.42}$$

where :

The second line is derived according to the following relations

$$\frac{\omega - k_j U}{\omega + k_j U} = \mp\sqrt{1-4\tau} \quad \text{for} \quad j = \begin{pmatrix} 1 \\ 2 \end{pmatrix} \tag{4.43}$$

$$\frac{\omega + k_j U}{\omega - k_j U} = \mp\sqrt{1+4\tau} \quad \text{for} \quad j = \begin{pmatrix} 3 \\ 4 \end{pmatrix} \tag{4.44}$$

In fact, the components, associated with its acceleration and displacement, of hydrodynamic forces acting on the body oscillating and translating with a constant forward speed under a calm water do not work against the fluid if averaged values are taken over a period. The work done by the damping force over a period in the j-mode motion associated with the unit velocity potential corresponding to radiation potentials ψ_j is indicated as

$$W = \frac{1}{2} B_{jj} \tag{4.45}$$

where :

B_{jj} is the damping coefficient defined in Eq. (4.4) before.

The work done is equal to the outward energy flux and is expressed as

$$W = R_{+\infty} - R_{-\infty} \tag{4.46}$$

Combining both Eqs. (4.45) and (4.46), the relationship between damping coefficients B_{jj} and amplitudes a_1, a_2, a_3 and a_4 of the wave systems travelling away from the submerged body is described as

$$B_{jj} = \frac{\rho g \omega}{2}\left[\left(\frac{a_1^2}{k_1} + \frac{a_2^2}{k_2}\right)\sqrt{1-4\tau} + \left(-\frac{a_3^2}{k_3} + \frac{a_4^2}{k_4}\right)\sqrt{1+4\tau}\right] \tag{4.47}$$

In terms of the Kochin functions of radiation potentials ψ_j, the equation for the damping coefficient described above can be derived in an alternative form as

$$B_{jj} = \frac{1}{2}\rho\omega\left[\frac{\left|H_j^+(k_1)\right|^2 + \left|H_j^+(k_2)\right|^2}{\sqrt{1-4\tau}} + \frac{-\left|H_j^-(k_3)\right|^2 + \left|H_j^-(k_4)\right|^2}{\sqrt{1+4\tau}}\right] \quad (4.48)$$

4.6 Investigation of numerical computations

Here the numerical accuracy of the first order hydrodynamic forces by newly modified approaches (the discrete source distribution method and the direct Green function method) is achieved by analytically solving the logarithmic part of the Green function. For the case of two rigidly held apart cylinders as in Fig. 4.1, the detail numerical scheme to solve the integral equation and the analytical solution of the logarithmic part of the Green function will be described in Chapter Eight.

By obtaining numerical solutions for the velocity potential ϕ, the damping coefficient of the j-mode motion is calculated by direct pressure integration over the wetted surface of the body and from the energy flux consideration in the fluid domain. The damping coefficient by direct pressure integration is written as $B_{jj}(P)$ and the one by energy flux consideration is written as $B_{jj}(E)$. If the discrepancy between $B_{jj}(P)$ and $B_{jj}(E)$ is smaller, the body boundary condition is satisfied. The accuracy check of wave excitation forces is investigated by direct pressure integration over body boundary contours and by Haskind-Newman relation in terms of the Kochin function of the radiation problem.

Based on direct Green function approach, these computations are performed on the VAXstation 4000 VLC computer system. The numerical calculations on two rigidly held apart cylinder system with submergence depth ratio d/a = 2.0, separation distance ratio c/a = 4.0, Froude number Fn = 0.20 and no inclination in following waves is carried out by taking the dipole images as ten ($N_I = 10$) and the discretized elements of the left and right cylinders as fifty ($N_E = N_L = N_R = 50$).

The numerical accuracy of surge, heave and pitch damping coefficients by direct pressure integration and by energy flux consideration is investigated and the computed results are in excellent agreement as shown in Figs. 4.2 to 4.4.

Numerical investigations of wave excitation forces in terms of the Kochin functions with real and imaginary parts on twin hulled structure model under the combined actions of wave and current in surge, heave and pitch modes by the pressure integration and the Haskind-Newman relation are performed and all calculated results are in excellent agreement as shown in Figs. 4.5 to 4.10.

4.7 Parametric studies and discussions

Here parametric studies for different Froude numbers, submerged depths, separation distances and inclinations to predict radiation forces such as added mass and damping coefficients, wave excitation forces and dynamic motion responses of the twin hulled offshore structure in incident waves are carried out. The detail calculated results are categorized into four parts as follows.

(A) For different Froude numbers :

The effect of Froude number (equivalent current speed) on the predicted results of added mass and damping coefficients, wave excitation forces and motion responses of the structure are as presented in Figs. 4.11 to 4.22.

For non-dimensionalized added mass coefficients as in Figs. 4.11, 4.12 and 4.13 respectively, the discrepancy of the predicted results between Fn = 0.0 and 0.4 is larger in the very low frequency range (within Ka = 0.2 range). As noticed, the effect of forward speed is greater for the low frequency range of wave numbers. Just as in the single cylinder case, the added mass coefficient with forward speed effect (m-vector contribution) becomes infinitely large as the frequency approaches zero which is due to the second and third terms of Eq. (4.9). Negative added mass coefficients do occur at certain frequencies for the case of

surface piercing and oscillating cylinders (Ohkusu 1969).

For non-dimensionalized damping coefficients, the numerical results in surge, heave and pitch motions are presented in Figs. 4.14, 4.15 and 4.16 respectively. Effect of forward speed is clearly noticed at high Froude numbers.

For non-dimensionalized wave excitation forces as in Figs. 4.17 to 4.19, computed surge, heave and pitch results in following waves show considerable variation for the higher frequency range. The non-dimensionalized dynamic response amplitudes in surge, heave and pitch motions are presented in Figs. 4.20 to 4.22 and large discrepancies for surge and heave motions are noticed in the very low frequency range and this could be due to large added mass contribution from higher speed.

(B) For different submergence depths :

The effect of submergence depths on theoretical predictions of added mass and damping coefficients, wave excitation forces and dynamic motion responses of the twin hulled structure model are as in Figs. 4.23 to 4.34.

For non-dimensionalized added mass coefficients as in Figs. 4.23 to 4.25, predicted results show not much variation over the frequency range and it may be concluded that the submergence depth has no significant effect on added mass coefficients.

For non-dimensionalized damping coefficients, numerical results in surge, heave and pitch motions are presented in Figs. 4.26, 4.27 and 4.28. This indicates that submergence depth has considerable influence.

For non-dimensionalized wave excitation forces as in Figs. 4.29, 4.30 and 4.31, computed results of surge, heave and pitch modes in following waves have clear difference. The non-dimensionalized response amplitudes in surge, heave and

pitch motions are as in Figs. 4.32 to 4.34 and the discrepancies are due to large contribution from the wave excitation forces.

(C) For different separation distances :

The effect of separation distances on the theoretical calculations of added mass, damping coefficients, wave excitation forces and dynamic motion responses of twin hulled structure model are as in Figs. 4.35 to 4.46.

For non-dimensionalized added mass coefficients as in Figs. 4.35 to 4.37, predicted results show not much variation over the selected range of frequencies. In the case of non-dimensionalized damping coefficients, calculated results in surge, heave and pitch modes are in Figs. 4.38 to 4.40. The peak values appear in the lower range of frequencies and it may be concluded that separation effect is considerable.

For non-dimensionalized wave excitation forces as in Figs. 4.41 to 4.43, computed results for surge, heave and pitch modes in following waves show same tendencies as the damping coefficients. The non-dimensionalized response amplitudes in surge, heave and pitch motions are shown in Figs. 4.44 to 4.46 and the characteristics for surge, heave and pitch motions are similar to those of wave excitation forces and it can be concluded that the contribution from wave excitation forces is clearly effective.

(D) For different inclinations :

For the inclination effect, the numerical predictions of added mass, damping coefficients, wave excitation forces and dynamic motion responses of twin hulled structure model are as in Figs. 4.47 to. 4.58.

For non-dimensionalized added mass coefficients as in Figs. 4.47 to 4.49, predicted results make not much variation over the frequency range and it may be

concluded that small inclination effect is not of importance on the hydrodynamic characteristics of submerged geometries.

For non-dimensionalized damping coefficients, numerical results in surge, heave and pitch motions are as in Figs. 4.50 to 4.52. The predicted results show that large inclination always contribute a certain amount but not significant. Hence it can be concluded that the inclination effect is not dominant on damping coefficients.

For non-dimensionalized wave excitation forces as in Figs. 4.53 to 4.55, numerical predictions for surge, heave and pitch modes in following waves have clear discrepancies. In fact, wave excitation forces are slightly increased as the body is inclined. Non-dimensionalized response amplitudes in surge, heave and pitch motions are also presented in Figs. 4.56 to 4.58 and the tendencies in surge, heave and pitch motions are similar to those of wave excitation forces.

4.8 Conclusion

Here a valuable procedure for theoretical confirmation of numerical computations is developed and completely described. The numerical accuracy check of the damping coefficients is calculated by the consideration of the energy flux in the fluid domain and by the direct pressure integration over body boundary contours. The numerical results of wave excitation forces in terms of the Kochin functions in radiation problem with real and imaginary parts is checked out by the Haskind-Newman relation and by the direct pressure integration.

CHAPTER 5
THEORETICAL DERIVATION OF M-VECTOR CONTRIBUTIONS

5.1 Solutions of unsteady potentials for the single cylinder case

In order to solve the boundary value problem for the velocity potential ϕ over body boundary contours, the integral equation of Eq. (2.31) is made use of.

$$\frac{1}{2}\phi(P) = -\int_{S_H}\left[\frac{\partial\phi(Q)}{\partial n} - \phi(Q)\frac{\partial}{\partial n}\right]G(P,Q)ds \qquad (5.1)$$

where S_H denotes the boundary contour of the cylinder as shown in Fig. 2.1 and $G(P,Q)$ is the Green function as shown in Eq. (2.32), which should satisfy the free surface condition, the bottom condition and the radiation condition. Since the normal derivative of the velocity potential $\frac{\partial\phi}{\partial n}$ on the right hand side of Eq. (5.1) is already described on the body surface as in Eqs. (2.24) and (2.25), Eq. (5.1) is an integral equation for the unknown velocity potential ϕ on the body surface of the cylinder.

For the case of the non-zero forward speed radiation potential, the evaluation of the m-vector contribution defined in Eq. (2.22) is required to obtain the normal derivative of the velocity potential $\frac{\partial\phi}{\partial n}$ on the body surface.

5.2 Analytical derivation of m-vector contributions for the single elliptical cylinder case

Since the principal interest is concentrated on the submerged body case at this moment, it is natural to assume that the steady velocity potential φ_S in the vicinity

of the body is approximated by the velocity potential without the free surface. It is certainly possible to apply the steady velocity potential which already satisfies the linearized free surface condition even if it is rather complicated to calculate the m-vector contribution. However it is known that the steady velocity potential satisfying the linearized free surface condition does not necessarily have accurate solutions for the steady flow around the moving body. The mathematical derivation of the m-vector contribution based on this assumption for the case of an elliptical submerged cylinder is described as follows.

The elliptical coordinate (μ,ν) is introduced as shown in Fig. 5.1, which is related to another coordinate (θ,ξ), and rectilinear coordinate (x,y) with the origin at the centre of the ellipse as

$$x = \kappa\cos\theta\cosh\xi = \kappa\mu\nu \tag{5.2}$$

$$y = \kappa\sin\theta\sinh\xi = \kappa\sqrt{1-\mu^2}\sqrt{\nu^2-1} \tag{5.3}$$

where :

$$\kappa = a\sqrt{1-\varepsilon^2} \quad , \quad \varepsilon = \frac{b}{a} \tag{5.4}$$

and ' 2a ' is the major axis length and ' 2b ' the minor axis length of the ellipse.

The velocity potential for the steady translation of an elliptical cylinder in an unbounded fluid domain is already expressed in Lamb (1879) as

$$\varphi_s = -\overline{A}e^{-\xi}\cos\theta = -\overline{A}\mu\left(\nu-\sqrt{\nu^2-1}\right) \tag{5.5}$$

where :

$$\overline{A} = a\varepsilon\sqrt{\frac{1+\varepsilon}{1-\varepsilon}} \tag{5.6}$$

With these formulae on the coordinate transformation in terms of the generalized orthogonal coordinate, the derivatives of the velocity potential with respect to both x and y coordinates is derived as

$$\frac{\partial \varphi_s}{\partial x} = \frac{1}{h_1^2}\frac{\partial x}{\partial \mu}\frac{\partial \varphi_s}{\partial \mu} + \frac{1}{h_2^2}\frac{\partial x}{\partial \nu}\frac{\partial \varphi_s}{\partial \nu} = \frac{\overline{A}}{\kappa}\left[-1 + \frac{\nu\sqrt{\nu^2-1}}{\nu^2-\mu^2}\right] \qquad (5.7)$$

$$\frac{\partial \varphi_s}{\partial y} = \frac{1}{h_1^2}\frac{\partial y}{\partial \mu}\frac{\partial \varphi_s}{\partial \mu} + \frac{1}{h_2^2}\frac{\partial y}{\partial \nu}\frac{\partial \varphi_s}{\partial \nu} = \frac{\overline{A}}{\kappa}\left[\frac{\mu\sqrt{1-\mu^2}}{\nu^2-\mu^2}\right] \qquad (5.8)$$

where :

$$h_1 = \kappa\sqrt{\frac{\nu^2-\mu^2}{1-\mu^2}} \quad , \quad h_2 = \kappa\sqrt{\frac{\nu^2-\mu^2}{\nu^2-1}} \qquad (5.9)$$

By substituting these results in the definition of the m-vector contribution, as Eq. (2.22), the theoretical expressions of m_1 and m_2 vector are written as

$$\begin{aligned} m_1 &= -\frac{\partial}{\partial n}\left(\frac{\partial \varphi_s}{\partial x}\right) = -\frac{1}{h_2}\frac{\partial}{\partial \nu}\left(\frac{\partial \varphi_s}{\partial x}\right) \\ &= \frac{\overline{A}}{\kappa^2\left(\nu^2-\mu^2\right)^{3/2}}\left\{1 - 2\nu^2\frac{1-\mu^2}{\nu^2-\mu^2}\right\}_{\text{on body}} \end{aligned} \qquad (5.10)$$

$$\begin{aligned} m_2 &= -\frac{\partial}{\partial n}\left(\frac{\partial \varphi_s}{\partial y}\right) = -\frac{1}{h_2}\frac{\partial}{\partial \nu}\left(\frac{\partial \varphi_s}{\partial y}\right) \\ &= \frac{\overline{A}}{\kappa^2\left(\nu^2-\mu^2\right)^{5/2}}\left\{2\mu\nu\sqrt{1-\mu^2}\sqrt{\nu^2-1}\right\}_{\text{on body}} \end{aligned} \qquad (5.11)$$

Here the expressions are all in terms of the coordinates (μ, ν).

By using the body surface equation of

$$\nu = \frac{1}{\sqrt{1-\varepsilon^2}} \qquad (5.12)$$

By substituting Eqs. (5.7) and (5.8), final results are written as

$$m_1 = \frac{1}{a}\varepsilon(1+\varepsilon)\frac{\varepsilon^2\cos^2\theta - \sin^2\theta}{\left(\sin^2\theta + \varepsilon^2\cos^2\theta\right)^{5/2}} \tag{5.13}$$

$$m_2 = \frac{1}{a}\varepsilon^2(1+\varepsilon)\frac{\sin 2\theta}{\left(\sin^2\theta + \varepsilon^2\cos^2\theta\right)^{5/2}} \tag{5.14}$$

With these results, the derivatives of the steady velocity potential φ_s on the body surface of the cylinder is written as

$$\frac{\partial\varphi_s}{\partial x} = \varepsilon\left(\varepsilon\cos^2\theta - \sin^2\theta\right)/\Delta^2 \tag{5.15}$$

$$\frac{\partial\varphi_s}{\partial y} = \varepsilon(1+\varepsilon)\sin\theta\cos\theta/\Delta^2 \tag{5.16}$$

where:

$$\Delta = \left(\sin^2\theta + \varepsilon^2\cos^2\theta\right)^{1/2} \tag{5.17}$$

The components of the n-vector contribution are written in terms of the elliptical coordinates as

$$n_1 = \frac{1}{h_2}\frac{\partial x}{\partial v} = \varepsilon\cos\theta/\Delta \tag{5.18}$$

$$n_2 = \frac{1}{h_2}\frac{\partial y}{\partial v} = \sin\theta/\Delta \tag{5.19}$$

$$n_3 = xn_2 - yn_1 = a\left(1-\varepsilon^2\right)\sin\theta\cos\theta/\Delta \tag{5.20}$$

When n_1 and n_2, m_1 and m_2 are substituted into the definition of the m_3 vector contribution, as Eq. (2.22), the expression of m_3 vector is written as

$$m_3 = xm_2 - ym_1 + \left(-1 + \frac{\partial \varphi_s}{\partial x}\right) n_2 - \frac{\partial \varphi_s}{\partial y} n_1$$
$$= (1-\varepsilon)(1+\varepsilon)^2 \sin\theta \left\{ \frac{\cos^2\theta}{\Delta^3} + \frac{\varepsilon^2 \cos^2\theta - \sin^2\theta}{\Delta^5} \right\} \qquad (5.21)$$

By setting $\varepsilon = 1$ in Eqs. (5.10) and (5.14), the mathematical expressions of the m-vector contribution for a circular cylinder of radius a can be readily obtained as

$$m_1 = \frac{2}{a} \cos 2\theta \qquad (5.22)$$

$$m_2 = \frac{2}{a} \sin 2\theta \qquad (5.23)$$

$$m_3 = 0 \qquad (5.24)$$

It is natural that there is no contribution to the m-vector when the circular cylinder undergoes pitching motions. Even after rotation (pitching motions) around the centre of the cross sectional circle, the normal velocity induced at a location on the cylinder surface by the steady flow is not different from that before the rotation.

5.3 Solutions of unsteady potentials for the twin cylinders case

The submerged two rigidly held apart cylinders without further modelling, advancing with a constant speed U in incident waves and performing sinusoidal oscillations of small amplitudes in surge, heave and pitch at a particular frequency ω about its mean position, is as in Fig. 4.1. This configuration can be realized as a simplified model of the typical form of offshore structures like twin hulled drilling rigs. The predictions of hydrodynamic loadings acting on twin hulled offshore structures under combined actions of wave and current, or moving in two combined modes of slow and fast frequency are always important from the point of view of operational safety in severe environmental conditions.

The midpoint of the line connecting the centres of the two cylinders is at submergence depth " d " under the free surface, " l " is half the distance between the centres of the two cylinders, " a " and " b " are the radii of downstream and upstream cylinders respectively. Symbols S_L and S_R denote the surface of downstream and upstream cylinders. Hereafter the downstream cylinder is called as " cylinder L " and the upstream cylinder as " cylinder R " for convenience.

The formulation of the boundary value problem for the unsteady potential ϕ is not different from what is described in Chapter Two. The integral equation for velocity potential ϕ over body boundary contours of the two cylinder case is written as

$$\frac{1}{2}\phi(P)-\left[\int_{S_L}+\int_{S_R}\right]\phi(Q)\frac{\partial}{\partial n}G(P,Q)ds$$
$$=-\left[\int_{S_L}+\int_{S_R}\right]\frac{\partial\phi(Q)}{\partial n}G(P,Q)ds \qquad (5.25)$$

Here G(P,Q) is the Green function described in Eq. (2.32) and ϕ is the unsteady velocity potential to be obtained. The point P will vary over the body boundary contours of the two cylinder structure. As in the single cylinder case, the estimation of the m-vector contribution is required to describe the normal derivative of the velocity potential of $\frac{\partial\phi}{\partial n}$ on the body surface, with taking into account effects of forward speed and interactions between the two hulls.

5.4 Theoretical formulation of m-vector contributions for the twin cylinders case

The theoretical derivation of the m-vector contribution is detailedly formulated to take into account the interaction effect between the two circular cylinders submerged under a free surface. The mathematical approach can be extended to predict the interaction effect of twin hulled marine vehicles in head and following waves for different diameter ratios, submerged depths, Froude number, separation

distance and inclinations.

5.4.1 Description of the Milne-Thomson's circle theorem

As shown in Fig. 5.2, a doublet at (x, y) position is assumed and an inclining angle β with the x-axis is made. The velocity potential can then be formulated as

$$f(z) = -\frac{\mu}{z - ce^{i\alpha}} \quad , \quad \mu = |\mu| e^{i\beta} \tag{5.26}$$

and the expression can be rewritten as

$$\begin{aligned}
\overline{f\left(\frac{a^2}{\bar{z}}\right)} &= -\bar{\mu}\frac{1}{\frac{a^2}{z} - ce^{-i\alpha}} = -\bar{\mu}\frac{z}{a^2 - zce^{-i\alpha}} \\
&= \bar{\mu}\frac{1}{ce^{-i\alpha}}\frac{z - \frac{a^2}{c}e^{i\alpha} + \frac{a^2}{c}e^{i\alpha}}{z - \frac{a^2}{c}e^{i\alpha}} = \frac{\bar{\mu}}{ce^{-i\alpha}}\left\{1 + \frac{a^2}{c}e^{i\alpha}\frac{1}{z - \frac{a^2}{c}e^{i\alpha}}\right\} \\
&= -|\mu|\frac{a^2}{c^2}e^{i(2\alpha - \pi - \beta)}\frac{1}{z - \frac{a^2}{c}e^{i\alpha}} + \text{const.}
\end{aligned} \tag{5.27}$$

This means that the image is in α direction and at a distance $\frac{a^2}{c}$. The strength of the doublet is $\left(\frac{a}{c}\right)^2$ times and the direction is $(2\alpha - \pi - \beta)$. In fact, this concept of dipole image method to formulate the complex velocity potential can be applied to derive analytical expression of m-vector contributions for two rigidly connected cylinder case.

5.4.2 Analytical derivation of m-vector contributions for the twin cylinders case

The prediction of the m-vector contribution requires a solution for the steady potential φ_S. In order to avoid numerical difficulties, the infinite-fluid solution which is valid for the deeply submerged body is applied.

The two cylinders, composed of the left circular cylinder of radius a (referred to as cylinder L) and the right circular cylinder of radius b (cylinder R), with a separation distance between both cylinder centres c and an angle of inclination α. The two cylinders are assumed to move with a forward speed U in the x-direction as shown in Fig. 4.1. The steady velocity potential is then described as

$$\varphi_S = U\left(\varphi^L + \varphi^R\right) \tag{5.28}$$

Then the body boundary conditions to be satisfied by φ^L and φ^R are derived as follows.

$$\frac{\partial \varphi^L}{\partial r} = \cos\theta \quad , \quad \frac{\partial \varphi^R}{\partial r} = 0 \qquad \text{on cylinder L} \tag{5.29}$$

$$\frac{\partial \varphi^R}{\partial r'} = \cos\theta' \quad , \quad \frac{\partial \varphi^L}{\partial r'} = 0 \qquad \text{on cylinder R} \tag{5.30}$$

Physically φ^L describes the velocity potential, in which only cylinder L moves with cylinder R at rest. Similarly φ^R is also for the velocity potential where only cylinder R moves with cylinder L at rest.

At first the velocity potential φ^L for cylinder L is considered. If cylinder R is not present, the flow past cylinder L is represented by a point doublet located at the origin and if the strength is assumed as μ_0. Then

$$\varphi_0{}^L = -\mu_0 \frac{\cos\theta}{r} \quad , \quad c_0 = 0 \quad , \quad \mu_0 = a^2 \quad , \quad \beta_0 = 0 \tag{5.31}$$

The change caused by the existence of restrained cylinder R is represented by image doublet at the ' mirror-image ' point inside cylinder R. Milne-Thomson's circle theorem is then applied as follows.

$$f(z) = -\tilde{\mu}\frac{1}{z - ce^{i(\alpha-\pi)}} \tag{5.32}$$

$$\overline{f\left(\frac{b^2}{\bar{z}}\right)} = -\tilde{\mu}\left(\frac{b}{c}\right)^2 e^{i(2\alpha-\pi)}\frac{1}{z - \frac{b^2}{c}e^{i(\alpha-\pi)}} + \text{const.} \tag{5.32a}$$

If the image of the doublet with cylinder R, as observed from cylinder L, the mathematical expression is written as

$$c_1 = c - \frac{b^2}{c - c_0} \quad , \quad \frac{\mu_1}{\mu_0} = \left(\frac{b}{c - c_0}\right)^2 \quad , \quad \beta_1 = 2\alpha - \pi \tag{5.33}$$

and in turn the effect of the image doublet on cylinder L is taken into account by introducing the image doublet inside cylinder L. Now this image will form another image inside cylinder R and that is described as

$$c_2 = \frac{a^2}{c_1} \quad , \quad \frac{\mu_2}{\mu_1} = \left(\frac{a}{c_1}\right)^2 \quad , \quad \beta_2 = 0 \tag{5.34}$$

Similarly following expressions are systematically written as

$$c_3 = c - \frac{b^2}{c - c_2} \quad , \quad \frac{\mu_3}{\mu_2} = \left(\frac{b}{c - c_2}\right)^2 \quad , \quad \beta_3 = 2\alpha - \pi \tag{5.35}$$

$$c_4 = \frac{a^2}{c_3} \quad , \quad \frac{\mu_4}{\mu_3} = \left(\frac{a}{c_3}\right)^2 \quad , \quad \beta_4 = 0 \tag{5.36}$$

$$c_5 = c - \frac{b^2}{c - c_4} \quad , \quad \frac{\mu_5}{\mu_4} = \left(\frac{b}{c - c_4}\right)^2 \quad , \quad \beta_5 = 2\alpha - \pi \tag{5.37}$$

Likewise a velocity potential φ^R for cylinder R is considered. If cylinder L is not present, the flow past cylinder R is represented by a image doublet located at the centre of cylinder R. From its coordinate system, the following formulation can

then be described as

$$\varphi_0{}^R = -\mu_0' \frac{\cos\theta'}{r'} \quad , \quad \mu_0' = b^2 \quad , \quad \beta_0' = 0 \quad , \quad c_0' = c \qquad (5.38)$$

If the image of the doublet with cylinder L as observed from cylinder R is observed, the expression is written as

$$c_1' = \frac{a^2}{c} \quad , \quad \frac{\mu_1'}{\mu_0'} = \left(\frac{a}{c}\right)^2 \quad , \quad \beta_1' = 2\alpha - \pi \qquad (5.39)$$

and in turn the effect of the image doublet on cylinder R is taken into account by introducing the image doublet inside cylinder R. Now this image will form another image inside cylinder L and thus it is described as

$$c_2' = c - \frac{b^2}{c - c_1'} \quad , \quad \frac{\mu_2'}{\mu_1'} = \left(\frac{b}{c - c_1'}\right)^2 \quad , \quad \beta_2' = 0 \qquad (5.40)$$

Similarly following expressions are systematically written as

$$c_3' = \frac{a^2}{c_2'} \quad , \quad \frac{\mu_3'}{\mu_2'} = \left(\frac{a}{c_2'}\right)^2 \quad , \quad \beta_3' = 2\alpha - \pi \qquad (5.41)$$

$$c_4' = c - \frac{b^2}{c - c_3'} \quad , \quad \frac{\mu_4'}{\mu_3'} = \left(\frac{b}{c - c_3'}\right)^2 \quad , \quad \beta_4' = 0 \qquad (5.42)$$

$$c_5' = \frac{a^2}{c_4'} \quad , \quad \frac{\mu_5'}{\mu_4'} = \left(\frac{a}{c_4'}\right)^2 \quad , \quad \beta_5' = 2\alpha - \pi \qquad (5.43)$$

In compliance with above relations, following expressions are arranged as

$$\gamma_0 = 0 \quad , \quad \mu_0 = 1 \quad , \quad \beta_0 = 0 \qquad (5.44a)$$

$$\gamma_1 = \gamma - \frac{\varepsilon^2}{\gamma - \gamma_0} \quad , \quad \frac{\mu_1}{\mu_0} = \left(\frac{\varepsilon}{\gamma - \gamma_0}\right)^2 \quad , \quad \beta_1 = 2\alpha - \pi \qquad (5.44b)$$

$$\gamma_2 = \frac{1}{\gamma_1} \quad , \quad \frac{\mu_2}{\mu_1} = \left(\frac{1}{\gamma_1}\right)^2 \quad , \quad \beta_2 = 0 \qquad (5.44c)$$

$$\gamma_3 = \gamma - \frac{\varepsilon^2}{\gamma - \gamma_2} \quad , \quad \frac{\mu_3}{\mu_2} = \left(\frac{\varepsilon}{\gamma - \gamma_2}\right)^2 \quad , \quad \beta_3 = 2\alpha - \pi \qquad (5.44d)$$

$$\gamma_4 = \frac{1}{\gamma_3} \quad , \quad \frac{\mu_4}{\mu_3} = \left(\frac{1}{\gamma_3}\right)^2 \quad , \quad \beta_4 = 0 \qquad (5.44e)$$

$$\gamma_5 = \gamma - \frac{\varepsilon^2}{\gamma - \gamma_4} \quad , \quad \frac{\mu_5}{\mu_4} = \left(\frac{\varepsilon}{\gamma - \gamma_4}\right)^2 \quad , \quad \beta_5 = 2\alpha - \pi \qquad (5.44f)$$

Likewise

$$\gamma_0' = \gamma \quad , \quad \mu_0' = \varepsilon^2 \quad , \quad \beta_0' = 0 \qquad (5.45a)$$

$$\gamma_1' = \frac{1}{\gamma_0'} \quad , \quad \frac{\mu_1'}{\mu_0'} = \left(\frac{1}{\gamma_0'}\right)^2 \quad , \quad \beta_1' = 2\alpha - \pi \qquad (5.45b)$$

$$\gamma_2' = \gamma - \frac{\varepsilon^2}{\gamma - \gamma_1'} \quad , \quad \frac{\mu_2'}{\mu_1'} = \left(\frac{\varepsilon}{\gamma - \gamma_1'}\right)^2 \quad , \quad \beta_2' = 0 \qquad (5.45c)$$

$$\gamma_3' = \frac{1}{\gamma_2'} \quad , \quad \frac{\mu_3'}{\mu_2'} = \left(\frac{1}{\gamma_2'}\right)^2 \quad , \quad \beta_3' = 2\alpha - \pi \qquad (5.45d)$$

$$\gamma_4' = \gamma - \frac{\varepsilon^2}{\gamma - \gamma_3'} \quad , \quad \frac{\mu_4'}{\mu_3'} = \left(\frac{\varepsilon}{\gamma - \gamma_3'}\right)^2 \quad , \quad \beta_4' = 0 \qquad (5.45e)$$

$$\gamma_5' = \frac{1}{\gamma_4'} \quad , \quad \frac{\mu_5'}{\mu_4'} = \left(\frac{1}{\gamma_4'}\right)^2 \quad , \quad \beta_5' = 2\alpha - \pi \qquad (5.45f)$$

In the same way, the velocity potential φ^R for cylinder R is also represented by an infinite series of image doublets, with the leading term being a point doublet located at the origin of cylinder R.

As a result of repeating such procedures, the velocity potential φ^L for cylinder L is described by an infinite series of image doublets within cylinder L and cylinder R. In terms of the complex velocity potential, it is described as follows.

$$f^L(z) = -a\sum_{j=0}^{\infty} \frac{\mu_j e^{i\beta_j}}{z - \gamma_j e^{i\alpha}} \quad , \quad z = re^{i\theta} \tag{5.46}$$

where :

$$\gamma_0 = 0 \quad , \quad \gamma_{2n-1} = \gamma - \frac{\varepsilon^2}{\gamma - \gamma_{2n-2}} \quad , \quad \gamma_{2n} = \frac{1}{\gamma_{2n-1}} \tag{5.47a}$$

$$\mu_0 = 1 \quad , \quad \frac{\mu_{2n-1}}{\mu_{2n-2}} = \left(\frac{\varepsilon}{\gamma - \gamma_{2n-2}}\right)^2 \quad , \quad \frac{\mu_{2n}}{\mu_{2n-1}} = \left(\frac{1}{\gamma_{2n-1}}\right)^2 \tag{5.47b}$$

$$\beta_0 = 0 \quad , \quad \beta_{2n-1} = 2\alpha - \pi \quad , \quad \beta_{2n} = 0 \tag{5.47c}$$

where :

$$\gamma = \frac{c}{a} \quad , \quad \varepsilon = \frac{b}{a} \qquad (n = 1,2,\cdots\infty) \tag{5.48}$$

Similarly, the velocity potential φ^R for cylinder R is also represented by an infinite series of image doublets, with the leading term being a point doublet located at the origin of cylinder R. In the coordinate system with the origin at the centre of cylinder R, φ^R is described as the real part of the complex potential of the form

$$f^R(z) = -a\sum_{j=0}^{\infty} \frac{\mu'_j e^{i\beta'_j}}{z - \gamma'_j e^{i\alpha}} \tag{5.49}$$

where :

$$\gamma_0' = \gamma \quad , \quad \gamma_{2n-1}' = \frac{1}{\gamma_{2n-2}'} \quad , \quad \gamma_{2n}' = \gamma - \frac{\varepsilon^2}{\gamma - \gamma_{2n-1}'} \tag{5.50a}$$

$$\mu_0' = \varepsilon^2 \quad , \quad \frac{\mu_{2n-1}'}{\mu_{2n-2}'} = \left(\frac{1}{\gamma_{2n-2}'}\right)^2 \quad , \quad \frac{\mu_{2n}'}{\mu_{2n-1}'} = \left(\frac{\varepsilon}{\gamma - \gamma_{2n-1}'}\right)^2 \tag{5.50b}$$

$$\beta_0' = 0 \quad , \quad \beta_{2n-1}' = 2\alpha - \pi \quad , \quad \beta_{2n}' = 0 \quad (n = 1,2,\cdots\infty) \tag{5.50c}$$

In order to calculate the m-vector contribution, a typical complex potential is written as

$$f(z) = -a\frac{\mu e^{i\beta}}{z - \gamma e^{i\alpha}} = -\frac{\mu e^{i\beta}}{z - ce^{i\alpha}} \tag{5.51}$$

Then

$$f'(z) = u - iv = \frac{\mu e^{i\beta}}{\left(z - ce^{i\alpha}\right)^2} \equiv \mu e^{i\beta} g(r,\theta) \tag{5.52}$$

where :

$$z = re^{i\theta} \tag{5.52a}$$

Substituting this expression into the definition of m-vector contribution, m-vector contribution can be readily obtained as

$$m_1 - im_2 = -\frac{\partial}{\partial n}(u - iv) = -\frac{\partial}{a\partial r} f'(z)\Big|_{r=1} \tag{5.53}$$

$$= -\frac{\partial}{\partial r} f'(z)\Big|_{r=1} = -\mu e^{i\beta}\frac{\partial}{\partial r} g(r,\theta) \tag{5.54}$$

where :

$$g(r,\theta)=\frac{1}{\left(re^{i\theta}-ce^{i\alpha}\right)^2} \tag{5.54a}$$

Then

$$m_1-im_2=\frac{2\mu e^{i\beta}e^{i\theta}}{\left(re^{i\theta}-ce^{i\alpha}\right)^3}\bigg|_{r=a}=\frac{2}{a}\left(\frac{\mu}{a^2}\right)\frac{e^{-i(2\theta-\beta)}}{\left(1-\frac{c}{a}e^{i(\alpha-\theta)}\right)^3} \tag{5.55}$$

Here

$$\begin{aligned}\frac{1}{1-\gamma e^{i(\alpha-\theta)}}&=\frac{1-\gamma e^{i(\theta-\alpha)}}{\left\{1-\gamma e^{i(\alpha-\theta)}\right\}\left\{1-\gamma e^{-i(\alpha-\theta)}\right\}}\\&=\frac{1-\gamma e^{i(\theta-\alpha)}}{1-2\gamma\cos(\theta-\alpha)+\gamma^2}\end{aligned} \tag{5.56}$$

where :

$$\gamma=\frac{c}{a} \tag{5.56a}$$

Thus

$$\begin{aligned}m_1-im_2&=\frac{2}{a}\left(\frac{\mu}{a^2}\right)\frac{e^{-i(2\theta-\beta)}\left\{1-\gamma e^{i(\theta-\alpha)}\right\}^3}{\left\{1-2\gamma\cos(\theta-\alpha)+\gamma^2\right\}^3}\\&=2\mu\left\{\frac{1-\gamma e^{i(\theta-\alpha)}}{1-2\gamma\cos(\theta-\alpha)+\gamma^2}\right\}^3 e^{-i(2\theta-\beta)}\end{aligned} \tag{5.57}$$

Here

$$\begin{aligned}\left\{1-\gamma e^{i(\theta-\alpha)}\right\}^3&=1-3\gamma e^{i(\theta-\alpha)}+3\gamma^2e^{i2(\theta-\alpha)}-\gamma^3e^{i3(\theta-\alpha)}\\&\equiv\tilde{R}+i\tilde{S}\end{aligned} \tag{5.58}$$

where :

$$\tilde{R} = 1 - 3\gamma\cos(\theta-\alpha) + 3\gamma^2\cos 2(\theta-\alpha) - \gamma^3\cos 3(\theta-\alpha) \qquad (5.59a)$$

$$\tilde{S} = -3\gamma\sin(\theta-\alpha) + 3\gamma^2\sin 2(\theta-\alpha) - \gamma^3\sin 3(\theta-\alpha) \qquad (5.59b)$$

Thus

$$m_1 - im_2 = \frac{2}{a}\left(\frac{\mu}{a^2}\right)\frac{e^{-i(2\theta-\beta)}\left(\tilde{R}+i\tilde{S}\right)}{\left\{1-2\gamma\cos(\theta-\alpha)+\gamma^2\right\}^3} \qquad (5.60)$$

$$m_1 = \frac{2}{a}\left(\frac{\mu}{a^2}\right)\frac{\tilde{R}\cos(2\theta-\beta)+\tilde{S}\sin(2\theta-\beta)}{\left\{1-2\gamma\cos(\theta-\alpha)+\gamma^2\right\}^3} \qquad (5.61)$$

$$m_2 = \frac{2}{a}\left(\frac{\mu}{a^2}\right)\frac{\tilde{R}\sin(2\theta-\beta)-\tilde{S}\cos(2\theta-\beta)}{\left\{1-2\gamma\cos(\theta-\alpha)+\gamma^2\right\}^3} \qquad (5.62)$$

In accordance with above relations, the strength of the doublet is normalised by a^2 and the image point can then be considered as an infinite series in the following form

$$f(z) = -a^2\sum_{j=0}^{\infty}\left\{\frac{\mu_j e^{i\beta_j}}{z-c_j e^{i\alpha}} + \frac{\mu'_j e^{i\beta'_j}}{z-c'_j e^{i\alpha}}\right\} \qquad (5.63)$$

Therefore

$$m_1^{L} = \frac{2}{a}\sum_{j=0}^{\infty}\left[\begin{array}{l}\mu_j\dfrac{\tilde{R}_j\cos(2\theta-\beta_j)+\tilde{S}_j\sin(2\theta-\beta_j)}{\left\{1-2\gamma_j\cos(\theta-\alpha)+\gamma_j^2\right\}^3} \\ +\mu'_j\dfrac{\tilde{R}'_j\cos(2\theta-\beta'_j)+\tilde{S}'_j\sin(2\theta-\beta'_j)}{\left\{1-2\gamma'_j\cos(\theta-\alpha)+\gamma_j'^2\right\}^3}\end{array}\right] \qquad (5.64)$$

$$m_2^{L} = \frac{2}{a}\sum_{j=0}^{\infty}\left[\begin{array}{l}\mu_j\dfrac{\tilde{R}_j\sin(2\theta-\beta_j)-\tilde{S}_j\cos(2\theta-\beta_j)}{\left\{1-2\gamma_j\cos(\theta-\alpha)+\gamma_j^2\right\}^3} \\ +\mu'_j\dfrac{\tilde{R}'_j\sin(2\theta-\beta'_j)-\tilde{S}'_j\cos(2\theta-\beta'_j)}{\left\{1-2\gamma'_j\cos(\theta-\alpha)+\gamma_j'^2\right\}^3}\end{array}\right] \qquad (5.65)$$

where :

$$\tilde{R}_j = 1 - 3\gamma_j \cos(\theta-\alpha) + 3\gamma_j^2 \cos 2(\theta-\alpha) - \gamma_j^3 \cos 3(\theta-\alpha) \quad (5.66a)$$

$$\tilde{S}_j = -3\gamma_j \sin(\theta-\alpha) + 3\gamma_j^2 \sin 2(\theta-\alpha) - \gamma_j^3 \sin 3(\theta-\alpha) \quad (5.66b)$$

$$\tilde{R}'_j = 1 - 3\gamma'_j \cos(\theta-\alpha) + 3\gamma'^2_j \cos 2(\theta-\alpha) - \gamma'^3_j \cos 3(\theta-\alpha) \quad (5.66c)$$

$$\tilde{S}'_j = -3\gamma'_j \sin(\theta-\alpha) + 3\gamma'^2_j \sin 2(\theta-\alpha) - \gamma'^3_j \sin 3(\theta-\alpha) \quad (5.66d)$$

Since the m-vector contribution for cylinder L is calculated from the sum of Eq. (5.46) and Eq. (5.49), Eq. (5.53) can be deduced as

$$m_1^{\,L} = 2\sum_{j=0}^{\infty}\begin{bmatrix}\mu_j\{R_j\cos(2\theta-\beta_j)+S_j\sin(2\theta-\beta_j)\}\\ +\mu'_j\{R'_j\cos(2\theta-\beta'_j)+S'_j\sin(2\theta-\beta'_j)\}\end{bmatrix} \quad (5.67)$$

$$m_2^{\,L} = 2\sum_{j=0}^{\infty}\begin{bmatrix}\mu_j\{R_j\sin(2\theta-\beta_j)-S_j\cos(2\theta-\beta_j)\}\\ +\mu'_j\{R'_j\sin(2\theta-\beta'_j)-S'_j\cos(2\theta-\beta'_j)\}\end{bmatrix} \quad (5.68)$$

where :

$$R_j = F(\gamma_j) \quad , \quad S_j = G(\gamma_j) \quad (5.69a)$$

$$R'_j = F(\gamma'_j) \quad , \quad S'_j = G(\gamma'_j) \quad (5.69b)$$

$$\begin{bmatrix}F(\gamma)\\ G(\gamma)\end{bmatrix} = \frac{\sum_{k=0}^{3} a_k \gamma^k \begin{bmatrix}\cos k(\theta-\alpha)\\ \sin k(\theta-\alpha)\end{bmatrix}}{\{1-2\gamma\cos(\theta-\alpha)+\gamma^2\}^3} \quad (5.70)$$

$$a_0 = 1 \quad , \quad a_1 = -3 \quad , \quad a_2 = 3 \quad , \quad a_3 = -1 \quad (5.71)$$

Next the formulation of the m-vector contribution for cylinder R is

performed. The only necessary task is to rewrite Eq. (5.46) and Eq. (5.49) in the coordinate system with the origin at the centre of the circle R. The positions to the doublet are $c - c_j$ and $c - c_j'$ and it is sufficient if α is replaced by $(\alpha - \pi)$. The axis of the doublet is the same as β_j and β_j'.

$$m_1^R - im_2^R = \frac{2}{b}\left(\frac{\mu}{b^2}\right)\frac{e^{-i(2\theta-\beta)}}{\left\{1-\frac{\tilde{c}}{b}e^{i(\alpha-\theta)}\right\}^3}$$

$$= \left(\frac{a}{b}\right)^3 \frac{2}{a}\left(\frac{\mu}{a}\right)\frac{e^{-i(2\theta-\beta)}\left\{1-\delta e^{i(\theta-\alpha)}\right\}^3}{\left\{1-2\delta\cos(\theta-\alpha)+\delta^2\right\}^3} \qquad (5.72)$$

where :

$$\delta_j = -\frac{1}{b}(c-c_j) = -\frac{1}{\varepsilon}(\gamma-\gamma_j) = \frac{1}{\varepsilon}(\gamma_j-\gamma) \qquad (5.73)$$

In the same way, the m-vector contribution for cylinder R can be described as

$$m_1^R = \frac{2}{a\varepsilon^3}\sum_{j=0}^{\infty}\left[\begin{array}{l}\mu_j \dfrac{\tilde{P}_j\cos(2\theta-\beta_j)+\tilde{Q}_j\sin(2\theta-\beta_j)}{\left\{1-2\delta_j\cos(\theta-\alpha)+\delta_j^2\right\}^3} \\ +\mu_j' \dfrac{\tilde{P}_j'\cos(2\theta-\beta_j')+\tilde{Q}_j'\sin(2\theta-\beta_j')}{\left\{1-2\delta_j'\cos(\theta-\alpha)+\delta_j'^2\right\}^3}\end{array}\right] \qquad (5.74)$$

$$m_2^R = \frac{2}{a\varepsilon^3}\sum_{j=0}^{\infty}\left[\begin{array}{l}\mu_j \dfrac{\tilde{P}_j\sin(2\theta-\beta_j)-\tilde{Q}_j\cos(2\theta-\beta_j)}{\left\{1-2\delta_j\cos(\theta-\alpha)+\delta_j^2\right\}^3} \\ +\mu_j' \dfrac{\tilde{P}_j'\sin(2\theta-\beta_j')-\tilde{Q}_j'\cos(2\theta-\beta_j')}{\left\{1-2\delta_j'\cos(\theta-\alpha)+\delta_j'^2\right\}^3}\end{array}\right] \qquad (5.75)$$

where :

$$\tilde{P}_j = 1-3\delta_j\cos(\theta-\alpha)+3\delta_j^2\cos 2(\theta-\alpha)-\delta_j^3\cos 3(\theta-\alpha) \qquad (5.76a)$$

$$\tilde{Q}_j = -3\delta_j\sin(\theta-\alpha)+3\delta_j^2\sin 2(\theta-\alpha)-\delta_j^3\sin 3(\theta-\alpha) \qquad (5.76b)$$

$$\tilde{P}_j' = 1 - 3\delta_j' \cos(\theta - \alpha) + 3\delta_j'^2 \cos 2(\theta - \alpha) - \delta_j'^3 \cos 3(\theta - \alpha) \quad (5.76c)$$

$$\tilde{Q}_j' = -3\delta_j' \sin(\theta - \alpha) + 3\delta_j'^2 \sin 2(\theta - \alpha) - \delta_j'^3 \sin 3(\theta - \alpha) \quad (5.76d)$$

Denoting the complex variable in this new coordinate system by z' and z is

$$z = z' + \gamma e^{i\alpha} \quad (5.77)$$

On the surface of the circle R, $z' = \varepsilon e^{i\theta}$ should be carefully specified. With these relations taken into account, the m-vector contribution for cylinder R is easily derived in the same manner as for cylinder L obtained above. Final expressions are expressed as

$$m_1^R = \frac{2}{\varepsilon^3} \sum_{j=0}^{\infty} \begin{bmatrix} \mu_j \{P_j \cos(2\theta - \beta_j) + Q_j \sin(2\theta - \beta_j)\} \\ + \mu_j' \{P_j' \cos(2\theta - \beta_j') + Q_j' \sin(2\theta - \beta_j')\} \end{bmatrix} \quad (5.78)$$

$$m_2^R = \frac{2}{\varepsilon^3} \sum_{j=0}^{\infty} \begin{bmatrix} \mu_j \{P_j \sin(2\theta - \beta_j) - Q_j \cos(2\theta - \beta_j)\} \\ + \mu_j' \{P_j' \sin(2\theta - \beta_j') - Q_j' \cos(2\theta - \beta_j')\} \end{bmatrix} \quad (5.79)$$

where :

$$P_j = F(\delta_j) \quad , \quad Q_j = G(\delta_j) \quad (5.80a)$$

$$P_j' = F(\delta_j') \quad , \quad Q_j' = G(\delta_j') \quad (5.80b)$$

where :

$$\delta_j = \frac{1}{\varepsilon}(\gamma_j - \gamma) \quad , \quad \delta_j' = \frac{1}{\varepsilon}(\gamma_j' - \gamma) \quad (5.81)$$

The rotation of two cylinder system around a point is considered to be the summation of each vertical and horizontal displacements of the cylinders, in which

cylinder L and R displacements occur in the reverse directions, and the rotation around each cylinder centre. The rotation of each circular cylinder around its centre does not contribute to the m-vector. Then expressions of the m_3 vector on each cylinder L and R are written as

$$m_3^{L} = -\left(m_2^{L}\cos\alpha - m_1^{L}\sin\alpha\right) \tag{5.82}$$

$$m_3^{R} = \left(m_2^{R}\cos\alpha - m_1^{R}\sin\alpha\right) \tag{5.83}$$

and the expression of n_3 vector is also written as

$$n_3^{L} = -l\sin(\theta - \alpha) \tag{5.84}$$

$$n_3^{R} = +l\sin(\theta - \alpha) \tag{5.85}$$

The distance between the centres of cylinder L and R is considerably large compared with the cylinder cross section of twin hulled marine structures. In this configuration, the series for the m-vector contribution can be truncated after several terms to obtain sufficient accuracy. In practical numerical computations, the infinite series can be reasonably truncated to ten (10) mirror images to converge the series for different submerged depths, Froude number, separation distance and inclinations.

5.5 Investigations of numerical computations

Under the linear assumption of the boundary value problem taking into consideration the m-vector contribution, the velocity potential can be obtained by numerical solutions of the integral equation over body boundary contours exactly. The numerical check of the first order hydrodynamic problems for such twin hulled marine vehicles under combined actions of wave and current, achieved by analytically solving the logarithmic part of the Green function, is well confirmed as

investigated by both numerical methods in Chapter Four.

By taking the image number as ten (10) and discretized element number as fifty (50) for individual left and right cylinders, the predicted results with and without the m-vector contribution can be compared. Both results of added mass coefficients in surge, heave and pitch motions with and without m-vector contribution match well and are as in Figs. 5.3, 5.4 and 5.5. For the damping coefficients, calculations in surge, heave and pitch modes also show excellent agreement as in Figs. 5.6, 5.7 and 5.8.

As regards the predicted results of the real and imaginary parts of the Kochin functions, these can be obtained by direct solution of the radiation problem and by the Haskind-Newman relation from wave excitation forces. Principally all numerical results of surge, heave and pitch Kochin functions for both real and imaginary parts are satisfied with good agreement and systematically shown in Figs. 5.9 to 5.14 respectively. In fact this theoretical formulation with the m-vector contribution is quite satisfactory to investigate such hydrodynamic problems with forward speed effect in waves.

5.6 Parametric studies and discussions

As the numerical investigation is satisfied, parametric studies on the hydrodynamic characteristics of twin hulled offshore structures in head waves with and without the m-vector contribution are extensively performed for different Froude number, submerged depths, separation distance and inclinations. The detail results are categorized into four major groups and discussed as follows.

(A) For forward speed effect :

Numerical results of non-dimensionalized surge, heave added mass coefficients and pitch added moment of inertia are as in Figs. 5.15 to 5.17. In the

very low frequency range (within Ka = 0.10), the significant variation is due to m-vector contribution and not much difference is seen for the remaining frequency range. As for the damping coefficients, the m-vector effect is not considerable for the selected range of frequencies as in Figs. 5.18 to 5.20. For the real and imaginary part of surge, heave and pitch Kochin functions, not much variation is due to the m-vector contribution as in Figs. 5.21 to 5.26.

Numerical results of non-dimensionalized surge and heave added mass coefficients and pitch added moment of inertia are presented in Figs. 5.27 to 5.29. The m-vector contribution shows very significant effect in the low frequency range (within Ka = 0.30), and a slight difference is shown for the remaining frequency range. As for the damping coefficients as in Figs. 5.30 to 5.32, the m-vector effect is quite dominant in the low frequency range (within Ka = 0.20) and not much contribution for the remaining range of frequencies. For the real and imaginary part of surge, heave and pitch Kochin functions, the amplitudes are mostly smaller than those without m-vector effect over the range of frequencies as in Figs. 5.33 to 5.38 respectively and it noticed that higher forward speed always contribute much to the m-vector effect.

(B) For deeper submergence depth :

Numerical computations of non-dimensionalized surge, heave added mass coefficients and pitch added moment of inertia are as in Figs. 5.39 to 5.41. In the very low frequency range (within Ka = 0.10), large discrepancy is shown due to the m-vector effect and not much difference for the remaining frequency range. As for damping coefficients as in Figs. 5.42 to 5.44, the m-vector effect shows no much contribution due to deeper submergence. For the real and imaginary part of surge, heave and pitch Kochin functions, a similar tendency is shown and as in Figs. 5.45 to 5.50.

(C) For larger separation distance :

Predicted results of non-dimensionalized surge, heave added mass

coefficients and pitch added moment of inertia are as in Figs. 5.51 to 5.53. The m-vector effect is considerable in the very low frequency range (within Ka = 0.10) and no significant difference is shown for the remaining frequency range. As for the non-dimensionalized damping coefficients as in Figs. 5.54 and 5.55, the m-vector effects in surge and heave modes have much contribution at certain frequency range (within Ka = 0.30 and 0.60). For pitch motion case, larger discrepancy occurs within Ka = 0.20 and 0.40 and as in Fig. 5.56. The results of the real and imaginary part of surge, heave and pitch Kochin functions are as in Figs. 5.57 to 5.62.

(D) For inclination effect :

Numerical results of the non-dimensionalized surge, heave added mass coefficients and pitch added moment of inertia are as in Figs. 5.63 to 5.65. Again large discrepancy is shown due to the m-vector effect in the very low frequency range (within Ka = 0.20) and not much difference for the remaining frequency range. As for non-dimensionalized damping coefficients as in Figs. 5.66 to 5.68, the m-vector effect shows not much contribution except for certain frequency ranges. For the real and imaginary part of surge, heave and pitch Kochin functions, a similar tendency is shown as in Figs. 5.69 to 5.74.

Numerical computations of non-dimensionalized surge, heave added mass coefficients and pitch added moment of inertia are as in Figs. 5.75 to 5.77. The m-vector contribution shows very significant effect in the low frequency range (within Ka = 0.20) and not much difference is shown for the remaining frequency range. As for the damping coefficients as in Figs. 5.78 to 5.80, the m-vector effect is considerable for certain frequencies. For the real and imaginary part of surge, heave and pitch Kochin functions, the amplitudes are almost smaller than those without m-vector effect over all the range of frequencies as in Figs. 5.81 to 5.86 and it is confirmed that inclination is not effective enough to affect hydrodynamic characteristics on submerged structures due to the m-vector effect.

5.7 Conclusion

Predicted results of the hydrodynamic loadings with the m-vector contribution are compared with those without taking the m-vector contribution into consideration. For non-forward speed case which the m-vector contribution is not considered, numerical computations are investigated and both results match very well. It is confirmed that this theoretical approach with the m-vector contribution is effective and reliable enough for practical engineering applications.

CHAPTER 6
THEORETICAL DERIVATION OF RESTORING FORCES DUE TO THE FORWARD SPEED EFFECT FOR TWO RIGIDLY HELD APART CYLINDERS

6.1 General description

The theoretical derivation of the hydrodynamic restoring forces due to forward speed effect (equivalent current effect) which is proportional to the unsteady displacement of the twin hulled marine structure is formulated, taking into consideration interaction effects between two hulls submerged under a free surface. The theoretical formulation of the restoring forces due to forward speed effect is analytically derived for the case of a single submerged cylinder and analytical solutions of hydrodynamic restoring coefficients due to forward speed effect for the single circular cylinder case, as shown in Appendix B, are applied to confirm numerical computations for the two rigidly connected cylinder system.

Under a linear assumption of the boundary value problem, numerical results are exactly obtained by solving the integral equation for the velocity potential over the body boundary contours and the numerical technique of the direct Green function method is applied. Numerical results of the damping coefficients are checked out by previous researches such as Varyani (1988) with satisfactory accuracy and motion responses of an inclined twin hulled offshore structure with and without hydrodynamic restoring forces due to the forward speed effect in head and following waves are investigated.

This mathematical approach is extensively applied to investigate dynamic motion responses of twin hulled marine vehicles, taking into account effects of forward speed and interactions between two hulls for different submerged depths,

Froude number, separation distance and inclinations in head and following waves. The dynamic motion behaviour of twin hulled marine vehicles in the low frequency region at resonance is also investigated.

6.2 Mathematical formulation of the coefficients of restoring forces due to forward speed effect for two rigidly held apart cylinders

Since the interest is concentrated on the submerged body case, it is natural to assume that the steady velocity potential φ_S around submerged bodies is approximated by velocity potential without taking the free surface effect into consideration.

It is certainly possible to apply the velocity potential which satisfies the linearized free surface condition even if it is rather intricate to calculate hydrodynamic restoring forces (referred to as the m-vector contribution). However it is known that the steady velocity potential satisfying the linearized free surface condition does not necessarily provide an accurate solution of the steady flow around the moving body. Using Eq. (4.2) and neglecting the second and higher order terms, the linearized expression of the hydrodynamic pressure is described as

$$p(x,y) = -\rho\left\{\left(i\omega + U\bar{V}\cdot\nabla\right)\phi + \frac{U^2}{2}(\tilde{\alpha}\cdot\nabla)\bar{V}^2\right\} \qquad (6.1)$$

The theoretical expression for hydrodynamic pressure forces acting on an offshore structure advancing under combined actions of wave and current can be presented as

$$F_i = -\int_{S_H} p(x,y) n_i dl \quad (i = 1, 2, 3) \qquad (6.2)$$

where :

$$n = n_1\vec{i} + n_2\vec{j} \qquad (6.3)$$

The last term in Eq. (6.1) introduces a hydrodynamic force proportional to the unsteady displacement of the body, hence this additional buoyancy force due to the forward speed effect corresponds to the hydrodynamic restoring force. This hydrodynamic restoring force due to the unsteady displacement of the moving body can be derived as

$$F_i = \frac{\rho U^2}{2}\int_{S_H}(\vec{\alpha}\cdot\nabla)\vec{V}^2 n_i dl \qquad (6.4)$$

where :

a). Description of motion responses of cylinder L with inclination effects

$$\vec{i}\left\{\xi_1^L + \xi_3^L(l\sin\alpha - y)\right\} + \vec{j}\left\{\xi_2^L - \xi_3^L(l\cos\alpha - x)\right\} \qquad (6.5a)$$

b). Description of motion responses of cylinder R with inclination effects

$$\vec{i}\left\{\xi_1^R - \xi_3^R(l\sin\alpha + y)\right\} + \vec{j}\left\{\xi_2^R + \xi_3^R(l\cos\alpha + x)\right\} \qquad (6.5b)$$

The hydrodynamic restoring force on cylinder L is then described as

$$F_i^L = \frac{\rho U^2}{2}\int_{S_L}\begin{bmatrix}\left\{\xi_1^L + \xi_3^L(l\sin\alpha - y)\right\}\dfrac{\partial}{\partial x}\\ +\left\{\xi_2^L - \xi_3^L(l\cos\alpha - x)\right\}\dfrac{\partial}{\partial y}\end{bmatrix}\left\{\left(-1+\frac{\partial\varphi_S}{\partial x}\right)^2 + \left(\frac{\partial\varphi_S}{\partial y}\right)^2\right\} n_i dl \qquad (6.6a)$$

$$\begin{aligned}
&= \rho U^2\xi_1^L\int_{S_L}\left[\left(-1+\frac{\partial\varphi_S}{\partial x}\right)\frac{\partial^2\varphi_S}{\partial x^2} + \frac{\partial\varphi_S}{\partial y}\frac{\partial^2\varphi_S}{\partial x\partial y}\right] n_i dl\\
&+\rho U^2\xi_2^L\int_{S_L}\left[\left(-1+\frac{\partial\varphi_S}{\partial x}\right)\frac{\partial^2\varphi_S}{\partial y\partial x} + \frac{\partial\varphi_S}{\partial y}\frac{\partial^2\varphi_S}{\partial y^2}\right] n_i dl\\
&+\rho U^2\xi_3^L\{(l\sin\alpha)\int_{S_L}\left[\left(-1+\frac{\partial\varphi_S}{\partial x}\right)\frac{\partial^2\varphi_S}{\partial x^2} + \frac{\partial\varphi_S}{\partial y}\frac{\partial^2\varphi_S}{\partial x\partial y}\right] n_i dl\\
&-\int_{S_L}(y)\left[\left(-1+\frac{\partial\varphi_S}{\partial x}\right)\frac{\partial^2\varphi_S}{\partial x^2} + \frac{\partial\varphi_S}{\partial y}\frac{\partial^2\varphi_S}{\partial x\partial y}\right] n_i dl
\end{aligned}$$

$$-(1\cos\alpha)\int_{S_L}\left[\left(-1+\frac{\partial\varphi_S}{\partial x}\right)\frac{\partial^2\varphi_S}{\partial y\partial x}+\frac{\partial\varphi_S}{\partial y}\frac{\partial^2\varphi_S}{\partial y^2}\right]n_i dl$$
$$+\int_{S_L}(x)\left[\left(-1+\frac{\partial\varphi_S}{\partial x}\right)\frac{\partial^2\varphi_S}{\partial y\partial x}+\frac{\partial\varphi_S}{\partial y}\frac{\partial^2\varphi_S}{\partial y^2}\right]n_i dl\Bigg\} \qquad (6.6b)$$

Thus such coefficients of the hydrodynamic restoring forces due to forward speed effect for cylinder L of the twin hulled marine structure are respectively written as

$$C_{i1}{}^{L}=\int_{S_L}\left[\left(-1+\frac{\partial\varphi_S}{\partial x}\right)\frac{\partial^2\varphi_S}{\partial x^2}+\frac{\partial\varphi_S}{\partial y}\frac{\partial^2\varphi_S}{\partial x\partial y}\right]n_i dl \qquad (6.7a)$$

$$C_{i2}{}^{L}=\int_{S_L}\left[\left(-1+\frac{\partial\varphi_S}{\partial x}\right)\frac{\partial^2\varphi_S}{\partial y\partial x}+\frac{\partial\varphi_S}{\partial y}\frac{\partial^2\varphi_S}{\partial y^2}\right]n_i dl \qquad (6.7b)$$

$$\begin{aligned}C_{i3}{}^{L}=l\Bigg\{&-\int_{S_L}(\sin\alpha)\left[\left(-1+\frac{\partial\varphi_S}{\partial x}\right)\frac{\partial^2\varphi_S}{\partial x^2}+\frac{\partial\varphi_S}{\partial y}\frac{\partial^2\varphi_S}{\partial x\partial y}\right]n_i dl\\&-\int_{S_L}\left(\frac{y}{l}\right)\left[\left(-1+\frac{\partial\varphi_S}{\partial x}\right)\frac{\partial^2\varphi_S}{\partial x^2}+\frac{\partial\varphi_S}{\partial y}\frac{\partial^2\varphi_S}{\partial x\partial y}\right]n_i dl\\&-\int_{S_L}(\cos\alpha)\left[\left(-1+\frac{\partial\varphi_S}{\partial x}\right)\frac{\partial^2\varphi_S}{\partial y\partial x}+\frac{\partial\varphi_S}{\partial y}\frac{\partial^2\varphi_S}{\partial y^2}\right]n_i dl\\&+\int_{S_L}\left(\frac{x}{l}\right)\left[\left(-1+\frac{\partial\varphi_S}{\partial x}\right)\frac{\partial^2\varphi_S}{\partial y\partial x}+\frac{\partial\varphi_S}{\partial y}\frac{\partial^2\varphi_S}{\partial y^2}\right]n_i dl\Bigg\}\end{aligned} \qquad (6.7c)$$

where :

$$n_1{}^{L}=\cos\theta \quad , \quad n_2{}^{L}=\sin\theta \quad , \quad n_3{}^{L}=l\{-\sin(\theta-\alpha)\}=al\{-\sin(\theta-\alpha)\}$$
(for an inclining angle α) (6.8)

Similarly the coefficients of the hydrodynamic restoring forces due to forward speed effect for cylinder R of the twin hulled marine vehicle in waves can also be presented as

$$C_{i1}{}^{R}=\int_{S_R}\left[\left(-1+\frac{\partial\varphi_S}{\partial x}\right)\frac{\partial^2\varphi_S}{\partial x^2}+\frac{\partial\varphi_S}{\partial y}\frac{\partial^2\varphi_S}{\partial x\partial y}\right]n_i dl \qquad (6.9a)$$

$$C_{i2}^{R} = \int_{S_R}\left[\left(-1+\frac{\partial\varphi_s}{\partial x}\right)\frac{\partial^2\varphi_s}{\partial y\partial x}+\frac{\partial\varphi_s}{\partial y}\frac{\partial^2\varphi_s}{\partial y^2}\right]n_i dl \qquad (6.9b)$$

$$\begin{aligned}C_{i3}^{R} = l\Bigg\{&-\int_{S_R}(\sin\alpha)\left[\left(-1+\frac{\partial\varphi_s}{\partial x}\right)\frac{\partial^2\varphi_s}{\partial x^2}+\frac{\partial\varphi_s}{\partial y}\frac{\partial^2\varphi_s}{\partial x\partial y}\right]n_i dl\\ &-\int_{S_R}\left(\frac{y}{l}\right)\left[\left(-1+\frac{\partial\varphi_s}{\partial x}\right)\frac{\partial^2\varphi_s}{\partial x^2}+\frac{\partial\varphi_s}{\partial y}\frac{\partial^2\varphi_s}{\partial x\partial y}\right]n_i dl\\ &+\int_{S_R}(\cos\alpha)\left[\left(-1+\frac{\partial\varphi_s}{\partial x}\right)\frac{\partial^2\varphi_s}{\partial y\partial x}+\frac{\partial\varphi_s}{\partial y}\frac{\partial^2\varphi_s}{\partial y^2}\right]n_i dl\\ &+\int_{S_R}\left(\frac{x}{l}\right)\left[\left(-1+\frac{\partial\varphi_s}{\partial x}\right)\frac{\partial^2\varphi_s}{\partial y\partial x}+\frac{\partial\varphi_s}{\partial y}\frac{\partial^2\varphi_s}{\partial y^2}\right]n_i dl\Bigg\} \qquad (6.9c)\end{aligned}$$

where :

$$n_1^{R} = \cos\theta \quad , \quad n_2^{R} = \sin\theta \quad , \quad n_3^{R} = l\{+\sin(\theta-\alpha)\} = bl\left\{+\frac{1}{\varepsilon}\sin(\theta-\alpha)\right\}$$

(for an inclining angle α) (6.10)

6.3.1 Theoretical formulation of the derivatives of restoring coefficients for two rigidly held apart cylinders submerged under a free surface

In order to calculate the hydrodynamic restoring coefficients, a reliable solution for the steady velocity potential φ_S is required. In order to avoid several numerical and theoretical problems which are still difficult to overcome at moments, the infinite fluid solution, which is valid for a deeply submerged body, is applied. The theoretical concept to derive mathematical expression of m-vector contribution due to forward speed effect has been discussed in Chapter Five. In the same way, it can be conveniently applied to develop theoretical formulation of restoring forces due to forward speed effect of twin hulled marine vehicles in incident waves.

The two rigidly held apart cylinders are composed of the left circular cylinder

of radius " a " (referred to as cylinder L) and the right circular cylinder of radius " b " (cylinder R), with a separation distance between both cylinder centres " c " and an angle of inclination " α ". These two cylinders of twin hulled marine vehicles are assumed to move with forward speed U in the x direction as shown in Fig. 4.1. The velocity potential of the two rigidly connected cylinder system is then formulated as

$$\varphi_S = U\left(\varphi^L + \varphi^R\right) \tag{6.11}$$

The body boundary conditions, to be satisfied by velocity potentials φ^L and φ^R for both cylinders, are derived in the following form

$$\frac{\partial\varphi^L}{\partial r} = \cos\theta \quad , \quad \frac{\partial\varphi^R}{\partial r} = 0 \qquad \text{on cylinder L} \tag{6.12a}$$

$$\frac{\partial\varphi^R}{\partial r'} = \cos\theta' \quad , \quad \frac{\partial\varphi^L}{\partial r'} = 0 \qquad \text{on cylinder R} \tag{6.12b}$$

Physically φ^L describes the velocity potential, in which only cylinder L moves with cylinder R at rest. Similarly φ^R is also for the velocity potential where only cylinder R moves with cylinder L at rest.

In order to investigate in detail the hydrodynamic restoring forces due to the forward speed effect of twin hulled marine vehicles in incident waves, a typical complex potential is introduced as

$$f(z) = -\frac{\mu e^{i\beta}}{z - ce^{i\alpha}} = -\frac{\mu e^{i\beta}}{\left(re^{i\theta} - ce^{i\alpha}\right)} \tag{6.13}$$

where :

$$z = re^{i\theta} \tag{6.13a}$$

Based on the polar coordinate system, the derivative expressions are written as

$$\frac{\partial}{\partial x} = \cos\theta \frac{\partial}{\partial r} - \frac{\sin\theta}{r} \frac{\partial}{\partial \theta} \tag{6.14a}$$

$$\frac{\partial}{\partial y} = \sin\theta \frac{\partial}{\partial r} + \frac{\cos\theta}{r} \frac{\partial}{\partial \theta} \tag{6.14b}$$

The first order derivatives of the complex velocity potential with respect to both x and y coordinates can be obtained respectively as

$$\begin{aligned}
\frac{\partial}{\partial x}\{f(z)\} &= \cos\theta \frac{\partial}{\partial r}\left\{\frac{-\mu e^{i\beta}}{\left(re^{i\theta} - ce^{i\alpha}\right)}\right\} - \frac{\sin\theta}{r}\frac{\partial}{\partial \theta}\left\{\frac{-\mu e^{i\beta}}{\left(re^{i\theta} - ce^{i\alpha}\right)}\right\} \\
&= \cos\theta\left\{\frac{\mu e^{i\beta} e^{i\theta}}{\left(re^{i\theta} - ce^{i\alpha}\right)^2}\right\} - \frac{\sin\theta}{r}\left\{\frac{\mu e^{i\beta} ire^{i\theta}}{\left(re^{i\theta} - ce^{i\alpha}\right)^2}\right\} \\
&= \frac{\mu e^{i\beta} e^{i\theta}}{\left(re^{i\theta} - ce^{i\alpha}\right)^2}\{\cos\theta - i\sin\theta\} \\
&= \frac{\mu e^{i\beta}}{\left(re^{i\theta} - ce^{i\alpha}\right)^2} \\
&= \left(\frac{\mu}{r^2}\right)\frac{e^{-i(2\theta-\beta)}}{\left\{1 - \frac{c}{r}e^{i(\alpha-\theta)}\right\}^2} \\
&= \left(\frac{\mu}{a^2}\right)\frac{e^{-i(2\theta-\beta)}}{\left\{1 - \gamma e^{i(\alpha-\theta)}\right\}^2} \\
&= \left(\frac{\mu}{a^2}\right)\frac{e^{-i(2\theta-\beta)}\left\{1 - \gamma e^{i(\theta-\alpha)}\right\}^2}{\left\{1 - 2\gamma\cos(\theta-\alpha) + \gamma^2\right\}^2}
\end{aligned} \tag{6.15}$$

and

$$\begin{aligned}
\frac{\partial}{\partial y}\{f(z)\} &= \sin\theta \frac{\partial}{\partial r}\left\{\frac{-\mu e^{i\beta}}{\left(re^{i\theta} - ce^{i\alpha}\right)}\right\} + \frac{\cos\theta}{r}\frac{\partial}{\partial \theta}\left\{\frac{-\mu e^{i\beta}}{\left(re^{i\theta} - ce^{i\alpha}\right)}\right\} \\
&= \sin\theta\left\{\frac{\mu e^{i\beta} e^{i\theta}}{\left(re^{i\theta} - ce^{i\alpha}\right)^2}\right\} + \frac{\cos\theta}{r}\left\{\frac{\mu e^{i\beta} ire^{i\theta}}{\left(re^{i\theta} - ce^{i\alpha}\right)^2}\right\} \\
&= \frac{\mu e^{i\beta} e^{i\theta}}{\left(re^{i\theta} - ce^{i\alpha}\right)^2}\{\sin\theta + i\cos\theta\} \\
&= \frac{i\mu e^{i\beta}}{\left(re^{i\theta} - ce^{i\alpha}\right)^2}
\end{aligned}$$

$$= \left(\frac{\mu}{r^2}\right)\frac{ie^{-i(2\theta-\beta)}}{\left\{1-\frac{c}{r}e^{i(\alpha-\theta)}\right\}^2}$$

$$= \left(\frac{\mu}{a^2}\right)\frac{ie^{-i(2\theta-\beta)}}{\left\{1-\gamma e^{i(\alpha-\theta)}\right\}^2} \qquad (6.16)$$

where :

$$\frac{1}{1-\gamma e^{i(\alpha-\theta)}} = \frac{1-\gamma e^{i(\theta-\alpha)}}{\left\{1-\gamma e^{i(\alpha-\theta)}\right\}\left\{1-\gamma e^{-i(\alpha-\theta)}\right\}}$$

$$= \frac{1-\gamma e^{i(\theta-\alpha)}}{1-2\gamma\cos(\theta-\alpha)+\gamma^2} \qquad (6.17)$$

and

$$\gamma = \frac{c}{a} \qquad (6.18)$$

Similar mathematical expressions mentioned above can be derived further by

$$\left\{1-\gamma e^{i(\theta-\alpha)}\right\}^2 = \left\{1-2\gamma e^{i(\theta-\alpha)}+\gamma^2 e^{i2(\theta-\alpha)}\right\} \equiv \tilde{C}+i\tilde{D} \qquad (6.19)$$

where :

$$\tilde{C} = 1-2\gamma\cos(\theta-\alpha)+\gamma^2\cos 2(\theta-\alpha) \qquad (6.20a)$$

$$\tilde{D} = -2\gamma\sin(\theta-\alpha)+\gamma^2\sin 2(\theta-\alpha) \qquad (6.20b)$$

The first order derivatives of this complex velocity potential is then described as follows.

$$\frac{\partial f(z)}{\partial x} = \left(\frac{\mu}{a^2}\right)\frac{e^{-i(2\theta-\beta)}\left(\tilde{C}+i\tilde{D}\right)}{\left\{1-2\gamma\cos(\theta-\alpha)+\gamma^2\right\}^2}$$

$$= \left(\frac{\mu}{a^2}\right) \frac{\tilde{C} * \cos(2\theta - \beta) + \tilde{D} * \sin(2\theta - \beta)}{\left\{1 - 2\gamma\cos(\theta - \alpha) + \gamma^2\right\}^2} \qquad (6.21)$$

$$\frac{\partial f(z)}{\partial y} = \left(\frac{\mu}{a^2}\right) \frac{ie^{-i(2\theta-\beta)}\left(\tilde{C} + i\tilde{D}\right)}{\left\{1 - 2\gamma\cos(\theta - \alpha) + \gamma^2\right\}^2}$$

$$= \left(\frac{\mu}{a^2}\right) \frac{-\tilde{D} * \cos(2\theta - \beta) + \tilde{C} * \sin(2\theta - \beta)}{\left\{1 - 2\gamma\cos(\theta - \alpha) + \gamma^2\right\}^2} \qquad (6.22)$$

For the two rigidly held apart cylinders, the strength of the doublet is normalised by a^2 and the image point can be considered as an infinite series in the following form

$$f(z) = -a^2 \sum_{j=0}^{\infty} \left\{ \frac{\mu_j e^{i\beta_j}}{z - c_j e^{i\alpha}} + \frac{\mu'_j e^{i\beta'_j}}{z - c'_j e^{i\alpha}} \right\} \qquad (6.23)$$

The Eq. (6.19) can be written as

$$\frac{\partial f(z)}{\partial x} = \sum_{j=0}^{\infty} \left[\begin{array}{l} \mu_j \left\{ C_j \cos\left(2\theta - \beta_j\right) + D_j \sin\left(2\theta - \beta_j\right) \right\} \\ + \mu'_j \left\{ C'_j \cos\left(2\theta - \beta'_j\right) + D'_j \sin\left(2\theta - \beta'_j\right) \right\} \end{array} \right] \qquad (6.24)$$

$$\frac{\partial f(z)}{\partial y} = \sum_{j=0}^{\infty} \left[\begin{array}{l} \mu_j \left\{ -D_j \cos\left(2\theta - \beta_j\right) + C_j \sin\left(2\theta - \beta_j\right) \right\} \\ + \mu'_j \left\{ -D'_j \cos\left(2\theta - \beta'_j\right) + C'_j \sin\left(2\theta - \beta'_j\right) \right\} \end{array} \right] \qquad (6.25)$$

where :

$$C_j = F\left(\gamma_j\right) \quad , \quad D_j = G\left(\gamma_j\right) \qquad (6.26a)$$

$$C'_j = F\left(\gamma'_j\right) \quad , \quad D'_j = G\left(\gamma'_j\right) \qquad (6.26b)$$

$$\left[\begin{array}{c} F\left(\gamma_j\right) \\ G\left(\gamma_j\right) \end{array} \right] = \frac{\sum_{k=0}^{2} a_k \gamma_j^{\,k} \left[\begin{array}{c} \cos k(\theta - \alpha) \\ \sin k(\theta - \alpha) \end{array} \right]}{\left\{1 - 2\gamma_j \cos(\theta - \alpha) + \gamma_j^{\,2}\right\}^2} \qquad (6.27a)$$

$$a_0 = 1 \quad , \quad a_1 = -2 \quad , \quad a_2 = 1 \tag{6.27b}$$

Similarly the second order derivatives of the complex velocity potential with both x and y coordinates are derived as

$$\frac{\partial}{\partial x}\left\{\frac{\partial f(z)}{\partial x}\right\} = \frac{\partial^2 f(z)}{\partial x^2} \tag{6.28a}$$

$$= \cos\theta \frac{\partial}{\partial r}\left\{\frac{\mu e^{i\beta}}{\left(re^{i\theta} - ce^{i\alpha}\right)^2}\right\} - \frac{\sin\theta}{r}\frac{\partial}{\partial\theta}\left\{\frac{\mu e^{i\beta}}{\left(re^{i\theta} - ce^{i\alpha}\right)^2}\right\}$$

$$= \cos\theta\left\{\frac{-2\mu e^{i\beta}e^{i\theta}}{\left(re^{i\theta} - ce^{i\alpha}\right)^3}\right\} - \frac{\sin\theta}{r}\left\{\frac{-2\mu e^{i\beta} ire^{i\theta}}{\left(re^{i\theta} - ce^{i\alpha}\right)^3}\right\}$$

$$= \frac{-2\mu e^{i\beta}e^{i\theta}}{\left(re^{i\theta} - ce^{i\alpha}\right)^3}\{\cos\theta - i\sin\theta\}$$

$$= \frac{-2\mu e^{i\beta}}{\left(re^{i\theta} - ce^{i\alpha}\right)^3}$$

$$= -2\left(\frac{\mu}{r^3}\right)\frac{e^{-i(3\theta-\beta)}}{\left\{1 - \frac{c}{r}e^{i(\alpha-\theta)}\right\}^3}$$

$$= \frac{-2}{a}\left(\frac{\mu}{a^2}\right)\frac{e^{-i(3\theta-\beta)}\left\{1 - \gamma e^{i(\theta-\alpha)}\right\}^3}{\left\{1 - \gamma e^{i(\alpha-\theta)}\right\}^3\left\{1 - \gamma e^{i(\theta-\alpha)}\right\}^3}$$

$$= \frac{-2}{a}\left(\frac{\mu}{a^2}\right)\frac{e^{-i(3\theta-\beta)}\left\{1 - \gamma e^{i(\theta-\alpha)}\right\}^3}{\left\{1 - 2\gamma\cos(\theta-\alpha) + \gamma^2\right\}^3} \tag{6.28b}$$

and

$$\frac{\partial}{\partial y}\left\{\frac{\partial f(z)}{\partial x}\right\} = \frac{\partial^2 f(z)}{\partial y \partial x} \tag{6.29a}$$

$$= \sin\theta \frac{\partial}{\partial r}\left\{\frac{\mu e^{i\beta}}{\left(re^{i\theta} - ce^{i\alpha}\right)^2}\right\} + \frac{\cos\theta}{r}\frac{\partial}{\partial\theta}\left\{\frac{\mu e^{i\beta}}{\left(re^{i\theta} - ce^{i\alpha}\right)^2}\right\}$$

$$= \sin\theta\left\{\frac{-2\mu e^{i\beta}e^{i\theta}}{\left(re^{i\theta} - ce^{i\alpha}\right)^3}\right\} + \frac{\cos\theta}{r}\left\{\frac{-2\mu e^{i\beta} ire^{i\theta}}{\left(re^{i\theta} - ce^{i\alpha}\right)^3}\right\}$$

$$= \frac{-2\mu e^{i\beta}e^{i\theta}}{\left(re^{i\theta} - ce^{i\alpha}\right)^3}\{\sin\theta + i\cos\theta\}$$

$$= \frac{-2\mu e^{i\beta}e^{i\theta}}{\left(re^{i\theta} - ce^{i\alpha}\right)^3}\left\{e^{i\frac{\pi}{2}}e^{-i\theta}\right\}$$

$$= \frac{-2i\mu e^{i\beta}}{\left(re^{i\theta} - ce^{i\alpha}\right)^3}$$

$$= -2\left(\frac{\mu}{r^3}\right)\frac{ie^{-i(3\theta-\beta)}}{\left\{1-\frac{c}{r}e^{i(\alpha-\theta)}\right\}^3}$$

$$= \frac{-2}{a}\left(\frac{\mu}{a^2}\right)\frac{ie^{-i(3\theta-\beta)}\left\{1-\gamma e^{i(\theta-\alpha)}\right\}^3}{\left\{1-\gamma e^{i(\alpha-\theta)}\right\}^3\left\{1-\gamma e^{i(\theta-\alpha)}\right\}^3}$$

$$= \frac{-2}{a}\left(\frac{\mu}{a^2}\right)\frac{ie^{-i(3\theta-\beta)}\left\{1-\gamma e^{i(\theta-\alpha)}\right\}^3}{\left\{1-2\gamma\cos(\theta-\alpha)+\gamma^2\right\}^3} \qquad (6.29b)$$

and

$$\frac{\partial}{\partial y}\left\{\frac{\partial f(z)}{\partial y}\right\} = \frac{\partial^2 f(z)}{\partial y^2} \qquad (6.30a)$$

$$= \sin\theta\frac{\partial}{\partial r}\left\{\frac{i\mu e^{i\beta}}{\left(re^{i\theta} - ce^{i\alpha}\right)^2}\right\} + \frac{\cos\theta}{r}\frac{\partial}{\partial\theta}\left\{\frac{i\mu e^{i\beta}}{\left(re^{i\theta} - ce^{i\alpha}\right)^2}\right\}$$

$$= \sin\theta\left\{\frac{-2i\mu e^{i\beta}e^{i\theta}}{\left(re^{i\theta} - ce^{i\alpha}\right)^3}\right\} + \frac{\cos\theta}{r}\left\{\frac{-2i\mu e^{i\beta}ire^{i\theta}}{\left(re^{i\theta} - ce^{i\alpha}\right)^3}\right\}$$

$$= \frac{2\mu e^{i\beta}e^{i\theta}}{\left(re^{i\theta} - ce^{i\alpha}\right)^3}\{\cos\theta - i\sin\theta\}$$

$$= \frac{2\mu e^{i\beta}}{\left(re^{i\theta} - ce^{i\alpha}\right)^3}$$

$$= 2\left(\frac{\mu}{r^3}\right)\frac{e^{-i(3\theta-\beta)}}{\left\{1-\frac{c}{r}e^{i(\alpha-\theta)}\right\}^3}$$

$$= \frac{2}{a}\left(\frac{\mu}{a^2}\right)\frac{e^{-i(3\theta-\beta)}\left\{1-\gamma e^{i(\theta-\alpha)}\right\}^3}{\left\{1-\gamma e^{i(\alpha-\theta)}\right\}^3\left\{1-\gamma e^{i(\theta-\alpha)}\right\}^3}$$

$$= \frac{2}{a}\left(\frac{\mu}{a^2}\right)\frac{e^{-i(3\theta-\beta)}\left\{1-\gamma e^{i(\theta-\alpha)}\right\}^3}{\left\{1-2\gamma\cos(\theta-\alpha)+\gamma^2\right\}^3} \qquad (6.30b)$$

Similarly the expressions mentioned above is rewritten as

$$\left\{1-\gamma e^{i(\theta-\alpha)}\right\}^3 = 1 - 3\gamma e^{i(\theta-\alpha)} + 3\gamma^2 e^{i2(\theta-\alpha)} - \gamma^3 e^{i3(\theta-\alpha)}$$

$$\equiv \tilde{R} + i\tilde{S} \qquad (6.31)$$

where :

$$\tilde{R} = 1 - 3\gamma\cos(\theta-\alpha) + 3\gamma^2\cos 2(\theta-\alpha) - \gamma^3\cos 3(\theta-\alpha) \qquad (6.32a)$$

$$\tilde{S} = -3\gamma\sin(\theta-\alpha) + 3\gamma^2\sin 2(\theta-\alpha) - \gamma^3\sin 3(\theta-\alpha) \qquad (6.32b)$$

The mathematical expression for the second order derivatives of the complex velocity potential is written as

$$\frac{\partial^2 f(z)}{\partial x^2} = \frac{-2}{a}\left(\frac{\mu}{a^2}\right)\frac{e^{-i(3\theta-\beta)}\left(\tilde{R}+i\tilde{S}\right)}{\left\{1-2\gamma\cos(\theta-\alpha)+\gamma^2\right\}^3}$$
$$= \frac{-2}{a}\left(\frac{\mu}{a^2}\right)\frac{\tilde{R}*\cos(3\theta-\beta)+\tilde{S}*\sin(3\theta-\beta)}{\left\{1-2\gamma\cos(\theta-\alpha)+\gamma^2\right\}^3} \qquad (6.33)$$

and

$$\frac{\partial^2 f(z)}{\partial y \partial x} = \frac{-2}{a}\left(\frac{\mu}{a^2}\right)\frac{e^{-i(3\theta-\beta)}i\left(\tilde{R}+i\tilde{S}\right)}{\left\{1-2\gamma\cos(\theta-\alpha)+\gamma^2\right\}^3}$$
$$= \frac{-2}{a}\left(\frac{\mu}{a^2}\right)\frac{-\tilde{S}*\cos(3\theta-\beta)+\tilde{R}*\sin(3\theta-\beta)}{\left\{1-2\gamma\cos(\theta-\alpha)+\gamma^2\right\}^3} \qquad (6.34)$$

and

$$\frac{\partial^2 f(z)}{\partial y^2} = \frac{2}{a}\left(\frac{\mu}{a^2}\right)\frac{e^{-i(3\theta-\beta)}\left(\tilde{R}+i\tilde{S}\right)}{\left\{1-2\gamma\cos(\theta-\alpha)+\gamma^2\right\}^3}$$
$$= \frac{2}{a}\left(\frac{\mu}{a^2}\right)\frac{\tilde{R}*\cos(3\theta-\beta)+\tilde{S}*\sin(3\theta-\beta)}{\left\{1-2\gamma\cos(\theta-\alpha)+\gamma^2\right\}^3} \qquad (6.35)$$

For the two rigidly held apart cylinder system, the strength of the doublet is normalised by a^2 and the image point can be also presented as an infinite series in the following form

$$f(z) = -a^2\sum_{j=0}^{\infty}\left\{\frac{\mu_j e^{i\beta_j}}{z-c_j e^{i\alpha}} + \frac{\mu'_j e^{i\beta'_j}}{z-c'_j e^{i\alpha}}\right\} \qquad (6.36)$$

The mathematical description for the second order derivatives of the complex velocity potential of twin hulled marine vehicles in waves is obtained as

$$\frac{\partial^2 f(z)}{\partial x^2} = \frac{-2}{a}\sum_{j=0}^{\infty}\left[\begin{array}{l}\mu_j \dfrac{\tilde{R}_j\cos(3\theta-\beta_j)+\tilde{S}_j\sin(3\theta-\beta_j)}{\left\{1-2\gamma_j\cos(\theta-\alpha)+\gamma_j^2\right\}^3} \\ +\mu_j' \dfrac{\tilde{R}_j'\cos(3\theta-\beta_j')+\tilde{S}_j'\sin(3\theta-\beta_j')}{\left\{1-2\gamma_j'\cos(\theta-\alpha)+\gamma_j'^2\right\}^3}\end{array}\right] \qquad (6.37)$$

and

$$\frac{\partial^2 f(z)}{\partial y \partial x} = \frac{-2}{a}\sum_{j=0}^{\infty}\left[\begin{array}{l}\mu_j \dfrac{-\tilde{S}_j\cos(3\theta-\beta_j)+\tilde{R}_j\sin(3\theta-\beta_j)}{\left\{1-2\gamma_j\cos(\theta-\alpha)+\gamma_j^2\right\}^3} \\ +\mu_j' \dfrac{-\tilde{S}_j'\cos(3\theta-\beta_j')+\tilde{R}_j'\sin(3\theta-\beta_j')}{\left\{1-2\gamma_j'\cos(\theta-\alpha)+\gamma_j'^2\right\}^3}\end{array}\right] \qquad (6.38)$$

and

$$\frac{\partial^2 f(z)}{\partial y^2} = \frac{2}{a}\sum_{j=0}^{\infty}\left[\begin{array}{l}\mu_j \dfrac{\tilde{R}_j\cos(3\theta-\beta_j)+\tilde{S}_j\sin(3\theta-\beta_j)}{\left\{1-2\gamma_j\cos(\theta-\alpha)+\gamma_j^2\right\}^3} \\ +\mu_j' \dfrac{\tilde{R}_j'\cos(3\theta-\beta_j')+\tilde{S}_j'\sin(3\theta-\beta_j')}{\left\{1-2\gamma_j'\cos(\theta-\alpha)+\gamma_j'^2\right\}^3}\end{array}\right] \qquad (6.39)$$

where :

$$\tilde{R}_j = 1-3\gamma_j\cos(\theta-\alpha)+3\gamma_j^2\cos 2(\theta-\alpha)-\gamma_j^3\cos 3(\theta-\alpha) \qquad (6.40a)$$

$$\tilde{S}_j = -3\gamma_j\sin(\theta-\alpha)+3\gamma_j^2\sin 2(\theta-\alpha)-\gamma_j^3\sin 3(\theta-\alpha) \qquad (6.40b)$$

$$\tilde{R}_j' = 1-3\gamma_j'\cos(\theta-\alpha)+3\gamma_j'^2\cos 2(\theta-\alpha)-\gamma_j'^3\cos 3(\theta-\alpha) \qquad (6.40c)$$

$$\tilde{S}_j' = -3\gamma_j'\sin(\theta-\alpha)+3\gamma_j'^2\sin 2(\theta-\alpha)-\gamma_j'^3\sin 3(\theta-\alpha) \qquad (6.40d)$$

Based on the above formulations, as shown in Eqs. (6.37), (6.38) and (6.39), the theoretical expression of the second order derivatives of the velocity potential for cylinder L of the twin hulled marine vehicle due to forward speed effect in incident waves is deduced as

$$\frac{\partial^2 f(z)}{\partial x^2} = \frac{-2}{a}\sum_{j=0}^{\infty}\begin{bmatrix}\mu_j\{R_j\cos(3\theta-\beta_j)+S_j\sin(3\theta-\beta_j)\}\\ +\mu_j'\{R_j'\cos(3\theta-\beta_j')+S_j'\sin(3\theta-\beta_j')\}\end{bmatrix} \qquad (6.41)$$

and

$$\frac{\partial^2 f(z)}{\partial y \partial x} = \frac{-2}{a}\sum_{j=0}^{\infty}\begin{bmatrix}\mu_j\{-S_j\cos(3\theta-\beta_j)+R_j\sin(3\theta-\beta_j)\}\\ +\mu_j'\{-S_j'\cos(3\theta-\beta_j')+R_j'\sin(3\theta-\beta_j')\}\end{bmatrix} \qquad (6.42)$$

and

$$\frac{\partial^2 f(z)}{\partial y^2} = \frac{2}{a}\sum_{j=0}^{\infty}\begin{bmatrix}\mu_j\{R_j\cos(3\theta-\beta_j)+S_j\sin(3\theta-\beta_j)\}\\ +\mu_j'\{R_j'\cos(3\theta-\beta_j')+S_j'\sin(3\theta-\beta_j')\}\end{bmatrix} \qquad (6.43)$$

where :

$$R_j = M(\gamma_j) \quad , \quad S_j = N(\gamma_j) \qquad (6.44a)$$

$$R_j' = M(\gamma_j') \quad , \quad S_j' = N(\gamma_j') \qquad (6.44b)$$

$$\begin{bmatrix}M(\gamma_j)\\ N(\gamma_j)\end{bmatrix} = \frac{\sum_{k=0}^{3} c_k \gamma_j^k \begin{bmatrix}\cos k(\theta-\alpha)\\ \sin k(\theta-\alpha)\end{bmatrix}}{\{1-2\gamma_j\cos(\theta-\alpha)+\gamma_j^2\}^3} \qquad (6.45a)$$

$$c_0 = 1 \quad , \quad c_1 = -3 \quad , \quad c_2 = 3 \quad , \quad c_3 = -1 \qquad (6.45b)$$

Next the mathematical formulation of the second order derivatives of the

velocity potential for cylinder R of twin hulled marine vehicles under combined actions of wave and current is also derived. The necessary task to rewrite Eqs. (6.13) and (6.34) in the coordinate system with the origin at the centre of cylinder R only. The positions to the doublet are $c - c_j$ and $c - c_j'$ and it is sufficient if α is replaced by $(\alpha - \pi)$. The axis of the doublet is the same as β_j and β_j', in other words, the expression of γ_j and γ_j' are replaced by δ_j and δ_j'.

Here all the relations are written as

$$\delta_j = \frac{\tilde{c}}{b} = -\frac{1}{b}(c - c_j) = -\frac{1}{\varepsilon}(\gamma - \gamma_j) = \frac{1}{\varepsilon}(\gamma_j - \gamma) \qquad (6.46a)$$

$$\delta_j' = \frac{1}{\varepsilon}(\gamma_j' - \gamma) \qquad (6.46b)$$

$$\frac{\mu}{b^3} = \frac{1}{b}\cdot\frac{\mu}{b^2} = \left(\frac{1}{\varepsilon a}\right)\frac{1}{\varepsilon^2}\left(\frac{\mu}{a}\right) \qquad (6.47a)$$

$$\frac{\mu}{b^2} = \frac{\mu}{\varepsilon^2 a^2} = \frac{1}{\varepsilon^2}\left(\frac{\mu}{a^2}\right) \qquad (6.47b)$$

where :

For the $\varepsilon = 1$ case, it means that both left and right cylinders of the twin hulled marine structure have identical diameters.

6.3.2 Summary of mathematical approach for numerical computations

Here the detail of the mathematical expression of all the derivatives of complex velocity potentials for both cylinder L and cylinder R of twin hulled marine vehicle in incident waves are summarised. At first, the first order derivatives of velocity potential for cylinder L of twin hulled offshore structure in waves are expressed as

$$\frac{\partial f(z)^L}{\partial x} = \sum_{j=0}^{\infty} \begin{bmatrix} \mu_j \{ V_j \cos(2\theta - \beta_j) + W_j \sin(2\theta - \beta_j) \} \\ + \mu_j' \{ V_j' \cos(2\theta - \beta_j') + W_j' \sin(2\theta - \beta_j') \} \end{bmatrix} \quad (6.48)$$

$$\frac{\partial f(z)^L}{\partial y} = \sum_{j=0}^{\infty} \begin{bmatrix} \mu_j \{ -W_j \cos(2\theta - \beta_j) + V_j \sin(2\theta - \beta_j) \} \\ + \mu_j' \{ -W_j' \cos(2\theta - \beta_j') + V_j' \sin(2\theta - \beta_j') \} \end{bmatrix} \quad (6.49)$$

where :

$$V_j = F(\gamma_j) \quad , \quad W_j = G(\gamma_j) \quad (6.50a)$$

$$V_j' = F(\gamma_j') \quad , \quad W_j' = G(\gamma_j') \quad (6.50b)$$

$$\begin{bmatrix} F(\gamma_j) \\ G(\gamma_j) \end{bmatrix} = \frac{\sum_{k=0}^{2} a_k \gamma_j^{\,k} \begin{bmatrix} \cos k(\theta - \alpha) \\ \sin k(\theta - \alpha) \end{bmatrix}}{\{ 1 - 2\gamma_j \cos(\theta - \alpha) + \gamma_j^{\,2} \}^2} \quad (6.51a)$$

$$a_0 = 1 \quad , \quad a_1 = -2 \quad , \quad a_2 = 1 \quad (6.51b)$$

Second order derivatives of the velocity potential for cylinder L of twin hulled offshore structures in waves are also deduced as

$$\frac{\partial^2 f(z)^L}{\partial x^2} = \frac{-2}{a} \sum_{j=0}^{\infty} \begin{bmatrix} \mu_j \{ R_j \cos(3\theta - \beta_j) + S_j \sin(3\theta - \beta_j) \} \\ + \mu_j' \{ R_j' \cos(3\theta - \beta_j') + S_j' \sin(3\theta - \beta_j') \} \end{bmatrix} \quad (6.52)$$

$$\frac{\partial^2 f(z)^L}{\partial y \partial x} = \frac{-2}{a} \sum_{j=0}^{\infty} \begin{bmatrix} \mu_j \{ -S_j \cos(3\theta - \beta_j) + R_j \sin(3\theta - \beta_j) \} \\ + \mu_j' \{ -S_j' \cos(3\theta - \beta_j') + R_j' \sin(3\theta - \beta_j') \} \end{bmatrix} \quad (6.53)$$

$$\frac{\partial^2 f(z)^L}{\partial y^2} = \frac{2}{a} \sum_{j=0}^{\infty} \begin{bmatrix} \mu_j \{ R_j \cos(3\theta - \beta_j) + S_j \sin(3\theta - \beta_j) \} \\ + \mu_j' \{ R_j' \cos(3\theta - \beta_j') + S_j' \sin(3\theta - \beta_j') \} \end{bmatrix} \quad (6.54)$$

where :

$$R_j = M(\gamma_j) \quad , \quad S_j = N(\gamma_j) \tag{6.55a}$$

$$R'_j = M(\gamma'_j) \quad , \quad S'_j = N(\gamma'_j) \tag{6.55b}$$

$$\begin{bmatrix} M(\gamma_j) \\ N(\gamma_j) \end{bmatrix} = \frac{\sum_{k=0}^{3} c_k \gamma_j{}^k \begin{bmatrix} \cos k(\theta-\alpha) \\ \sin k(\theta-\alpha) \end{bmatrix}}{\left\{1 - 2\gamma_j \cos(\theta-\alpha) + \gamma_j^2\right\}^3} \tag{6.56a}$$

$$c_0 = 1 \quad , \quad c_1 = -3 \quad , \quad c_2 = 3 \quad , \quad c_3 = -1 \tag{6.56b}$$

Similarly the first order derivatives of the velocity potential for cylinder R of twin hulled offshore structures in waves are also described as

$$\frac{\partial f(z)^R}{\partial x} = \frac{1}{\varepsilon^2} \sum_{j=0}^{\infty} \begin{bmatrix} \mu_j \left\{ T_j \cos(2\theta - \beta_j) + U_j \sin(2\theta - \beta_j) \right\} \\ + \mu'_j \left\{ T'_j \cos(2\theta - \beta'_j) + U'_j \sin(2\theta - \beta'_j) \right\} \end{bmatrix} \tag{6.57}$$

$$\frac{\partial f(z)^R}{\partial y} = \frac{1}{\varepsilon^2} \sum_{j=0}^{\infty} \begin{bmatrix} \mu_j \left\{ -U_j \cos(2\theta - \beta_j) + T_j \sin(2\theta - \beta_j) \right\} \\ + \mu'_j \left\{ -U'_j \cos(2\theta - \beta'_j) + T'_j \sin(2\theta - \beta'_j) \right\} \end{bmatrix} \tag{6.58}$$

where :

$$T_j = F(\delta_j) \quad , \quad U_j = G(\delta_j) \tag{6.59a}$$

$$T'_j = F(\delta'_j) \quad , \quad U'_j = G(\delta'_j) \tag{6.59b}$$

$$\delta_j = \frac{\tilde{c}}{b} = -\frac{1}{b}(c - c_j) = -\frac{1}{\varepsilon}(\gamma - \gamma_j) = \frac{1}{\varepsilon}(\gamma_j - \gamma) \tag{6.60a}$$

$$\delta'_j = \frac{1}{\varepsilon}(\gamma'_j - \gamma) \tag{6.60b}$$

$$\begin{bmatrix} F(\delta_j) \\ G(\delta_j) \end{bmatrix} = \frac{\sum_{k=0}^{2} a_k \delta_j^{\,k} \begin{bmatrix} \cos k(\theta-\alpha) \\ \sin k(\theta-\alpha) \end{bmatrix}}{\left\{1-2\delta_j \cos(\theta-\alpha)+\delta_j^{\,2}\right\}^2} \qquad (6.61a)$$

$$a_0 = 1 \quad , \; a_1 = -2 \quad , \; a_2 = 1 \qquad (6.61b)$$

Second order derivatives of the velocity potential for cylinder R of the twin hulled offshore structure in waves are also deduced as

$$\frac{\partial^2 f(z)^R}{\partial x^2} = \frac{1}{\varepsilon^2}\left(\frac{-2}{a\varepsilon}\right)\sum_{j=0}^{\infty}\begin{bmatrix} \mu_j\left\{P_j \cos(3\theta-\beta_j)+Q_j \sin(3\theta-\beta_j)\right\} \\ +\mu_j'\left\{P_j' \cos(3\theta-\beta_j')+Q_j' \sin(3\theta-\beta_j')\right\} \end{bmatrix} \qquad (6.62)$$

$$\frac{\partial^2 f(z)^R}{\partial y \partial x} = \frac{1}{\varepsilon^2}\left(\frac{-2}{a\varepsilon}\right)\sum_{j=0}^{\infty}\begin{bmatrix} \mu_j\left\{-Q_j \cos(3\theta-\beta_j)+P_j \sin(3\theta-\beta_j)\right\} \\ +\mu_j'\left\{-Q_j' \cos(3\theta-\beta_j')+P_j' \sin(3\theta-\beta_j')\right\} \end{bmatrix} \qquad (6.63)$$

$$\frac{\partial^2 f(z)^R}{\partial y^2} = \frac{1}{\varepsilon^2}\left(\frac{2}{a\varepsilon}\right)\sum_{j=0}^{\infty}\begin{bmatrix} \mu_j\left\{P_j \cos(3\theta-\beta_j)+Q_j \sin(3\theta-\beta_j)\right\} \\ +\mu_j'\left\{P_j' \cos(3\theta-\beta_j')+Q_j' \sin(3\theta-\beta_j')\right\} \end{bmatrix} \qquad (6.64)$$

where :

$$P_j = M(\delta_j) \quad , \quad Q_j = N(\delta_j) \qquad (6.65a)$$

$$P_j' = M(\delta_j') \quad , \quad Q_j' = N(\delta_j') \qquad (6.65b)$$

$$\begin{bmatrix} M(\delta_j) \\ N(\delta_j) \end{bmatrix} = \frac{\sum_{k=0}^{3} c_k \delta_j^{\,k} \begin{bmatrix} \cos k(\theta-\alpha) \\ \sin k(\theta-\alpha) \end{bmatrix}}{\left\{1-2\delta_j \cos(\theta-\alpha)+\delta_j^2\right\}^3} \qquad (6.66a)$$

$$c_0 = 1 \quad , \quad c_1 = -3 \quad , \quad c_2 = 3 \quad , \quad c_3 = -1 \qquad (6.66b)$$

6.4 Investigation of numerical computations

The theoretical formulation of hydrodynamic restoring forces acting on twin hulled offshore structures in head and following waves by taking into consideration effects of forward speed and interactions between two hulls is derived in detail. The numerical accuracy of the damping coefficients is checked by direct pressure integration over the body boundary contours and by energy flux consideration in the infinite fluid. Nevertheless the accuracy of numerical solutions of the integral equation is improved by increasing the numbers of discrete elements and images of the dipoles.

Based on the direct Green function method, practical computations are carried out by taking the dipole image as ten ($N_I = 10$) and the discrete element of left and right cylinders as fifty ($N_E = N_L = N_R = 50$) on a twin hulled offshore structure for submergence depth ratio d/a = 2.0, separation distance ratio c/a = 4.0, Froude number Fn = 0.20 and no inclination in waves. The mathematical formulations of the coupled and uncoupled restoring coefficients due to the forward speed effect for the single cylinder and two cylinders cases in incident waves are derived theoretically. The predicted results of these hydrodynamic restoring coefficients due to forward speed effect (equivalent current effect) for the twin cylinder case by numerical computations are compared with those for the single cylinder case by analytical solutions and it is confirmed that both results for different separation distance, inclination, depths of submergence match well as in Table 6.1.

It can be found that if the separation distance between two cylinders is kept far away enough, computational discrepancies of hydrodynamic restoring coefficients between the single and two cylinder cases are insignificant. It means that the downstream cylinder is not influenced much by the flow field induced by the upstream cylinder. For the effect of submerged depth, no difference for different submerged depths can be easily realised for deeply submerged concept.

For numerical investigation of practical computations, both theoretical approaches are formulated to study motion responses of twin hulled ocean structures with and without hydrodynamic restoring terms due to forward speed effect under combined actions of wave and current and the detail of mathematical model is introduced in Chapter Four. In head wave condition, relative errors of damping coefficients for surge, heave and pitch modes show good agreement with those from previous researches such as Varyani (1988) and Wu (1992) et al and computed results lie within errors less than 0.1 % over the wave number range as shown in Figs. 6.1 to 6.3. The comparison of the CPU time between both approaches makes no much difference and is as in Fig. 6.4. The non-dimensionalized motion amplitudes for surge, heave and pitch motions with and without such restoring effects are as in Figs. 6.5 to 6.7. In particular slight discrepancy of motion responses in the low frequency region may be due to resonance.

In following wave condition, the relative errors of damping coefficients for surge, heave and pitch modes show good accuracy again and predicted results show errors less than 0.1 % over the wave number range as in Figs. 6.8 to 6.10. The CPU time calculated by the present approach shows a little bit more which is due to numerical computations of such hydrodynamic restoring forces due to forward speed effect and compared results are presented as in Fig. 6.11. The non-dimensionalized motion amplitudes for surge, heave and pitch motions with and without such restoring effects are as in Figs. 6.12 to 6.14. The restoring forces together with inertial forces due to mass and acceleration produce natural frequencies of those modes of motions. If the frequency of the wave excitation force is close to the natural frequency, the resonance occurs and it leads to significant influence of motions. Thus the slight discrepancy of motion responses at the low frequency region is similarly happened and it is confirmed that it is due to resonance.

6.5 Parametric studies and discussions

A parametric study is performed to investigate low frequency motion responses due to forward speed effect on twin hulled offshore vehicles for different submerged depths, Froude number, separation distance and inclinations in head and following waves. The detail results are categorised into two groups as follows.

(A) In head wave condition :

(a) For different Froude numbers :

The predicted results of motion responses for surge, heave and pitch amplitudes on twin hulled marine vehicles are as in Figs. 6.15 to 6.17 for different Froude numbers. Apparently if forward speed is getting higher, the peaks of dynamic motion responses in surge and heave modes after ka = 0.60 decrease dramatically and critical peaks also decrease and shift slightly.

(b) For different submergence depths :

Calculations of motion responses on twin hulled marine vehicles for surge, heave and pitch amplitudes are as in Figs. 6.18 to 6.20 for different submergence depths. Calculated results of dynamic motion amplitudes in surge, heave and pitch modes for deeper submergence ratio d/a = 4.0 show decreasing tendencies over the wave frequency range. Particularly the significant discrepancy of the critical peak in pitch motion may be due to hydrodynamic contributions from damping and restoring coefficients as discussed in Chapter Four.

(c) For different separation distances :

Predicted results of motion responses on twin hulled marine vehicles for. Surge, heave and pitch motion amplitudes are as in Figs. 6.21 to 6.23 for different separation distances. The discrepancies of the dynamic motion behaviour in surge, heave and pitch modes are clearly affected by the separation distance and when dynamic motion responses approach to zero point, it is clear that the wave

excitation forces acting on twin hulled offshore structures are compensated altogether.

(d) For different inclinations :

Calculated results of motion responses on twin hulled marine vehicles for surge, heave and pitch modes are as in Figs. 6.24 to 6.26 for different inclinations and numerical results show slight discrepancies. It is clear that the inclination is not significant enough to affect the hydrodynamic performance on submerged geometries of twin hulled offshore structures in waves.

(B) In following wave condition :

(a) For different Froude numbers :

The predicted results of motion responses on twin hulled marine vehicles for surge, heave and pitch modes are as in Figs. 6.27 to 6.29. If forward speed increases, the peaks of the dynamic motion responses in surge and heave modes when ka value is greater than 0.60 decrease dramatically and critical peaks also decrease and shift slightly. Particularly as Fn = 0.2 or 0.4, larger dynamic amplitude in pitch motion is noticed. In fact, it is noticed that the motion behaviour in following waves is rather different from that of head waves

(b) For different submergence depths :

Dynamic motion responses of twin hulled marine vehicles for surge, heave and pitch modes are as in Figs. 6.30 to 6.32 for different submergence depths. Calculations of motion amplitudes in surge, heave and pitch modes have significant peak at very low frequency point within ka = 0.40 and for deeper submergence of d/a = 4.0, they show decreasing tendencies with smaller amplitude over the wave frequency range. For deeper submergence depth, motion responses in surge and heave modes approach zero when wave number ka value is greater than 0.7 and pitch response has similar tendency at ka = 1.5. Particularly the discrepancy of the

critical peak in pitch motion may be affected by damping and restoring contributions and it is clear that the submergence depth effect is important.

(c) For different separation distances :

The predicted results of motion responses on twin hulled marine vehicles for surge, heave and pitch modes are as in Figs. 6.33 to 6.35 for different separation distances. The discrepancies of dynamic motion responses in surge, heave and pitch modes are due to the separation distance effect. When dynamic motion responses approach zero, the wave excitation forces acting on twin hulled offshore structures are compensated altogether and the detailed description of this hydrodynamic behaviour is discussed in Chapter Four. Calculated results for deeper submergence are presented for technical reference as in Figs. 6.36 to 6.38. For larger separation distance of c/a = 6.0, pitch motion responses in following waves show more significant magnitude than those in head waves at low frequency range within wave number ka = 0.4.

(d) For different inclinations :

Calculated results of motion responses on twin hulled marine vehicles for surge, heave and pitch modes are as in Figs. 6.39 to 6.41 for different inclinations. The predicted results show slight discrepancies for different inclinations. Calculated results for deeper submergence of d/a = 4.0, show the cross effect between submergence and separation distance as in Figs. 6.42 to 6.44. Similarly it is noticed that the inclination is not effective enough to dominate the hydrodynamic behaviour on submerged geometries of twin hulled marine structures in waves.

6.6 Conclusions

In principal, the mathematical formulation of the hydrodynamic restoring forces due to forward speed effect is theoretically derived for the two rigidly held

apart cylinders. The analytical solutions of such restoring coefficients due to forward speed effect for the single submerged cylinder are also worked out to confirm numerical computations of the two cylinder case.

Dynamic motion responses of twin hulled offshore structures in head and following waves are investigated by taking into consideration hydrodynamic restoring forces due to the effects of forward speed and interactions between two hulls and calculated results are compared. The non-dimensionalized motion amplitudes in surge, heave and pitch motions with and without such restoring forces due to effects of forward speed and interactions between two hulls are compared and discussed. In particular a slight discrepancy of motion responses by both theoretical approaches in the low frequency range may be due to resonance. The numerical accuracy of the damping coefficients checked by direct pressure integration and energy conservation relation is well satisfied and with errors less than 0.1 % in general.

A theoretical approach to predict dynamic motion responses of an inclined offshore structure in head waves with the hydrodynamic restoring terms due to forward speed effect has been proposed and is extended to calculate the dynamic motion responses in following waves. It is found that the hydrodynamic behaviour in following waves is more significant than in head waves. Such hydrodynamic restoring forces together with inertial forces due to mass and acceleration effects produce natural frequencies of those modes of dynamic motions. If the frequency of the wave excitation force is close to the natural frequency, the resonance occurs and it leads to large magnitude of motion. It is noted that the large amplitude of dynamic motions experienced by twin hulled offshore structures in low frequency range is due to the resonance.

CHAPTER 7
SECOND ORDER HYDRODYNAMIC FORCES

7.1 General description

When the body is moving into incident waves at a constant forward speed but not restrained in its oscillatory motions, the flow field surrounding the body may be described by the velocity potential in Eq. (2.2). $\xi_j e^{i\omega t}$ is the j mode motion of the body which can be obtained by solving the equations of motions in Eq. (4.18). In this situation the excess steady horizontal force acts on the body over the steady force which would act if it should move under a calm water. This excess force is of the second order with respect to the magnitude of the unsteady flow and is called as the added resistance of ships and the second order horizontal force for offshore structures.

In fact the second order velocity potentials satisfying the second order free surface condition and the second order body boundary condition have to be involved in numerical computations of second order hydrodynamic forces in general. However second order velocity potentials contain no steady part and in this case, only the square terms of the first order velocity potential presented in previous chapters contribute to second order steady forces (Ogilvie 1963).

The second order steady force acting in the horizontal direction can be calculated by the momentum flux concept, particularly evaluated far away, of the waves generated by the body. The average over a period of the momentum flux in the x direction through a vertical plane at the x position is expressed by the integral as

$$I_x = \overline{\int_{\eta_\omega}^{\infty} \left[P + \rho \left(\frac{\partial \Phi}{\partial x} \right)^2 \right] dy} \qquad (7.1)$$

where η_ω is the wave depression including the steady as well as unsteady parts. By Bernoulli's equation, the mathematical expression of hydrodynamic pressure P is written as

$$P = -\rho \left[\frac{\partial \Phi}{\partial t} + \frac{1}{2} \nabla \Phi \nabla \Phi - gy \right] + \frac{1}{2} \rho U^2 \qquad (7.2)$$

After substituting the expression in Eq. (2.2) for velocity potential Φ into Eq. (7.1), the terms associated only with respect to the steady velocity potential φ_S are excluded, as the excess steady force over the steady force due to the steady velocity potential φ_S are concerned here. Then the momentum flux can be written as

$$I_x = \overline{\int_{\zeta_\omega}^{\infty} \left[P + \rho \frac{\partial \phi_u}{\partial x} \left(\frac{\partial \phi_u}{\partial x} - U \right) \right] dy} - \rho U m_0 \qquad (7.3)$$

where the unsteady velocity potential including the time factor is denoted by $\phi_u = \mathrm{Re}\left(\phi e^{i\omega t} \right)$ as in Chapter Four. ζ_ω is the unsteady part of the wave depression which is given as in Eq. (4.23).

The hydrodynamic pressure of Eq. (7.3) must be the contribution associated with ϕ_u and written as

$$P = -\rho \left[\left(\frac{\partial \phi_u}{\partial t} - U \frac{\partial \phi_u}{\partial x} \right) + \frac{1}{2} \nabla \phi_u \nabla \phi_u - gy \right] \qquad (7.4)$$

m_0 in the last term of Eq. (7.3) is the average of the mass flux through the vertical plane at x position. Since this term does not contribute to second order forces as mentioned later, the term of $\rho U m_0$ is suppressed hereafter from the expression for the momentum flux I_x.

Now the mean value of the above integral of the momentum flux with the expression for ϕ_u and ζ_ω is evaluated. It should be noted that ϕ_u and ζ_ω and all its derivatives have zero mean values. In all the following computations, the second order terms with respect to ϕ_u are the only quantities required. I_x is then written as

$$I_x = \rho\int_0^{-\infty}\overline{\left[\left(\frac{\partial\phi_u}{\partial x}\right)^2 - \frac{1}{2}(\nabla\phi_u)^2\right]}dy + \rho\int_{\zeta_\omega}^{0}\overline{\left[-\frac{\partial\phi_u}{\partial t} + gy\right]}dy$$
$$= \frac{1}{2}\rho\int_0^{-\infty}\overline{\left[\left(\frac{\partial\phi_u}{\partial x}\right)^2 - \left(\frac{\partial\phi_u}{\partial y}\right)^2\right]}dy + \frac{\rho}{2g}\overline{\left(\frac{\partial\phi_u}{\partial t} - U\frac{\partial\phi_u}{\partial x}\right)}*\overline{\left(\frac{\partial\phi_u}{\partial t} + U\frac{\partial\phi_u}{\partial x}\right)}_{y=0} \tag{7.5}$$

The formula in Eq. (4.24) is used for transforming Eq. (7.5) into the expression in term of the velocity potential ϕ, then the final expression is written as

$$I_x = \frac{\rho}{4}\int_0^{-\infty}\left\{\frac{\partial\phi}{\partial x}\frac{\partial\phi^*}{\partial x} - \frac{\partial\phi}{\partial y}\frac{\partial\phi^*}{\partial y}\right\}dy + \frac{\rho}{4g}\left\{\omega^2\phi\phi^* - U^2\frac{\partial\phi}{\partial x}\frac{\partial\phi^*}{\partial x}\right\}_{y=0} \tag{7.6}$$

7.2 Description of second order horizontal forces in head waves

When incident waves are coming from ahead of the body (in head waves) with the encounter frequency ω, the velocity potential ϕ far upstream $x = +\infty$ is the sum of the velocity potential $(gA/i\omega_0)\varphi_I$ of the incident waves of the amplitude A and the velocity potential ϕ_2 of the k_2- wave of the amplitude A_2 where τ is smaller than 0.25 (referred to Eq. 2.42).

$$\phi = A\sqrt{\frac{g}{k_4}}e^{-k_4y+ik_4x} - A_2\sqrt{\frac{g}{k_2}}e^{-k_2y-ik_2x-i\delta_2}$$
$$= \frac{gA}{\omega - k_4U}e^{-k_4y+ik_4x-i\frac{\pi}{2}} - \frac{gA_2}{\omega + k_2U}e^{-k_2y-ik_2x-i\delta_2} \tag{7.7}$$

It should be noted that the wave number of the incident waves coincides with the wave number k_4 described by (2.37) at the encounter frequency ω in the head

wave conditions. As described in Chapter Two, the body moving at constant speed U in incident waves with encounter frequency ω have one of the wave numbers k_1, k_2, k_3 and k_4 necessarily. Only the k_4- wave is in the head wave. The second order line of Eq. (7.7) is obtained from the definition (2.37) of the wave numbers k_l (l = 1, 2, 3, 4).

By substituting Eq. (7.7) into Eq. (7.6), the momentum flux I_∞ at far ahead of the body can be described as

$$I_\infty = \frac{1}{4}\rho g\left\{ A^2 \frac{\omega + k_4 U}{\omega - k_4 U} + A_2{}^2 \frac{\omega - k_2 U}{\omega + k_2 U}\right\}$$
$$+\frac{\rho g A A_2}{(\omega + k_2 U)(\omega - k_4 U)}\left\{ g\frac{k_2 k_4}{k_2 - k_4} - \frac{1}{2}\left(\omega^2 + U^2 k_2 k_4\right)\right\}\cos\left\{(k_2 + k_4)x + \delta_2 - \frac{\pi}{2}\right\} \tag{7.8}$$

The cross terms of the incident waves and the k_2- wave in Eq. (7.8) are proved to be zero as follows and the reciprocals of k_l are easily obtained from their definitions in Eq. (2.37) as

$$\frac{1}{k_j} = \frac{g}{2\omega^2}\left\{1 - 2\tau \mp \sqrt{1 - 4\tau}\right\} \qquad j = \begin{pmatrix} 1 \\ 2 \end{pmatrix} \tag{7.9}$$

$$\frac{1}{k_l} = \frac{g}{2\omega^2}\left\{1 + 2\tau \mp \sqrt{1 + 4\tau}\right\} \qquad l = \begin{pmatrix} 3 \\ 4 \end{pmatrix} \tag{7.10}$$

Such mathematical relations can be combined to obtain

$$g\left(\frac{k_l k_j}{k_l + k_j} - \frac{U^2}{2g} k_l k_j\right) - \frac{1}{2}\omega^2 = \frac{1}{2\left(\frac{1}{k_l} + \frac{1}{k_j}\right)}\left\{2g - U^2\left(k_l + k_j\right)\right\} - \frac{1}{2}\omega^2 = 0 \tag{7.11}$$

and the cross terms of Eq. (7.8) are zero.

Finally the momentum flux I_{∞} in far upstream can be written as

$$I_{\infty} = \frac{1}{4}\rho g\left\{ A^2 \frac{\omega + k_4 U}{\omega - k_4 U} + A_2{}^2 \frac{\omega - k_2 U}{\omega + k_2 U} \right\}$$
$$= \frac{1}{4}\rho g\left\{ A^2\sqrt{1+4\tau} + A_2{}^2\sqrt{1-4\tau} \right\} \qquad (7.12)$$

The velocity potential ϕ far downstream $x = -\infty$ is the sum of the velocity potentials ϕ_1, ϕ_3 and ϕ_4 of the k_1-, k_3- and k_4- waves as presented in Eq. (2.42).

Their amplitudes are defined to be A_1, A_3 and A_4 respectively. The k_4-wave includes the incident waves as well as the waves generated by the body ; A_4 includes A as its component.

$$\phi = -A_1\sqrt{\frac{g}{k_1}}e^{-k_1 y - ik_1 x - i\delta_1} - A_3\sqrt{\frac{g}{k_3}}e^{-k_3 y + ik_3 x + i\delta_3} - A_4\sqrt{\frac{g}{k_4}}e^{-k_4 y + ik_4 x + i\delta_4}$$
$$= -\frac{gA_1}{\omega + k_1 U}e^{-k_1 y - ik_1 x - i\delta_1} + \frac{gA_3}{\omega - k_3 U}e^{-k_3 y + ik_3 x + i\delta_3} - \frac{gA_4}{\omega - k_4 U}e^{-k_4 y + ik_4 x + i\delta_4} \qquad (7.13)$$

With this expression substituted into Eq. (7.6), the momentum flux $I_{-\infty}$ far downstream is written as

$$I_{-\infty} = \frac{1}{4}\rho g\left[\frac{A_1{}^2}{(\omega + k_1 U)^2}(\omega^2 - U^2 k_1{}^2) + \frac{A_3{}^2}{(\omega - k_3 U)^2}(\omega^2 - U^2 k_3{}^2) + \frac{A_4{}^2}{(\omega - k_4 U)^2}(\omega^2 - U^2 k_4{}^2) \right]$$
$$+\rho g\left[\begin{array}{l} \dfrac{A_1 A_3}{(\omega + k_1 U)(\omega - k_3 U)}\left\{ g\dfrac{k_1 k_3}{k_1 - k_3} - \dfrac{1}{2}(\omega^2 + U^2 k_1 k_3) \right\} * \cos\{(k_1 + k_3)x + \delta_1 + \delta_3\} \\ \dfrac{A_1 A_4}{(\omega + k_1 U)(\omega - k_4 U)}\left\{ g\dfrac{k_1 k_4}{k_1 - k_4} - \dfrac{1}{2}(\omega^2 + U^2 k_1 k_4) \right\} * \cos\{(k_1 + k_4)x + \delta_1 + \delta_4\} \\ \dfrac{1}{2}\dfrac{A_3 A_4}{(\omega - k_3 U)(\omega - k_4 U)}(\omega^2 - U^2 k_3 k_4) * \cos\{(k_3 - k_4)x + \delta_3 - \delta_4\} \end{array} \right] \qquad (7.14)$$

The cross terms associated with A_1A_3 and A_1A_4 are once again zero and using the relation of Eq. (7.11). Another cross term in Eq.(7.14) is also zero since

the following relation is valid from the definition of k_3 and k_4.

$$U^2 k_3 k_4 = \frac{g^2}{4U^2} 4\tau^2 = \omega^2 \tag{7.15}$$

The momentum flux over a period going outward through the surfaces at $x = +\infty$ and $x = -\infty$, the body surface and the free surface enclosing a fluid domain must be zero. Accordingly as the momentum flux across the free surface is zero, the second order force $\overline{F}_1$ acting upon the body into the x direction can be expressed as

$$\overline{F}_1 = I_{-\infty} - I_{+\infty} \tag{7.16}$$

In deriving this expression, the mass flux term $\rho U m_0$ does not contribute to the solutions, because the mass flux appears in both $I_{-\infty}$ and $I_{+\infty}$ are equal in magnitude to satisfy the continuity equation in the fluid domain.

For further simplification of Eq. (7.16), the principle of energy conservation is applied. By substituting Eq. (7.7) into Eq. (4.25), the mean of the energy flux $R_{+\infty}$ across the vertical plane at $x = +\infty$, in almost identical manner to obtain Eq. (7.12), can be written as

$$R_{+\infty} = -\frac{1}{4}\rho g\omega\left\{\frac{A^2}{k_4}\sqrt{1+4\tau}\right\} + \frac{1}{4}\rho g\omega\left\{\frac{A_2^{\,2}}{k_2}\sqrt{1-4\tau}\right\} \tag{7.17}$$

The energy flux $R_{-\infty}$ through the vertical plane at $x = -\infty$ is derived in the same way as

$$R_{-\infty} = -\frac{\rho g A_1^{\,2}\omega}{4k_1}\sqrt{1-4\tau} + \frac{\rho g A_3^{\,2}\omega}{4k_3}\sqrt{1+4\tau} - \frac{\rho g A_4^{\,2}\omega}{4k_4}\sqrt{1+4\tau} \tag{7.18}$$

In the case of freely oscillating body in waves, no work is done by the body

against the fluid because no external force acts on the body except for the force, which does no work, keeping its mean position steadily in the fluid flow. It means that $R_{+\infty} - R_{-\infty}$ is zero and then the following relation is written

$$\left(A_4^2 - A^2\right)\sqrt{1+4\tau} = -k_4\left(\frac{A_1^2}{k_1} + \frac{A_2^2}{k_2}\right)\sqrt{1-4\tau} + k_4\frac{A_3^2}{k_3}\sqrt{1+4\tau} \tag{7.19}$$

Based on this relation, the expression of Eq. (7.16) for the second order horizontal force $\overline{F}_1$ can be simplified as

$$\overline{F}_1 = -\frac{1}{4}\rho g\left[\left\{\left(1+\frac{k_4}{k_1}\right)A_1^2 + \left(1+\frac{k_4}{k_2}\right)A_2^2\right\}\sqrt{1-4\tau} + \left(1-\frac{k_4}{k_3}\right)A_3^2\sqrt{1+4\tau}\right] \tag{7.20}$$

This expression clearly shows that the second order horizontal force $\overline{F}_1$ acts necessarily in the negative direction, in other words, the steady second order horizontal force in head waves is always resistance. If the k_1- and k_2- waves do not exist for τ larger than 0.25, the expression for this steady force $\overline{F}_1$ by setting A_1 and A_2 equal to zero.

Non-dimensionalized second order horizontal force (similar to the added resistance for ships) in head waves is written in terms of the Kochin functions of velocity potentials ϕ except incident waves as

$$\begin{aligned}\frac{R_{aw}}{\frac{1}{2}\rho g A^2} &= \frac{-\overline{F}_1}{\frac{1}{2}\rho g A^2} \\ &= \frac{1}{2}\left[\frac{\left|H^+(k_1)\right|^2}{\sqrt{1-4\tau}}\left(1+\frac{k_1}{k_4}\right) + \frac{\left|H^+(k_2)\right|^2}{\sqrt{1-4\tau}}\left(1+\frac{k_2}{k_4}\right) + \frac{\left|H^-(k_3)\right|^2}{\sqrt{1+4\tau}}\left(\frac{k_3}{k_4}-1\right)\right]\end{aligned} \tag{7.21}$$

7.3 Description of second order horizontal forces in following waves

The wave number of the following waves at encounter frequency ω should be identical to one of these wave numbers k_1, k_2 and k_3. When it coincides with a wave number k_1 or k_2, the following waves pass the structure ahead. This is the case that the phase speed C of the waves is higher than the body translating speed U. The phase speed of the following wave with the wave number k_3 is lower than the forward speed U and the waves in this case appear to propagate to the negative x direction from an observer fixed to the structure.

The mathematical expressions for the second order horizontal forces in following waves with each wave number are systematically described as follows.

(1) For wave number $k = k_1$ $(\frac{1}{2} \le \frac{U}{C} \le 1)$:

The velocity potential ϕ at $x = +\infty$, far ahead of the structure, is expressed as

$$\phi = \frac{gA}{\omega + k_1 U} e^{-k_1 y - ik_1 x - i\frac{\pi}{2}} - \frac{gA_2}{\omega + k_2 U} e^{-k_2 y - ik_2 x - i\delta_2} \qquad (7.22)$$

where the first term represents the following incident wave and the second one the disturbance. Apparently τ is smaller than 0.25 when the wave number of the following wave happens to agree with the wave number k_1.

In almost the same way, as Eq. (7.14) was derived, the momentum flux at $x = +\infty$ can be written as

$$\begin{aligned} I_{+\infty} &= \frac{1}{4}\rho g\left\{ A^2 \frac{\omega - k_1 U}{\omega + k_1 U} + {A_2}^2 \frac{\omega - k_2 U}{\omega + k_2 U} \right\} \\ &= \frac{1}{4}\rho g\left({A_2}^2 - A^2 \right)\sqrt{1 - 4\tau} \end{aligned} \qquad (7.23)$$

For far downstream case, the velocity potential has the same form as Eq. (7.13) excepting that A_1 instead of A_4 includes the incident waves of amplitude A. Therefore the momentum flux at $x = -\infty$ is written by the same expression as Eq. (7.14).

Then the mean second order horizontal force acting on the body can be written as

$$\begin{aligned}\overline{F}_1 &= I_{-\infty} - I_{+\infty} \\ &= -\frac{1}{4}\rho g\left[\left(A_1^2 + A_2^2 - A^2\right)\sqrt{1-4\tau} + \left(A_3^2 - A_4^2\right)\sqrt{1+4\tau}\right] \quad (7.24)\end{aligned}$$

By the principal of energy conservation, the following relation similar to Eq. (7.19) can be obtained as

$$\left(A_1^2 - A^2\right)\sqrt{1-4\tau} = -k_1\left(\frac{-A_3^2}{k_3} + \frac{A_4^2}{k_4}\right)\sqrt{1+4\tau} - k_1\frac{A_2^2}{k_2}\sqrt{1-4\tau} \quad (7.25)$$

When this relation is substituted into Eq. (7.24), a little more simplified expression for this second order force $\overline{F}_1$ can be expressed as

$$\overline{F}_1 = \frac{1}{4}\rho g\left[\left(\left(\frac{k_1}{k_2} - 1\right)A_2^2\sqrt{1-4\tau} + \left\{-\left(1+\frac{k_1}{k_3}\right)A_3^2 + \left(1+\frac{k_1}{k_4}\right)A_4^2\right\}\sqrt{1+4\tau}\right] \quad (7.26)$$

Then the normalized second order horizontal force can be described in terms of the Kochin functions as

$$\frac{\overline{F}_1}{\frac{1}{2}\rho g A^2} = \frac{1}{2}\left[-\frac{\left|H^+(k_2)\right|^2}{\sqrt{1-4\tau}}\left(1-\frac{k_2}{k_1}\right) + \frac{\left|H^-(k_3)\right|^2}{\sqrt{1+4\tau}}\left(1+\frac{k_3}{k_1}\right) - \frac{\left|H^-(k_4)\right|^2}{\sqrt{1+4\tau}}\left(1+\frac{k_4}{k_1}\right)\right] \quad (7.27)$$

(2). For wave number $k = k_2$ $(0 \le \frac{U}{C} \le \frac{1}{2})$:

The final expressions of this second order horizontal force $\overline{F}_1$ for the following cases are systematically expressed here to avoid the mathematical repetition since the derivation of the second order horizontal force is principally similar to that for the case of (1).

$$\overline{F}_1 = -\frac{1}{4}\rho g\left[\left(1-\frac{k_2}{k_1}\right)A_1^{\,2}\sqrt{1-4\tau}+\left\{\left(1+\frac{k_2}{k_3}\right)A_3^{\,2}-\left(1+\frac{k_2}{k_4}\right)A_4^{\,2}\right\}\sqrt{1+4\tau}\right] \tag{7.28}$$

and

$$\frac{\overline{F}_1}{\frac{1}{2}\rho g A^2} = \frac{1}{2}\left[\frac{\left|H^+(k_1)\right|^2}{\sqrt{1-4\tau}}\left(\frac{k_1}{k_2}-1\right)+\frac{\left|H^-(k_3)\right|^2}{\sqrt{1+4\tau}}\left(1+\frac{k_3}{k_2}\right)-\frac{\left|H^-(k_4)\right|^2}{\sqrt{1+4\tau}}\left(1+\frac{k_4}{k_2}\right)\right] \tag{7.29}$$

(3). For wave number $k = k_3$ $(\frac{U}{C} \ge 1)$:

The theoretical expressions of the second order horizontal force in following waves for this case are also written as follows.

$$\overline{F}_1 = -\frac{1}{4}\rho g\left[\left\{\left(1+\frac{k_3}{k_1}\right)A_1^{\,2}+\left(1+\frac{k_3}{k_2}\right)A_2^{\,2}\right\}\sqrt{1-4\tau}+\left(\frac{k_3}{k_4}-1\right)A_4^{\,2}\sqrt{1+4\tau}\right] \tag{7.30}$$

and

$$\frac{\overline{F}_1}{\frac{1}{2}\rho g A^2} = \frac{1}{2}\left[\frac{\left|H^+(k_1)\right|^2}{\sqrt{1-4\tau}}\left(1+\frac{k_1}{k_3}\right)+\frac{\left|H^+(k_2)\right|^2}{\sqrt{1-4\tau}}\left(1+\frac{k_2}{k_3}\right)+\frac{\left|H^-(k_4)\right|^2}{\sqrt{1+4\tau}}\left(1-\frac{k_4}{k_3}\right)\right] \tag{7.31}$$

It should be noted that in this case τ can be either larger or smaller than 0.25. When τ is larger than 0.25, both A_1 and A_2 in Eq. (7.30), the first and second terms of Eq. (7.31) should be ignored.

7.4 Theoretical formulation of second order hydrodynamic forces

In principal, the theoretical prediction of such second order forces acting on twin hulled offshore structures in both horizontal and vertical directions by direct pressure integration over the body boundary contours is rather difficult to calculate from mathematical expressions. Referring to the far field approach proposed by Lee and Newman (1971) for the zero speed problem, the momentum flux across the bottom part of the fluid domain must be calculated to obtain the second order vertical force acting on the structure, but this is not easier than the direct evaluation of the hydrodynamic pressure over the body surface. Moreover several practical formulae to predict second order vertical forces on the single submerged body in a calm wave proposed by Ogilvie (1963), Goodman (1965), Lee-Newman (1971), Numata (1978), Morrall (1978) and Atlar (1986) are also summarized in Appendix C. Here based on the near field concept, steady second order forces are computed by direct pressure integration over body boundary contours and the numerical algorithm for the prediction of second order horizontal and vertical forces on the structure, moving with a specific forward speed in incident waves but with its oscillatory motions suppressed, is completely formulated.

Here there is no radiation wave and the unsteady velocity potential $\phi_u = \mathrm{Re}\left(\phi e^{i\omega t}\right)$ are described as the summation of velocity potentials of incident waves and diffraction waves. The major efforts are concentrated on the excess forces over those due to steady velocity potential φ_S and the second order pressure with respect to velocity potential ϕ contributing to second order forces. Then the theoretical formulation of second order horizontal and vertical forces and clockwise pitch moments around the origin of the coordinate system Oxy by direct pressure integration over body boundary contours are derived in detail as follows.

$$\overline{F_j} = \frac{\rho}{2}\int_{S_H}\overline{\left[\left(\frac{\partial \phi_u}{\partial x}\right)^2 + \left(\frac{\partial \phi_u}{\partial y}\right)^2\right]} n_j \, ds$$

$$= \frac{\rho}{4}\int_{S_H}\left[\left(\frac{\partial \phi_u}{\partial x}\right)\left(\frac{\partial \phi_u}{\partial x}\right)^* + \left(\frac{\partial \phi_u}{\partial y}\right)\left(\frac{\partial \phi_u}{\partial y}\right)^*\right] n_j \, ds \qquad (7.32)$$

where j = 1 signifies the force into the x direction, j = 2 for the force into the y direction and j = 3 the moment.

The sum of incident wave potential $(gA/i\omega_0)\varphi_I$ of amplitude A and diffraction wave potential $(gA/i\omega_0)\varphi_D$ is substituted into velocity potential ϕ of Eq. (7.32), then the mathematical expression for the steady second order forces on the structure under the combined action of wave and current can be written as

$$\overline{F_j} = \frac{\rho g A^2}{4k}\int_{S_H}\left[\frac{\partial}{\partial x}(\varphi_I + \varphi_D)\frac{\partial}{\partial x}(\varphi_I^* + \varphi_D^*) + \frac{\partial}{\partial y}(\varphi_I + \varphi_D)\frac{\partial}{\partial y}(\varphi_I^* + \varphi_D^*)\right] n_j \, ds \qquad (7.33)$$

The expression of Eq. (7.33) looks simple, but in order to evaluate this integral, detail mathematical orthogonal properties are required to be used for numerical computation purposes.

7.5 Description of steady tilt moments due to steady second order forces

Here the detail formulation of steady tilt moments due to second order horizontal and vertical forces on twin hulled offshore structures under the combined action of wave and current will be completely derived by direct pressure integration over body boundary contours. At first as an example, the theoretical formulation of the second order horizontal forces acting on the structure is written as

$$\overline{F}_x = -\int_{S_H}\left[\overline{\rho\frac{\partial\Phi}{\partial x}\left(\frac{\partial\Phi}{\partial n} - Un_x\right) + Pn_x}\right]dl \qquad (7.34)$$

and the hydrodynamic pressure acting on the surface of the structure is written as

$$P = -\rho\left[\frac{\partial\Phi}{\partial x} - U\frac{\partial\Phi}{\partial x} + \frac{1}{2}\nabla\Phi\nabla\Phi\right] \qquad (7.35)$$

The mathematical expression of this second order horizontal force can then be derived as

$$\overline{F}_x = -\int_{S_H}\left[\rho\frac{\partial\Phi}{\partial x}\frac{\partial\Phi}{\partial n} - \rho U\frac{\partial\Phi}{\partial x}n_x - \rho\frac{\partial\Phi}{\partial x}n_x + \rho U\frac{\partial\Phi}{\partial x}n_x - \frac{1}{2}\rho\nabla\Phi\nabla\Phi n_x\right]dl \qquad (7.36)$$

By neglecting all the first order terms, the final expression of the second order steady forces is detailedly derived as follows.

$$\overline{F}_x = -\int_{S_H}\left[\rho\frac{\partial\Phi}{\partial x}\frac{\partial\Phi}{\partial n} - \frac{1}{2}\rho\nabla\Phi\nabla\Phi n_x\right]dl \qquad (7.37)$$

$$= -\int_{S_H}\left[\rho\frac{\partial\Phi}{\partial x}\left(\frac{\partial\Phi}{\partial x}n_x + \frac{\partial\Phi}{\partial y}n_y\right) - \frac{\rho}{2}\left\{\left(\frac{\partial\Phi}{\partial x}\right)^2 + \left(\frac{\partial\Phi}{\partial y}\right)^2\right\}n_x\right]dl$$

$$= -\int_{S_H}\left[\rho\frac{\partial\Phi}{\partial x}\frac{\partial\Phi}{\partial x}n_x + \rho\frac{\partial\Phi}{\partial x}\frac{\partial\Phi}{\partial y}n_y - \frac{\rho}{2}\left\{\left(\frac{\partial\Phi}{\partial x}\right)^2 + \left(\frac{\partial\Phi}{\partial y}\right)^2\right\}n_x\right]dl$$

$$= -\int_{S_H}\left[\begin{array}{l}\dfrac{\rho}{2}\dfrac{\partial\Phi}{\partial x}\dfrac{\partial\Phi^*}{\partial x}n_x + \dfrac{\rho}{4}\left(\dfrac{\partial\Phi}{\partial x}\dfrac{\partial\Phi^*}{\partial y} + \dfrac{\partial\Phi^*}{\partial x}\dfrac{\partial\Phi}{\partial y}\right)n_y \\ -\dfrac{\rho}{4}\left\{\dfrac{\partial\Phi}{\partial x}\dfrac{\partial\Phi^*}{\partial x} + \dfrac{\partial\Phi}{\partial y}\dfrac{\partial\Phi^*}{\partial y}\right\}n_x\end{array}\right]dl$$

$$= -\int_{S_H}\left[\frac{\rho}{4}\frac{\partial\Phi}{\partial x}\frac{\partial\Phi^*}{\partial x}n_x + \frac{\rho}{4}\left(\frac{\partial\Phi}{\partial x}\frac{\partial\Phi^*}{\partial y} + \frac{\partial\Phi^*}{\partial x}\frac{\partial\Phi}{\partial y}\right)n_y - \frac{\rho}{4}\frac{\partial\Phi}{\partial y}\frac{\partial\Phi^*}{\partial y}n_x\right]dl$$

$$= -\frac{\rho}{4}\frac{g^2A^2}{\omega_0^2}\int_{S_H}\left[\frac{\partial\Phi}{\partial x}\frac{\partial\Phi^*}{\partial x}n_x + \frac{\partial\Phi}{\partial x}\frac{\partial\Phi^*}{\partial y}n_y + \frac{\partial\Phi^*}{\partial x}\frac{\partial\Phi}{\partial y}n_y - \frac{\partial\Phi}{\partial y}\frac{\partial\Phi^*}{\partial y}n_x\right]dl \qquad (7.38)$$

and the non-dimensionalized form of the second order horizontal force acting on

the structure is described as

$$\frac{\overline{F}_x}{\frac{1}{2}\rho g A^2} = -\frac{1}{2k_0}\int_{S_H}\left[\frac{\partial\Phi}{\partial x}\frac{\partial\Phi^*}{\partial x}n_x + \frac{\partial\Phi}{\partial x}\frac{\partial\Phi^*}{\partial y}n_y + \frac{\partial\Phi^*}{\partial x}\frac{\partial\Phi}{\partial y}n_y - \frac{\partial\Phi}{\partial y}\frac{\partial\Phi^*}{\partial y}n_x\right]dl \tag{7.39}$$

In the same way, the generalized expression of the second order horizontal and vertical forces acting on the structure is expressed as follows.

$$\begin{aligned}\overline{F}_j &= -\int_{S_H}\overline{P}n_j dl \qquad (7.40)\\ &= \frac{\rho}{2}\int_{S_H}\overline{\nabla\Phi\nabla\Phi}n_j dl\\ &= \frac{\rho}{2}\int_{S_H}\overline{\left[\left(\frac{\partial\varphi}{\partial x}\right)^2+\left(\frac{\partial\varphi}{\partial y}\right)^2\right]}n_j dl\\ &= \frac{\rho}{4}\mathrm{Re}\int_{S_H}\left(\frac{\partial\varphi}{\partial x}\frac{\partial\varphi^*}{\partial x}+\frac{\partial\varphi}{\partial y}\frac{\partial\varphi^*}{\partial y}\right)n_j dl \qquad (7.41)\end{aligned}$$

The sum of the incident wave potential $(gA/i\omega_0)\varphi_I$ and diffraction wave potential $(gA/i\omega_0)\varphi_D$ is substituted into the velocity potential ϕ of Eq. (7.41). The mathematical expression for the steady second order forces acting on the structure at a constant forward speed in incident waves is rewritten as

$$F_j = \frac{\rho}{4}\mathrm{Re}\int_{S_H}\left[\begin{array}{l}\left(\frac{\partial\varphi_D}{\partial x}+\frac{\partial\varphi_I}{\partial x}\right)\left(\frac{\partial\varphi_D^*}{\partial x}+\frac{\partial\varphi_I^*}{\partial x}\right)\\ +\left(\frac{\partial\varphi_D}{\partial y}+\frac{\partial\varphi_I}{\partial y}\right)\left(\frac{\partial\varphi_D^*}{\partial y}+\frac{\partial\varphi_I^*}{\partial y}\right)\end{array}\right]n_j dl \tag{7.42}$$

$$F_j = \frac{1}{4}\frac{\rho g^2 A^2}{\omega_0^2}\int_{S_H}\left[\begin{array}{l}\left(\frac{\partial\varphi_D}{\partial x}+\frac{\partial\varphi_I}{\partial x}\right)\left(\frac{\partial\varphi_D^*}{\partial x}+\frac{\partial\varphi_I^*}{\partial x}\right)\\ +\left(\frac{\partial\varphi_D}{\partial y}+\frac{\partial\varphi_I}{\partial y}\right)\left(\frac{\partial\varphi_D^*}{\partial y}+\frac{\partial\varphi_I^*}{\partial y}\right)\end{array}\right]n_j dl \tag{7.43}$$

and the non-dimensionalized form of the second order forces is written as

$$\frac{F_j}{\frac{1}{2}\rho g A^2} = \frac{1}{2k_0}\int_{S_H}\left[\begin{array}{l}\left(\frac{\partial\varphi_D}{\partial x}+\frac{\partial\varphi_I}{\partial x}\right)\left(\frac{\partial\varphi_D^*}{\partial x}+\frac{\partial\varphi_I^*}{\partial x}\right)\\ +\left(\frac{\partial\varphi_D}{\partial y}+\frac{\partial\varphi_I}{\partial y}\right)\left(\frac{\partial\varphi_D^*}{\partial y}+\frac{\partial\varphi_I^*}{\partial y}\right)\end{array}\right]n_j dl \qquad (7.44)$$

where :

$$\phi_I = \frac{gA}{i\omega}e^{-ky\pm ikx} = \frac{gA}{i\omega}e^{-k(y\mp ix)} = \frac{gA}{i\omega}\varphi_I \qquad (7.45)$$

$$\phi_I^* = -\frac{gA}{i\omega}e^{-ky\mp ikx} = -\frac{gA}{i\omega}e^{-k(y\pm ix)} = -\frac{gA}{i\omega}\varphi_I^* \qquad (7.46)$$

$$\phi_D = \frac{gA}{i\omega}\varphi_D \qquad (7.47)$$

$$\phi_D^* = -\frac{gA}{i\omega}\varphi_D^* \qquad (7.48)$$

All the derivatives of incident wave potential is then expressed as follows.

$$\frac{\partial\varphi_I}{\partial x} = \pm ike^{-k(y\mp ix)} \qquad (7.49)$$

$$\frac{\partial\varphi_I}{\partial y} = -ke^{-k(y\mp ix)} \qquad (7.50)$$

$$\frac{\partial\varphi_I^*}{\partial x} = \mp ike^{-k(y\pm ix)} \qquad (7.51)$$

$$\frac{\partial\varphi_I^*}{\partial y} = -ke^{-k(y\pm ix)} \qquad (7.52)$$

Here the formulation of second order horizontal and vertical forces acting on the left body of the twin hulled marine vehicle taking into consideration the effects of forward speed and interactions between two hulls are presented as

$$\frac{F_j^L}{\frac{1}{2}\rho g A^2} = \frac{1}{2k_0}\int_{S_L}\left[\begin{array}{l}\left(\frac{\partial\varphi_D}{\partial x}+\frac{\partial\varphi_I}{\partial x}\right)\left(\frac{\partial\varphi_D^*}{\partial x}+\frac{\partial\varphi_I^*}{\partial x}\right)\\ +\left(\frac{\partial\varphi_D}{\partial y}+\frac{\partial\varphi_I}{\partial y}\right)\left(\frac{\partial\varphi_D^*}{\partial y}+\frac{\partial\varphi_I^*}{\partial y}\right)\end{array}\right]n_j dl \quad (\text{for } j = 1, 2) \tag{7.53}$$

where :

$$\varphi_I = \varphi_I^L + \varphi_I^R \tag{7.54}$$

$$\varphi_D = \varphi_D^L + \varphi_D^R \tag{7.55}$$

Here the derivatives of the incident velocity potential with respect to both horizontal and vertical directions for left and right bodies of twin hulled marine vehicles are written as follows.

$$\frac{\partial\varphi_I}{\partial x} = \frac{\partial\varphi_I^L}{\partial x} + \frac{\partial\varphi_I^R}{\partial x} \tag{7.56}$$

$$\frac{\partial\varphi_I}{\partial y} = \frac{\partial\varphi_I^L}{\partial y} + \frac{\partial\varphi_I^R}{\partial y} \tag{7.57}$$

$$\frac{\partial\varphi_I^*}{\partial x} = \frac{\partial\varphi_I^{*L}}{\partial x} + \frac{\partial\varphi_I^{*R}}{\partial x} \tag{7.58}$$

$$\frac{\partial\varphi_I^*}{\partial y} = \frac{\partial\varphi_I^{*L}}{\partial y} + \frac{\partial\varphi_I^{*R}}{\partial y} \tag{7.59}$$

and similarly the diffraction velocity potential is obtained as

$$\frac{\partial\varphi_D}{\partial x} = \frac{\partial\varphi_D^L}{\partial x} + \frac{\partial\varphi_D^R}{\partial x} \tag{7.60}$$

$$\frac{\partial\varphi_D}{\partial y} = \frac{\partial\varphi_D^L}{\partial y} + \frac{\partial\varphi_D^R}{\partial y} \tag{7.61}$$

$$\frac{\partial \varphi_D^*}{\partial x} = \frac{\partial \varphi_D^{*L}}{\partial x} + \frac{\partial \varphi_D^{*R}}{\partial x} \tag{7.62}$$

$$\frac{\partial \varphi_D^*}{\partial y} = \frac{\partial \varphi_D^{*L}}{\partial y} + \frac{\partial \varphi_D^{*R}}{\partial y} \tag{7.63}$$

In principal, the theoretical formulation of the diffracted wave potential for the body is derived as follows.

$$\phi = -2\int_{S_H}\left(\frac{\partial \phi}{\partial n} - \phi\frac{\partial}{\partial n}\right)T ds \tag{7.64}$$

$$\begin{aligned} &= -2\int_{S_H}\frac{\partial \phi}{\partial n}T ds + 2\int_{S_H}\phi\frac{\partial}{\partial n}T ds \\ &= -2\int_{S_H}\frac{\partial \phi}{\partial n}T ds + 2\int_{S_H}\phi\frac{\partial}{\partial s}U ds \\ &= -2\int_{S_H}\frac{\partial \phi}{\partial n}T ds + 2\phi\int_{S_H} dU \\ &= -2\int_{S_H}\frac{\partial \phi}{\partial n}T ds + 2\phi U\Big|_j^{j+1} \end{aligned} \tag{7.65}$$

where :

$$\frac{\partial T}{\partial n} = \frac{dU}{ds} \tag{7.66}$$

In compliance with the relations between both velocity potential and stream function in the fluid flow, the equations are written as follows.

$$\frac{dx}{dn} = -\frac{dy}{ds} = \frac{dx}{dG} = -\frac{dy}{d\psi} \tag{7.67}$$

and

$$\frac{dG}{dn}ds = \frac{d\psi}{ds}ds = d\psi \tag{7.68}$$

The relation can then be obtained as

$$\frac{dG}{d\xi} = \frac{d\psi}{d\eta} \tag{7.69}$$

and

$$\frac{dG}{d\xi} d\eta = d\psi \tag{7.70}$$

All the derivatives in the equation of the diffracted wave potential are completely worked out and detailedly described as follows. The derivative of the diffracted wave potential in terms of the Green function with respect to the x direction is written as

$$T_x = \frac{\partial G}{\partial x} = -\frac{1}{2\pi}\left[\frac{(x-\xi)}{(x-\xi)^2+(y-\eta)^2} - \frac{(x-\xi)}{(x-\xi)^2+(y+\eta)^2} + \frac{K_0(-i)}{(k_1-k_2)}\{k_1S_1 - k_2S_2\} + \frac{K_0(i)}{(k_3-k_4)}\{k_3S_3 - k_4S_4\}\right] \tag{7.71}$$

The derivative of the diffracted wave potential in terms of the Green function with respect to the y direction is also written as

$$T_y = \frac{\partial G}{\partial y} = -\frac{1}{2\pi}\left[\frac{(y-\eta)}{(x-\xi)^2+(y-\eta)^2} - \frac{(y-\eta)}{(x-\xi)^2+(y+\eta)^2} + \frac{K_0(-1)}{(k_1-k_2)}\{k_1S_1 - k_2S_2\} + \frac{K_0(-1)}{(k_3-k_4)}\{k_3S_3 - k_4S_4\}\right] \tag{7.72}$$

In the same way, the second order derivative of the wave diffraction potential with respect to the x direction is also derived as

$$\frac{dT_x}{\partial x} = -\frac{1}{2\pi}\left[\begin{array}{l}\dfrac{\left[(x-\xi)^2+(y-\eta)^2\right](1)}{\left[(x-\xi)^2+(y-\eta)^2\right]^2} - \dfrac{2(x-\xi)^2}{\left[(x-\xi)^2+(y-\eta)^2\right]^2} \\ -\left\{\dfrac{\left[(x-\xi)^2+(y+\eta)^2\right](1)}{\left[(x-\xi)^2+(y+\eta)^2\right]^2} - \dfrac{2(x-\xi)^2}{\left[(x-\xi)^2+(y+\eta)^2\right]^2}\right\} \\ +\dfrac{K_0(-i)(-ik)}{(k_1-k_2)}\{k_1S_1-k_2S_2\} + \dfrac{K_0(i)(ik)}{(k_3-k_4)}\{k_3S_3-k_4S_4\}\end{array}\right]$$

$$= -\frac{1}{2\pi}\left[\begin{array}{l}\dfrac{1}{(x-\xi)^2+(y-\eta)^2} - \dfrac{2(x-\xi)^2}{\left[(x-\xi)^2+(y-\eta)^2\right]^2} \\ -\left\{\dfrac{1}{(x-\xi)^2+(y+\eta)^2} - \dfrac{2(x-\xi)^2}{\left[(x-\xi)^2+(y+\eta)^2\right]^2}\right\} \\ +\dfrac{K_0(-k)}{(k_1-k_2)}\{k_1S_1-k_2S_2\} + \dfrac{K_0(-k)}{(k_3-k_4)}\{k_3S_3-k_4S_4\}\end{array}\right] \tag{7.73}$$

Finally these expression are detailedly presented as follows.

$$\frac{dT_x}{dx}dy = -\frac{1}{2\pi}\left[\begin{array}{l}\dfrac{1}{(x-\xi)}\tan^{-1}\left(\dfrac{y-\eta}{x-\xi}\right) - 2(x-\xi)^2\left\{\dfrac{(y-\eta)}{2(x-\xi)^2\left[(x-\xi)^2+(y-\eta)^2\right]} + \dfrac{1}{2(x-\xi)^2(x-\xi)}\tan^{-1}\left(\dfrac{y-\eta}{x-\xi}\right)\right\} \\ -\left\{\dfrac{1}{(x-\xi)}\tan^{-1}\left(\dfrac{y+\eta}{x-\xi}\right) - 2(x-\xi)^2\left\{\dfrac{(y+\eta)}{2(x-\xi)^2\left[(x-\xi)^2+(y+\eta)^2\right]} + \dfrac{1}{2(x-\xi)^2(x-\xi)}\tan^{-1}\left(\dfrac{y+\eta}{x-\xi}\right)\right\}\right\} \\ +\dfrac{K_0}{(k_1-k_2)}\dfrac{(-k)}{(-k)}\{k_1S_1-k_2S_2\} + \dfrac{K_0}{(k_3-k_4)}\dfrac{(-k)}{(-k)}\{k_3S_3-k_4S_4\}\end{array}\right]$$

$$= -\frac{1}{2\pi}\left[\begin{array}{l}\left\{\frac{1}{(x-\xi)}\tan^{-1}\left(\frac{y-\eta}{x-\xi}\right)-\frac{(y-\eta)}{\left[(x-\xi)^2+(y-\eta)^2\right]}-\frac{1}{(x-\xi)}\tan^{-1}\left(\frac{y-\eta}{x-\xi}\right)\right\} \\ -\left\{\frac{1}{(x-\xi)}\tan^{-1}\left(\frac{y+\eta}{x-\xi}\right)-\frac{(y+\eta)}{\left[(x-\xi)^2+(y+\eta)^2\right]}-\frac{1}{(x-\xi)}\tan^{-1}\left(\frac{y+\eta}{x-\xi}\right)\right\} \\ +\frac{K_0}{(k_1-k_2)}\{k_1S_1-k_2S_2\}+\frac{K_0}{(k_3-k_4)}\{k_3S_3-k_4S_4\}\end{array}\right]$$

$$= -\frac{1}{2\pi}\left[\begin{array}{l}\left\{-\frac{(y-\eta)}{\left[(x-\xi)^2+(y-\eta)^2\right]}\right\}-\left\{-\frac{(y+\eta)}{\left[(x-\xi)^2+(y+\eta)^2\right]}\right\} \\ +\frac{K_0}{(k_1-k_2)}\{k_1S_1-k_2S_2\}+\frac{K_0}{(k_3-k_4)}\{k_3S_3-k_4S_4\}\end{array}\right] \quad (7.74)$$

By the mathematical technique of the coordinate transformation, the expression is rewritten as

$$\frac{dT_x}{d\xi}d\eta = -\frac{1}{2\pi}\left[\begin{array}{l}-\frac{(y-\eta)}{\left[(x-\xi)^2+(y-\eta)^2\right]}-\frac{(y+\eta)}{\left[(x-\xi)^2+(y+\eta)^2\right]} \\ -\frac{K_0}{(k_1-k_2)}\{k_1S_1-k_2S_2\}-\frac{K_0}{(k_3-k_4)}\{k_3S_3-k_4S_4\}\end{array}\right]$$

$$= \frac{1}{2\pi}\left[\begin{array}{l}\frac{(y-\eta)}{\left[(x-\xi)^2+(y-\eta)^2\right]}+\frac{(y+\eta)}{\left[(x-\xi)^2+(y+\eta)^2\right]} \\ +\frac{K_0}{(k_1-k_2)}\{k_1S_1-k_2S_2\}+\frac{K_0}{(k_3-k_4)}\{k_3S_3-k_4S_4\}\end{array}\right] \quad (7.75)$$

Similarly the following equation is also obtained as

$$\frac{dT_y}{d\xi}d\eta = -\frac{1}{2\pi}\left[\begin{array}{l}\frac{(x-\xi)}{\left[(x-\xi)^2+(y-\eta)^2\right]}+\frac{(x-\xi)}{\left[(x-\xi)^2+(y+\eta)^2\right]} \\ +\frac{iK_0}{(k_1-k_2)}\{k_1S_1-k_2S_2\}+\frac{(-i)K_0}{(k_3-k_4)}\{k_3S_3-k_4S_4\}\end{array}\right]$$

$$= -\frac{1}{2\pi}\left[\frac{(x-\xi)}{\left[(x-\xi)^2+(y-\eta)^2\right]}+\frac{(x-\xi)}{\left[(x-\xi)^2+(y+\eta)^2\right]}\right.$$
$$\left.+i\left[\frac{K_0}{(k_1-k_2)}\{k_1S_1-k_2S_2\}-\frac{K_0}{(k_3-k_4)}\{k_3S_3-k_4S_4\}\right]\right] \tag{7.76}$$

In order to make such theoretical derivations possible, certain mathematical formulae for function derivatives and integrations are also summarized here as follows.

$$d\left(\frac{u}{v}\right)=\frac{vdu-udv}{v^2} \tag{7.77}$$

$$\int\frac{dx}{x^2+a^2}=\frac{1}{a}\tan^{-1}\frac{x}{a} \tag{7.78}$$

$$\int\frac{dx}{\left(x^2+a^2\right)^2}=\frac{x}{2a^2\left(x^2+a^2\right)}+\frac{1}{2a^3}\tan^{-1}\frac{x}{a} \tag{7.79}$$

Finally total second order horizontal and vertical forces and steady tilt moments due to second order horizontal and vertical forces, taking into consideration the effects of forward speed (equivalent current speed) and interactions between two hulls, are written as follows.

$$R_j=R_j^{\,L}+R_j^{\,R} \qquad (\text{for } j=1,2) \tag{7.80}$$

$$R_j=\left\{R_2^{\,L}(1\cos\alpha)-R_1^{\,L}(1\sin\alpha)-R_2^{\,R}(1\cos\alpha)+R_1^{\,R}(1\sin\alpha)\right\}$$
$$(\text{for } j=3) \tag{7.81}$$

and the non-dimensionalized expression of the steady tilt moments due to both second order horizontal and vertical forces acting on the left and right bodies of the twin hulled offshore structure is written as

$$\frac{R_3}{\frac{1}{2}\rho g A^2 l} \equiv \left\{\left(R_2{}^L - R_2{}^R\right)\cos\alpha - \left(R_1{}^L - R_1{}^R\right)\sin\alpha\right\} \qquad (7.82)$$

where :

α is the inclining angle of the two rigidly held apart bodies system. The non-dimensionalized second order horizontal and vertical forces are respectively written as

$$R_1 \equiv \frac{\bar{F}_1}{\frac{1}{2}\rho g A^2} \qquad (7.83)$$

$$R_2 \equiv \frac{\bar{F}_2}{\frac{1}{2}\rho g A^2} \qquad (7.84)$$

7.6 Investigation of numerical computations

The numerical accuracy of the second order hydrodynamic problems for twin hulled offshore structures is achieved by analytically solving the logarithmic part of the Green function. For the twin cylinders case as shown in Fig. 4.1, the detail of both numerical techniques, the discrete source distribution method and direct Green function approach, to solve the classical integral equation and analytical solution of the logarithmic part of the Green function will be discussed in Chapter Eight.

By solving the diffraction velocity potential, the second order horizontal and vertical forces acting on twin hulled offshore structures are predicted by direct pressure integration over the body boundary contours exactly. For the second order force in horizontal direction, theoretical formulations of both direct pressure integration (near field approach) and momentum flux consideration in terms of the Kochin functions (far field approach) are derived in detail and calculated results are also compared to confirm numerical accuracy. For the second order vertical force in

the vertical direction, comparison studies of both theoretical methods such as the direct pressure integration and Lee-Newman (1971) approach for the non-forward speed case are carried out to check numerical computations.

Numerical computations in Table 7.1 and 7.2 are for a twin hulled offshore structure model with submergence depth ratio d/a = 2.0, separation distance ratio c/a = 4.0, no tilt in head waves and for different Froude numbers. The computations were performed by taking the image number as ten (10) and discretized element number of both left and right cylinders as fifty (50). Numerical results of second order horizontal forces by both theoretical near field and far field approaches are compared and good agreement are also obtained as indicated in Table 7.1. The second order horizontal forces are of very small magnitude and are found not to make much difference, so the accuracy of numerical solutions is quite satisfactory.

As for the second order vertical forces, the numerical results of second order vertical forces, proposed by Lee-Newman (1971), on twin hulled marine structures with submergence depth ratio d/a = 2.0, separation distance ratio c/a = 4.0 and no tilt in a calm water are detailedly presented in Fig. 7.1 and the detail mathematical model to calculate such second order vertical forces is also described in Appendix C. The numerical accuracy check of the second order vertical forces by both theoretical approaches is performed for two different submergence depth ratio, i.e. d/a = 2.0 and 4.0 respectively. Here the CPU time for both computations is compared as in Fig. 7.2 and calculated results for accuracy check confirm reasonable agreement as in Figs. 7.3 and 7.4. Slight discrepancies as in Table 7.2 are due to the fact that Lee-Newman (1971) approach does not take into consideration the effects of forward speed and interactions between two submerged hulls.

7.7 Parametric studies and discussions

The parametric studies are performed for different Froude numbers (equivalent current speed), submerged depths, separation distances and inclinations to predict second order horizontal and vertical forces and steady tilt moment due to second order forces on twin hulled marine structures in head and following waves. The detail results are classified into two main categories as follows.

(A) In head wave condition :

(a) For different Froude numbers :

The calculated results of the non-dimensionalized second order horizontal and vertical forces and steady tilt moments due to these steady forces are detailedly presented in Tables 7.1 to 7.3 and those of second order vertical forces are presented in Fig. 7.5. In numerical computations, predicted results show no much difference over the frequency range and results of second order horizontal and vertical forces by both theoretical approaches are also compared.

(b) For different submergence depths :

The predictions of second order vertical forces are as in Fig. 7.6 and large discrepancies confirm the significant effect of the submergence depth. The calculated results of non-dimensionalized second order horizontal and vertical forces and steady tilt moments are detailedly indicated in Tables 7.4 to 7.6. In computations, all calculated results show that the magnitude of the second order force is clearly decreased for deeper immersions.

(c) For different separation distances :

Numerical results of non-dimensionalized second order horizontal and vertical forces and steady tilt moments due to these steady forces are detailedly presented in Tables 7.7 to 7.9 and the second order vertical forces are as in Fig. 7.7. In numerical computations, second order horizontal and vertical forces are of

small magnitude and the predicted results show no much difference over the frequency range. It may be concluded that the separation distance between two hulls has no significant contribution to the second order forces.

(d) For different inclinations :

The numerical calculations of non-dimensionalized second order horizontal and vertical forces and steady tilt moments are as in Figs. 7.8 to 7.10 and more detail in Tables 7.10 to 7.12. In the computations, calculated results of second order horizontal forces are of small amplitude and have no much difference as shown in Fig. 7.8. For the second order vertical forces and steady tilt moments as shown in Figs. 7.9 and 7.10, the inclination effect is significantly dominant over the range of frequencies.

(B) In following wave condition :

(a) For different Froude numbers :

The calculated results of the non-dimensionalized second order horizontal and vertical forces and steady tilt moments due to these steady forces are detailedly indicated in Tables 7.13 to 7.15 and the second order vertical forces are as in Fig. 7.11. In the numerical computations, predicted results show no much difference over the frequency range and results of the second order horizontal and vertical forces by both theoretical approaches are also compared. For higher current speed (Fn = 0.40) in following waves, the significant effect is due to the second order vertical forces and steady tilt moments. It may be concluded that forward speed effect is clearly dominant in the steady tilt behaviour of twin hulled marine vehicles under combined actions of wave and current.

(b) For different submergence depths :

The predictions of second order vertical forces are as in Fig. 7.12 and large discrepancies show the significant contribution due to the submergence depth. The

calculated results of non-dimensionalized second order horizontal and vertical forces and steady tilt moments are detailedly indicated in Tables 7.16 to 7.18. In the computations, all calculated results show that the magnitude of the second order vertical force is clearly decreased by deeper immersion, for example 50 % decrease of magnitude at certain frequency points of ka = 0.30 or 0.50 and much more in the remaining frequency range.

(c) For different separation distances :

Numerical results of non-dimensionalized second order horizontal and vertical forces and steady tilt moments due to these steady forces are detailedly presented in Tables 7.19 to 7.21 and the second order vertical forces are as in Fig. 7.13. In the numerical computations, second order horizontal and vertical forces are of small magnitude and predicted results show less than 1.0 % difference over the range of all frequencies. It may be concluded that the second order forces have no significant effect due to separation distance between two hulls.

(d) For different inclinations :

The numerical calculations of the non-dimensionalized second order horizontal and vertical forces and steady tilt moments are as in Figs. 7.14 to 7.16 and the detail results are as in Tables 7.22 to 7.24. In the computations, calculated results of second order horizontal forces are of small amplitude and have no much difference as shown in Fig. 7.14. For the second order vertical forces and steady tilt moments as shown in Figs. 7.15 and 7.16, the inclination effect at high current speed (Fn = 0.40) shows dominant behaviour of more than 35 % increase in magnitude in second order vertical forces and 2.5 times in steady tilt moments. The increase in magnitude of the second order vertical force and steady tilt moment is due to the tilt of the structure. The amplitudes of the second order vertical force and steady tilt moment are greater in following waves than in head waves. These variations sometimes are of the order of 30 % increase.

7.8 Conclusions

The second order horizontal forces acting on twin hulled marine vehicles in head and following waves by both direct pressure integration (near field approach) and momentum flux consideration in terms of the Kochin functions (far field approach) are theoretically formulated. In accordance with the near field concept, the second order horizontal and vertical forces are mathematically derived to take into consideration the effects of forward speed and interactions between two submerged hulls. The steady tilt moments due to the effects of second order forces, based on near field approach, on an inclined twin hulled offshore structure can be predicted to investigate its steady tilt behaviours in head and following waves taking into consideration the second order forces in both horizontal and vertical directions.

In the numerical investigations, calculated results of second order horizontal forces on twin hulled structures by both theoretical approaches match well and both predicted results have errors less than 0.1 % in general. As for the second order vertical forces, there is about 10 % variation between the pressure integration method and Lee-Newman approach for the selected range of wave frequencies. The reason for this variation is that the Lee-Newman (1971) approach does not take into consideration the effects of forward speed and interactions between two submerged hulls.

CHAPTER 8
NUMERICAL COMPUTATION OF HYDRODYNAMIC INTERACTION OF THE TWO RIGIDLY HELD APART CYLINDERS SUBMERGED UNDER THE FREE SURFACE

8.1 General description

Two numerical methods have been modified to predict hydrodynamic loadings acting on twin hulled offshore structures advancing in incident waves. The velocity potentials in these methods are calculated by the discrete source distribution technique and by the direct solution of the classical integral equation method. These new theoretical modifications, accomplished by analytically solving the logarithmic part of the Green function, have helped to improve the numerical accuracy and computational efficiency for the prediction of hydrodynamic forces acting on the twin hulled offshore structures in waves.

In the field of computational fluid dynamics, computational efficiency and numerical accuracy are two principal concerns of researchers in marine hydrodynamics. Here the logarithmic part of the Green function is newly derived to improve the computational efficiency, in other words, it can cut down the CPU time considerably.

It is obvious that as the number of the discrete elements on the body surface is increased, the numerical accuracy is improved. Hence there is a need to carry out the numerical computations which could help researchers to choose the optimum numbers of discrete elements and the images of the dipoles.

8.2 General introduction of both numerical approaches

Under the linear assumption of the boundary value problems, described in Chapter Two., the solutions of the velocity potential on the body surface of twin hulled marine vehicles can be exactly obtained by solving the integral equations numerically. The computational algorithm of both numerical approaches are described as follows.

8.2.1 Discrete source distribution approach

If the discrete source distribution method is applied to the Green function and the strength of velocity potential is solved, the following expression of the velocity potential can be derived and when the field point P = (x,y) situated on the body surface.

$$\varphi_L = -\int_{S_L} \gamma_L G ds \tag{8.1}$$

$$\varphi_R = -\int_{S_R} \gamma_R G ds \tag{8.2}$$

and

$$\varphi = \varphi_L + \varphi_R = -\int_{S_L} \gamma_L G dl - \int_{S_R} \gamma_R G dl \tag{8.3}$$

Then if the field point is on cylinder L, the boundary equation is to be satisfied as

$$\frac{\gamma_L}{2} - \int_{S_L} \gamma_L \frac{\partial G}{\partial n_L} dl - \int_{S_R} \gamma_R \frac{\partial G}{\partial n_L} dl = \frac{\partial \varphi}{\partial n_L} \tag{8.4}$$

Similarly if the field point is on cylinder R, the boundary equation is as

$$\frac{\gamma_R}{2} - \int_{S_L} \gamma_L \frac{\partial G}{\partial n_R} dl - \int_{S_R} \gamma_R \frac{\partial G}{\partial n_R} dl = \frac{\partial \varphi}{\partial n_R} \tag{8.5}$$

where :

S_L and S_R denote the body surfaces of the left and right cylinders respectively. The normal derivatives of n_L and n_R on the right hand side are given by the body condition, so that Eq. (8.4) and Eq. (8.5) are the boundary equations for the velocity potential on the body surface.

The boundary equations mentioned above can be rewritten as

$$\frac{\gamma_L}{2} - \int_{S_L} \gamma_L \frac{\partial G(x_L, y_L; \xi_L, \eta_L)}{\partial n_L} dl - \int_{S_R} \gamma_R \frac{\partial G(x_L, y_L; \xi_R, \eta_R)}{\partial n_L} dl = \frac{\partial \varphi}{\partial n_L} \tag{8.6}$$

$$\frac{\gamma_R}{2} - \int_{S_L} \gamma_L \frac{\partial G(x_R, y_R; \xi_L, \eta_L)}{\partial n_R} dl - \int_{S_R} \gamma_R \frac{\partial G(x_R, y_R; \xi_R, \eta_R)}{\partial n_R} dl = \frac{\partial \varphi}{\partial n_R} \tag{8.7}$$

8.2.2 Direct Green function approach

If Green's theorem is applied to this Green function and the velocity potential is solved, the following expression can be derived and when the field point P = (x,y) situated on the body surface.

$$\frac{1}{2}\phi(P) - \left[\int_{S_L} + \int_{S_R}\right] \phi(Q) \frac{\partial}{\partial n} G(P,Q) dl = -\left[\int_{S_L} + \int_{S_R}\right] \frac{\partial \phi}{\partial n} G(P,Q) dl \tag{8.8}$$

where :

S_L and S_R denote the body surfaces of left and right cylinders respectively. The normal derivative $\frac{\partial \phi}{\partial n}$ on the right hand side is given by the body condition, so that Eq. (8.8) is the integral equation for the velocity potential on the body surface.

8.3 Numerical solutions of the integral equations

The numerical scheme to solve the integral equation is described. The wetted boundary contours of both right and left cylinders in the integral equation can be discretized with the N_L and N_R elements as shown in Fig. 8.1 respectively and the velocity potential is assumed to be constant over each element over the body boundary surface of the twin hulled marine vehicles as shown in Fig. 8.2. The approximation of the integral equation is then written as

$$\sum_{j=1}^{(N_L+N_R)} \left\{ \frac{1}{2}\delta_{ij} - D_{ij} \right\} \phi_j = - \sum_{j=1}^{(N_L+N_R)} \left(\frac{\partial \phi}{\partial n} \right)_j \overline{C}_{ij} \qquad (i = 1, 2, 3, \ldots\ldots N) \qquad (8.9)$$

where :

$$\overline{C}_{ij} = \left[\int_{S_{Lj}} + \int_{S_{Rj}} \right] G(P_i, Q) ds(Q) \qquad (8.10a)$$

$$D_{ij} = \left[\int_{S_{Lj}} + \int_{S_{Rj}} \right] \frac{\partial}{\partial n_Q} G(P_i, Q) ds(Q) \qquad (8.10b)$$

where :

ϕ_j denotes the value of the velocity potential on the j-th element.

$\left(\frac{\partial \phi}{\partial n} \right)_j$ is the normal derivative of the velocity potential on the j-th element.

n_Q is outward normal at the point Q and the integral equation, Eq. (8.9), is required to be satisfied at the point $P_i(x,y)$ on each element over the body boundary contours and the integration of Eqs. (8.10a) and (8.10b) is to be performed over the j-th element with respect to $Q(\xi,\eta)$ in which ξ and η are the x and y coordinates of the point Q. δ_{ij} is Kronecker's delta.

As the velocity potential is a complex quantity, the integral equation, separated into the real and imaginary parts, can be reduced to a linear system of

simultaneous equations with the $2(N_L + N_R)$ unknowns and it can be solved by direct matrix inversion method.

When the point Q coincides with the field point P_i where the body boundary condition is to be satisfied, the logarithmic part of the Green function, the first term of Eq. (2.32), becomes singular. Thus numerical computations of integrals in Eqs. (8.10a) and (8.10b) must be dealt with care in this case. The integration of the logarithmic part of the Green function over each element of the body boundary surface of twin hulled marine structures is analytically derived as

$$\vartheta = \int_{(\xi_j,\eta_j)}^{(\xi_{j+1},\eta_{j+1})} \ln\sqrt{(x-\xi)^2+(y-\eta)^2}\, ds \qquad (8.11a)$$

$$\begin{aligned} &= -D + \frac{1}{2}\Big[\Big\{(x_i-\xi_j)\cos\delta + (y_i-\eta_j)\sin\delta\Big\} * \ln\Big\{(x_i-\xi_j)^2 + (y_i-\eta_j)^2\Big\} \\ &\quad - \Big\{(x_i-\xi_{j+1})\cos\delta + (y_i-\eta_{j+1})\sin\delta\Big\} * \ln\Big\{(x_i-\xi_{j+1})^2 + (y_i-\eta_{j+1})^2\Big\}\Big] \\ &\quad + \Big|(x_i-\xi_j)\sin\delta - (y_i-\eta_j)\cos\delta\Big| * \Big[\tan^{-1}\frac{(x_i-\xi_j)\cos\delta + (y_i-\eta_j)\sin\delta}{\Big|(x_i-\xi_j)\sin\delta - (y_i-\eta_j)\cos\delta\Big|} \\ &\quad - \tan^{-1}\frac{(x_i-\xi_{j+1})\cos\delta + (y_i-\eta_{j+1})\sin\delta}{\Big|(x_i-\xi_j)\sin\delta - (y_i-\eta_j)\cos\delta\Big|}\Big] \end{aligned} \qquad (8.11b)$$

where :

$$D = \sqrt{(\xi_{j+1}-\xi_j)^2 - (\eta_{j+1}-\eta_j)^2} \qquad (8.12)$$

$$\cos\delta = \frac{(\xi_{j+1}-\xi_j)}{D} \qquad (8.13a)$$

$$\sin\delta = \frac{(\eta_{j+1}-\eta_j)}{D} \qquad (8.13b)$$

and (ξ_j, η_j) and (ξ_{j+1}, η_{j+1}) are the coordinates of two ends of the j-th element.

Under the linear assumption of the boundary value problem, the numerical

solutions can be exactly obtained by solving the integral equation of the velocity potential on the body boundary surface of twin hulled offshore structures in head and following waves. In fact the numerical solutions of the velocity potentials are calculated for the radiation potential ψ_j and the diffraction potential φ_D on each segment of twin hulled offshore structures in waves. Then the added mass and damping coefficients are obtained by Eqs. (4.9) and (4.10) integrated over body boundary contours, the wave excitation forces by Eq. (4.12) with the effects of incident and diffraction wave potentials together and the steady second order horizontal forces by Eq. (4.14) too. In these numerical computations, the numerical integration is just replaced by the summation of the contributions from each element of the body boundary surface of the twin hulled offshore structures in waves.

The numerical accuracy check is of major concern to researchers in computational fluid dynamics. The accuracy of the numerical solutions of the integral equation, Eqs. (8.6), (8.7) and (8.8), is improved by increasing the numbers of the discrete elements and the images of the dipoles.

8.4 Description of numerical computations on hydrodynamic forces of twin hulled structures

The theoretical approach for the numerical solutions of the integral equation, Eq. (8.1), for the two cylinders case is almost the same as that for the single cylinder case. The unique difference is that the integral equation should be satisfied over the both body boundary contours of the twin hulled offshore structures. Once the predicted solutions of the unsteady velocity potential, ϕ, is obtained on each element of the two cylinder surfaces, S_L and S_R, at their equilibrium positions, the added mass and damping coefficients of the two rigidly connected cylinders of the twin hulled marine vehicles can be calculated. The total added mass coefficients, evaluated by Eq. (4.9), of twin hulled structures can be summarized by that of the left and right cylinders respectively and then described as

$$A_{kj} = A_{kj}^{L} + A_{kj}^{R} \qquad (8.14)$$

where A_{kj}^{L} and A_{kj}^{R} denote the added mass coefficients of the respective cylinder L and R of the twin hulled structures which are evaluated by the direct pressure integration on each cylinder surface of S_L and S_R instead of over the two cylinders. Subscripts k and j represent the added mass coefficient associated with the hydrodynamic force in the k-th direction due to the j-th mode of the motion.

Similarly the damping coefficients, evaluated by Eq. (4.10), is expressed as

$$B_{kj} = B_{kj}^{L} + B_{kj}^{R} \qquad (8.15)$$

in which B_{kj}^{L} and B_{kj}^{R} are the damping coefficients of each cylinder of the twin hulled structure which the effect of the forward speed and interactions between two hulls is already taken into consideration.

The wave excitation forces are also computed by Eq. (4.12) over the body boundary surface of the twin hulled marine vehicles $S_L + S_R$ instead of S_H. The wave excitation forces on each cylinder L and R are also defined by integrating Eq. (4.12) over the body boundary surface of twin hulled structure S_L and S_R. Hence in the same manner, the total wave excitation forces acting on the twin hulled structure are summarized as

$$E_j = E_j^{L} + E_j^{R} \qquad (8.16)$$

The wave excitation forces acting on twin hulled structure can also be evaluated by the Haskind - Newman relation in terms of the Kochin functions of the radiation waves as mentioned previously. However this relation is an appropriate approach to confirm numerical computations on the theoretical side.

The second order horizontal forces such as the added resistance for ships and steady second order vertical forces are also predicted by the theoretical procedures described in Chapter Seven.

The restoring forces due to the forward speed effect evaluated by Eq. (6.4) for the single cylinder case can be extended and briefly described for the two cylinders case as

$$C_{k1} = \frac{-\rho U^2}{2} \int_{S_L+S_R} \frac{\partial}{\partial x}\left(\vec{V}\right)^2 n_k \, ds \tag{8.17}$$

$$C_{k2} = \frac{-\rho U^2}{2} \int_{S_L+S_R} \frac{\partial}{\partial y}\left(\vec{V}\right)^2 n_k \, ds \tag{8.18}$$

$$C_{k3} = \frac{-\rho U^2}{2} \left[\sin\alpha \int_{S_L+S_R} \frac{\partial}{\partial x}\left(\vec{V}\right)^2 - \cos\alpha \int_{S_L+S_R} \frac{\partial}{\partial y}\left(\vec{V}\right)^2 \right] n_k \, ds \tag{8.19}$$

where $\vec{V}$ is the steady velocity field around the two cylinders and can be evaluated by taking the interaction effect between two hulls into consideration. In fact, the mathematical expression for the velocity $\vec{V}$ in the vicinity of the two cylinders case is not as simple as that for the single cylinder case and the integrals of Eq. (6.21), described in Chapter Six detailedly, have to be performed by the numerical computations.

8.5 Description of motion equations of twin hulled marine vehicles

The dynamic motion responses of the two rigidly connected cylinders of twin hulled offshore structures in head and following waves responding to the first order hydrodynamic forces can be obtained above. With the assumption that the density of both cylinders is the same as that of the fluid, the following simultaneous linear equations are applied to describe the coupled motions which are in surge, heave and pitch modes.

$$\sum_{j=1}^{3} \left\{ -\omega^2 \left(m_i \delta_{ij} + A_{ij} \right) + i\omega B_{ij} \right\} \xi_j = E_i \qquad (j = 1, 2, 3) \tag{8.20}$$

If the hydrodynamic restoring forces due to forward speed effect are considered, the dynamic motion equations of the twin hulled marine vehicles in the head and following waves is written as

$$\sum_{j=1}^{3}\left\{\left[-\omega^2\left(m_i\delta_{ij}+A_{ij}\right)+C_{ij}\right]+i\omega B_{ij}\right\}\xi_j = E_i \quad (j = 1, 2, 3) \tag{8.21}$$

where :

$$A_{ij} = 2\pi\rho a^2 A'_{ij} \tag{8.22a}$$

$$B_{ij} = 2\pi\rho a^2 \omega B'_{ij} \tag{8.22b}$$

$$C_{ij} = \rho U^2 C'_{ij} = 2\pi\rho a^2\omega^2\left[\left(\frac{U}{\omega a}\right)^2\left(\frac{1}{2\pi}\right)\right]C'_{ij} \tag{8.22c}$$

$$\begin{aligned} E_i &= 2\rho g A a E'_i = 2\pi\rho a^2\omega^2\left[\left(\frac{g}{\omega^2 a}\right)\left(\frac{A}{\pi}\right)\right]E'_i \\ &\equiv 2\pi\rho a^2\omega^2\left(\frac{A}{\pi k}\right)E'_i \end{aligned} \tag{8.22d}$$

Then the dynamic motion equation of twin hulled marine vehicles in head and following waves is written as

$$\sum_{j=1}^{3}\left\{\left[-\left(\delta_{ij}+A'_{ij}\right)+C'_{ij}\left(\frac{1}{2\pi}\right)\left(\frac{U}{\omega a}\right)^2\right]+iB'_{ij}\right\}\left(\frac{\xi_j}{A}\right)=\left(\frac{E'_i}{\pi k}\right) \tag{8.23}$$

In numerical computations, the absolute value of the " complex " motion amplitude can be presented for the two rigidly connected cylinders in head and following waves. It is found that the forward speed affects the body motion to reduce its amplitude in the head waves, whereas, in following waves, the motion amplitude increases with the increasing Froude numbers.

8.6 Computational investigations and discussions of numerical approaches

All numerical computations by both discrete source distribution method (D.S. method) and direct Green function method (Direct method), are carried out on the VAXstation 4000 VLC computer system. The results of CPU time versus numbers of elements and images for different submergence depth are as in Figs. 8.3 and 8.4. The numerical values are indicated in Tables 8.1 and 8.2. It is found that the effect of submergence depths has no much influence on computational efficiency.

The predicted results of the percentage error in damping coefficients for surge, heave and pitch modes for different submergence depths and for varying discrete element numbers and ten (10) dipole images are as in Figs. 8.5 to 8.10. The numerical values are as in Tables 8.3 to 8.5. Relative errors of all damping coefficients are less than 1.0 % as discrete element numbers are larger than thirty (30) and it is clear that if the discrete element number is taken as fifty (50), it is accurate and efficient.

The numerical accuracy of the damping coefficients in surge, heave and pitch motions for different submergence depths and for varying diploe image numbers and fifty (50) discrete elements is as in Figs. 8.11 to 8.16. Numerical results are as in Tables 8.6 to 8.8. The calculated results show very stable tendency for all computations as the dipole image numbers increase. It may be concluded that the selection of dipole image number as ten (10) is appropriate.

On the accuracy check of the numerical computations, numerical results of surge, heave and pitch damping coefficients by both direct pressure integration and energy flux consideration match well and are detailedly presented in Tables 8.9 to 8.11. The numerical check of surge, heave and pitch Kochin functions has good agreement as in Tables 8.12 to 8.14. The discrepancies in the damping coefficients and Kochin functions are significant when submerged bodies (d/a =

1.0) approach the free surface. This may be due to the fluctuations of the sinks and sources on body boundary surfaces.

The comparison of both methods against CPU time is as in Fig. 8.17 for different wave frequencies. The numerate values are as in Table 8.15. These results indicate that the direct Green function method is about three (3) times more efficient than the discrete source distribution method.

A comparison of relative errors in surge, heave and pitch damping coefficients is shown in Figs. 8.18 to 8.20 and numerical values are as in Tables 8.16 to 8.18. From the calculated results it is clear that the direct Green function method can predict hydrodynamic loadings much more accurately than the discrete source distribution method over frequency range in calculations.

With respect to accuracy check of both numerical approaches, predicted results of damping coefficients in surge, heave and pitch motions by direct pressure integration and energy flux consideration are in good agreement and detailedly presented in Tables 8.19 to 8.21 respectively. The numerical check of surge, heave and pitch Kochin functions are as in Tables 8.22 to 8.24.

As for the second order horizontal forces shown in Table 8.25, the percentage errors of second order horizontal forces, in comparison with damping forces, seem to be a little bit more because these forces are of higher order and much smaller than damping forces. In fact such steady second order horizontal forces by direct pressure integration (near field concept) and momentum flux consideration (far field concept) are found not to make much difference.

Dynamic surge, heave and pitch responses, predicted by both numerical approaches, in head waves are as in Figs. 8.21 to 8.23. The numerical values are as in Tables 8.26 to 8.28. Principally the calculated results of motion amplitudes in surge and heave modes match well as shown in Figs. 8.21 and 8.22. A slight discrepancy of pitch amplitudes at certain specific frequencies, shown in Fig. 8.23, could be due to more accurate prediction of hydrodynamic loadings such as

added mass and damping coefficients and wave excitation forces by the direct Green function method. From these calculated results, it is clear that the direct Green function method is much more accurate and efficient than the discrete source distribution method in numerical computations.

8.7 Conclusions

Here a valuable procedure for theoretical confirmation of numerical computations is newly developed. The numerical accuracy of the damping coefficients is calculated by the energy flux consideration in the fluid domain and by the direct pressure integration over body boundary contours. The results of the wave excitation forces in terms of the Kochin functions is checked out by the Haskind-Newman relation. The accuracy check of second order horizontal forces on twin hulled structures under combined actions of wave and current is investigated by direct pressure integration (near field approach) and by momentum flux consideration (far field approach). The numerical accuracy of second order vertical forces with forward speed effects is also confirmed by the Lee-Newman (1971) approach for single submerged body in non-forward speed condition.

The numerical accuracy of the damping coefficients, wave excitation forces and steady second order horizontal force is extensively investigated by energy conservation principle, Haskind Newman relation and momentum conservation principle respectively. In general, the errors in all numerical accuracy check are confirmed to be less than 0.1 % and the computation time has also decreased dramatically.

In fact it is concluded that the direct Green function method is a more effective and efficient approach than the discrete source distribution method to deal with different kinds of hydrodynamic problems in a better way as far as the numerical accuracy and computational efficiency are concerned.

CHAPTER 9
EXPERIMENTAL WORK IN DYNAMIC POSITIONING ASPECTS OF TWIN HULLED MARINE VEHICLES

9.1 General description

The mathematical approach using the linear optimal control theory to investigate the dynamic positioning behaviour of twin hulled marine structures under combined actions of wind, wave and current is briefly introduced. A series of experiments on twin hulled structure for different submerged depths, drift and trim angles at a constant forward speed, simulating the ocean current effect, are carried out to measure the sway forces and yaw moment acting on the twin hulled marine structure advancing under the free surface.

The setup of the two aluminium strain gauged bars for the manoeuvring experiment is briefly described. The recorded data can be well presented on the screen of the VAXstation 3100-M38 micro computer and the comparison of analysed results are performed on the Macintosh Plus computer system.

The sway force and yaw moment are measured with the aid of two aluminium strain gauged bars. The experimental results are based on first and second order curve fitting technique to obtain several newly developed formulae for predicting the dynamic positioning behaviour of twin hulled marine vehicles. These mathematical formulae can be utilized to simulate the dynamic positioning performance of newly designed twin hulled offshore structures at the preliminary design stage.

9.2 Mathematical model of dynamic positioning system

The fundamental concept and algorithm of the linear optimal regulator control approach to study the dynamic positioning performance of twin hulled marine vehicles is briefly described as follows.

A) Offshore structures are usually required to keep their positions under the unsteady external forces such as ocean current, wind and wave etc. In general, PID (Proportional, Integral and Differential system) control theory is applied to design the control system of offshore structures for surge, sway and yaw motions respectively.

B) The type and arrangement of thrusters have much influence on the performance of the control system. The performance of the control system for two types of thruster system such as tunnel-type thrusters or rotatable thrusters under unsteady external forces is introduced.

C) The external forces such as ocean current and wind have much influence on the horizontal motion of twin hulled offshore structures. The Dynamic Positioning System (DPS) by the optimal regulator control theory for twin hulled offshore structures under unsteady external forces is briefly described.

The coordinate system to study the dynamic positioning behaviour of twin hulled marine vehicles under combined actions of wind, wave and current is shown in Fig. 9.1 and the mathematical model is briefly described as follows.

$$(m+m_x)\dot{u}-(m+m_y)vr-(m_x-m_y)V_C r\sin(\psi-\alpha)=X_C+X_W+\tau_x$$

$$(m+m_y)\dot{v}+(m+m_x)ur-(m_y-m_x)V_C r\cos(\psi-\alpha)=Y_C+Y_W+\tau_y$$

$$(I_z+i_z)\dot{r}=N_C+N_W+\tau_z \qquad (9.1)$$

where :

u is the velocity of the twin hulled offshore structure in the x direction.

v is the velocity of the twin hulled offshore structure in the y direction.

r is the angular velocity of the twin hulled offshore structure in the z direction.

m is the mass of the twin hulled offshore structure.

I_z is the moment of inertia with respect to the z axis.

m_x is the added mass in the x direction.

m_y is the added mass in the y direction.

i_z is the added moment of inertia in the z direction.

X_C is the current force in the x direction.

Y_C is the current force in the y direction.

N_C is the current-induced moment in the z direction.

X_W is the wind force in the x direction.

Y_W is the wind force in the y direction.

N_W is the wind-induced moment in the z direction.

τ_x is the thrust driving force in the x direction.

τ_y is the thrust driving force in the y direction.

τ_z is the thrust driving moment in the z direction.

V_C is the current speed.

The mathematical expression of the total relative velocity of the twin hulled offshore structure due to current effect is written as

$$V_C^* = \sqrt{u_C^* + v_C^*} \tag{9.2}$$

$$u_C^* = u + V_C \cos(\psi - \alpha) \tag{9.3a}$$

$$v_C^* = v - V_C \sin(\psi - \alpha) \tag{9.3b}$$

$$\beta^* = \tan^{-1}\left(\frac{u_C^*}{v_C^*}\right) \tag{9.3c}$$

and the external hydrodynamic surge and sway forces and yaw moment due to current effect acting on twin hulled offshore vehicle are written as

$$X_C = \frac{1}{2}\rho A V_C^{*2} C_{Cx} \tag{9.4a}$$

$$Y_C = \frac{1}{2}\rho A V_C^{*2} C_{Cy} \tag{9.4b}$$

$$N_C = \frac{1}{2}\rho A L_{OA} V_C^{*2} C_{Cz} \tag{9.4c}$$

where :

ρ is the density of the sea water.

A is the transversal projected area of the twin hulled offshore structure under the water surface.

L_{OA} is the overall length of the twin hulled offshore structure.

C_{Cx} is the coefficient of the current force in the x direction.

C_{Cy} is the coefficient of the current force in the y direction.

C_{Cz} is the coefficient of the current induced moment in the z direction

Similarly the mathematical expression of the total relative velocity of twin hulled offshore structure due to wind effect is described as

$$V_W^* = \sqrt{u_W^* + v_W^*} \tag{9.5}$$

$$u_W^* = u + V_W \cos(\psi - \gamma) \tag{9.6a}$$

$$v_W^* = v - V_W \sin(\psi - \gamma) \tag{9.6b}$$

$$\gamma^* = \tan^{-1}\left(\frac{u_W^*}{v_W^*}\right) \tag{9.6c}$$

and the external surge, sway forces and yaw moment due to wind effect acting on twin hulled offshore vehicle are also written as

$$X_W = \frac{1}{2}\rho_a A_a V_W^{*2} C_{Wx} \qquad (9.7a)$$

$$Y_W = \frac{1}{2}\rho_a A_a V_W^{*2} C_{Wy} \qquad (9.7b)$$

$$N_W = \frac{1}{2}\rho_a A_a L_{OA} V_W^{*2} C_{Wz} \qquad (9.7c)$$

where :

ρ_a is the air density.

A_a is the transverse-projected area of the twin hulled offshore structure above the water surface.

L_{OA} is the overall length of the twin hulled offshore structure.

C_{Wx} is the coefficient of the wind force in the x direction.

C_{Wy} is the coefficient of the wind force in the y direction.

C_{Wz} is the coefficient of the wind induced moment in the z direction.

In conclusion, the mathematical model to predict the dynamic positioning behaviour of twin hulled marine vehicles under combined action of wind, wave and current is described. Also to investigate this dynamic positioning work further, optimal control theory is applied and briefly introduced in the next section.

9.3 Introduction of optimal control approach in dynamic positioning aspects of twin hulled marine vehicles

The optimal control concept to study the dynamic positioning behaviour of twin hulled marine vehicles under external unsteady forces such as wind, wave and current is briefly reviewed and practical prediction of dynamic positioning behaviour of twin hulled marine vehicles under external forces can be carried out by the 4th order Runge Kutta integration method for real time simulation in time domain.

The analytical solutions of such dynamic motion equations of twin hulled offshore vehicles under combined action of wind, wave and current are detailedly derived as

$$\dot{u} = \frac{1}{(m+m_x)}\left\{(m_x - m_y)V_C r\sin(\psi-\alpha) + (m+m_y)vr + X_C + X_W + \tau_x\right\}$$

$$\dot{v} = \frac{1}{(m+m_y)}\left\{(m_y - m_x)V_C r\cos(\psi-\alpha) - (m+m_x)ur + Y_C + Y_W + \tau_y\right\}$$

$$\dot{r} = \frac{1}{(I_z+i_z)}\left\{N_C + N_W + \tau_z\right\}$$

$$\dot{x} = u\cos\psi - v\sin\psi$$

$$\dot{y} = v\cos\psi + u\sin\psi$$

$$\dot{\psi} = r \qquad (9.8)$$

The mathematical formulation of the optimal control approach with state space notation is briefly described and the governing equations of such state variables in compliance with Euler type discretization concept are written as follows.

$$\vec{x}(k+1) = P\vec{x}(k) + Q\vec{u}(k) \qquad (9.9a)$$

$$\vec{x}(k) = [u, v, r, x, y, \psi]^T \qquad (9.9b)$$

$$\vec{u}(k) = \left[\frac{\tau_x}{m+m_x}, \frac{\tau_y}{m+m_y}, \frac{\tau_z}{I_z+i_z}\right]^T \qquad (9.10)$$

The objective function of this control system for dynamic positioning assessment of twin hulled marine vehicles is defined as

$$J = \sum_{k=0}^{\infty} \left\{ \bar{x}^T(k) R_1 \bar{x}(k) + \bar{u}^T(k) R_2 \bar{u}(k) \right\} \tag{9.11}$$

$$R_1 = \begin{bmatrix} \omega_1 & 0 & 0 & 0 & 0 & 0 \\ 0 & \omega_1 & 0 & 0 & 0 & 0 \\ 0 & 0 & \omega_1 & 0 & 0 & 0 \\ 0 & 0 & 0 & \omega_2 & 0 & 0 \\ 0 & 0 & 0 & 0 & \omega_2 & 0 \\ 0 & 0 & 0 & 0 & 0 & \omega_2 \end{bmatrix}, \quad R_2 = \begin{bmatrix} \omega_3 & 0 & 0 \\ 0 & \omega_3 & 0 \\ 0 & 0 & \omega_3 \end{bmatrix} \tag{9.12}$$

where :

ω_1 is the velocity associated term.

ω_2 is the displacement associated term.

ω_3 is the input associated term.

In accordance with minimum energy consideration, optimal values of input variables in linear state equations can be obtained by minimizing the objective function of the control system. The following mathematical expression proposed by Riccati must be satisfied for solutions of the non-linear discrete equations in terms of matrix expression as

$$H = P^T H P - P^T H Q \left(R_2 + Q^T H Q \right)^{-1} Q^T H P + R_1 \tag{9.13}$$

The solution of Equation above can be obtained as $H = H^0$. The feedback gain matrix G is expressed and calculated accordingly as follows.

$$G = \left(R_2 + Q^T H^0 Q \right)^{-1} Q^T H^0 P \tag{9.14}$$

The optimal values of input variables to estimate dynamic positioning behaviour of twin hulled marine vehicles is written as

$$\bar{u}^0(k) = -G\bar{x}(k) \tag{9.15}$$

and the optimal values of input forces and moments generated by thrusters in surge, sway and yaw directions are derived as

$$\vec{u}^0(k)=\left[\frac{\tau_x^0}{m+m_x},\frac{\tau_y^0}{m+m_y},\frac{\tau_z^0}{I_z+i_z}\right]^T \qquad (9.16)$$

where:

τ_x^0 is the optimal value of the driving force in the x direction.
τ_y^0 is the optimal value of the driving force in the y direction.
τ_z^0 is the optimal value of the driving force in the z direction.

Also the power-sharing of optimal driving forces and moments by thrusters is briefly described for two different kinds of arrangements as follows.

Type A arrangement :

The thruster arrangement of type A where three pairs of thrusters are required is shown in Fig. 9.2. The thrust driving force in surge direction is generated by thruster no. 1 and 2 and the thrust driving force in sway direction is generated by thruster no. 3 and 4. As regards the driving yaw moment, it is generated from the thrust driving force by thruster no. 5 and 6 in sway direction. The optimal driving forces by each pair of thrusters are determined as follows.

$$T_1 = \tau_x^0/2 \qquad (9.17a)$$

$$T_2 = \tau_y^0/2 \qquad (9.17b)$$

$$T_3 = \tau_z^0/(2x_1) \qquad (9.17c)$$

where :

T_1 is the thrust driving force generated by thruster no. 1 and 2 in x direction.

T_2 is the thrust driving force generated by thruster no. 3 and 4 in y direction.

T_3 is the thrust driving force generated by thruster no. 5 and 6 in y direction.

x_1 is the distance between centre of gravity and location of thruster no. 5 (or 6) in x direction.

Type B arrangement :

The thruster arrangement of type B where four individual thrusters are applied is as in Fig. 9.3. Based on Lagrangian indeterminate coefficient method, the optimal driving forces and acting directions by the four thrusters are described in detail as

$$T_i = \sqrt{T_{xi}^2 + T_{yi}^2} \tag{9.18}$$

$$T_{xi} = \frac{1}{4}\tau_x^0 - \frac{1}{2} y_{Ti} \frac{\tau_z^0}{\sum_{j=1}^{4}\left(x_{Tj}^2 + y_{Tj}^2\right)} \tag{9.19a}$$

$$T_{yi} = \frac{1}{4}\tau_y^0 + \frac{1}{2} x_{Ti} \frac{\tau_z^0}{\sum_{j=1}^{4}\left(x_{Tj}^2 + y_{Tj}^2\right)} \tag{9.19b}$$

$$\phi_i = \tan^{-1}\left(\frac{T_{xi}}{T_{yi}}\right) \quad \text{for } i = 1,2,3,4 \tag{9.19c}$$

where :

x_{Ti} is the x coordinate of the location of the i-th thruster.

y_{Ti} is the y coordinate of the location of the i-th thruster.

T_i is the driving force generated by the i-th thruster.

ϕ_i is the direction of the driving force generated by the i-th thruster.

9.4 Description of model experiment

A series of model experiments on twin hulled model for different submergence depths, drift and trim angles at a constant forward speed, simulating the current effect, are carried out to measure the sway forces and yaw moment acting on twin hulled marine structure advancing under the free surface. The principal objective of this manoeuvring experiment is to determine such hydrodynamic loadings acting on the twin circular cylinder model under the ocean current effect as described before. For the determination of wind loadings acting on the upper structure of twin hulled models, the same concept of this experiment can be applied to obtain several mathematical equations from experimental data for practical prediction of the dynamic positioning behaviour of twin hulled marine vehicles.

The simplified model consists of twin circular cylinder hulls, which were made of PVC pipes with steel framework to connect the hulls as shown in Figs. 9.4 and 9.5 and the principal particulars are indicated in Fig. 9.6. The framework has four rods supporting the cylinders at each end and two transverse and two longitudinal beams connecting these rods together at their top end. The whole frame work is constructed of rectangular cross section steel rods (1 in x 1 in) with different draft marks and this kind of material provides adequate rigidity to keep the system stable. A small platform is designed on the framework for adjusting the ballast to the required submergence depth for testing the model.

When the twin hulled model is put in the experimental tank, the buoyancy of this model is generated. In order to get the correct position for attachment under the two straight bar device as shown in Fig. 9.7, some ballasting work must be done to compensate the buoyancy of the model. When the model is ballasted and adjusted to the right position, the attachment of the two straight bar device and the model is mounted by three pairs of steel bolts as arranged on each side.

In order to get the correct drift angle, a turnplate facility as in Fig. 9.8 fitted

with several holes for specific drift angles such as 0,+2, +4, +6, +8, +10, -2, -4 and -10 degrees are designed and mounted on the top of the two straight bar device. Two sets of wooden wedges are made in advance to obtain the specific trim angles such as +2 (trim by stern), +4, -2 (trim by bow) and -4 degrees for this experiment and they are attached between the two straight bar device and the model as in Fig. 9.9.

A series of experiments for two submergence depths (d/a = 3.0 and 4.0), drift and trim angles at a constant forward speed, simulating the current effect, were carried out in the towing tank of the Hydrodynamics Laboratory at Glasgow University.

9.5 Layout of manoeuvring experiment

The data measuring facility including the turnplate, two straight bars and testing model is assembled together and fixed by several bolts on the framework of the main carriage. The speed of the main carriage for the testing condition is automatically controlled by MicroVitec 452 computer system.

The sway force and yaw moment acting on twin hulled model advancing under the free surface are measured by two straight bar device (load cell transducers) as shown in Fig. 9.7 and they are made up from the existing facility in the laboratory by converting each straight bar into load cells with the aid of foil type electrical resistance strain gauges. By calibrating the load cell to read in load units other than strain, wave load on each bar is measured directly. In order to measure the sway force, two pairs of opposite strain gauges are fitted in the transverse direction on face-2 and face-4 of each bar perpendicular to the carriage moving direction. To measure the yaw moment, one torque strain gauge is fitted on each bar. The detailed arrangement of load cell transducers on two straight bar device is indicated in Fig. 9.10.

As described above, the load cell is composed of strain gauges which are passive resistors. Therefore there is a need for a power source in order to interpret the changes in the resistance caused by mechanical strain (or loads) measured. This can be achieved by a bridge circuit which produces an out of balance voltage. This voltage must be amplified and displayed so as to indicate the required force units. At this stage the **Wheatstone Bridge**, which is the most common bridge circuit, is applied as a direct readout device where the output voltage is measured or related to strain (or load). The four active strain gauges are placed in the bridge with one in each of four arm - for the full bridge arrangement. Since the lead wires from the measuring point to the instrumentation are outside the measuring circuit, this kind of arrangement increases the sensitivity of the measuring system and provides improved temperature compensation and minimal errors due to connection of the system. Before the system is loaded to the Wheatstone Bridge, it should be balanced as the output voltage is equal to zero. As the system is loaded a change in resistance will unbalance the bridge and induce an output voltage across the output terminal. By measuring this voltage and using the calibration curve, the voltage readout can be converted into the corresponding load value.

The calibration of two straight bar device as shown in Fig. 9.7 is performed before it is clamped onboard. After taking the zero readings from the load cells, the testing weights simulating hydrodynamic loadings are step by step increased from 0.1 to 1.5 kg. During this procedure the change in the output voltage of the bridge is recorded for each increment of the test weight. All relations of these calibration data, which are converted from induced voltages to actual loads, show linear behaviour.

The signals of hydrodynamic loadings picked up by two straight bar device are recorded into ten (10) individual data channels and experimental data are sampled at a rate of two hundred (200) samples per second per channel for ten (10) or twenty (20) seconds.

9.6 Description of data acquisition and analysis system

A comprehensive description of the experimental data acquisition and analysis system for manoeuvring experiment is explained and the details are as follows.

A. The data acquisition system :

The experimental data can be collected by Macintosh-2CLA microcomputer system when the speed of the main carriage reaches the most steady and consistent level. The speed of the main carriage for the experimental condition is controlled by MicroVitec 452 computer system and easily confirmed with the design speed requirement of this experiment automatically as shown in Fig. 9.11 (see pp489).

The hydrodynamic sway force and yaw moment are recorded through the two straight bar facility which is designed for hydrodynamic experiments on manoeuvring. The experimental signals by two straight bar device are picked up into the FLYDE amplifier and filter system. The signals are then processed and passed through the Data Collecting System (32 channel analogue to digital converter). Finally the experimental data are recorded in the DATASPAN 2000 system. Simultaneously the experimental signals after data processing can be displayed from the monitor of the Macintosh-2CLA microcomputer system for preliminary confirmation of the experimental validity test as in Fig. 9.12.

B. The data analysis system :

The experimental data are acquired by the two straight bar device, FLDYE amplifier and filter system, Data Collecting system, DATASPAN 2000 system and recorded in the Macintosh-2CLA microcomputer system. The experimental data files are transferred through the recording tape from the DATASPAN 2000 system and loaded in the digital VAXstation 3100-M38 microcomputer system. The detail procedure of the data analysis and checking work is described as follows.

a). At the experimental stage, a preliminary validity test of the experimental data acquisition can be checked from the screen of the Macintosh-2CLA micro computer system.

b). At the computation stage, experimental data files are analysed by the Fast Fourier Transform technique on the VAXstation 3100 M38 micro computer system.

c). At the data analysis stage, experimental data, analysed by the Fast Fourier Transform technique, are computed on the Micro Vax 3600 computer system to obtain the sway force and yaw moment acting on twin hulled structure model.

d). At the data presentation stage, such hydrodynamic forces acting on twin hulled model advancing under the free surface for different drift and trim angles can be transferred to the Macintosh Plus computer system and the experimental results are based on the technique of curve fitting to obtain several newly developed formulae for predicting the manoeuvring (dynamic positioning) performance of twin hulled marine vehicles.

e). At the data checking stage, analysis results are compared with that of previous research work to confirm the effectiveness of experimental work.

9.7 Presentation of experimental results and discussions

A series of experiments are performed for nine (9) drift, four (4) trim angles and two (2) submergence depths (d/a = 3.0 and 4.0) to measure the sway force and yaw moment acting on twin hulled model advancing under the free surface.

The signals of hydrodynamic loadings picked up by two straight bar device are recorded in ten (10) individual data channels as in Fig. 9.13 and experimental data are sampled at a rate of two hundred (200) samples per second per channel for

ten (10) seconds. The contents of measuring signals recorded in each channel are described as follows.

Channel 1 : Torque in Bar 1 (M1)
Channel 2 : Torque in Bar 2 (M2)
Channel 3 : Moment on face-1 and face-3 of Bar 1 bottom (M3)
Channel 4 : Moment on face-1 and face-3 of Bar 1 top (M4)
Channel 5 : Moment on face-1 and face-3 of Bar 2 bottom (M5)
Channel 6 : Moment on face-1 and face-3 of Bar 2 top (M6)
Channel 7 : Moment on face-2 and face-4 of Bar 1 bottom (M7)
Channel 8 : Moment on face-2 and face-4 of Bar 1 top (M8)
Channel 9 : Moment on face-2 and face-4 of Bar 2 bottom (M9)
Channel 10 : Moment on face-2 and face-4 of Bar 2 top (M10)

The mean amplitudes of moments from all experimental data channels are calculated by the Fast Fourier Transform technique on the VAXstation 3100 M38 micro computer system. The non-dimensionalized amplitudes of the sway force and yaw moment acting on twin hulled model under current action is predicted on Micro Vax 3600 (VMS) computer system and the mathematical equations to calculate surge, sway forces and yaw moment acting on the twin hulled model under current action by beam theory is simplified for small magnitude signals as follows.

$$X = \frac{(M4 - M3) + (M6 - M5)}{0.2} \qquad (9.20a)$$

$$Y = \frac{(M8 - M7) + (M10 - M9)}{0.2} \qquad (9.20b)$$

$$N = M1 + M2 \qquad (9.20c)$$

Here the value of 0.2 (m) is the distance between the top and bottom positions of each bar and non-dimensionalized amplitudes of forces and yaw moment is written as

$$X' = \frac{X}{\frac{1}{2}\rho V^2 A} \qquad (9.21a)$$

$$Y' = \frac{Y}{\frac{1}{2}\rho V^2 A} \qquad (9.21b)$$

$$N' = \frac{N}{\frac{1}{2}\rho V^2 AL} \qquad (9.21c)$$

where :

A denotes the transversal area of the submerged cylinder (= DL).
V is the moving speed of the main carriage in experiment.

The non-dimensionalized sway force and yaw moment acting on the twin hulled model under current action are calculated from experimental data for different drift and trim angles and submergence depths. In accordance with the technique of curve fitting, several newly developed equations are obtained. The experimental results and mathematical equations for different submergence depths are categorized as follows.

A) For submerged depth ratio d/a = 4.0 :

The experiments of the twin hulled model advancing under the free surface are performed to measure sway force and yaw moment acting on it for different drift and trim angles. The results are analysed and mathematical equations are fitted for different trim angle conditions. In general all experimental results show linear tendencies and the details are as follows.

a) For 2 degree trim by stern condition :

The mathematical equations of non-dimensionalized sway force and yaw moment

are obtained from experimental results with good accuracy as in Figs. 9.14 and 9.15.

$$Y' = -2.9009 \times 10^{-2} - 4.1773 \times 10^{-2}\beta \qquad (9.22a)$$

$$N' = 1.3167 \times 10^{-3} + 2.2528 \times 10^{-3}\beta \qquad (9.22b)$$

b) For 2 degree trim by bow condition :

The mathematical equations of the sway force and yaw moment in terms of drift angles from the experimental data in Figs. 9.16 and 9.17 are as follows.

$$Y' = -1.2742 \times 10^{-2} - 2.8602 \times 10^{-2}\beta \qquad (9.23a)$$

$$N' = -1.5038 \times 10^{-3} + 1.9532 \times 10^{-3}\beta \qquad (9.23b)$$

c) For 4 degree trim by bow condition :

The mathematical equations of the sway force and yaw moment in terms of drift angles from the experimental data in Figs. 9.18 and 9.19 are as follows.

$$Y' = -5.9479 \times 10^{-2} - 3.3513 \times 10^{-2}\beta \qquad (9.24a)$$

$$N' = 1.0482 \times 10^{-3} + 1.1933 \times 10^{-3}\beta \qquad (9.24b)$$

d) For 4 degree trim by stern condition :

The mathematical equations of the sway force and yaw moment in terms of drift angles from the experimental data in Figs. 9.20 and 9.21 are as follows.

$$Y' = 1.3920 \times 10^{-2} - 5.7884 \times 10^{-2}\beta \qquad (9.25a)$$

$$N' = 1.2017 \times 10^{-3} + 2.3182 \times 10^{-3}\beta \qquad (9.25b)$$

where :

β denotes the drift angle in degree and the positive value for starboard side.

For larger (4 degree) trim by bow condition, the least square error of mathematical equations by the curve fitting method is slight greater within 10 % for sway force and 1.2 % for yaw moment. The results for the sway force and yaw moment are for the deep submergence only. Comparison of the non-dimensionalized sway force and yaw moment acting on twin hulled model under current action is presented for different trim conditions as in Figs. 9.22 and 9.23.

Typical signals from experimental measurement for several specific conditions are as in Figs. 9.24 to 9.33. Typical motion behaviour of twin hulled model in experiments are also indicated in Figs. 9.34 (see pp491) to 9.40.

B) For submergence depth ratio d/a = 3.0 :

Similarly the sway force and yaw moment acting on twin hulled model under current action are measured for different drift and trim angles in submerged depth (d/a =3.0) condition. The results show linear relationships and mathematical equations are systematically presented for different trim conditions as follows.

a) For no trim condition :

The mathematical equations fitted with reasonable accuracy are obtained and experimental results are as in Figs. 9.41 and 9.42.

$$Y' = -3.6348 \times 10^{-2} - 1.5076 \times 10^{-2}\beta \qquad (9.26a)$$

$$N' = -8.7511 \times 10^{-3} + 4.3686 \times 10^{-3}\beta \qquad (9.26b)$$

b) For 2 degree trim by stern condition :

Experimental results are shown in Figs. 9.43 and 9.44 and mathematical equations with good accuracy of less than 0.1 % least square error are obtained as follows.

$$Y' = -4.8445 \times 10^{-2} - 1.7342 \times 10^{-2}\beta \qquad (9.27a)$$

$$N' = -6.5561 \times 10^{-3} + 5.2147 \times 10^{-3}\beta \qquad (9.27b)$$

c) For 4 degree trim by stern condition :

Experimental results are presented in Figs. 9.45 and 9.46 and mathematical equations are expressed as follows.

$$Y' = -4.0246 \times 10^{-2} - 1.9692 \times 10^{-2}\beta \qquad (9.28a)$$

$$N' = -5.6641 \times 10^{-3} + 5.5626 \times 10^{-3}\beta \qquad (9.28b)$$

d) For 2 degree trim by bow condition :

Experimental results for the sway force and yaw moment as in Figs. 9.47 and 9.48 show discontinuity behaviour at certain drift angles and the least square errors of the mathematical equations are 20 % and 5 % respectively as follows.

$$Y' = -8.8996 \times 10^{-2} - 4.5188 \times 10^{-2}\beta \qquad (9.29a)$$

$$N' = 1.4673 \times 10^{-3} + 1.3918 \times 10^{-3}\beta \qquad (9.29b)$$

e) For 4 degree trim by bow condition :

The experimental results show rather different tendencies as compared with previous results. Hence more tests were repeated for the same condition for

confirmation of the experimental measurement. The comparison of experimental results for different tests still show scattering behaviour as illustrated in Figs. 9.49 and 9.50 respectively. For the trim by bow condition as scatter behaviour was observed, experiments were once again repeated and these results show fluctuations as the bodies approach the free surface.

For larger (4 degree) trim by bow condition, the tendency of testing results show scatter behaviour. Comparison of non-dimensionalized sway force and yaw moment acting on twin hulled model under current action is presented for different trim conditions as in Figs. 9.51 and 9.52.

Comparison study of non-dimensionalized sway force and yaw moment acting on twin hulled model under current action is performed for different submerged depths and trim angles and experimental results are detailedly presented in Figs. 9.53 to 9.60. For trim by stern conditions, analysed results show rather linear relationships for different submergence depth conditions and the difference between the slopes is significant as shown in Figs. 9.53, 9.54, 9.57 and 9.58. For the non-dimensionalized sway force, the slope for submergence depth ratio d/a = 4.0 case is about two (2) times greater than that for submergence depth ratio d/a = 3.0 case and about three (3) times smaller for non-dimensionalized yaw moment. For trim by bow conditions, linear tendencies are roughly indicated, but not much discrepancy is shown for two different submergence depth conditions as in Figs. 9.55, 9.56, 9.59 and 9.60. In particular the results of non-dimensionalized sway force for submerged depth ratio d/a = 3.0 and 4 degree trim by bow condition show rather flat behaviour over the range of drift angles as in Fig. 9.59 and it is clear that this is due to the complicated behaviour of flow field around submerged bodies when they approach free surface. Finally one set of typical measuring signals for this draught condition are also presented as in Figs. 9.61 to 9.70.

9.8 Conclusions

The mathematical approach using the linear optimal control concept to study the dynamic positioning behaviour of twin hulled marine vehicles is briefly introduced. Experimental work on the dynamic positioning aspects of a twin hulled structure is described. Detailed description of the data acquisition and analysis system for the experimental work is also described.

The setup of the manoeuvring experiment is described and the design for data measurement facility such as the two straight bar device and data acquisition system is introduced. The standard procedure of the data analysis system for the experimental investigation is discussed in detail.

A series of experiments were carried out in the Hydrodynamics Laboratory for different submergence depths, trim and drift angles for measuring the sway force and yaw moment. The experimental results are based on the technique of curve fitting to obtain several newly developed formulae which can be used by researchers for simulation analyses on manoeuvring performance and dynamic positioning of twin hulled marine vehicles.

CHAPTER 10
PRACTICAL ENGINEERING APPLICATIONS AND TECHNICAL DISCUSSIONS

10.1 General description

Much research work has been contributed for accurate prediction of dynamic motions of offshore structures in waves. In spite of such efforts, several problems still remain to be solved or to be contributed further for correct evaluation of their motion characteristics and safety at sea as follows.

A) There are certain forces acting on marine structures to restore their motions in waves and buoyancy variation is the origin of such restoring forces for heave, roll and pitch motions. The restoring forces together with inertia forces associated with mass and acceleration create natural frequencies of those modes of motions. If the frequency of the wave excitation force is close to the natural frequency, resonance occurs to lead to significant magnitude of motions.

Offshore structures have the restoring force even for the motions in horizontal plane, where no buoyancy variation contributes, because of the reaction of mooring lines. Magnitude of such restoring forces due to the mooring system is very small compared with the mass of offshore structures, so the natural periods of surge, sway and yaw motions are so long as 100 to 200 seconds.

In principal, sea waves can be assumed to be composed of many components of waves with different frequency. Linear wave excitation forces are superposition of components with frequencies corresponding to the component waves which means that they do not contain a long period component as 100 seconds. However second order forces due to these multi-frequency waves can have components with

the difference frequency of every two wave components. If the waves have components whose frequencies are very close to each other, the second order force will have very long period as 100 seconds and may induce resonance of motions in the horizontal plane. This will affect safer design of the mooring system as discussed by Hsu and Blenkern (1970), Arai et al (1976).

In such situations, the motions must be combined modes, one of which is fast frequency and small amplitude motion corresponding to the linear wave force and another is low frequency and large amplitude due to the second order force. Effect of the low frequency motion on the fast frequency motion has by no means been studied and this effect might be considered to be forward speed effect (or backward speed effect) on the oscillatory motions.

B) Accurate prediction of damping forces is important to calculate the motion responses of the low frequency oscillations, since the low frequency motions are considerably large only at resonance and magnitude of such damping forces determines magnitude of motion responses. Several researches have been done on which wave making or viscous effect is dominant in the damping forces in such a slow motion as published by Wichers and van Sluijs (1979), Saito et al (1984). Saito proposed an approach to determine the damping forces proportional to the velocity of the low frequency oscillation from the second order horizontal forces in waves. If such second order horizontal forces are plotted against the body velocity, the slope of the curve at zero velocity is supposed to obtain a coefficient of the damping force proportional to the velocity.

C) Stability of offshore structures is always of concern to designers and operators. Nevertheless they do not have a long history of research and practical experience. In fact regulations on stability are still at primitive level (ABS 1968). In United Kingdom, Japan as well as other countries, a lot of project studies have been concentrated on the stability of offshore structures in waves to find rational foundation for reasonable stability regulations such as Morrall (1978), Martin (1978), Numata (1978),Takarada et al (1984), Arai and Takaishi (1986), Atlar

(1986) and Takezawa (1987) et al. Two principal points emphasized in those studies are related to this research work, i.e. the second order forces acting on single or twin hulled marine vehicles lead to further inclination and steady tilt moments acting on offshore structures under combined actions of wave and current are to be predicted.

The configuration of the twin hulled marine vehicle is very complicated but the most are typically of two submerged long bodies (cylinders) with slender vertical surface piercing columns. So the hydrodynamic characteristics in beam seas are supposed to be realized even with very simple configuration of two circular cylinders with the wave crests parallel to their axis. The low frequency motion of very large amplitude is approximated as quasi-steady movement in numerical computations of hydrodynamic loadings.

The calculated results of the hydrodynamic coefficients between both Tasai's practical and present fundamental approaches are compared and discussed. The results of the steady tilt moments by direct pressure integration are compared with those of experimental work performed in Japan (Maeda 1984 and Ikeda 1985 et al) and a parametric study for different inclinations in varying current speeds is carried out. The predictions of steady tilt moments acting on twin hulled vehicles from previous theoretical approaches are compared and discussed. The calculated results from the present approach is compared with those from previous theoretical and experimental work. In particular the work performed by Martin et al (1978) is reviewed and the concept of Martin's model is discussed. The results of both approaches are investigated. The effects due to forward speed and interactions between two hulls using the Martin-type twin hulled model are extensively investigated and numerical results are discussed in detail. The effects of the viscous and waterline forces acting on the vertical surface piercing columns on steady tilt behaviour of an inclined offshore structure are studied and discussed. Finally the predicted results for a typical offshore twin hulled structure model, based on the present theoretical approach, are presented to demonstrate the overall value of this research work for engineering applications to twin hulled marine vehicles under the combined actions of wave and current.

10.2 Results comparison between Tasai's approximate approach and present fundamental approach

The practical approach to predict hydrodynamic loadings and motion responses of twin hulled marine structures in waves was proposed by Tasai (1970) and calculated results meet with engineering accuracy as discussed in Chapter One. The fundamental approach by direct pressure integration over body boundary contours is described in detail and completely investigated in earlier chapters. Comparison of computed results such as added mass and damping coefficients between practical and fundamental approaches are discussed as follows.

Calculations of hydrodynamic loadings on a twin hulled marine structure are performed for submergence depth ratio d/a = 4.18, separation distance ratio c/a = 7.73 and no inclination in waves. The predicted results of non-dimensionalized surge added mass coefficient show similar tendency and the prediction by Tasai approximate method is constant as in Fig. 10.1. In heave and pitch motions, both results match well as in Figs. 10.2 and 10.3. Added mass coefficients are assumed to be constant over the wave period range and show reasonable accuracy of less than 5 % discrepancy with the fundamental approach.

As for non-dimensionalized damping coefficients, predicted results in surge, heave and pitch motions by direct pressure integration method show fluctuating behaviour for all wave periods and the discrepancies of both predictions are not significant as in Figs. 10.4 to 10.6. In fact it is confirmed that the Tasai approximate approach is an economical and efficient tool for practical predictions on motion dynamics of twin hulled marine structures in waves.

10.3 Practical applications on Japan SR-1988 twin hulled model

In order to confirm theoretical predictions of steady tilt moments due to second order effects on twin hulled marine vehicle under combined actions of wave

and current, calculated results of present theoretical approach by direct pressure integration over body boundary contours are compared with three dimensional experimental work from Japan and the details are discussed here.

Based on the SR-192 twin hulled model of Japanese Ship Research Institute as shown in Fig. 10.7, parametric studies of steady tilt moments due to second order forces taking into consideration effects of forward speed (equivalent current effect) and interactions between two hulls are systematically investigated for different inclinations of ±5, ±10 and ±15 degrees in varying ±2 and ±4 knots current speeds. The present theoretical work on steady tilt moment is compared with experimental results and the theoretical prediction compares with full scale results from experiments (Takerada et al 1984).

Parametric studies of non-dimensionalized steady tilt moments acting on twin hulled marine vehicle with submergence depth ratio d/a = 2.59 and separation distance ratio c/a = 9.71 are performed for different current speeds and inclinations in waves. The predictions of steady tilt moments are carried out for different current speeds of +2 (referred to as following waves), -2 (referred to as head waves), +4 and -4 knots in positive 10 degree tilt (into incident wave) condition as shown in Fig. 10.8. Calculated results in following waves are larger for higher current speed, but those in head waves show adverse tendencies except for short wave period (within T = 0.60) range. For negative 10 degree tilt (following incident wave) condition, calculations of steady tilt moments are shown for different current speeds of +2, -2, +4 and -4 knots as in Fig. 10.9. The calculated results in negative tilt condition show similar magnitude and tendency as those of positive tilt condition, but in the reverse direction. In general as the current speed is higher, the peak value shifts to higher wave period. The peak value of the non-dimensionalized steady tilt moment for period of 1.0 second and for current velocity of 4 knots in positive 10 degree tilt condition is 1.0.

As for the positive and negative 15 degree tilt conditions, predicted results of non-dimensionalized steady tilt moments for different current speeds are presented

as shown in Figs. 10.10 and 10.11. From such results, significant contribution due to large inclination for higher current speed in following waves occurs and it can be concluded that such severe environmental conditions such as higher current speed (Fn = 0.40) and larger inclination (15 degree) in following waves should be more carefully studied to investigate the steady tilt behaviour of sea-going ships and marine vehicles.

Calculated results of non-dimensionalized steady tilt moments for different current speeds in positive and negative 5 degree tilt conditions are presented in Figs. 10.12 and 10.13. All results show similar tendency with smaller magnitude (less than 0.40 at peak value) and no much discrepancy for different current speeds. It means that the steady tilt behaviour of twin hulled marine vehicles in head and following waves is rather safe in small tilt (for example less than 5 degree) conditions.

Theoretical predictions of steady tilt moments due to second order effects on twin hulled marine vehicle in head and following waves are compared with three dimensional experimental work (Maeda and Ikeda 1985 et al) and both theoretical and experimental results match well as shown in Figs. 10.14 to 10.25 for different inclinations of 10, 15 and 5 degree and current speeds respectively. For positive 10 degree tilt condition, the compared results for different -2 and +2 knot current speeds have good agreement as presented in Fig. 10.14 and same conclusions are for different -4 and +4 knot current speeds as in Fig. 10.15. For negative 10 degree tilt condition, compared results are also shown in Figs. 10.16 and 10.17. From such comparison study between theoretical and experimental work, it is found that the second order forces acting on the submerged hulls are dominant, compared with that of the vertical surface piercing columns (Martin 1978 and Atlar 1986 et al), and the motion amplitude of the twin hulled marine structure in the beam sea condition can be assumed to be small from the viewpoint of physical and practical engineering applications. It is clear that the present pressure integration approach can be applied as an effective and useful tool for designers and engineers to predict the steady tilt behaviour of twin hulled marine vehicles under combined actions of wave and current.

As theoretical predictions have been confirmed with experimental results, the full scale predictions, based on SR-192 twin hulled model, by experimental results from model tests are carried out for different ±2 and ±4 knot current speeds in ±15 degree tilt conditions and all calculated results are as in Figs. 10.26 to 10.29. Both full scale and theoretical results are compared and the full scale predictions are almost three (3) times smaller than those from theoretical results for such severe conditions. In fact it is clear that the scale effect always exists and more research efforts concentrated on reasonable correlation between model and full scale results are still required.

10.4 Practical applications and comparison studies on U.K. Glasgow HL-1986 work

A technical review of past research work, such as Ogilvie (1963), Numata (1978), Morrall (1978), Martin (1978) and Atlar (1986), on steady tilt moments due to second order forces acting on submerged structures in waves is extensively surveyed. The practical approaches in these researches are simplified and the twin hulled vehicle is assumed as two rigidly held apart cylinders submerged under a free surface for zero speed case. The prediction of steady tilt moments acting on twin hulled marine vehicles is based on the empirical formula of the second order force in vertical direction only which takes no effect of forward speed and interaction between two submerged hulls into consideration.

In present theoretical approach, the steady tilt moments acting on twin hulled vehicles due to the effect of second order forces in both horizontal and vertical directions are considered. A comparison study on steady tilt moments on twin hulled marine vehicles between several previous practical approaches and present theoretical approach is investigated in detail and predicted results of second order vertical forces acting on the submerged left and right hulls and steady tilt moments on the twin hulled marine vehicle under a free surface for non-forward speed case are extensively investigated. A parametric study on steady tilt moments due to

second order forces is performed for different submerged depths, separation distance and inclinations in zero current speed condition.

Parametric studies based on several different kinds of empirical formula, such as Morrall (1978), Numata (1978), Lee-Newman modified by Atlar (1986), Lee-Newman modified by Wu (1993) and present fundamental approach (1993) by direct pressure integration over body boundary contours is performed to predict second order vertical forces acting on the submerged left and right hulls and steady tilt moments on the twin hulled marine vehicle under a free surface for non-forward speed case are extensively investigated. The calculated results of the twin hulled model for different submergence depths, separation distance and inclinations for zero speed case are classified into three major categories and are as follows.

A) For submergence depth ratio d/a = 2.0, separation distance ratio c/a = 4.0 condition :

For the non-dimensionalized second order vertical forces acting on the left hull of twin hulled structure in 10 degree tilt condition, all predicted results have similar tendencies and a peak value predicted by pressure integration occurs at low frequency ka = 0.40 point as shown in Fig. 10.30. In general all calculations match well in low frequency (within ka = 0.60) range but significant discrepancy for the remaining range of frequencies. Moreover the results predicted by Atlar (1986) and Wu (1993), modified from Lee-Newman (1971) approach, are about three (3) times smaller than that of Morrall (1978) and two (2) times for Numata (1978). It is found that the predictions by Lee-Newman modified approaches are rather small but those by Morrall and Numata approaches are almost larger. The predictions by direct pressure integration just lie between these four results and have a critical value in the low frequency region and it may be noted that this present theoretical approach can predict more accurate hydrodynamic loadings in the low frequency range.

For the non-dimensionalized second order vertical forces acting on the right

hull of twin hulled structure in 10 degree tilt condition, all results meet with good agreement and reasonable accuracy over the range of frequencies as in Fig. 10.31. It is clear that the numerical results predicted by all five different approaches are reliable for practical design applications.

For non-dimensionalized steady tilt moments acting on twin hulled structure in 10 degree tilt condition, all results have similar behaviour as presented in Fig. 10.32. In general all calculations match well for the low frequency (within ka = 0.65) range but significant discrepancy is seen for the remaining range of frequencies. Similarly calculated results by Atlar (1986) and Wu (1993), modified from Lee-Newman (1971) approach, are about three (3) times smaller than those from Morrall (1978) and two (2) times for Numata (1978). Predictions by Lee-Newman modified approaches are rather small but those by Morrall and Numata approaches are larger. The predictions by direct pressure integration just lie between these four results and have a critical value in the low frequency region.

For the non-dimensionalized second order vertical forces and steady tilt moments acting on the twin hulled structure in 5 degree tilt condition, all predicted results show reasonable agreement as in Figs. 10.33 to 10.35 and have similar tendencies as those of 10 degree tilt condition. In 15 degree tilt condition, calculated results of forces and steady tilt moments are also presented as in Figs. 10.36 to 10.38. On comparison of the results, good agreement is found for forces acting on the right hulls and significant discrepancies in forces acting on the left hull and steady tilt moments on twin hulled marine vehicles predicted by five different approaches. It is clear that these four different kinds of practical approaches take no interaction effect between two submerged hulls into consideration exactly.

In conclusions, predicted results of second order vertical forces acting on the left hull are always larger than that on the right hull. For greater inclination condition, second order vertical forces on left hull and steady tilt moments on twin hulled structures show greater magnitude but forces on right hull have adverse tendencies.

B) For submergence depth ratio d/a = 4.0, separation distance ratio c/a = 4.0 condition :

For deeper submergence, all predictions of non-dimensionalized second order vertical forces and steady tilt moments on twin hulled structure in 10 degree tilt condition match very well as illustrated in Figs. 10.39 to 10.41 and calculated results are smaller than those of shallower submergence (d/a = 2.0) condition. As for numerical results in 5 and 15 degree inclinations, these are systematically presented as in Figs. 10.42 to 10.47. The only discrepancy in low frequency (within ka = 0.50) range is predicted by Wu (1993) and this approach is modified from Lee-Newman (1971). It is clear that the five different approaches are convenient and effective to predict the steady tilt behaviour of twin hulled marine vehicles in waves.

C) For submergence depth ratio d/a = 2.0, separation distance ratio c/a = 6.0 condition :

Calculations of non-dimensionalized second order vertical forces acting on left hull of twin hulled structure in 10 degree tilt condition show similar behaviour as those of category (A) and peak values predicted by both pressure integration and Wu (1993) approaches occur at low frequency ka = 0.50 point as in Fig. 10.48. All calculations show clear discrepancies over all frequency range and numerical results predicted by Atlar (1986) and Wu (1993) are about three (3) times smaller than that of Morrall (1978) and two (2) times for Numata (1978). It is found that the predictions by Lee-Newman modified approaches are rather small but those from Morrall and Numata approaches are larger. Predicted results by pressure integration lie between these four results and have a critical value in the low frequency region.

For non-dimensionalized second order vertical forces acting on the right hull of twin hulled structure in 10 degree tilt condition, all results have good agreement over all frequency range except for results predicted by Wu (1993) as in Fig.

10.49. For non-dimensionalized steady tilt moments acting on twin hulled structure in 10 degree tilt condition, all results show similar behaviour as in Fig. 10.50. In general all calculations have significant discrepancy for the range of frequencies. Similarly predicted results by Atlar (1986) and Wu (1993) are about three (3) times smaller than that of Morrall (1978) and two (2) times for Numata (1978). Indeed numerical predictions from Lee-Newman modified approaches are almost small but those by Morrall and Numata approaches are larger.

For non-dimensionalized second order vertical forces and steady tilt moments acting on the twin hulled structure in 5 degree tilt condition, all results have rather reasonable agreement as in Figs. 10.51 to 10.53 and have same tendencies as those of 10 degree tilt condition. In 15 degree tilt condition, calculated results of such forces and steady tilt moments are also presented as in Figs. 10.54 to 10.56. For second order vertical forces acting on the left hull and steady tilt moments on twin hulled marine vehicles predicted by five different approaches, significant discrepancy in calculated results are as in Figs. 10.54 and 10.56. Results calculated by Morrall and Numata approaches show divergent behaviour in the higher frequency range and those from Lee-Newman modified approaches are always under-estimated. In principal it can be realized that these four different kinds of practical approaches which take no interaction effect between two submerged hulls into consideration cannot be effectively applied to investigate the steady tilt behaviour of twin hulled marine vehicles in such severe conditions.

10.5 Practical applications on U.K. Martin-1978 twin hulled model

The work performed by Martin et al (1978) is reviewed and the concept of the Martin-type model is discussed. The calculated results of steady tilt moments on twin hulled marine vehicle, based on the Martin (1978) twin hulled vehicle model as in Fig. 10.57, are investigated and compared with those from present and previous work. A comparison study with all previous work, based on the Martin (1978) twin hulled vehicle model, for second order vertical forces acting on

individual left and right hulls and steady tilt moments of the inclined twin hulled marine vehicle in waves for non-forward speed case is carried out. Calculated results by pressure integration and Wu (1993) approaches are compared for different Froude numbers of Fn = 0.0, 0.2 and 0.4 in 10 degree tilt condition and a parametric study is also carried out for different Froude number and inclinations.

In Martin (1978) approach, it is assumed that the submerged pontoons are sufficiently long enough and a two dimensional formulation is satisfactory. All columns and bracings are ignored in calculating wave forces and are assumed to contribute only in the hydrostatics. The ocean is assumed to be inviscid, incompressible, of infinite depth, and the irrotational solution can be presented in terms of a velocity potential by using the second order wave theory. The mathematical problem is formulated and solved by the multipole expansion method to predict second order forces and steady tilt moments acting on twin hulled marine vehicles.

The outline of this approach is briefly described as follows. It is supposed that a particular displaced mean position is artificially imposed by applying a suitable steady force and moment. The coupled rigid body and hydrodynamic problems are expanded in powers of wave steepness ε, supposing that motions about the mean position are also of order ε. The first order problem admits the required oscillatory solution and the second order problem indicates how the steady force and tilt moment are calculated in the presence of the first order oscillation. Results are presented at this stage for various mean displaced motions artificially imposed. Finally the mean position may be adjusted until the resulting steady wave upthrust and moment are exactly balanced by hydrostatic restoring forces. No artificially imposed upthrust or moment is then required. In general this procedure will lead to a mean elevation as well as a mean tilt. Solutions of the first order problem for various aspects have been studied by Wang (1970) for the case of forces heaving with the cylinders at equal depth by Schnute (1971) for the scattering problem on cylinders of arbitrary radii fixed at arbitrary depths. In fact this approach does not solve the boundary value problem exactly and only steady tilt moments acting on twin hulled structures in waves for non-forward speed case

is discussed.

Based on the Martin (1978) twin hulled vehicle model, a comparison study with all previous work including Martin's approach for second order vertical forces acting on individual left and right hulls and steady tilt moments of the inclined twin hulled marine vehicle in waves for non-forward speed case is extensively carried out as follows.

The calculations are performed for second order vertical forces acting on left and right hulls and steady tilt moments on this twin hulled structure with submergence depth ratio d/a = 3.17, separation distance ratio c/a = 10.0 in no tilt and zero current speed condition and predicted results are as in Figs. 10.58 to 10.60. All calculated results show reasonable agreement over the range of frequencies. The predicted result of non-dimensionalized second order vertical forces on left hull by Wu (1993) have infinite peak value in low frequency (at ka = 0.05) range and show significant discrepancy with other four different approaches as indicated in Fig. 10.58. It may be noted that the Wu (1993) approach is not suitable enough for practical design applications. From Fig. 10.60, it is clear that approaches such as Morrall (1978), Numata (1978) and Atlar (1986) take into consideration no effect of interactions between the two submerged hulls and can provide no information about hull interaction effect of twin hulled marine vehicles in no tilt condition. It may be noticed that the present theoretical approach by pressure integration is the most effective tool for practical engineering applications.

Predicted results of second order vertical forces acting on left and right hulls and steady tilt moments on twin hulled structure for submergence depth ratio d/a = 3.17, separation distance ratio c/a = 10.0 in 5 and 10 degree tilt conditions are presented as in Figs. 10.61 to 10.66 respectively. Basically all calculated results show reasonable agreement over the range of frequencies except for predicted results by Wu (1993) which have infinite peak value in the low frequency (at ka = 0.05) range as in Figs. 10.61 and 10.64 and show significant discrepancy with other four different approaches as in Figs. 10.62 and 10.65. For non-

dimensionalized steady tilt moments, predicted results by Martin (1978) approach show large difference with five other theoretical approaches and are always underestimated as in Figs. 10.63 and 10.66. It is found that the Martin approach is not suitable enough to provide useful information on steady tilt aspects.

Calculated results by pressure integration and Wu (1993) approaches are compared on the Martin twin hulled model with submergence depth ratio d/a = 3.17 and separation distance ratio c/a = 10.0 for different Froude numbers, i.e. Fn = 0.0, 0.2 and 0.4 in 10 degree tilt condition to investigate the discrepancy of forces and steady tilt moments due to current effect. The non-dimensionalized second order vertical forces and steady tilt moments acting on this twin hulled model are in Figs. 10.67 to 10.75. In general the predictions of such forces and tilt moments by Wu (1993) have a more significant peak than those of pressure integration in the low frequency range and less contribution from the remaining range of frequencies. Hence it is concluded that the Wu (1993) approach modified from Lee-Newman work is not reliable.

A parametric study for different Froude number and inclinations is performed to investigate the steady tilt behaviour of twin hulled marine vehicles under combined actions of wave and current further. The theoretical predictions of second order vertical forces and steady tilt moments of twin hulled marine vehicles in waves for different Froude numbers, i.e. Fn = 0.0, 0.2 and 0.4 in 10 degree tilt condition are carried out and numerical results are shown as presented in Figs. 10.76 to 10.78. There is not much variation between the results due to current effect. For the inclination effect, the significant discrepancy is clearly presented as in Figs. 10.79 to 10.81. Hence it may be concluded that larger inclination always induces severe steady tilt behaviour on twin hulled marine vehicles under combined actions of wave and current, particularly in following waves as discussed in Chapter Seven.

10.6 Investigation of effects due to forward speed and hull interactions on Martin-type twin hulled model

Here theoretical investigations are extensively performed for the effects due to forward speed and hull interactions on the Martin-type twin hulled (two rigidly held apart cylinder) model and numerical results such as added mass and damping coefficients, wave excitation forces, motion responses, second order horizontal and vertical forces, steady tilt moments and computation time etc, are systematically presented for submergence depth ratio d/a = 2.0, separation distance ratio c/a = 4.0 and no tilt in head and following waves. Numerical predictions of the hydrodynamic characteristics of twin hulled marine vehicles in head and following waves are categorized into five (5) major groups as follows.

A) For second order horizontal and vertical forces :

Application is performed on twin hulled structure model. The two caissons are simulated by circular cylinders to investigate the damping coefficient of the low frequency motion. Several researches concluded by Wicher and van Sluijs (1979), Saito (1984) et al have shown that the wave making or viscous effect is dominant in the damping forces in a slow motion. Saito (1984) et al presented an approach to determine damping forces proportional to the velocity of the low frequency oscillation forces from second order forces in waves. If the second order force is plotted against the velocity of the body, the slope of the curve at zero velocity is supposed to give a coefficient of the damping force proportional to the velocity. These results are for a surface piercing body. It can be concluded that it is also valid for submerged body. Similarly the second order forces for different positive and negative Froude numbers are calculated. The results clearly indicate that the curve is flat at zero when the cross section of the submerged caisson is almost circular. It may be concluded that viscous effect is dominant on the damping forces of low frequency motion with the caisson part of the offshore structures.

Theoretical calculations of second order horizontal and vertical forces acting on twin hulled marine vehicles in head and following waves are performed for

Froude number Fn = +1.5 to -1.5. For wave number ka = 0.10, predicted results of second order horizontal forces by both approaches, i.e. direct pressure integration and momentum flux consideration match well and the effects of forward speed and interactions between two hulls are clearly indicated as shown in Fig. 10.82. The results clearly indicate that the curve is flat at zero. Moreover the predictions of second order vertical forces by both theoretical approaches are presented and large discrepancy between both results, particularly an infinite value at Fn = -1.0 (in following waves), may be due to Lee-Newman (1971) work which does not consider the effects of forward speed and interactions between two hulls as shown in Fig. 10.83. Again the results show that the curve is flat at zero. In fact this conclusion is originally valid for a surface piercing body and it is also confirmed to be valid for submerged body.

For wave numbers ka = 0.20, 0.30, 0.40, 0.50 and 0.60, calculated results of second order horizontal and vertical forces against Fn = +1.5 to -1.5 are systematically presented as in Figs. 10.84 to 10.93. As to the result comparison for different wave numbers ka = 0.10 to 0.60, both results of second order horizontal and vertical forces by present theoretical approach are indicated to give certain information about the effects of forward speed and interactions between two hulls as shown in Figs. 10.94 and 10.95. In general such results clearly indicate that significant magnitude is experienced in following waves within Fn = -0.5 to -1.0 range.

B) For added mass coefficients and computation time :

Calculations of surge and heave added mass coefficients and pitch added moment of inertia of twin hulled marine vehicles in head and following waves are carried out for Froude number Fn = +1.5 to -1.5. For wave number ka = 0.10, numerical results of surge and heave added mass coefficients are as in Figs. 10.96 and 10.97 respectively and the non-dimensionalized amplitudes are greater in following waves as current speed increases. For non-dimensionalized pitch added moment of inertia coefficient, predicted results clearly show two knuckle points in

head and following waves, i.e. one at Fn = +0.5 (in head waves) and the other at Fn = -0.7 (in following waves) and it may be due to the effect of interactions between two hulls as shown in Fig. 10.98. The computation time for this numerical calculation is as in Fig. 10.99 and two significant peaks within the range of Fn = -0.5 to +0.5 are due to the hull interaction effect.

For wave number ka = 0.50, predicted results of surge and heave added mass coefficients, pitch added moment of inertia and the computation time against Fn = +1.5 to -1.5 are systematically indicated for technical reference as in Figs. 10.100 to 10.103. As to result comparison for different wave numbers ka = 0.10 to 0.60, all results of surge and heave added mass coefficients, pitch added moment of inertia and computation time by present theoretical approach are shown to give certain information about the effects of forward speed and interactions between two hulls as in Figs. 10.104 and 10.107. In general these results clearly indicate that the significant effect is indicated within Fn = -0.5 to +0.5 range.

C) For damping coefficients and steady tilt moments :

Numerical computations of non-dimensionalized surge, heave and pitch damping coefficients of twin hulled marine vehicles in head and following waves are carried out for Froude number Fn = +1.5 to -1.5. For wave number ka = 0.10, numerical results of surge, heave and pitch damping coefficients are as in Figs. 10.108 to 10.110 and the predicted is flat at Fn = 0.0 point and negative occurs for Fn = -1.5 and Fn = +1.2. Two knuckle points of all results are seen in head and following waves, one at Fn = +0.5 (in head waves) and the other at Fn = -0.7 (in following waves) and for pitch mode significant negative value at Fn = -1.5 (following waves) as in Fig. 10.110. Non-dimensionalized steady tilt moments in head and following waves are as in Fig. 10.111 and the peak value at Fn = -0.7 confirms the hull interaction effect.

For wave number ka = 0.50, predictions of surge, heave and pitch damping coefficients and steady tilt moments in head and following waves are as in Figs.

10.112 to 10.115. On comparison of surge, heave and pitch damping coefficients and steady tilt moments for different wave numbers, i.e. ka = 0.10 to 0.60, by present theoretical approach shown certain information about the effects of forward speed and interactions between two hulls as in Figs. 10.116 and 10.119. In general such results clearly indicate that the significant effect is indicated beyond Fn = -0.5 range.

D) For dynamic motion responses :

Theoretical calculations of non-dimensionalized motion responses in surge, heave and pitch modes in head and following waves are performed for Froude number Fn = +1.5 to -1.5. For wave number ka = 0.10, numerical results of surge and heave motion responses are as in Figs. 10.120 and 121 respectively and predicted results show only one peak value at Fn = 0.0 point. For pitch mode significant peak value at Fn = -0.7 (following waves) indicate the importance of the steady tilt behaviour in following waves as in Fig. 10.122.

For wave number ka = 0.30 and 0.50, numerical results of dynamic motion responses in surge, heave and pitch modes of twin hulled marine structures in head and following waves are as in Figs. 10.123 to 10.128. On comparison for different wave numbers ka = 0.10 to 0.60, the predictions of surge, heave and pitch motion responses by present theoretical approach provide certain information about the effects of forward speed and interactions between two hulls as in Figs. 10.129 and 10.131.

E) For wave excitation forces :

Numerical predictions of non-dimensionalized surge, heave excitation forces and pitch moments of twin hulled marine vehicles in head and following waves are investigated for Froude number Fn = +1.5 to -1.5. For wave number ka = 0.10, calculated results of surge and heave wave excitation forces are as in Figs. 10.132 and 133 respectively and predicted results show two peak values at Fn = -0.5 and -0.7 points. For pitch moment significant peak value at Fn = -0.7 (following waves)

indicate the effect to the steady tilt behaviour in following waves as in Fig. 10.134.

For wave number ka = 0.30 and 0.50, numerical results of wave excitation forces and moments in surge, heave and pitch modes in head and following waves are as in Figs. 10.135 to 10.140. On comparison for different wave numbers ka = 0.10 to 0.60, calculated results of forces and moments by present theoretical approach are useful for design applications as shown in Figs. 10.141 and 10.143.

10.7 Investigation of effects due to viscous and waterline forces on vertical surface piercing columns of twin hulled vehicles

The effects of viscous forces acting on vertical surface piercing columns of a twin hulled marine vehicle are studied to investigate the steady tilt behaviour of an inclined twin hulled offshore structure in waves. The mathematical formulation, based on Morrison approach, of viscous horizontal forces acting on single vertical surface piercing column are described as shown in Appendix D. The steady tilt moments due to such viscous horizontal forces acting on vertical surface piercing columns and the second order effect on submerged hulls are discussed. A comparison study of steady tilt moments acting on twin hulled offshore structures for different GM values is performed.

The comparison study of steady tilt moments due to such viscous horizontal forces acting on vertical surface piercing columns, predicted by Morrison(Wu) 1993 approach, and the second order effect on submerged two hulls, calculated by Morrall (1978), Numata (1978) and L-N(Atlar) 1986 approaches, are performed on a twin hulled marine vehicle with submergence depth ratio d/a = 2.0, separation distance ratio c/a = 4.0 and 5 degree tilt condition. All calculated results, predicted by these four different kinds of practical approaches such as Morrall (1978), Numata (1978), L-N(Atlar) 1986 and Morrison(Wu) 1993, are performed for different GM values and discussed as follows.

A) For the ratio of GM/a = 0.30 :

The predictions of non-dimensionalized steady tilt moments acting on two submerged hulls of twin hulled structures by Morrall (1978), Numata (1978) and L-N(Atlar) 1986 are compared with those including viscous horizontal forces on four vertical surface piercing columns by Morrison(Wu) 1993. A slight discrepancy between both results are as in Figs. 10.144 to 10.146. Calculated results of steady tilt moments on two submerged hulls are compared with viscous forces on columns and it is found that the contribution due to viscous horizontal forces on vertical columns is rather insignificant as in Fig. 10.147.

B) For the ratio of GM/a = 0.40 :

Similarly computed results of non-dimensionalized steady tilt moments acting on two submerged hulls of twin hulled structures by Morrall (1978), Numata (1978) and L-N(Atlar) 1986 are compared with those cases including viscous horizontal forces on four vertical surface piercing columns by Morrison(Wu) 1993. All calculations show not much difference as in Figs. 10.148 to 10.150. Calculated results of steady tilt moments acting on two submerged hulls are compared with viscous forces on vertical columns and it is clear that viscous horizontal forces acting on vertical columns show small effect on total steady tilt moments acting on twin hulled marine vehicles in waves as in Fig. 10.151.

C) For the ratio of GM/a = 0.50 :

Calculated results of non-dimensionalized steady tilt moments acting on two submerged hulls of twin hulled structures by Morrall (1978), Numata (1978) and L-N(Atlar) 1986 are compared with those cases including viscous horizontal forces on four vertical surface piercing columns by Morrison(Wu) 1993 as in Figs. 10.152 to 10.154. Predicted results of steady tilt moments on two submerged hulls are compared with viscous horizontal forces on vertical columns and it is noticed that the viscous effect on vertical columns is insignificant on steady tilt behaviour

as indicated in Fig. 10.155. Conclusion by pervious researches confirms that the second order forces acting on submerged hulls are clearly dominant as compared with forces acting on vertical surface piercing columns (Martin 1978 and Atlar 1986 et al). If the value of GM increases, the contribution due to viscous forces becomes greater and it may be concluded that the viscous effect in the horizontal direction acting on vertical surface piercing columns help to reduce steady tilt behaviour.

A comparison study of steady tilt moments is performed for submergence depth ratio d/a = 2.0, separation distance ratio c/a = 4.0 and 5 degree inclination for different GM values. Based on Morrall (1978), Numata (1978) and L-N(Atlar) 1986 approaches, calculations are carried out on steady tilt moments with viscous contribution for different GM values, i.e. GM/a = 0.3, 0.4 and 0.5 and all results are as in Figs. 10.156 to 10.158. Predictions of steady tilt moments due to viscous effect on vertical columns are compared and the contribution due to greater GM value is as in Fig. 10.159.

Finally the predictions, by Morrall (1978), Numata (1978) and L-N(Atlar) 1986, of non-dimensionalized steady tilt moments including viscous effect on vertical columns are compared with that of viscous effect on columns only and the calculated results for different GM values are presented as in Figs. 10.160, 10.161 and 10.162.

As for theoretical predictions of waterline forces acting on surface piercing body without forward speed effect in waves, previous research work performed by Pinkster (1980) and Wichers (1988) et al are reviewed. The five main components of such mean wave steady forces as proposed by Pinkster (1980) are briefly described as follows.

A) Contribution I (wave elevation) is due to the relative wave elevation which can be referred as the contribution to the waterline force. The first order hydrodynamic forces are predicted by direct pressure integration over the mean wetted surface of the body. When the hydrostatic decay of this pressure including

diffraction effect is taken into consideration from the mean waterline to the instantaneous free surface, this produces an additional steady force over one wave period and the general equation is written as

$$F_{I_{mean}} = -\int_{WL} \frac{1}{2}\rho g \zeta_r^{(1)^2} \vec{n}\, dl_{mean} \qquad (10.1)$$

where the integrand in this case always represents a pressure increase acting inwardly at the waterline.

B) Contribution II (velocity head) is due to the square of the velocity potential. The Bernoulli equation describes a dynamic pressure in terms of the quadratic first order wave particle velocity including the diffraction effect. The direct integration of this pressure over the mean wetted surface represents the steady force and the general formulation is described as

$$F_{II_{mean}} = -\iint_{S_0} -\frac{1}{2}\rho \left|\overline{\nabla}\phi^{(1)}\right|^2 \vec{n}\, dS_{mean} \qquad (10.2)$$

Here the integrand denotes a pressure decrease acting outwardly on the mean wetted surface of the body. In general the fluid velocity tends to be largest on the coming wave side and such results in a mean force component is directed into the waves.

C) Contribution III (body translation) is due to the translational displacement of the body. The first order hydrodynamic force can be realized that the pressure always acts on the mean position of the body. In fact the pressure field may slightly change due to the translational surge, sway and heave motions. Thus such steady forces can be predicted from direct integration of the product of this pressure gradient by the translational body displacement and the general equation is indicated as

$$F_{III_{mean}} = -\iint_{S_0} -\rho\left(\overline{\xi}^{(1)} \cdot \overline{\nabla}\phi_t^{(1)}\right) \vec{n}\, dS_{mean} \qquad (10.3)$$

Since this is a mixed product of the first order motion and pressure gradient, it is not possible to predict the sign of this quantity and the sign depends on the phase angles of both quantities.

D) Contribution IV (body rotation) is due to the product of the angular motion and acceleration. As the body rotates in roll, pitch and yaw modes, the pressure field also change slightly. For example a roll angle will incline the bottom of a rectangular caisson so that the pressure in the vertical direction will induce a horizontal force component which is the product of the heave pressure and the roll angle. The general formulation of this force is written as

$$F_{IV_{mean}} = \overline{\alpha}^{(1)}\left(M \cdot \ddot{\overline{\xi}}^{(1)}\right)_{mean} \qquad (10.4)$$

Hence the wave pressure integrated over the body surface is expressed in terms of the body acceleration and is the product of the first order rotational motion and body mass and acceleration.

E) Contribution V (second order effect) is due to the second order effect of velocity potential. This force is induced by the pressure gradient in second order waves and the detailed expression is formulated as proposed by Pinkster (1980).

In general the potential accuracy of this numerical approach is sufficient for the prediction of the first order hydrodynamic problem and second order horizontal forces of marine vehicles with non-forward speed effect in waves. As to forward speed case, certain difficulties of numerical approaches for theoretical computations still remain. More research efforts concentrated on this subject are possible to accurately predict the first and second order hydrodynamic problems of single or twin hulled marine vehicles in waves.

10.8 Example presentation of a twin hulled marine vehicle

The predicted results of a typical offshore twin hulled structure model, based on the present pressure integration approach, are presented to show the overall value of this theoretical work. Calculated results are divided into three major categories as follows.

A) First order hydrodynamic forces :

(a) The added mass coefficients for individual left and right ones of two rigidly held apart cylinders are predicted for different current speeds, submergence depths, separation distances and inclinations in head and following waves as in Figs. 10.163 to 10.165 and for the total system, they are as in Chapter Four.

(b) The damping coefficients for individual left and right ones of two rigidly held apart cylinders are calculated for different current speeds, submergence depths, separation distances and inclinations in head and following waves as in Figs. 10.166 to 10.168 and for the total system, they are as in Chapter Four.

(c) The wave excitation forces for individual left and right ones of two rigidly held apart cylinders are predicted for different current speeds, submergence depths, separation distances and inclinations in head and following waves as in Figs. 10.169 to 10.174 and for the total system, they are as in Chapter Four.

(d) The numerical results of the real and imaginary parts of Kochin functions in head and following waves are as in Chapter Five.

(e) The numerical results of the m-vector contribution due to forward speed effect are as in Chapter Five.

(f) The numerical results of motion responses in head and following waves with and without hydrodynamic restoring forces due to forward speed effect as in

Chapter Six.

B) Second order hydrodynamic forces :

(a) The second order horizontal forces acting on individual left and right ones and two rigidly held apart cylinders are calculated for different current speeds, submergence depths, separation distances and inclinations in head and following waves as in Chapter Seven.

(b) The second order vertical forces acting on individual left and right ones and two rigidly held apart cylinders are predicted for different current speeds, submergence depths, separation distances and inclinations in head and following waves as in Chapter Seven.

(c) The steady tilt moments due to second order horizontal and vertical forces are computed for different current speeds, submergence depths, separation distances and inclinations in head and following waves as in Chapter Seven.

C) Accuracy check of numerical computations :

(a) The numerical accuracy check of damping coefficients is checked out by the consideration of energy flux in the fluid domain and by direct pressure integration over the body boundary contours as in Chapters Four and Eight.

(b) The numerical results of wave excitation forces in terms of the Kochin functions is investigated by the Haskind and Newman relation as in Chapters Four and Eight.

(c) The numerical results of the m-vector contribution due to forward speed effect are compared with zero forward speed effect as in Chapter Five.

(d) The numerical results of the hydrodynamic restoring coefficients due to forward speed effect of two cylinder case are confirmed by analytical solutions of

single cylinder case as in Chapter Six.

(e) The numerical accuracy of second order horizontal forces is checked by direct pressure integration over the body boundary contours (near field approach) and by momentum flux consideration in the fluid domain (far field approach) as in Chapters Seven and Eight.

(f) The numerical accuracy of second order vertical forces is investigated by direct pressure integration over body boundary contours (near field approach) and momentum flux consideration in the fluid domain (far field approach proposed by Lee-Newman 1971) as in Chapter Seven.

(g) The numerical accuracy of the steady tilt moments is confirmed by three dimensional experimental work (Maeda 1984 and Ikeda 1985 et al) as in Chapter Ten.

10.9 Discussions and conclusions

All predicted results are systematically presented and the main conclusions are as follows.

A) The calculated results of the hydrodynamic coefficients between both Tasai's practical and present fundamental approaches are compared and discussed. In practical approach, added mass coefficients are assumed to be constant over all wave frequency range and show reasonable accuracy with the fundamental approach. As for non-dimensionalized damping coefficients, predicted results in surge, heave and pitch motions by direct pressure integration method show fluctuating behaviour over all wave periods and the discrepancies in both predictions are not significant. In fact it is confirmed that the Tasai (1970) approximate approach (Wu 1991) is an efficient and useful tool for practical predictions on motion dynamics of twin hulled marine structures in waves.

B) The results of the steady tilt moments by direct pressure integration are compared with three dimensional experimental work (Maeda 1984 and Ikeda 1985 et al) and a parametric study for different inclinations and varying current speeds is carried out. It is noticed that in the case of severe condition like current speed (Fn = 0.40) and large inclination (15 degree) in following waves, great care should be taken.

C) The predictions of steady tilt moments acting on twin hulled vehicles from previous theoretical approaches (Morrall 1978, Numata 1978, Atlar 1986 et al) are compared and discussed. The above five theoretical approaches are a useful tool to designers. It may be concluded that the empirical approaches mentioned above do not take into consideration the effect of forward speed and hull interactions. Hence they are not preferred, especially when it comes to predicting the steady tilt behaviour in severe conditions. It is clear that the pressure integration approach can be comfortably applied to predict more accurate hydrodynamic loadings and steady tilt behaviour of twin hulled marine structures in waves.

D) Work performed by Martin et al (1978) is reviewed and the concept of Martin's model is discussed. Predicted results by Martin (1978) approach show large difference with five other theoretical approaches are underestimated. It is found that the Martin approach is not suitable enough to provide useful information on steady tilt aspects.

Calculated results by both pressure integration and Wu (1993) approaches are compared with the Martin twin hulled model for submergence depth ratio d/a = 3.17, separation distance ratio c/a = 10.0, different Froude numbers, i.e. Fn = 0.0, 0.2 and 0.4 and 10 degree tilt condition to investigate the discrepancy in forces and steady tilt moments due to current speed effect. In general the predictions of such forces and tilt moments by Wu (1993) almost have more significant peak than those from pressure integration in the low frequency range and less contribution for the remaining range of frequencies. Hence it may conclude that the Wu (1993) approach modified from Lee-Newman work is not reliable.

E) The results of second order forces show that the curve is flat at zero. In fact this conclusion is originally valid for a surface piercing body and it is also confirmed to be valid for submerged body and viscous effect is dominant on the damping forces of low frequency motion on the caisson part of offshore structures.

For non-dimensionalized pitch added moment of inertia coefficient, predicted results clearly show two knuckle points in head and following waves and it may be due to the effect of interactions between two hulls. The computation time for this numerical calculation indicates that two significant peaks within the range of Fn = -0.5 to +0.5 are shown to demonstrate the hull interaction effect.

Two knuckle points in damping coefficients are shown in head and following waves, one at Fn = +0.5 (in head waves) and the other at Fn = -0.7 (in following waves) and for pitch mode significant negative value at Fn = -1.5 (following waves). For non-dimensionalized steady tilt moments in head and following waves the peak value at Fn = -0.7 point confirms the hull interaction effect.

In general a significant effect on pitch motion and pitch excitation moment is indicated in following waves and this gives some hints regarding the prediction of steady tilt behaviour in following waves.

F) Calculated results of steady tilt moments on two submerged hulls are compared with that of steady tilt moments due to viscous effect on vertical columns and it is clear that the contribution due to viscous horizontal forces on vertical columns is rather insignificant and provides certain positive benefit to steady tilt behaviour.

Conclusion by pervious researches (Martin 1978 and Atlar 1986 et al) confirms that the second order forces acting on submerged hulls are more dominant as compared with that of the vertical surface piercing columns. If the value of GM increases, the contribution due to viscous forces acting on twin hulled structures becomes greater and it may be concluded that the viscous effect in the horizontal direction acting on such vertical surface piercing columns has effective contribution

to the steady tilt behaviour.

As GM value increases, the effect of the column contribution in the steady tilt behaviour is significant. However in most cases the column effect helps to reduce the steady tilt behaviour.

CHAPTER 11
ACHIEVEMENTS, CONCLUSIONS AND RECOMMENDATIONS

11.1 Achievements and conclusions

A systematical review on the main findings of this research work is presented here with emphasis on the overall conclusions and several recommendations for future work as follows.

(1) A preliminary study of practical applications in the ocean engineering field was performed at the earlier stage. Practical engineering predictions of the Froude Krylov forces acting on floating buoys and twin hulled vehicles in waves were studied. The mathematical equations to predict hydrodynamic forces acting on floating buoys and twin hulled structures in the heeled condition were formulated by direct pressure integration over the body boundary contours. The predicted results are in good agreement with previous more approximate theoretical researches (Tasai 1983) and experimental work (Wu 1991).

The mathematical approach to predict the hydrodynamic behaviour of floating buoys with the mooring systems in waves were extended to twin hulled offshore structures. Approximate predictions based on the Froude Krylov approach show good agreement with that of previous researches (Tasai 1970, 1983). Results of experimental work (Wu 1991) performed for three different kinds of buoy models are compared with such calculations and generally fall within 10 % accuracy which is reasonable in engineering. In fact this practical approach has revealed that it can provide reliable predictions in CPU times less than 2 or 3 seconds and it can also be conveniently computed on desktop calculators for practical design and offshore engineering work.

For approximate calculations of twin hulled offshore structures in regular waves, there is good agreement with previous research work (Tasai 1970). Both theoretical and experimental results show good agreement with less than 5 % discrepancies in general.

All predicted results are compared with previous theoretical and experimental research work with reasonable engineering accuracy. On an analysis of the computation time taken for these calculations, it is found that the CPU time is only less than 5 seconds on the VAX 3600 micro computer system.

(2) The theoretical formulation of the boundary value problem with forward speed effect is described in detail. Under these linear assumptions, numerical solutions can be obtained by solving the integral equation of the velocity potential on the body surface. It is noted that not only non-linear effect on body boundary and free surface conditions make such problems mathematically intractable but also the instantaneous surfaces of such boundaries are difficult to be determined. These boundary conditions have to be linearized to a certain extent so that practical solutions can be obtained by numerical computations. Mathematical expressions of the radiation and diffraction wave depressions far upstream and far downstream are also described in terms of Kochin functions.

(3) The fundamental formulation of the most generalized form of Green function to predict hydrodynamic forces is theoretically derived for the boundary value problem of a single submerged body advancing at a constant forward speed and oscillating in incident waves and its derivatives are also described for the solution of velocity potential over body boundary contours in the integral equations. The theoretical formulation of this Green function which can be applied to arbitrary cross sections of submerged structures is fully derived and mathematical manipulation of the Green function which makes numerical computations more convenient is also achieved.

(4) The comprehensive derivation of analytical expressions for radiation and

wave excitation forces acting on the submerged structure in incident waves is described in detail. These are of first order with respect to motion responses and wave amplitudes. Due to forward speed effects, there is a contribution from the hydrodynamic restoring force terms proportional to body displacement. Based on such radiation and wave excitation forces, motion equations of dynamic responses of submerged structure translating at constant forward speed (equivalent current speed) in incident waves, but left to oscillate, are systematically formulated.

A valuable procedure for theoretical confirmation of numerical computations is developed and completely described. The numerical accuracy check of the damping coefficients is calculated by consideration of the energy flux in the fluid domain and by the direct pressure integration over body boundary contours. The numerical results of wave excitation forces in terms of the Kochin functions in the radiation problem with real and imaginary parts is checked out by the Haskind-Newman relation and by direct pressure integration as well. The numerical accuracy of this newly modified approach, achieved by analytically solving the logarithmic part of the Green function, is extensively investigated and all predicted results are well satisfied with errors less than 0.5 % in general.

(5) The formulation of the m-vector contribution due to forward speed and interactions between two submerged hulls is theoretically derived by the dipole image method and the mathematical expression of the m-vector contribution for single submerged circular or elliptical cylinder case is also described for possible applications. The predicted results of hydrodynamic loadings with m-vector contribution are compared with those without taking into consideration the m-vector contribution and for non-forward speed case both results of numerical computations match very well with no discrepancy. It is confirmed that this theoretical approach with the m-vector contribution is effective and reliable enough for practical engineering applications.

(6) The mathematical formulations of hydrodynamic restoring forces associated with the forward speed effect for the submerged single and two circular cylinder cases are derived in detail and numerical results of the submerged two circular

cylinder case show much less than 5 % errors when compared with the analytical solution derived mathematically for the submerged single circular cylinder case. The dynamic motion responses of an inclined offshore structure with and without restoring forces due to forward speed effects in head and following waves are extensively investigated and a parametric study for different submerged depths, Froude numbers, separation distances and inclinations in head and following waves are also performed to provide information on motion responses. In fact it is found that the hydrodynamic behaviour of the single or twin hulled marine vehicles in following waves is more significant than that of head waves.

(7) The second order horizontal forces including the effects of forward speed and interactions between two submerged hulls in head and following waves by the momentum flux consideration in fluid domain are theoretically formulated. The theoretical formulation of the second order forces due to forward speed and hull interaction effects acting on the submerged two circular cylinders in waves by the direct pressure integration over the body boundary contours is derived in detail and predicted results are also compared with that of previous work (Kashiwagi 1987 and Varyani 1988) and are found to meet with a good level of engineering accuracy. It is concluded that the outer solution of the near field approach and the inner solution of the far field approach in present numerical calculations of second order horizontal forces match well within errors less than 1 %. For second order forces in the vertical direction, calculated results are compared with those predicted by Lee-Newman (1971) approach and discrepancies less than 10 % for zero speed case in the far field and near field approaches are due to the Lee-Newman (1971) approach which does not take into consideration effects of forward speed and interaction between two submerged hulls.

The steady tilt moments due to second order forces with the forward speed effect are calculated and numerical results have good agreement of less than 1 % discrepancy with the three dimensional experimental work (Maeda 1984 and Ikeda 1985 et al). Predicted results of parametric studies on steady tilt moment for different submergence depths, current velocities, separation distances and

inclinations in head and following waves are extensively investigated to improve knowledge which is necessary for practical design consideration.

(8) In the field of computational fluid dynamics, the computational efficiency and numerical accuracy are two major concerns of researchers. In the present study, both numerical approaches such as the discrete source distribution method and the direct Green function method are newly modified and formulated in detail. The logarithmic part of the Green function is analytically derived to improve the computational efficiency, in other words, it considerably cuts down the CPU time.

The numerical results based on both numerical approaches are extensively investigated. From a consideration of CPU time against incident wave numbers, the results show that the direct Green function method is almost three (3) times more efficient than the discrete source distribution method for practical computations. The errors in damping coefficients confirms that the direct Green function method is about ten (10) times more accurate than the discrete source distribution method in computation accuracy.

It is obvious that as the number of discrete elements on the body surface increases, the numerical accuracy is improved. Nevertheless a major concern is the computational efficiency. Hence it is very important to carry out numerical computations which will help researchers to choose the optimum numbers of discrete elements and images of the dipoles.

(9) A mathematical approach with linear optimal control theory to study the dynamic positioning behaviour of twin hulled marine structures under combined action of wind, wave and current is briefly introduced. A detail description of the experimental data acquisition and analysis system at the Hydrodynamics Laboratory of Glasgow University is described. Series of experiments were carried out to measure the sway force and yaw moment acting on twin hulled structure model for different submergence depth, trim and drift angle conditions.

The experimental results show linear relationships and they are based on the technique of curve fitting to obtain several newly developed formulae of hydrodynamic forces and moments. These mathematical equations are proposed so that designers and researchers can make use of these results in simulation analyses to predict the manoeuvring performance and dynamic positioning behaviour of twin hulled marine vehicles for practical engineering applications.

(10) The practical approach, based on the approximation method proposed by Tasai (1970), for predicting the hydrodynamic behaviour of twin hulled marine vehicles in waves is well developed within adequate engineering accuracy. The calculated results of the added mass and damping coefficients of a twin hulled marine structure in waves are compared between Tasai's approximate (1970) and pressure integration approaches with errors less than 5 %. It may be concluded that the Tasai's approximate approach is economical and efficient to designers and engineers and the pressure integration approach is useful to researchers for more fundamental grasp of the ocean engineering field.

The predicted results of steady tilt moments, due to the effect of second order forces, are compared with that of the three dimensional experimental work (Maeda 1984 and Ikeda 1985 et al) and they show good agreement within errors less than 1.0 % for different current velocities and inclinations. A parametric study is performed to investigate to predict steady tilt moments acting on SR-192 twin hulled offshore structure model for different current velocities and inclinations in head and following waves.

A review of the past research work on steady tilt moment due to second order forces is extensively studied. Approaches proposed by Ogilvie (1963), Lee-Newman (1971), Morrall (1978), Numata (1978), Atlar (1986) and Wu (1993) modified from Lee-Newman approach etc are simplified and the twin hulled vehicle is taken as two rigidly held apart cylinders submerged under a free surface. For the zero speed case, the results of steady tilt moments do not incorporate the interaction effect between two hulls. In the present research work, the theory is developed to solve the boundary value problem of a typical twin hulled vehicle model including

the effects of forward speed and interactions between two submerged hulls fundamentally. The prediction of steady tilt moments due to second order forces in both horizontal and vertical directions is taken into consideration. The discrepancies in previous approaches on the theoretical side are discussed and new major contributions of the present research by direct pressure integration (1993) are also described in detail. Several calculated results, based on typical twin hulled structure model, are compared with that of previous research work. From the calculated results, it is found that these theoretical approaches provide reasonable predictions for certain ordinary conditions such as deep submergence and small inclinations. But for the most severe conditions such as 15 degree inclination condition, predicted results by Morrall (1978) and Numata (1978) approaches show divergent behaviour and those from both Atlar (1986) and Wu (1993) approaches, modified from Lee-Newman (1971), are in the conservative side. In fact, it is concluded that all five approaches can be conveniently applied to predict steady tilt moments acting on twin hulled marine vehicles in calm water for ordinary conditions. However for more complicate and severe conditions, the present pressure integration approach is the only effective and reliable tool for practical engineering applications.

A simplified version of a twin hulled offshore structure as submerged two circular cylinders model is generally proposed to study the steady tilt moments due to second order vertical forces for zero speed and incident wave condition. Martin's theoretical approach (1978) is briefly described and predicted results, based on Martin's twin hulled structure model, are compared with all previous research work, Wu (1993), modified from Lee-Newman (1971) approach, and present pressure integration approach. On comparison of results, it is noticed that the Martin approach shows underestimated behaviour of 2 or 3 times smaller than others over the frequency range. Hence it is clear that this approach is applied in more conservative manner for practical applications.

The mathematical formulation of the viscous horizontal forces acting on vertical surface piercing columns to investigate the steady tilt behaviour of an inclined offshore twin hulled structure is derived. On comparison of the steady tilt

moment due to viscous horizontal forces on vertical columns and second order forces on two submerged hulls are performed for different theoretical approaches such as Morrall (1978), Numata (1978), Atlar (1986), Wu(1993) and Morrison (Wu) 1993 etc. It is clear that the contribution of the second order forces on steady tilt moment due to the lower hulls is more than that of vertical columns. A comparison study on the steady tilt moments for different GM values of twin hulled structures in waves is performed. It is concluded that as the GM value increases, the viscous effect in the horizontal direction of vertical surface piercing column shows certain contribution to steady tilt moment. The theoretical formulation of the first and second order hydrodynamic problems with respect to waterline forces on surface piercing columns of twin hulled offshore structures are briefly described and certain research work to improve numerical algorithm for computational fluid dynamics is suggested.

11.2 Recommendations

The present research work is concentrated on the steady tilt moments due to the second order effect of typical twin hulled marine structure in beam sea condition and the boundary value problem takes into consideration the effects of forward speed and the interaction between two submerged hulls. Although the present theoretical work is already dealt well, further work needs to be done as follows.

Further experimental work can be performed on twin hulled marine vehicles under current action for different loading conditions in manoeuvring and dynamic positioning aspects. More mathematical equations can be fitted from experimental measurement to check the effectiveness of recent theoretical approaches and improve the accuracy of mathematical modelling for practical predictions of the dynamic positioning behaviour of twin hulled marine vehicles under the combined action of wind, wave and current.

In compliance with the theories of the optimal control system such as the

Extended Kalman Filter technique, Applied Parameter Estimation and Uncertain Dynamic System etc, the mathematical approach of real time simulation can be exactly formulated and effectively applied to predict the dynamic positioning behaviour of twin hulled marine vehicles under the combined action of wind, wave and current. Indeed this work is an economical and efficient tool for designers to assess the preliminary manoeuvring performance of ships and twin hulled marine vehicles in waves and also a useful one for engineers to operate the dynamic positioning behaviour of marine vehicles in severe environmental conditions.

REFERENCES

Abramowitz, M., Stegun, I.A., " *Handbook of Mathematical Functions* ", Dover Publications, Inc., New York, June 1964.

Atlar, M., Miller, N.S., " The Tilt Problem in Semi-submersibles ", International Conference on Marine Safety, Department of Naval Architecture and Ocean Engineering, University of Glasgow, 1983.

Atlar, M., Lai, P.S.K., " *A Two-Dimensional Method for Estimating Hydrodynamic Loads and Motions of a Twin-Hulled Semi-Submersible Associated with Some Hydrodynamic Aspects in Regular Beam Seas* ", NAOE-85-34, Department of Naval Architecture and Ocean Engineering, University of Glasgow, February 1985.

Atlar, M., " *SWATH Wave Load Program, Method of Solution for 5 Degrees of Freedom Coupled Equations of Motions of a SWATH Ship* ", NAOE-86-36, Department of Naval Architecture and Ocean Engineering, University of Glasgow, September 1986.

Atlar, M., " *Towards an Understanding of the Steady Tilt Phenomena in Semi-Submersibles* ", Ph.D. Thesis, Department of Naval Architecture and Ocean Engineering, University of Glasgow, Glasgow, Scotland, November 1986.

Bhattacharyya, R., " *Dynamics of Marine Vehicles* ", Wiley-Interscience Publication, 1972.

Chakrabarti, S.K., " *Hydrodynamics of Offshore Structures* ", Computational mechanics publications, Springer-Verlag, Berlin, 1978.

Chakrabarti, S.K., " Steady and Oscillating Drift Forces on Floating Objects ", Journal of Waterway, Port, Coastal and Ocean Division, ASCE, WW2, pp205-228, 1980.

Chakrabarti, S.K., " Steady Drift Force on Vertical Cylinder - Viscous vs. Potential ", Applied Ocean Research, Vol. 6, No. 2, pp73-82, 1984.

Clarke, D., " Assessment of Manoeuvring Performance ", British Maritime Technology Limited, the International Conference on Ship Manoeuvrability, April 1987.

Clough, R.W., Penzien, J., " *Dynamics of Structures* ", McGraw-Hill, New York, 1974.

Dally, J.W., William, F.R., " *Experimental Stress Analysis* ", The 2rd Edition, McGraw-Hill Book Company, pp216-271, 1978.

" DATASPAN 2000, Operating Instructions for Strain Gauge Amplifier Type 2028 ", RDP Electronics Ltd., West Midlands, 1978.

Dean, W.R., " On the Reflection of Surface Waves by a Submerged Cylinder ", Proceedings of Cambridge Philosophy Society, Vol. 46, pp483-491, 1948.

Edwards, R.Y., " Hydrodynamic Forces on Vessels Stationed in a Current ", Offshore Technology Conference, Paper No. 5032, 1985.

Faulkner, D., Cameron, R.M., Ferguson, A.M., Livingstone, M., Miller, N.S., " *Semi-Submersibles, Some Design Considerations* ", Lectures Given for a Course in the Department of Naval Architecture and Ocean Engineering, University of Glasgow, September 1974.

" *Foil Strain Gauges and Accessories (Terminal/Cement)* ", Technical Notes, Showa Measuring Instruments Co, Ltd., Tokyo, Japan, 1985.

Frank, W., " *Oscillation of Cylinders in or below the Free Surface of Deep Fluid* ", Report No. 2375, Naval Ship Research and Development Centre, 1967.

Grue, J., Palm, E., " Wave Radiation and Wave Diffraction from a Submerged Body in a Uniform Current ', Journal of Fluid Mechanics, Vol. 151, pp257-278, 1985.

Hogben, N., Standing, R.G., " Wave Loads on Large Bodies ", Proceedings of International Symposium of the Dynamics of Marine Vehicles and Structures in Waves, London, 1974.

Holiter, G.S., " *Experimental Stress Analysis - Principles and Methods* ", Cambridge University Press, 1967.

Hooft, J.P., " *Hydrodynamic Aspects of Semi-Submersible Platforms* ", Ph.D. Thesis, Publication No. 400, Netherlands Ship Model Basin, Wageningen, Netherlands, 1972.

Hooft, J.P., " *Advanced Dynamics of Marine Structures* ", John Wiley and Sons, New York, 1982.

Ikeda, Y., Takagi, M., Tanaka, N., " On Viscous Forces Acting upon Moving Semisubmersible ", Journal of Kansai Society of Naval Architects, Vol. 198, Japan, 1985.

Inglis, R.B., Price, W.G., " A Three Dimensional Ship Motion Theory-Comparison between Theoretical Prediction and Experimental Data of the Hydrodynamic Coefficient with Forward Speed ", Transactions of the Royal Institution of Naval Architects, Vol. 124, 1981.

Kagemoto, H., Yue, D.K.P., " Hydrodynamic Interaction among Multiple Three Dimensional Bodies : An Exact Algebraic Method ", Journal of Fluid Mechanics, Vol. 166, pp189-209, 1986.

Kashiwagi, M., Varyani, K.S., Ohkusu, M., " Hydrodynamic Forces Acting on a Submerged Elliptic Cylinder Translating and Oscillating in Waves ", Transactions of the West-Japan Society of Naval Architects, Vol. 74, Japan, August 1987.

Kashiwagi, M., Varyani, K.S., Ohkusu, M., " *Forward-Speed Effects on Hydrodynamic Forces Acting on a Submerged Cylinder in Waves* ", Reports of Research Institute for Applied Mechanics, Kyushu University, Vol. XXXIV, No. 102, Kyushu, Japan, September 1987.

Kashiwagi, M., Varyani, K.S., " Interaction Forces on Oscillating and Translating Two Cylinders Submerged Under a Free Surface ", Journal of the Society of Naval

Architects in Japan, Vol. 162, pp223-233, November 1987.

Kijima, K., Furukawa, Y., Takahira, T., Tanaka, S., " On a Study for Dynamic Positioning System of Offshore Platform ", Transactions of the West-Japan Society of Naval Architects, No.82, PP93-104, May 1991.

Kijima, K., Furukawa, Y., Washio, Y., " Dynamic Positioning System for an Offshore Platform under Unsteady External Forces ", Transactions of the West-Japan Society of Naval Architects, No.83, pp91-102, November 1991.

Kijima, K., Furukawa, Y., " Dynamic Positioning System for an Offshore Platform under Unsteady External Forces (Continued) ", Transactions of West-Japan Society of Naval Architects, No. 84, pp121-129, May 1992.

Kim, C.H., " *The Hydrodynamic Interaction between Two Cylindrical Bodies Floating in Beam Seas* ", Stevens Institute of Technology, Report SIT-OE-72-10, Hoboken, 1972.

Kim, C.H., Chou, F.S., " Motions of a Semi-submersible Drilling Platform in Head Seas ", Marine Technology, pp112-123, April 1973.

Kuo, C., Lee, A., Welya, Y., Martin, J., " Semi-submersible Intact Stability - Static and Dynamic Assessment and Steady Tilt in Waves ", Offshore Technology Conference, Paper No. 2976, 1977.

Kyozuka, Y., Makamura, S., Jakagi, M., " On the Unstable Swaying Motions of a Moored Cylinder in Regular Waves ", Journal of the Society of Naval Architects of Japan Vol. 142, December 1977. (in Japanese)

Lamb, H., " *Hydrodynamics* ", Dover Publication, 6th Edition, The Cambridge University Press, 1962.

Lee, C.M., Newman, J.N., " The Vertical Mean Force and Moment of Submerged Bodies Under Waves ", Journal of Ship Research, September 1971.

Lee, C.M., Bedel, J.W., " *Added Mass and Damping Coefficients of Heaving Twin Cylinders in a Free Surface* ", DTNSRDC Report No. 3695, 1971.

Lin, C.W., " *Fundamental Programs for Engineering Applications* ", Department of Civil Engineering, National Taiwan University, Taiwan, Republic of China, 1980.

Lin, W.C., Reed, A., " The Second Order Steady Force and Moment on a Ship Moving in an Oblique Seaway ", 11th International Symposium on Naval Hydrodynamics, University College, pp333-351, London, 1976.

Maeda, H., " Wave Exciting Forces on Two Dimensional Ship of Arbitrary Section ", Journal of Society of Naval Architects of Japan, Vol. 126, 1969.

Meada, H., Nishimoto, K., Eguchi, S., " Study of Components of Wind and Current Loads on Semisubmersibles ", Journal of Society of Naval Architects of Japan, 1984.

Martin, J. et al, " Calculations for the Steady Tilt of Semi-submersibles in Regular Waves ", Transaction of the Royal Institute of Naval Architects, Vol. 121, pp87-101, Spring Meetings 1978.

Martin, J., Kuo, C., " The Steady Tilt of Semi-submersibles in Regular Waves : Calculations and a Simple Experiment ", Mechanics of Wave-Induced Forces on Cylinders, University of Bristol, Pitman Advanced Publishing Ltd., pp704-713, 1979.

Maruo, H., " The Excess Resistance of a Ship in Rough Seas ", International Ship Building Progress, Vol. 4, No. 35, pp337-345, July, 1957.

Maruo, H., " The Drift Force of a Floating Body in Waves ", Journal of Ship Research, Vol. 4, No. 3, pp1-10, 1960.

Michelsen, F.C., Faltinsen, O., " Motions of Large Structures in Waves at Zero Froude Number ", Proceedings of International Symposium of the Dynamics of Marine Vehicles and Structures in Waves, London, 1974.

Milne-Thomson, L.M., " *Theoretical Hydrodynamics* ', 3rd Edition, MacMillan & Co Ltd., London, 1955.

Morrison, J.R., O'brien, M.P., Schaaf, S.A., " The Force Exerted by Surface Waves on Piles ", Petroleum Transactions, AIME, Vol. 189, 1950.

Morrall, A., " *The Influence of the Steady Vertical Component of Wave Force on the Stability of Semi-submersibles* ", NMI Report, NMI R46, OT-R-7833, National Maritime Institute, United Kingdom, October 1978.

Naftzger, R.A., Chakrabarti, S.K., " Dynamic Behaviour of Floating Storage Vessel ", Journal of Waterway, Port, Coastal and Ocean Division, ASCE, WW2, pp157-167, 1980.

Naito, S., Nakamura, S., Nishigushi, A., " Added Resistance in Short Length Waves of Ship Forms with Blunt Bow ", Journal of Kansai Society of Naval Architects, No. 197, Japan, 1985.

Natvig, B.J., Pendered, J.W., " Nonlinear Motion Response of Floating Structures to Wave Excitation ", Offshore Technology Conference, Paper No. 2796, pp525-536, May 1977.

Newman, J.N., " The Exciting Force on a Moving Body in Waves ", Journal of Ship Research, Vol. 9, 1965.

Newman, J.N., " *Marine Hydrodynamics* ", Massachusett Institute of Technology, Cambridge Press, 1977.

Numata, E., McClure, A.C., " Experimental Study of Stability Limits for Semi-submersible Drilling Platforms ", Offshore Technology Conference, Paper No. 2285, Houston, Texas, 1975.

Numata, E., Michel, W.H., McClure, A.C., " Assessment of Stability Requirements for Semi-Submersible Units ", Transactions of Society of Naval Architects and Marine Engineers Vol. 84, November 1976.

Ogilvie, T.F., " First and Second Order Forces on a Cylinder Submerged under a Free Surface ", Journal of Fluid Mechanics, Vol. 44, pp451-472, 1963.

Ohkusu, M., " On the Motion of Multi-Hull Ship in Waves ", Journal of Society of Naval Architects of West-Japan, No. 40, Japan, 1970.

Ohkusu, M., " Hydrodynamic Forces on Multiple Cylinders in Waves ", Proceedings of international Symposium on Dynamics of Marine Vehicles and Structures in Waves, Paper No. 12, pp107-112, London, United Kingdom, 1974.

Ohkusu, M., " Added Resistance in Waves of Hull Forms with Blunt Bow ", Proceedings of the 15th Symposium on Naval Hydrodynamics, 1984.

Ohkusu, M., Iwashita, H., " Radiation and Diffraction Wave Pattern of Ships with Forward Speed ", Journal of Society of Naval Architects of West-Japan, No. 73, Japan, 1987.

Paulling, J.R., Hong, Y.S., " Analysis of Semi-submersible Catamaran Type Platforms ", Offshore Technology Conference, Paper No. 2975, Houston, 1977.

Pinkster, J.A., " *Low Frequency Second Order Wave Exciting Forces on Floating Structures* ", Ph.D. Thesis, Netherlands Ship Model Basin, Wageningen, Netherlands, 1980.

Pinkster, J.A., " Dynamic Positioning of Large Vessels at Sea ", Offshore Technology Conference, Paper No. 5208, Houston, 1986.

Press, W.H., Flannery, B.P., Teukolsky, S.A., Vetterling, W.T., " *Numerical Recipes, the Art of Scientific Computing* ", Cambridge University Press, 1986.

Saito, K., Takagi, M., Ohkubo, H., Hirashima, M., " On the Low Frequency Damping Forces on a Moored Body in Waves ", Journal of Kansai Society of Naval Architects, Vol. 195, Japan, 1984.

Salvesen, N., Tuck, E.O., Faltinsen, O., " Ship Motions and Sea Loads ", Transactions of SNAME, Vol. 78, pp250-287, 1970.

Sarpkaya, T., Isaacson, M., " *Mechanics of Wave Forces on Offshore Structures* ", Van Nostrand Reihold Co., 1981.

Soylemez, M., " *Motion Response Simulation of Damaged Floating Platforms* ", Ph.D. Thesis, Department of Naval Architecture and Ocean Engineering, University of Glasgow, Scotland, January 1990.

Takagi, M., Ohkusu, M., " Ship Motion Theory ", The 2nd Seakeeping Symposium, Society of Naval Architects of Japan, 1977.

Takarada, N., Obakata, J., Inoue, R., Nakajima, T., Kobayashi, K., " The Stability on Semi-Submersible Platform in Waves (On the Capsizing of Moored Semi-Submersible Platform) ", Proceedings of 2nd International Conference on Stability of Ships and Ocean Vehicles, Japan, 1982.

Takarada, N., Nakajima, T., Inoue, R., " A Study on the Capsizing Mechanism of Semi-Submersible Platforms (1st, 2nd and 3rd Reports) ", Journal of Society of Naval Architects of Japan, Vol. 155, 156 and 157, Japan, June 1984.

Takezawa, S., Hirayama, T., " Safety of Moored Semi-Submersible Platform under Extreme Complex External Loads ", Proceedings of the 5th International Symposium on Offshore Mechanics and Arctic Engineering, 1986.

Tasai, F., " On the Damping Forces and Added Mass of Ships Heaving and Pitching ", Journal of Society of Naval Architects of Japan, Vol. 105, 1959.

Tasai, F., Takagi, M., " Theory of Ship Motions in Regular Waves ", Proceedings of Seakeeping Symposium, Society of Naval Architects of Japan, 1969.

Tasai, F., Arakrwa, H., Kurihara, M., " *A Study on the Motions of a Semi-Submersible Catamaran Hull in Regular Waves* ", Report No. 60, Research institute of Applied Mechanics, Kyushu University, Japan, 1970.

Tasai, F., " *Lecture notes on the Hydrodynamic Forces Acting on a Floating Offshore Structure and its Motion in Waves* ", Bulletin of the Society of Naval Architects of Japan, Kyushu, Japan, No. 649, 1983. (in Japanese)

Tomonaga, Y., Hatakenaka, K., " Measurements of the Drifting Force and Moment on Floating Type Offshore Structures in Waves ", Transactions of the West-Japan Society of Naval Architects, No. 59, December 1989.

Triantafyllow, M.S., " A Consistent Hydrodynamic Theory for Moored and Positioned Vessel ", Journal of Ship Research, Vol. 26, 1982.

Varyani, K.S., " *The Effect of Forward Speed on Hydrodynamic Forces Acting on Cylindrical Bodies in Waves* ", Ph.D. Thesis, Research Institute of Applied Mechanics, Kyushu University, Japan, April 1988.

Varyani, K.S., " Experimental Approach to Hydrodynamics of Towed Body ", Department of Ship Technology, Cochin University, 1989.

Varyani, K.S., " Two-Dimensional Green Function for an Oscillating and Translating Body ", Seminar on Recent Trends in Research and Teaching in Naval Architecture, Department of Ship Technology, Cochin University, India, 1989.

Varyani, K.S., " Wave Radiation and Diffraction from a Submerged Translating and Oscillating elliptical Cylinder ", Seminar on Trends in Research and Teaching in Naval Architecture, Department of Ship Technology, Cochin University, India, 1989.

Varyani, K.S., " Froude-Krylov Force Acting on Offshore Structure in Heeled Condition ", Proceedings of 9th Annual International Conference on Offshore Mechanics and Arctic Engineering, Houston, 1990.

Wang, S., Wahab, R., " Heaving Oscillations of Twin Cylinders in a Free Surface ", Journal of Ship Research, Vol. 15, No. 1, pp33-48, 1971.

Wichers, J.E.W., van Sluijs, M.F., " The Influence of Waves on the Low-Frequency Hydrodynamic Coefficients of Moored Vessel ", Offshore Technology Conference, Paper No. 3825, 1979.

Wu, T.M., " *Motion Response Predictions of a Semi-Submersible Catamaran Hull Form in Regular Waves* ", NAOE-91-18, Department of Naval Architecture and Ocean Engineering, University of Glasgow, July 1991.

Wu, T.M., " *Program Manual ; Motion Dynamics of Semi-Submersible Catamaran Hulls* ", NAOE-91-19, Department of Naval Architecture and Ocean Engineering, University of Glasgow, August 1991.

Wu, T.M., " *Froude Krylov Forces on Buoys and Semi-submersibles in Heeled Condition* ", NAOE-91-22, Department of Naval Architecture and Ocean Engineering, University of Glasgow, August 1991.

Wu, T.M., " *Program Manual ; Froude Krylov Forces on an Offshore Structure in Heeled Conditions* ", NAOE-91-23, Department of Naval Architecture and Ocean Engineering, University of Glasgow, August 1991.

Wu, T.M., " *Dynamic Response Analysis of Floating Buoys* ", NAOE-91-28, DEpartment of Naval Architecture and Ocean Engineering, University of Glasgow, August 1991.

Wu, T.M., " *Program Manual ; Motion Dynamics of a Floating Buoy* ", NAOE-91-25, Department of Naval Architecture and Ocean Engineering, University of Glasgow, September 1991.

Wu, T.M., " Research Notes on Spectral Analysis on Motion Dynamics of Floating Offshore Structures ", Glasgow, March 1992.

Wu, T.M., " Research Notes on Program Manual ; Spectral Analysis on Motion Dynamics of Floating Buoys ", Glasgow, April 1992.

Wu, T.M., Varyani, K.S., " Practical Approach to Hydrodynamic Forces on Buoys and Semi-submersibles ", 4th International Conference on Computer Aided Design, Manufacture and Operation in the Marine and Offshore Industries, Madrid, Spain, October 1992.

Wu, T.M., Varyani, K.S., " Effect of Second Order Forces and Capsizing Moments on an Inclined Offshore Structure Advancing in Waves ", 8th International Workshop on Water Waves and Floating Bodies, St. John's, Canada, May 1993.

Wu, T.M., Varyani, K.S., " Dynamic Motion Responses on an Inclined Offshore Structure Including Restoring Forces Due to Forward Speed Effect ", Proceedings of 12th Annual International Conference on Offshore Mechanics and Arctic Engineering, Glasgow, United Kingdom, June 1993.

Wu, T.M., Varyani, K.S., " Motion Responses and Second Order Forces on an Inclined Offshore Structure Under Combined Action of Wave and Current ", 8th International Conference on the Numerical Methods in Laminar and Turbulent Flow ", Swansea, United Kingdom, July 1993.

Wu, T.M., " Hydrodynamic Loadings Acting on Submerged Bodies Advancing in Waves - An Assessment of Accuracy ", 3rd International Conference on Applications of Supercomputers in Engineering, Bath, United Kingdom, September 1993. (under journal review)

Wu, T.M., " A Practical Approach and Computer Program to Predict Hydrodynamic Behaviours on Offshore Semi-Submersible Structures with Different Configurations in Regular Waves ", International NEVA 93 Conference, St. Petersburg, Russia, September 1993.

Wu, T.M., " *Experimental investigation on Motion Dynamics of Floating Buoys and Semi-submersibles* ", Department of Naval Architecture and Ocean Engineering, University of Glasgow, August 1993. (to be published)

Wu, T.M., Varyani, K.S., " Effect of Second Order Forces on Steady tilt Behaviours of an Inclined Offshore Structure Advancing in Waves ", 4th International Offshore and Polar Engineering Conference, Osaka, Japan, April 1994. (accepted for review)

Wu, T.M., " A Practical Approach to Predict Hydrodynamic Characteristics on Floating Offshore Buoys with Different Configurations in Regular Waves ", 5th International Conference on Computer Aided Design, Manufacture and Operation in the Marine and Offshore Industries, Southampton, September 1994. (to be published)

BIBLIOGRAPHY

Aalbers, A., Nienhuis, U., " Recent Development in Simulation and Real Time Control of Dynamic Positioning and Tracking ", Proceedings of MARIN Jubilee Meeting, Wageningen, May 1992.

Abkowitz, M.A., " *Stability and Control of Ocean Vehicles* ", The MIT Press, ppI-1, I-14, Cambridge, Massachusett and London, 1969.

Atlar, M., " *A Study of the Frank Close-Fit Method; Theory, Application and Comparison with Other Methods* ", NAOE-81-09, Department of Naval Architecture and Ocean Engineering, University of Glasgow, February 1982.

Atlar, M., " *Method for Predicting First-Order Hydrodynamic Loads on Single and Twin Sections by the Frank Close-Fit Technique* ", NAOE-85-41, Department of Naval Architecture and Ocean Engineering, University of Glasgow, October 1985.

Arai, S., Nekado, Y., Takagi, M., " Study on the Motions of a Moored Vessel among the Irregular Waves ", Journal of Society of Naval Architects of Japan, Vol. 140, 1976.

Arai, H., Takaishi, Y, " Tendency of Rules on Safety of Offshore Structures ", Proceedings of the 3rd Marine Dynamics Symposium, Society of Naval Architects of Japan, 1986.

Butland, J., " *User Manual of SIMPLEPLOT MARK 2* ", Revised Edition, Bradford University Software Services Ltd. (BUSS), 1985.

Caldeira-Saraiva, F., Clarke, D., " Application of Multivariable Control Techniques to the Active Motion Control of SWATH Craft ", British Ship Research Association, the International Conference on SWATH Ships and Advanced Multi-Hulled Vessels, London, April 1985.

Caldeira-Saraiva, F., Clarke, D., " The Active Control of SWATH Motions ", 8th Ship Control Systems Symposium, British Maritime Technology Limited, Hague, 1987.

Chakrabarti, S.K., Cotter, D.C., " Analysis of a Tower-Tanker System ", Proc. of the 10th Annual Offshore Technology conference, Paper No. 3202, pp1301-1310, Houston, 1978.

Chakrabarti, S.K., Cotter, D.C., " Hydrodynamic Coefficients of a Mooring Tower ", Journal of Energy Resources Technology, ASME, Vol. 106, pp183-190, 1984.

Chakrabarti, S.K., Cotter, D.C., " Motions of Articulated Towers and Floating Structures ", Proceedings. of the 7th Annual International Conference on Offshore Mechanics and Arctic Engineering, ASME, Houston, 1988.

Chan, H.S., " *A Three-Dimensional Technique for Predicting First and Second Order Hydrodynamic Forces on a Marine Vehicle Advancing in Waves* ", Ph.D. Thesis, Department of Naval Architecture and Ocean Engineering, University of Glasgow, Scotland, August 1990.

Chun, H.H., " *Theoretical and Experimental Studies on the Resistance of SWATH Ships* ", Ph.D. Thesis, Department of Naval Architecture and Ocean Engineering, University of Glasgow, Scotland, May 1988.

Chun, H.H., Djatmiko, E.B., McGregor, R.C., " A Wide Ranging Study on the SWATH Ships with and without Forward Speeds ", Department of Naval Architecture and Ocean Engineering, University of Glasgow, 1989.

De Souza, P.M.F.M., Miller, N.S., " The Intact and Damaged Stability Behaviour of Two Semi-Submersible Models under Wind and Wave Loading ", Offshore Technology Conference, Paper No. 3298, Houston, May 1978.

Djatmiko, E.B., " *Experimental Investigation into SWATH Ship Motions and Loadings* ", M.Sc. Thesis, Department of Naval Architecture and Ocean Engineering, University of Glasgow, 1987.

Djatmiko, E.B., Chun, H.H., McGregor, R.C., McGregor, J.R., " Hydrodynamic Behaviour of a SWATH Fishing Vessel ", CSME Mechanical Engineering Forum 1990.

Faulkner, D. et. al., " *Semi-Submersibles and Tethered Buoyant Platforms, Some Design Considerations* ", Lectures given for a Course in the Department of Naval Architecture and Ocean Engineering, University of Glasgow, September 1977.

Faulkner, D., Incecik, A. et. al., " Advanced Design for Ships and Offshore Floating Systems ", Lectures given for a UETP/COMETT Course in the Department of Naval Architecture and Ocean Engineering, University of Glasgow, Glasgow, Scotland, September 1992.

Gregory, J.B., Smith, C.E., " *Technology Assessment and Research Program for Offshore Minerals Operation* ", OCS Report MMS 84-0001, United States Dept. of the Interior Mineral Management Service, 1984.

Grekoussis, C., " *On the Resistance Prediction of Offshore Mobile Platforms* ", M.Sc Thesis, Department of Naval Architecture and Ocean Engineering, University of Glasgow, Scotland, June 1977.

Helvacioglu, I.H., " *Dynamic Analysis of Coupled Articulated Tower and Floating Production Systems* ", Ph.D. Thesis, Department of Naval Architecture and Ocean Engineering, University of Glasgow, Glasgow, Scotland, November 1990.

Hooft, J.P., " A Mathematical Method of Determining Hydrodynamically induced Forces on a Semi-Submersible ", SNAME, November 1971.

Hsu, F.A.,Blenkarn, K.A., " Analysis of Peak Mooring Forces by Slow Vessel-Drift Oscillations in Random Seas ", Offshore Technology Conference, Paper No. 1159, 1970.

Incecik, A., " *Design Aspects of the Hydrodynamic and Structural Loading on Floating offshore Platforms Under Wave Excitation* ", Ph.D. Thesis, Department of Naval Architecture and Ocean Engineering, University of Glasgow, Scotland, 1982.

Incecik, A., " The Effect of Non-colinear Wave, Wind and Current Loading on Dynamic Response of a Tension Leg ", Proceedings of 12th Annual International Conference on Offshore Mechanics and Arctic Engineering, Glasgow, Scotland, June 1993.

" *International Conference on Ship Manoeuvrability-Prediction and Achievements* ", Vol. 1., the Royal Institution of Naval Architects, London, April 1987.

" *International Conference on Ship Manoeuvrability-Prediction and Achievements* ", Vol. 2., the Royal Institution of Naval Architects, London, April 1987.

Khattab, O., " Prediction of the Manoeuvring Characteristics of a SWATH Ship in Design Stage ", British Maritime Technology Limited, the International Conference on SWATH Ships and Advanced Multi-Hull Vessels II, London, November 1988.

Kim, C.H., Chou, F.S., Tien, O., " Motions and Hydrodynamic Loads of a Ship Advancing in Oblique Waves ", Transaction of SNAME, Vol. 88, 1980.

Kim, C.H., Luh, P.A., " Prediction of Pitching Motions and Loads of an Articulated Loading Platform in Waves ", Proceedings of the 14th Annual Offshore Technology conference, Paper No. 4247, Houston, 1982.

Kirk, C.L., Jain, R.K., " Response of Articulated Towers to Waves and Current ", Proceedings of the 9th Annual Offshore Technology Conference, Paper No. 2798, Houston, 1977.

Korn, G.A., Wait, J.V., " *Digital Continuous System Simulation* ", Prentice-Hall Inc., Englewood, Cliffs, New Jersey, 1978.

Lager, G., " Development of Dynamic Positioning ", Offshore Technology Conference, Paper No. 1498, Houston, 1971.

Lee, C.M., Curphey, R.M., " Prediction of Motion, Stability and Wave Load of Small-water-area, Twin-hull Ships ", Transaction of SNAME, Vol. 85, pp94-103, 1977.

Leonard, J.W., Young, R.A., " Coupled Response of Compliant Offshore Platforms ", Engineering Structures Vol. 7., pp74-84, April 1985.

MacGregor, J.R., MacGregor, R.C., Zheng, X., Miller, N.S., " Computer Aided SWATH Ship Design and Seakeeping Analysis ", the International Conference on SWATH Ships and Advanced Multi-Hull Vessels II, London, November 1988.

" *MATHTYPE User Manual* ", Department of Naval Architecture and Ocean Engineering, University of Glasgow, Scotland, 1990.

McClean and Nelson, " *Theory and Problems in Engineering Mechanics, Statics and Dynamics* ", Schaum's Outline Series, 1962.

McCormick, M.E., " *Ocean Engineering Wave Mechanics* ", A Wiley-Interscience Publication, New York, U.S.A., 1973.

Miller, N.S., " *Model Tests on the Stability of Semi-Submersibles* ", Department of Naval Architecture and Ocean Engineering, University of Glasgow, January 1977.

Miller, N.S., " *Stability Tests on Two Designs of Semi-Submersibles in Regular Waves* ", Report NAOE-HL-77-01, Department of Naval Architecture and Ocean Engineering, University of Glasgow, January 1977.

Miller, N.S., Bassiouny, A.H., de Souza, P.F.M., Strahan, J, " Some Aspects of Semi-Submersible and Tethered Buoyant Platform Design ", Paper No. 1449, The Institution of Engineers and Shipbuilders in Scotland (IESIS), Glasgow, Scotland, January 1983.

Mork, K., Lerstad, A., " Development of Dynamic Positioning in Relation to Offshore Loading in the Norwegian Sector ", Proceedings of MARIN Jubilee Meeting, Wageningen, May 1992.

Newman, J.N., Sortand, B., Vinje, T., " Added Mass and Damping of Rectangular Bodies Close to the Free Surface ", Journal of Ship Research, Vol. 28, No. 4, pp219-225, 1984.

Nienhuis, U., " Simulation of Low Frequency Motions of Dynamically Positioned Offshore Structure ", Transaction of Royal Institute of Naval Architects, 1986.

Nienhuis, U., " *Analysis of Thruster Effectivity for Dynamic Positioning and Low Speed Manoeuvring* ", Thesis, Delft University of Technology, 1992.

Nordenstrom, N., Faltinsen, O., Pedersen, B., " Prediction of Wave-induced Motions and Loads for Catamarans ", Offshore Technology Conference, Paper No. 1418, Houston, 1971.

" *Notes of FORTRAN 77 Lectures* ", Computing Services, University of Glasgow, Scotland, October 1990.

Ogilvie, T.F., Tuck, E.O., " *Rational Strip Theory for Ship Motions (Part One)* ", Report No. 013, Department of Naval Architecture and Marine Engineering, University of Michigan, 1969.

Ohkusu, M., " *On the Heaving Motion of Two Circular Cylinders on the Surface of a Fluid* ", Report of Research Institute of Applied Mechanics, Kyushu University, Vol. 17, No. 58, Japan, 1969.

" *Outer Continental Shelf Frontier Technology* ", Proceedings of a Symposium, National Academy of Sciences, December 1979.

Parkingson, S.T., Saren, M.A., " *Offshore Technology : a Forecast and Review* ", The Financial Times Business Information LTD., 1981.

Paulling, J.R., Hong, Y.S., Stiansen, S.G., Chen, H.H., " Structural Loads on Twin-hull Semi-submersible Platforms ", Offshore Technology Conference, Paper No. 3246, Houston, 1978.

Pinkster, J.A., " Wave - Feed - Forward As a Means to Improve Dynamic Positioning ", Offshore Technology Conference, Paper No. 3057, 1978.

Price, W.G., Bishop, R.E.D., " *Probabilistic Theory of Ship Dynamics* ", London, Chapman and Hall, 1974.

Price, W.G., Temarel, P., Yousheng, W., " Structural Response of a SWATH or Multi-hull Vessel Travelling in Waves ", Proceedings of International Conference on SWATH Ships and Advanced Multi-hulled Vessels ", RINA, Paper 13, London, 1984.

Ryu, J.S., Yun, C.B., " Nonlinear Stochastic Analysis of Guyed Towers ", Proceedings of the 6th Annual International Conference on Offshore Mechanics and Arctic Engineering, Vol. 1, pp53-59, March 1987.

Schnute, J.T., " The Scattering of Surface Waves by Two Submerged Cylinders ", Preceedings of Cambridge Philosophy Society, Vol. 69, pp201-215, 1971.

Seren, D.B., Atlar, M., " *An Overview of the Concepts Employed to Predict the Hydrodynamic Forces Imposed on an Unappended SWATH Ship Proceeding in a Seaway* ", NAOE-84-63, Department of Naval Architecture and Ocean Engineering, University of Glasgow, December 1984.

Shatto, H.K., Van Calcar, H., " Improving Dynamic Positioning Performance in Deep Water, High Current, Rough Water Environment ", Offshore Technology Conference, Paper No. 4749, Houston, 1984.

Soylemez, M., Incecik, A., " Identification of Non-Linear Effects in Predicting the Motion Response of Mobile Platforms ", Proceedings of 9th Annual International Conference on Offshore Mechanics and Arctic Engineering, June 1990.

Standing, R.G., Dacunha, N.M.C., Matten, R.B., " *Mean Wave Drift Forces : Theory and Experiments* ", National Maritime Institute, Report OT-R-8175 NMI R124, Feltham, 1981.

St. Denis, Pierson, W.J., " On the Motions of Ships in Confused Seas ", Transactions of Society of Naval Architects and Marine Engineers, Vol. 61, 1953.

Takezawa, S., Hirayama, T., Nishimoto, K., " Study on Longitudinal Motion and Bending Moment of a Container Ship in Following Seas ", Journal of Society of Naval Architects of Japan, Vol. 150, 1981.

Takezawa, S., Hirayama, T., Nishimoto, K., " Study on Longitudinal Motions and Vertical Wave Loads of a Ship in Following Seas ", Journal of Society of

Naval Architects of Japan, Vol. 151, 1982.

Taylor, E., Knoop, J., " Dynamic Instability of Freely Floating Platform in Waves ", Transaction of Royal Institute of Naval Architects, United Kingdom, 1981.

Timman, R., Newman, J.N., " The Coupled Damping Coefficients of a Symmetric Ship ", Journal of Ship Research, Vol. 5, 1962.

Triantafyllow, M.S., " Strip Theory of Ship Motions in the Presence of Current ", Journal of Ship Research, Vol. 24, 1980.

Thompson, J.M.T., Bokaian, A.R., Ghaffari, R., " Subharmonic and Chaotic Motions of Compliant Offshore Structures and Articulated Mooring Towers ", Journal of Energy Research Technology Vol. 106, 1984.

Thorpe, T., Farrell, K.P., " Permanent Moorings ", Institution of Naval Architects, September 1947.

Tsinipizoglou, S.G., " *A Computer Program for the Dynamic Response of a Spar Buoy* ", NAOE-79-08, Department of Naval Architecture and Ocean Engineering, University of Glasgow, march 1979.

Tsinipizoglou, S.G., " *Dynamics of Mooring Buoys* ", Ph.D. Thesis, NAOE-83-84, Department of Naval Architecture and Ocean Engineering, University of Glasgow, December 1982.

Ursell, F., " On the Heaving Motion of a Circular Cylinder on the Surface of a Fluid ", Journal of Mechanics and Applied Mathematics, 2-3, 1949.

Ursell, F., " Surface Waves on Deep Water in the Presence of a Submerged Circular Cylinder ", Proceedings of Cambridge Philosophy Society, Vol. 46, pp141-152, 1950.

Van Walree, F., " Wind, Wave and Current Loads on Semi-submersibles ", Offshore Technology Conference, Paper No. 6521, Houston, 1991.

" *VAX/VMS Handbook* ", Computing Services, University of Glasgow,

Scotland, October 1989.

Wang, S., " On the Hydrodynamic Forces of Twin Hull Vessels ", Proceedings of 12th Coastal Engineering Conference, Vol. III, pp1700-1721, Washington DC, 1970.

Wichers, J.E.W., " Progress in Computer Simulations of SPM Moored Vessels ", Offshore Technology Conference, Paper No. 5175, May 1986.

Wichers, J.E.W., " *A Simulation Model for a Single Point Moored Tanker* ", Publication No. 797, Maritime Research Institute Netherlands, Wageningen, Netherlands, 1988.

Wilson, J.F., " *Dynamics of Offshore Structures* ", Duke University, New York, A Wiley-Interscience Publication, 1984.

Window, A.L., Holister, G.S., " *Strain Gauge Technology* ", Applied Science Publishers Ltd., 1982.

Wu, J.Y., " *SWATH Vertical Motions with Emphasis on Fixed Fin Control* ", Ph.D. Thesis, Department of Naval Architecture and Ocean Engineering, University of Glasgow, Scotland, December 1985.

Yilmaz, O., " *Experiments with Conical and Cylindrical Moored Buoys* ", NAOE-90-20, Department of Naval Architecture and Ocean Engineering, University of Glasgow, May 1990.

Yilmaz, O., Incecik, A., " Non-Linear Dynamic Interaction Between Mooring Systems and a Floating Structure under Environmental Forces ", Proceedings. of 9th Annual International Conference on Offshore Mechanics and Arctic Engineering, June 1990.

Zheng, X., " *Prediction of Motion and Wave Load of Mono and Twin Hull Ships in Waves* ", Ph.D. Thesis, Department of Naval Architecture and Ocean Engineering, University of Glasgow, United Kingdom, June 1988.

Zienkiewicz, O.C., Lewis, R.W., Stagg, K.G., " *Numerical Methods in Offshore Engineering* ", A Wiley- Interscience Publication, John Wiley & Sons, 1978.

APPENDIX

A. Mathematical derivation of the velocity identity

The mathematical manipulation of the quantity described before is considered as follows.

$$\vartheta = \left[i\omega\bar{\alpha} + \nabla \times \left(\bar{\alpha} \times \bar{V} \right) \right] \cdot \bar{n} \qquad \text{(A1)}$$

where :

The i-th components of these vectors $\bar{\alpha}$, $\bar{V}$ and $\bar{n}$ are presented as α_i, v_i and n_i respectively.

At first, mathematical conventions of the indicial notation relevant to the vector calculation are summarized and a dot product of the vectors is written as

$$\bar{A} \cdot \bar{B} = \sum_{i=1}^{3} A_i B_i = A_i B_i \qquad \text{(A2)}$$

In fact, if the same subscript, for example " i ", appears in a term of the above equation, the summation with respect to " i " is supposed to be performed.

The i-th component of the divergence of a scalar quantity is written as

$$\frac{\partial \phi}{\partial x_i} \equiv \partial_i \phi \qquad \text{(A3)}$$

The i-th component of a vector cross product is indicated as

$$\left(\vec{A}\times\vec{B}\right)_i = \varepsilon_{ijk}A_jB_k \qquad \text{(A4)}$$

where :

The mathematical convention of the summation, as shown in Eq. (A2), applies for j and k and the alternating tensor ε_{ijk} is used, which is equal to +1 for the indices in cyclic order (123, 231, 312) ; equal to -1 for the indices in a cyclic order (132, 213, 321) ; equal to 0 if any pair of the indices are identical.

In relation to the alternating tensor, the following mathematical property is applied as

$$\varepsilon_{ijk}\varepsilon_{ipq} = \delta_{jp}\delta_{kq} = \delta_{kp}\delta_{jq} \qquad \text{(A5)}$$

Here δ_{ij} is the Kronecker's delta which is equal to 1 for i = j and equal to 0 for the others.

A. For the translational motions

With the mathematical conventions introduced above and the assumptions of $\alpha_1 = \xi_1$, $\alpha_2 = \xi_2$ and $\alpha_3 = 0$, the quantity ϑ described in Eq. (A1) can be rewritten as

$$\begin{aligned}\vartheta &\equiv \left[i\omega\vec{\alpha} + \nabla\times\left(\vec{\alpha}\times\vec{V}\right)\right]\cdot\vec{n} = i\omega n_j\alpha_j + n_i\varepsilon_{ijk}\partial_j\varepsilon_{kpq}\alpha_p v_q \\ &= i\omega n_j\alpha_j + n_i\left(\delta_{ip}\delta_{jq} - \delta_{iq}\delta_{jp}\right)\partial_j\alpha_p v_q \\ &= i\omega n_j\alpha_j + n_i\left(\alpha_i\partial_j v_j + v_j\partial_j\alpha_i - \alpha_j\partial_j v_i - v_i\partial_j\alpha_j\right) \qquad \text{(A6)}\end{aligned}$$

Here the mathematical relations are written as follows.

$$\partial_j\alpha_i = 0, \quad \partial_j\alpha_j = 0 \qquad \text{(A7)}$$

$\partial_j v_j = 0$; that is the equation of the fluid continuity. (A8)

$\partial_j v_i = \partial_i v_j$; that is the irrotational flow property. (A9)

By substituting the Eqs. (A7), (A8) and (A9) into the Eq. (A6), the following equation can be derived as

$$\vartheta = i\omega n_j \alpha_j - n_i \partial_i v_j \alpha_j = \left\{ i\omega \vec{n} - (\vec{n} \cdot \nabla)\vec{V} \right\} \vec{\alpha} \qquad \text{(A10)}$$

B. For the rotational motions

Here several mathematical expressions are assumed as follows.

$$\alpha_i = \varepsilon_{ijk} \theta_j x_k \qquad \text{(A11a)}$$

$$\theta_1 = \theta_2 = 0 \ , \ \theta_3 = \xi_3 \qquad \text{(A11b)}$$

$$x_1 = x \ , \ x_2 = y - d \ , \ x_3 = 0 \qquad \text{(A11c)}$$

By substituting the above relations, Eq. (A11), into the Eq. (A1) with several reduction, the following equation can be derived as

$$\begin{aligned} \vartheta &= i\omega n_i \varepsilon_{ijk} \theta_j x_k + n_i \varepsilon_{ijk} \partial_j \varepsilon_{kpq} \left(\varepsilon_{plm} \theta_l x_m \right) v_q \\ &= i\omega \theta_j \varepsilon_{jki} x_k n_i - \theta_k \varepsilon_{kij} n_i v_j + n_i \varepsilon_{ijk} \left(\theta_q x_k - \theta_k x_q \right) \partial_j v_q \end{aligned} \qquad \text{(A12)}$$

Here the third term of the Eq. (A12) can be rewritten as

$$\begin{aligned} n_i \varepsilon_{ijk} \left(\theta_q x_k - \theta_k x_q \right) \partial_j v_q &= n_i \varepsilon_{ijk} \varepsilon_{pqk} \left(\vec{\theta} \times \vec{r}_0 \right)_p \partial_j v_q \\ &= -\left(\vec{\theta} \times \vec{r}_0 \right)_j n_i \partial_i v_j = -\theta_k \varepsilon_{kmj} x_m n_i \partial_i v_j \end{aligned} \qquad \text{(A13)}$$

where :

$\vec{\theta}$ and $\vec{r}_0$ are newly defined vectors and their components are $(0,0,\xi_3)$ and $(x, y-d, 0)$ respectively. The mathematical expression is then obtained as follows.

$$\vartheta = i\omega\theta_j\varepsilon_{jki}x_k n_i - \theta_j\varepsilon_{jki}n_k v_i - \theta_j\varepsilon_{jki}x_k n_m \partial_m v_i$$
$$= \left\{i\omega(\vec{r}_0 \times \vec{n}) - (\vec{n} \times \vec{V}) - \vec{r}_0 \times \left[(\vec{n} \cdot \nabla)\vec{V}\right]\right\}\vec{\theta} \qquad \text{(A14)}$$

The second and third terms of the Eq. (A14) can be rewritten as

$$-(\vec{n} \times \vec{V}) - \vec{r}_0 \times \left[(\vec{n} \cdot \nabla)\vec{V}\right] = -(\vec{n} \cdot \nabla)(\vec{r}_0 \times \vec{V}) \qquad \text{(A15)}$$

By substituting the Eq. (A15) into the Eq. (A14), the final mathematical expression is obtained as

$$\vartheta = \left\{i\omega(\vec{r}_0 \times \vec{n}) - (\vec{n} \cdot \nabla)(\vec{r}_0 \times \vec{V})\right\} \qquad \text{(A16)}$$

B. Analytical formulation of restoring coefficients due to forward speed effect for the submerged circular cylinder case

Since the interest is stressed on the case of submerged single circular cylinder, it is natural to assume that the steady velocity potential φ_s as

$$\varphi_s = -\frac{a^2}{r}\cos\theta \qquad \text{(B1)}$$

where :

$$x = r\cos\theta \quad , \quad y = r\sin\theta \qquad \text{(B2)}$$

$$\frac{\partial r}{\partial x} = \cos\theta \quad , \quad \frac{\partial \theta}{\partial x} = \frac{-\sin\theta}{r} \qquad \text{(B3a)}$$

$$\frac{\partial r}{\partial y} = \sin\theta \quad , \quad \frac{\partial \theta}{\partial y} = \frac{\cos\theta}{r} \qquad \text{(B3b)}$$

$$\frac{\partial}{\partial x} = (\cos\theta)\frac{\partial}{\partial r} - \left(\frac{\sin\theta}{r}\right)\frac{\partial}{\partial \theta} \qquad \text{(B4a)}$$

$$\frac{\partial}{\partial y} = (\sin\theta)\frac{\partial}{\partial r} + \left(\frac{\cos\theta}{r}\right)\frac{\partial}{\partial \theta} \qquad \text{(B4b)}$$

The derivatives of the steady velocity potential are systematically described as follows.

$$\frac{\partial \varphi_s}{\partial x} = \cos\theta\frac{\partial \varphi_s}{\partial r} - \frac{\sin\theta}{r}\frac{\partial \varphi_s}{\partial \theta}$$
$$= \frac{a^2}{r^2}\left\{\cos^2\theta - \sin^2\theta\right\} = \frac{a^2}{r^2}\cos 2\theta \qquad \text{(B5)}$$

$$\frac{\partial \varphi_s}{\partial y} = \sin\theta\frac{\partial \varphi_s}{\partial r} + \frac{\cos\theta}{r}\frac{\partial \varphi_s}{\partial \theta}$$
$$= \frac{a^2}{r^2}\sin 2\theta \qquad \text{(B6)}$$

$$\frac{\partial}{\partial x}\left(\frac{\partial \varphi_s}{\partial x}\right) = (\cos\theta)\frac{\partial}{\partial r}\left(\frac{\partial \varphi_s}{\partial x}\right) - \left(\frac{\sin\theta}{r}\right)\frac{\partial}{\partial \theta}\left(\frac{\partial \varphi_s}{\partial x}\right)$$
$$= \frac{2a^2}{r^3}\left\{3\cos\theta\sin^2\theta - \cos^3\theta\right\} \qquad \text{(B7)}$$

$$\frac{\partial}{\partial y}\left(\frac{\partial \varphi_s}{\partial x}\right) = (\sin\theta)\frac{\partial}{\partial r}\left(\frac{\partial \varphi_s}{\partial x}\right) + \left(\frac{\cos\theta}{r}\right)\frac{\partial}{\partial \theta}\left(\frac{\partial \varphi_s}{\partial x}\right)$$
$$= \frac{2a^2}{r^3}\left\{-3\sin\theta\cos^2\theta + \sin^3\theta\right\} \qquad \text{(B8)}$$

$$\frac{\partial}{\partial y}\left(\frac{\partial \varphi_s}{\partial y}\right) = (\sin\theta)\frac{\partial}{\partial r}\left(\frac{\partial \varphi_s}{\partial y}\right) + \left(\frac{\cos\theta}{r}\right)\frac{\partial}{\partial \theta}\left(\frac{\partial \varphi_s}{\partial y}\right)$$
$$= \frac{2a^2}{r^3}\left\{-3\sin^2\theta\cos\theta + \cos^3\theta\right\} \qquad \text{(B9)}$$

$$\frac{\partial}{\partial x}\left(\frac{\partial \varphi_s}{\partial y}\right) = (\cos\theta)\frac{\partial}{\partial r}\left(\frac{\partial \varphi_s}{\partial y}\right) - \left(\frac{\sin\theta}{r}\right)\frac{\partial}{\partial \theta}\left(\frac{\partial \varphi_s}{\partial y}\right)$$
$$= \frac{2a^2}{r^3}\left\{-3\sin\theta\cos^2\theta + \sin^3\theta\right\} = \frac{\partial}{\partial y}\left(\frac{\partial \varphi_s}{\partial x}\right) \qquad \text{(B10)}$$

For the case of r = a, the equations of these derivatives can be expressed as

$$\frac{\partial \varphi_S}{\partial x} = \cos 2\theta \qquad \text{(B11a)}$$

$$\frac{\partial \varphi_s}{\partial y} = \sin 2\theta \qquad \text{(B11b)}$$

$$\frac{\partial^2 \varphi_S}{\partial x^2} = \frac{1}{a}\left\{6\cos\theta\sin^2\theta - 2\cos^3\theta\right\} = \frac{-2}{a}\cos 3\theta \qquad \text{(B11c)}$$

$$\frac{\partial^2 \varphi_S}{\partial y \partial x} = \frac{1}{a}\left\{-6\sin\theta\cos^2\theta + 2\sin^3\theta\right\} = \frac{-2}{a}\sin 3\theta \qquad \text{(B11d)}$$

$$\frac{\partial^2 \varphi_S}{\partial y^2} = \frac{1}{a}\left\{-6\sin^2\theta\cos\theta + 2\cos^3\theta\right\} = \frac{2}{a}\cos 3\theta \qquad \text{(B11e)}$$

$$\frac{\partial^2 \varphi_S}{\partial x \partial y} = \frac{1}{a}\left\{-6\sin\theta\cos^2\theta + 2\sin^3\theta\right\} = \frac{-2}{a}\sin 3\theta \qquad \text{(B11f)}$$

Mathematical expressions of hydrodynamic restoring coefficients due to the forward speed effect for the submerged single circular cylinder case are written and analytical solutions are detailedly worked out as follows.

$$C_{i1} = \rho U^2 \int_0^{2\pi}\left[\left(-1 + \frac{\partial \varphi_S}{\partial x}\right)\frac{\partial^2 \varphi_S}{\partial^2 x} + \frac{\partial \varphi_s}{\partial y}\frac{\partial^2 \varphi_S}{\partial x \partial y}\right] n_i \, ds \qquad \text{(B12a)}$$

$$C_{i2} = \rho U^2 \int_0^{2\pi}\left[\left(-1 + \frac{\partial \varphi_S}{\partial x}\right)\frac{\partial^2 \varphi_S}{\partial y \partial x} + \frac{\partial \varphi_s}{\partial y}\frac{\partial^2 \varphi_S}{\partial y^2}\right] n_i \, ds \qquad \text{(B12b)}$$

where :

$$n_1 = \cos\theta \quad , \quad n_2 = \sin\theta \qquad \text{(B13)}$$

and

$$C_{11} = \rho U^2 \int_0^{2\pi} \begin{bmatrix} (-1+\cos^2\theta-\sin^2\theta)(6\cos\theta\sin^2\theta-2\cos^3\theta) \\ +(2\sin\theta\cos\theta)(-6\sin\theta\cos^2\theta+2\sin^3\theta) \end{bmatrix} \cos\theta\, d\theta$$

$$= \rho U^2 \int_0^{2\pi} [-8\cos\theta+8\cos^3\theta]\cos\theta\, d\theta = \rho U^2[-2\pi] \qquad \text{(B14)}$$

$$C_{21} = \rho U^2 \int_0^{2\pi} [-8\cos\theta+8\cos^3\theta]\sin d\theta = 0 \qquad \text{(B15)}$$

$$C_{12} = \rho U^2 \int_0^{2\pi} \begin{bmatrix} (-1+\cos^2\theta-\sin^2\theta)(-6\sin\theta\cos^2\theta+2\sin^3\theta) \\ +(2\sin\theta\cos\theta)(-6\sin^2\theta\cos\theta+2\cos^3\theta) \end{bmatrix} \cos\theta\, d\theta$$

$$= \rho U^2 \int_0^{2\pi} [4\sin\theta-8\sin^3\theta]\cos\theta\, d\theta = 0 \qquad \text{(B16)}$$

$$C_{22} = \rho U^2 \int_0^{2\pi} [4\sin\theta-8\sin^3\theta]\sin\theta\, d\theta = \rho U^2[-2\pi] \qquad \text{(B17)}$$

C. Formula of second order vertical forces for deeply submerged single body case

The previous research work on steady tilt moments due to the effect of second order forces of the twin hulled marine vehicles is reviewed extensively. Here theoretical approaches of second order vertical forces acting on both submerged hulls of the twin hulled marine structure in a calm water are summarized as follows.

A. Morrall 1978 approach :

By using the simple linear wave theory, mathematical equations for steady wave forces acting on the submerged pontoons of the twin hulled structure in calm water can be derived by taking the pressure difference, due to the velocities of the wave particles between the top and bottom surfaces of the submerged footings or pontoons, in the fluid flow field.

The mathematical equation for steady vertical wave forces acting on a

restrained vertical cylinder which represents a submerged footing type is expressed as

$$F = -\rho \frac{\pi^3 R^2 A^2}{T^2} e^{\frac{-4\pi h}{\lambda}} \sinh \frac{4\pi a}{\lambda} \qquad \text{(C1)}$$

where :

R is the radius of the submerged footing, A is the wave height and h is the submerged depth of the footing centroid under the free surface ; T and λ are the wave period and length respectively and a is half the depth of the submerged hull.

The corresponding equation for steady vertical wave forces acting on the restrained horizontal prism which represents the hull of the submerged pontoon is as follows.

$$F = -\rho \frac{\pi^2 BLA^2}{T^2} e^{\frac{-4\pi h}{\lambda}} \sinh \frac{4\pi a}{\lambda} \qquad \text{(C2)}$$

where :

B is the beam and L is the length of the submerged pontoon.

B. Numata 1978 approach :

The phenomenon of the wave induced steady tilt moment of twin hulled offshore structure in beam sea condition is related to the tendency of the submarine, hovering at the shallow submergence, to lift toward the sea surface. The steady vertical forces acting on the submerged body have been analyzed by a number of previous researchers who refer to it as a second order force, that is, varying as the square of the wave amplitude.

Ogilvie (1963) has given the solution of the second order vertical force acting

on a submerged circular cylinder under the waves whose crests are parallel to the cylinder axis. Complete numerical results were obtained for the two dimensional problem of a restrained cylinder and a free neutrally buoyant cylinder.

Goodman (1965) performed the direct pressure integration over the hull surface of a slender body of revolution hovering under the head and beam waves. The predicted solutions for the beam wave condition is rather equivalent to the Ogilvie's results in general.

Lee and Newman (1971) proposed a slender body approach which can carry out these calculations for the simple cylinders other than circular. The final expression for the steady vertical force is dependent in part on the longitudinal distribution of the sectional area and added mass coefficient in the sway and heave modes.

The solutions of all three theoretical approaches mentioned above are of the following general form in the deep water waves :

$$\frac{F}{L} \propto k^2 A^2 e^{-2kh}[f] \qquad \text{(C3)}$$

where :

The function [f] in the Goodman solution and in a simplification of the Ogilvie exact solution is a Bessel function of the wave number and body radius. In the Lee and Newman approach, [f] involves the effects of the body sectional area and added mass.

By the mathematical manipulation, the theoretical equation, proposed by Ogilvie (1963) and Goodman (1965), for the steady vertical wave forces acting on the restrained circular cylinder in the beam sea condition is obtained as follows

$$\frac{F}{L} = 2\rho g \pi a^2 k^2 A^2 \left[\frac{I_1(2ka)}{ka}\right] e^{-2kh} \qquad \text{(C4)}$$

where :

a is the radius of the submerged cylinder and approximated as

1) For the lower hulls of a barge form structure

$$a = \left(\frac{S_A}{\pi}\right)^{\frac{1}{2}} \qquad \text{(C5)}$$

where S_A is the midship sectional area of the lower hull

2) For the lower hulls of the footing type structure

$$a = \left(\frac{\nabla}{2\pi}\right)^{\frac{1}{3}} \qquad \text{(C6)}$$

where ∇ is the footing volume

C. Takarada and Nakajima 1985 approach :

When the submergence of the lower hull is relatively deep, the approximate prediction of the steady vertical wave forces acting on the single submerged structure in a calm water is proposed by Ogilvie (1963) for the circular cylinder case as

$$F = 4\pi a^2 k^2 f_0 \left[\frac{I_1(2ka)}{ka}\right] e^{-2kh} \qquad \text{(C7)}$$

and the practical equation proposed by Lee and Newman (1971) for the single submerged cylinder of an arbitrary section is

$$F = k^2 S_A f_0 (2 + m_{11} + m_{22}) e^{-2kh} \qquad \text{(C8)}$$

$$f_0 = \frac{1}{2}\rho g A^2 L \qquad \text{(C9)}$$

where :

I_1 is the modified first order Bessel function

k is the wave number

A is the wave amplitude

h is the submerged depth of the lower hull

a is the radius of the submerged circular cylinder and L is the length of the lower hull

S_A is the sectional area of the lower hull

m_{11}, m_{22} are the added mass coefficients of the sway and heave motion in the unbound fluid

D. Atlar 1986 approach :

Here the theoretical far field approach to predict the steady second order vertical forces acting on the submerged hull of the twin hulled structure in a calm water (equivalent non-forward speed effect), proposed by the Lee and Newman (1971), is applied and the mathematical expression is written as

$$F = \frac{1}{2}\rho g A^2 k^2 e^{-2kh} S_A (2 + m_{11} + m_{22}) \qquad \text{(C10)}$$

Here the determination of the added mass coefficients in the sway and heave modes, suggested by Numata (1976) et al., are reasonably applied to take the effect of the cross sectional shape into consideration and the predicted values can be interpolated by the aspect ratio about one (1).

E. Wu 1993 approach :

Here the far field approach to calculate the steady second order vertical forces

acting on the submerged hull of the twin hulled structure, proposed by the Lee and Newman (1971), is used and written as

$$F = \frac{1}{2}\rho g A^2 k^2 e^{-2kh} S_A (2 + m_{11} + m_{22}) \qquad \text{(C11)}$$

Here the values of the added mass coefficients in the sway and heave modes is predicted by solving the boundary value problem taking the effects of the forward speed (equivalent current effect) and interactions between two submerged hulls into consideration directly.

Here the heeling moment is described by the difference of the steady vertical forces acting on the individual left and right hulls of the twin hulled structure. The mathematical equation of the steady tilt moments due to the steady vertical wave forces acting on the twin hulled marine vehicles in calm water is categorized into two separate parts and is expressed as follows.

For the pontoon type of the twin hulled offshore structure, the steady vertical wave forces acting on both submerged pontoon of the twin hulled structure in calm water can be written, as Eqs. (C2), (C4), (C8) and (C10) respectively, by substituting the submerged depths due to the inclination effect on the twin hulled structure. Thus for the pontoon type of twin hulled structure setting $b_1 = b_2$, both mathematical expressions associated with the submerged depth for the left and right pontoon due to the inclination effect are written as

$$h_1 = (h_0 - b_1 \tan\phi)\cos\phi \qquad \text{(C12)}$$

$$h_2 = (h_0 + b_1 \tan\phi)\cos\phi \qquad \text{(C13)}$$

In the same manner for the footing type of twin hulled structure and setting $b_1 \neq b_2$, both mathematical expressions of the submerged depths for the left and right pontoon due to the inclination effect are written as

$$h_1 = (h_0 - b_2 \tan\phi)\cos\phi \qquad \text{(C14)}$$

$$h_2 = (h_0 + b_1 \tan\phi)\cos\phi \qquad \text{(C15)}$$

where :

h_0 denotes the submerged depth between the centre of gravity and the centroid of the pontoon in the upright condition and ϕ presents the heeling angle of the twin hulled structure. b_1 is the separation distance between the centre of gravity and the centroid of the left pontoon and h_1 is the submerged depth of the left pontoon due to the inclination. b_2 is the separation distance between the centre of gravity and the centroid of the right pontoon and h_2 is the submerged depth of the right pontoon due to the inclination.

Finally for the pontoon type of twin hulled offshore structure, the steady tilt moment about the centre of gravity can be presented in the following form

$$M = b_1 \cos\phi (F_1 - F_2) + d \sin\phi (F_1 + F_2) \qquad \text{(C16)}$$

and for the footing type of the twin hulled structure, it can be also written as

$$M = 2F_1 b_1 \cos\phi - F_2 b_2 \cos\phi + d \sin\phi (2F_1 + F_2) \qquad \text{(C17)}$$

The mathematical equations of the steady tilt moments due to the steady vertical wave forces acting on the twin hulled marine vehicle in a calm water are introduced here and applied to predict for different heeling angles up to fifteen (15) degrees practically.

D. Formulation of viscous forces on the single vertical surface piercing column case

Although the Morrison approach cannot describe the hydrodynamic loadings

in the theoretical aspects, it can take the viscous effect into consideration practically. In this approach, the flow velocity in the viscous drag term may include a constant part and a harmonic part. The constant part is induced by the mass transport of the waves (Stokes drift) and a possible current, whereas the harmonic part is induced by the wave particle motions.

The constant velocity components induce a steady " wave-current drag " force at a submerged location in terms of the form and friction factor and the latter is a very small part of the form drag. Since the wave particle velocity is harmonic, the drag force induced by this velocity at a submerged location has a zero mean over a wave period. Because of the variation of surface elevation along the splash zone of a vertical column, a mean " wave drag " force due to the horizontal wave particle velocities in the horizontal direction can be calculated.

Thus the viscous force acting on the vertical surface piercing column can be derived by the Morrison approach and written as

$$F_V = \frac{1}{2}\rho C_{Dc} A_{Pc}\, u|u| \qquad \text{(D1)}$$

where :

Subscript c indicates the quantities with respect to the column and

$$A_{Pc} = 2R_c dy \qquad \text{(D2)}$$

and the horizontal wave particle velocity at a depth of y is

$$u = -A\omega e^{-kh}\cos(kx - \omega t) \qquad \text{(D3)}$$

Based on the assumption of the small diameter member, the variation of the velocity across the diameter of the element dy is neglected. Moreover the variation of C_{Dc} along the submerged depth of the column and the hydrodynamic

interference between members are also ignored. Then the heeling moment due to the viscous forces in the horizontal direction about the centroid of the twin hulled offshore structure can be integrated from the bottom of the column up to the wave crest and formulated as

$$M_{V_c} = \frac{1}{2}\rho C_{Dc}(2R_c)(kgA^2) \int_{A\cos(kx-\omega t)}^{h} [ye^{-2ky} - \overline{OG}e^{-2ky}]\cos(kx-\omega t)|\cos(kx-\omega t)|dy \quad (D4)$$

EFFECT OF SECOND ORDER FORCES ON STEADY TILT BEHAVIOURS AND SOME APPLICATIONS IN DYNAMIC POSITIONING ASPECTS OF TWIN HULLED MARINE VEHICLES

"Thesis Figures"

(Volume II)

by

Tong-Ming WU, B.Sc., M.Sc.

This thesis is submitted for the degree of Doctor of Philosophy
in the Department of Naval Architecture and Ocean Engineering
University of Glasgow

June 1993

Great Britain

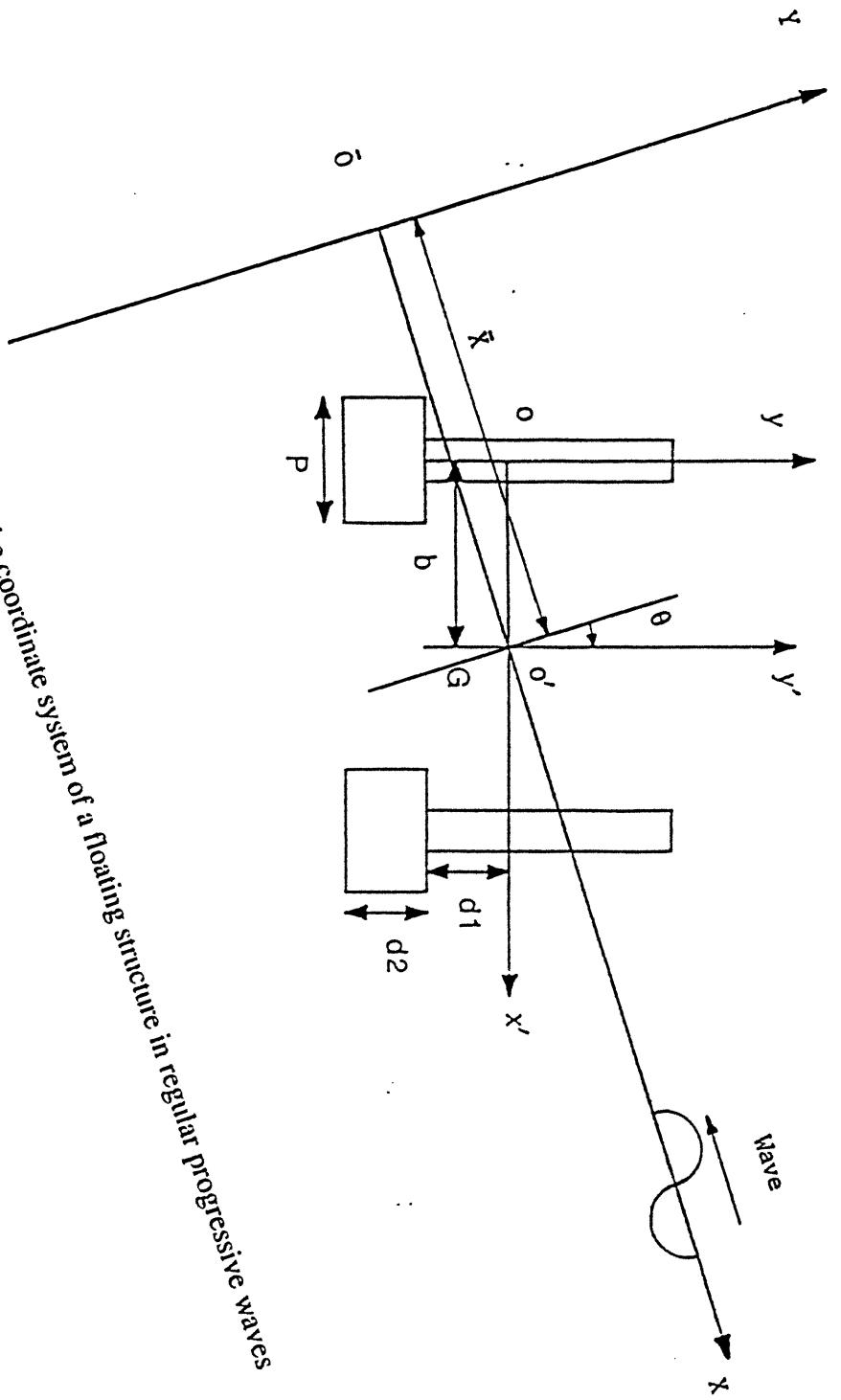

Fig.1.1 The coordinate system of a floating structure in regular progressive waves

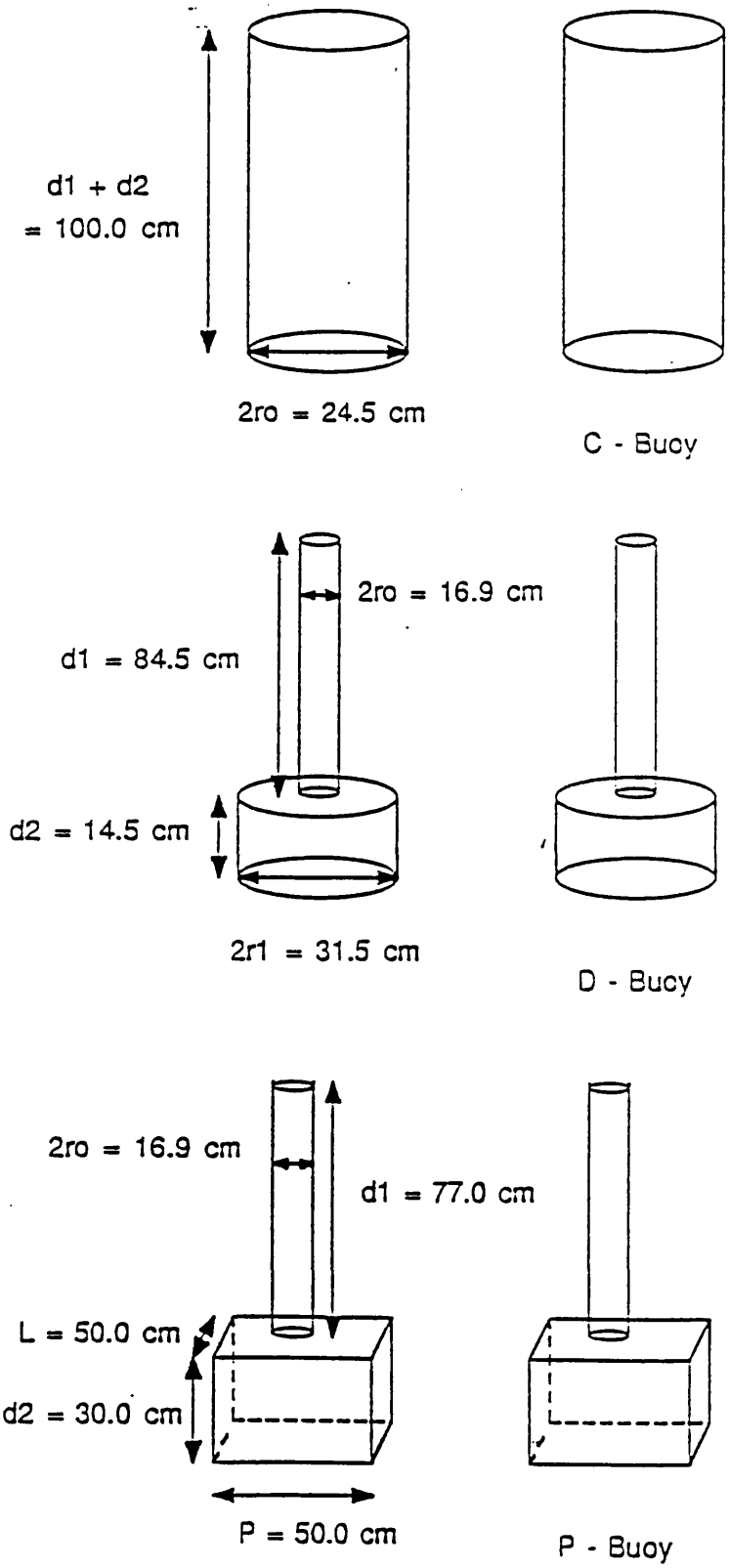

Fig.1.2 Basic configuration of C - buoy, D - buoy, P - buoy and simplified semi-submersible models

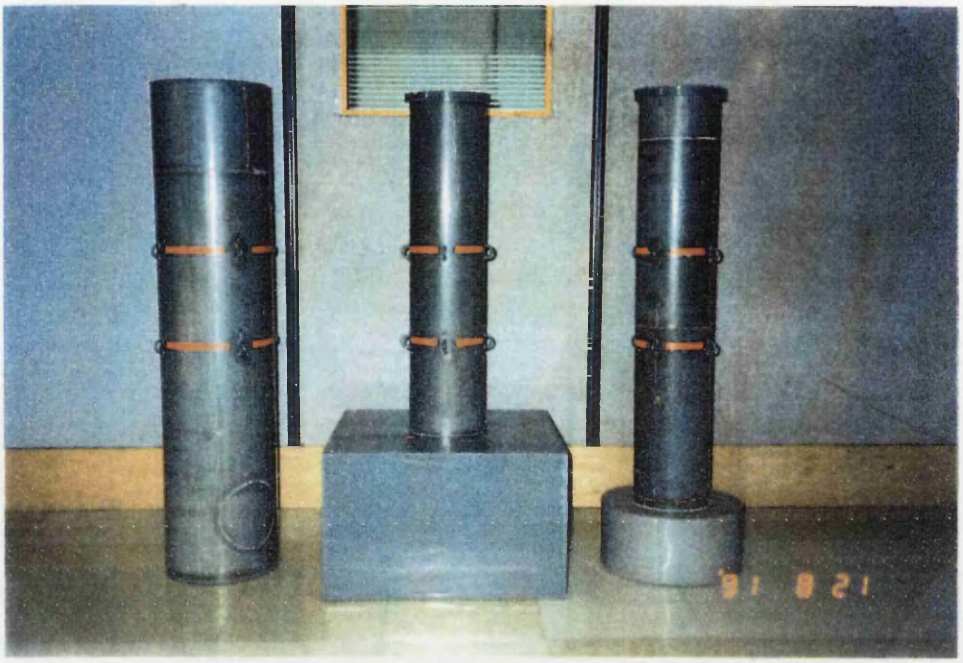

Fig.1.3 Three different kinds of buoy models for experiments

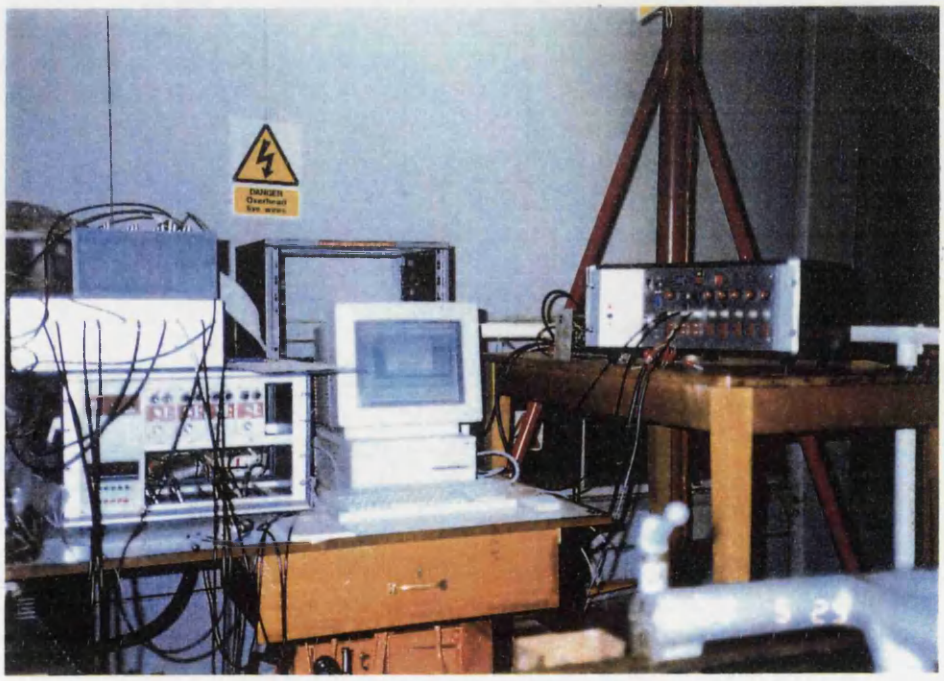

Fig.1.4 Layout of a data acquisition system for experiments

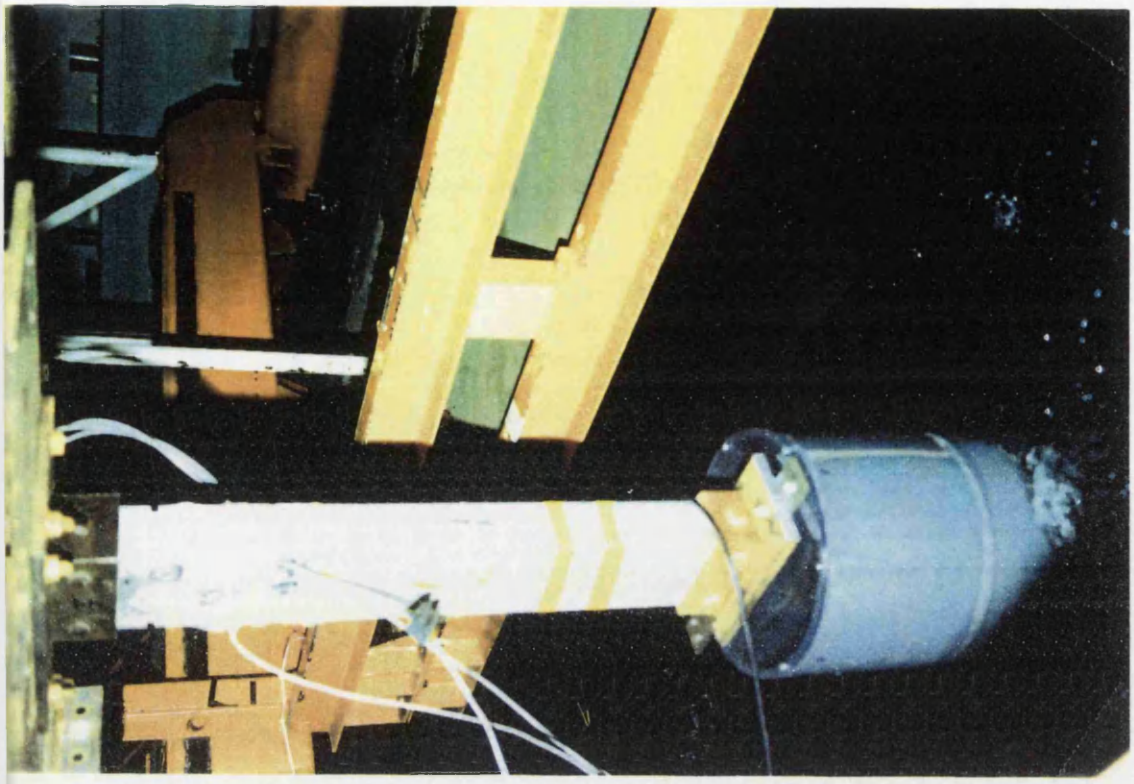

Fig.1.5 Layout of the straight bar devices in experiments

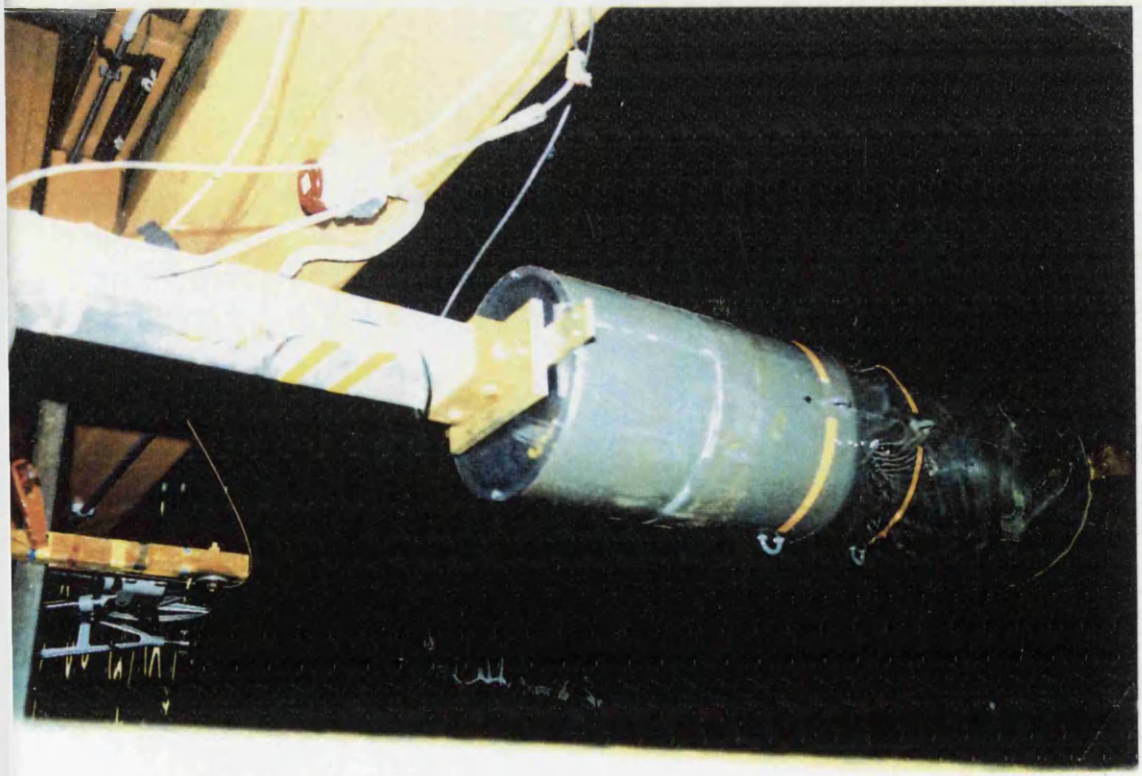

Fig.1.14 C - buoy model in experiments

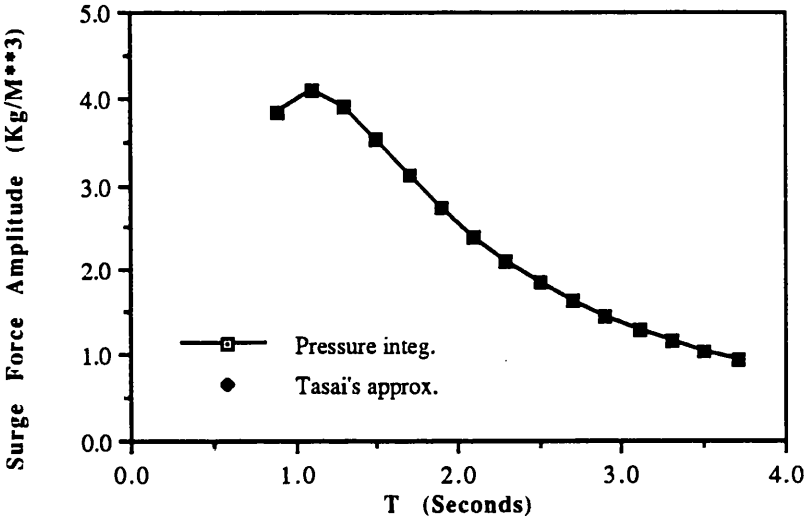

Fig.1.6 Comparison of surge forces for the P-buoy model

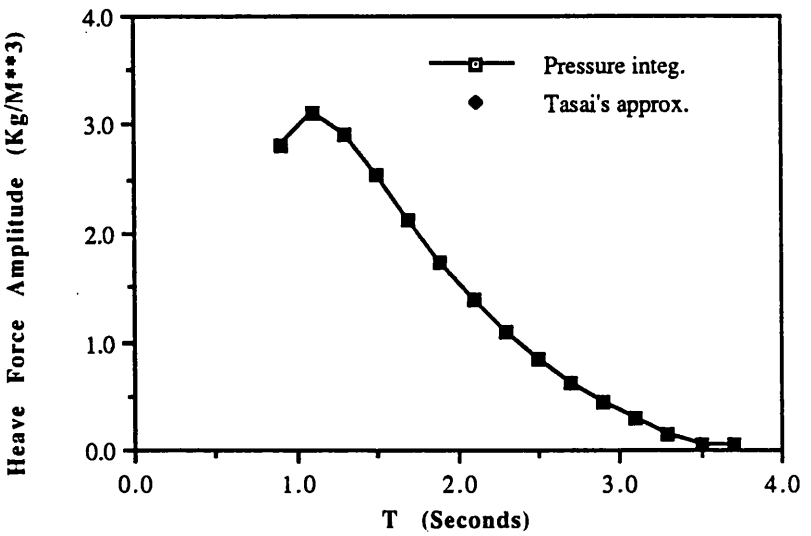

Fig.1.7 Comparison of heave forces for the P-buoy model

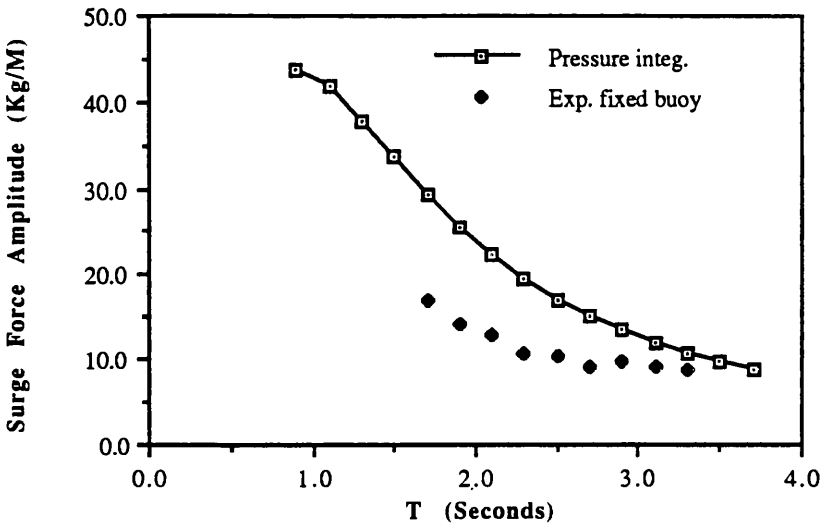

Fig.1.8 Comparison of surge forces for the C-buoy model

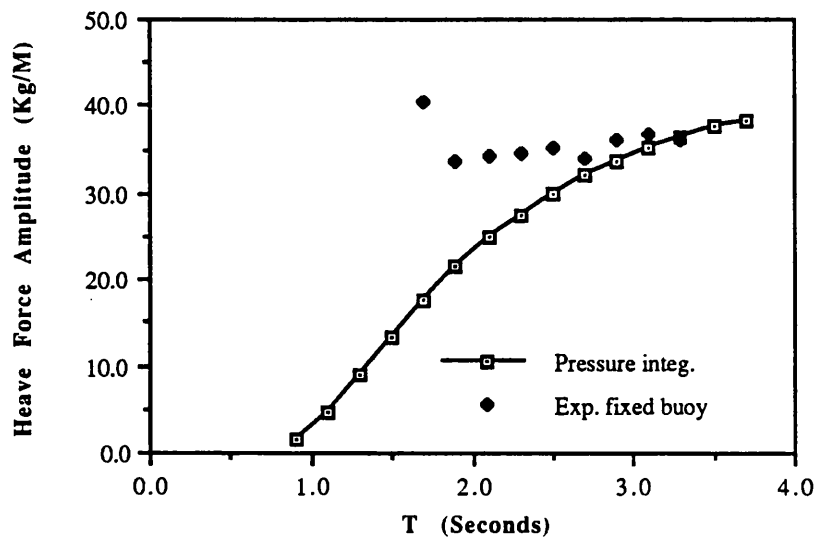

Fig.1.9 Comparison of heave forces for the C-buoy model

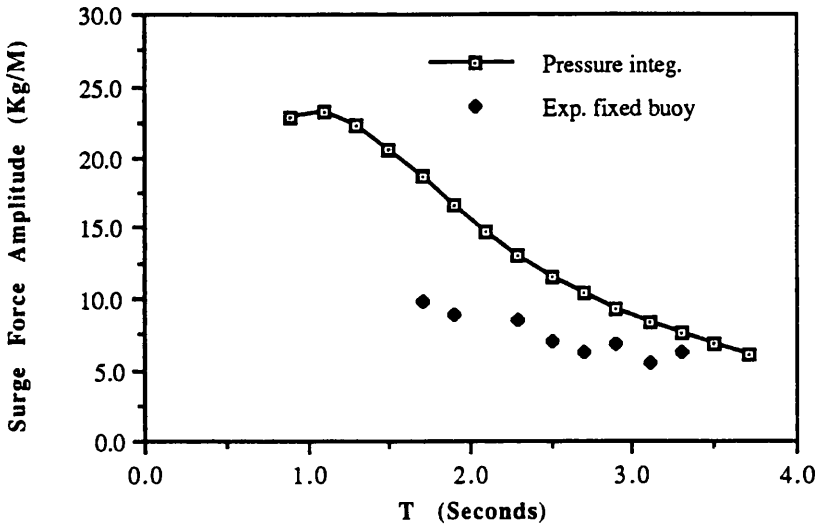

Fig.1.10 Comparison of surge forces for the D-buoy model

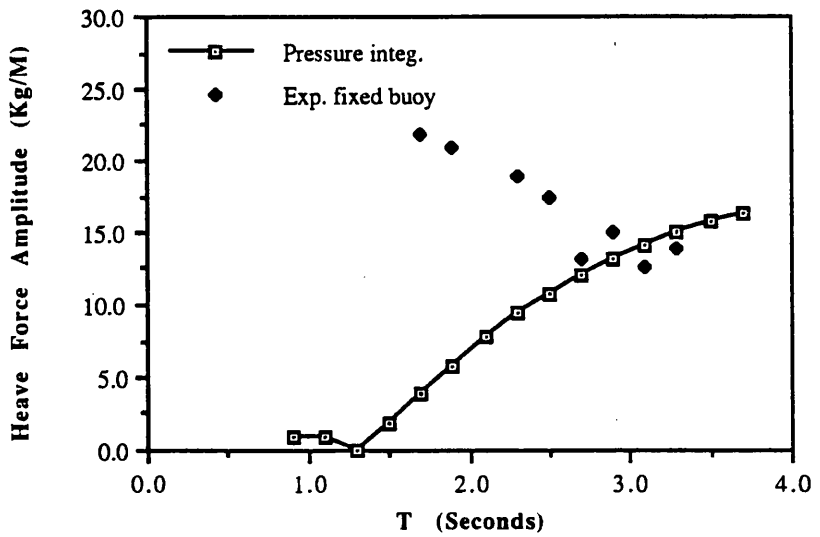

Fig.1.11 Comparison of heave forces for the D-buoy model

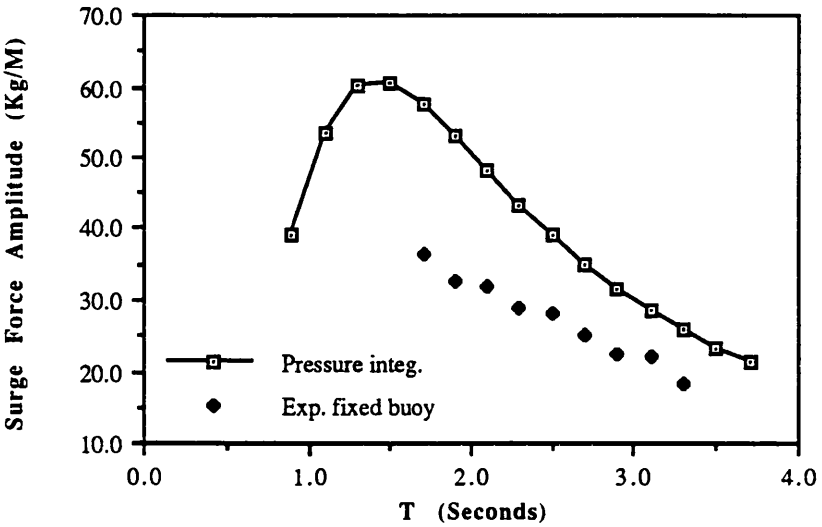

Fig.1.12 Comparison of surge forces for the P-buoy model

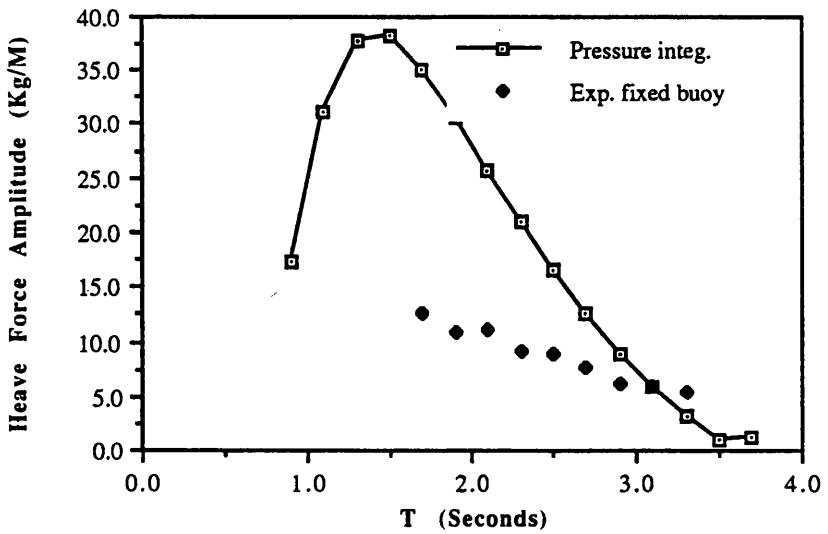

Fig.1.13 Comparison of heave forces for the P-buoy model

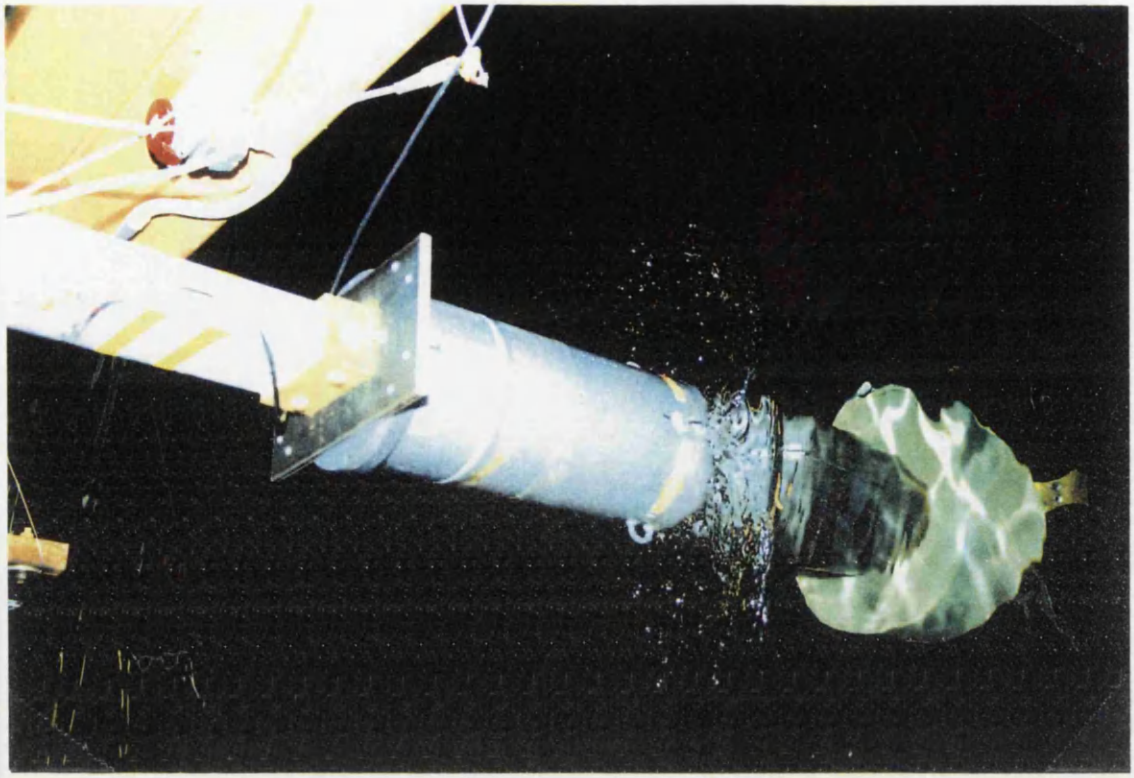

Fig.1.15 D - buoy model in experiments

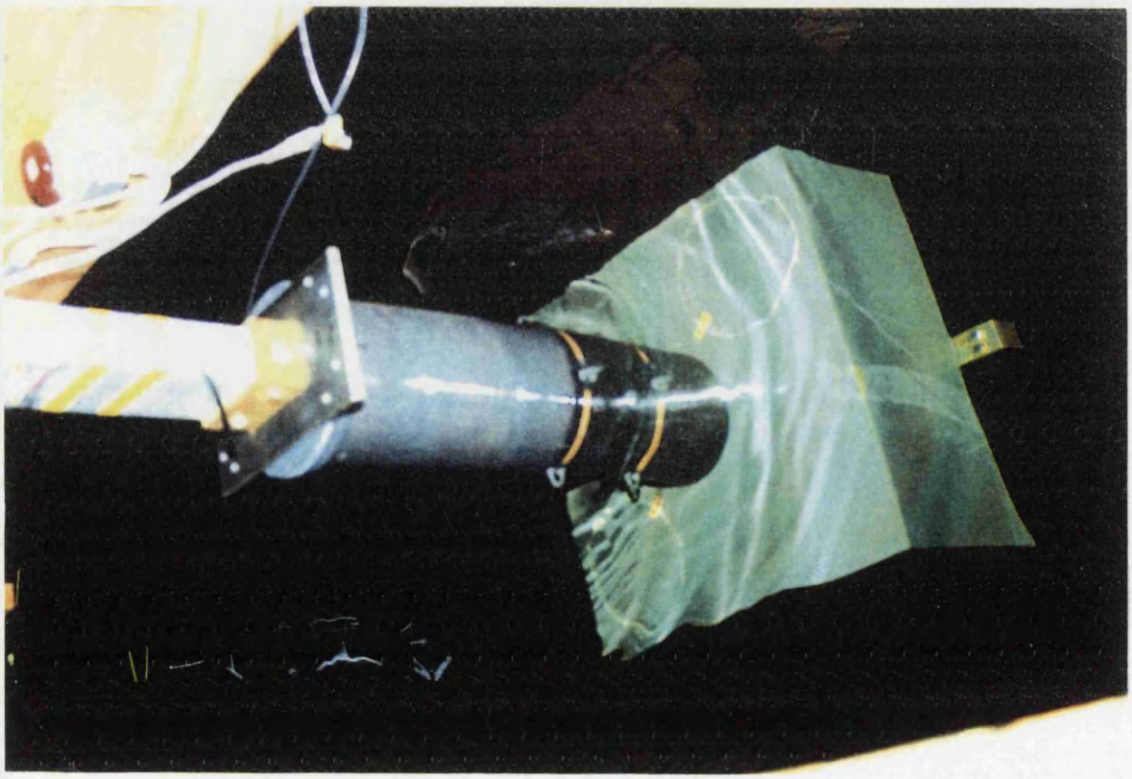

Fig.1.16 P - buoy model in experiments

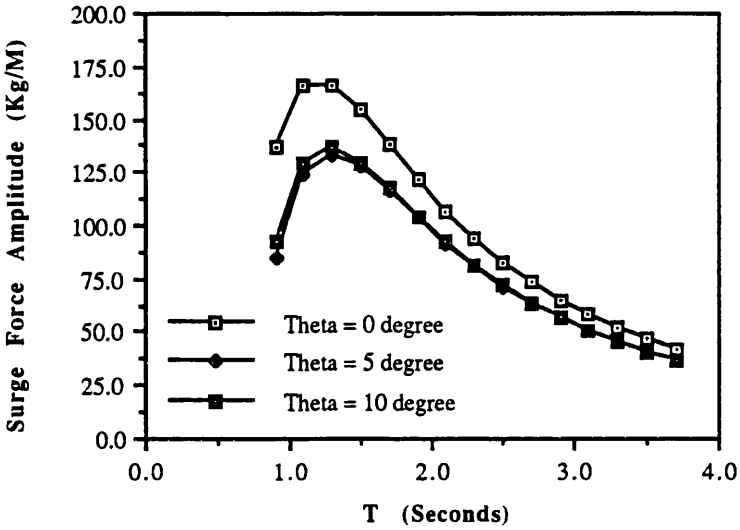

Fig.1.17 Surge forces due to inclination for the semi-submersible model (P-buoy)

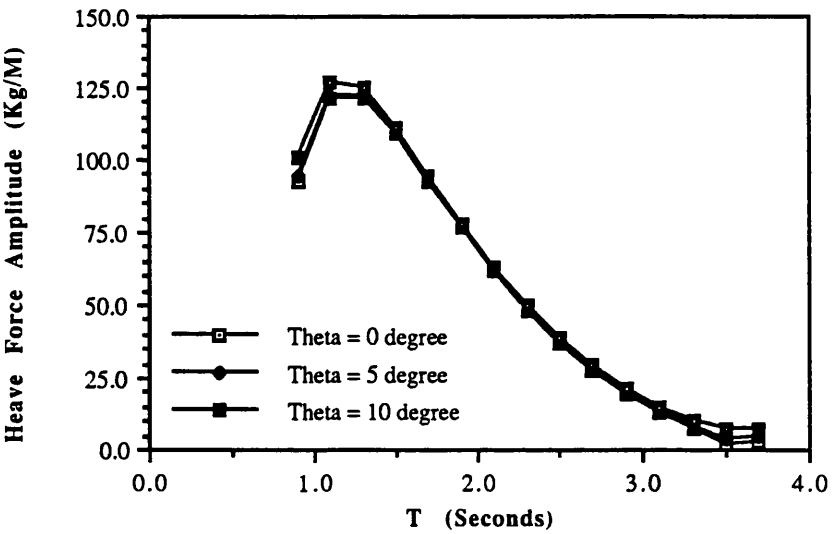

Fig.1.18 Heave forces due to inclination for the semi-submersible model (P-buoy)

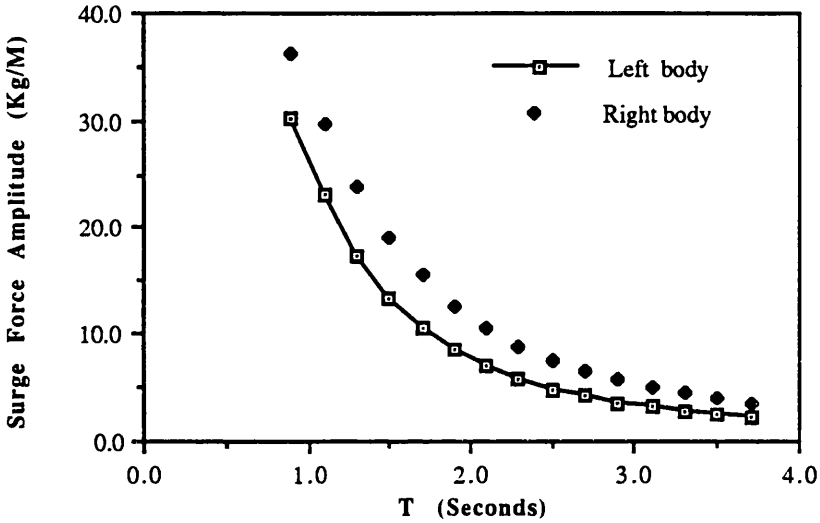

Fig.1.19 Comparison of surge forces for the sem-submersible model in 10 degree tilt condition

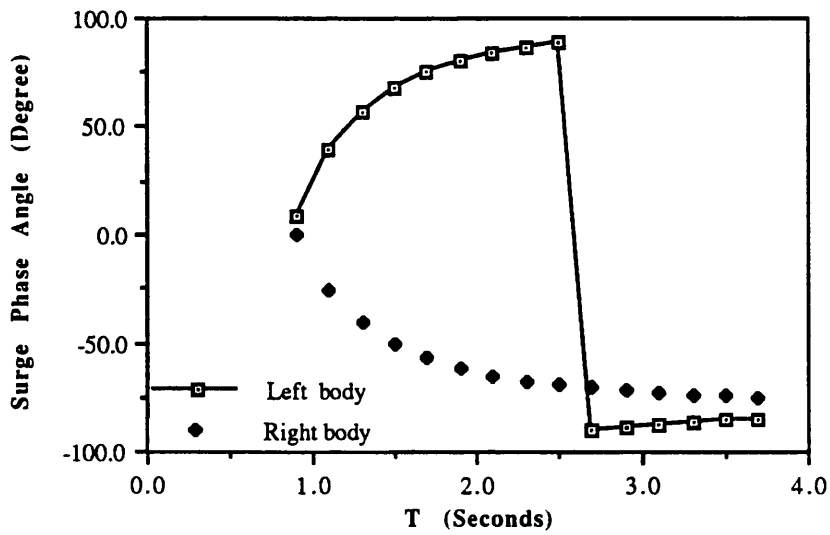

Fig.1.20 Comparison of surge phase angle for the semi-submersible model in 10 deg. tilt condition

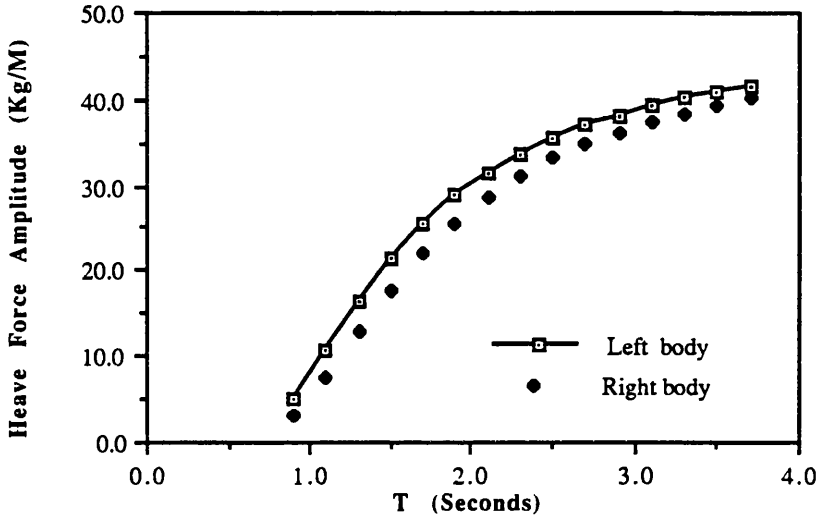

Fig.1.21 Comparison of heave forces for the semi-submersible model in 10 degree tilt condition

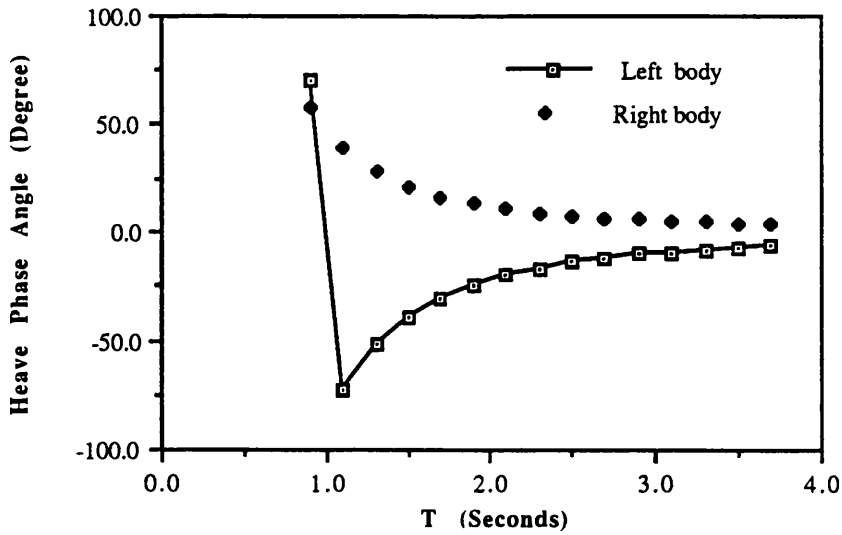

Fig.1.22 Comparison of heave phase angle for the semi-submersible model in 10 deg. tilt condition

Table

Main Particulars	
L =2.26m	d=0.16m
x_1=0.93m	∇=0.4765m
x_2=0.31m	W=169.48kg
h_0=0.40m	KB=0.1114m
h=0.28m	KG=0.1835m
l_1=0.12m	BM=0.1514m
f_1=0.2165m	GM=0.0793m
b=0.37m	BM_t=0.4560m
b_1=0.12m	GM_t=0.3839m

S.S.C.H. MODEL

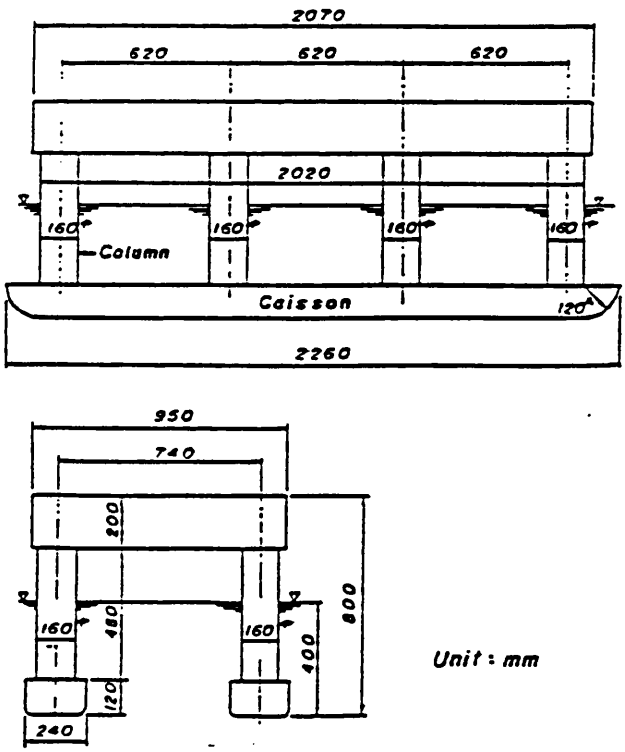

Fig.1.23 Basic configuration of twin hulled SSCH-1 model

Table of principal particulars

displacement	85.60 kg
draft	0.328 m
GM (transverse)	0.066 m
1). catamaran hull :	
length	1.803 m
breadth	0.183 m
depth	0.112 m
separation distance	0.940 m
2). column :	
diameter	0.132 m
	0.097 m
depth (under water)	0.260 m

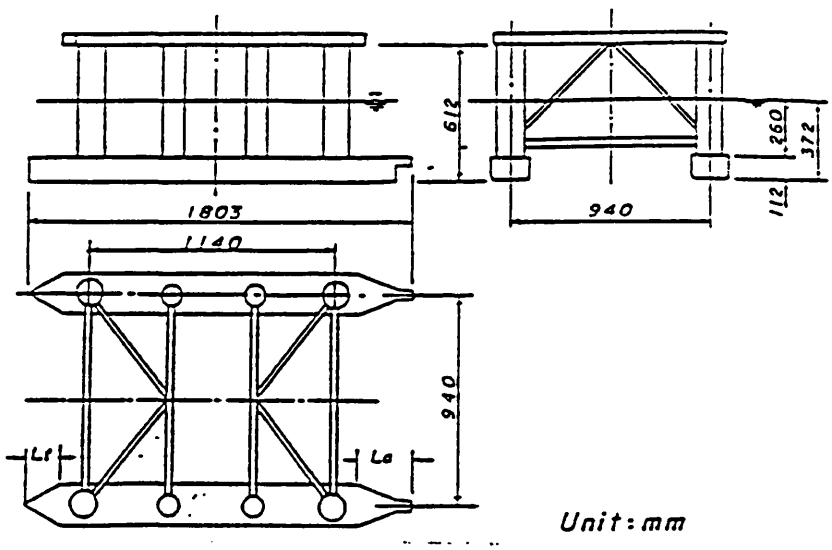

Fig.1.24 Basic configuration of twin hulled SSCH-2 model

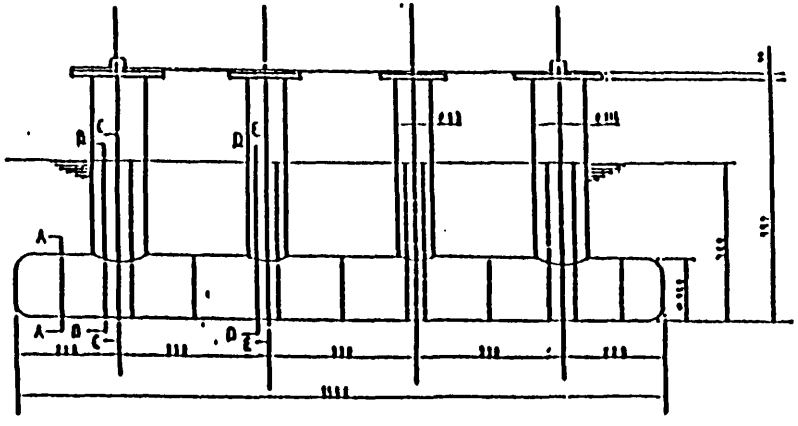

ELEVATION

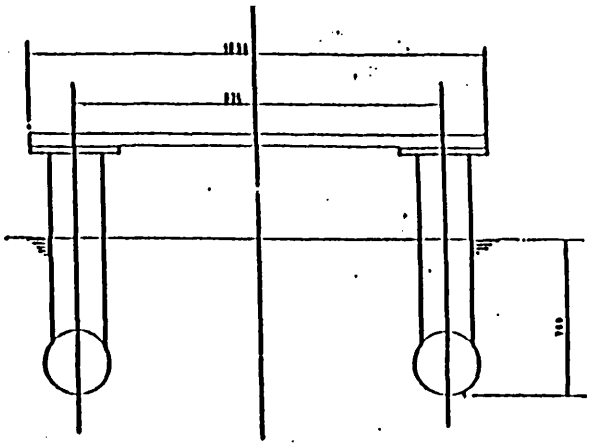

END VIEW

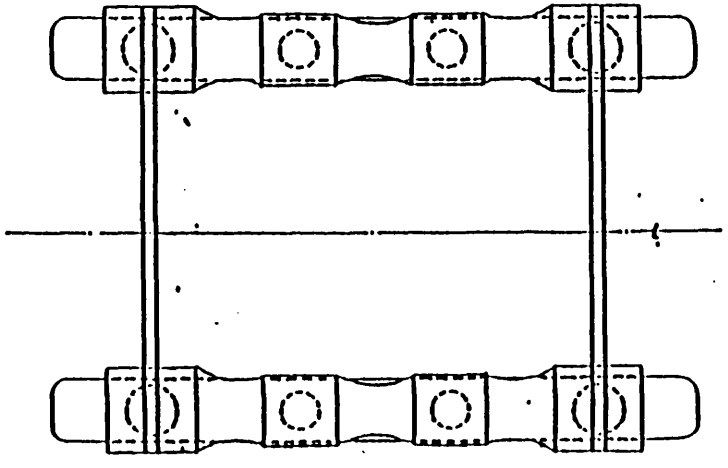

PLAN VIEW

TWIN CYLINDER HULL SEMI-SUBMERSIBLE

PRINCIPAL DIMENSIONS

Length of Pontoon	1.446 M
Radius of Pontoon	0.070 M
Pontoon Separation	0.834 M
Radius of Large Col.	0.057 M
Radius of Small Col.	0.0415 M
Draught	0.360 M

Fig.1.25 Basic configuration of twin hulled SSCH-3 model

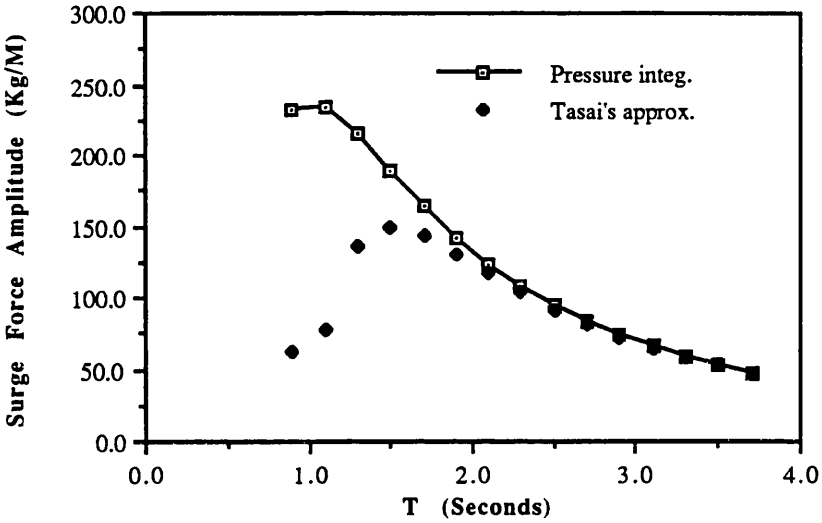

Fig.1.26 Comparison of surge forces for the SSCH-1 model

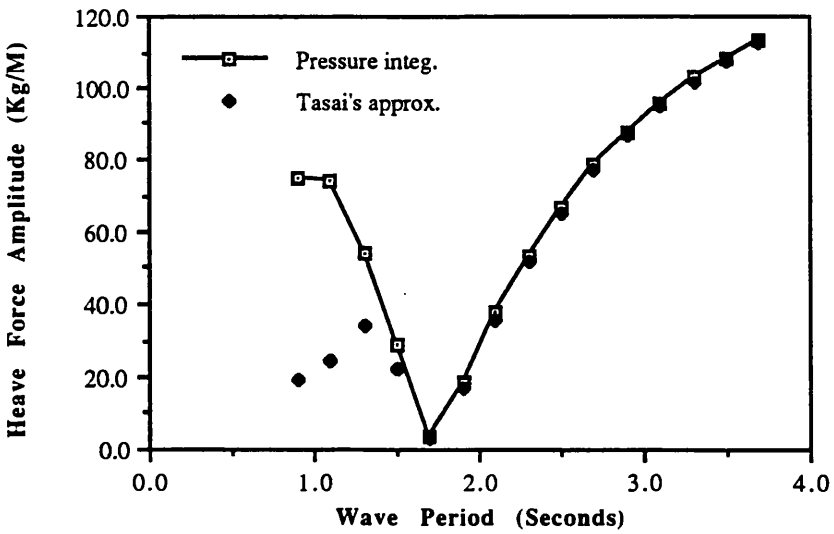

Fig.1.27 Comparison of heave forces for the SSCH-1 model

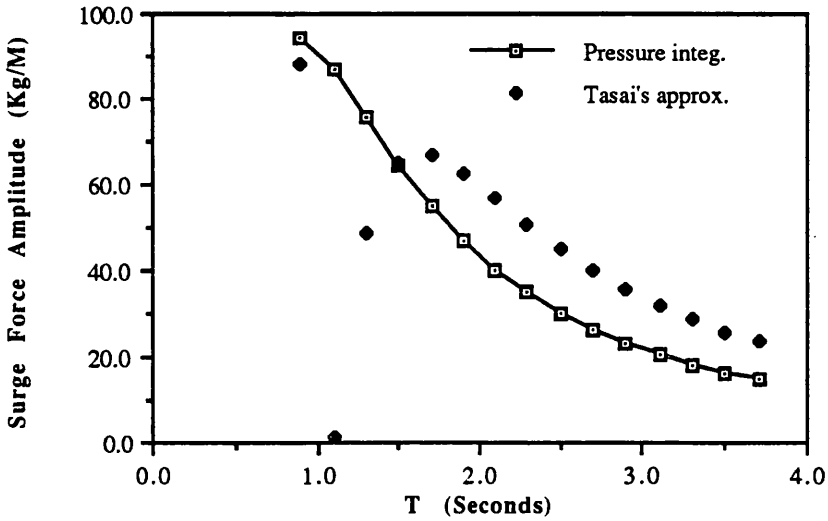

Fig.1.28 Comparison of surge forces for the SSCH-2 model

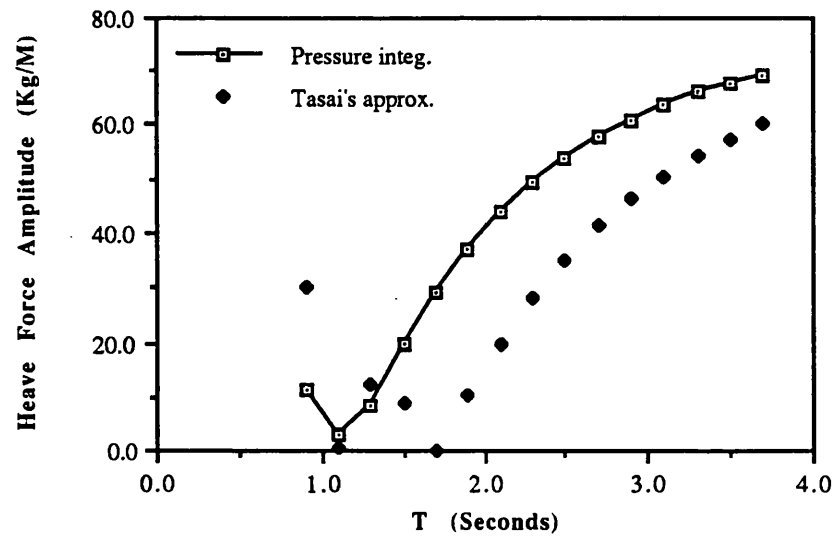

Fig.1.29 Comparison of heave forces for the SSCH-2 model

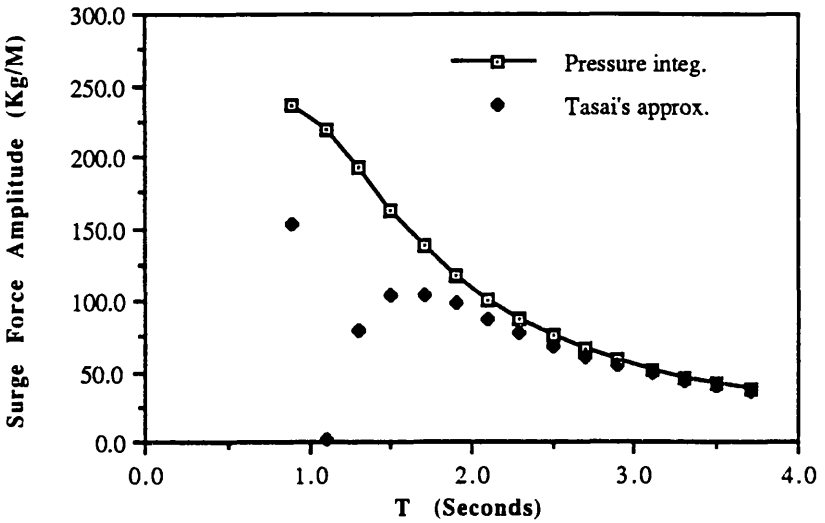

Fig.1.30 Comparison of surge forces for the SSCH-3 model

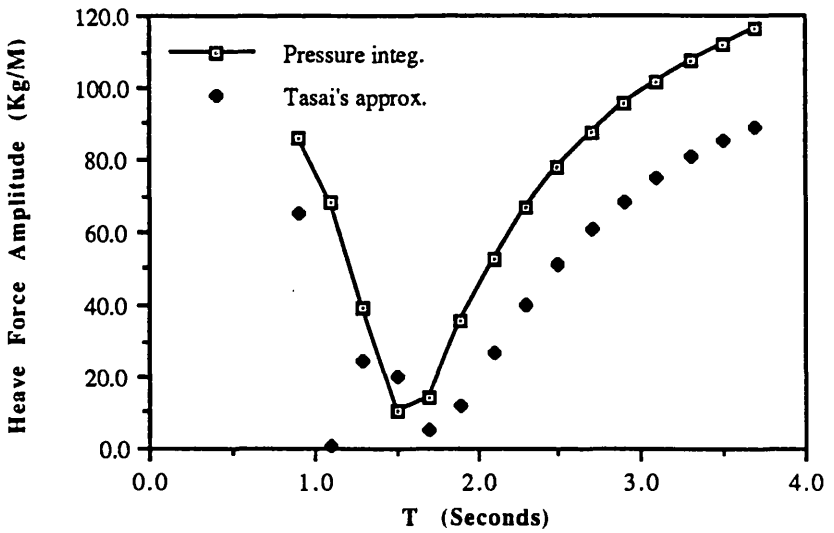

Fig.1.31 Comparison of heave forces for the SSCH-3 model

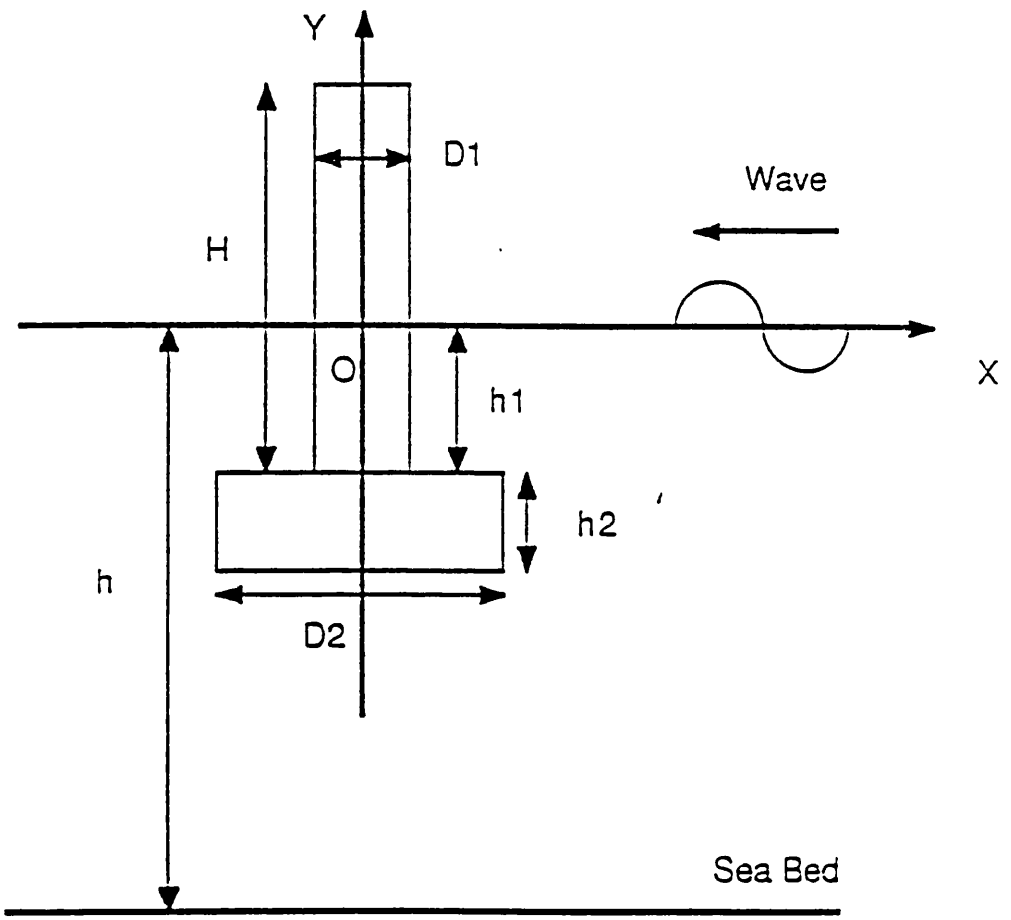

Fig.1.32 The coordinate system of a floating buoy in regular progressive waves

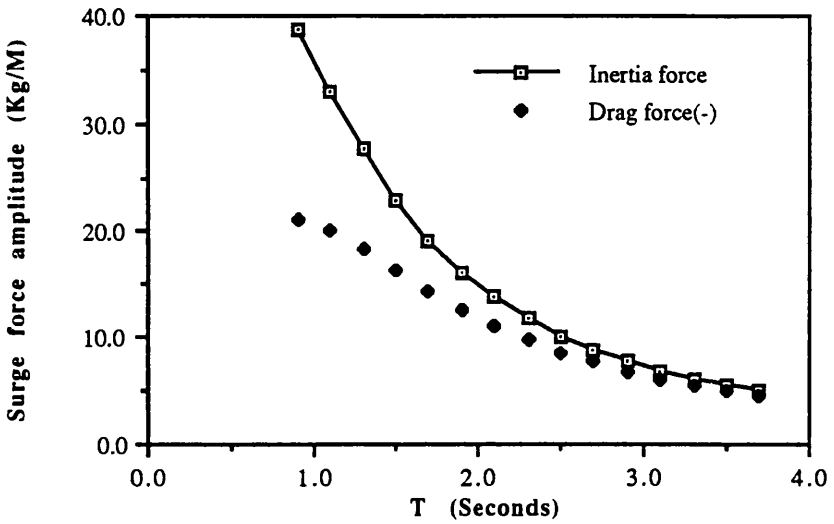

Fig.1.33 Surge force amplitude on the upper column of the P-buoy model

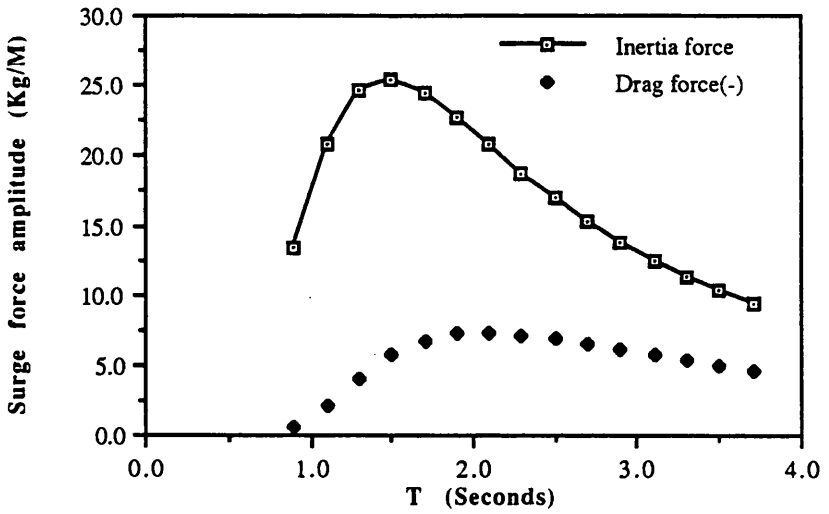

Fig.1.34 Surge force amplitude on the lower hull of the P-buoy model

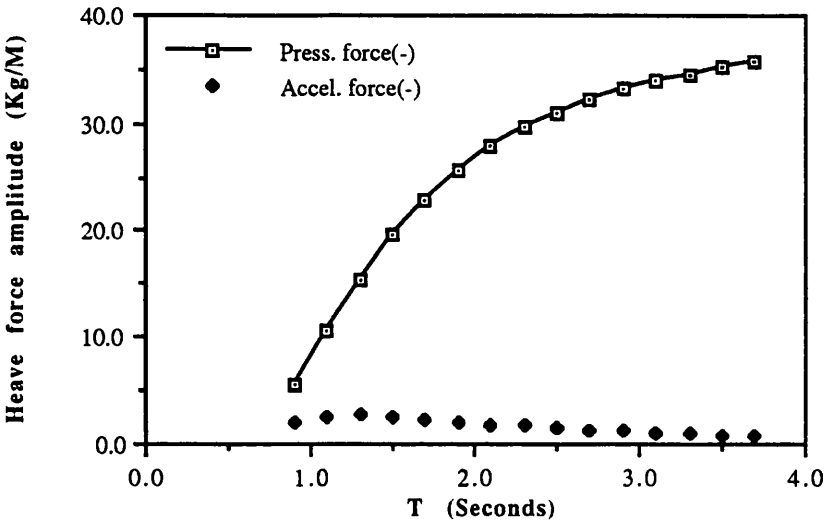

Fig.1.35 Heave force amplitude on upper column of the P-buoy model

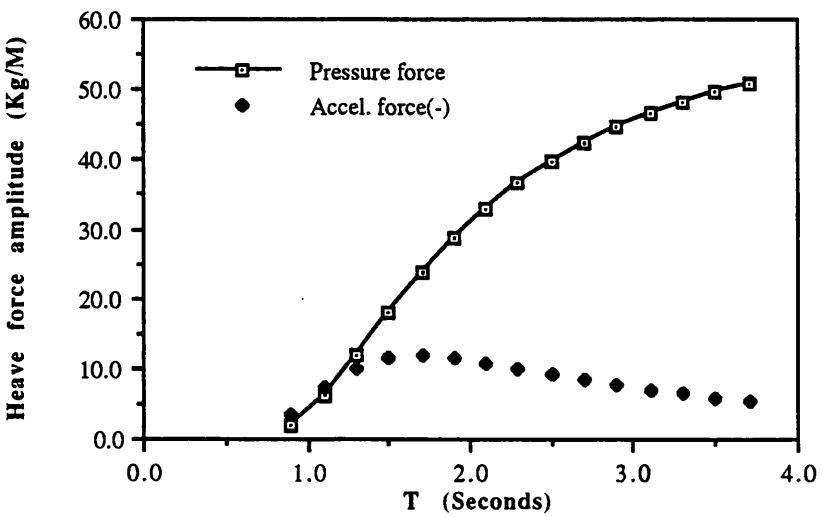

Fig.1.36 Heave force amplitude on lower hull of the P-buoy model

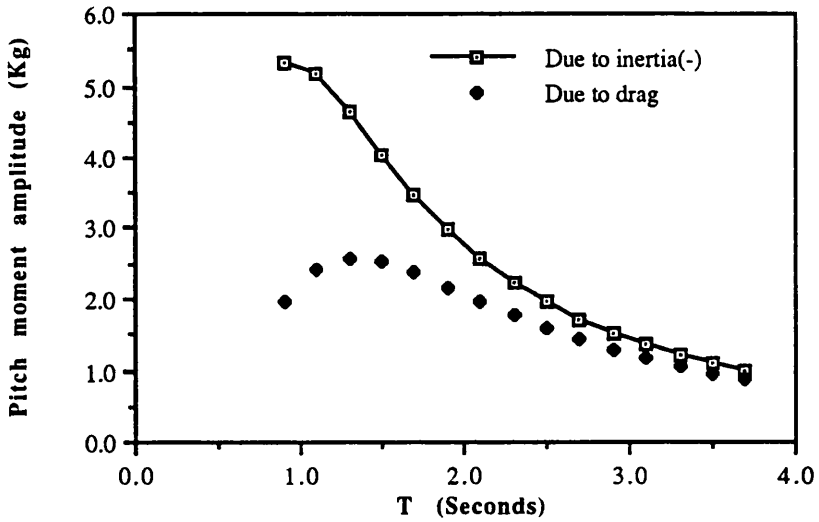

Fig.1.37 Pitch moment amplitude on upper column of the P-buoy model

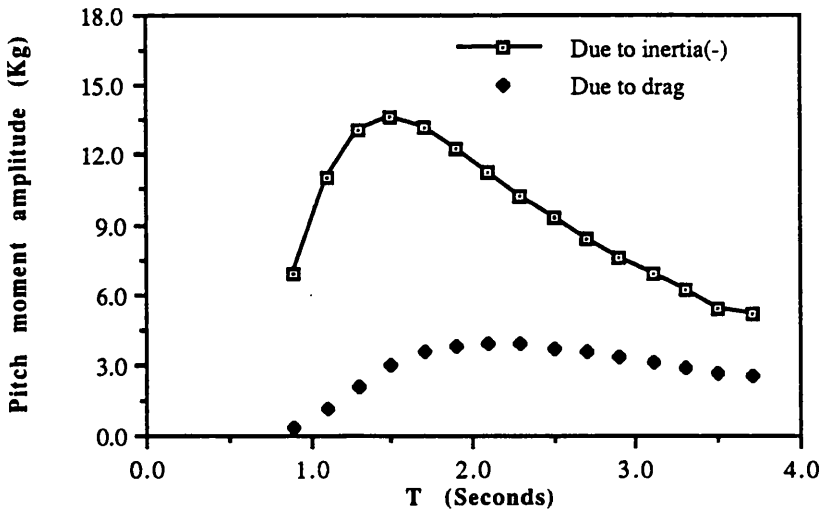

Fig.1.38 Pitch moment amplitude on lower hull of the P-buoy model

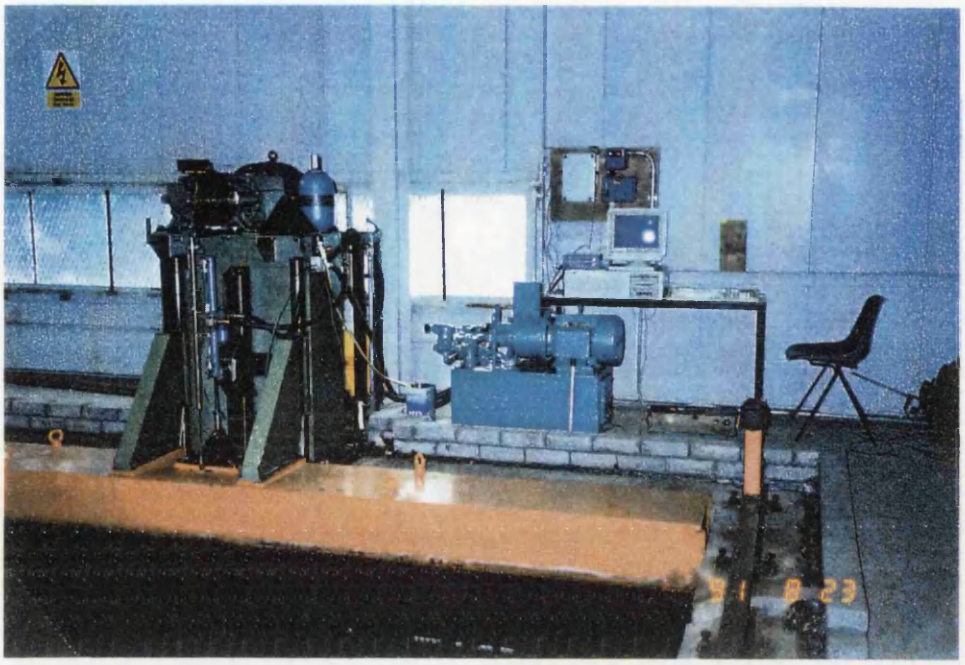

Fig.1.39 Layout of numerical-controlled wave making system

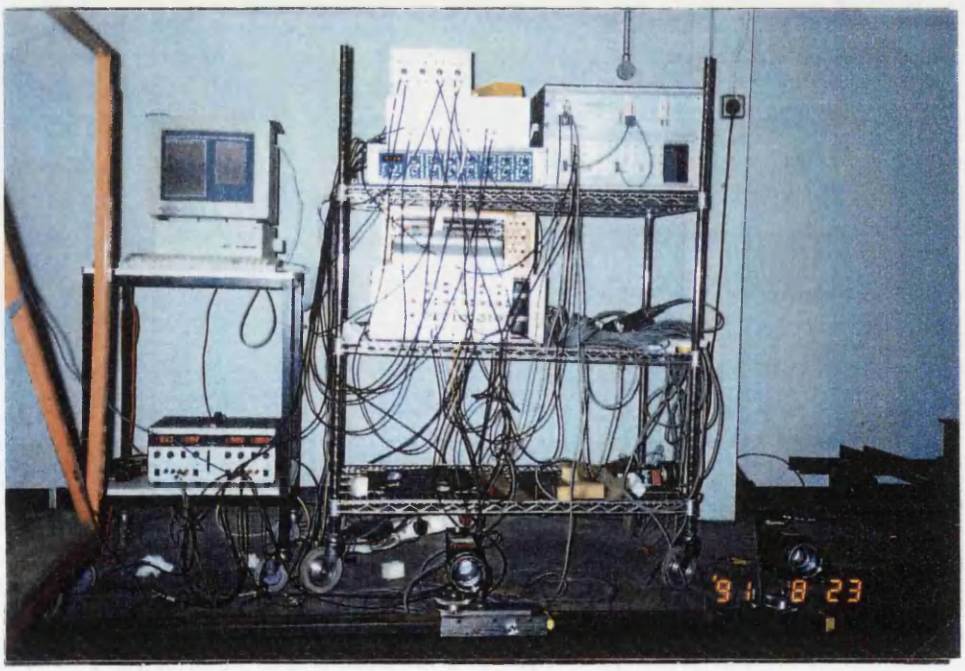

Fig.1.40 Layout of experimental data acquisition system

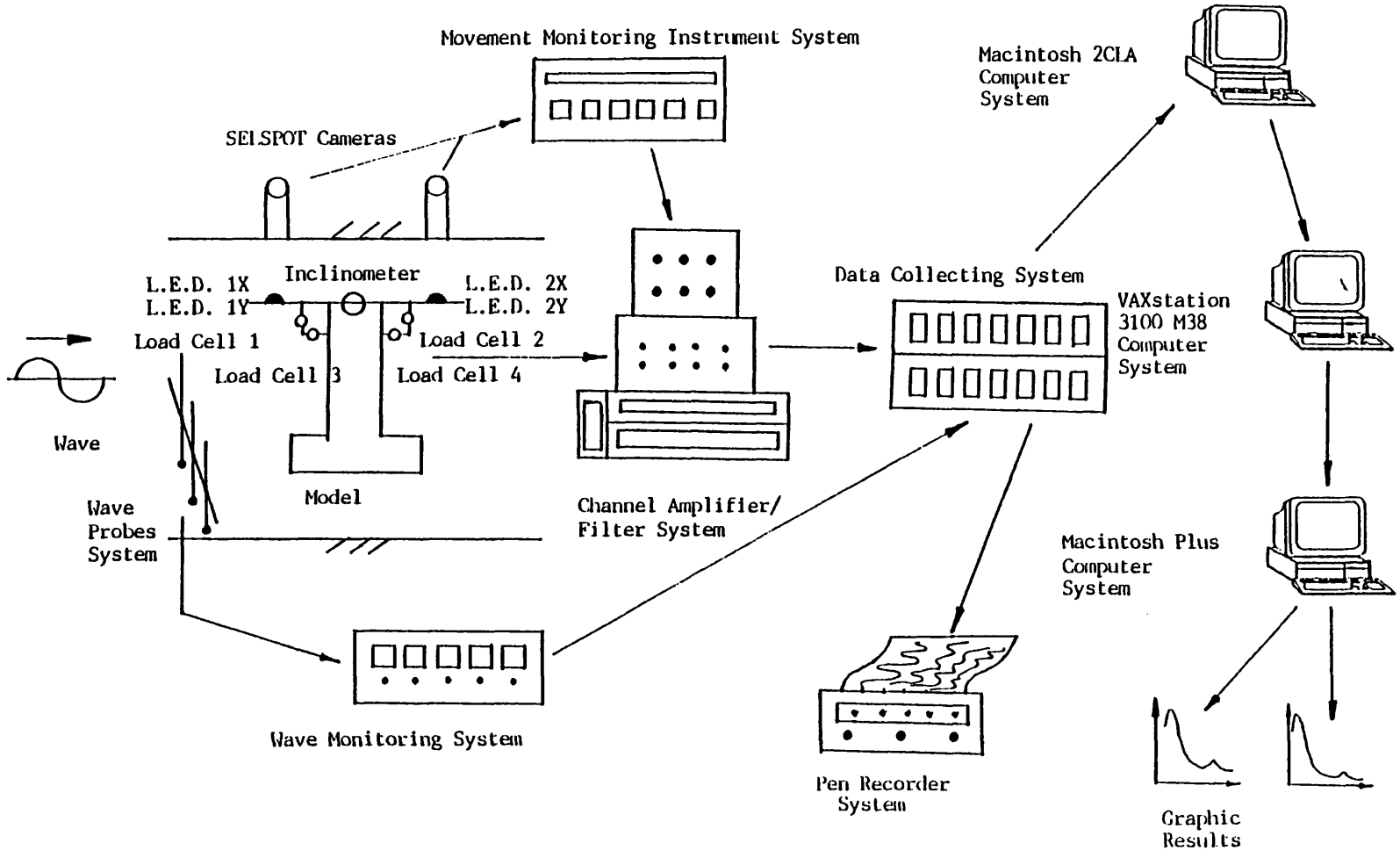

Fig.1.41 Flowing diagram of experimental data acquisition and analysis system

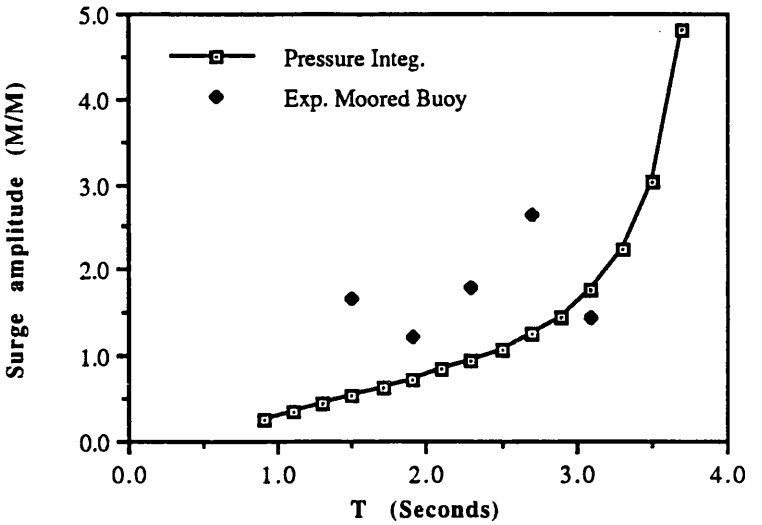

Fig.1.42 Comparison of surge amplitudes for the C-buoy model

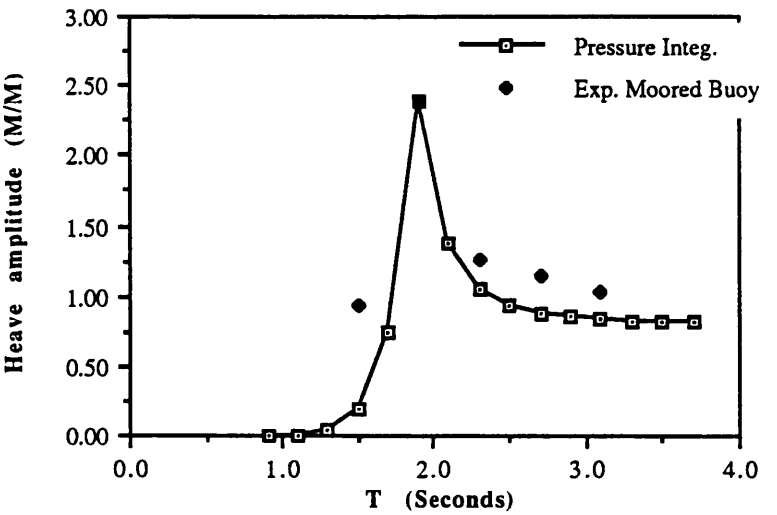

Fig.1.43 Comparison of heave amplitudes for the C-buoy model

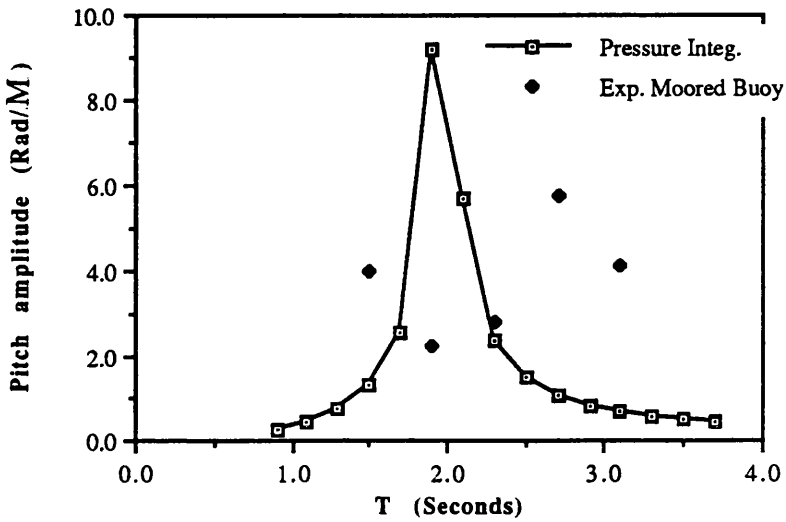

Fig.1.44 Comparison of pitch amplitudes for the C-buoy model

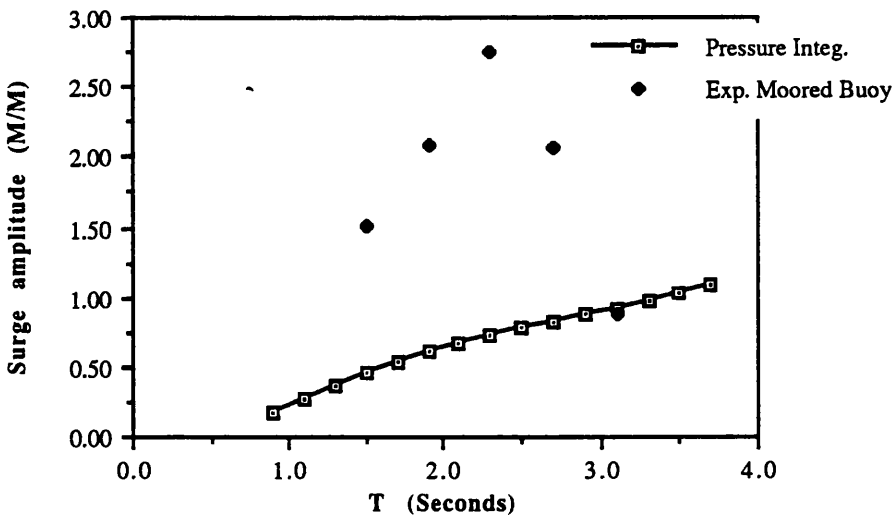

Fig.1.45 Comparison of surge amplitudes for the D-buoy model

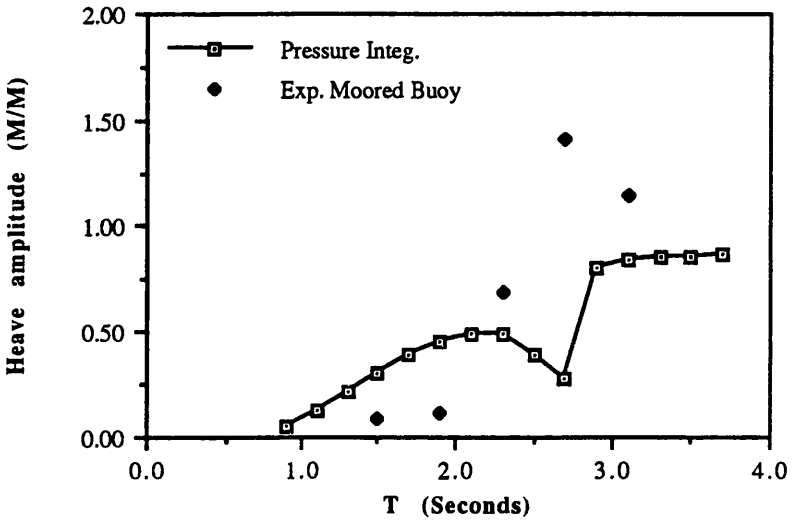

Fig.1.46 Comparison of heave amplitudes for the D-buoy model

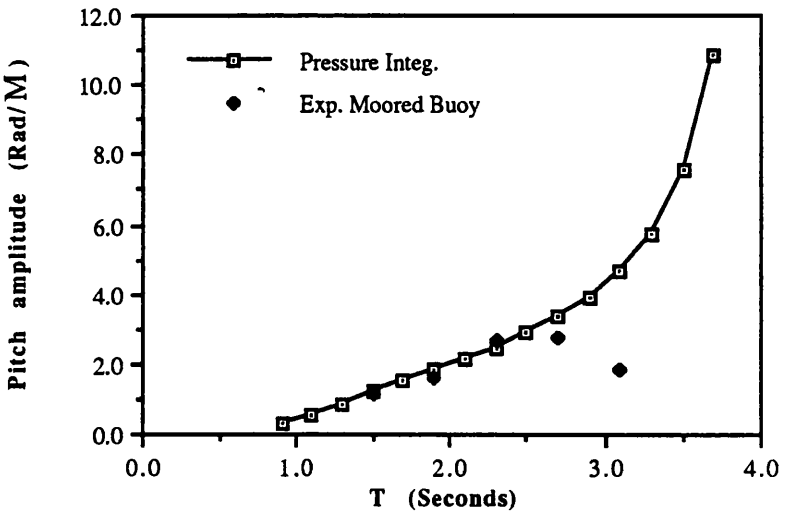

Fig.1.47 Comparison of pitch amplitudes for the D-buoy model

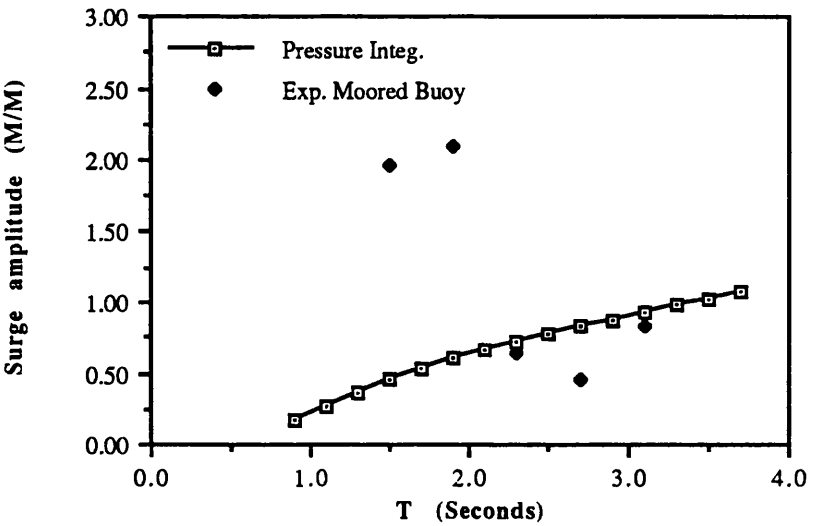

Fig.1.48 Comparison of surge amplitudes for the P-buoy model

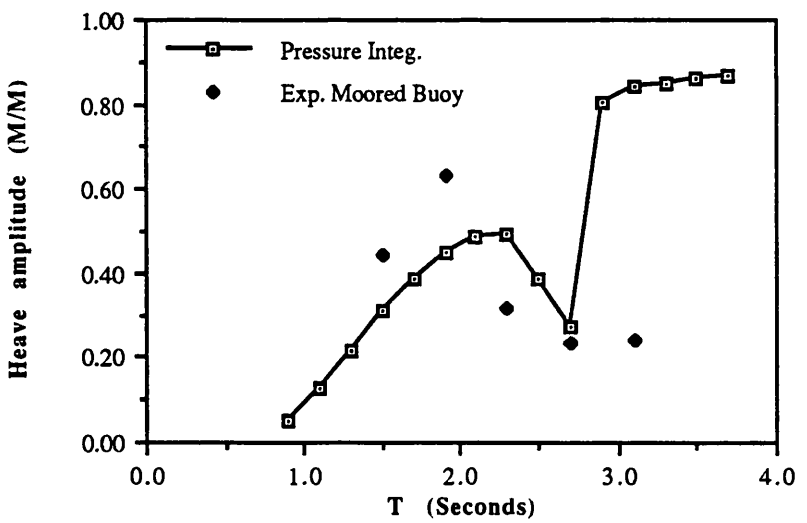

Fig.1.49 Comparison of heave amplitudes for the P-buoy model

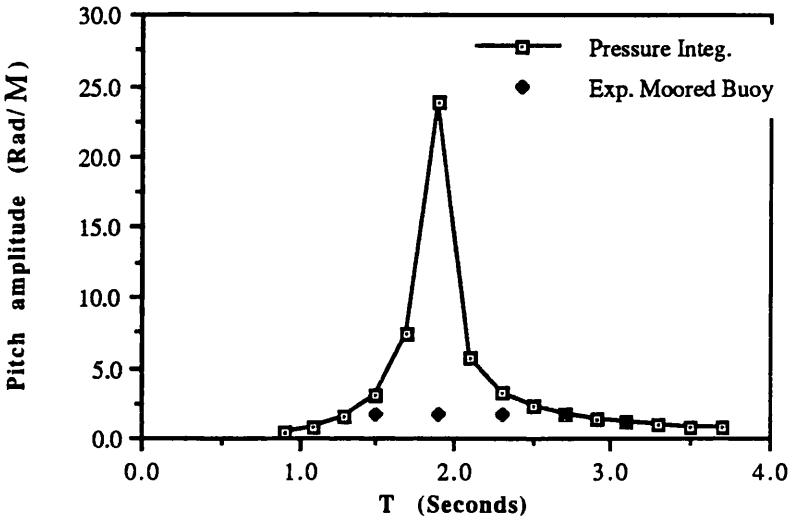

Fig.1.50 Comparison of pitch amplitudes for the P-buoy model

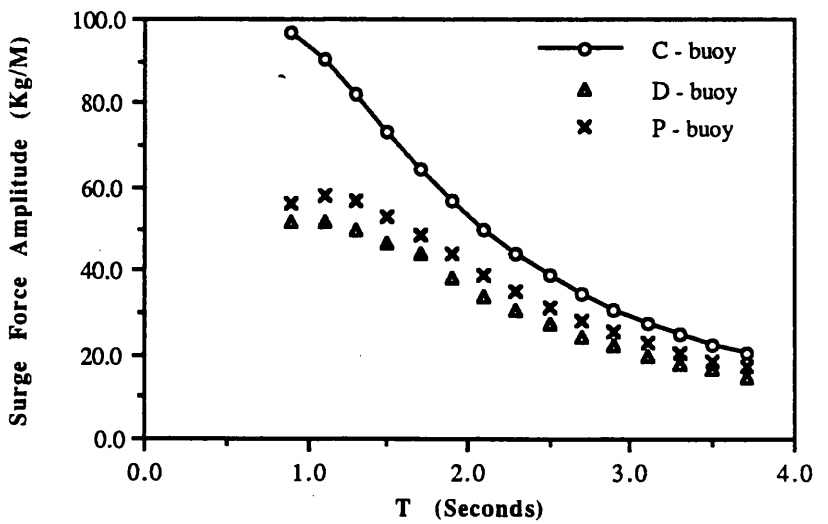

Fig.1.51 Comparison of surge force amp. for different buoy configurations

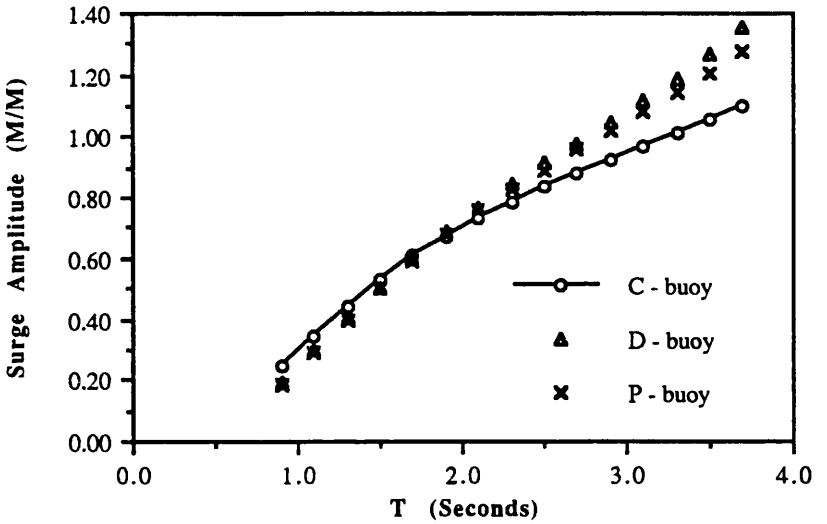

Fig.1.52 Comparison of surge amp. for different buoy configurations

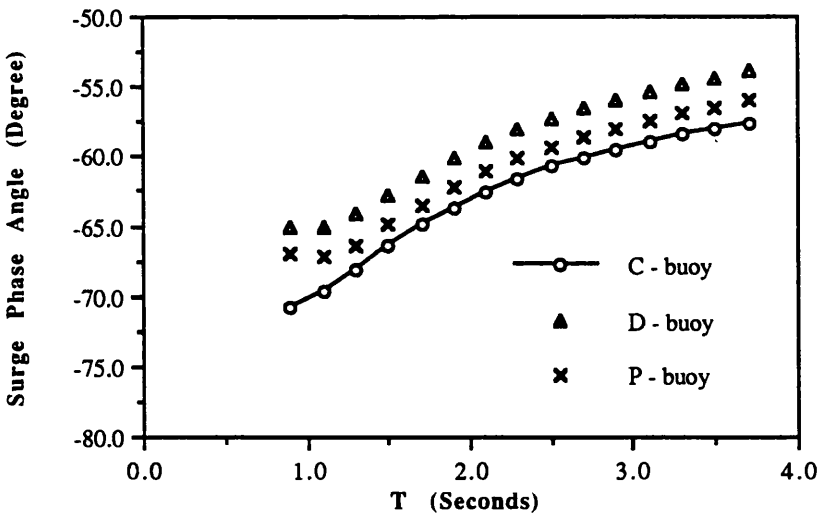

Fig.1.53 Comparison of surge phase angles for different buoy configurations

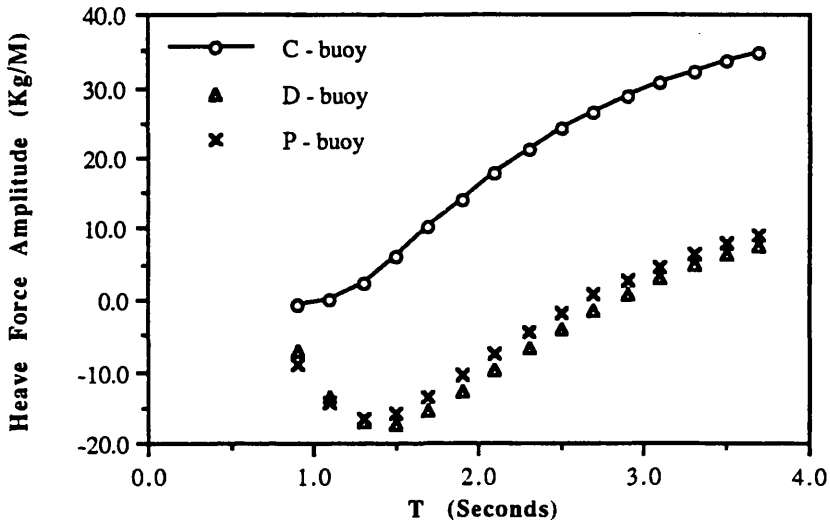

Fig.1.54 Comparison of heave force amp. for different buoy configurations

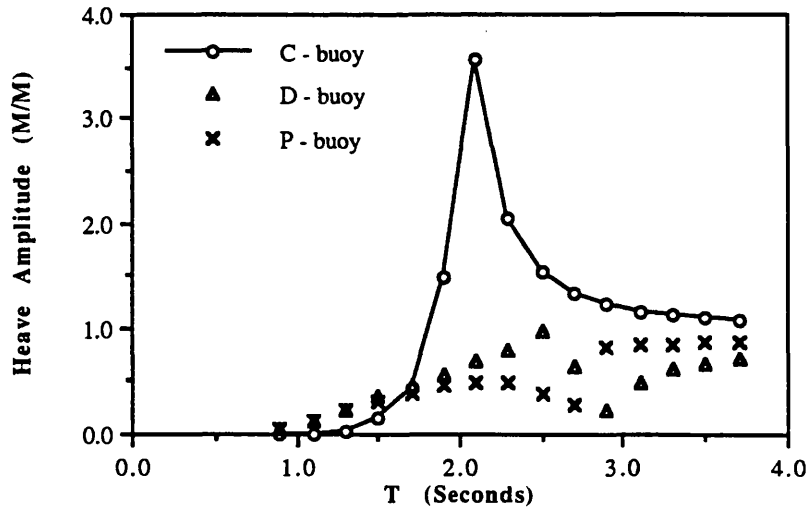

Fig.1.55 Comparison of heave amplitudes for different buoy configurations

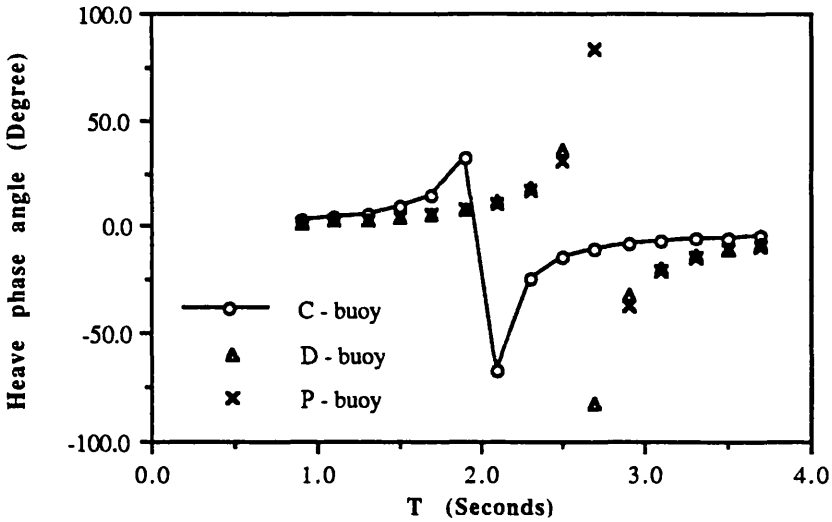

Fig.1.56 Comparison of heave phase angles for different buoy configurations

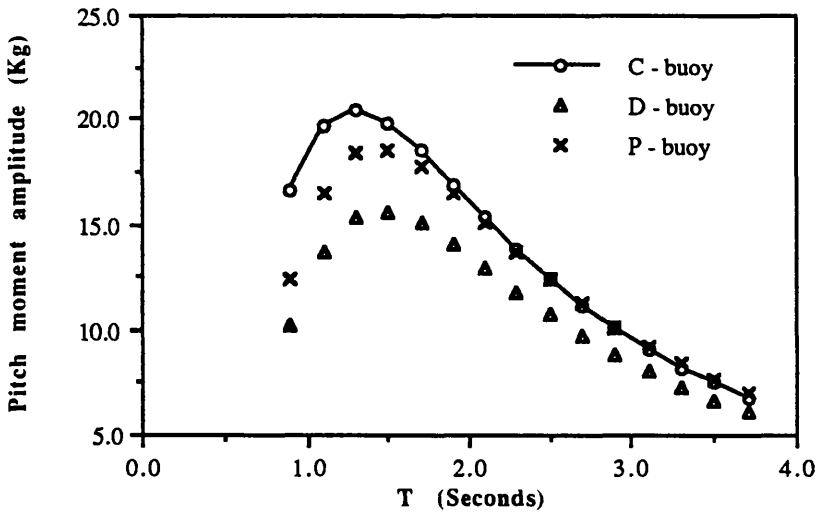

Fig.1.57 Comparison of pitch moment amp. for different buoy configurations

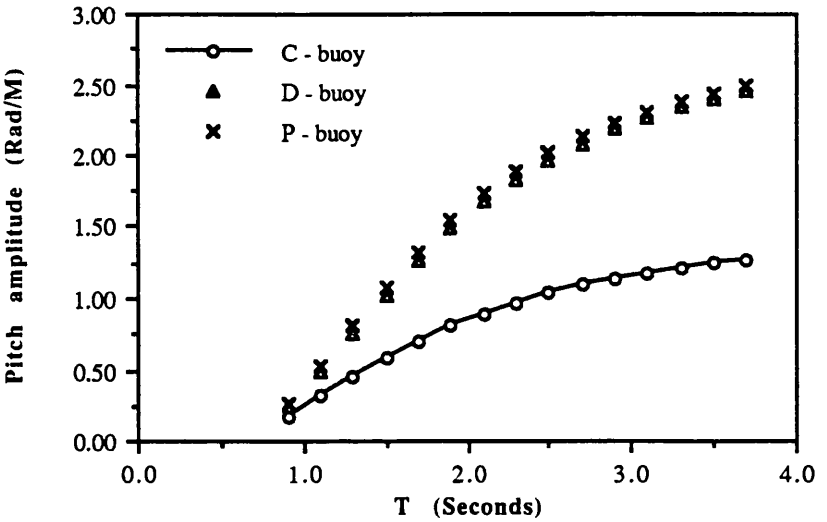

Fig.1.58 Comparison of pitch amplitudes for different buoy configurations

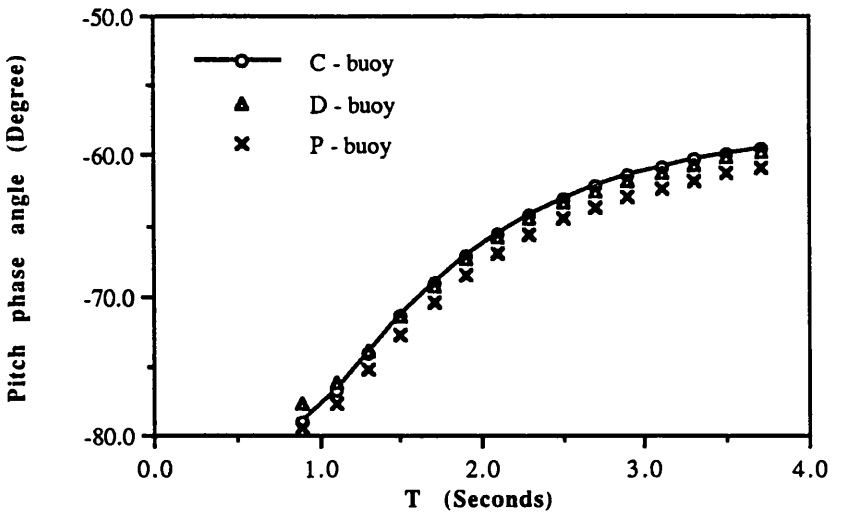

Fig.1.59 Comparison of pitch phase angles for different buoy configurations

Fig.1.60 The " C - buoy " model in dynamic motion experiments

Fig.1.61 The " D - buoy " model in dynamic motion experiments

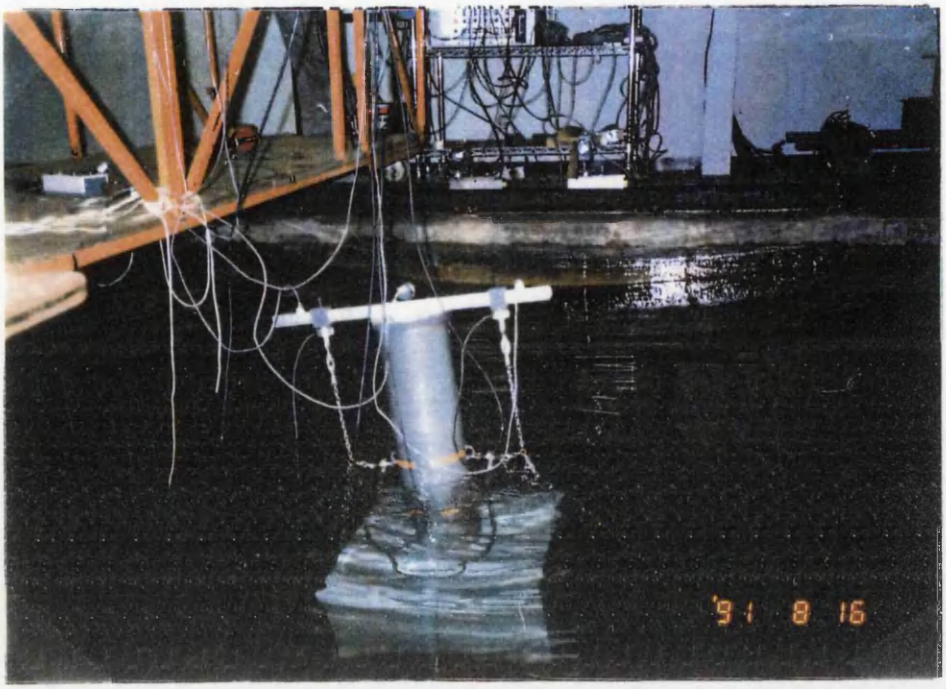

Fig.1.62 The " P - buoy " model in dynamic motion experiments

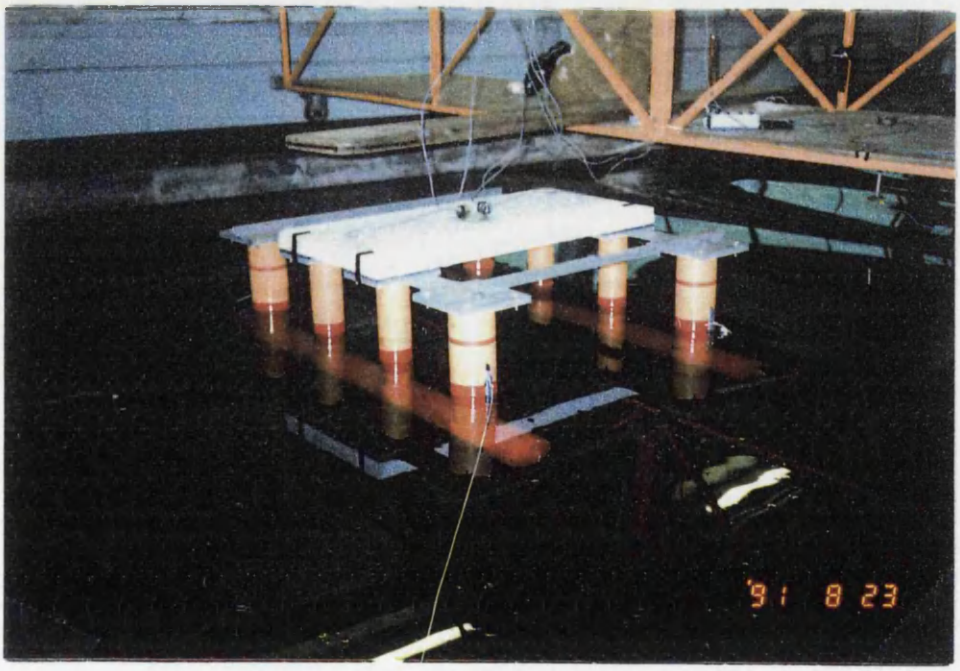

Fig.1.85 The twin hulled offshore structure in dynamic motion experiments

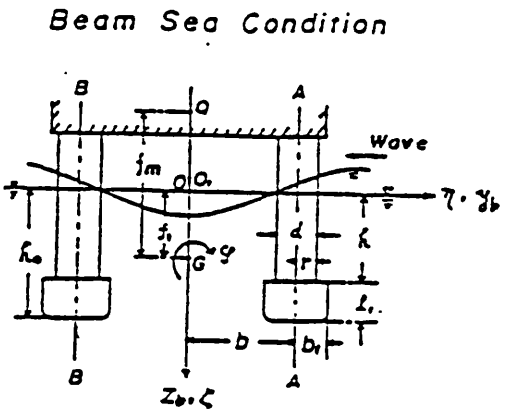

Fig.1.63 The coordinate system of a twin hulled structure in beam sea condition

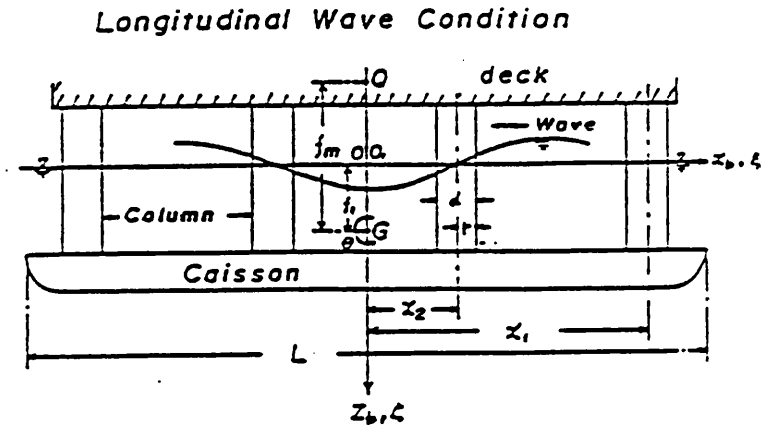

Fig.1.64 The coordinate system of a twin hulled structure in longitudinal wave condition

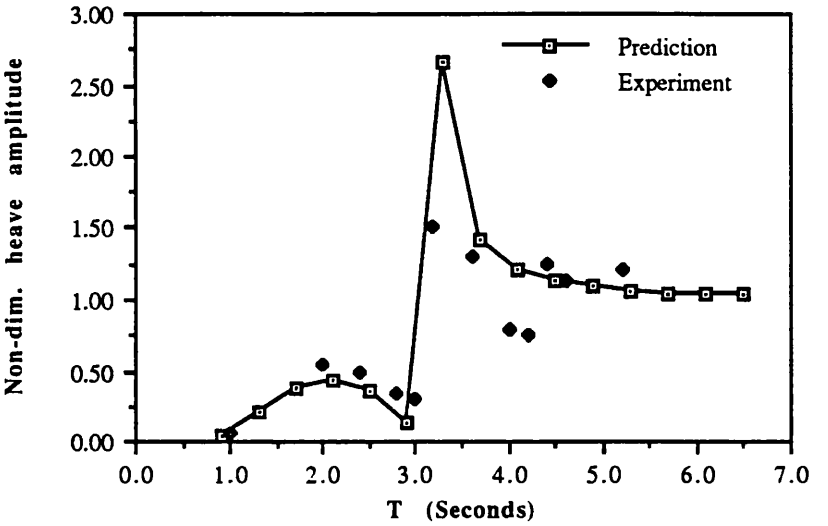

Fig.1.65 Comparison of non-dim. heave motion amplitude (SSCH-1)

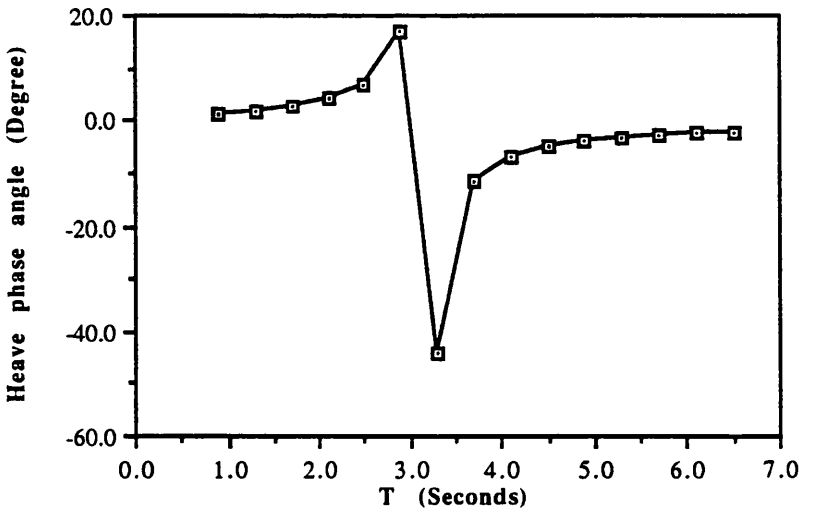

Fig.1.66 Phase angle for heave motion of the semi-submersible model (SSCH-1)

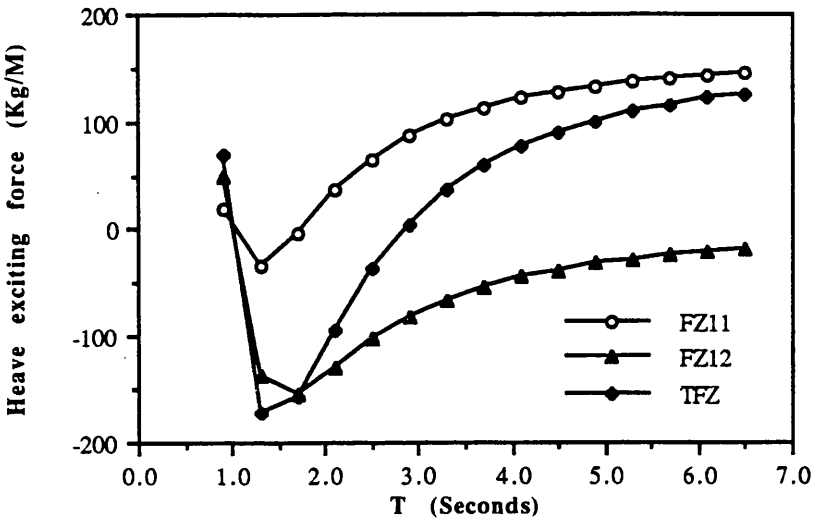

Fig.1.67 Wave exciting force per wave amplitude of heave motion (SSCH-1)

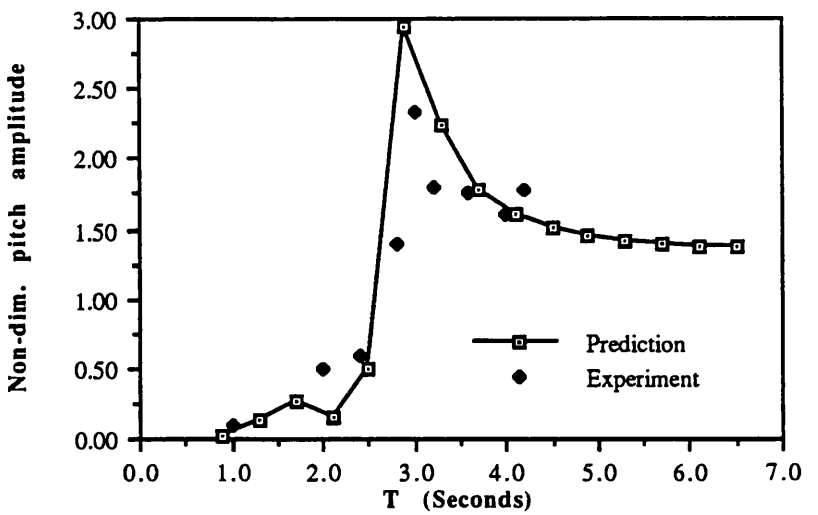

Fig.1.68 Comparison of non-dim. pitch amplitude (SSCH-1)

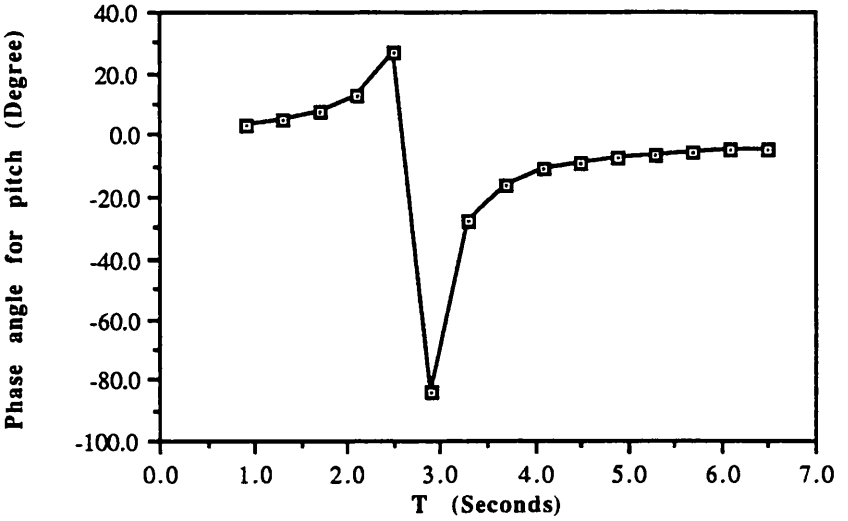

Fig.1.69 Phase angle for pitch motion of the semi-submersible model (SSCH-1)

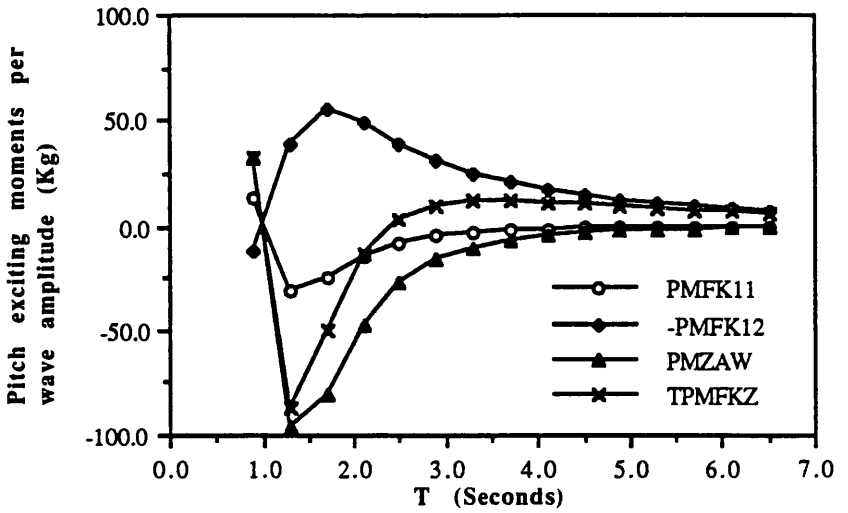

Fig.1.70 Froude-Krylov's moment per wave amplitude for pitching motion (SSCH-1)

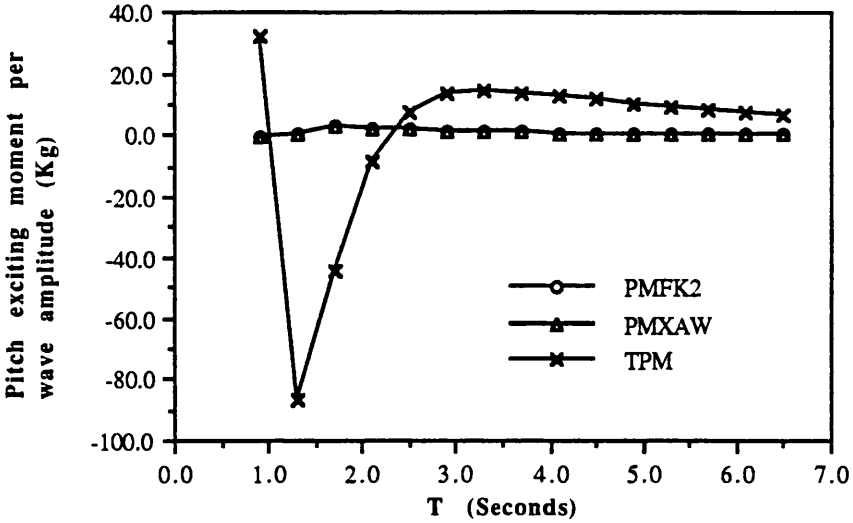

Fig.1.71 Wave exciting moment per wave amplitude for pitch motion (SSCH-1)

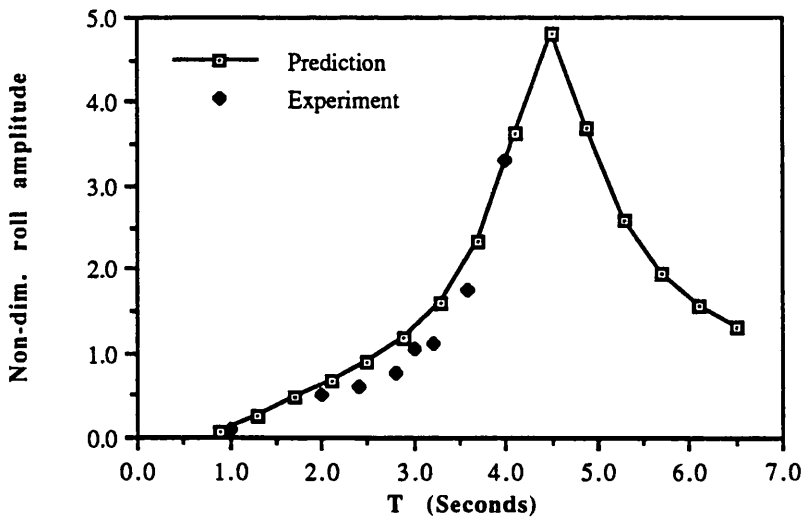

Fig.1.72 Comparison of non-dim. roll amplitude (SSCH-1)

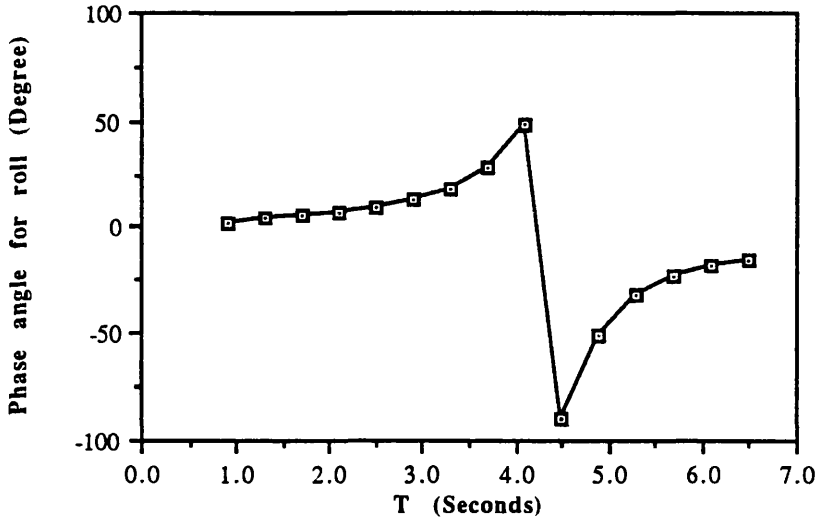

Fig.1.73 Phase angle for roll motion of the semi-submersible model (SSCH-1)

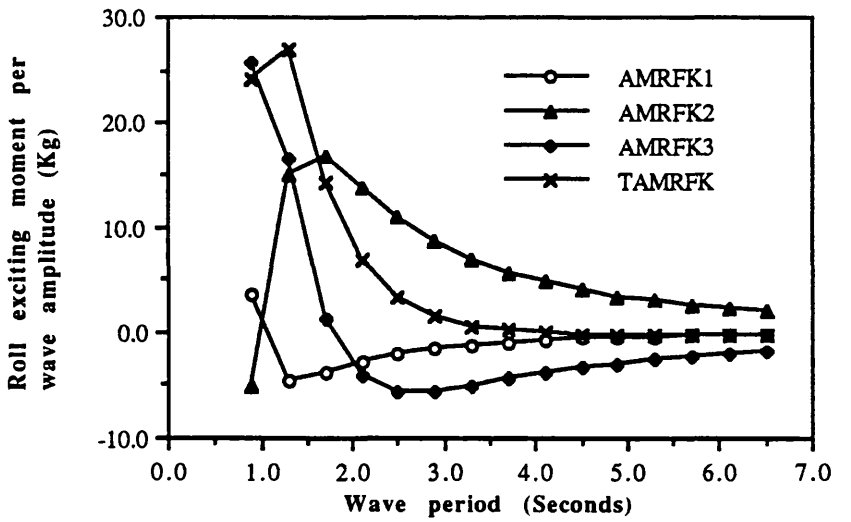

Fig.1.74 Froude-Krylov's moment per wave amplitude for roll motion (SSCH-1)

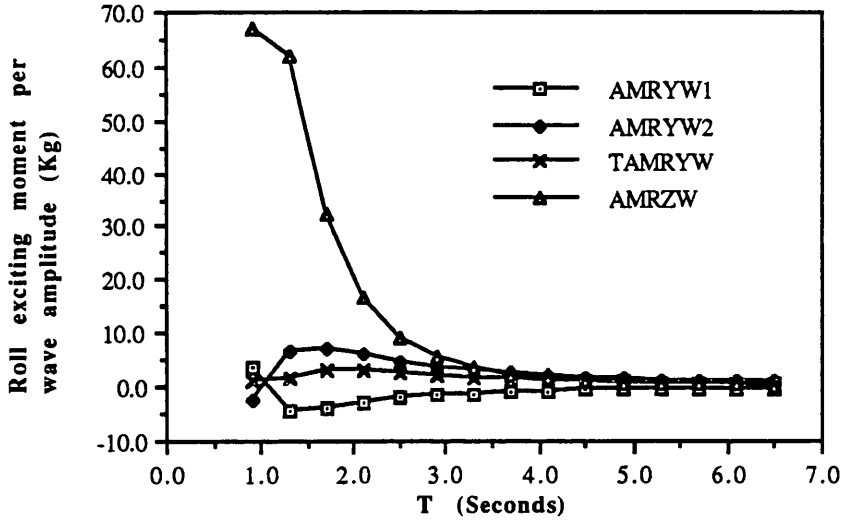

Fig.1.75 Wave diffraction moment per wave amplitude for roll motion (SSCH-1)

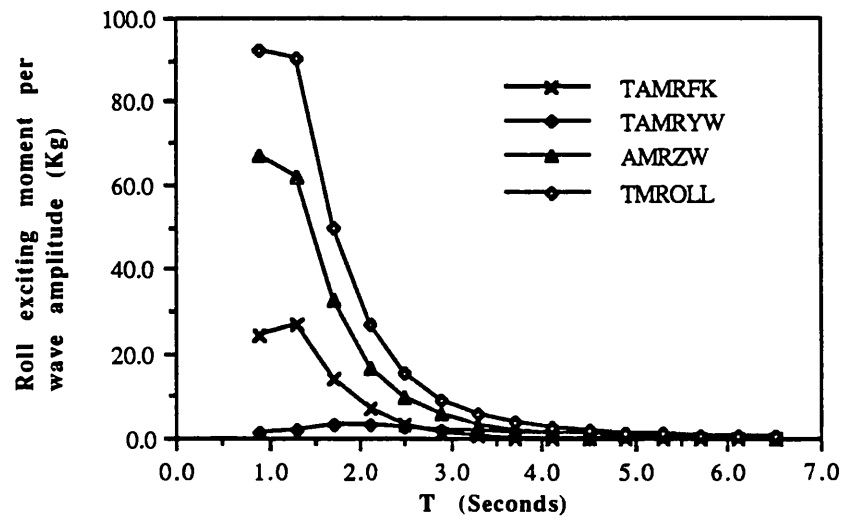

Fig.1.76 Wave exciting moment per wave amplitude for roll motion (SSCH-1)

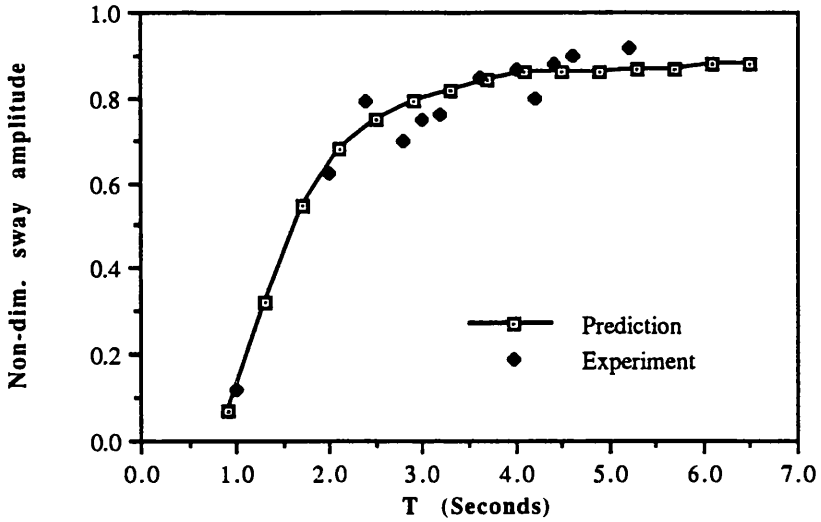

Fig.1.77 Comparison of non-dim. sway amplitude (SSCH-1)

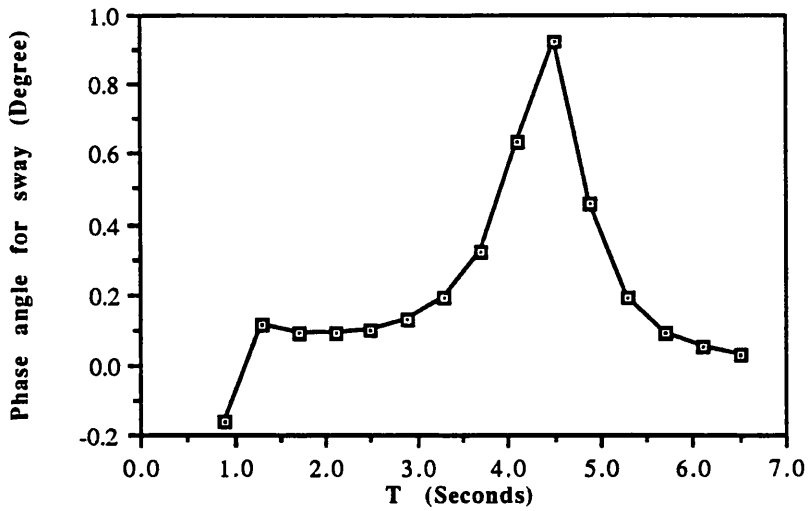

Fig.1.78 Phase angle for sway motion of the semi-submersible model (SSCH-1)

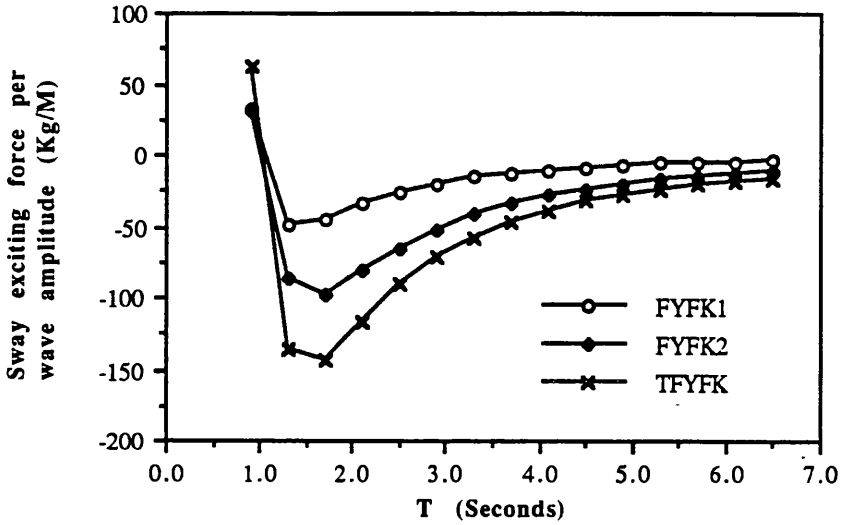

Fig.1.79 Froude-Krylov's force per wave amplitude for sway motion (SSCH-1)

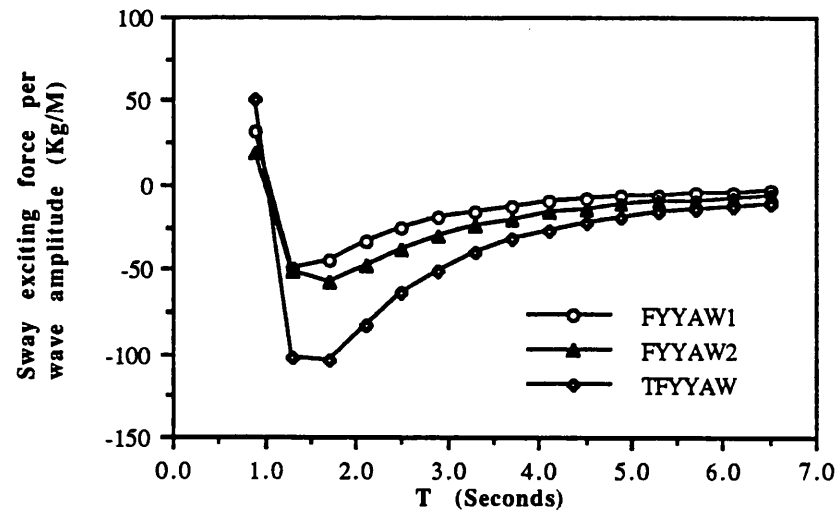

Fig.1.80 Wave diffraction force per wave amplitude for sway motion (SSCH-1)

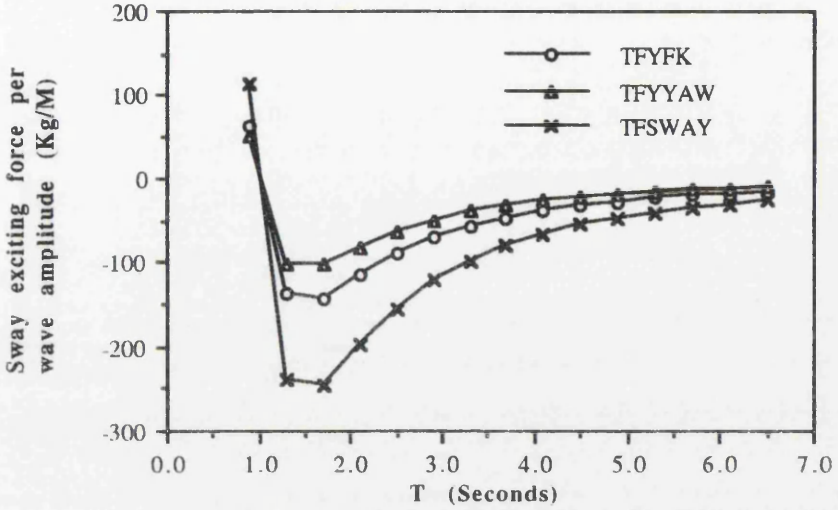

Fig.1.81 Wave exciting force per wave amplitude for sway motion (SSCH-1)

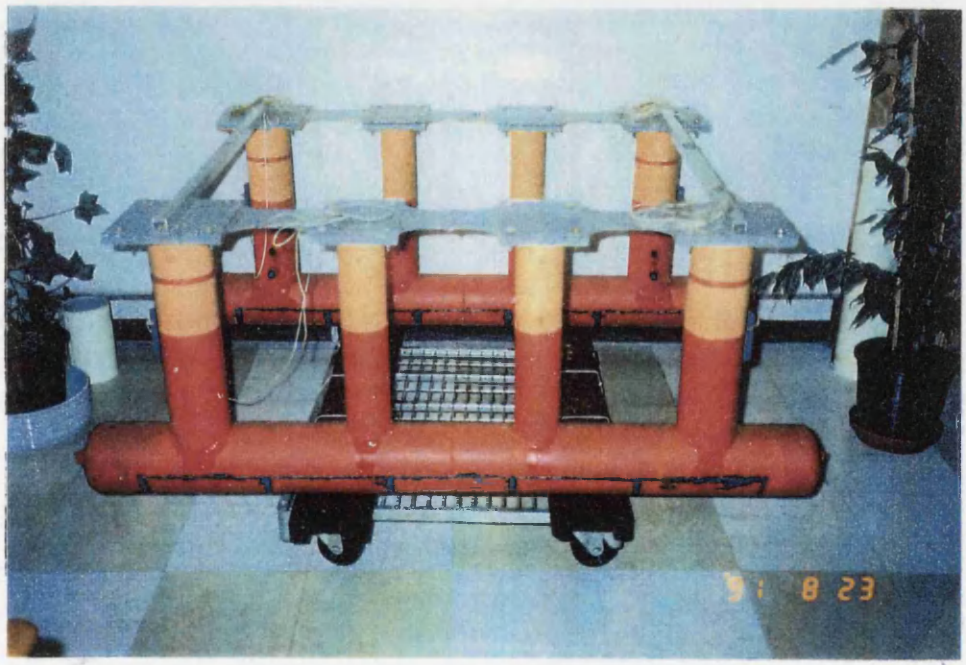

Fig.1.82 The twin hulled structure model for dynamic motion experiments

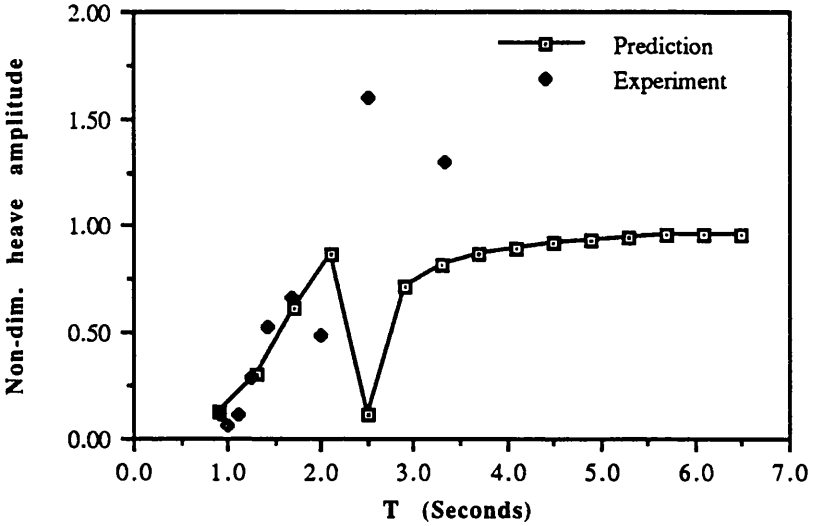

Fig.1.83 Comparison of non-dim. heave amplitude (SSCH-3)

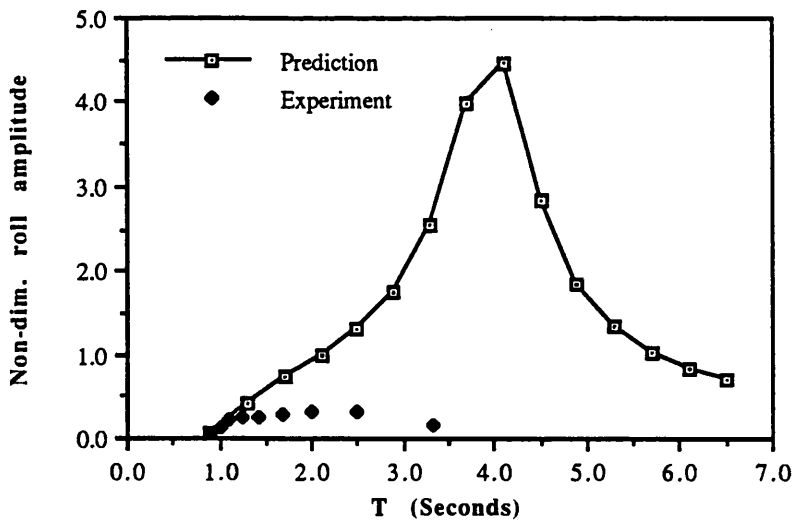

Fig.1.84 Comparison of non-dim. roll amplitude (SSCH-3)

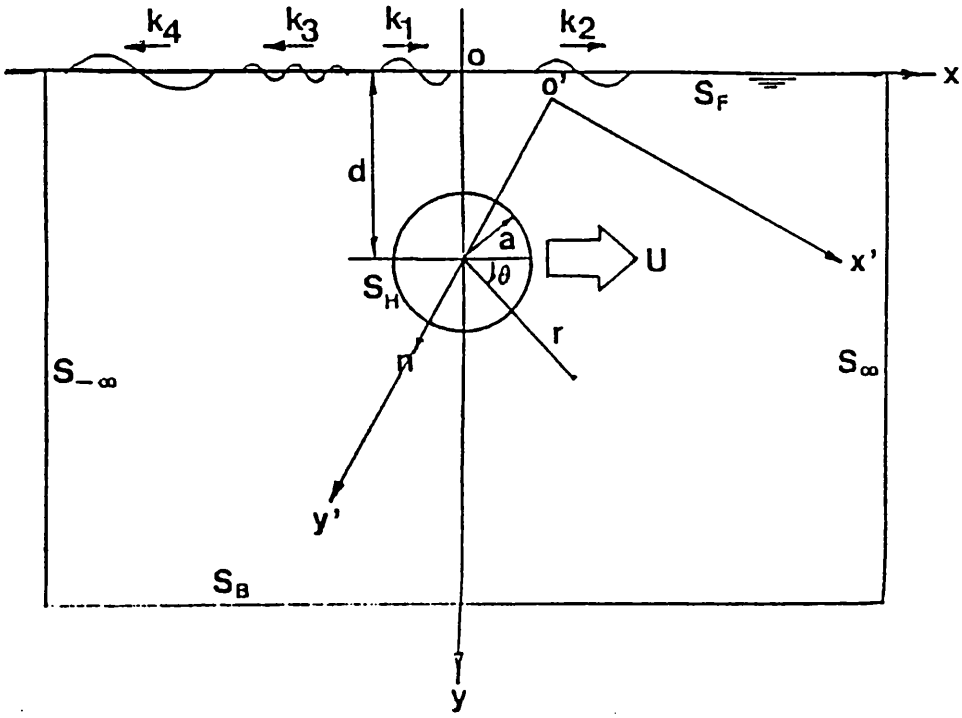

Fig.2.1 The coordinate system of an oscillating and translating circular cylinder

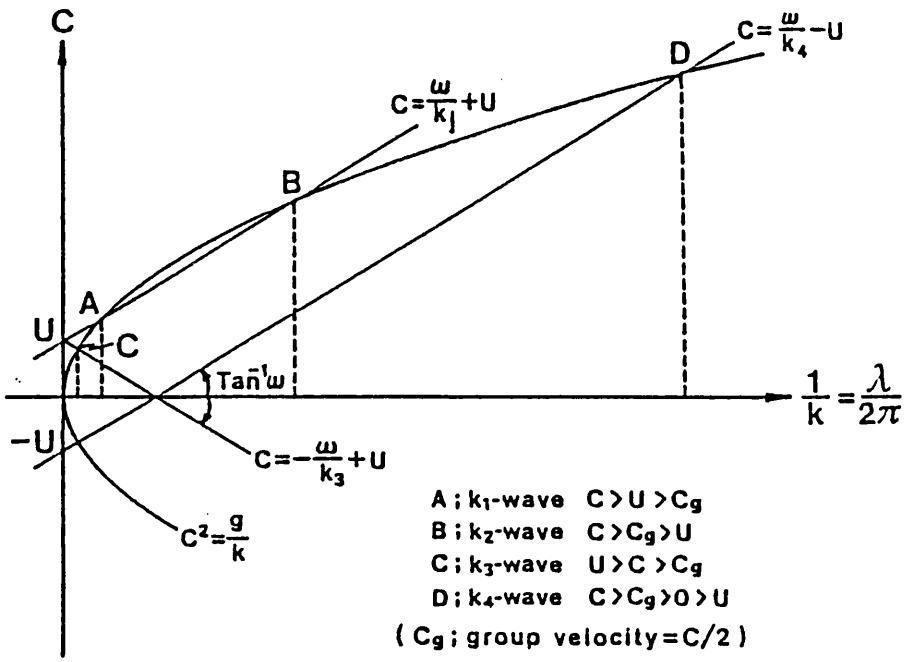

Fig.2.2 Relation between body speed, phase velocity and group velocity of waves

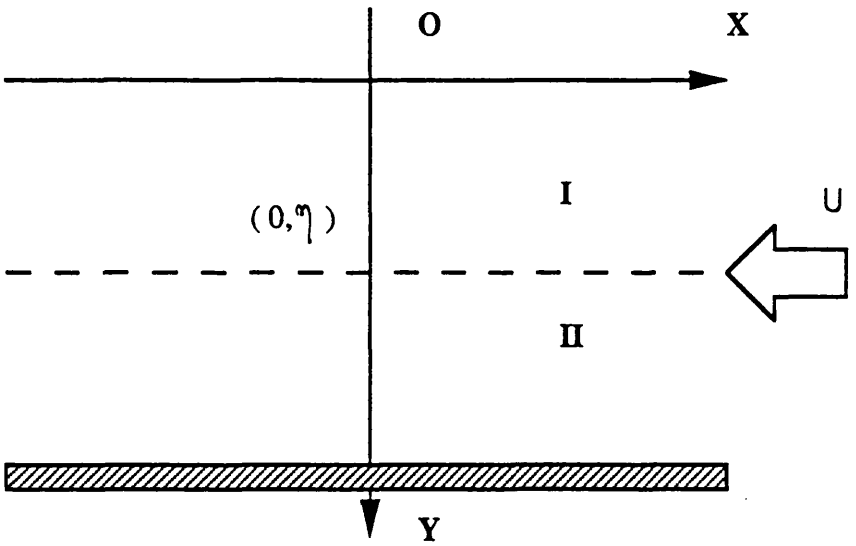

Fig.3.1 Coordinate system for problem formulation

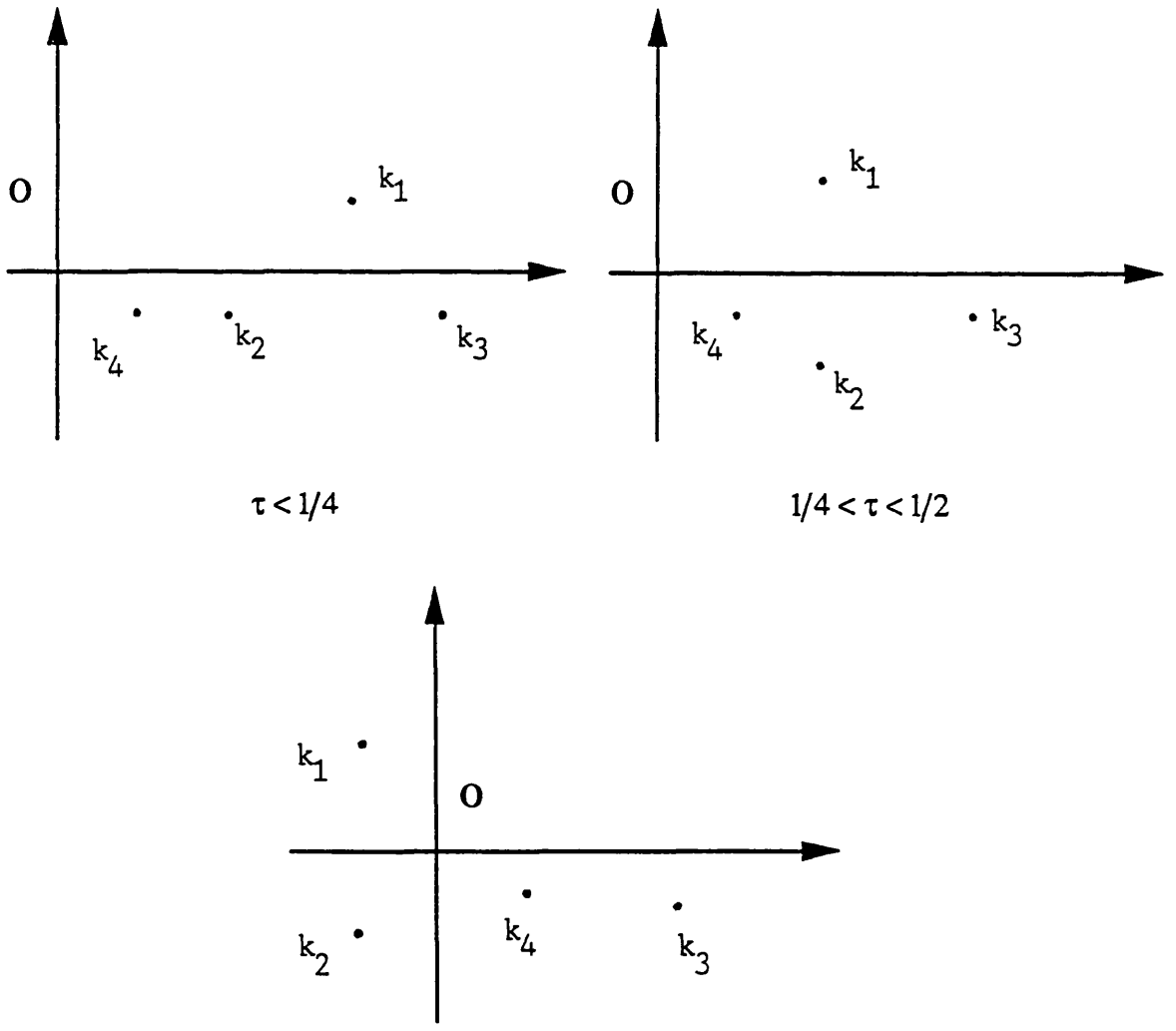

Fig.3.2 Pole locations in various τ ranges

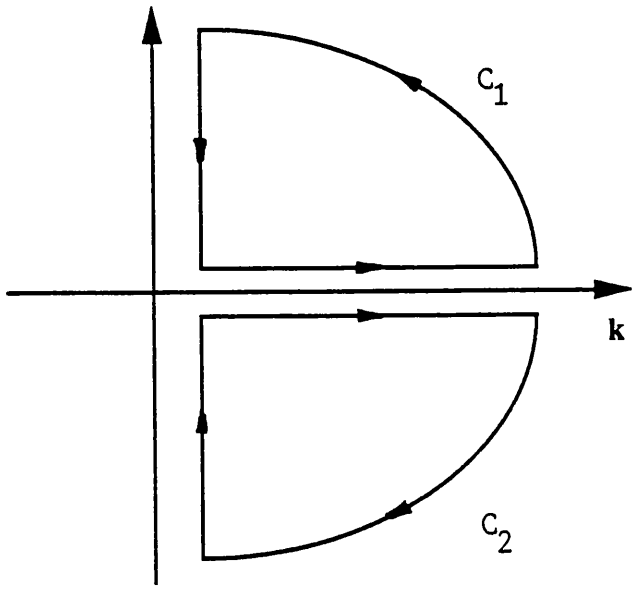

Fig.3.3 Path for numerical integration in the complex plane

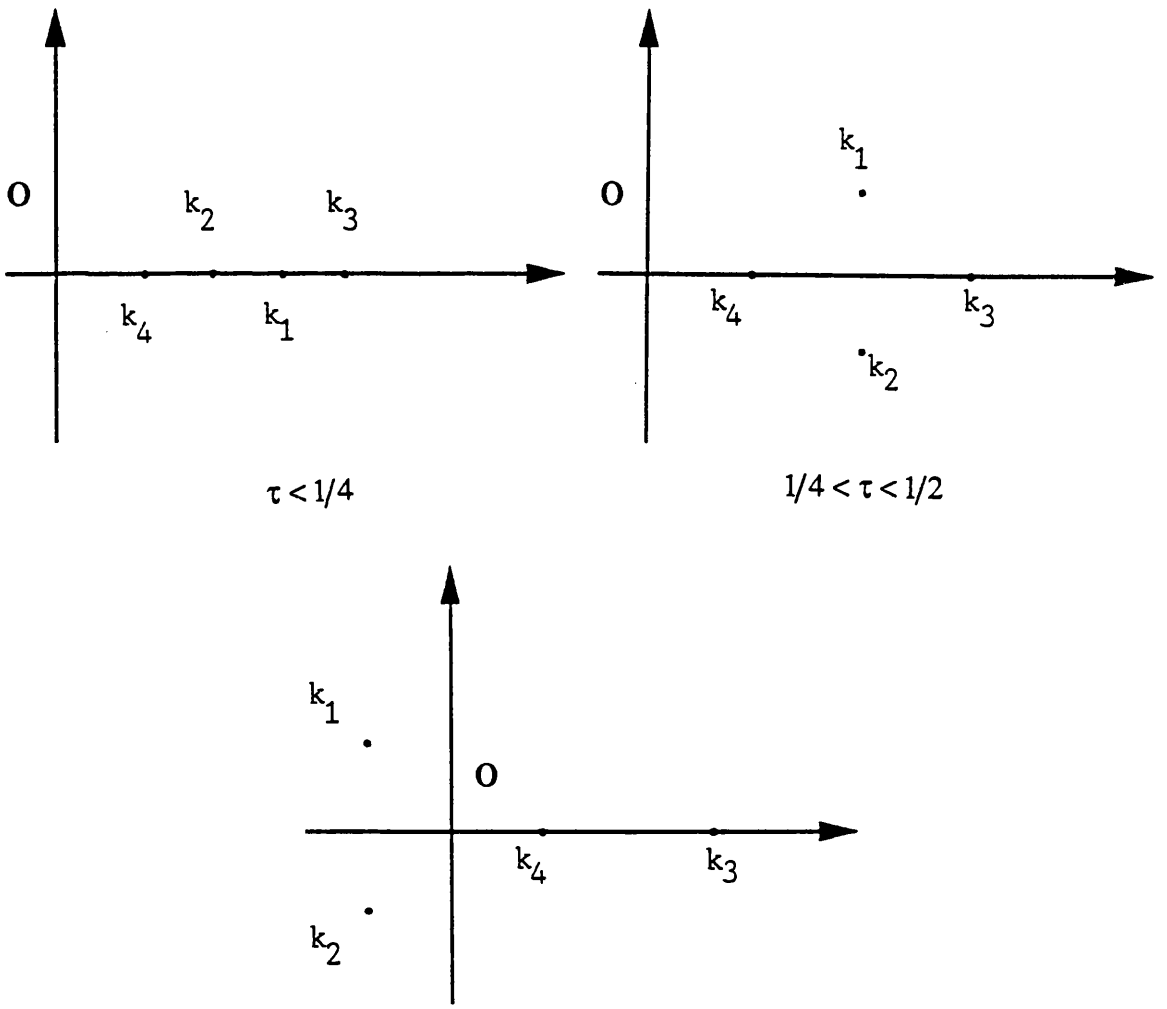

Fig.3.4 Pole locations for numerical computations in various τ ranges

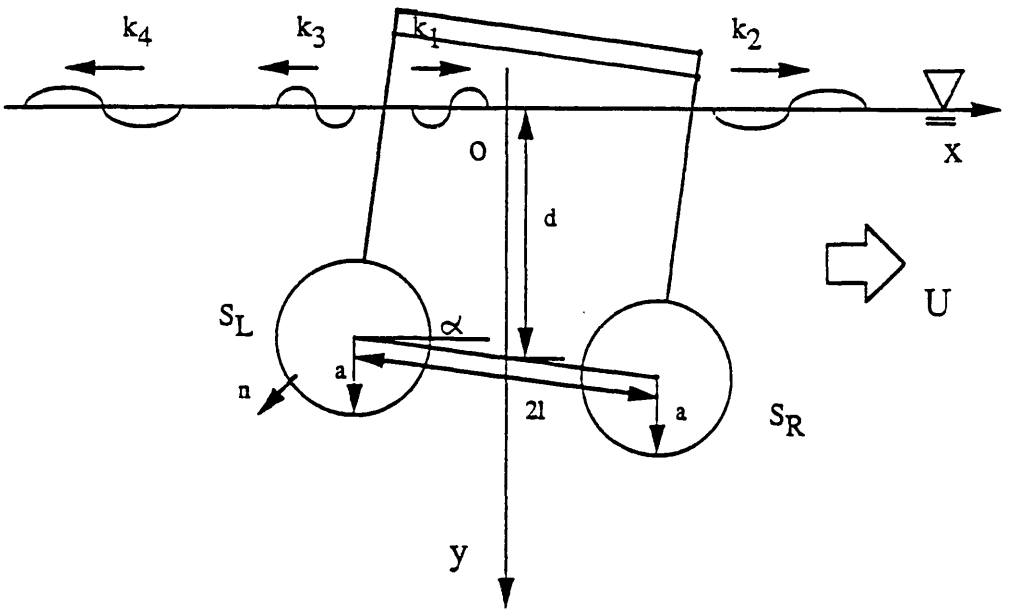

Fig.4.1 The coordinate system of an inclined offshore structure model and schematic representation of radiated waves

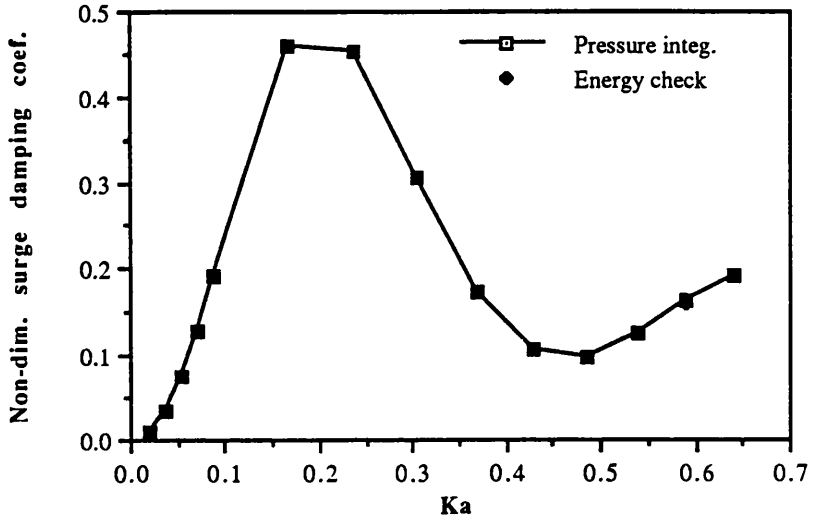

Fig.4.2 Comparison of numerical accuracy of non-dimen. surge damping coefficients (d/a=2, c/a=4, Fn=0.2 in following waves)

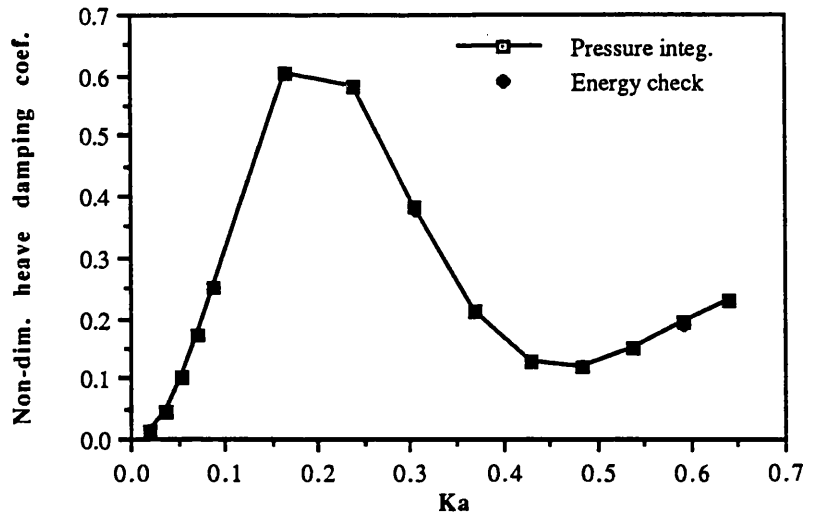

Fig.4.3 Comparison of numerical accuracy of non-dimen. heave damping coefficients (d/a=2, c/a=4, Fn=0.2 in following waves)

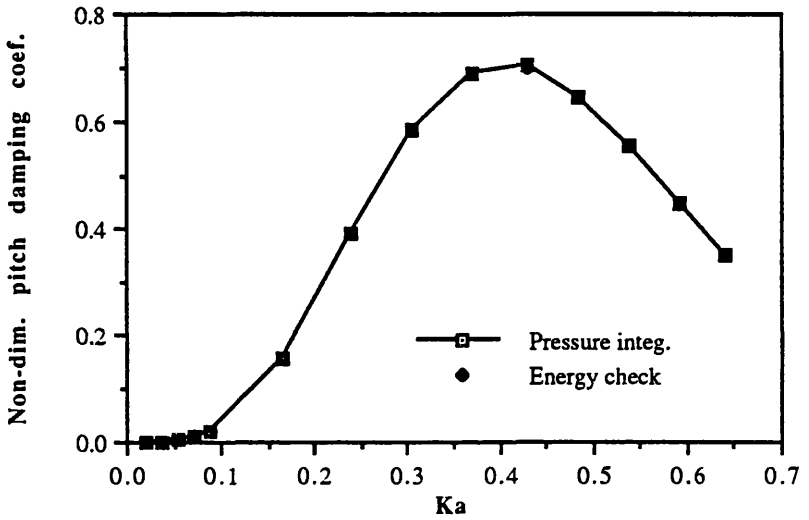

Fig.4.4 Comparsion of numerical accuracy of non-dimen. pitch damping coefficients (d/a=2, c/a=4, Fn=0.2 in following waves)

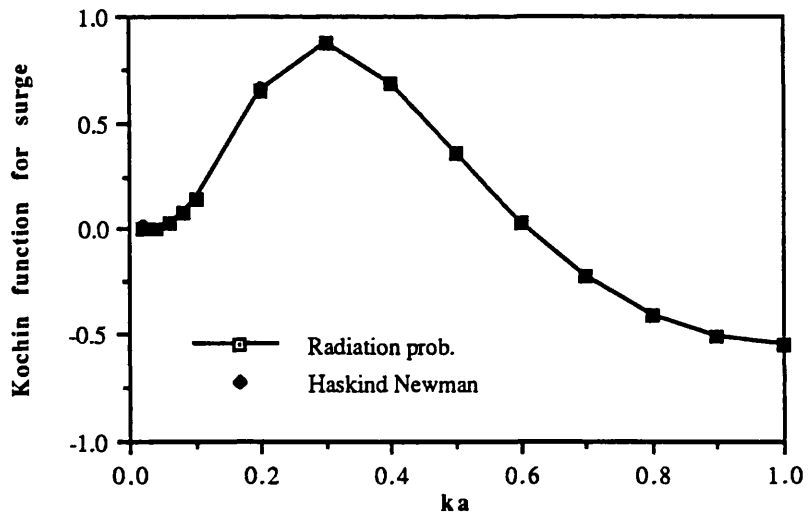

Fig.4.5 Comparison of numerical accuracy of the real part of surge Kochin function (d/a=2, c/a=4, Fn=0.2 in following waves)

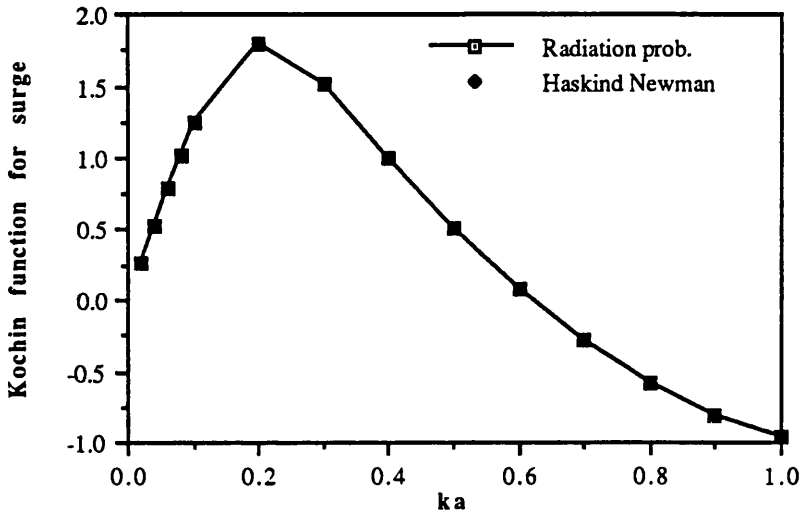

Fig.4.6 Comparison of numerical accuracy of imaginary part of surge Kochin function (d/a=2, c/a=4, Fn=0.2 in following waves)

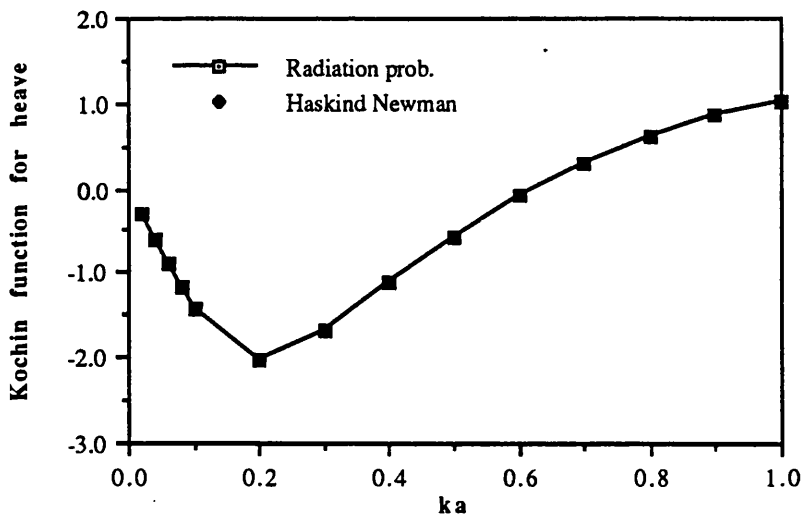

Fig.4.7 Comparison of numerical accuracy of the real part of heave Kochin function (d/a=2, c/a=4, Fn=0.2 in following waves)

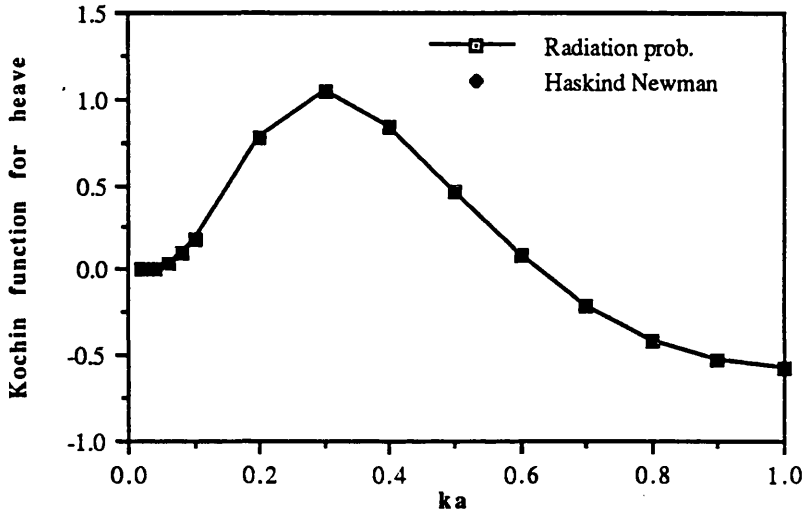

Fig.4.8 Comparison of numerical accuracy of imaginary part of heave Kochin function (d/a=2, c/a=4, Fn=0.2 in following waves)

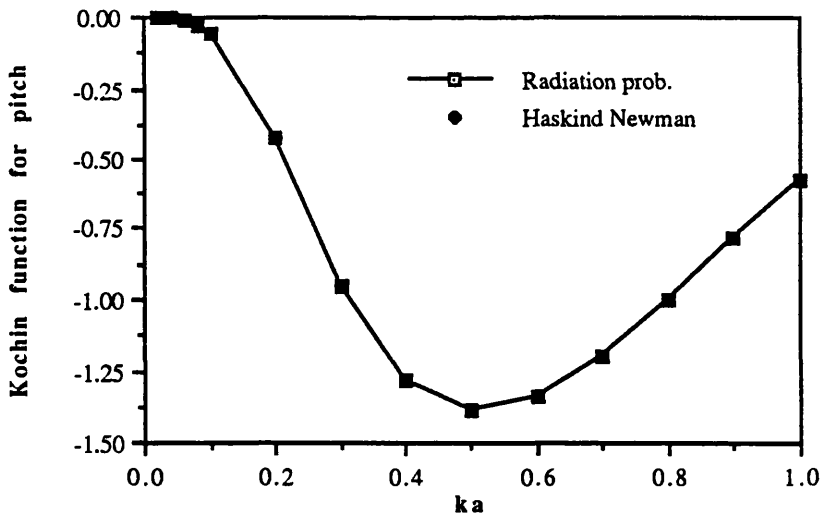

Fig.4.9 Comparison of numerical accuracy of the real part of pitch Kochin function (d/a=2, c/a=4, Fn=0.2 in following waves)

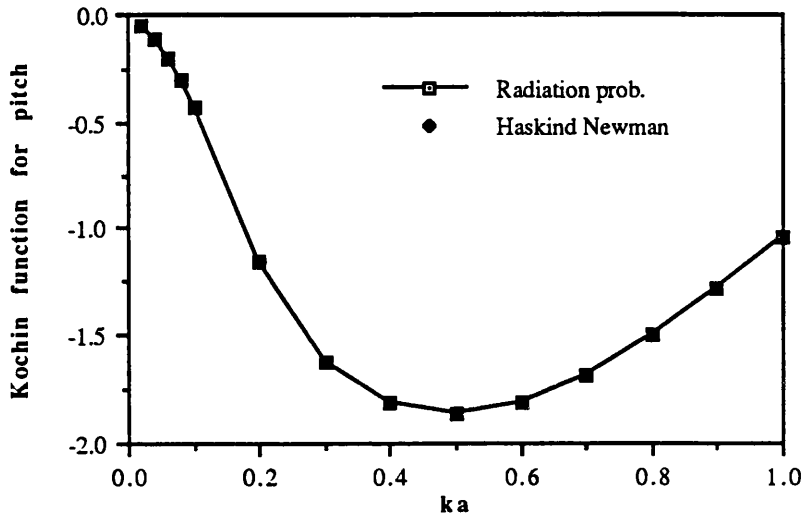

Fig.4.10 Comparison of numerical accuracy of imaginary part of pitch Kochin function (d/a=2, c/a=4, Fn=0.2 in following waves)

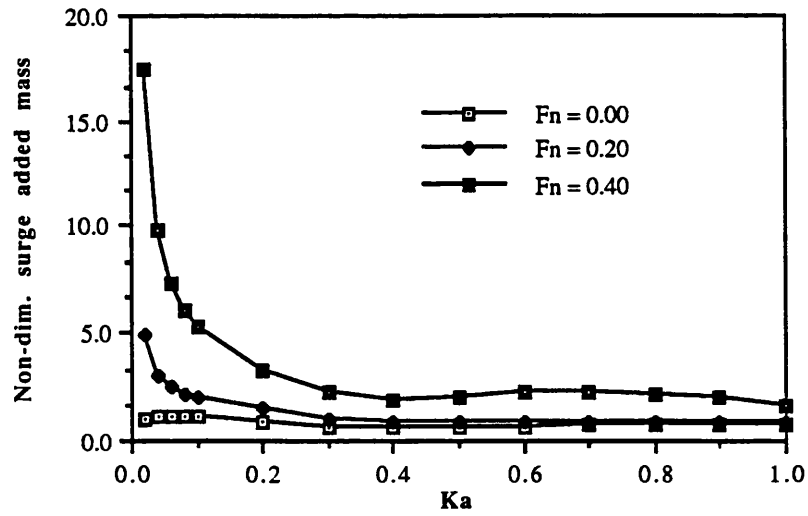

Fig.4.11 Non-dimensionalized surge added mass for different Froude numbers(d/a=2, c/a=4, no tilt in following waves)

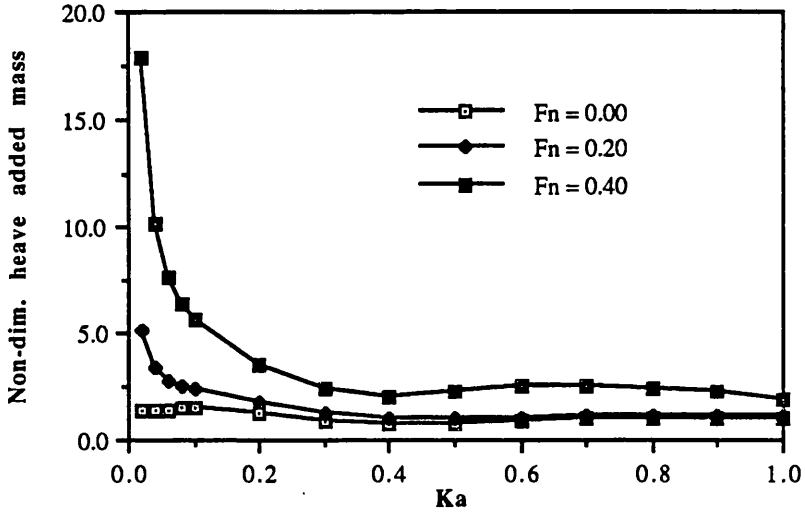

Fig.4.12 Non-dimensionalized heave added mass for diiferent Froude numbers(d/a=2, c/a=4, no tilt in following waves)

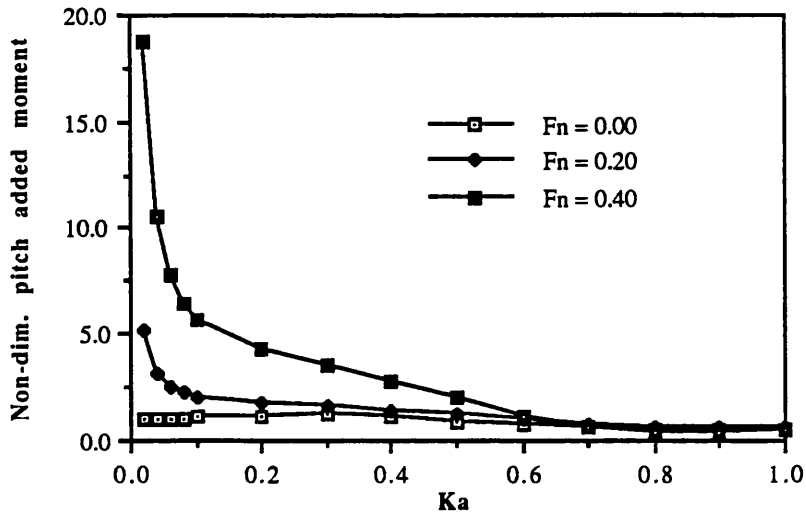

Fig.4.13 Non-dimensionalized pitch added moment for different Froude numbers (d/a=2, c/a=4, no tilt in following waves)

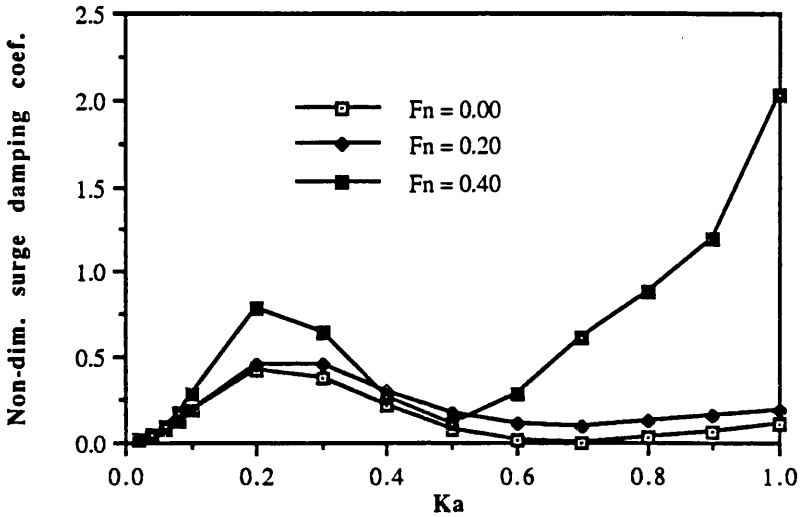

Fig.4.14 Non-dimensionalized surge damp. coefficients for different Froude numbers (d/a=2, c/a=4, no tilt in following waves)

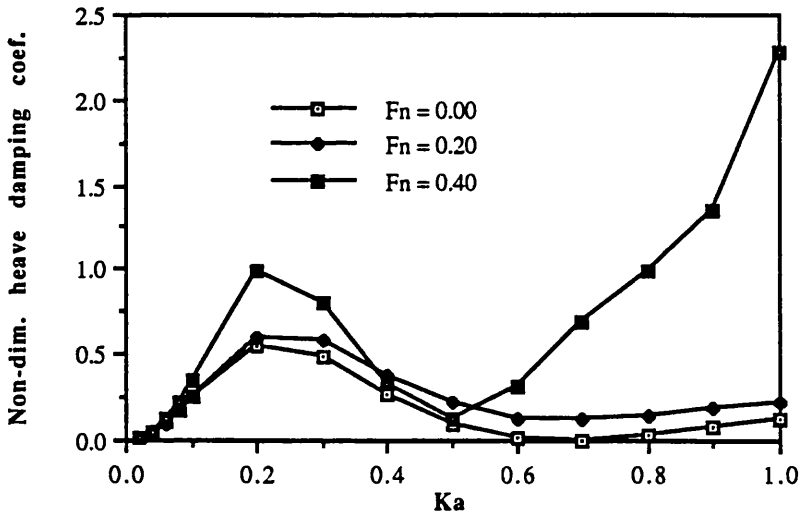

Fig.4.15 Non-dimensionalized heave damp. coefficients for different Froude numbers (d/a=2, c/a=4, no tilt in following waves)

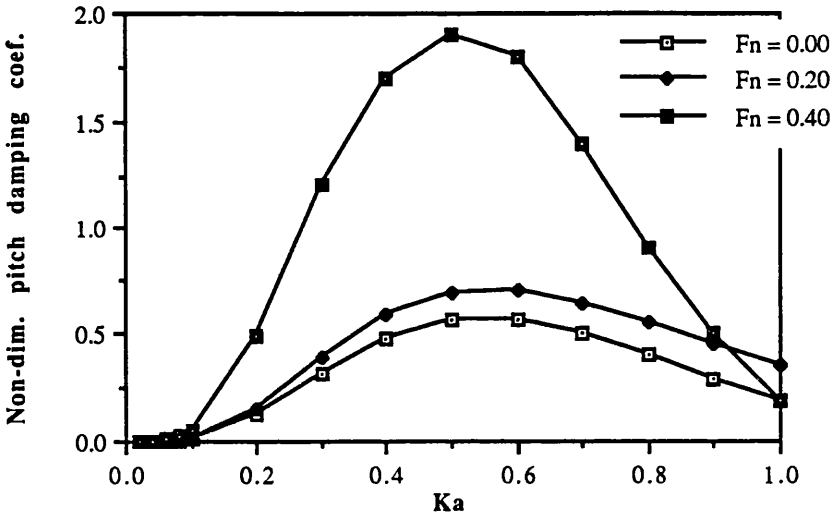

Fig.4.16 Non-dimensionalized pitch damp. coefficients for different Froude numbers (d/a=2, c/a=4, no tilt in following waves)

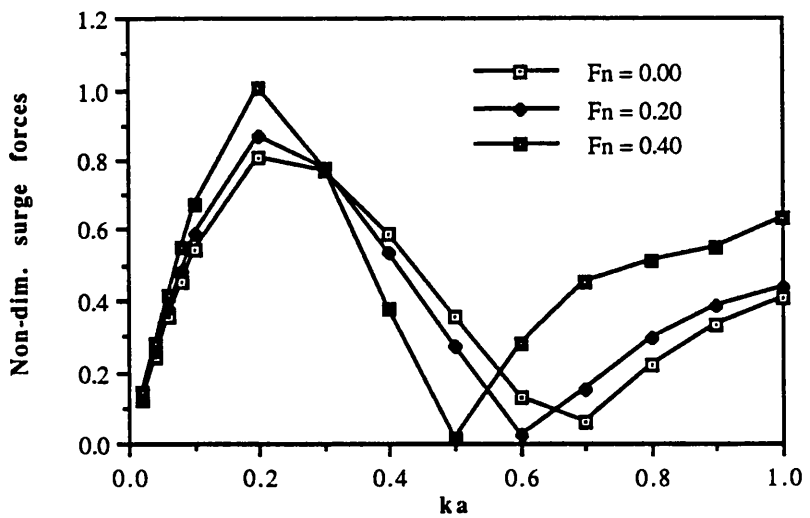

Fig.4.17 Non-dimensionalized surge forces for different Froude numbers(d/a=2,c/a=4, no tilt in following waves)

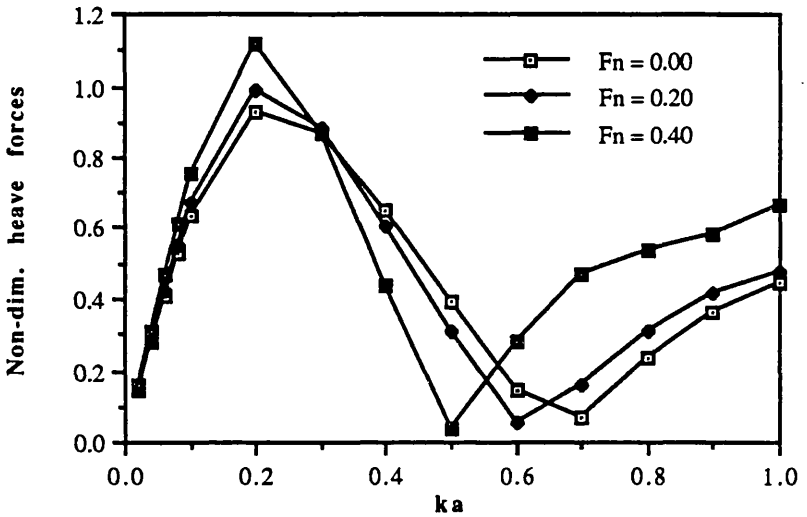

Fig.4.18 Non-dimensionalized heave forces for different Froude numbers(d/a=2,c/a=4, no tilt in following waves)

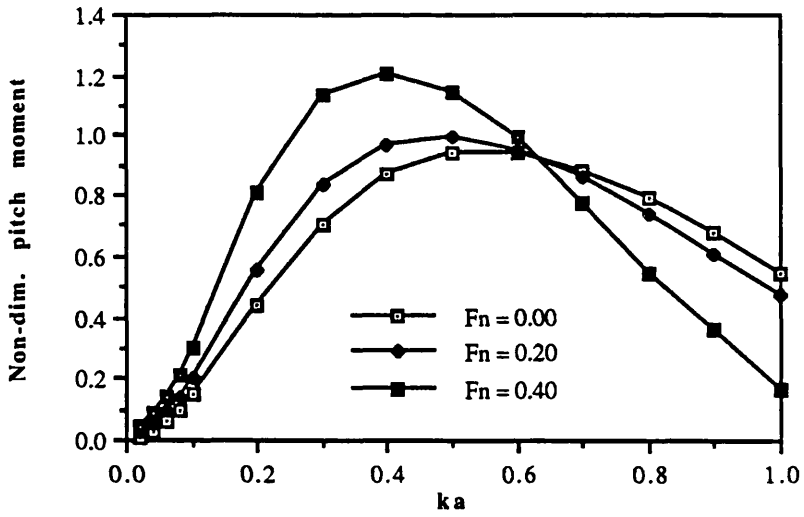

Fig.4.19 Non-dimensionalized pitch moment for different Froude numbers(d/a=2,c/a=4, no tilt in following Waves)

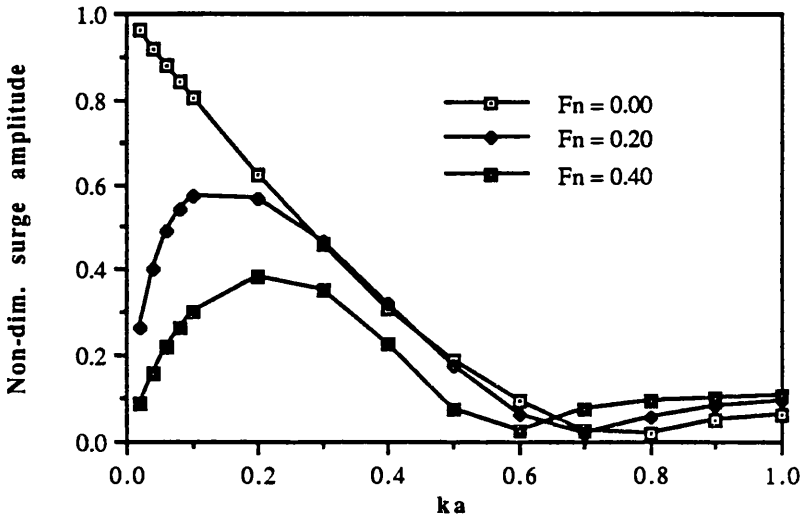

Fig.4.20 Non-dimensionalized surge amp. for different Froude numbers(d/a=2,c/a=4, no tilt in following waves)

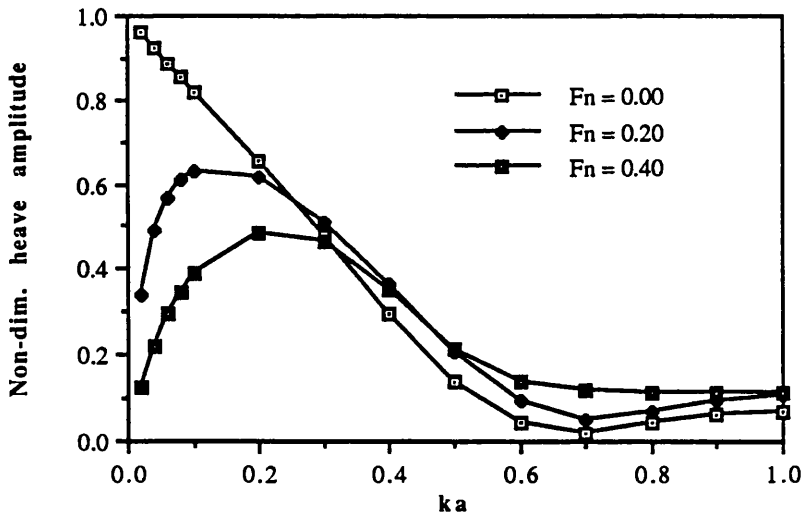

Fig.4.21 Non-dimensionalized heave amp. for different Froude numbers(d/a=2,c/a=4, no tilt in following waves)

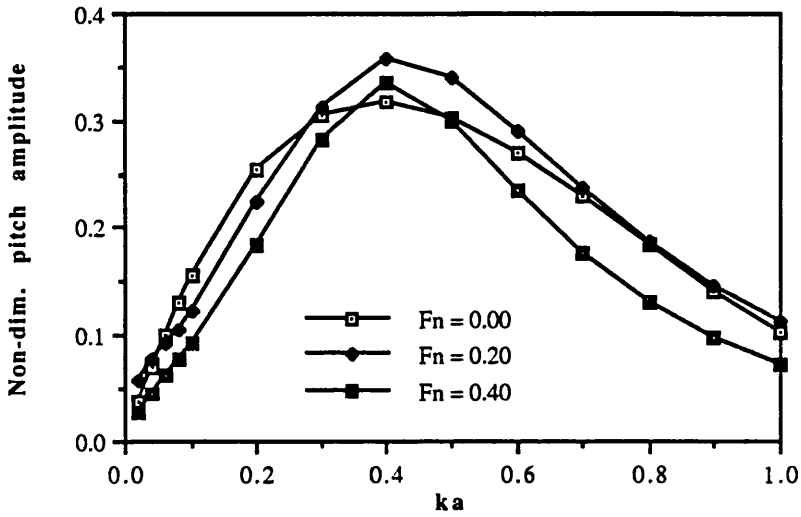

Fig.4.22 Non-dimensionalized pitch amp. for different Froude numbers(d/a=2,c/a=4, no tilt in following waves)

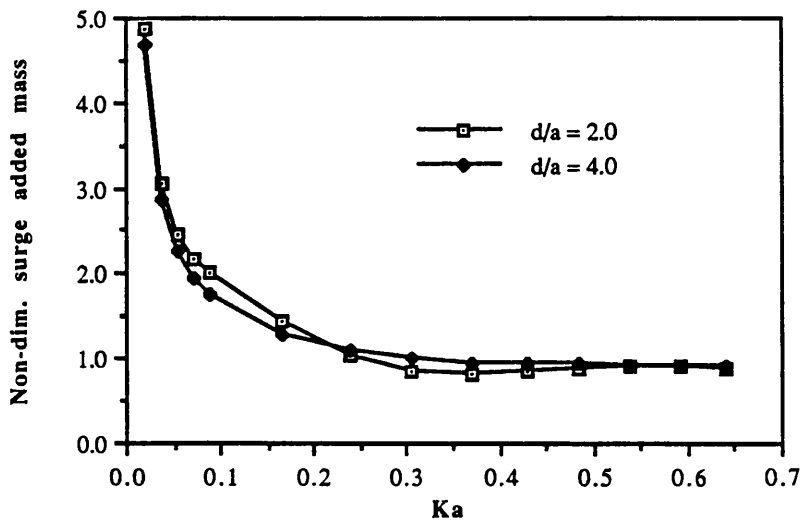

Fig.4.23 Non-dimensionalized surge added mass for different depths (c/a=4, Fn=0.2, no tilt in following waves)

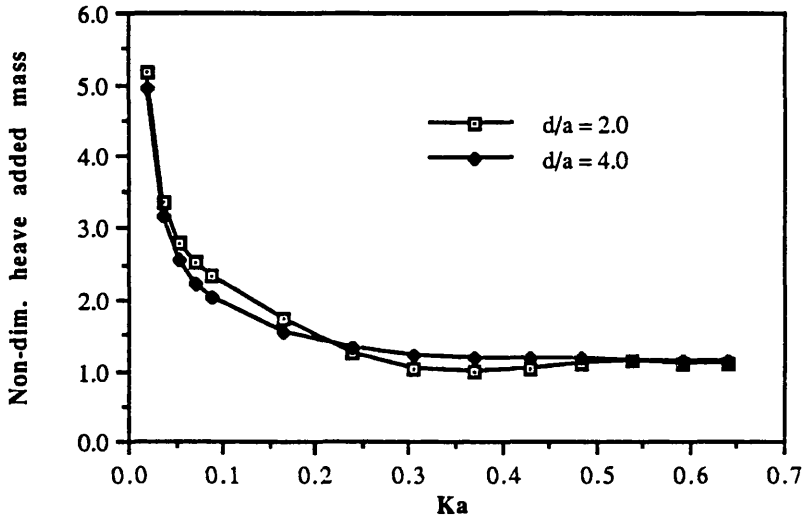

Fig.4.24 Non-dimensionalized heave added mass for different depths (c/a=4, Fn=0.2, no tilt in following waves)

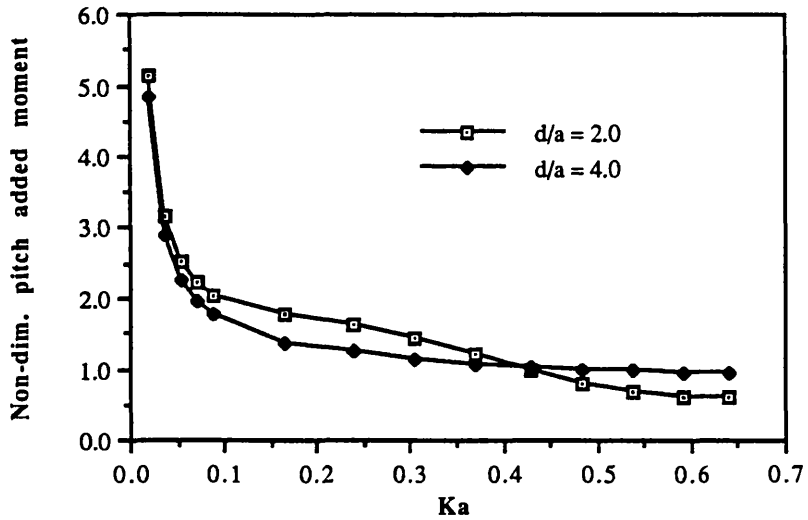

Fig.4.25 Non-dimensionalized pitch added moment for different depths (c/a=4,Fn=0.2, no tilt in following waves)

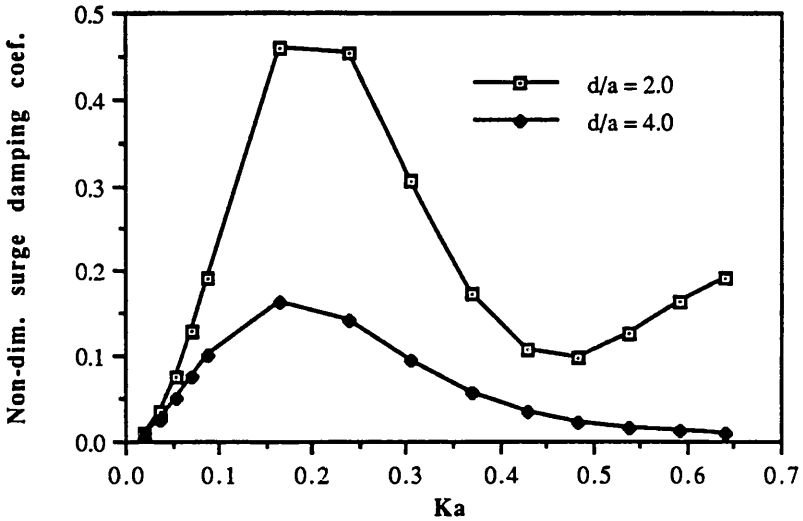

Fig.4.26 Non-dimensionalized surge damp. coefficients for different depths (c/a=4, Fn=0.2, no tilt in following waves)

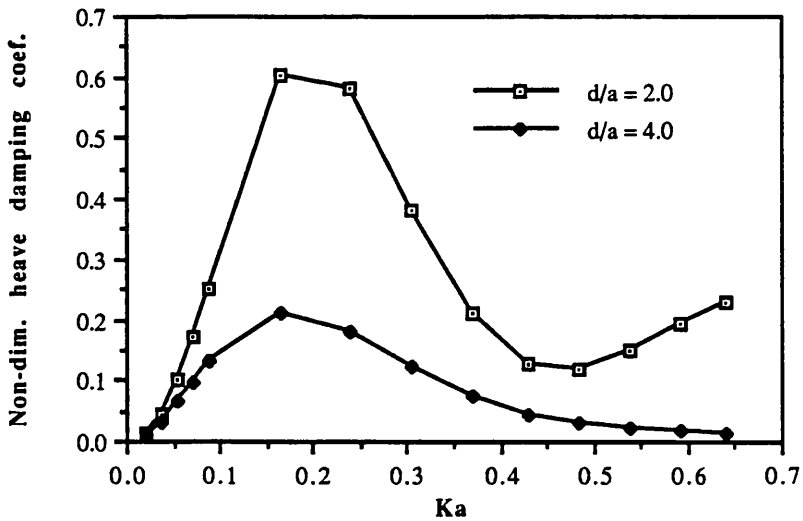

Fig.4.27 Non-dimensionalized heave damp. coefficients for different depths (c/a=4, Fn=0.2, no tilt in following waves)

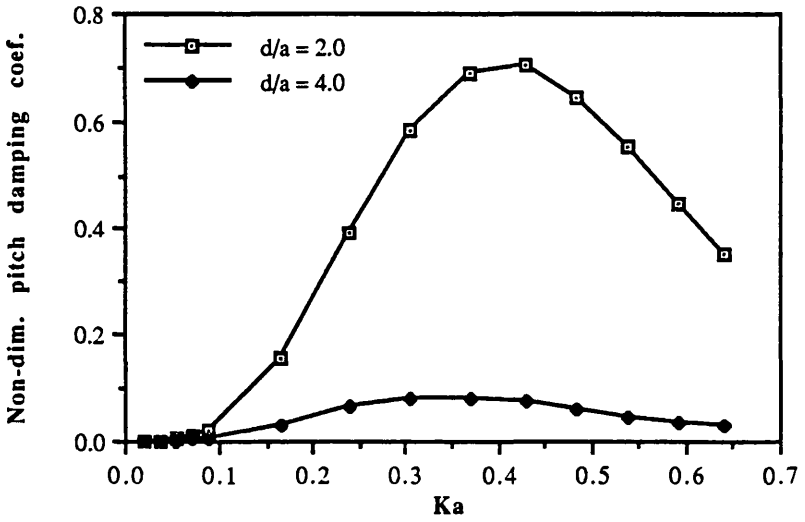

Fig.4.28 Non-dimensionalized pitch damp. coefficients for different depths (c/a=4, Fn=0.2, no tilt in following waves)

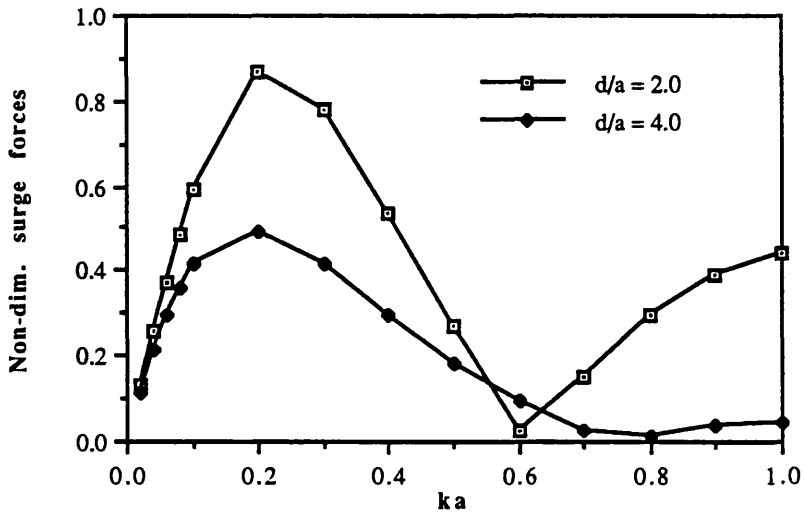

Fig.4.29 Non-dimensionalized surge forces for different depths (c/a=4.0, Fn=0.20, no tilt in following waves)

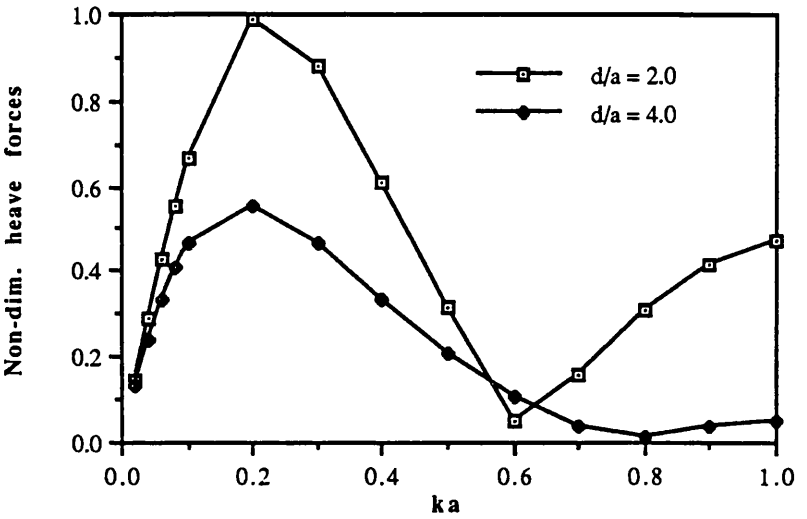

Fig.4.30 Non-dimensionalized heave forces for different depths (c/a=4.0, Fn=0.20, no tilt in following waves)

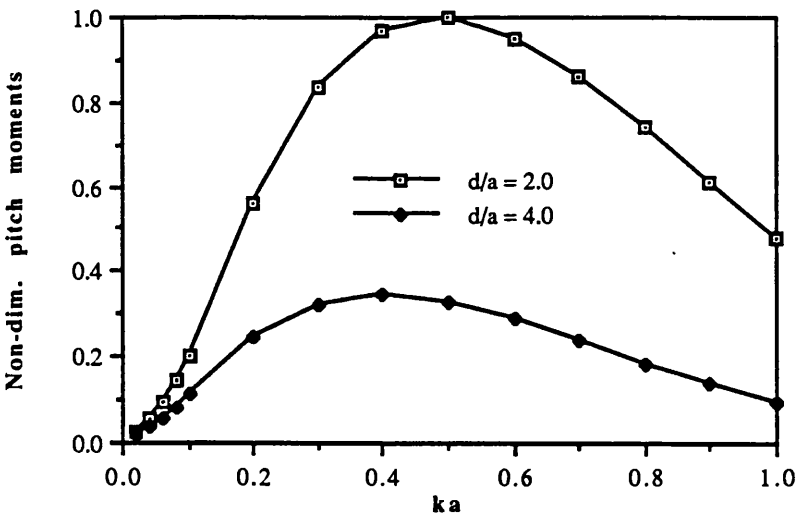

Fig.4.31 Non-dimensionalized pitch moment for different depths (c/a=4.0, Fn=0.20, no tilt in following waves)

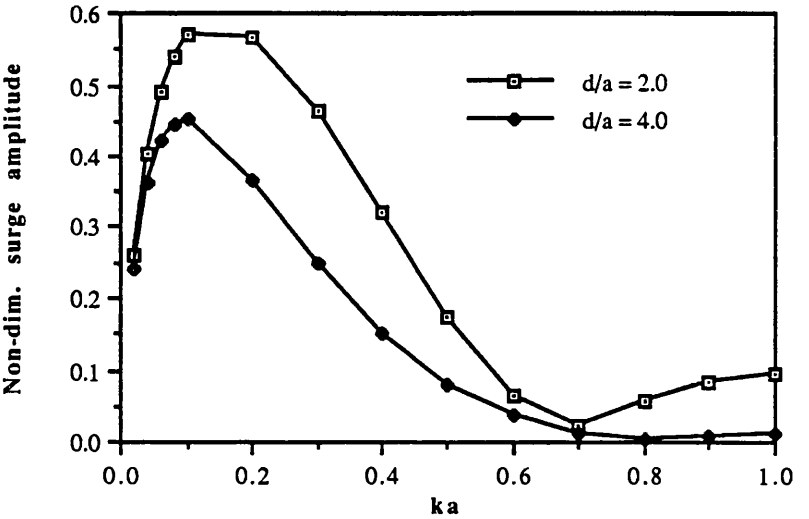

Fig.4.32 Non-dimensionalized surge amp. for different depths (c/a=4.0, Fn=0.20, no tilt in following waves)

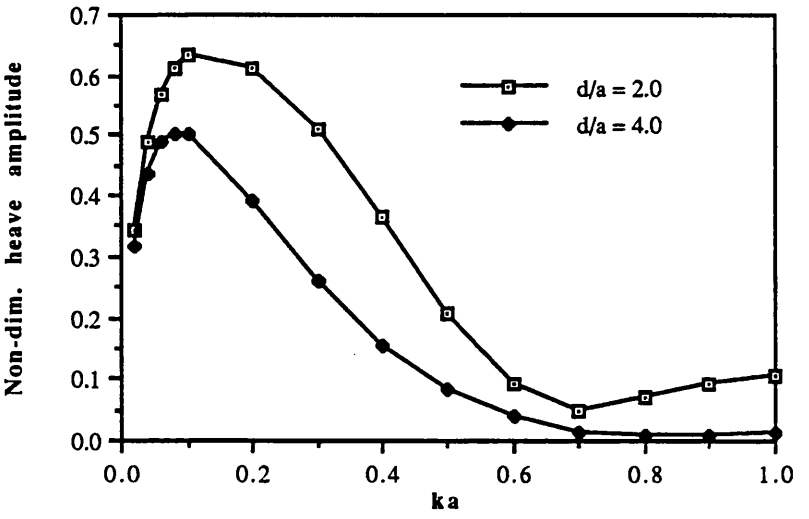

Fig.4.33 Non-dimensionalized heave amp. for different depths (c/a=4.0, Fn=0.20, no tilt in following waves)

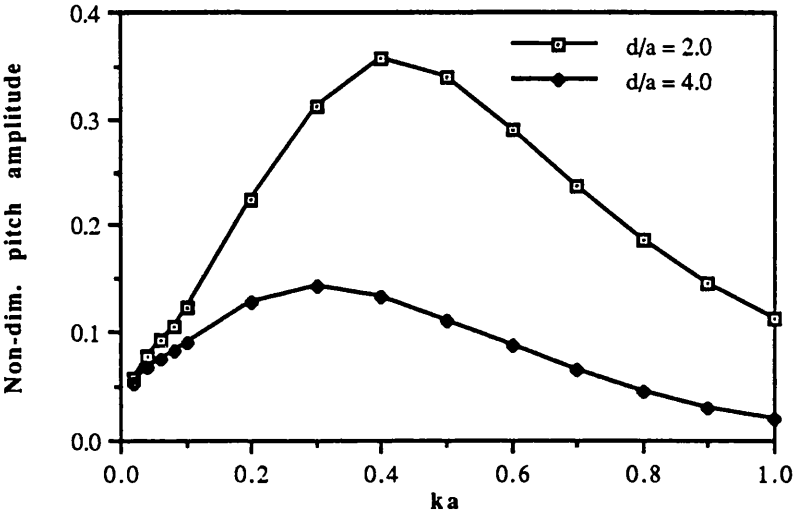

Fig.4.34 Non-dimensionalized pitch amp. for different depths (c/a=4.0, Fn=0.20, no tilt in following waves)

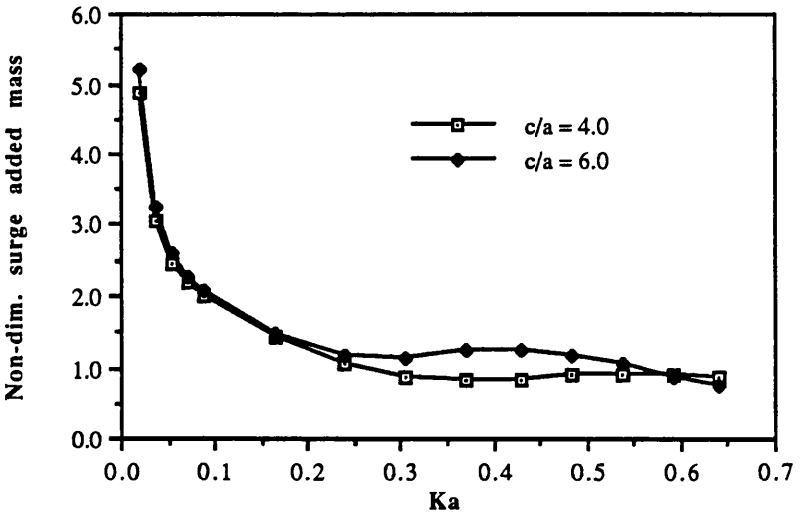

Fig.4.35 Non-dimensionalized surge added mass for different separation diastances (d/a=2, Fn=0.2, no tilt in following waves)

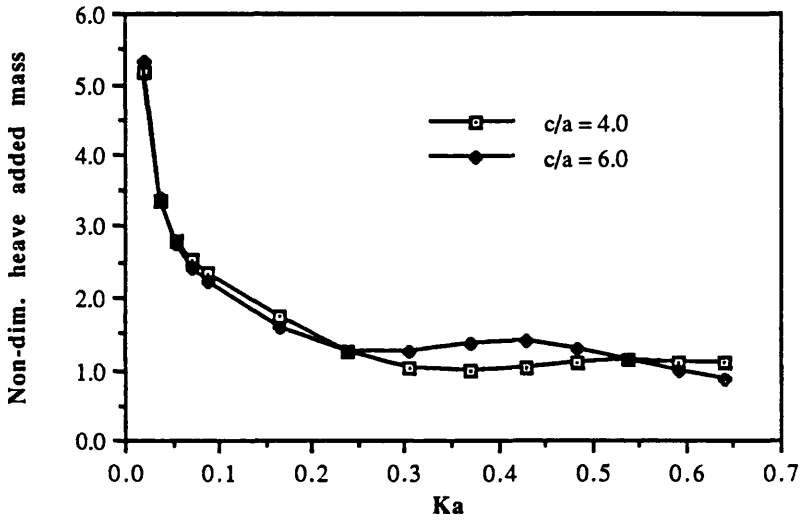

Fig.4.36 Non-dimensionalized heave added mass for different separation distances (d/a=2, Fn=0.2, no tilt in following waves)

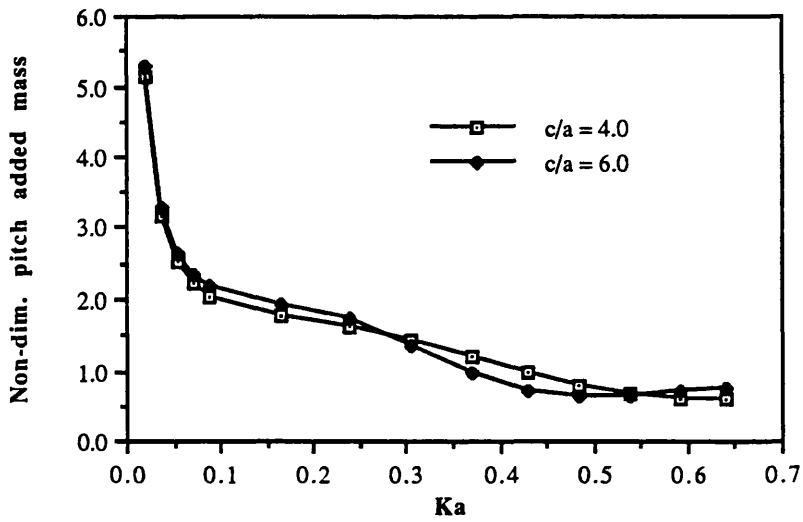

Fig.4.37 Non-dimensionalized pitch added moment for different separation distances (d/a=2,Fn=0.2, no tilt in following waves)

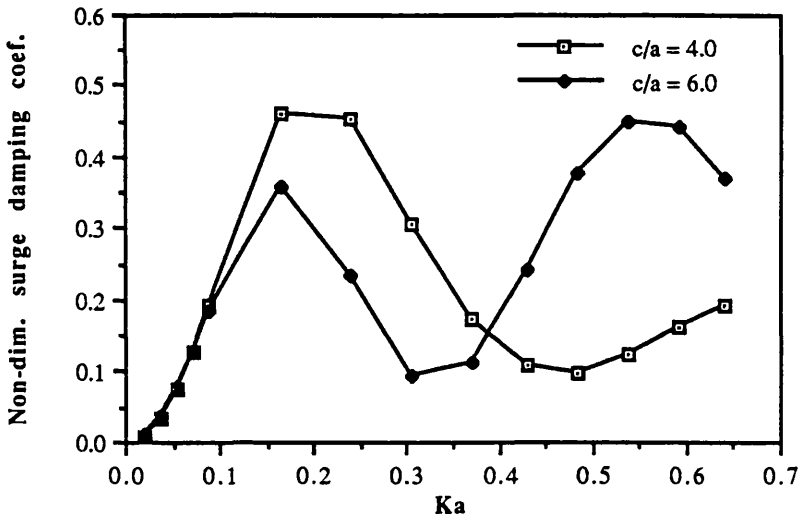

Fig.4.38 Non-dimensionalized surge damp. coefficients for different separations (d/a=2, Fn=0.2, no tilt in following waves)

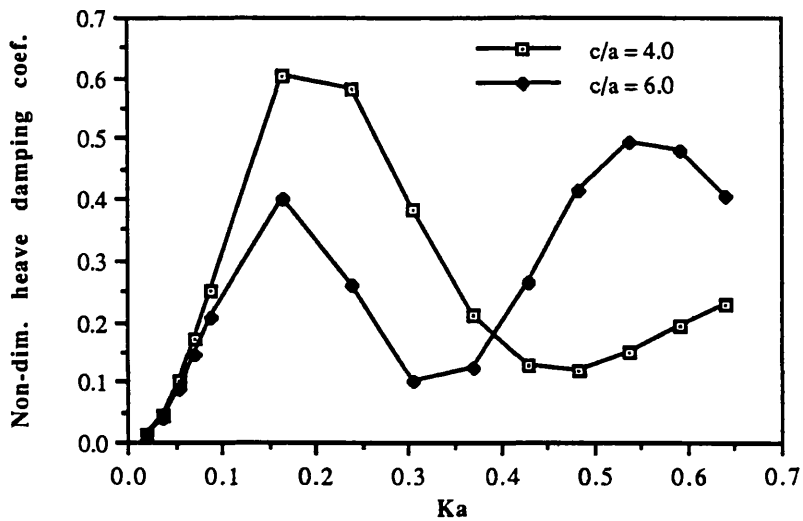

Fig.4.39 Non-dimensionalized heave damp. coefficients for different separations (d/a=2, Fn=0.2, no tilt in following waves)

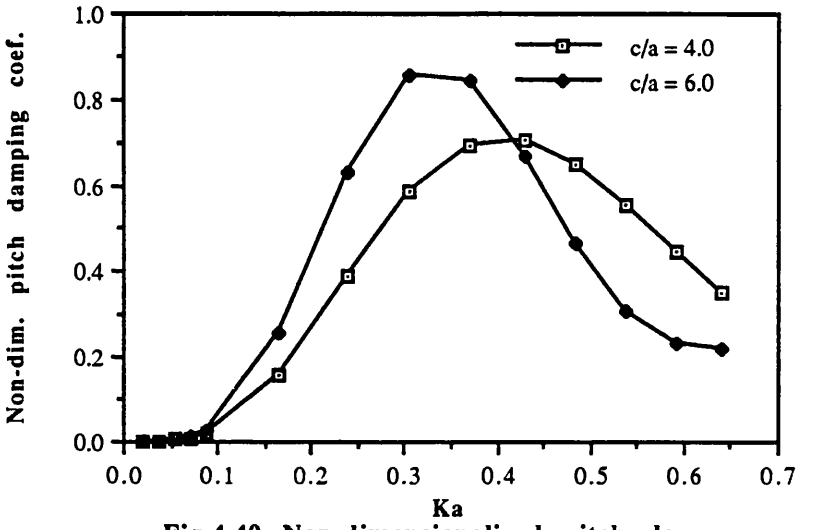

Fig.4.40 Non-dimensionalized pitch damp. coefficients for different separations (d/a=2, Fn=0.2, no tilt in following waves)

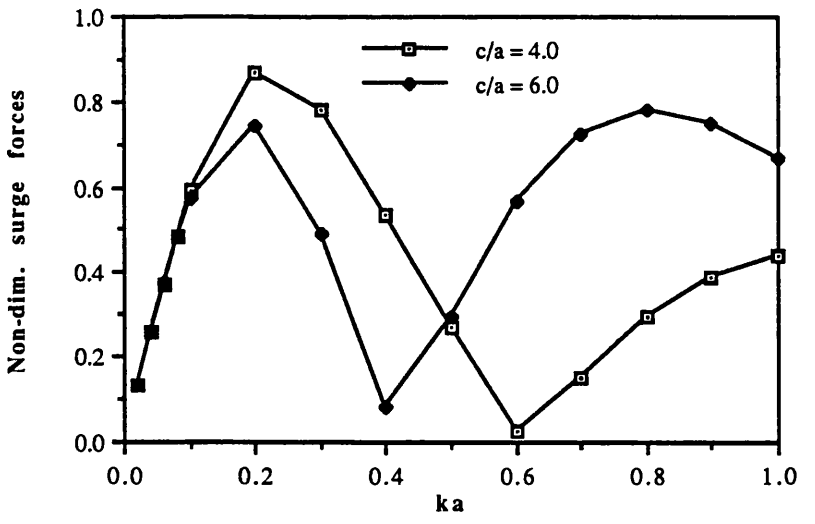

Fig.4.41 Non-dimensionalized surge forces for different separation distances(d/a=2, Fn=0.20, no tilt in following waves)

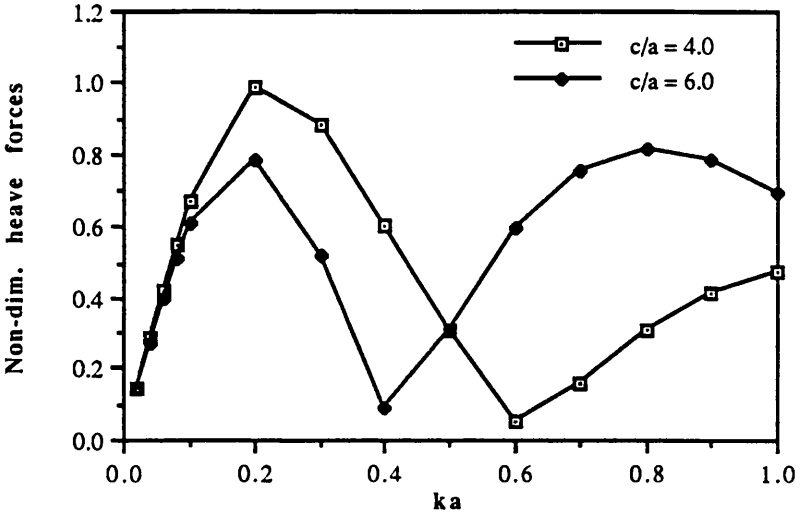

Fig.4.42 Non-dimensionalized heave forces for different separation distances(d/a=2, Fn=0.2, no tilt in following waves)

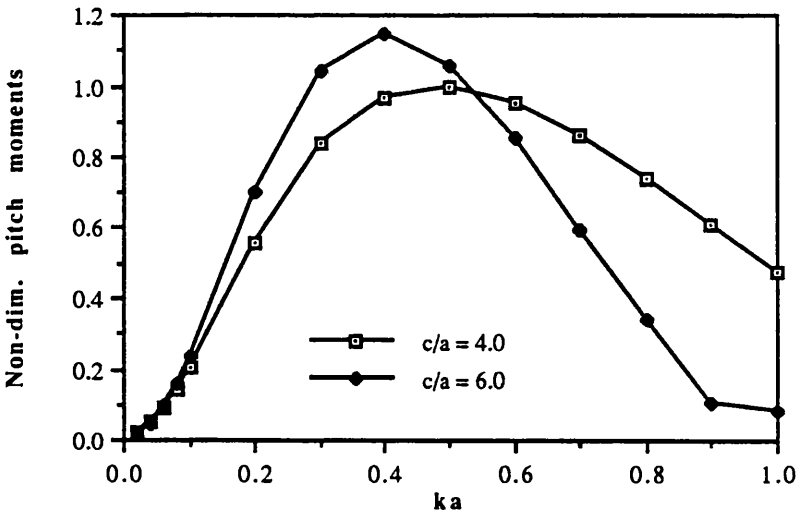

Fig.4.43 Non-dimensionalized pitch moment for different separation distances(d/a=2, Fn=0.2, no tilt in following waves)

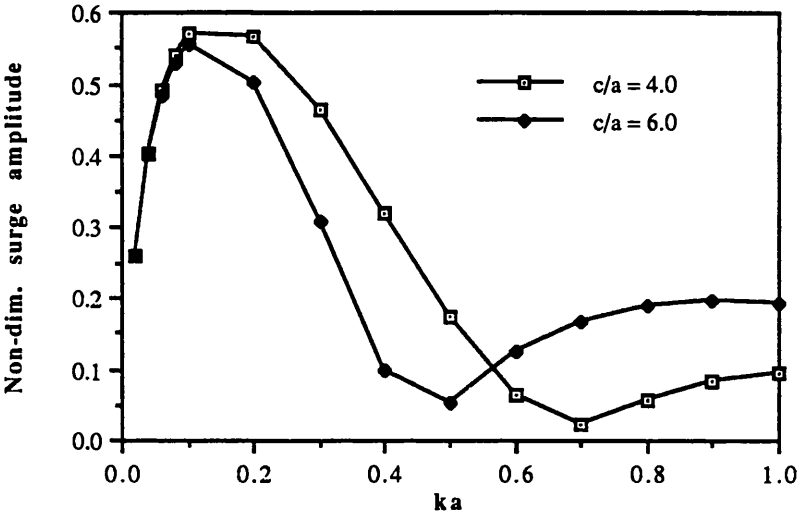

Fig.4.44 Non-dimensionalized surge amp. for different separation distances(d/a=2, Fn=0.2, no tilt in following waves)

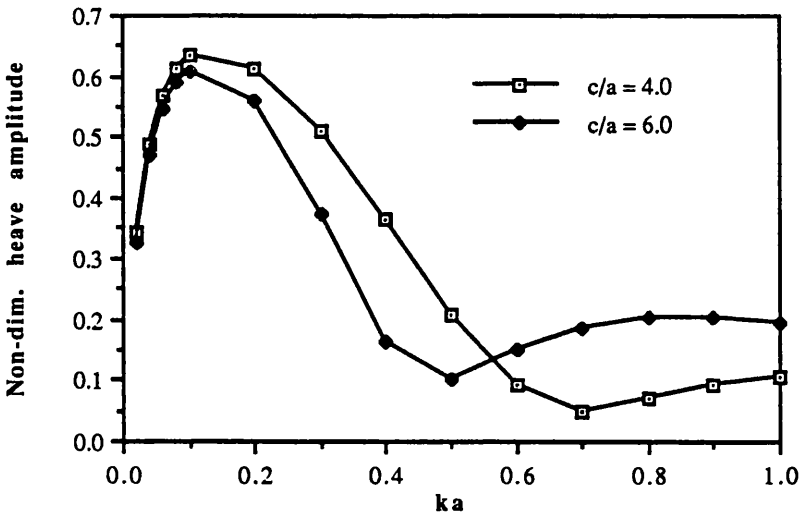

Fig.4.45 Non-dimensionalized heave amp. for different separation distances(d/a=2, Fn=0.2, no tilt in following waves)

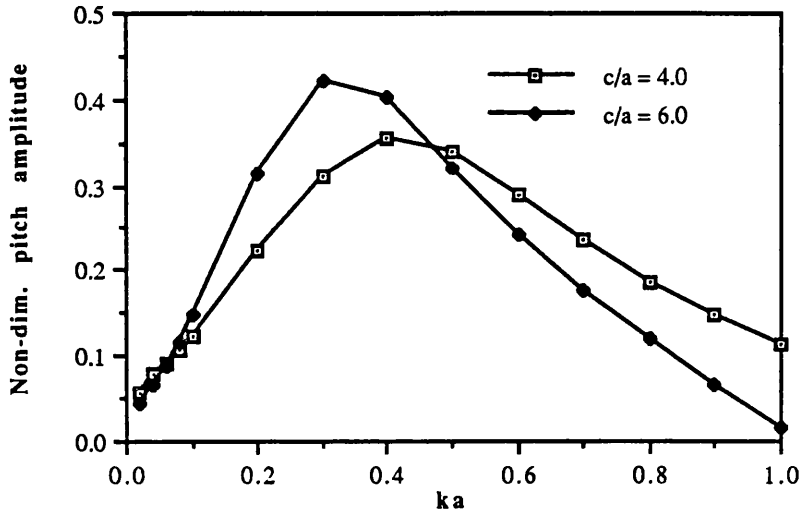

Fig.4.46 Non-dimensionalized pitch amp. for different separation distances (d/a=2, Fn=0.2, no tilt in following waves)

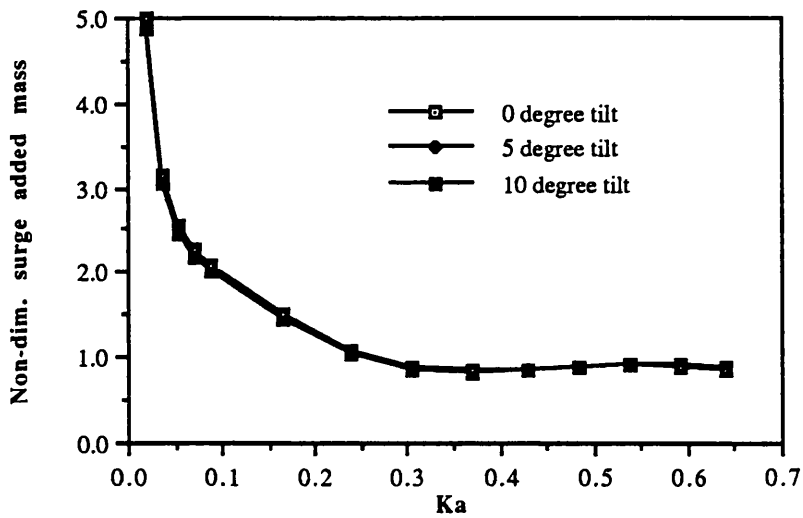

Fig.4.47 Non-dimensionalized surge added mass for different inclinations (d/a=2, c/a=4, Fn=0.2 in following waves)

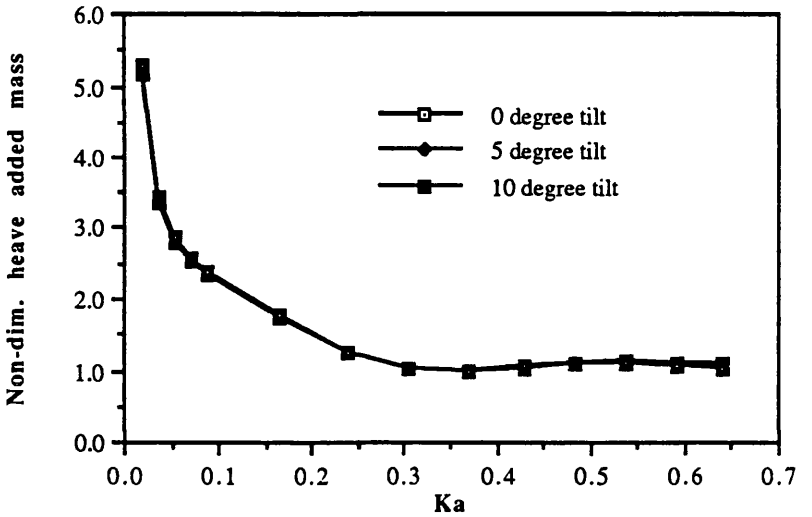

Fig.4.48 Non-dimensionalized heave added mass for different inclinations (d/a=2, c/a=4, Fn=0.2 in following waves)

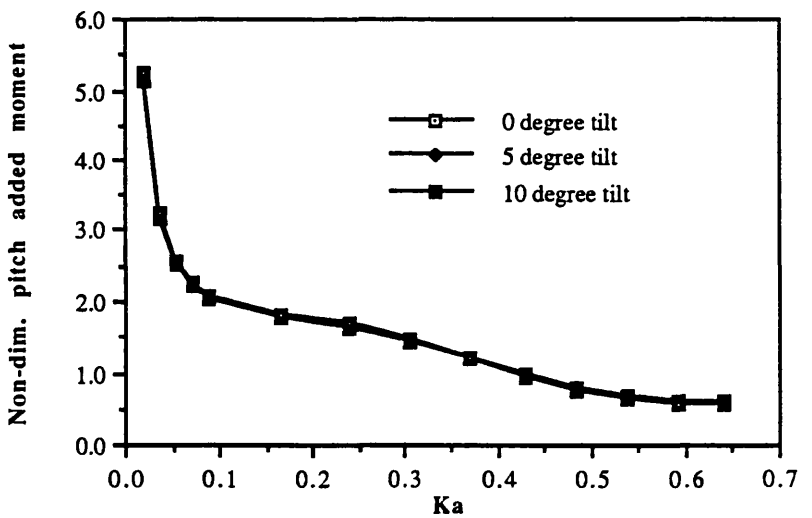

Fig.4.49 Non-dimensionalized pitch added moments for different inclinations(d/a=2, c/a=4, Fn=0.2 in following waves)

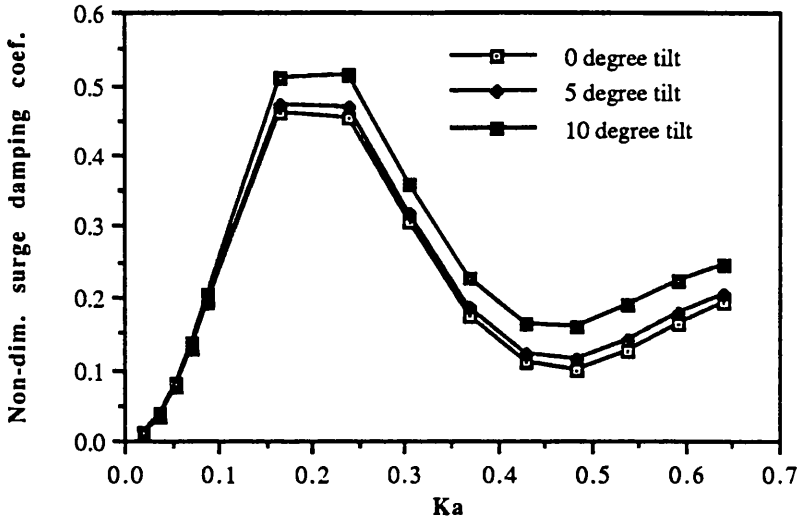

Fig.4.50 Non-dimensionalized surge damp. coeffcients for different inclinations (d/a=2, c/a=4, Fn=0.2 in following waves)

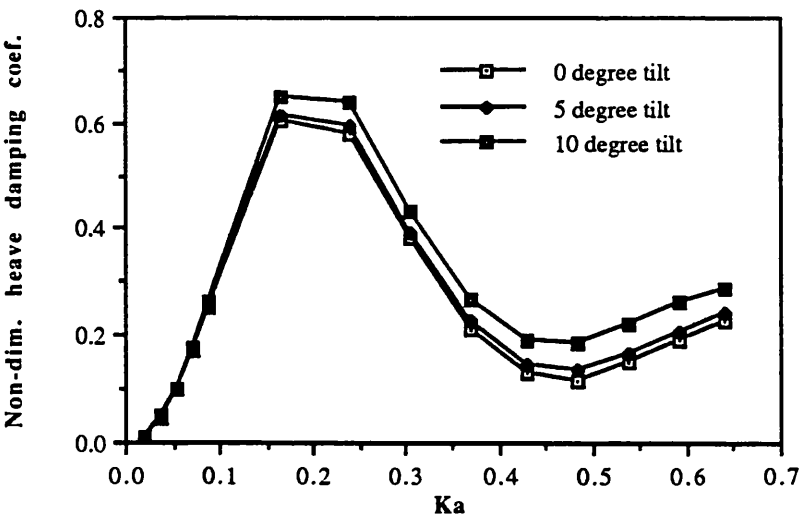

Fig.4.51 Non-dimensionalized heave damp. coefficients for different inclinations (d/a=2, c/a=4, Fn=0.2 in following waves)

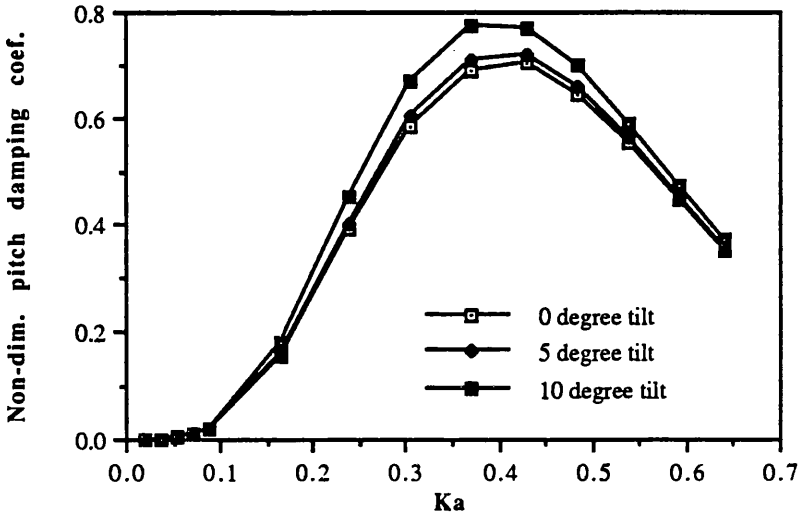

Fig.4.52 Non-dimensionalized pitch damp. coefficients for different inclinations (d/a=2, c/a=4, Fn=0.2 in following waves)

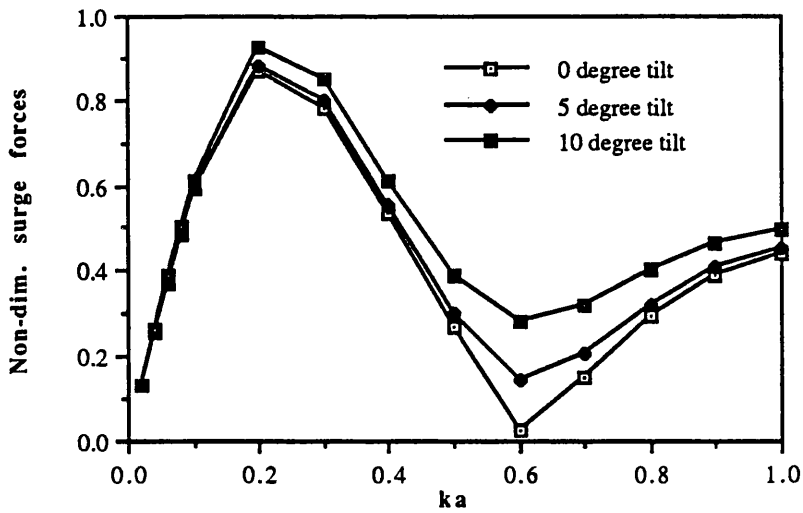

Fig.4.53 Non-dimensionalized surge forces for different inclinations (d/a=2, c/a=4, Fn=0.2 in following waves)

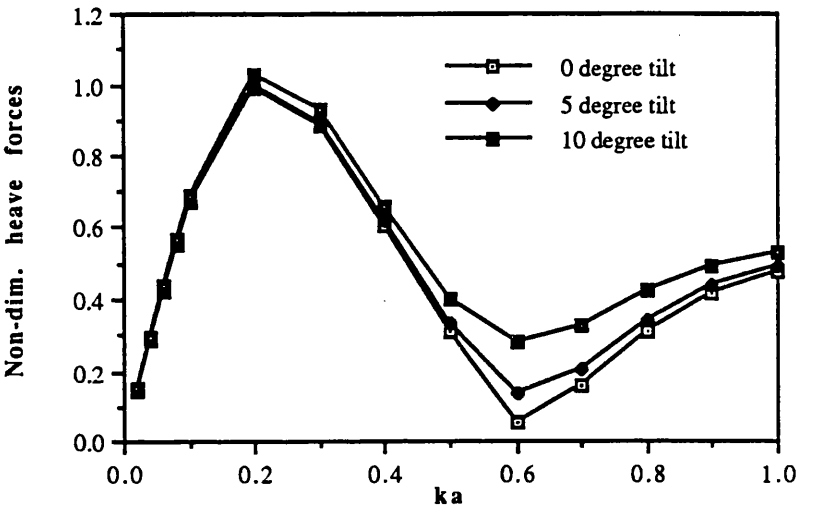

Fig.4.54 Non-dimensionalized heave forces for different inclinations (d/a=2, c/a=4, Fn=0.2 in following waves)

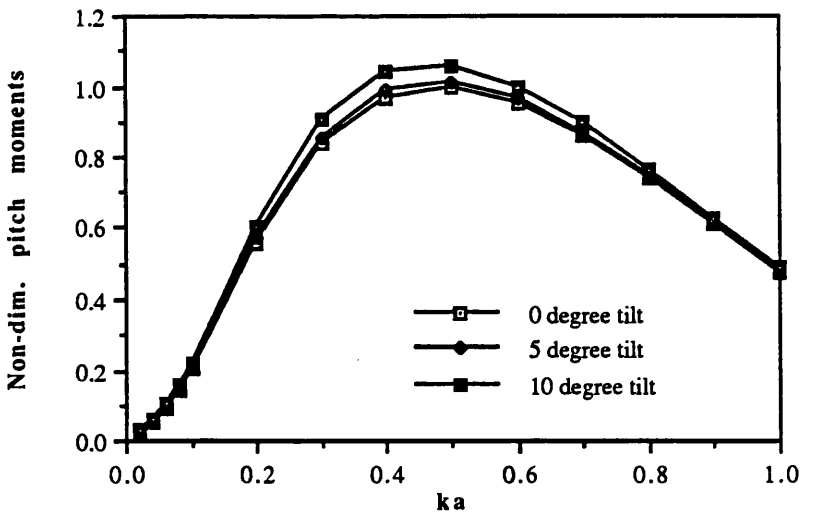

Fig.4.55 Non-dimensionalized pitch moment for different inclinations (d/a=2, c/a=4, Fn=0.2 in following waves)

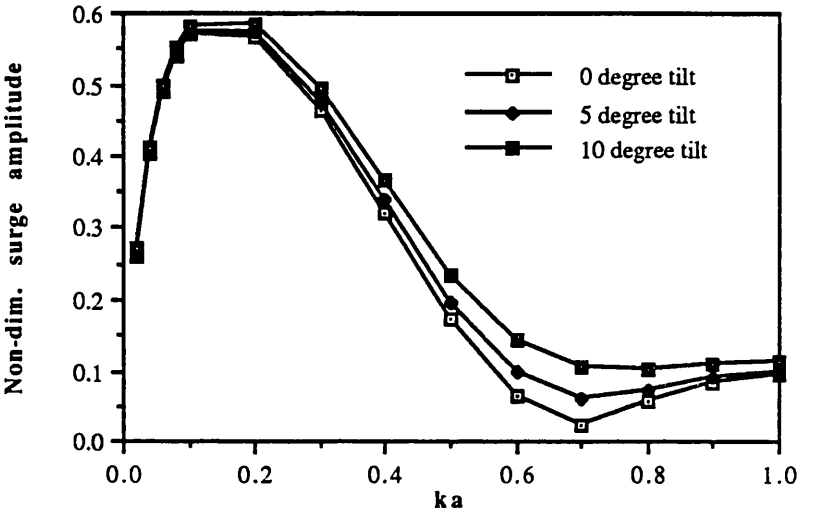

Fig.4.56 Non-dimensionalized surge amp. for different inclinations (d/a=2, c/a=4, Fn=0.2 in following waves)

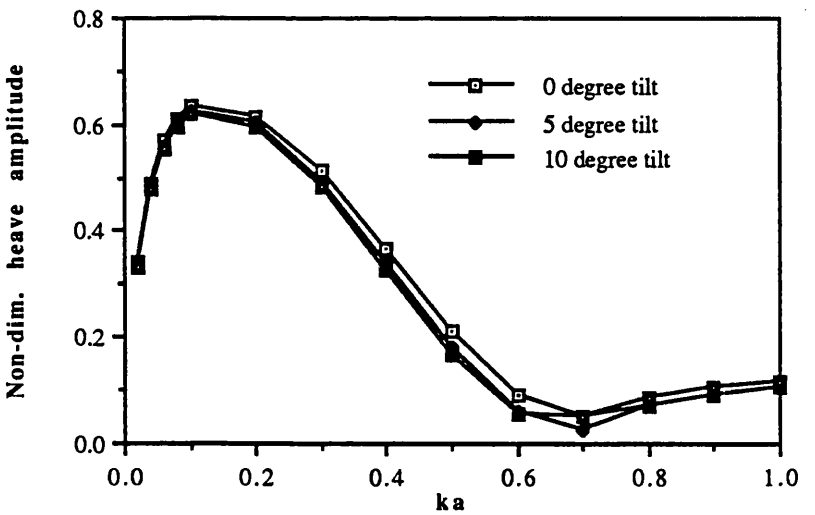

Fig.4.57 Non-dimensionalized heave amp. for different inclinations (d/a=2, c/a=4, Fn=0.2 in following waves)

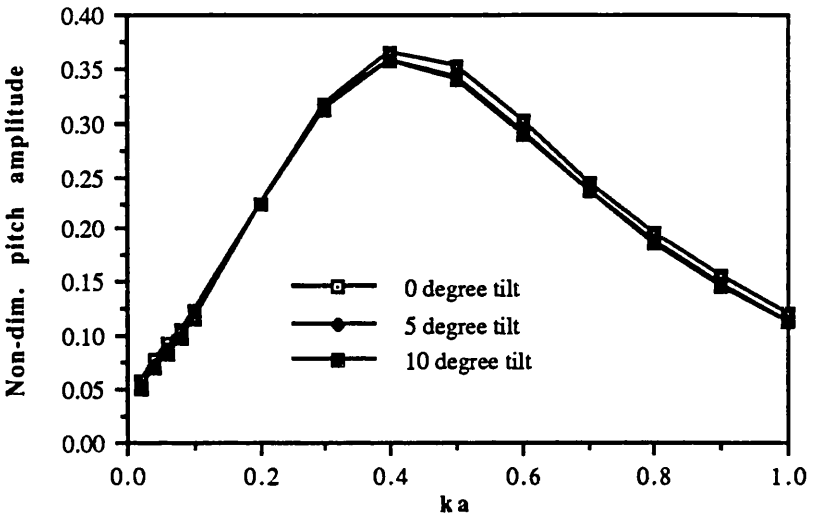

Fig.4.58 Non-dimensionalized pitch amp. for different inclinations (d/a=2, c/a=4, Fn=0.2 in following waves)

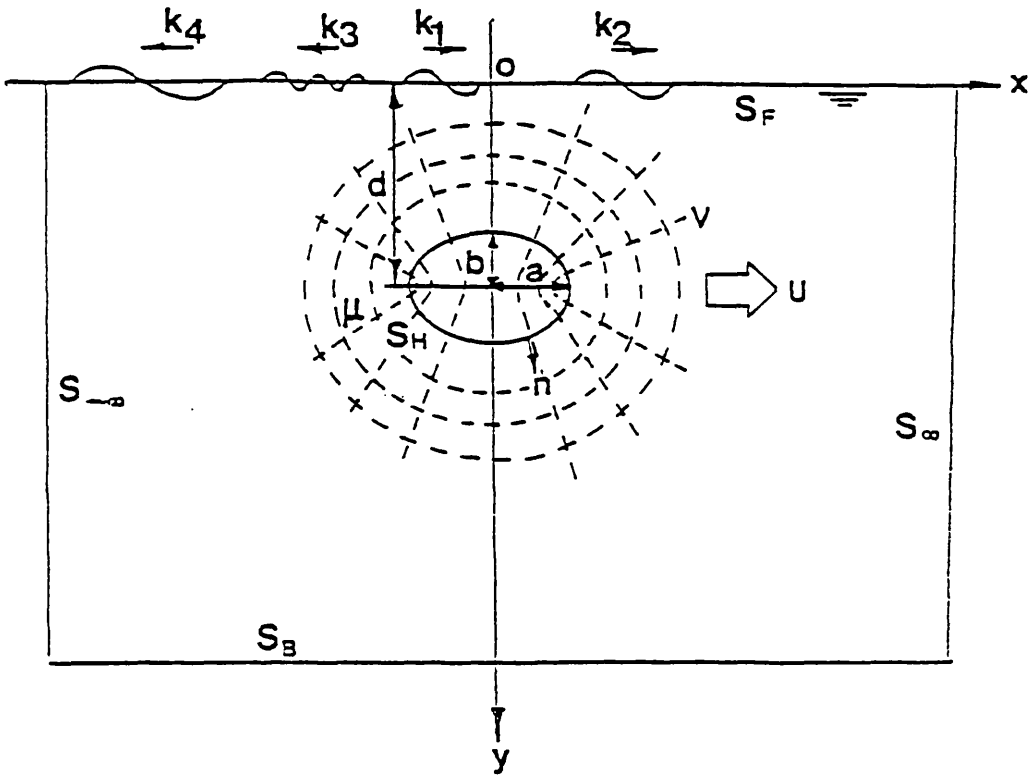

Fig.5.1 The coordinate system of an oscillating and translating elliptical cylinder

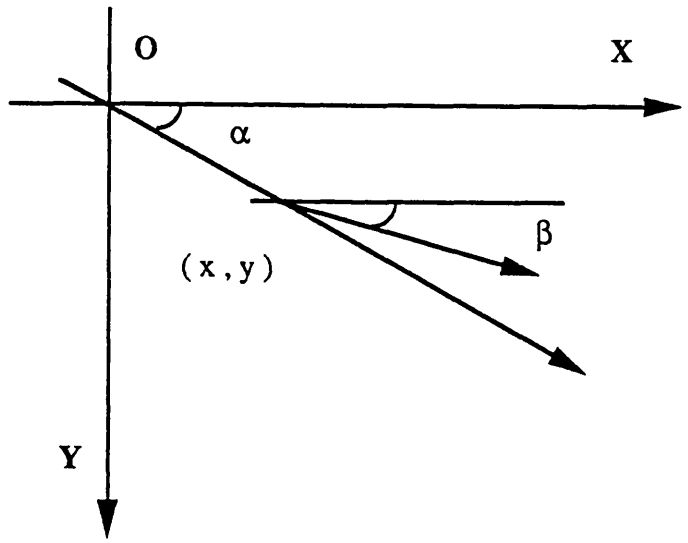

Fig.5.2 The coordinate system for the m-vector formulation by image method

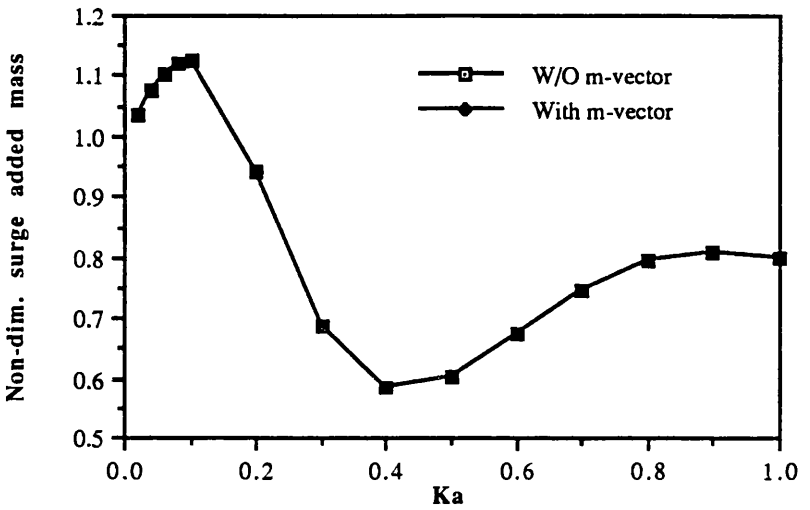

Fig.5.3 Comparison of non-dimensionalized surge added mass coefficients with m-vector(d/a=2,c/a=4,Fn=0.0 in head waves)

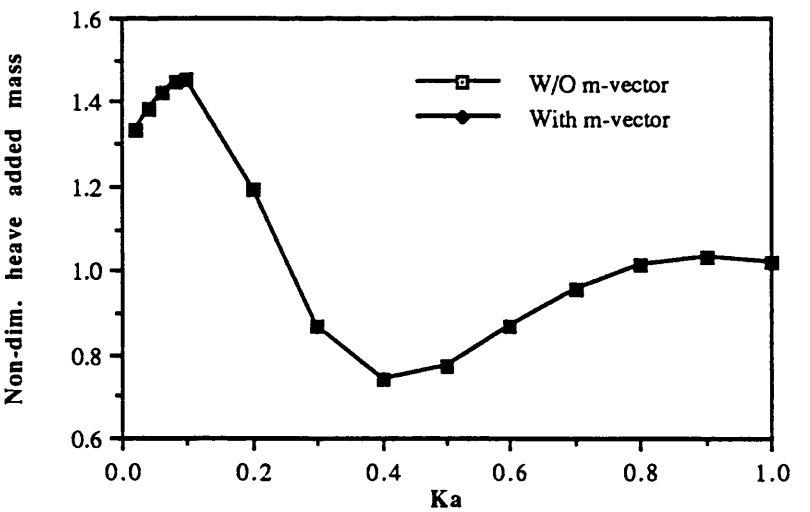

Fig.5.4 Comparison of non-dimensionalized heave added mass coefficients with m-vector(d/a=2,c/a=4,Fn=0.0 in head waves)

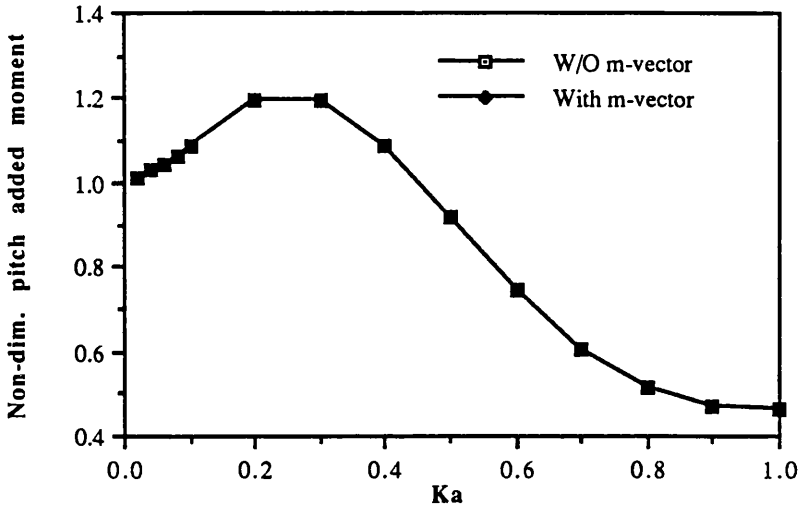

Fig.5.5 Comparison of non-dimensionalized pitch added moment of inertia with m-vector(d/a=2,c/a=4,Fn=0.0 in head waves)

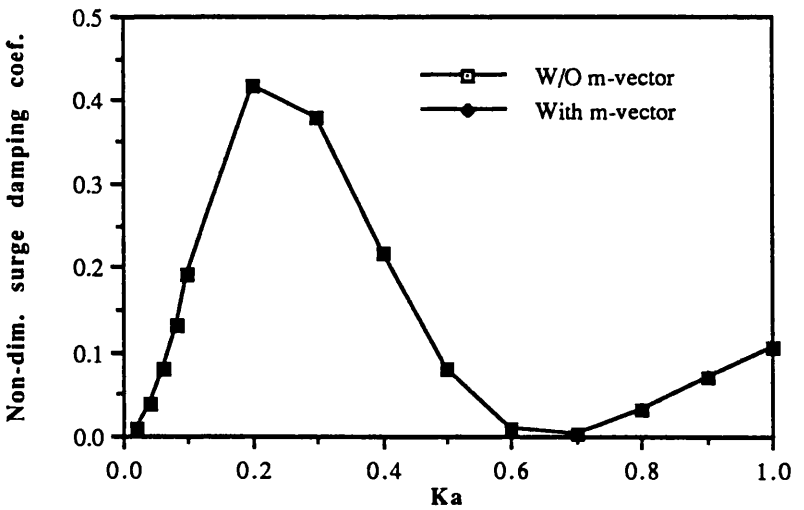

Fig.5.6 Comparison of non-dimensionalized surge damping coefficients with m-vector (d/a=2, c/a=4, Fn=0.0 in head waves)

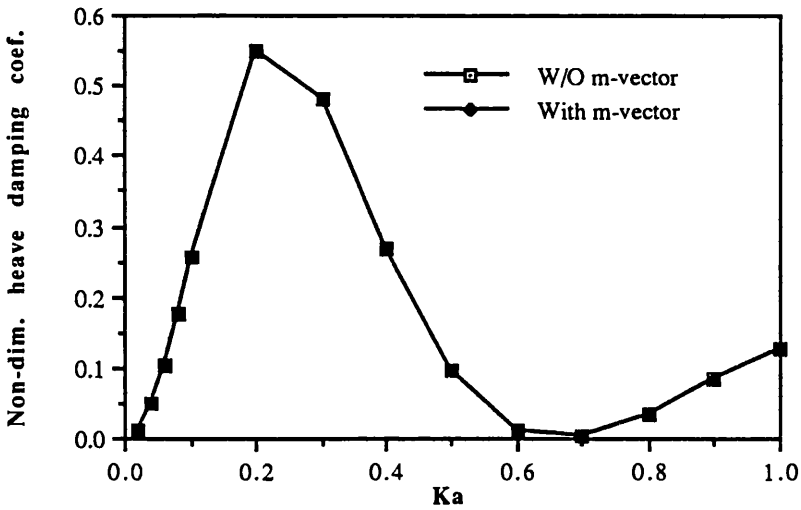

Fig.5.7 Comparison of non-dimensionalized heave damping coefficients with m-vector (d/a=2, c/a=4, Fn=0.0 in head waves)

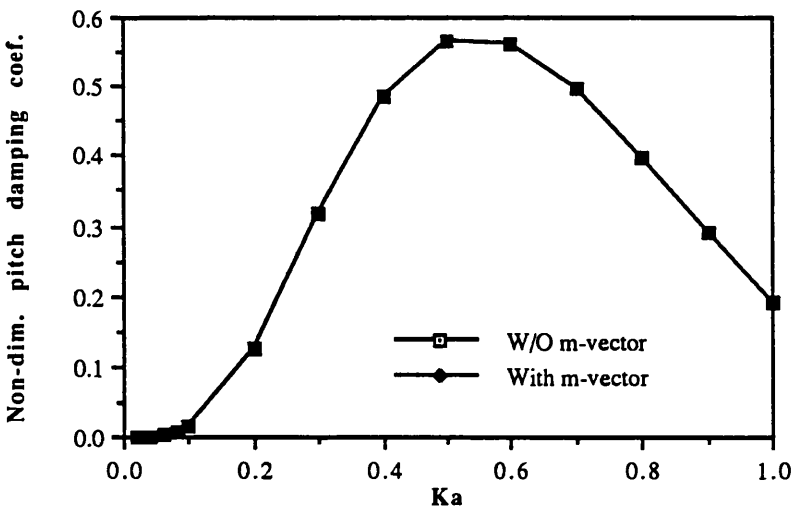

Fig.5.8 Comparison of non-dimensionalized pitch damping coefficients with m-vector (d/a=2, c/a=4, Fn=0.0 in head waves)

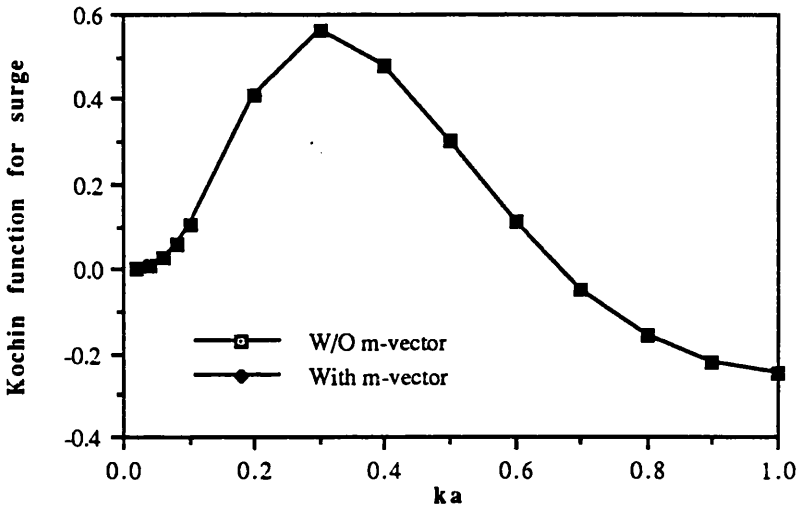

Fig.5.9 Comparison of the real part of surge Kochin function with m-vector contribution (d/a=2, c/a=4, Fn=0.0 in head waves)

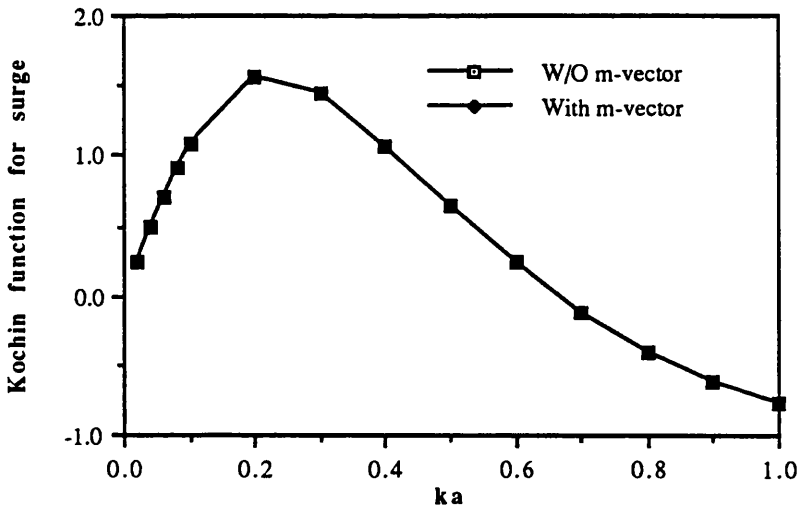

Fig.5.10 Comparison of imaginary part of surge Kochin function with m-vector (d/a=2, c/a=4, Fn=0.0 in head waves)

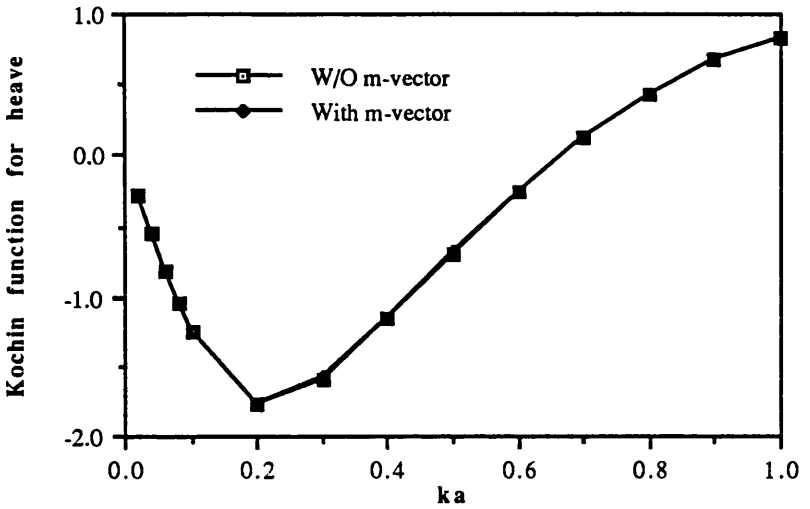

Fig.5.11 Comparison of real part of heave Kochin function with m-vector contribution (d/a=2, c/a=4, Fn=0.0 in head waves)

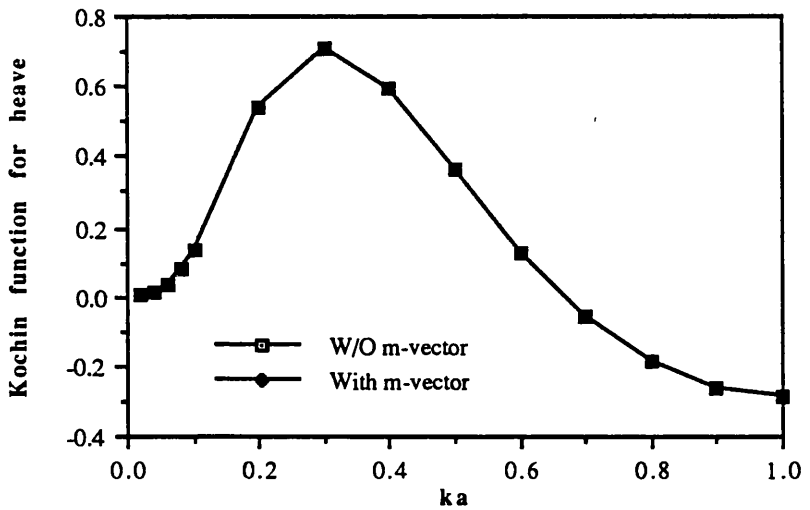

Fig.5.12 Comparison of the imaginary part of heave Kochin function with m-vector (d/a=2, c/a=4, Fn=0.0 in head waves)

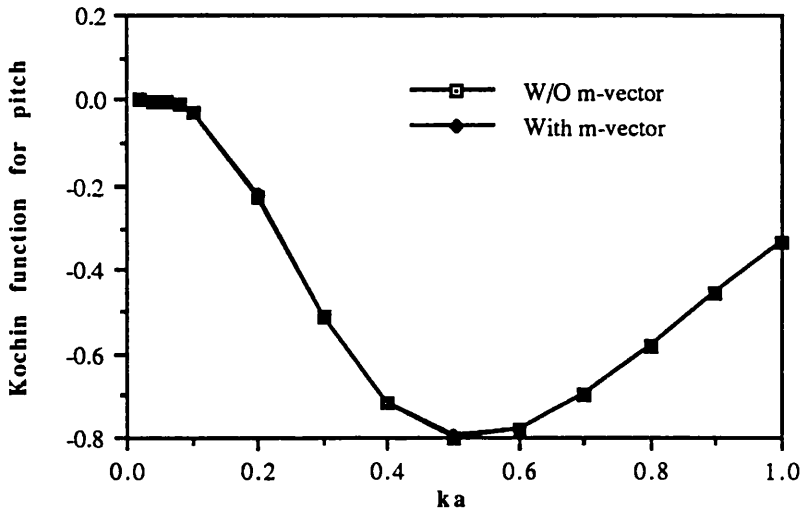

Fig.5.13 Comparison of real part of pitch Kochin function with m-vector contribution (d/a=2, c/a=4, Fn=0.0 in head waves)

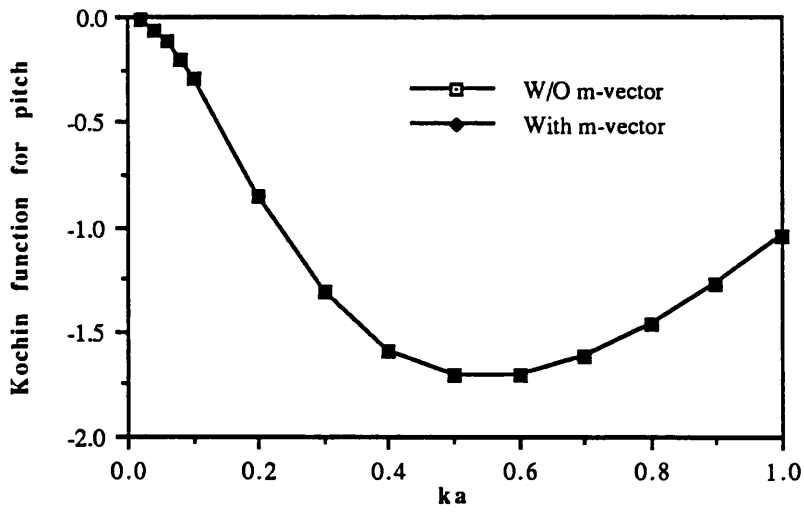

Fig.5.14 Comparison of imaginary part of pitch Kochin function with m-vector (d/a=2, c/a=4, Fn=0.0 in head waves)

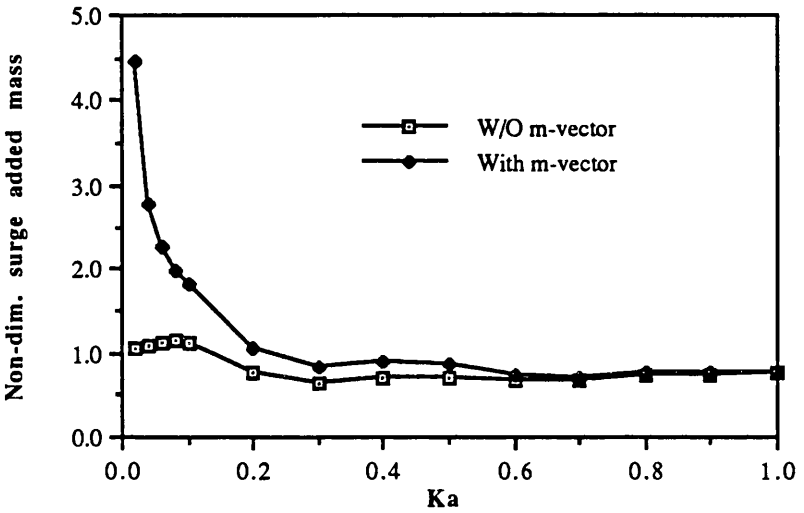

Fig.5.15 Comparison of non-dim. surge added mass coefficients with m-vector (d/a=2,c/a=4,Fn=0.2 in head waves)

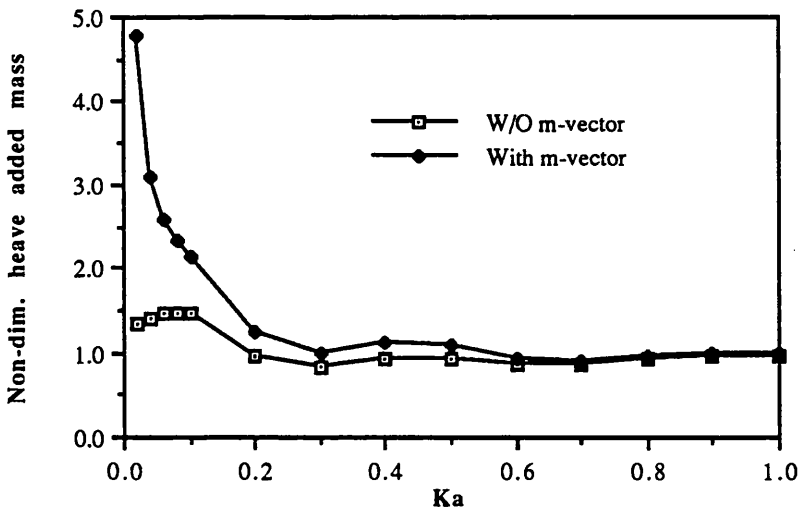

Fig.5.16 Comparison of non-dim. heave added mass coefficients with m-vector (d/a=2,c/a=4,Fn=0.2 in head waves)

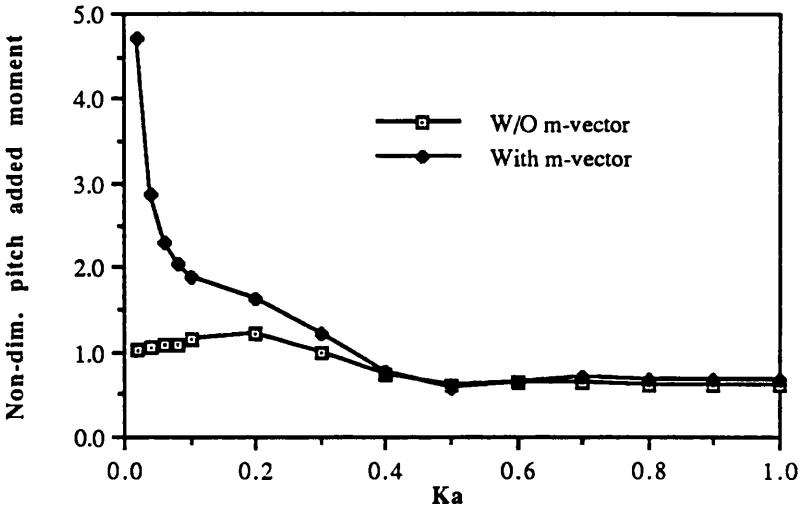

Fig.5.17 Comparison of non-dim. pitch added moment of inertia with m-vector (d/a=2,c/a=4,Fn=0.2 in head waves)

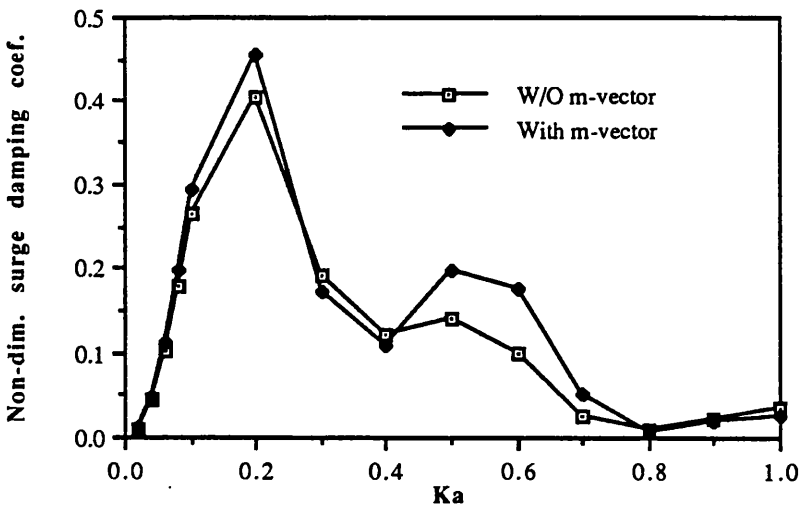

Fig.5.18 Comparison of non-dim. surge damping coefficients with m-vector (d/a=2, c/a=4, Fn=0.2 in head waves)

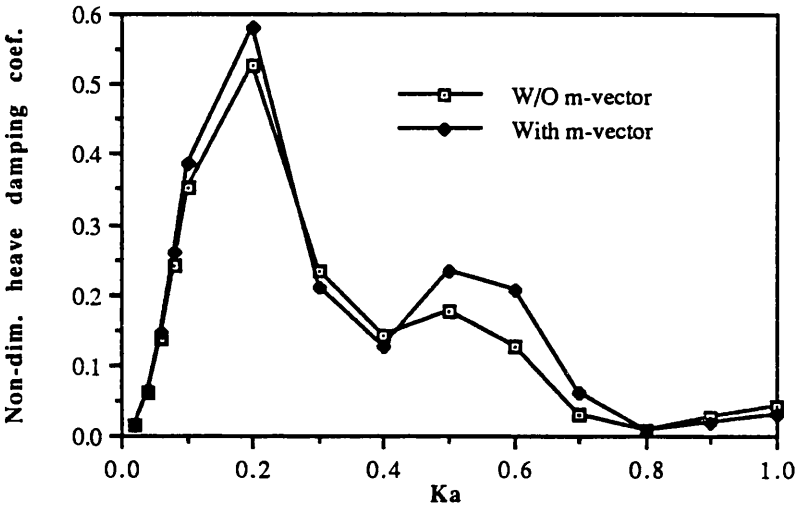

Fig.5.19 Comparison of non-dim. heave damping coefficients with m-vector (d/a=2, c/a=4, Fn=0.2 in head waves)

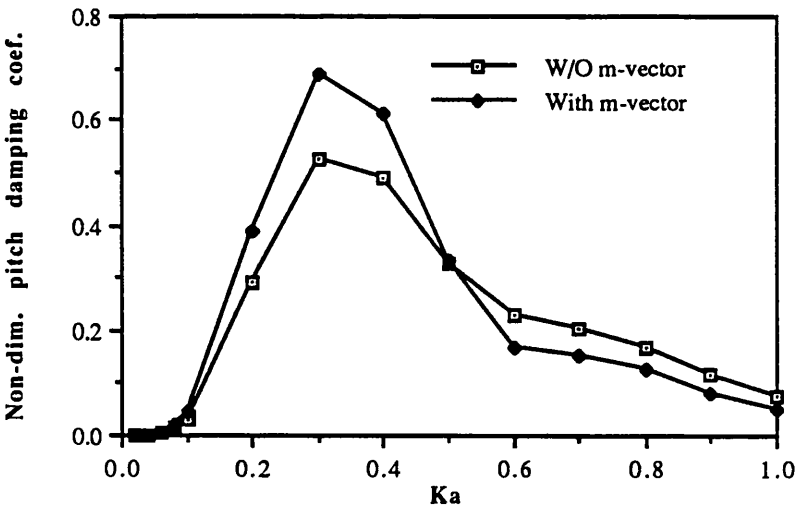

Fig.5.20 Comparison of non-dim. pitch damping coefficients with m-vector (d/a=2, c/a=4, Fn=0.2 in head waves)

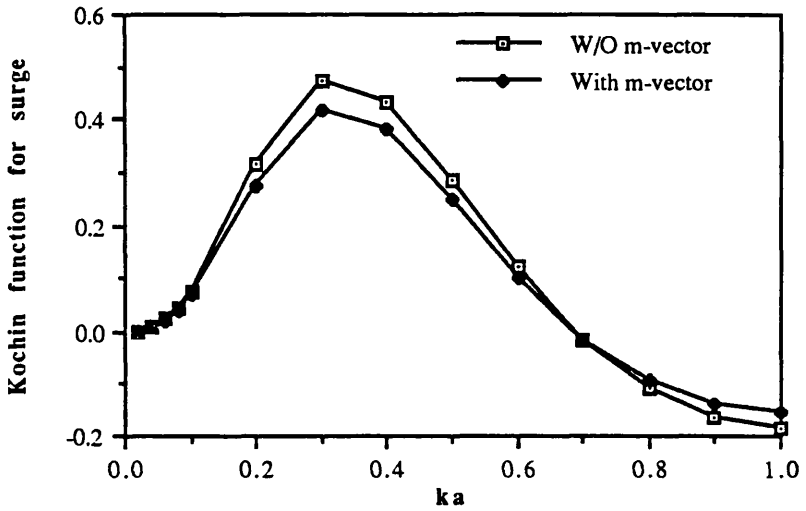

Fig.5.21 Comparison of real part of surge Kochin function with m-vector contribution (d/a=2, c/a=4, Fn=0.2 in head waves)

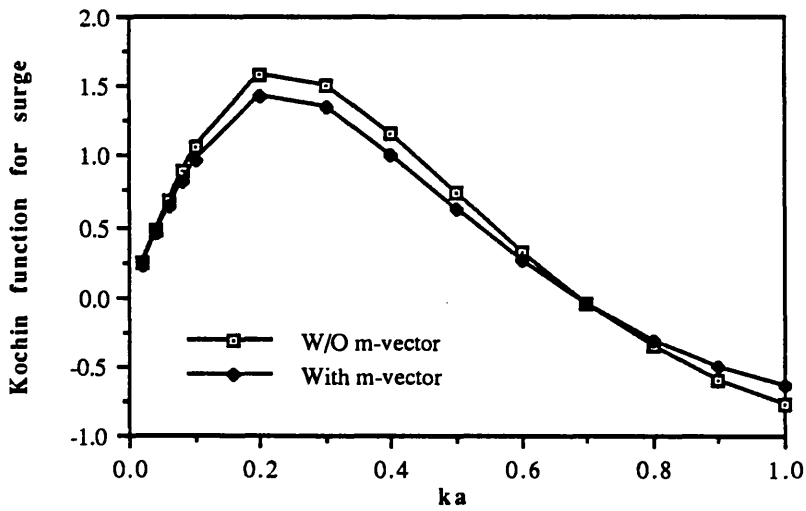

Fig.5.22 Comparison of imaginary part of surge Kochin function with m-vector (d/a=2, c/a=4, Fn=0.2 in head waves)

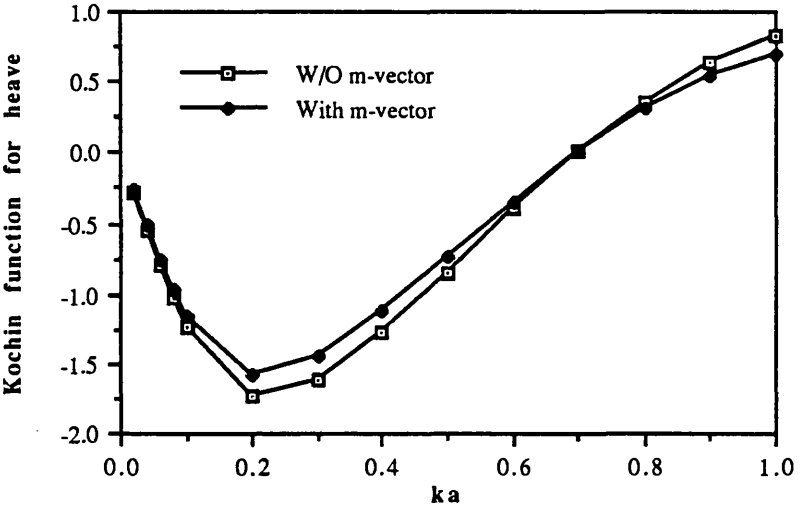

Fig.5.23 Comparison of real part of heave Kochin function with m-vector contribution (d/a=2, c/a=4, Fn=0.2 in head waves)

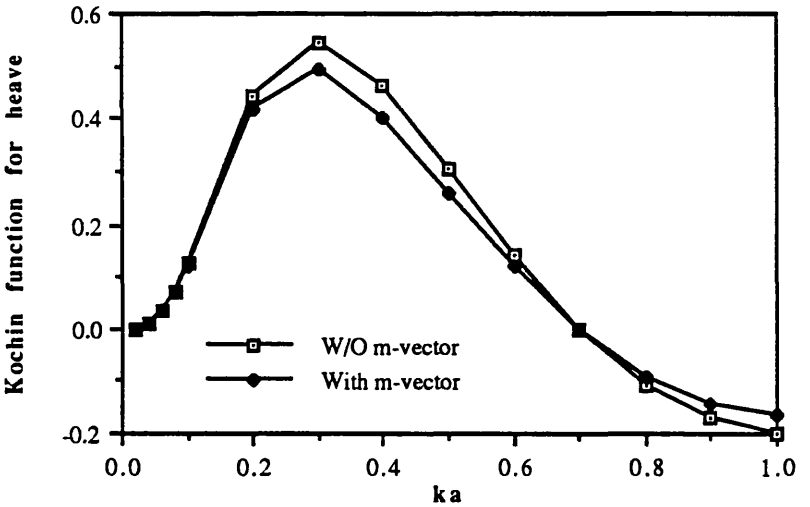

Fig.5.24 Comparison of the imaginary part of heave Kochin function with m-vector (d/a=2, c/a=4, Fn=0.2 in head waves)

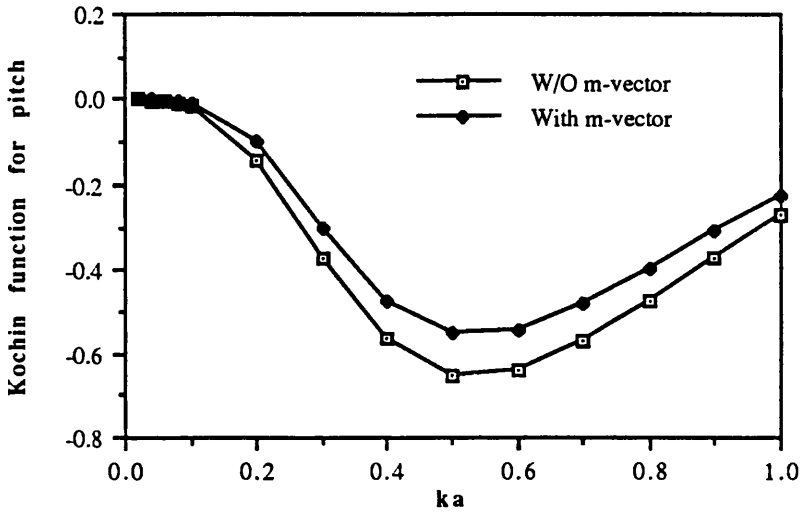

Fig.5.25 Comparison of real part of pitch Kochin function with m-vector contribution (d/a=2, c/a=4, Fn=0.2 in head waves)

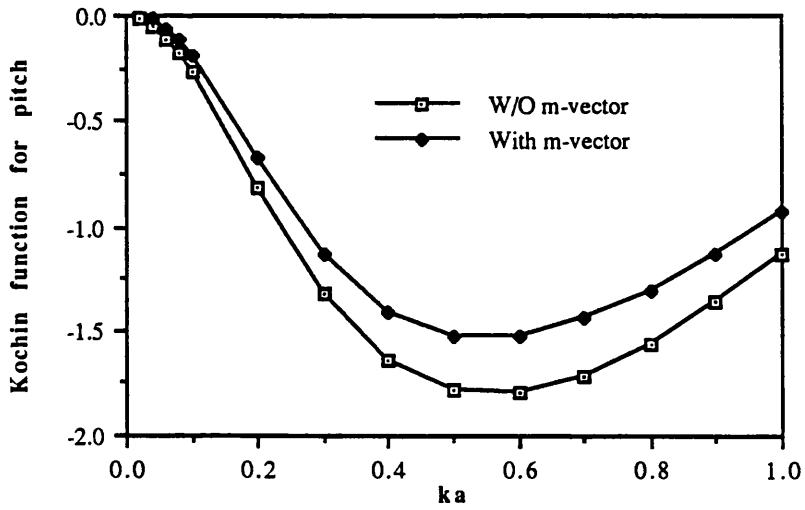

FIg.5.26 Comparison of imaginary part of pitch Kochin function with m-vector (d/a=2, c/a=4, Fn=0.2 in head waves)

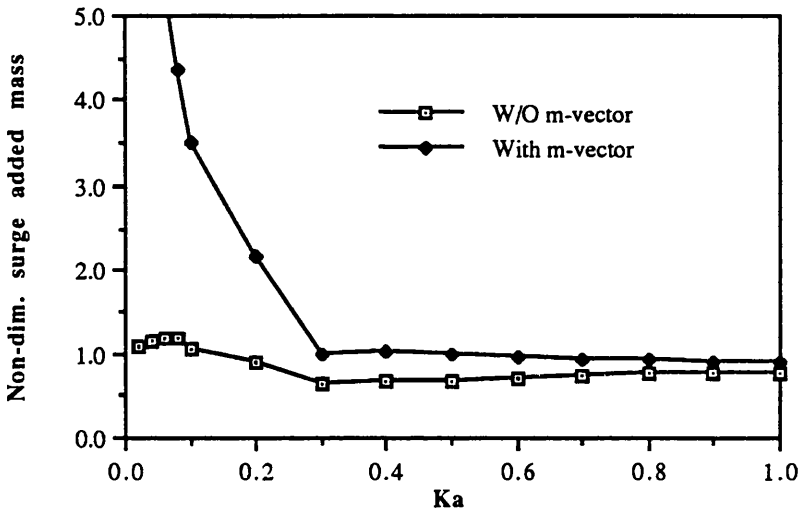

Fig.5.27 Comparison of non-dim. surge added mass coefficients with m-vector (d/a=2,c/a=4,Fn=0.4 in head waves)

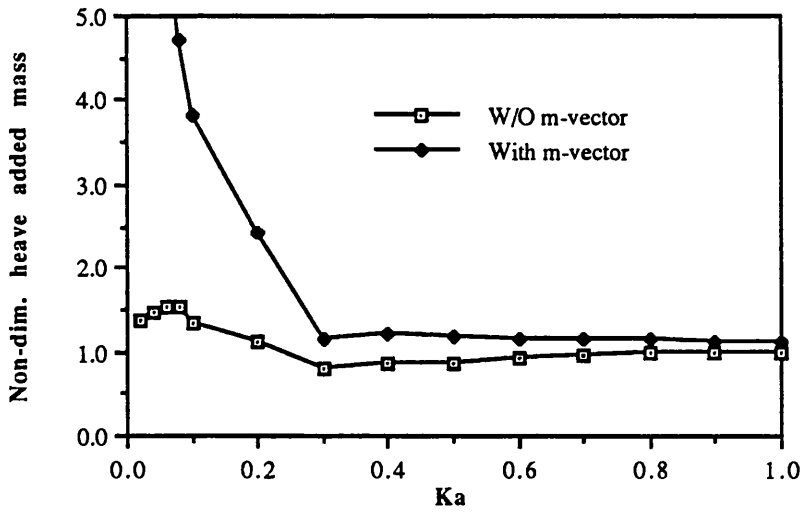

Fig.5.28 Comparison of non-dim. heave added mass coefficients with m-vector (d/a=2,c/a=4,Fn=0.4 in head waves)

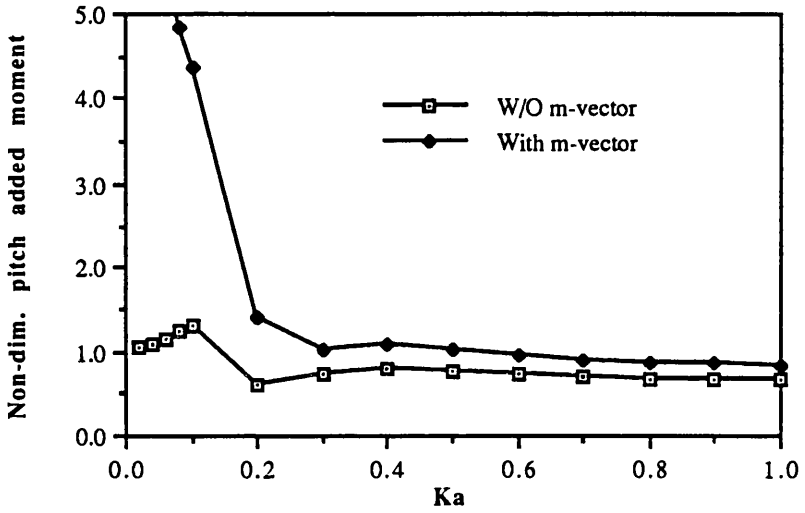

Fig.5.29 Comparison of non-dim. pitch added moment of inertia with m-vector (d/a=2,c/a=4,Fn=0.4 in head waves)

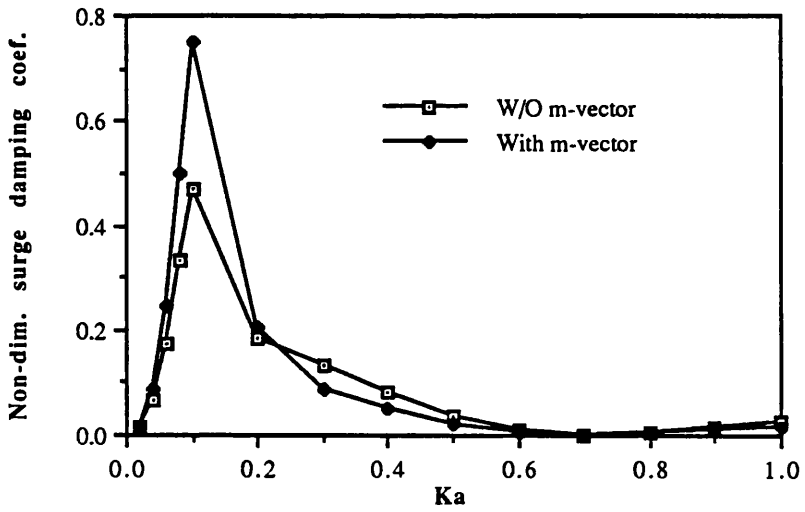

Fig.5.30 Comparison of non-dim. surge damping coefficients with m-vector (d/a=2, c/a=4, Fn=0.4 in head waves)

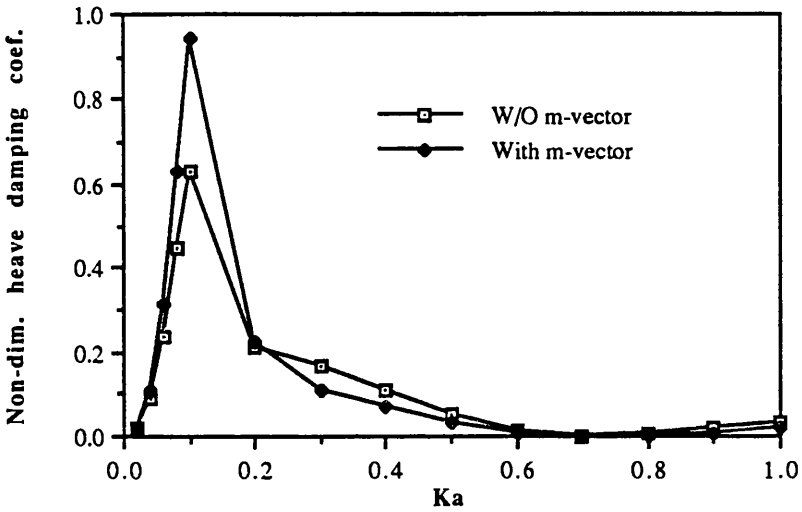

Fig.5.31 Comparison of non-dim. heave damping coefficients with m-vector (d/a=2, c/a=4, Fn=0.4 in head waves)

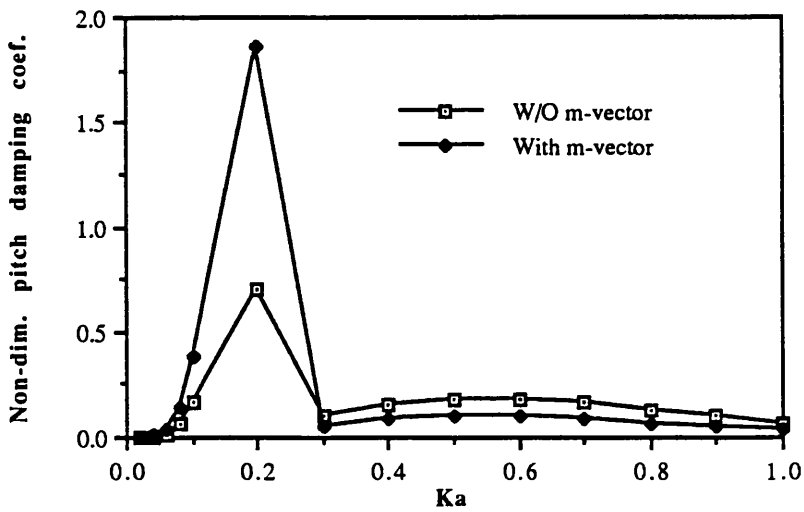

Fig.5.32 Comparison of non-dim. pitch damping coefficients with m-vector (d/a=2, c/a=4, Fn=0.4 in head waves)

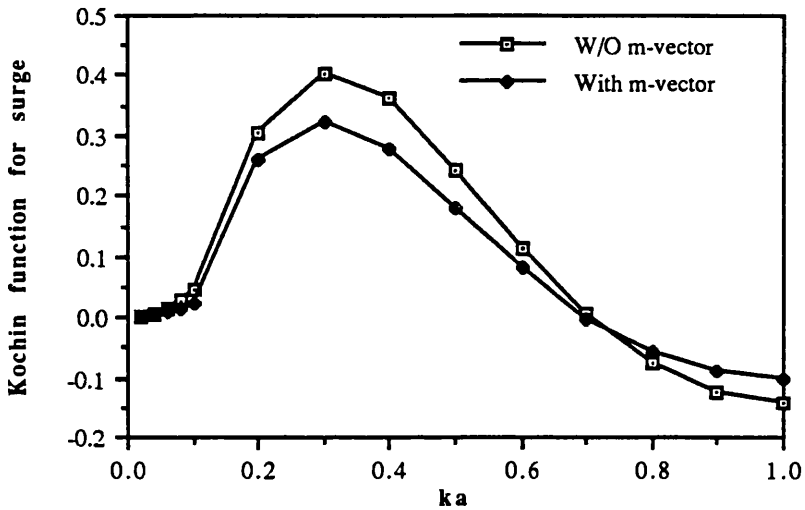

Fig.5.33 Comparison of real part of surge Kochin function with m-vector contribution (d/a=2, c/a=4, Fn=0.4 in head waves)

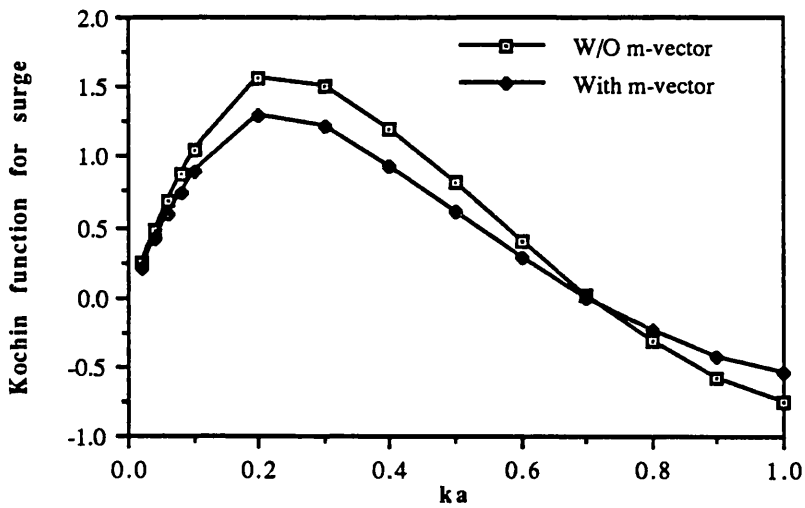

Fig.5.34 Comparison of imaginary part of surge Kochin function with m-vector (d/a=2, c/a=4, Fn=0.4 in head waves)

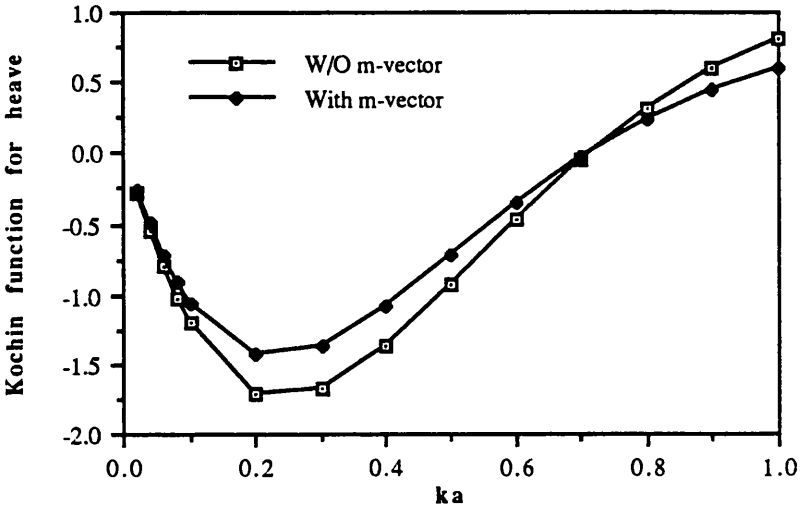

Fig.5.35 Comparison of real part of heave Kochin function with m-vector contribution (d/a=2, c/a=4, Fn=0.4 in head waves)

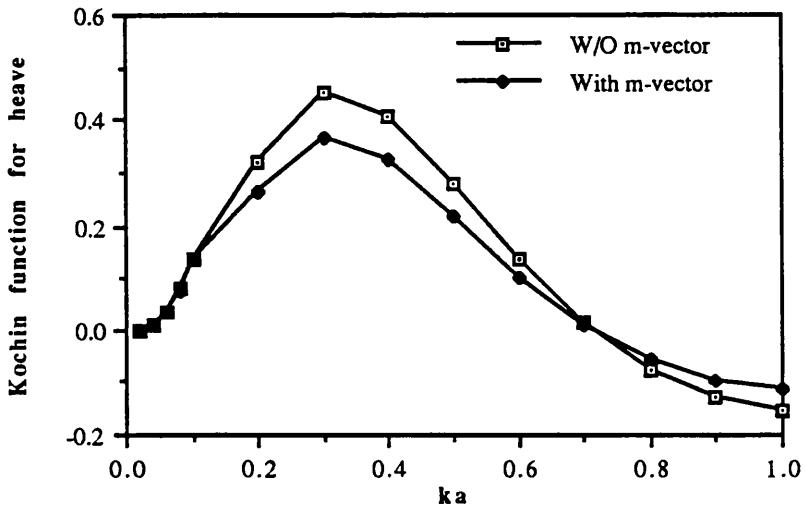

Fig.5.36 Comparison of the imaginary part of heave Kochin function with m-vector (d/a=2, c/a=4, Fn=0.4 in head waves)

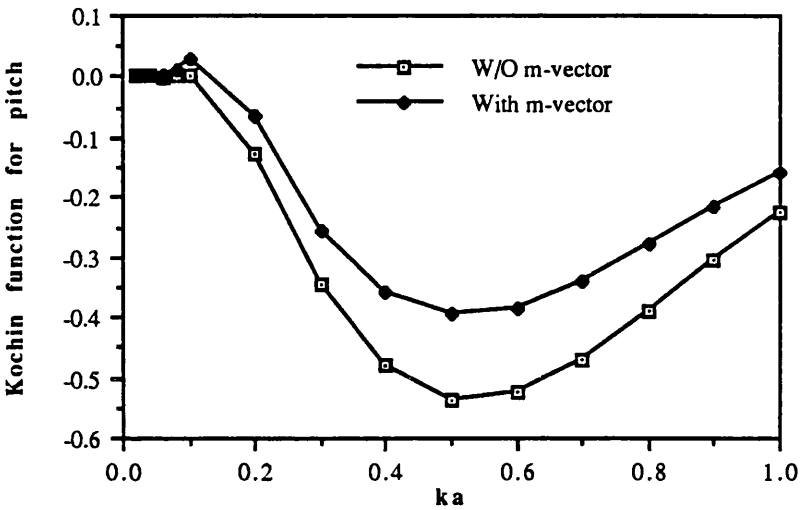

Fig.5.37 Comparison of real part of pitch Kochin function with m-vector contribution (d/a=2, c/a=4, Fn=0.4 in head waves)

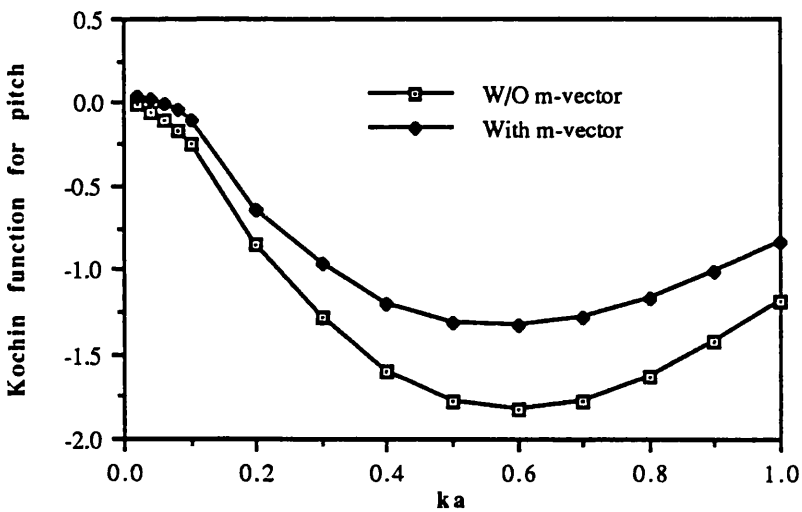

Fig.5.38 Comparison of imaginary part of pitch Kochin function with m-vector (d/a=2, c/a=4, Fn=0.4 in head waves)

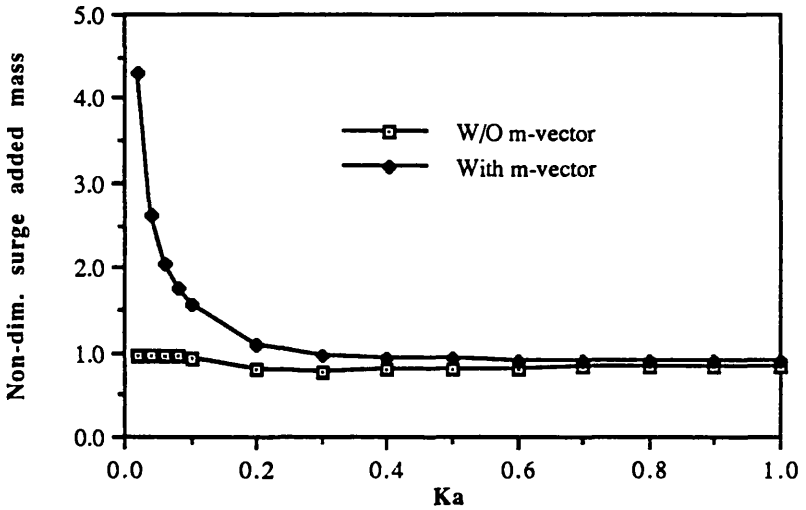

Fig.5.39 Comparison of non-dim. surge added mass coefficients with m-vector (d/a=4,c/a=4, Fn=0.2 in head waves)

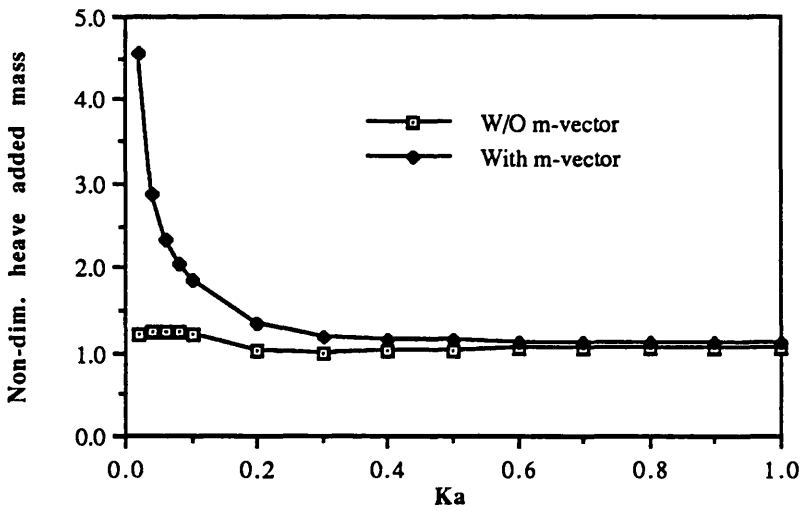

Fig.5.40 Comparison of non-dim. heave added mass coefficients with m-vector (d/a=4,c/a=4, Fn=0.2 in head waves)

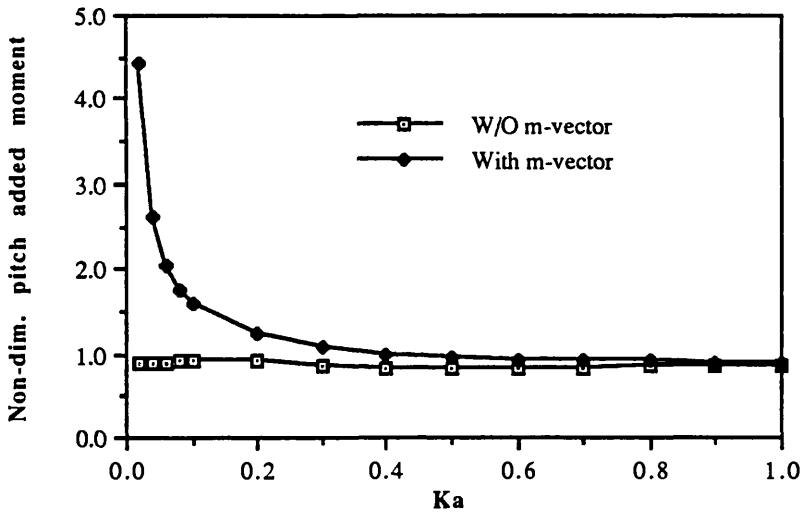

Fig.5.41 Comparison of non-dim. pitch added moment of inertia with m-vector (d/a=4, c/a=4, Fn=0.2 in head waves)

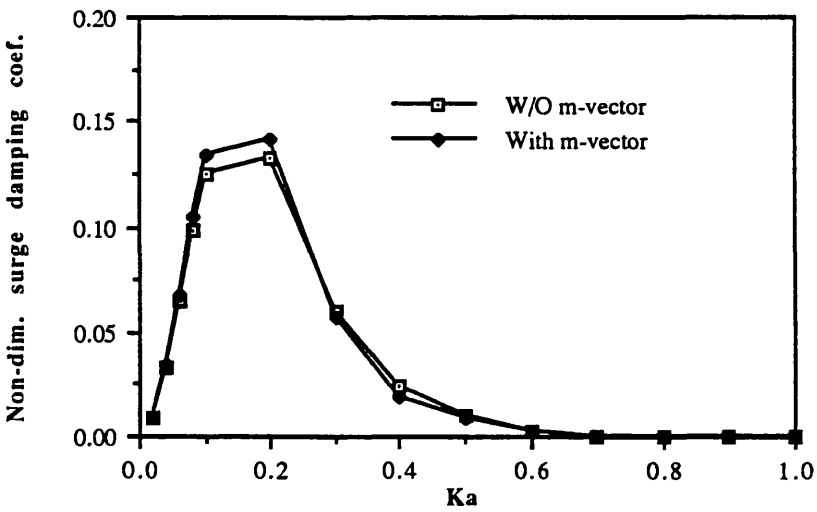

Fig.5.42 Comparison of non-dim. surge damping coefficients with m-vector (d/a=4, c/a=4, Fn=0.2 in head waves)

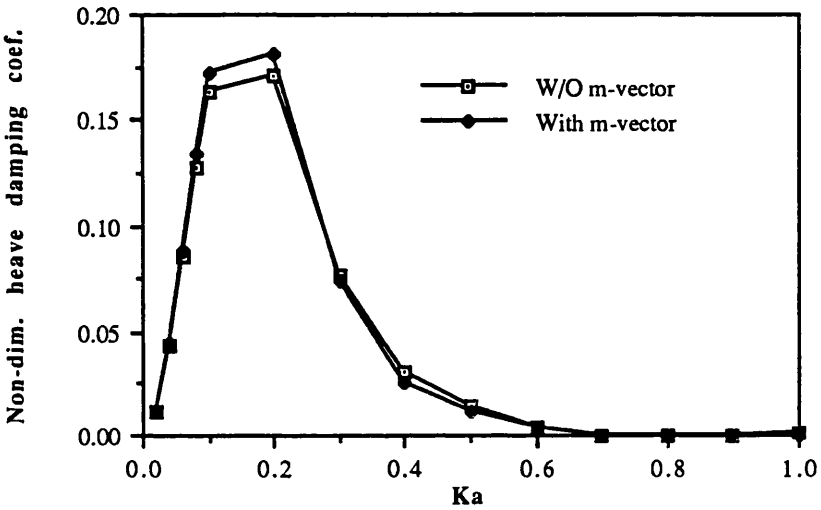

Fig.5.43 Comparison of non-dim. heave damping coefficients with m-vector (d/a=4, c/a=4, Fn=0.2 in head waves)

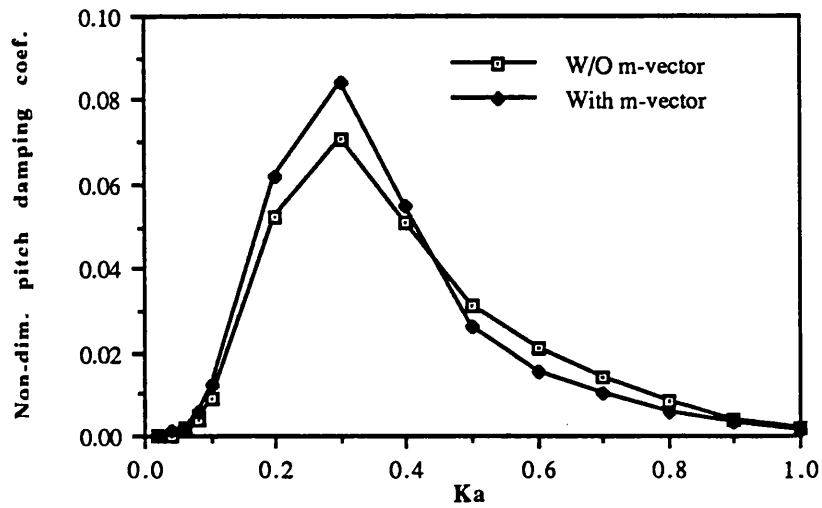

Fig.5.44 Comparison of non-dim. pitch damping coefficients with m-vector (d/a=4, c/a=4, Fn=0.2 in head waves)

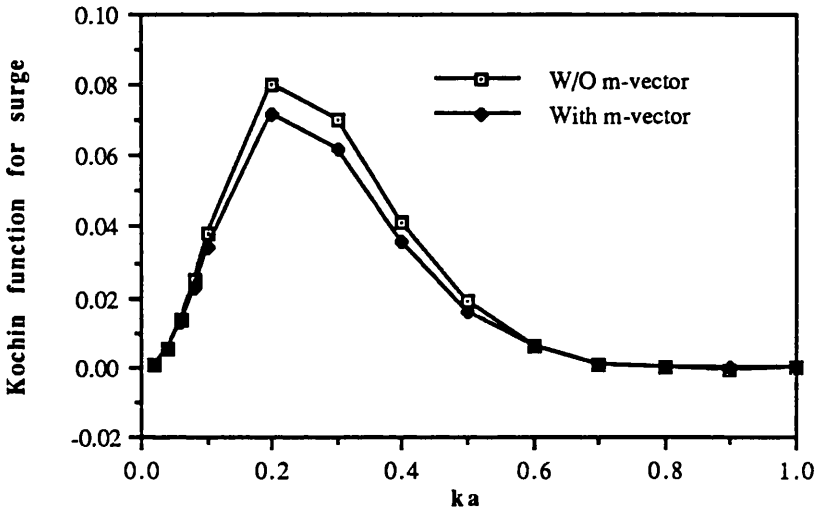

Fig.5.45 Comparison of real part of surge Kochin function with m-vector contribution (d/a=4, c/a=4, Fn=0.2 in head waves)

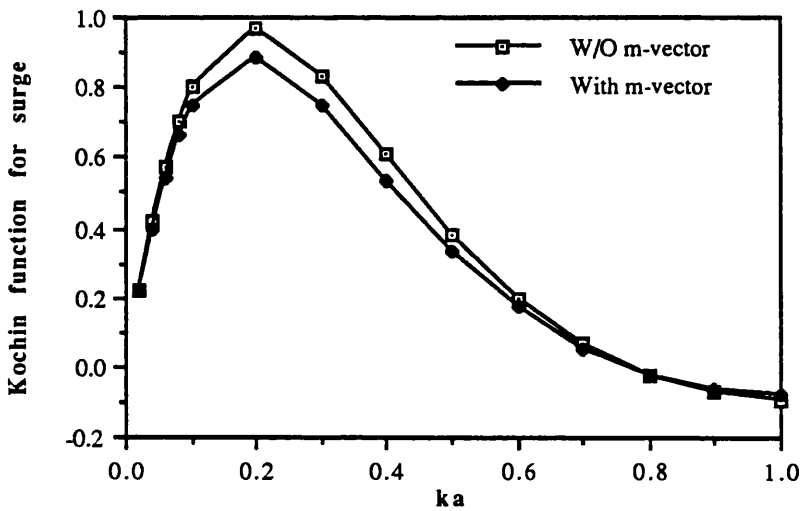

Fig.5.46 Comparison of imaginary part of surge Kochin function with m-vector (d/a=4, c/a=4, Fn=0.2 in head waves)

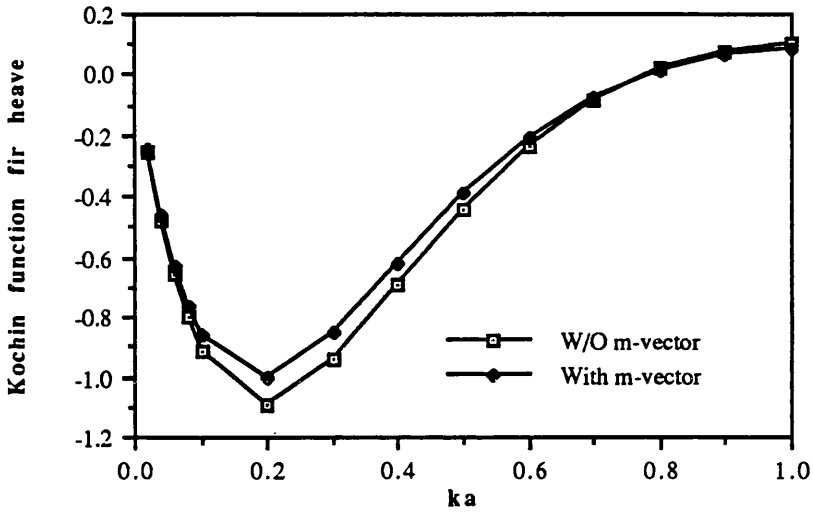

Fig.5.47 Comparison of real part of heave Kochin function with m-vector contribution (d/a=4, c/a=4, Fn=0.2 in head waves)

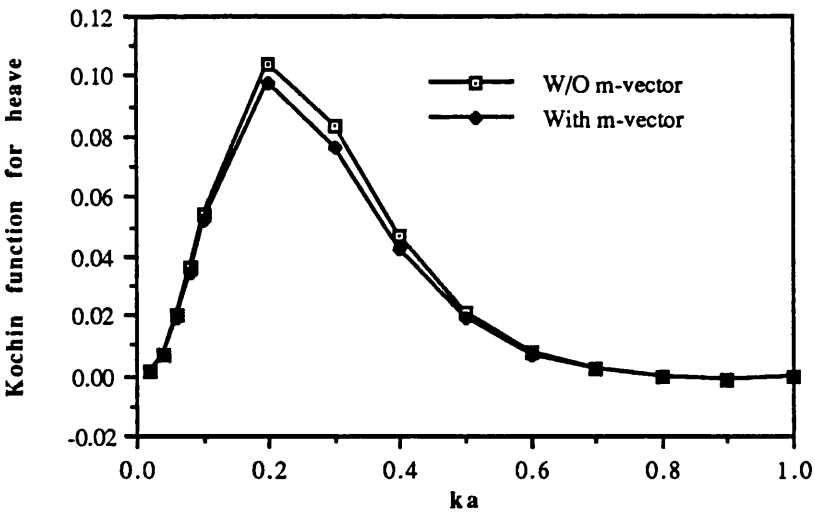

Fig.5.48 Comparison of the imaginary part of heave Kochin function with m-vector (d/a=4, c/a=4, Fn=0.2 in head waves)

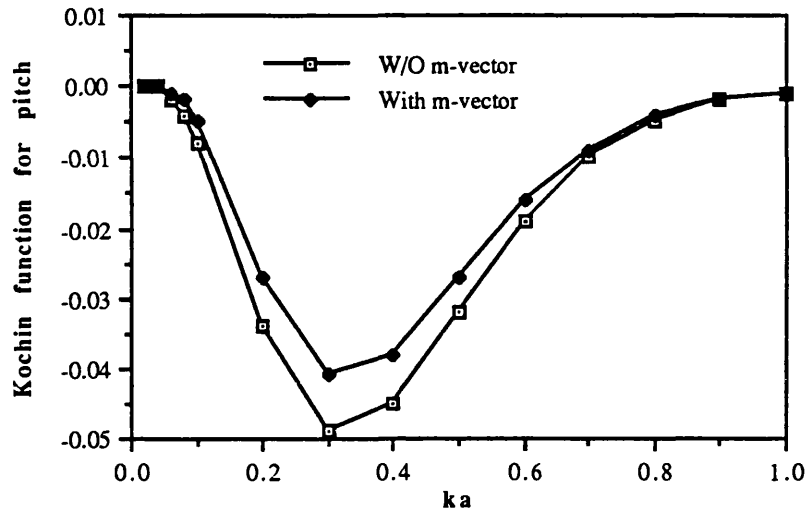

Fig.5.49 Comparison of real part of pitch Kochin function with m-vector contribution (d/a=4, c/a=4, Fn=0.2 in head waves)

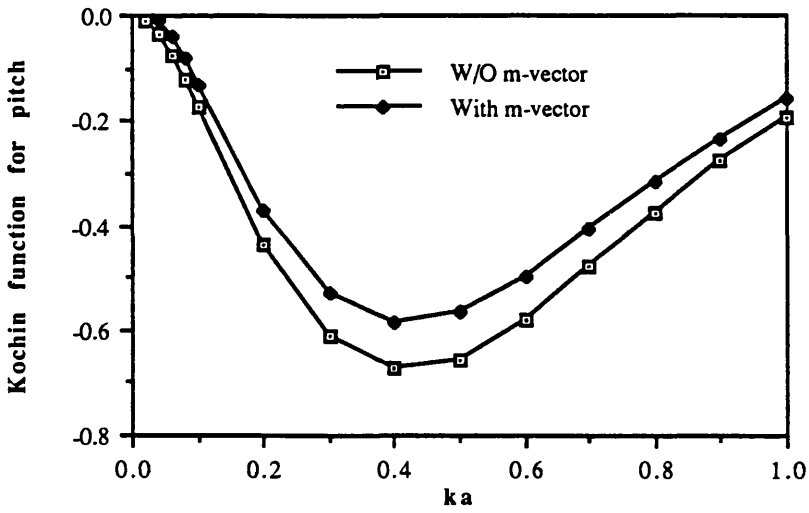

Fig.5.50 Comparison of imaginary part of pitch Kochin function with m-vector (d/a=4, c/a=4, Fn=0.2 in head waves)

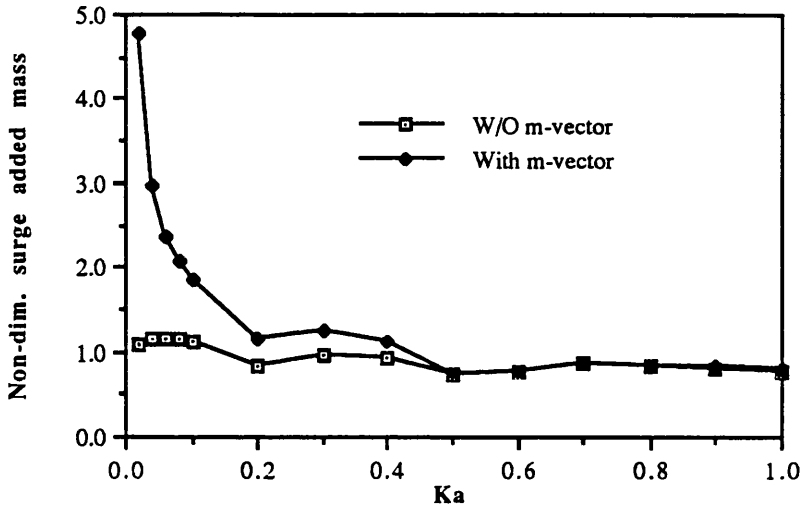

Fig.5.51 Comparison of non-dim. surge added mass coefficients with m-vector (d/a=2, c/a=6, Fn=0.2 in head waves)

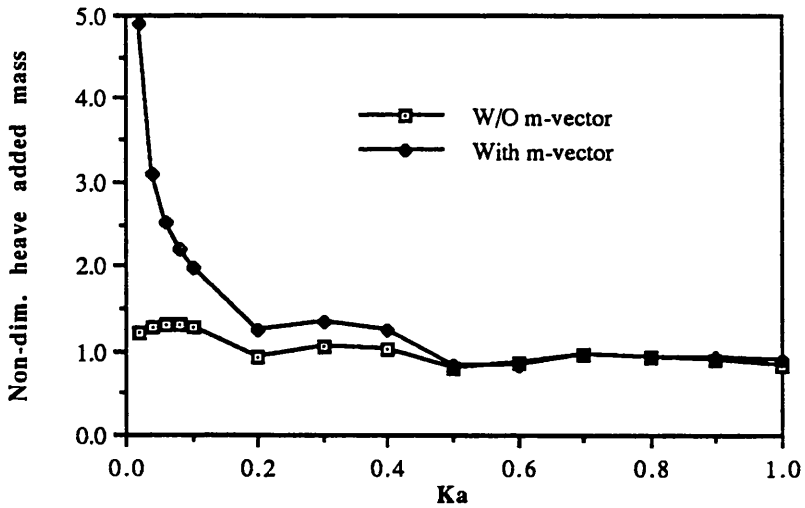

Fig.5.52 Comparison of non-dim. heave added mass coefficients with m-vector (d/a=2, c/a=6, Fn=0.2 in head waves)

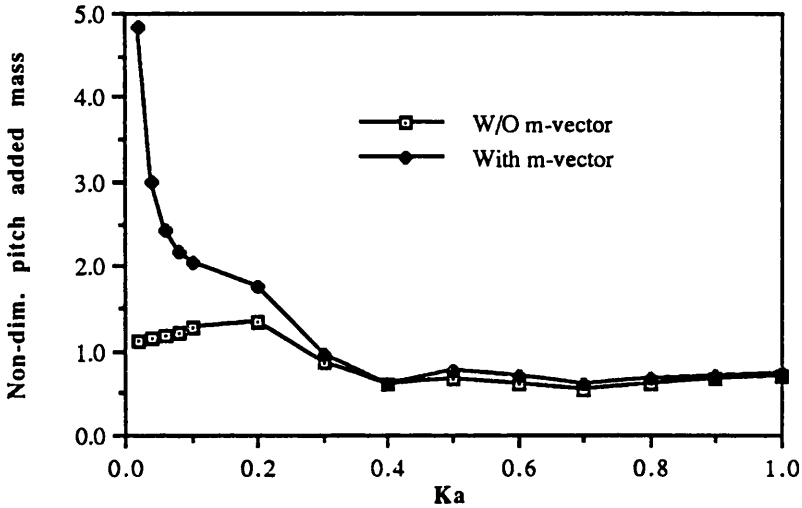

Fig.5.53 Comparison of non-dim. pitch added moment of inertia with m-vector (d/a=2, c/a=6, Fn=0.2 in head waves)

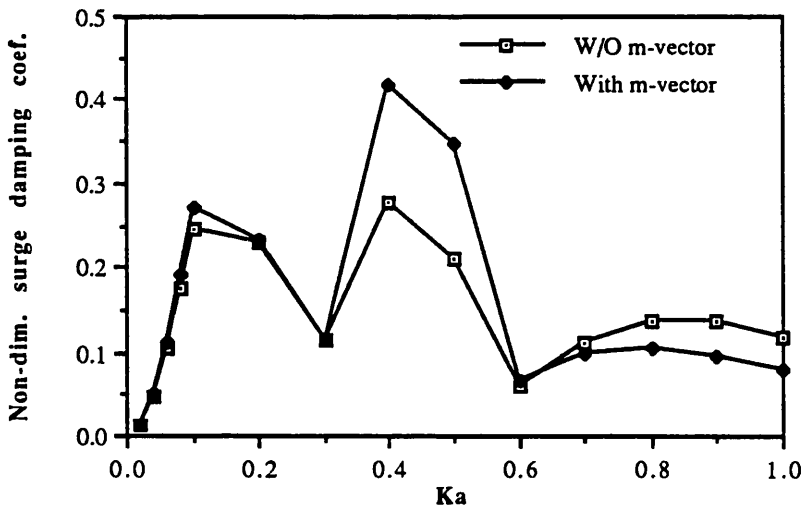

Fig.5.54 Comparison of non-dim. surge damping coeffcients with m-vector (d/a=2, c/a=6, Fn=0.2 in head waves)

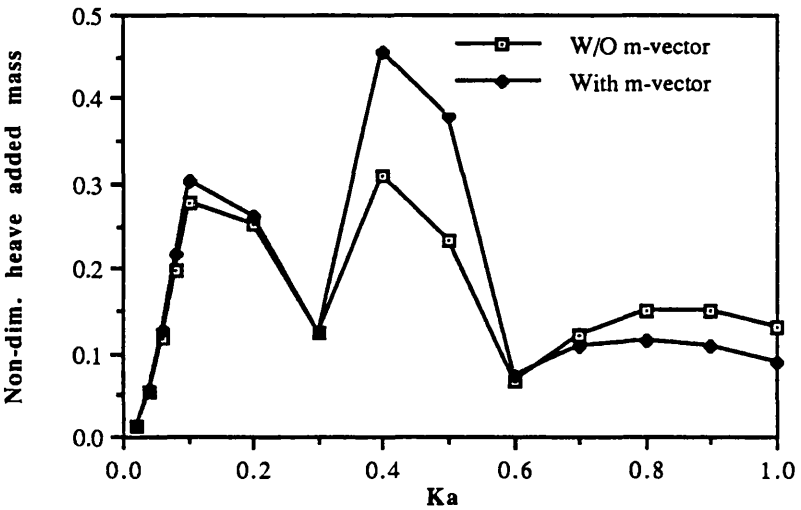

Fig.5.55 Comparison of non-dim. heave damping coefficients with m-vector (d/a=2, c/a=6, Fn=0.2 in head waves)

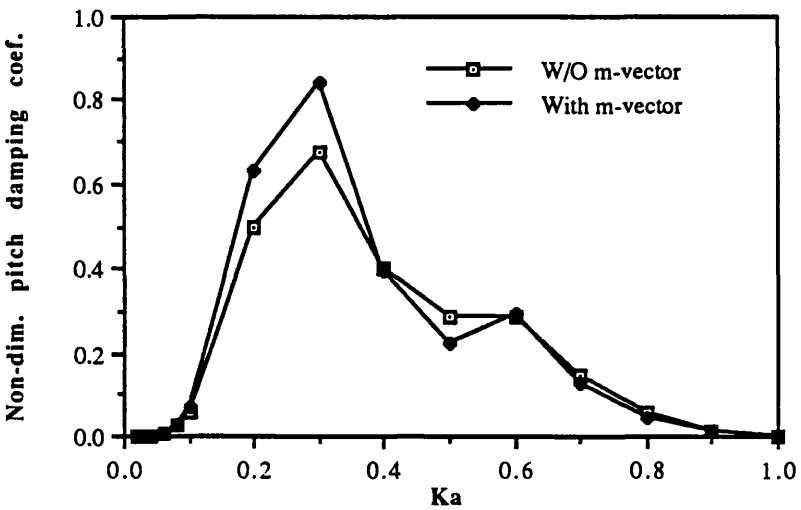

Fig.5.56 Comparison of non-dim. pitch damping coefficients with m-vector (d/a=2, c/a=6, Fn=0.2 in head waves)

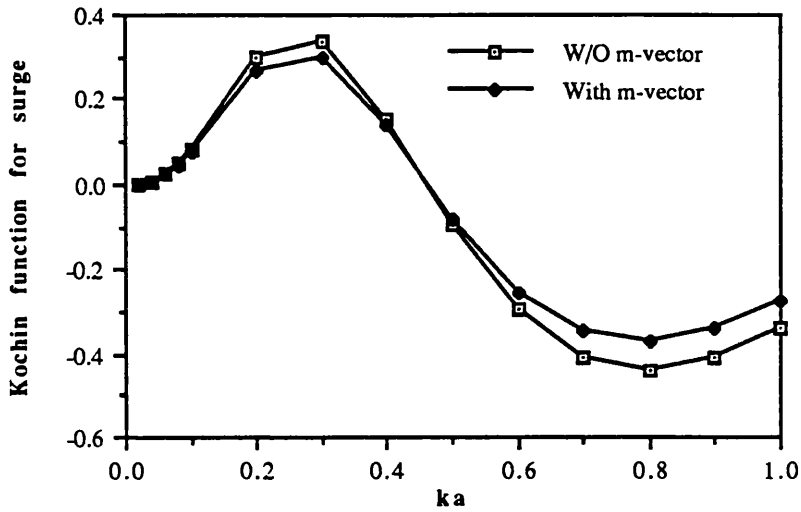

Fig.5.57 Comparison of real part of surge Kochin function with m-vector contribution (d/a=2, c/a=6, Fn=0.2 in head waves)

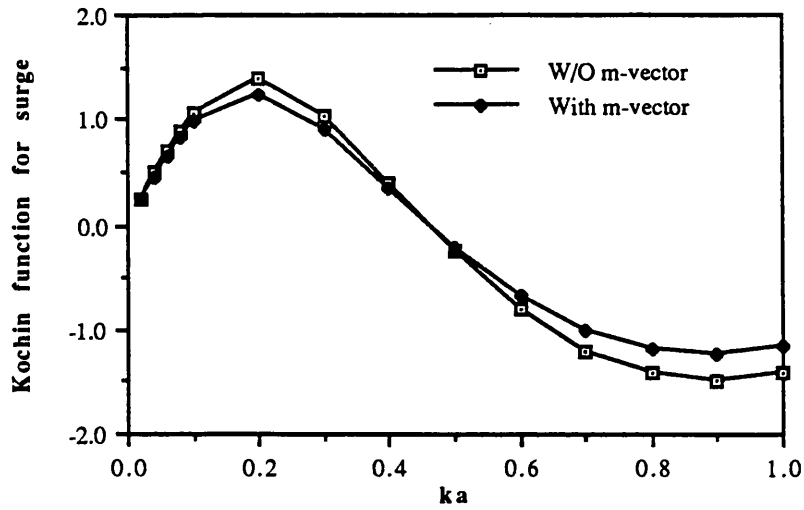

Fig.5.58 Comparison of imaginary part of surge Kochin function with m-vector (d/a=2, c/a=6, Fn=0.2 in head waves)

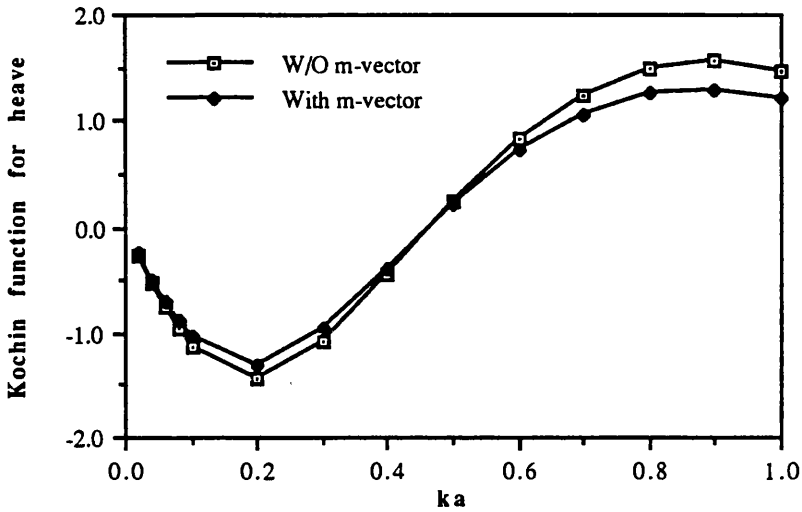

Fig.5.59 Comparison of real part of heave Kochin function with m-vector contribution (d/a=2, c/a=6, Fn=0.2 in head waves)

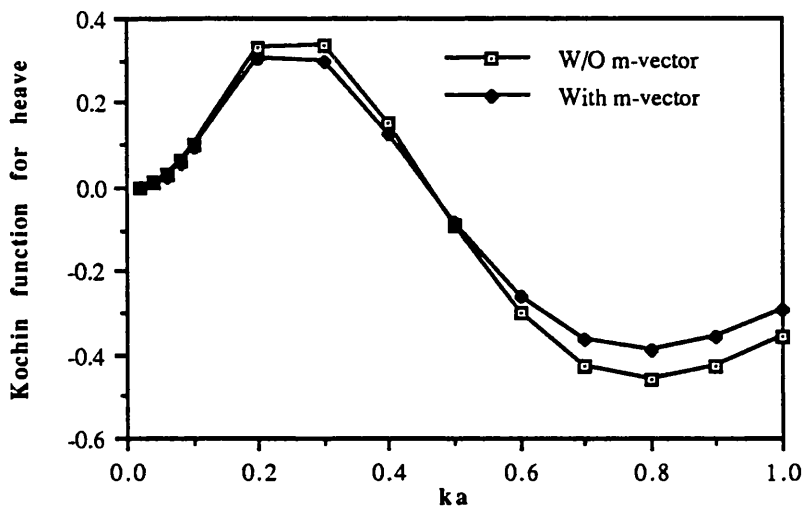

Fig.5.60 Comparison of the imaginary part of heave Kochin function with m-vector (d/a=2, c/a=6, Fn=0.2 in head waves)

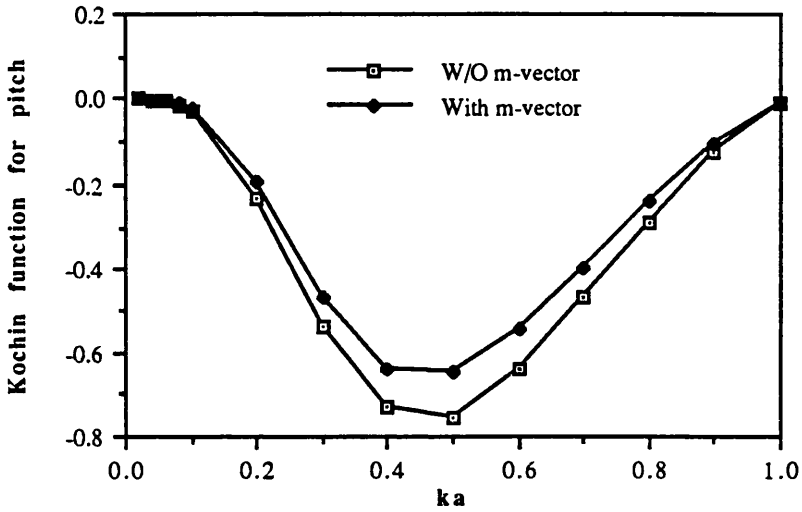

Fig.5.61 Comparison of real part of pitch Kochin function with m-vector contribution (d/a=2, c/a=6, Fn=0.2 in head waves)

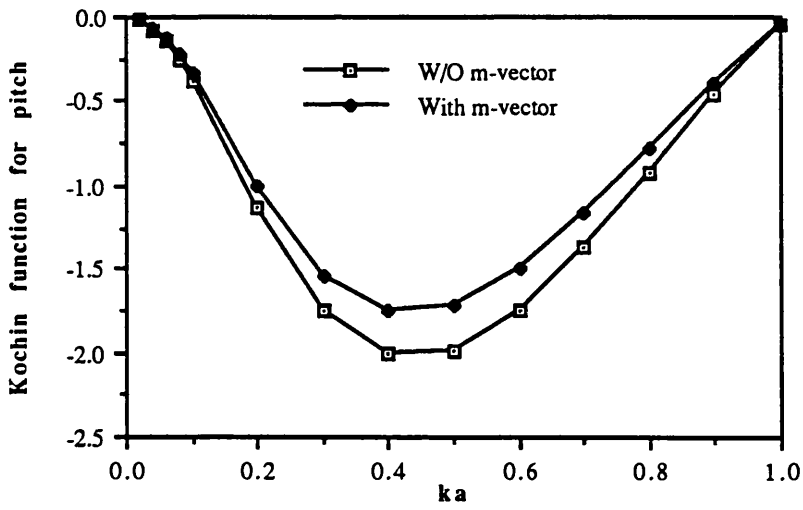

Fig.5.62 Comparison of imaginary part of pitch Kochin function with m-vector (d/a=2, c/a=6, Fn=0.2 in head waves)

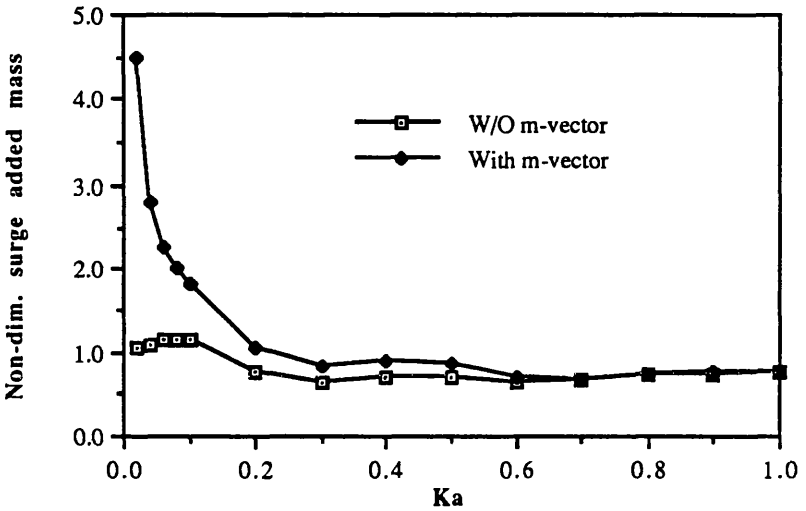

Fig.5.63 Comparison of non-dim. surge added mass coefficients with m-vector (d/a=2 ,c/a=4, 5 degree inclination)

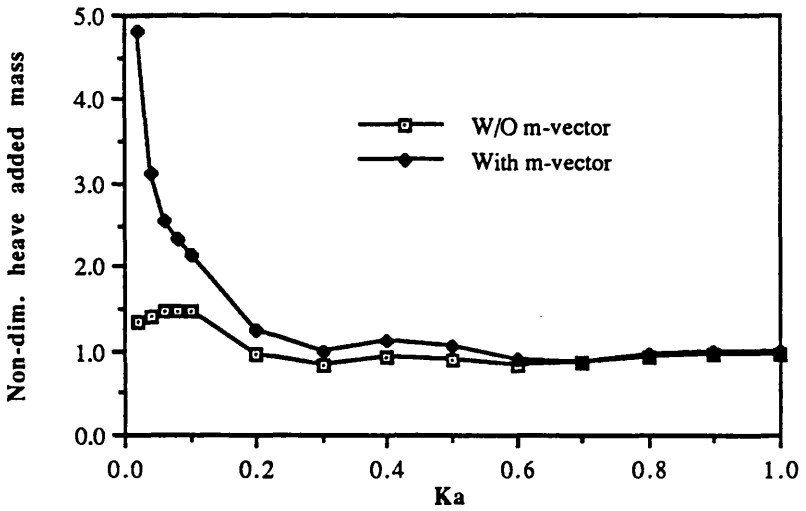

Fig.5.64 Comparison of non-dim. heave added mass coefficients with m-vector (d/a=2, c/a=4, 5 degree inclination)

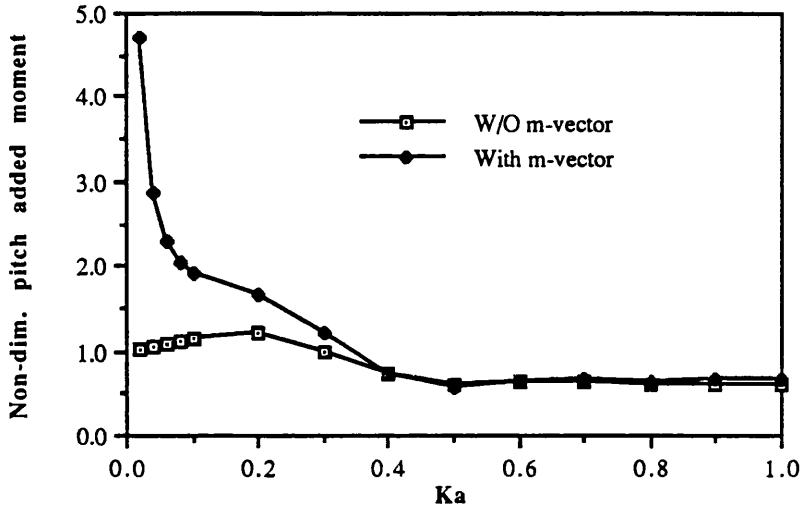

Fig.5.65 Comparison of non-dim. pitch added moment of inertia with m-vector (d/a=2, c/a=4, 5 degree inclination)

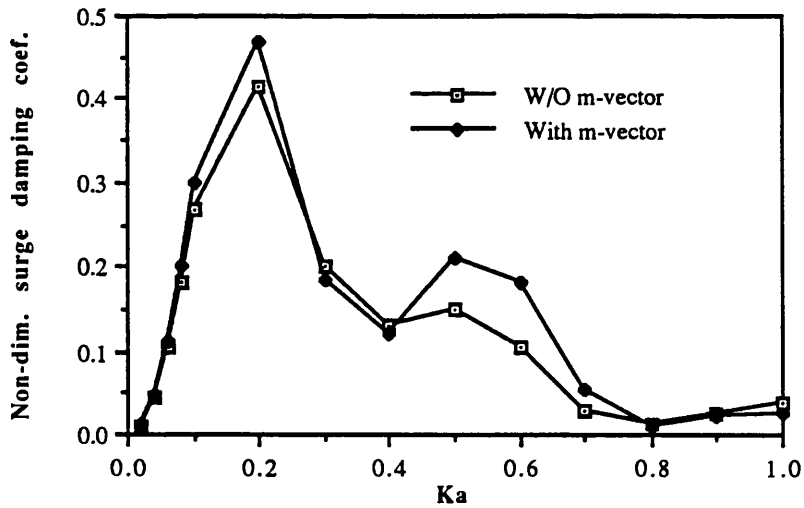

Fig.5.66 Comparison of non-dim. surge damping coefficients with m-contribution (d/a=2, c/a=4, 5 degree tilt in head waves)

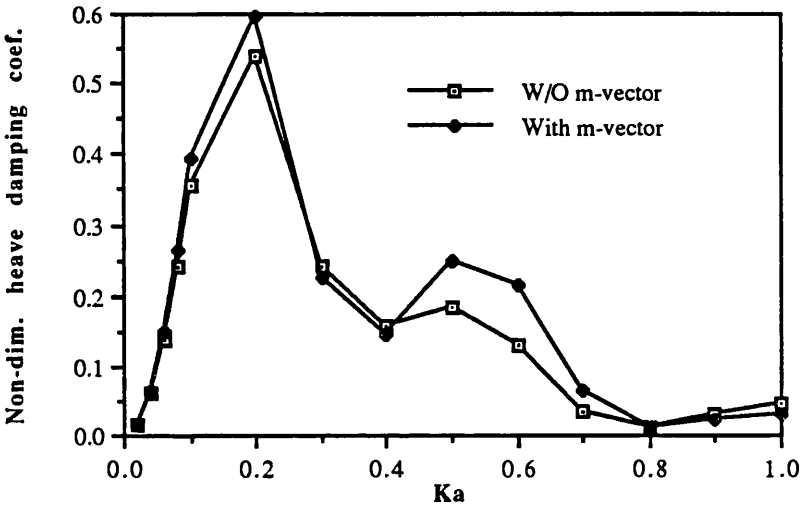

Fig.5.67 Comparison of non-dim. heave damping coefficients with m-contribution (d/a=2, c/a=4, 5 degree tilt in head waves)

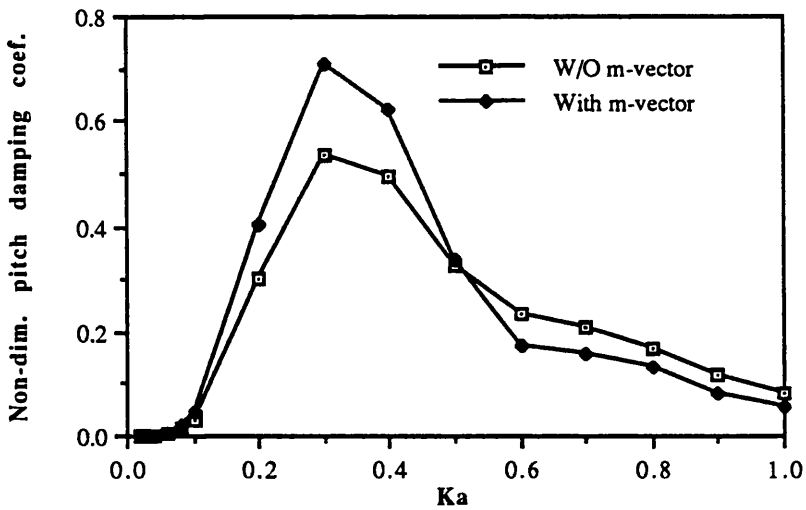

Fig.5.68 Comparison of non-dim. pitch damping coefficients with m-contribution (d/a=2, c/a=4, 5 degree tilt in head waves)

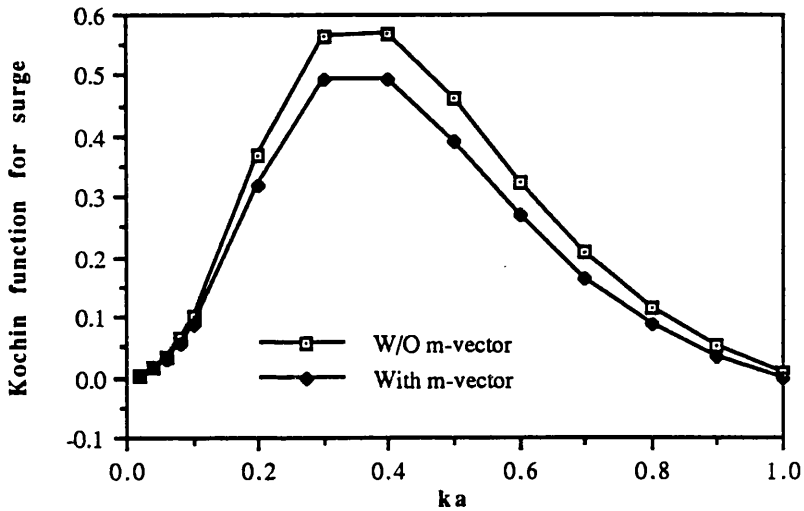

Fig.5.69 Comparison of real part of surge Kochin function with m-vector contribution (d/a=2, c/a=4, 5 degree tilt in head waves)

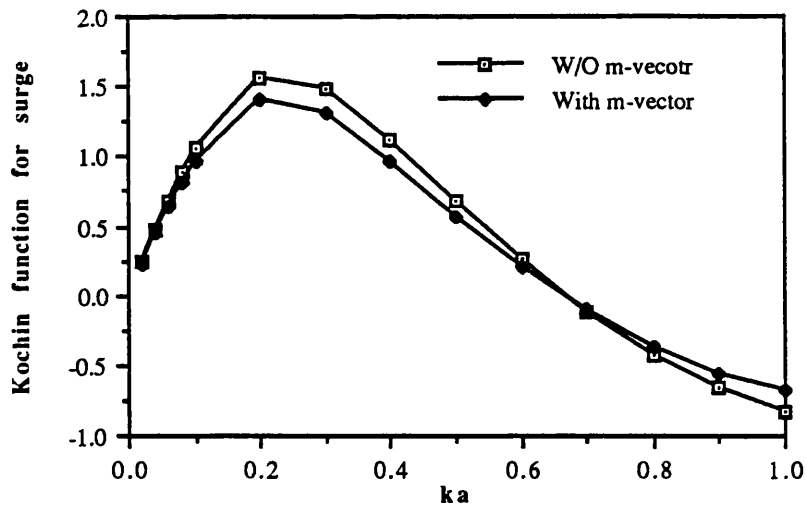

Fig.5.70 Comparison of the imaginary part of surge Kochin function with m-vector (d/a=2, c/a=4, 5 degree tilt in head waves)

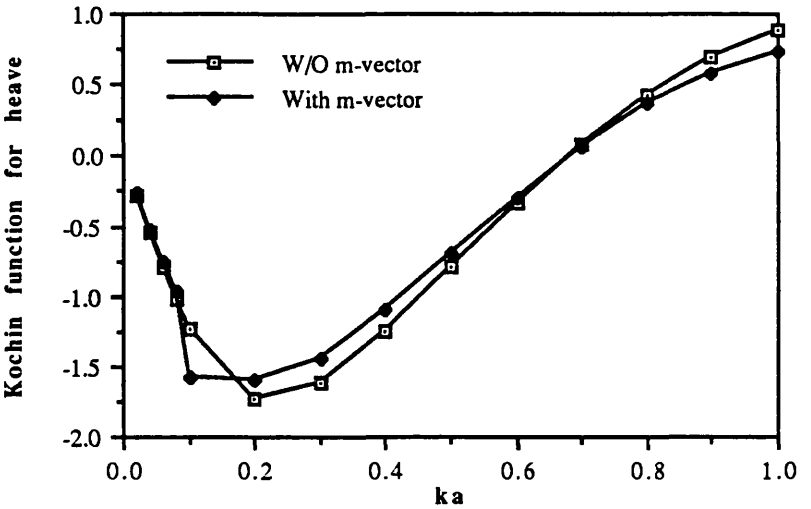

Fig.5.71 Comparison of real part of heave Kochin function with m-vector contribution (d/a=2, c/a=4, 5 degree tilt in head waves)

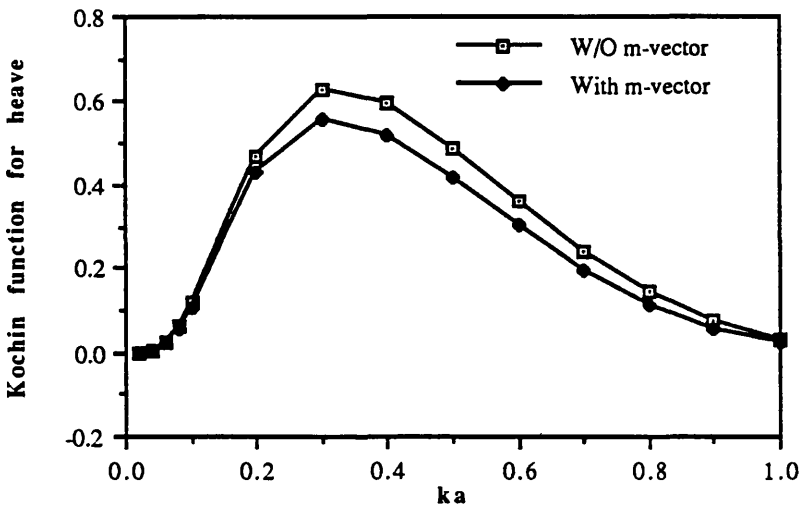

Fig.5.72 Comparison of the imaginary part of heave Kochin function with m-vector (d/a=2, c/a=4, 5 degree tilt in head waves)

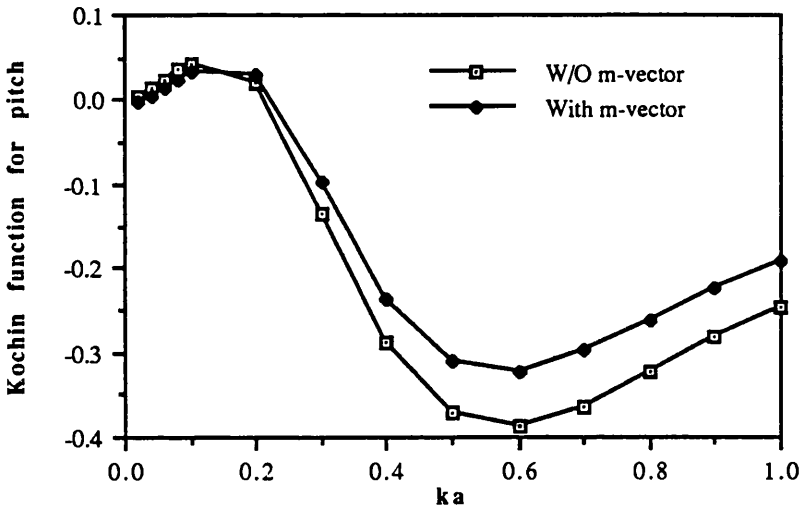

Fig.5.73 Comparison of real part of pitch Kochin function with m-vector contribution (d/a=2, c/a=4, 5 degree tilt in head waves)

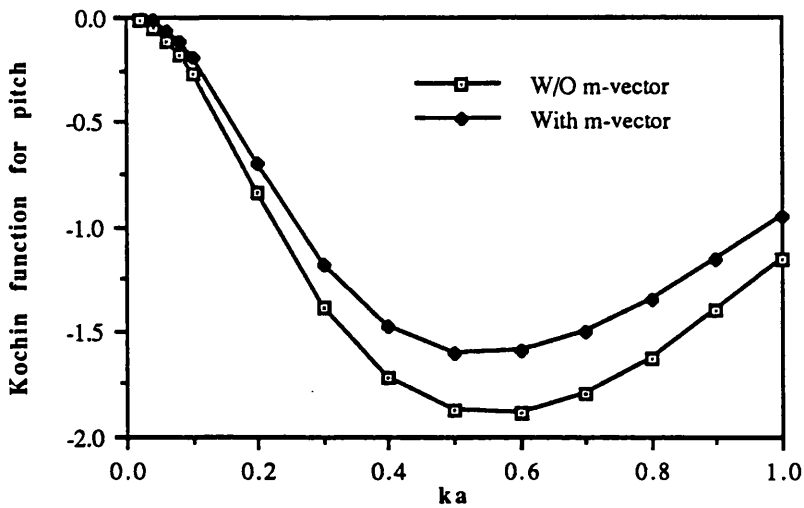

Fig.5.74 Comparison of the imaginary part of pitch Kochin function with m-vector (d/a=2, c/a=4, 5 degree tilt in head waves)

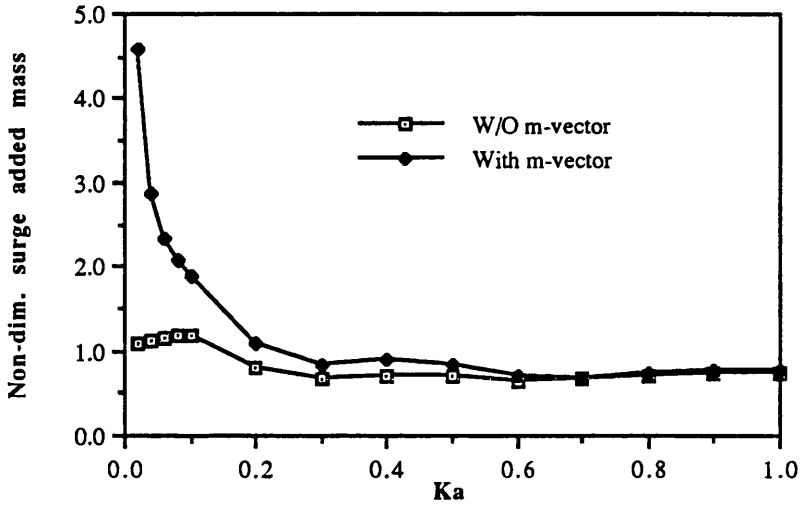

Fig.5.75 Comparison of non-dim. surge added mass coefficients with m-vector (d/a=2, c/a=4, 10 degree inclination)

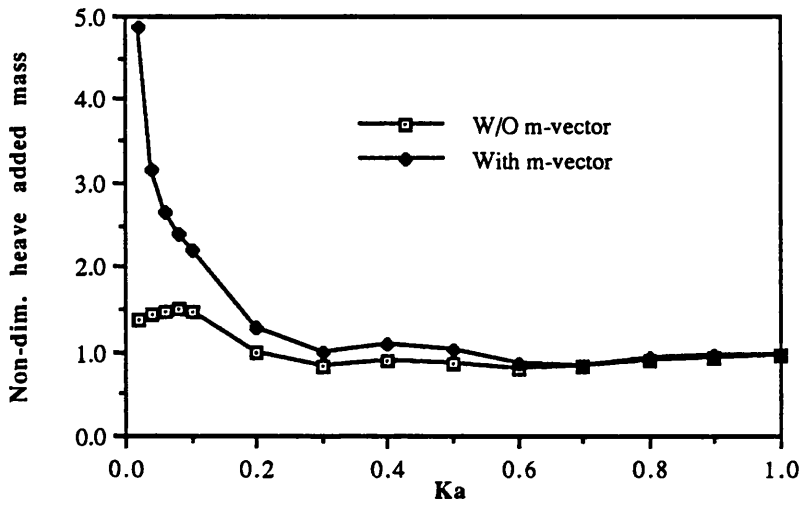

Fig.5.76 Comparison of non-dim. heave added mass coefficients with m-vector (d/a=2, c/a=4, 10 degree inclination)

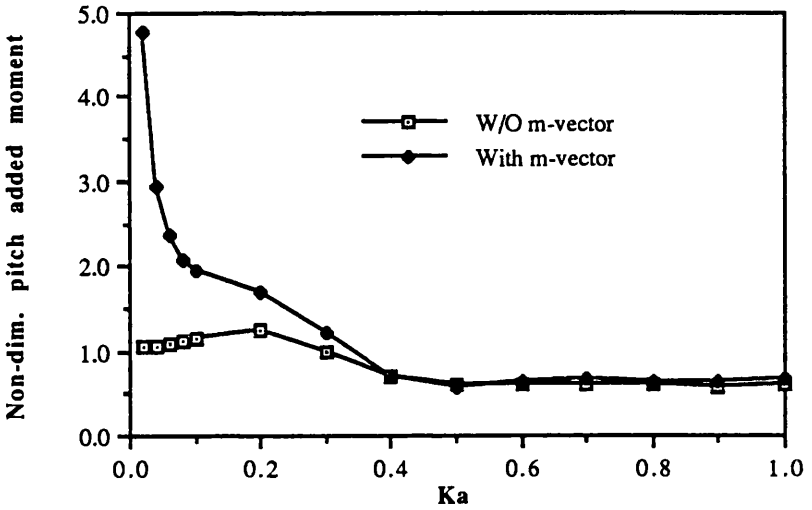

Fig.5.77 Comparison of non-dim. pitch added moment of inertia with m-vector (d/a=2, c/a=4, 10 degree inclination)

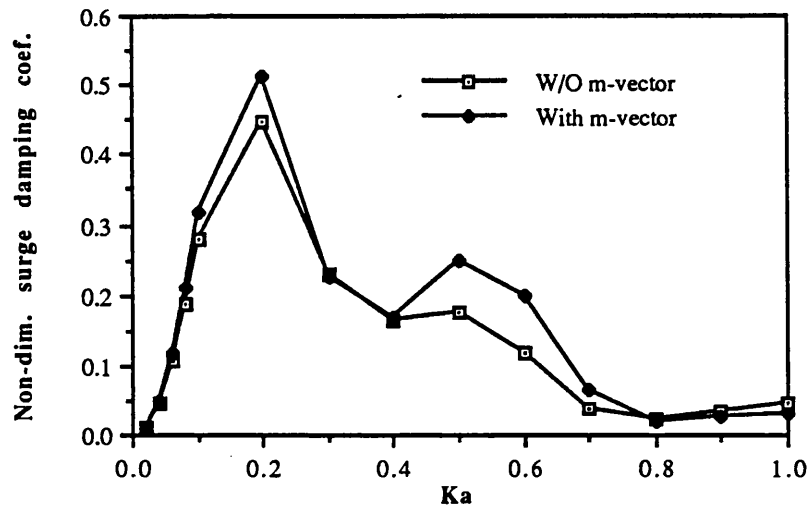

Fig.5.78 Comparison of non-dim. surge damping coefficients with m-contribution (d/a=2,c/a=4, 10 degree tilt in head waves)

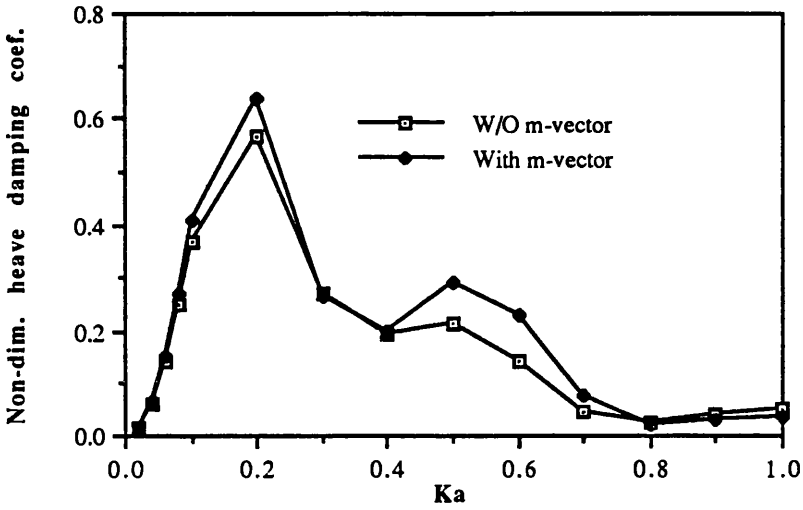

Fig.5.79 Comparison of non-dim. pitch damping coefficients with m-contribution (d/a=2,c/a=4, 10 degree tilt in head waves)

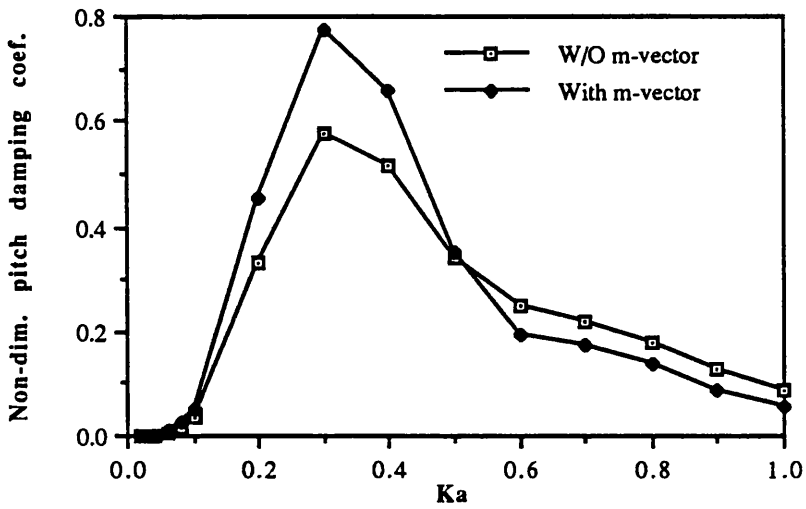

Fig.5.80 Comparison of non-dim. pitch damping coefficients with m-contribution (d/a=2,c/a=4, 10 degree tilt in head waves)

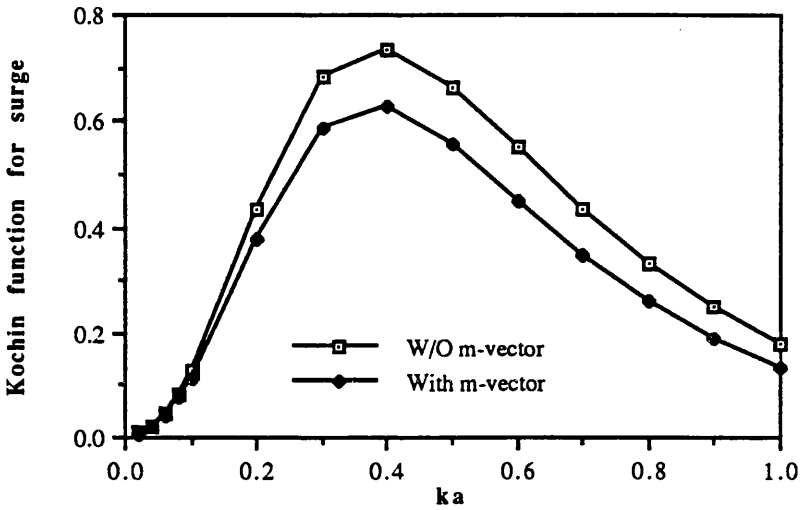

Fig.5.81 Comparison of real part of surge Kochin function with m-vector contribution (d/a=2,c/a=4, 10 degree tilt in head waves)

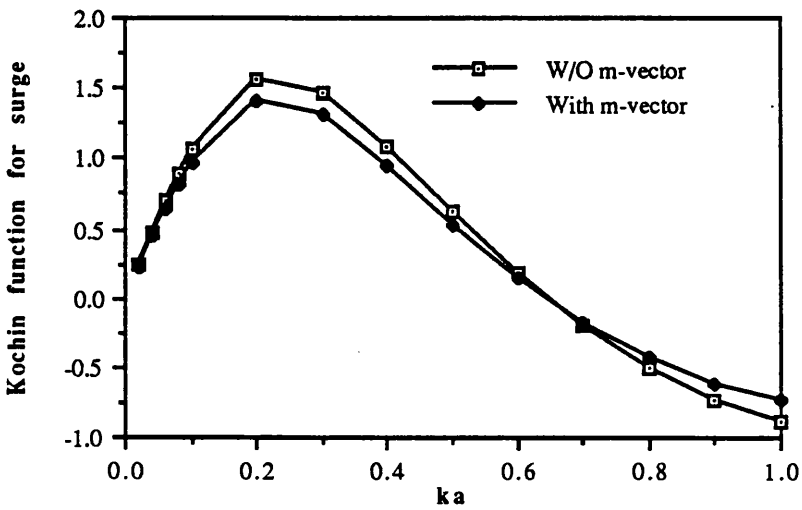

Fig.5.82 Comparison of the imaginary part of surge Kochin function with m-vector (d/a=2,c/a=4, 10 degree tilt in head waves)

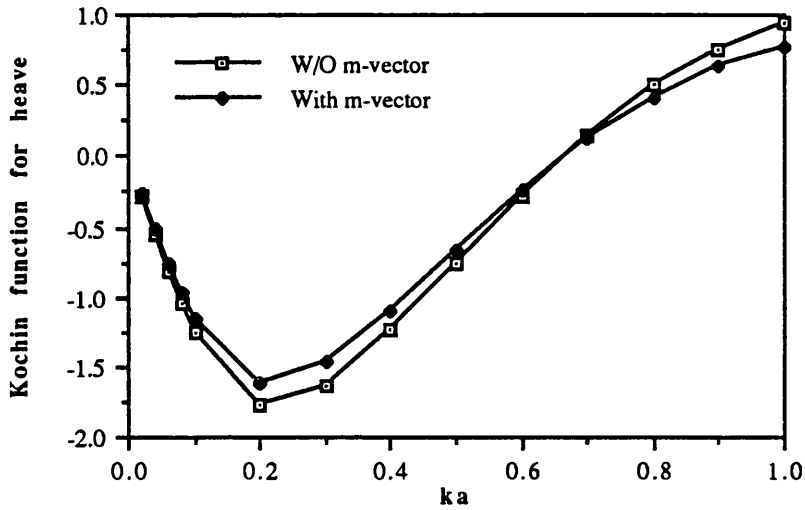

Fig.5.83 Comparison of real part of heave Kochin function with m-vector contribution (d/a=2,c/a=4, 10 degree tilt in head waves)

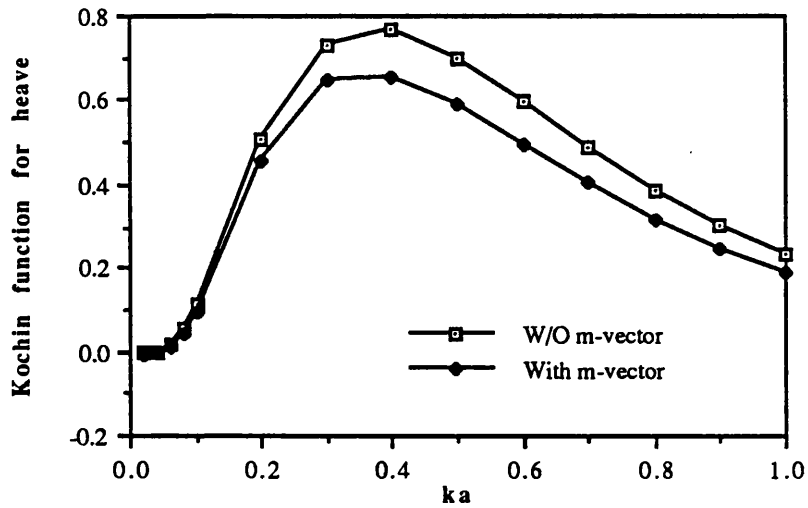

Fig.5.84 Comparison of the imaginary part of heave Kochin function with m-vector (d/a=2,c/a=4, 10 degree tilt in head waves)

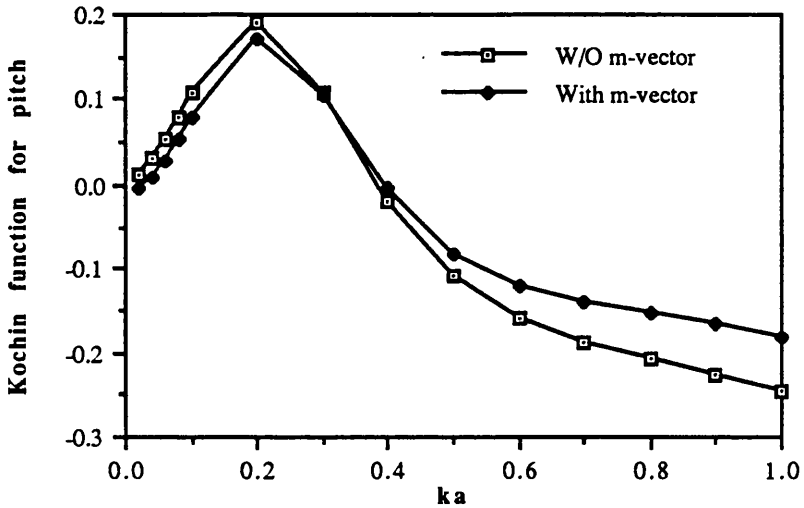

Fig.5.85 Comparison of real part of pitch Kochin function with m-vector contribution (d/a=2,c/a=4, 10 degree tilt in head waves)

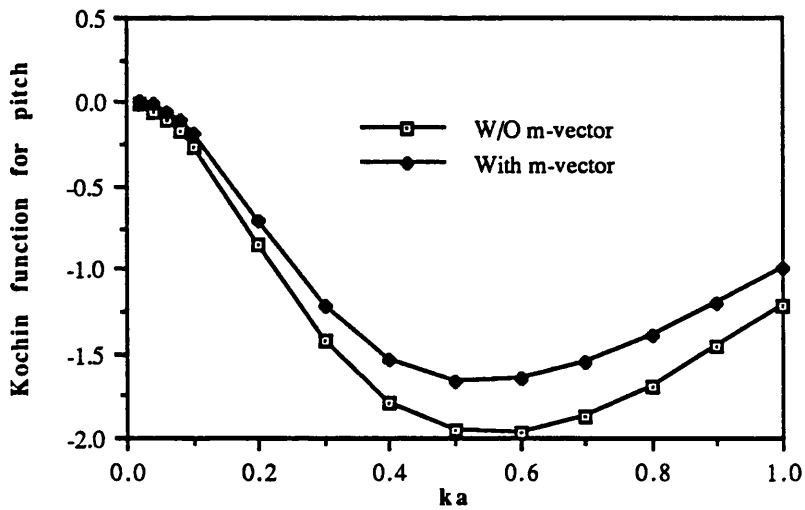

Fig.5.86 Comparison of the imaginary part of pitch Kochin function with m-vector (d/a=2,c/a=4, 10 degree tilt in head waves)

Table 6.1 Comparison of restoring coefficients between single and two cylinders for different separation distances, submerged depths and inclinations

Restoring Coefficients	C11	C12	C21	C22
Single Cylinder Case	-6.28318	0	0	-6.28318
Two Cylinders Case (c/a= 4)	-5.57357	1.65319E-15	8.71258E-17	-5.57357
Two Cylinders Case (c/a= 6)	-5.94529	1.51355E-15	2.80471E-17	-5.94529
Two Cylinders Case (d/a= 2)	-5.57357	1.65319E-15	8.71258E-17	-5.57357
Two Cylinders Case (d/a= 4)	-5.57357	1.65319E-15	8.71258E-17	-5.57357
Two Cylinders Case (0 degree tilt)	-5.57357	1.65319E-15	8.71258E-17	-5.57357
Two Cylinders Case (5 degree tilt)	-5.58581	6.42143E-13	6.40516E-13	-5.58581
Two Cylinders Case (10 degree tilt)	-5.62161	1.27257E-12	1.27107E-12	-5.62161

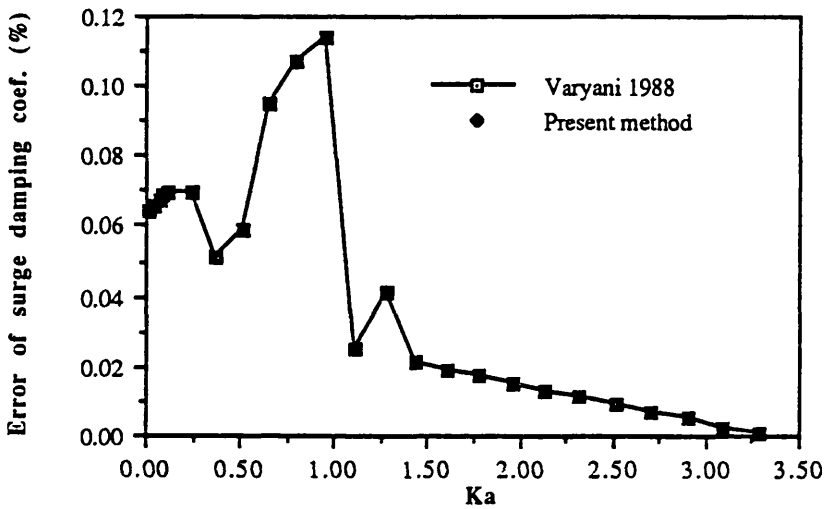

Fig.6.1 Error of surge damping coeffcients (d/a=2.0, c/a=4.0, Fn=0.20, no tilt in head waves)

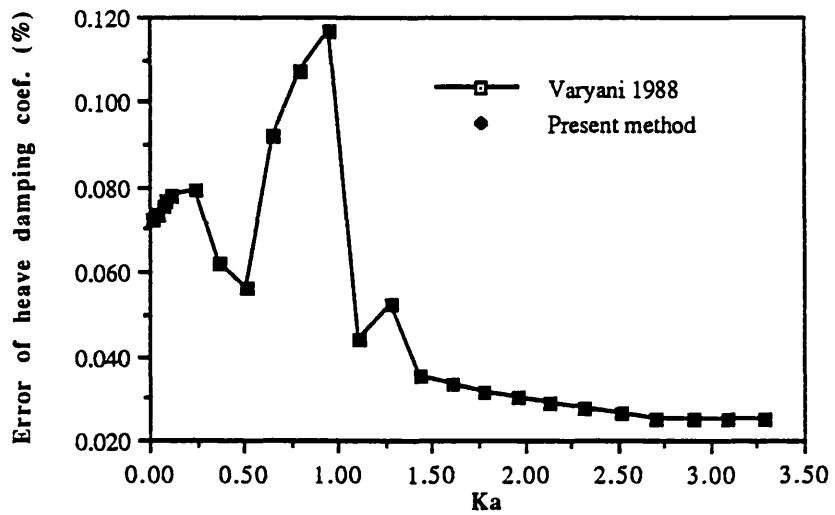

Fig.6.2 Error of heave damping coefficients (d/a=2.0, c/a=4.0, Fn=0.20, no tilt in head waves)

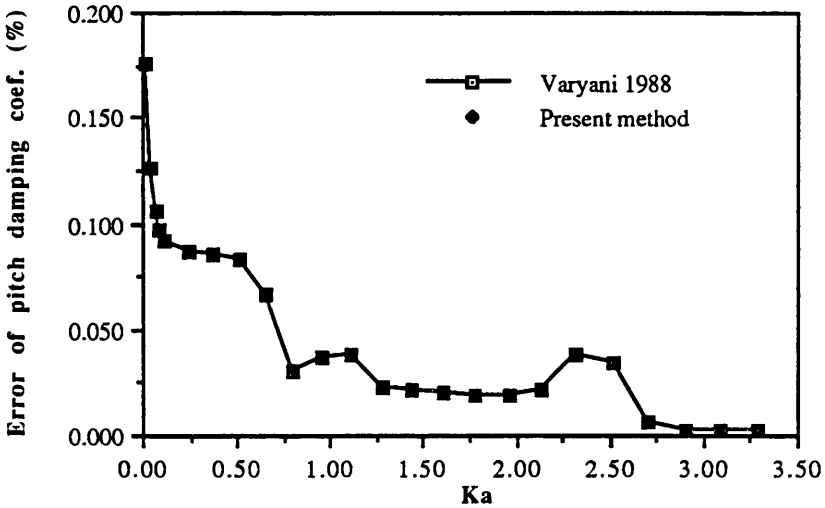

Fig.6.3 Error of pitch damping coefficients (d/a=2.0, c/a=4.0, Fn=0.20, no tilt in head waves)

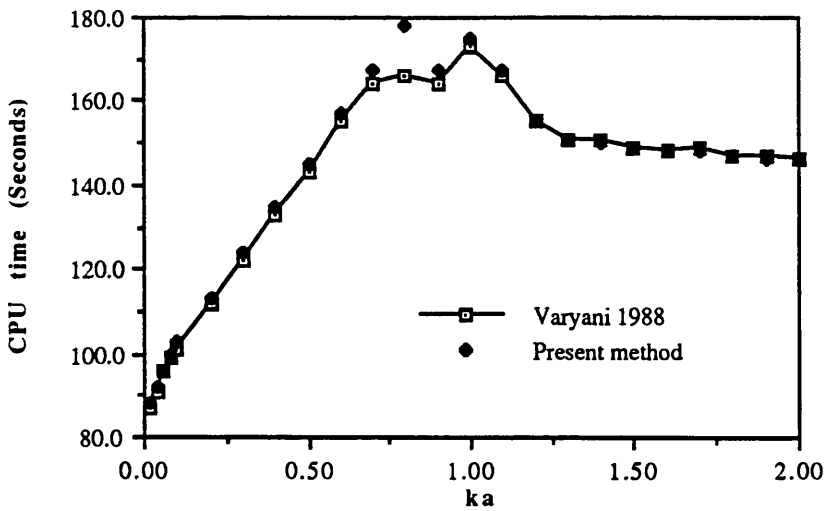

Fig.6.4 Comparison of CPU time for numerical methods (d/a=2,c/a=4,Fn=0.2, no tilt in head waves)

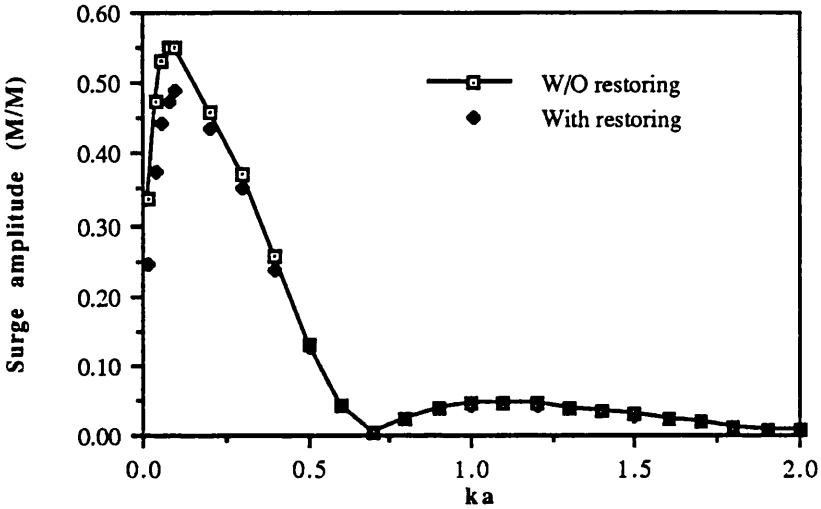

Fig.6.5 Comparison of surge amplitudes (d/a=2.0, c/a=4.0, Fn=0.20, no tilt in head waves)

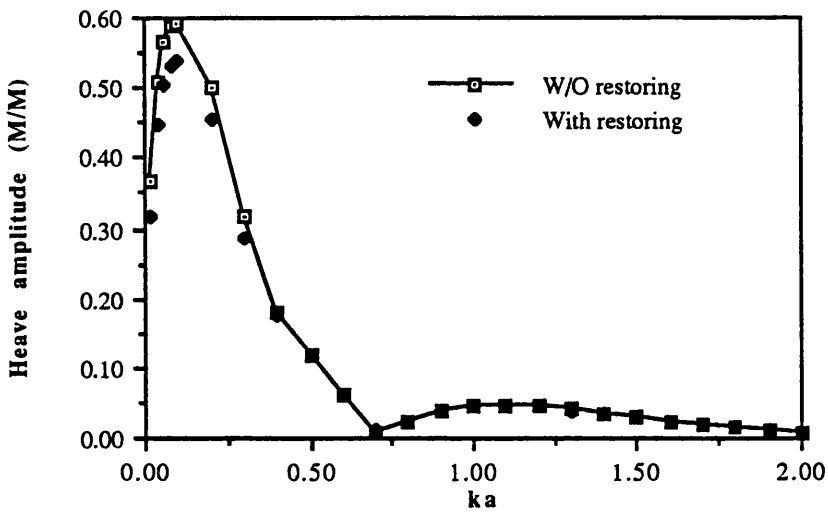

Fig.6.6 Comparison of heave amplitudes (d/a=2.0, c/a=4.0, Fn=0.20, no tilt in head waves)

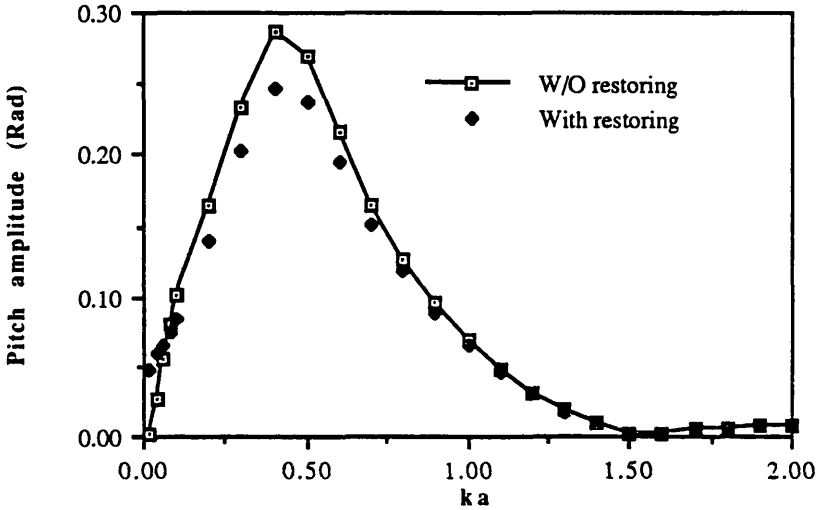

Fig.6.7 Comparison of pitch amplitudes (d/a=2.0, c/a=4.0, Fn=0.20, no tilt in head waves)

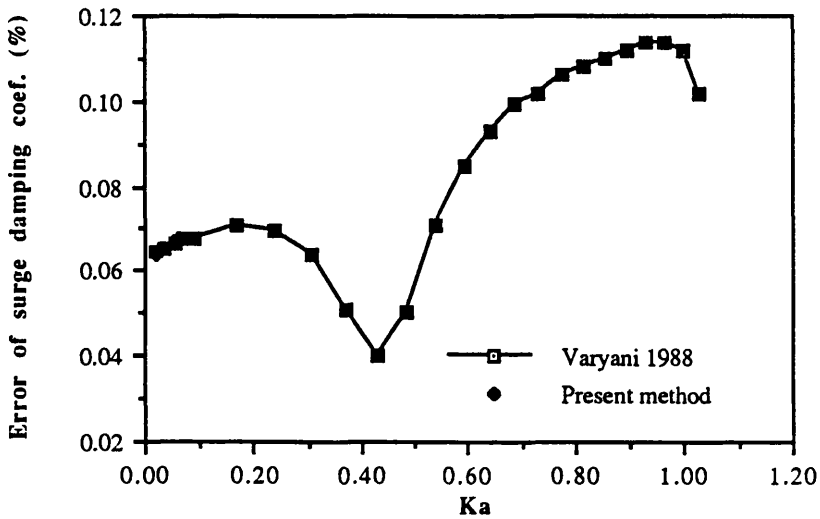

Fig.6.8 Error of surge damping coefficients (d/a=2.0, c/a=4.0, Fn=0.20, no tilt in following waves)

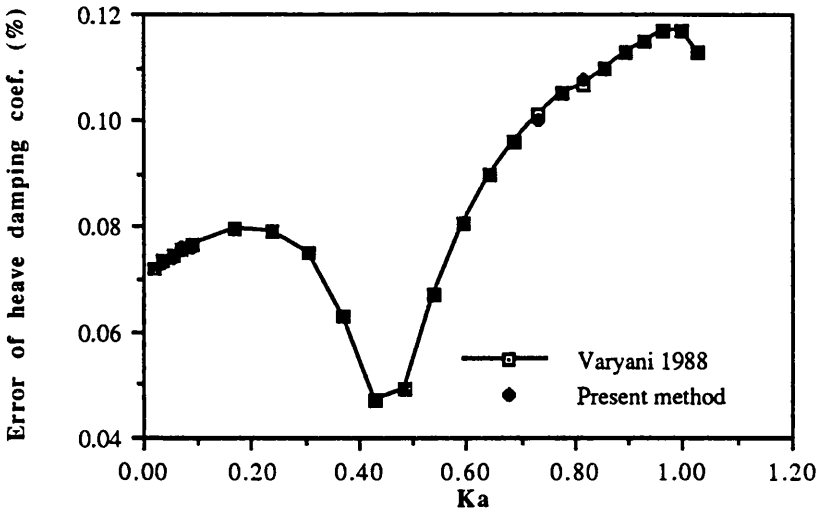

Fig.6.9 Error of heave damping coefficients (d/a=2.0, c/a=4.0, Fn=0.20, no tilt in following waves)

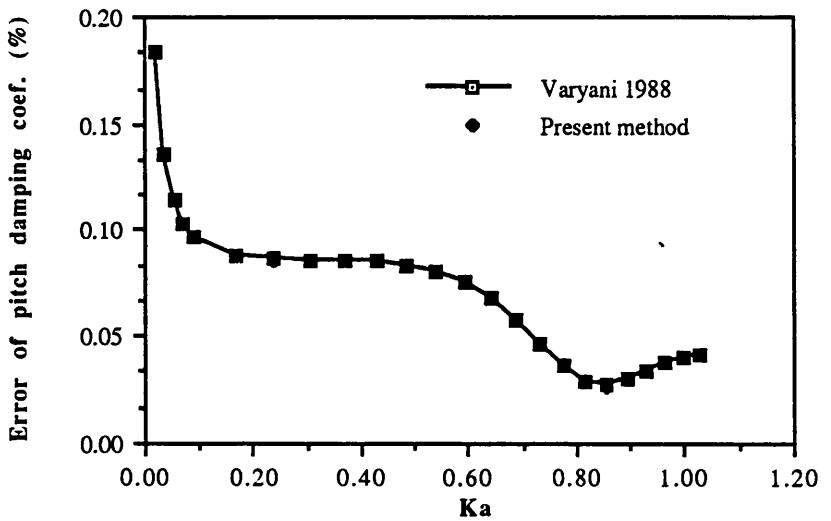

Fig.6.10 Error of pitch damping coefficients (d/a=2.0, c/a=4.0, Fn=0.20, no tilt in following waves)

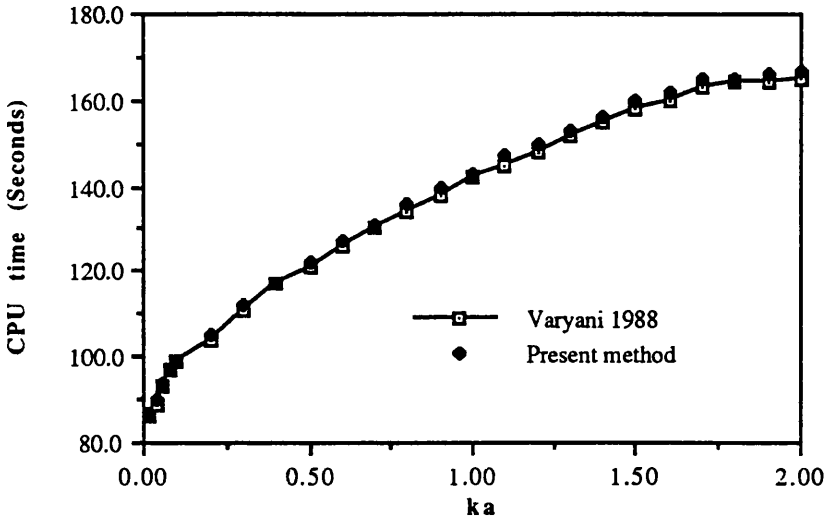

Fig.6.11 Comparison of CPU time for numerical methods (d/a=2,c/a=4,Fn=0.2, no tilt in following waves)

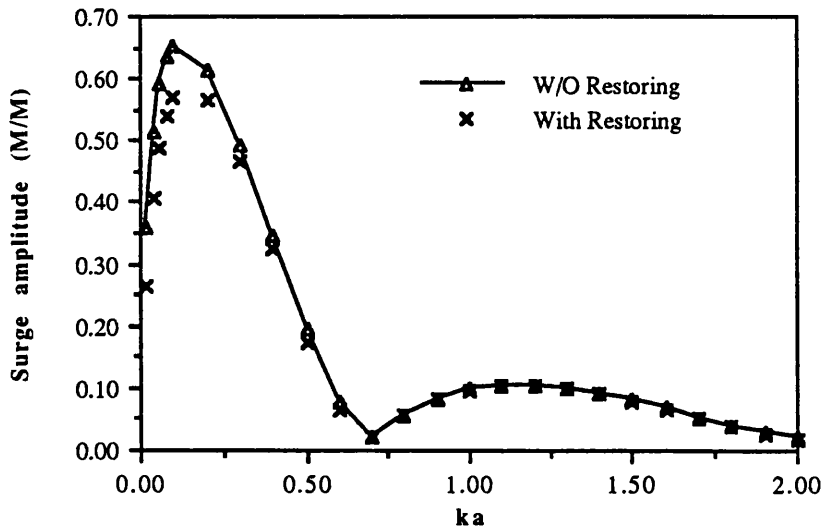

Fig.6.12 Comparison of surge amplitudes (d/a=2.0, c/a=4.0, Fn=0.20, no tilt in following waves)

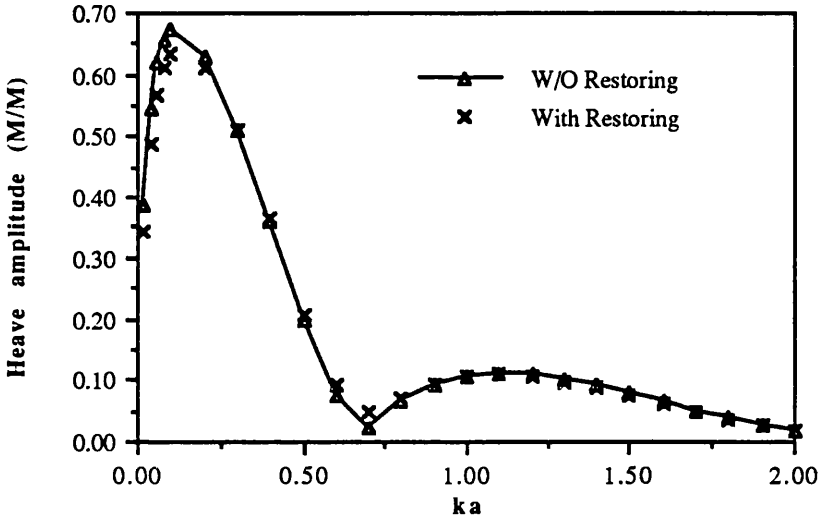

Fig.6.13 Comparison of heave amplitudes (d/a=2.0, c/a=4.0, Fn=0.20, no tilt in following waves)

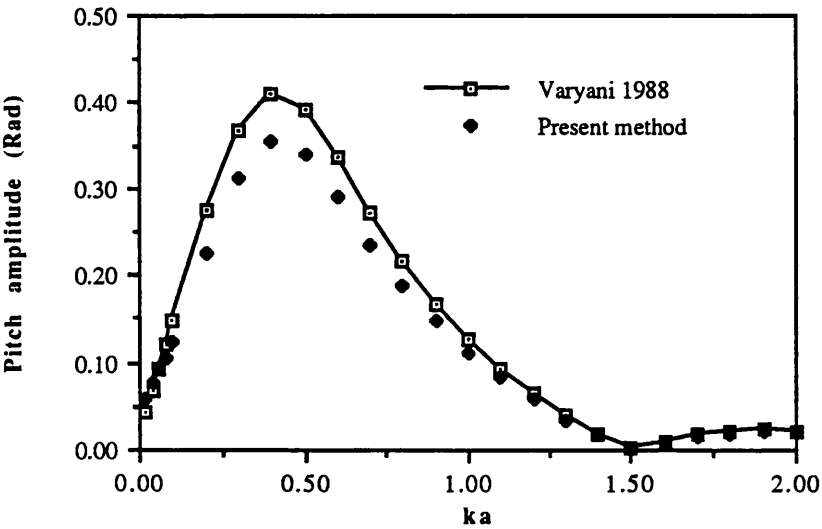

Fig.6.14 Comparison of pitch amplitudes (d/a=2.0, c/a=4.0, Fn=0.20, no tilt in following waves)

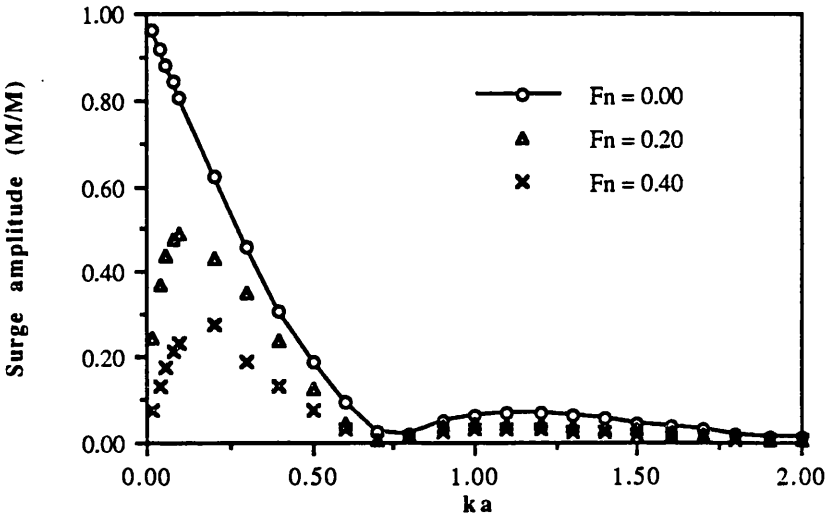

Fig.6.15 Comparison of surge motion amplitudes for different Froude numbers (d/a=2.0, c/a=4.0, no tilt in head waves)

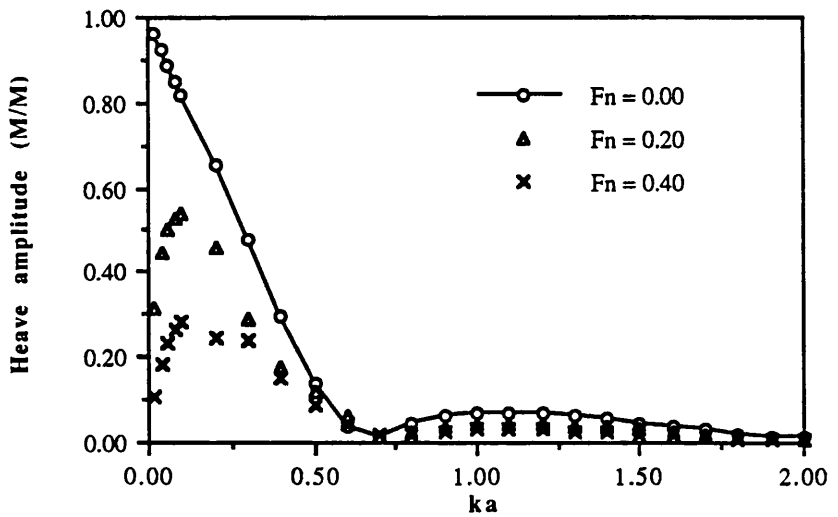

Fig.6.16 Comparison of heave motion amplitudes for different Froude numbers (d/a=2.0, c/a=4.0, no tilt in head waves)

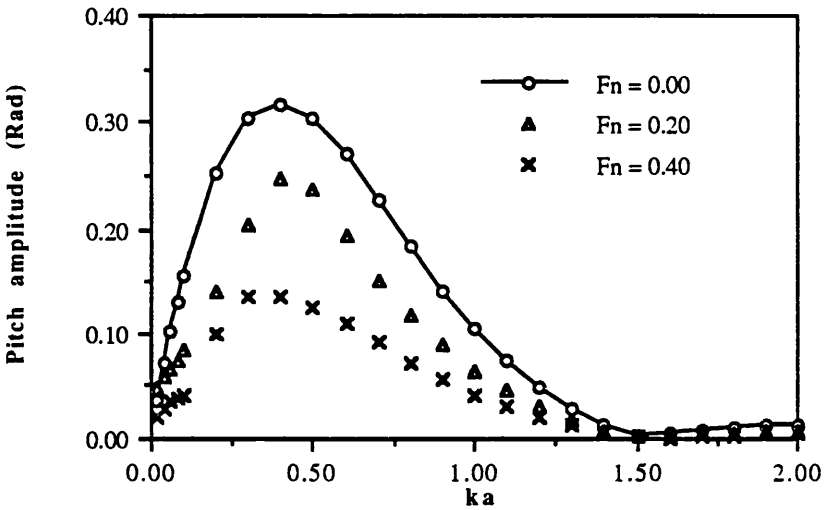

Fig.6.17 Comparison of pitch motion amplitudes for different Froude numbers (d/a=2.0, c/a=4.0, no tilt in head waves)

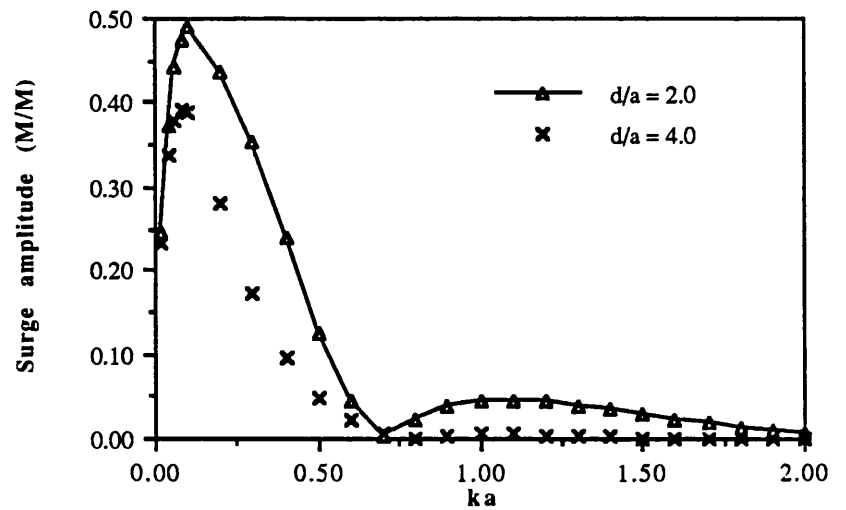

Fig.6.18 Comparison of surge motion amplitudes for different depths (c/a=4.0, Fn=0.20, no tilt in head waves)

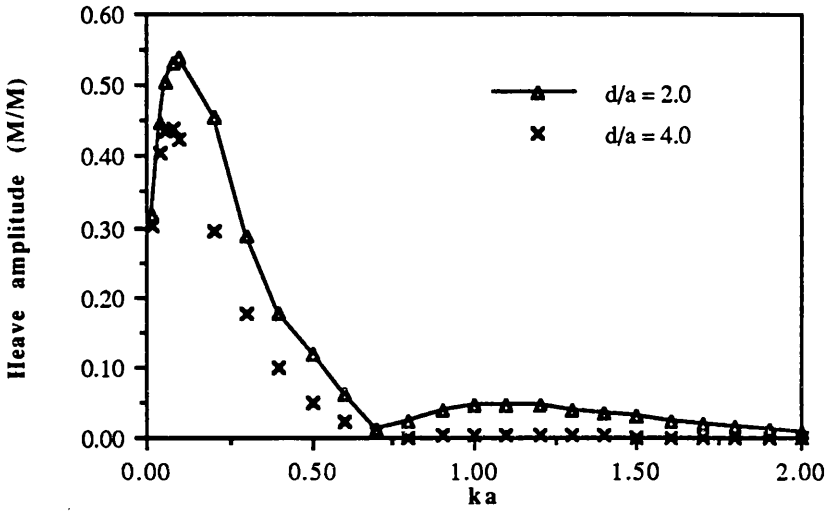

Fig.6.19 Comparison of heave motion amplitudes for different depths (c/a=4.0, Fn=0.20, no tilt in head waves)

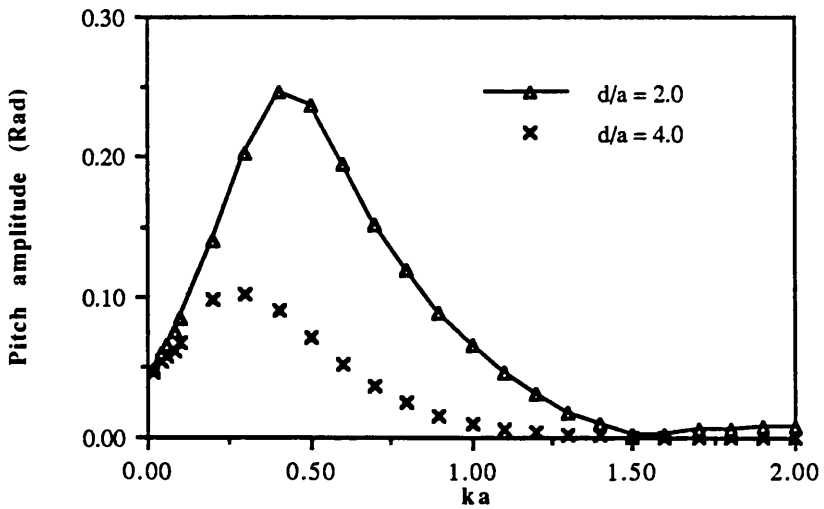

Fig.6.20 Comparison of pitch motion amplitudes for different depths (c/a=4.0, Fn=0.20, no tilt in head waves)

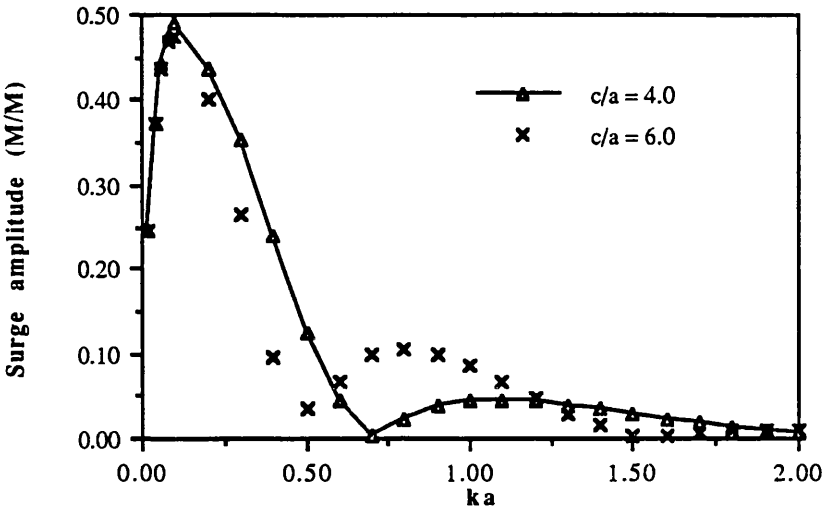

Fig.6.21 Comparison of surge motion amplitudes for different spacings (d/a=2.0, Fn=0.20, no tilt in head waves)

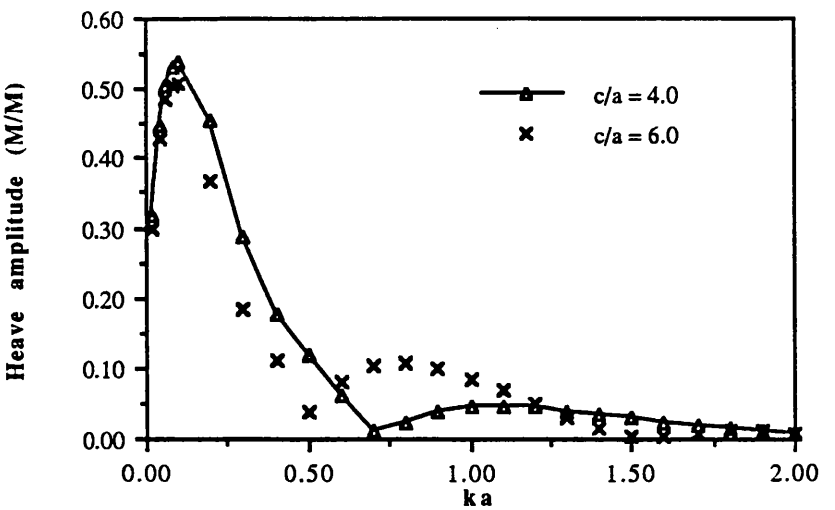

Fig.6.22 Comparison of heave motion amplitudes for different spacings (d/a=2.0, Fn=0.20, no tilt in head waves)

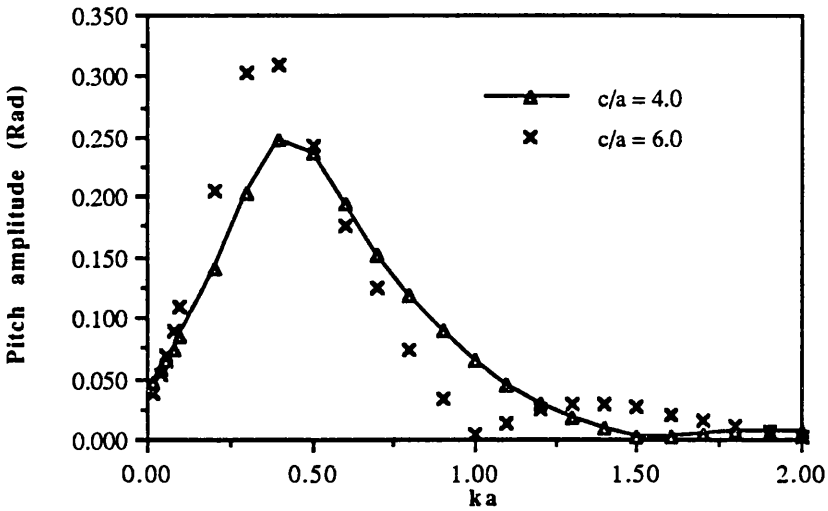

Fig.6.23 Comparison of pitch motion amplitudes for different spacings (d/a=2.0, Fn=0.20, no tilt in head waves)

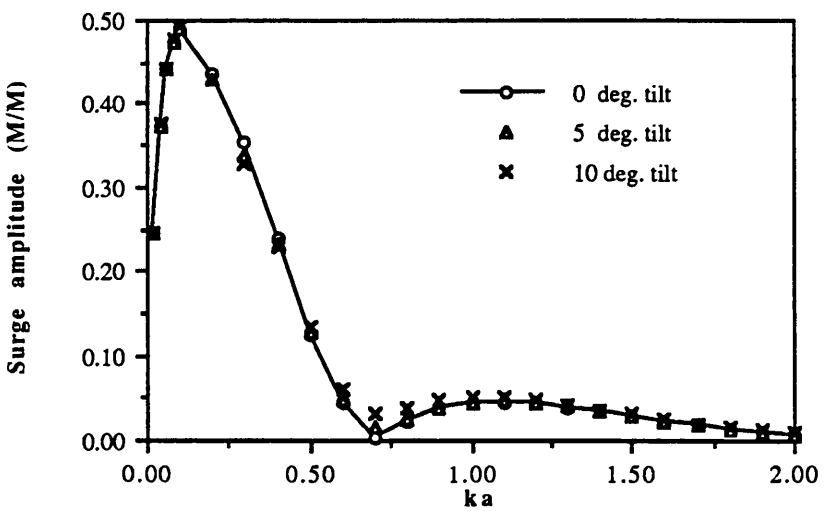

Fig.6.24 Comparison of surge motion amplitudes for different inclinations (d/a=2.0, c/a=4.0, Fn=0.20 in head waves)

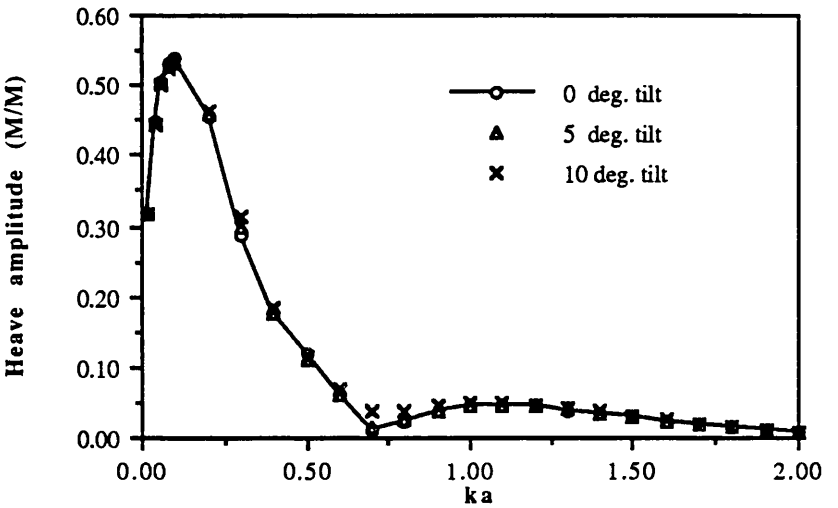

Fig.6.25 Comparison of heave motion amplitudes for different inclinations (d/a=2.0, c/a=4.0, Fn=0.20 in head waves)

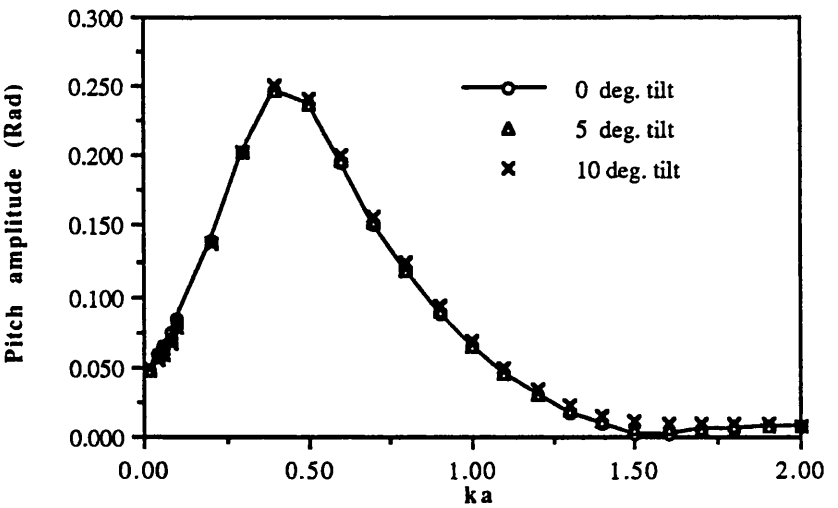

Fig.6.26 Comparison of pitch motion amplitudes for different inclinations (d/a=2.0, c/a=4.0, Fn=0.20 in head waves)

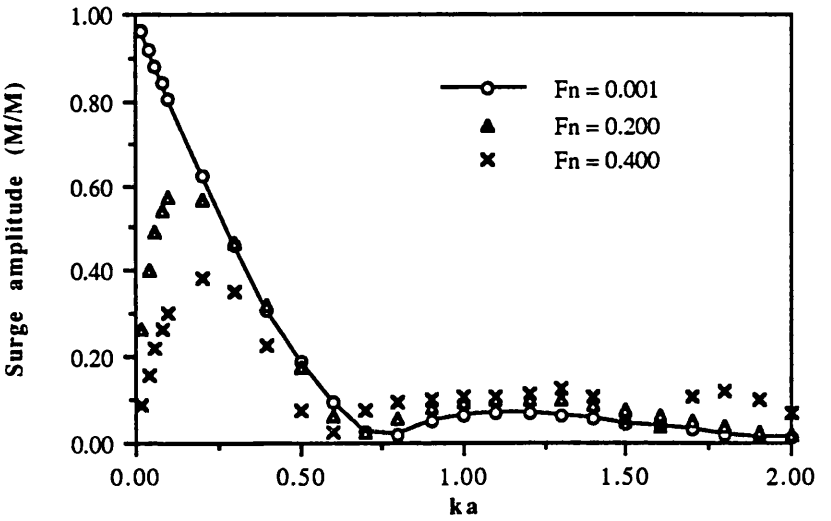

Fig.6.27 Comparison of surge amplitudes for different Froude numbers(d/a=2,c/a=4, no tilt in following waves)

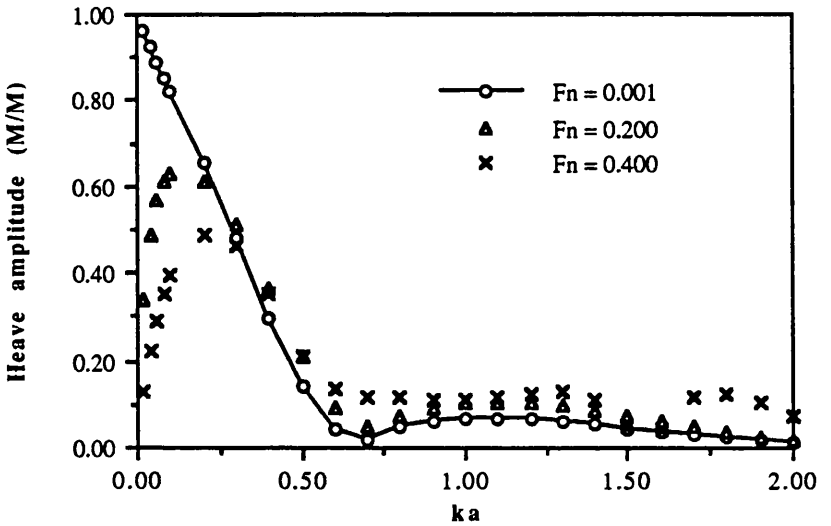

Fig.6.28 Comparison of heave amplitudes for different Froude numbers(d/a=2,c/a=4, no tilt in following waves)

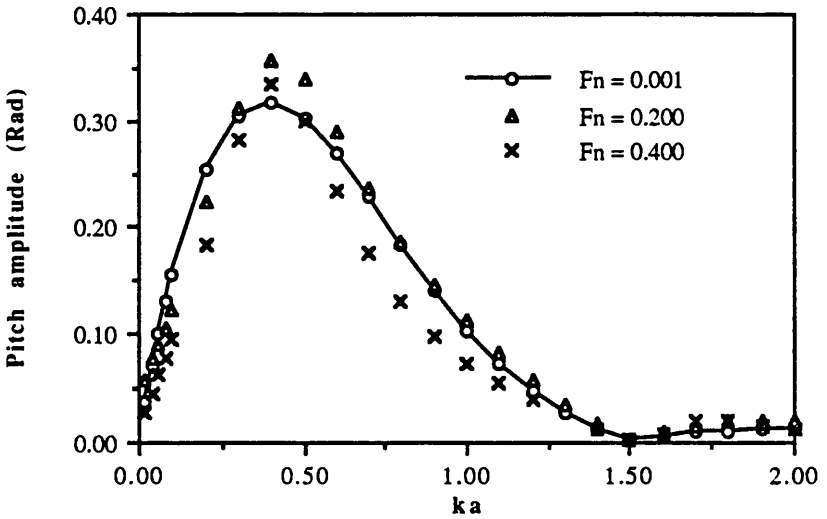

Fig.6.29 Comparison of pitch amplitudes for different Froude numbers(d/a=2,c/a=4, no tilt in following waves)

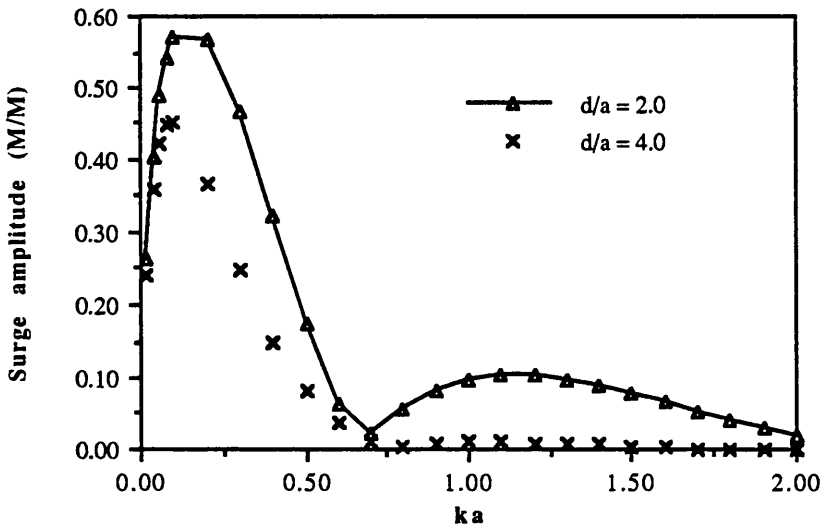

Fig.6.30 Comparison of surge amplitudes for different depths(c/a=4.0, Fn=0.20, no tilt in following waves)

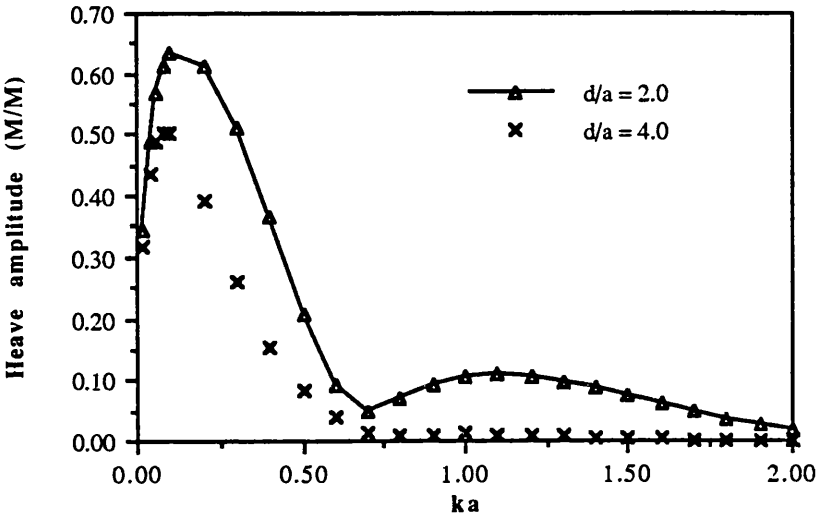

Fig.6.31 Comparison of heave amplitudes for different depths(c/a=4.0, Fn=0.20, no tilt in following waves)

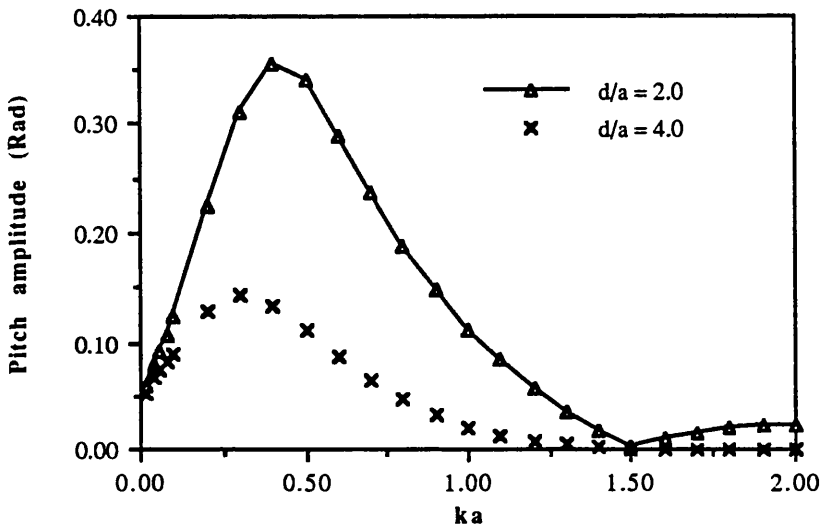

Fig.6.32 Comparison of pitch amplitudes for different depths(c/a=4.0, Fn=0.20, no tilt in following waves)

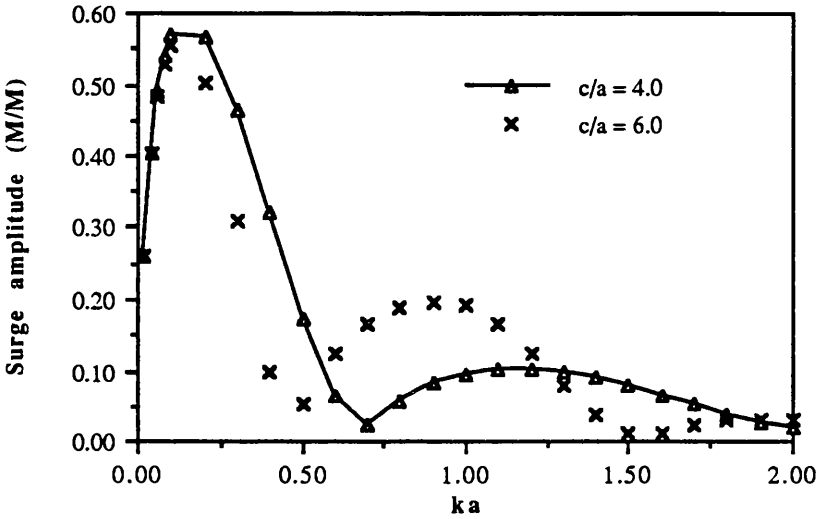

Fig.6.33 Comparison of surge amplitudes for different separation distances(d/a=2.0, Fn=0.20, no tilt in following waves)

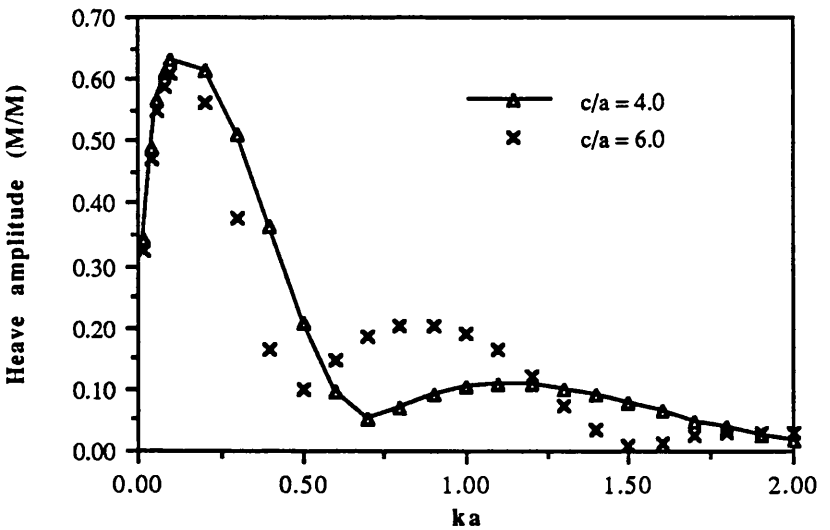

Fig.6.34 Comparison of heave amplitudes for different separation distances(d/a=2.0, Fn=0.20, no tilt in following waves)

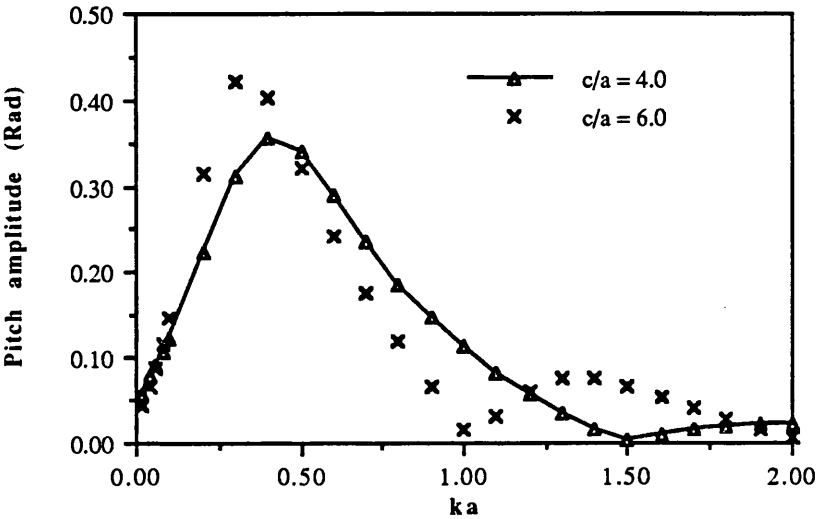

Fig.6.35 Comparison of pitch amplitudes for different separation distances(d/a=2.0, Fn=0.20, no tilt in following waves)

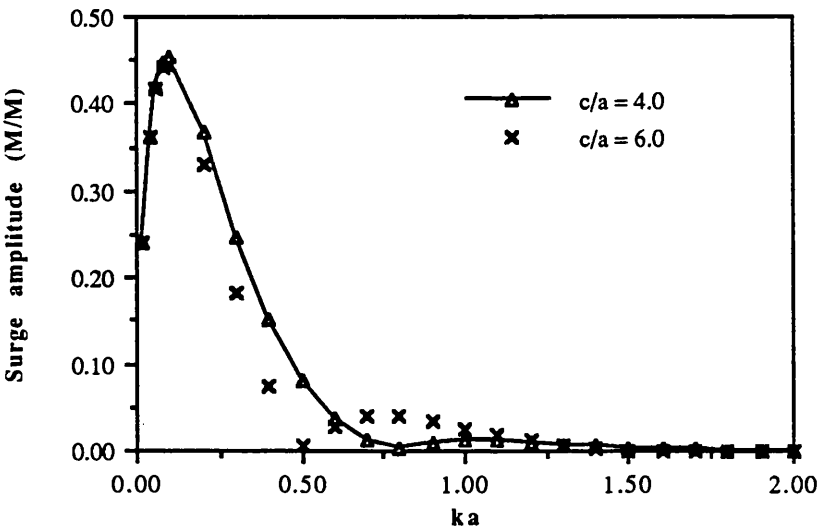

Fig.6.36 Comparison of surge amplitudes for different separation distances(d/a=4.0, Fn=0.20, no tilt in following waves)

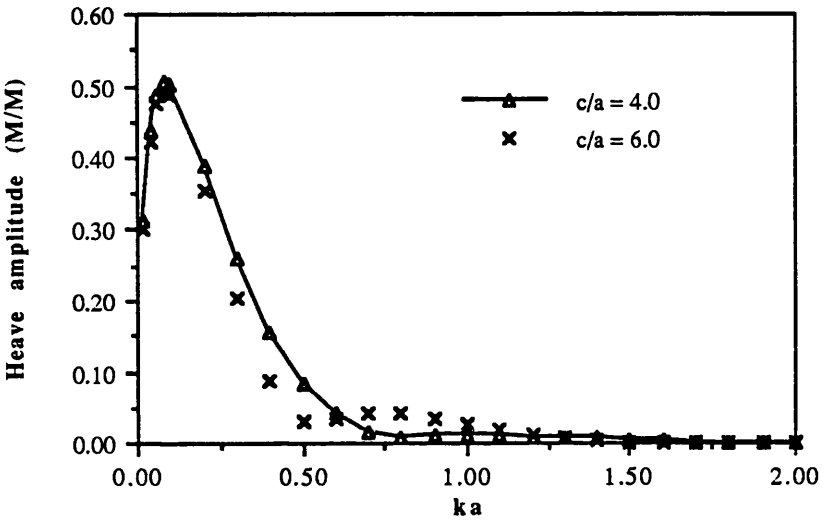

Fig.6.37 Comparison of heave amplitudes for different separationdistances(d/a=4.0, Fn=0.20, no tilt in following waves)

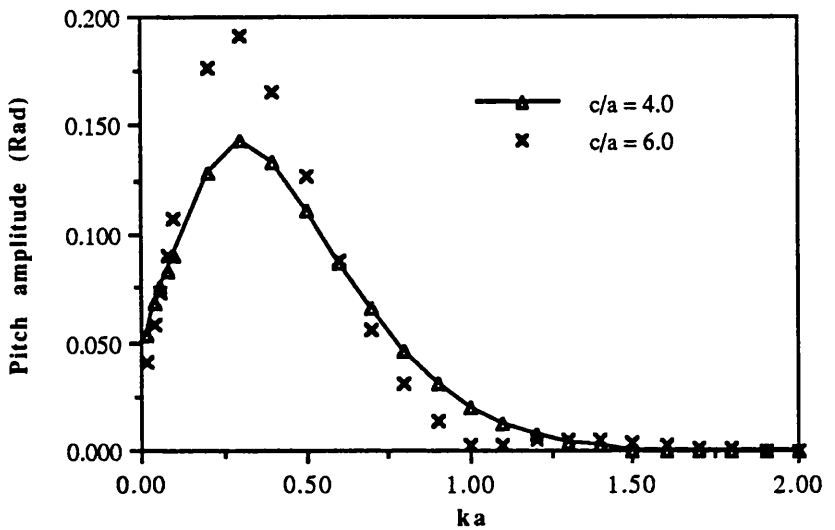

Fig.6.38 Comparison of pitch amplitudes for different separation distances(d/a=4.0, Fn=0.20, no tilt in following waves)

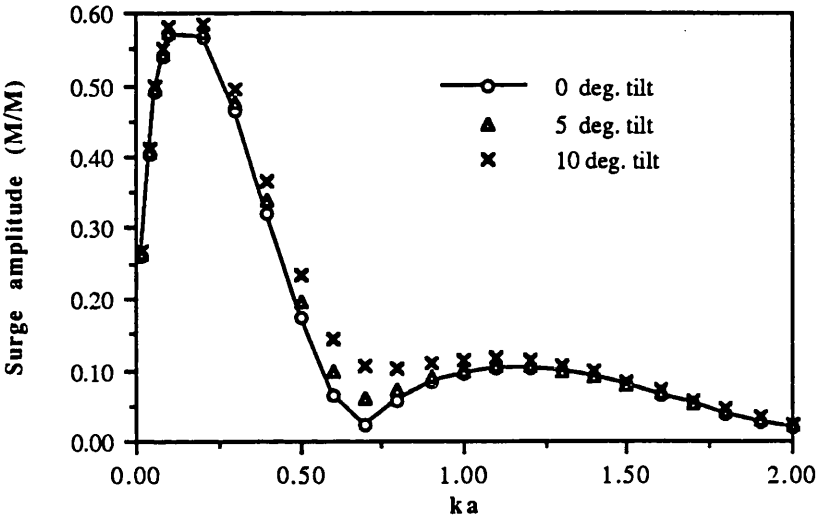

Fig.6.39 Comparison of surge amplitudes for different inclinations (d/a=2.0, c/a=4.0, Fn=0.20 in following waves)

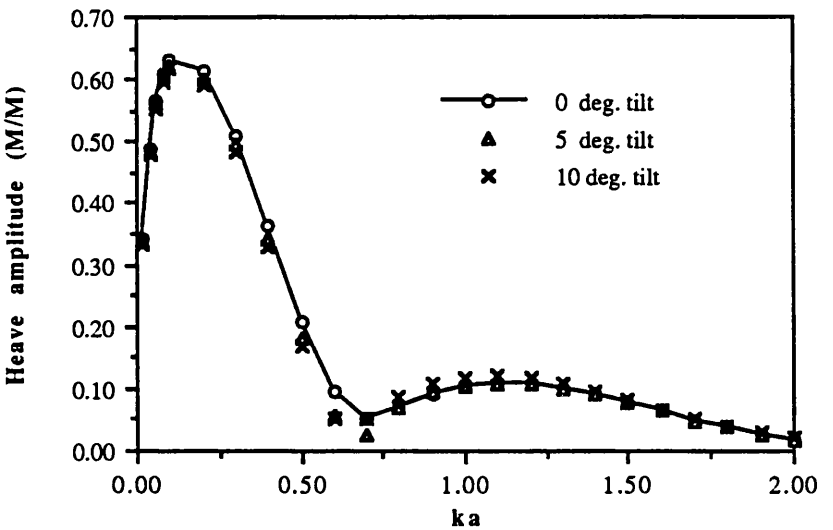

Fig.6.40 Comparison of heave amplitudes for different inclinations (d/a=2.0, c/a=4.0, Fn=0.20 in following waves)

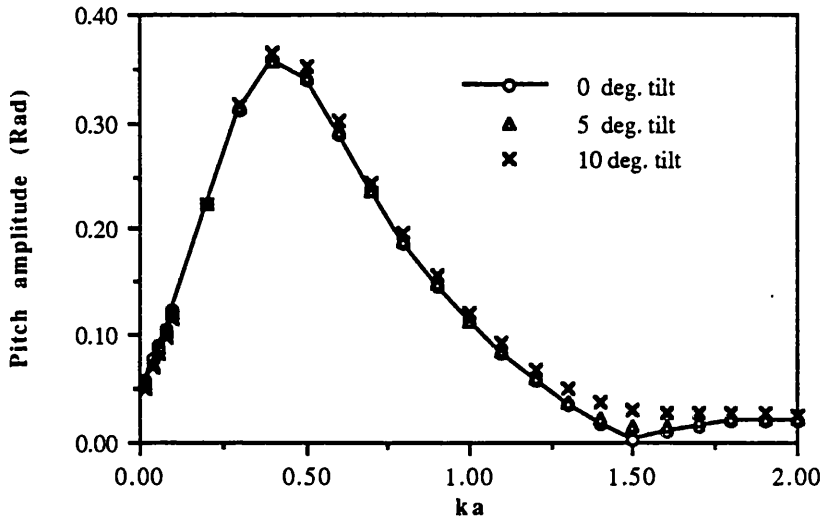

Fig.6.41 Comparison of pitch amplitudes for different inclinations (d/a=2.0, c/a=4.0, Fn=0.20 in following waves)

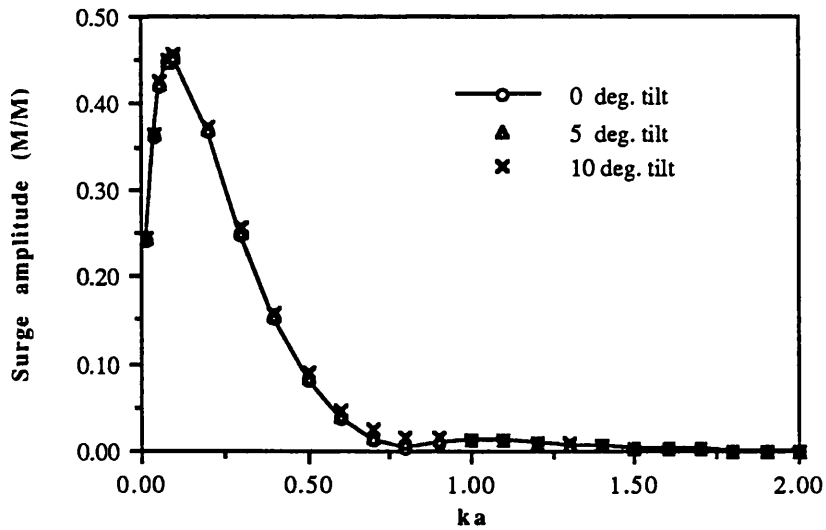

Fig.6.42 Comparison of surge amplitudes for different inclinations (d/a=4.0, c/a=4.0, Fn=0.20 in following waves)

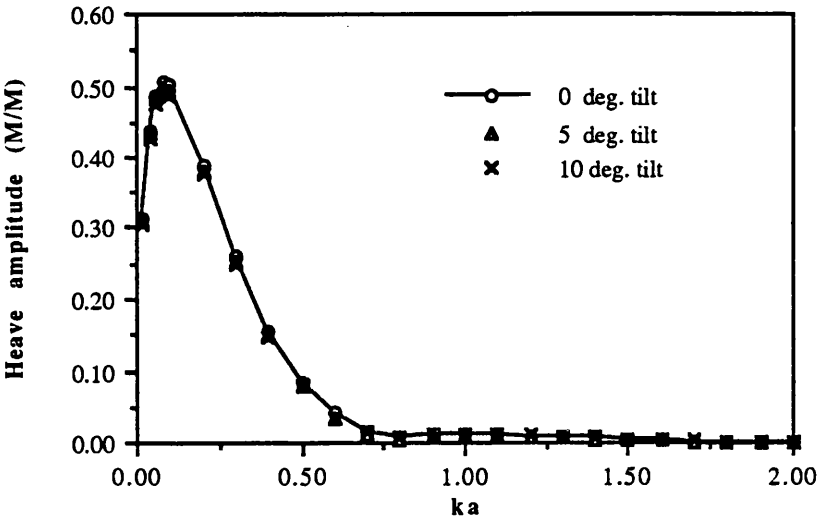

Fig.6.43 Comparison of heave amplitudes for different inclinations (d/a=4.0, c/a=4.0, Fn=0.20 in following waves)

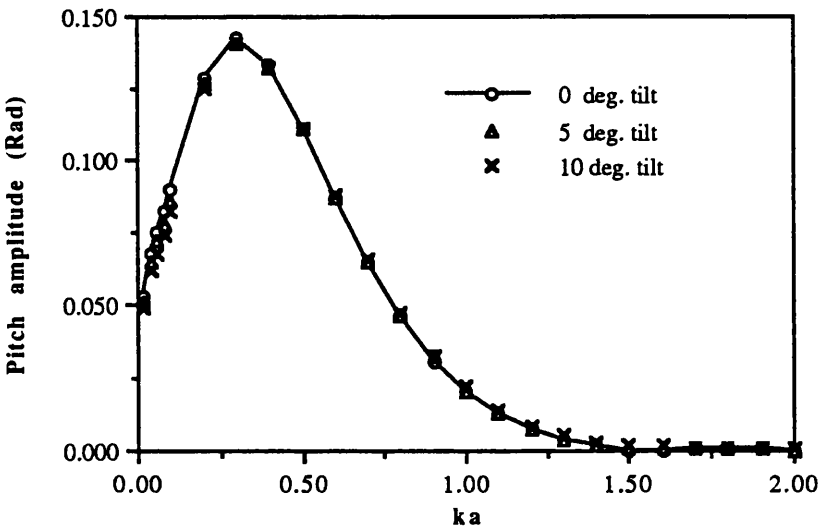

Fig.6.44 Comparison of pitch amplitudes for different inclinations (d/a=4.0, c/a=4.0, Fn=0.20 in following waves)

Table 7.1 Accuracy check of non-dimensionalized second order horizontal forces on submerged twin cylinders for different Froude numbers (d/a = 2.0, c/a = 4.0, no tilt in head waves)

Second order X forces	ka = 0.02	ka = 0.04	ka = 0.06	ka = 0.08	ka = 0.10	ka = 0.20	ka = 0.30	ka = 0.40
Fn=0.0 (Approx.)	4.88092E-07	7.35776E-06	3.48146E-05	0.000101288	0.000223212	0.00156039	0.00250893	0.00246412
Fn=0.0 (Press. Integ.)	4.02101E-07	6.69165E-06	3.26455E-05	9.63625E-05	0.000214085	0.00151234	0.00242036	0.00235715
Fn=0.2 (Approx.)	7.02209E-07	1.23886E-05	6.60805E-05	0.000210465	0.000492202	0.00293952	0.00295158	0.00160501
Fn=0.2 (Press. Integ.)	6.27455E-07	1.18691E-05	6.45522E-05	0.000207327	0.000486913	0.00291527	0.00290032	0.00153785
Fn=0.4 (Approx.)	1.09383E-06	2.43688E-05	0.000160316	0.000599693	0.00147695	0.00110611	5.98097E-12	4.65751E-12
Fn=0.4 (Press. Integ.)	1.01996E-06	2.39397E-05	0.000159394	0.000598702	0.00147696	0.00108642	4.24433E-05	4.92676E-05

ka = 0.50	ka = 0.60	ka = 0.70	ka = 0.80	ka = 0.90	ka = 1.00	ka = 1.10	ka = 1.20	ka = 1.30	ka = 1.40
0.00204911	0.00160056	0.00121015	0.000891435	0.000639409	0.000445602	0.000301048	0.000196833	0.000124419	7.60231E-05
0.00194406	0.00150918	0.00113685	0.000835927	0.000599018	0.000416884	0.000280769	0.000182406	0.000113983	6.83319E-05
0.000542326	7.33247E-05	3.55461E-06	3.47571E-05	1.18665E-05	2.76428E-09	2.41095E-35	9.79473E-35	2.93509E-35	5.96349E-37
0.000474358	1.42896E-05	4.28525E-05	5.53402E-07	1.24033E-05	1.68249E-05	1.16125E-05	8.12513E-06	5.82721E-06	4.28696E-06
8.95092E-13	3.53067E-14	1.23215E-14	2.66055E-14	1.53229E-14	4.89749E-15	8.50112E-16	2.91687E-17	2.85962E-17	6.93459E-17
4.71595E-05	3.99301E-05	3.10063E-05	2.26019E-05	1.57793E-05	1.07761E-05	7.36469E-06	5.14148E-06	3.70911E-06	2.76602E-06

ka = 1.50	ka = 1.60	ka = 1.70	ka = 1.80	ka = 1.90	ka = 2.00
4.49482E-05	2.57783E-05	1.44008E-05	7.88351E-06	4.26199E-06	2.29567E-06
3.92012E-05	2.14623E-05	1.11722E-05	5.49565E-06	2.52426E-06	1.05465E-06
1.80171E-36	2.07805E-36	5.65956E-37	0	0	6.13618E-38
3.20908E-06	2.41486E-06	1.80599E-06	1.33109E-06	9.62003E-07	6.80171E-07
5.72918E-17	3.06043E-17	1.19628E-17	3.35788E-18	5.45337E-19	8.69155E-21
2.09325E-06	1.59281E-06	1.20028E-06	8.87978E-07	6.41971E-07	4.52783E-07

Table 7.2 Accuracy check of non-dimensionalized second order vertical forces on submerged twin cylinders for different Froude numbers (d/a = 2.0, c/a = 4.0, no tilt in head waves)

Second order Y forces	ka = 0.02	ka = 0.04	ka = 0.06	ka = 0.08	ka = 0.10	ka = 0.20	ka = 0.30	ka = 0.40
Fn=0.0 (Lee-Newman)	0.0101411	0.0381841	0.0805533	0.133426	0.192752	0.467207	0.605196	0.674807
Fn=0.0 (Press. Integ.)	0.0266559	0.0769523	0.148518	0.237786	0.339911	0.848421	1.08838	1.11451
Fn=0.2 (Lee-Newman)	0.0261039	0.0675612	0.121589	0.184181	0.249939	0.484663	0.648626	0.811922
Fn=0.2 (Press. Integ.)	0.0254976	0.0720815	0.137235	0.217239	0.307504	0.752575	0.988649	1.04635
Fn=0.4 (Lee-Newman)	0.0713323	0.149372	0.235511	0.323149	0.393701	0.743427	0.706493	0.861939
Fn=0.4 (Press. Integ.)	0.0264741	0.0717061	0.133658	0.208749	0.292333	0.696388	0.931257	1.00816

ka = 0.50	ka = 0.60	ka = 0.70	ka = 0.80	ka = 0.90	ka = 1.00	ka = 1.10	ka = 1.20	ka = 1.30	ka = 1.40
0.717992	0.726634	0.692888	0.623422	0.533634	0.439144	0.351042	0.275041	0.212714	0.163201
1.058851	0.978606	0.892337	0.806031	0.722092	0.641917	0.566504	0.496574	0.432591	0.374775
0.834661	0.744938	0.667384	0.607461	0.522523	0.434073	0.351789	0.279825	0.219437	0.170166
1.02121	0.962774	0.890938	0.813786	0.735314	0.657962	0.583428	0.513031	0.447735	0.388169
0.885068	0.844083	0.764396	0.664981	0.560293	0.460204	0.370405	0.293348	0.229315	0.177352
1.00132	0.955883	0.892479	0.820529	0.744936	0.668781	0.594303	0.523227	0.456835	0.396002

ka = 1.50	ka = 1.60	ka = 1.70	ka = 1.80	ka = 1.90	ka = 2.00
0.124582	0.0947467	0.0717972	0.0541849	0.0407008	0.0304135
0.323142	0.277521	0.237591	0.202925	0.173018	0.147337
0.130756	0.0996906	0.0754792	0.0567851	0.0424688	0.0315869
0.334644	0.287194	0.245612	0.209517	0.178411	0.151733
0.135931	0.103369	0.0780597	0.0585751	0.0436997	0.0324285
0.341212	0.292599	0.250011	0.213071	0.181272	0.154033

Table 7.3 Comparison of non-dimensionalized steady tilt moments on submerged twin cylinders for different Froude numbers (d/a = 2.0, c/a = 4.0, no tilt in head waves)

Steady tilt moments	ka = 0.02	ka = 0.04	ka = 0.06	ka = 0.08	ka = 0.10	ka = 0.20	ka = 0.30	ka = 0.40
Fn = 0.00	-1.27287E-05	-9.66476E-05	-0.000307501	-0.000677628	-0.00120812	-0.00455816	-0.00543617	-0.00453347
Fn = 0.20	-1.72793E-05	-0.000149551	-0.000525498	-0.00124608	-0.00232267	-0.00711193	-0.00516482	-0.00237286
Fn = 0.40	-2.53571E-05	-0.000268489	-0.00113137	-0.00306788	-0.00586341	-0.00185081	-6.23209E-05	-8.98565E-05

ka = 0.50	ka = 0.60	ka = 0.70	ka = 0.80	ka = 0.90	ka = 1.00	ka = 1.10	ka = 1.20	ka = 1.30	ka = 1.40
-0.00341813	-0.00249261	-0.00177755	-0.00123681	-0.000836514	-0.000548582	-0.000348454	-0.000214455	-0.000128119	-7.45692E-05
-0.000782968	-0.000215034	-0.000145105	-0.000147516	-9.83841E-05	-6.89873E-05	-4.91556E-05	-3.35706E-05	-2.20865E-05	-1.40779E-05
-0.000103098	-0.000102792	-9.27365E-05	-7.73403E-05	-6.03867E-05	-4.45179E-05	-3.11865E-05	-2.08755E-05	-1.34253E-05	-8.34581E-06

ka = 1.50	ka = 1.60	ka = 1.70	ka = 1.80	ka = 1.90	ka = 2.00
-4.25286E-05	-2.39586E-05	-1.34639E-05	-7.62635E-06	-4.39317E-06	-2.58763E-06
-8.74961E-06	-5.34225E-06	-3.23167E-06	-1.95425E-06	-1.19107E-06	-7.35891E-07
-5.05171E-06	-3.00425E-06	-1.77432E-06	-1.05304E-06	-6.34848E-07	-3.91512E-07

Table 7.4 Accuracy check of non-dimensionalized second order horizontal forces on submerged twin cylinders for different submerged depths (c/a = 4.0, Fn = 0.2, no tilt in head waves)

Second order X forces	ka = 0.02	ka = 0.04	ka = 0.06	ka = 0.08	ka = 0.10	ka = 0.20	ka = 0.30	ka = 0.40
d/a=2.0 (Approx.)	7.02209E-07	1.23886E-05	6.60805E-05	0.000210465	0.000492202	0.00293952	0.00295158	0.00160501
d/a=2.0 (Press. Integ.)	6.27455E-07	1.18691E-05	6.45522E-05	0.000207327	0.000486913	0.00291527	0.00290032	0.00153785
d/a=4.0 (Approx.)	4.67267E-07	6.39536E-06	2.58831E-05	6.19475E-05	0.000109475	0.000234632	0.000119453	2.83523E-05
d/a=4.0 (Press. Integ.)	4.57848E-07	6.34755E-06	2.57847E-05	6.18091E-05	0.000109313	0.000234304	0.000118961	2.79762E-05

ka = 0.50	ka = 0.60	ka = 0.70	ka = 0.80	ka = 0.90	ka = 1.00	ka = 1.10	ka = 1.20	ka = 1.30	ka = 1.40
0.000542326	7.33247E-05	3.55461E-06	3.47571E-05	1.18665E-05	2.76428E-09	2.41095E-35	9.79473E-35	2.93509E-35	5.96349E-37
0.000474358	1.42896E-05	4.28525E-05	5.53402E-07	1.24033E-05	1.68249E-05	1.16125E-05	8.12513E-06	5.82721E-06	4.28696E-06
2.87879E-06	5.84058E-08	2.04475E-09	5.44271E-10	4.29253E-12	6.18908E-16	0	0	0	0
2.69649E-06	5.25816E-08	1.54538E-08	3.35054E-09	6.95579E-10	1.26924E-10	5.08696E-11	3.37515E-11	1.99494E-11	9.87608E-12

ka = 1.50	ka = 1.60	ka = 1.70	ka = 1.80	ka = 1.90	ka = 2.00
1.80171E-36	2.07805E-36	5.65956E-37	0	0	6.13618E-38
3.20908E-06	2.41486E-06	1.80599E-06	1.33109E-06	9.62003E-07	6.80171E-07
0	0	0	0	0	0
4.25471E-12	1.64482E-12	5.85432E-13	1.94251E-13	6.11317E-14	1.82803E-14

Table 7.5 Accuracy check of non-dimensionalized second order vertical forces on submerged twin cylinders for different submerged depths (c/a = 4.0, Fn = 0.20, no tilt in head waves)

Second order Y forces	ka = 0.02	ka = 0.04	ka = 0.06	ka = 0.08	ka = 0.10	ka = 0.20	ka = 0.30	ka = 0.40
d/a=2.0 (Lee-Newman)	0.0261039	0.0675612	0.121589	0.184181	0.249939	0.484663	0.648626	0.811922
d/a=2.0 (Press. Integ.)	0.0254976	0.0720815	0.137235	0.217239	0.307504	0.752575	0.988649	1.04635
d/a=4.0 (Lee-Newman)	0.0232233	0.0545421	0.0890155	0.122611	0.152508	0.224233	0.211748	0.166959
d/a=4.0 (Press. Integ.)	0.0116439	0.0369217	0.0693046	0.103612	0.136146	0.225976	0.216671	0.172278

ka = 0.50	ka = 0.60	ka = 0.70	ka = 0.80	ka = 0.90	ka = 1.00	ka = 1.10	ka = 1.20	ka = 1.30	ka = 1.40
0.834661	0.744938	0.667384	0.607461	0.522523	0.434073	0.351789	0.279825	0.219437	0.170166
1.02121	0.962774	0.890938	0.813786	0.735314	0.657962	0.583428	0.513031	0.447735	0.388169
0.116414	0.0749491	0.0457139	0.0267649	0.0151863	0.00840712	0.00456286	0.00243635	0.00128319	0.000667989
0.125091	0.0858229	0.0565029	0.0360136	0.0223599	0.0135898	0.00811904	0.00478431	0.00279114	0.00161531

ka = 1.50	ka = 1.60	ka = 1.70	ka = 1.80	ka = 1.90	ka = 2.00
0.130756	0.0996906	0.0754792	0.0567851	0.0424688	0.0315869
0.334644	0.287194	0.245612	0.209517	0.178411	0.151733
0.000344246	0.000175853	8.91399E-05	4.48762E-05	2.24545E-05	1.11739E-05
0.000929502	0.000532686	0.000304377	0.000173535	9.87551E-05	5.61037E-05

Table 7.6 Comparison of non-dimensionalized steady tilt moments on submerged twin cylinders for different submerged depths (c/a = 4.0, Fn = 0.20, no tilt in head waves)

Steady tilt moments	ka = 0.02	ka = 0.04	ka = 0.06	ka = 0.08	ka = 0.10	ka = 0.20	ka = 0.30	ka = 0.40
d/a = 2.0	-1.72793E-05	-0.000149551	-0.000525498	-0.00124608	-0.00232267	-0.00711193	-0.00516482	-0.00237286
d/a = 4.0	-1.10876E-05	-7.39452E-05	-0.000195532	-0.000344991	-0.000480299	-0.000482037	-0.000152019	-2.39676E-05

ka = 0.50	ka = 0.60	ka = 0.70	ka = 0.80	ka = 0.90	ka = 1.00	ka = 1.10	ka = 1.20	ka = 1.30	ka = 1.40
-0.000782968	-0.000215034	-0.000145105	-0.000147516	-9.83841E-05	-6.89873E-05	-4.91556E-05	-3.35706E-05	-2.20865E-05	-1.40779E-05
-1.65802E-06	-1.76855E-07	-7.86852E-08	-2.40452E-08	-6.48521E-09	-1.47112E-09	-2.38361E-10	-4.30716E-12	-1.70115E-11	9.10425E-12

ka = 1.50	ka = 1.60	ka = 1.70	ka = 1.80	ka = 1.90	ka = 2.00
-8.74961E-06	-5.34225E-06	-3.23167E-06	-1.95425E-06	-1.19107E-06	-7.35891E-07
3.31696E-12	9.79098E-13	2.38494E-13	4.46384E-14	3.79071E-15	-1.55592E-15

Table 7.7 Accuracy check of non-dimensionalized second order horizontal forces on submerged twin cylinders for different separation distances (d/a = 2.0, Fn = 0.20, no tilt in head waves)

Second order X forces	ka = 0.02	ka = 0.04	ka = 0.06	ka = 0.08	ka = 0.10	ka = 0.20	ka = 0.30	ka = 0.40
c/a=4.0 (Approx.)	7.02209E-07	1.23886E-05	6.60805E-05	0.000210465	0.000492202	0.00293952	0.00295158	0.00160501
c/a=4.0 (Press. Integ.)	6.27455E-07	1.18691E-05	6.45522E-05	0.000207327	0.000486913	0.00291527	0.00290032	0.00153785
c/a=6.0 (Approx.)	1.29836E-07	2.25399E-06	1.18186E-05	3.70034E-05	8.51828E-05	0.000484612	0.000418607	0.000129536
c/a=6.0 (Press. Integ.)	4.78325E-08	1.67509E-06	1.00668E-05	3.32635E-05	7.86036E-05	0.000454328	0.000364048	6.46091E-05

ka = 0.50	ka = 0.60	ka = 0.70	ka = 0.80	ka = 0.90	ka = 1.00	ka = 1.10	ka = 1.20	ka = 1.30	ka = 1.40
0.000542326	7.33247E-05	3.55461E-06	3.47571E-05	1.18665E-05	2.76428E-09	2.41095E-35	9.79473E-35	2.93509E-35	5.96349E-37
0.000474358	1.42896E-05	4.28525E-05	5.53402E-07	1.24033E-05	1.68249E-05	1.16125E-05	8.12513E-06	5.82721E-06	4.28696E-06
1.41439E-06	4.17051E-05	5.94505E-05	6.52786E-06	1.23924E-06	8.54364E-09	3.18456E-34	3.41387E-35	1.86069E-35	1.11208E-35
6.02117E-05	9.48233E-06	1.97345E-05	2.36754E-05	2.18717E-05	1.80313E-05	1.42095E-05	1.10724E-05	8.39437E-06	6.13631E-06

ka = 1.50	ka = 1.60	ka = 1.70	ka = 1.80	ka = 1.90	ka = 2.00
1.80171E-36	2.07805E-36	5.65956E-37	0	0	6.13618E-38
3.20908E-06	2.41486E-06	1.80599E-06	1.33109E-06	9.62003E-07	6.80171E-07
1.52738E-37	2.12241E-36	2.77651E-37	1.03257E-37	1.56391E-37	0
4.31809E-06	2.93851E-06	1.95316E-06	1.28606E-06	8.51711E-07	5.73638E-07

Table 7.8 Accuracy check of non-dimensionalized second order vertical forces on submerged twin cylinders for different separation distances (d/a = 2.0, Fn = 0.20, no tilt in head waves)

Second order Y forces	ka = 0.02	ka = 0.04	ka = 0.06	ka = 0.08	ka = 0.10	ka = 0.20	ka = 0.30	ka = 0.40
c/a=4.0 (Lee-Newman)	0.0261039	0.0675612	0.121589	0.184181	0.249939	0.484663	0.648626	0.811922
c/a=4.0 (Press. Integ.)	0.0254976	0.0720815	0.137235	0.217239	0.307504	0.752575	0.988649	1.04635
c/a=6.0 (Lee-Newman)	0.0270835	0.0688449	0.122226	0.182939	0.245658	0.497605	0.781576	0.886557
c/a=6.0 (Press. Integ.)	0.0256503	0.0706971	0.132628	0.207877	0.292243	0.711601	0.953672	1.03679

ka = 0.50	ka = 0.60	ka = 0.70	ka = 0.80	ka = 0.90	ka = 1.00	ka = 1.10	ka = 1.20	ka = 1.30	ka = 1.40
0.834661	0.744938	0.667384	0.607461	0.522523	0.434073	0.351789	0.279825	0.219437	0.170166
1.02121	0.962774	0.890938	0.813786	0.735314	0.657962	0.583428	0.513031	0.447735	0.388169
0.760132	0.737871	0.718644	0.612438	0.517791	0.423807	0.341673	0.272571	0.215421	0.168576
1.03614	0.991607	0.922068	0.838974	0.750524	0.662752	0.579834	0.504238	0.437014	0.378146

ka = 1.50	ka = 1.60	ka = 1.70	ka = 1.80	ka = 1.90	ka = 2.00
0.130756	0.0996906	0.0754792	0.0567851	0.0424688	0.0315869
0.334644	0.287194	0.245612	0.209517	0.178411	0.151733
0.130534	0.100018	0.0758929	0.0571035	0.0426653	0.0316933
0.326933	0.282368	0.243438	0.209295	0.179315	0.153051

Table 7.9 Comparison of non-dimensionalized steady tilt moments on submerged twin cylinders for different separation distances (d/a = 2.0, Fn = 0.20, no tilt in head waves)

Steady tilt moments	ka = 0.02	ka = 0.04	ka = 0.06	ka = 0.08	ka = 0.10	ka = 0.20	ka = 0.30	ka = 0.40
c/a = 4.0	-1.72793E-05	-0.000149551	-0.000525498	-0.00124608	-0.00232267	-0.00711193	-0.00516482	-0.00237286
c/a = 6.0	-2.13185E-06	-1.82097E-05	-6.31501E-05	-0.000147991	-0.000273456	-0.000856731	-0.000628849	-0.000278597

ka = 0.50	ka = 0.60	ka = 0.70	ka = 0.80	ka = 0.90	ka = 1.00	ka = 1.10	ka = 1.20	ka = 1.30	ka = 1.40
-0.000782968	-0.000215034	-0.000145105	-0.000147516	-9.83841E-05	-6.89873E-05	-4.91556E-05	-3.35706E-05	-2.20865E-05	-1.40779E-05
-0.000174954	-0.000216828	-0.000192273	-0.000123305	-9.10341E-05	-6.30554E-05	-4.25344E-05	-2.82267E-05	-1.86855E-05	-1.24251E-05

ka = 1.50	ka = 1.60	ka = 1.70	ka = 1.80	ka = 1.90	ka = 2.00
-8.74961E-06	-5.34225E-06	-3.23167E-06	-1.95425E-06	-1.19107E-06	-7.35891E-07
-8.28925E-06	-5.50758E-06	-3.60983E-06	-2.31521E-06	-1.44685E-06	-8.81502E-07

Table 7.10 Accuracy check of non-dimensionalized second order horizontal forces on submerged twin cylinders for different inclinations (d/a = 2.0, c/a = 4.0, Fn = 0.20 in head waves)

Second order X forces	ka = 0.02	ka = 0.04	ka = 0.06	ka = 0.08	ka = 0.10	ka = 0.20	ka = 0.30	ka = 0.40
0 degree tilt (Approx.)	7.02209E-07	1.23886E-05	6.60805E-05	0.000210465	0.000492202	0.00293952	0.00295158	0.00160501
0 degree tilt (Press. Int.)	6.27455E-07	1.18691E-05	6.45522E-05	0.000207327	0.000486913	0.00291527	0.00290032	0.00153785
5 degree tilt (Approx.)	7.07994E-07	1.25075E-05	6.68255E-05	0.000213251	0.000499741	0.00299287	0.00296386	0.00157901
5 degree tilt (Press. Int.)	5.85301E-07	1.18745E-05	6.50692E-05	0.000209697	0.000493752	0.00296483	0.00290471	0.00150114
10 degree tilt (Approx.)	7.26688E-07	1.28933E-05	6.92582E-05	0.000222408	0.000524687	0.00316846	0.00299125	0.00148774
10 degree tilt (Press. Int.)	5.22718E-07	1.20051E-05	6.68911E-05	0.000217644	0.000516608	0.00312958	0.00290956	0.00137897

ka = 0.50	ka = 0.60	ka = 0.70	ka = 0.80	ka = 0.90	ka = 1.00	ka = 1.10	ka = 1.20	ka = 1.30	ka = 1.40
0.000542326	7.33247E-05	3.55461E-06	3.47571E-05	1.18665E-05	2.76428E-09	2.41095E-35	9.79473E-35	2.93509E-35	5.96349E-37
0.000474358	1.42896E-05	4.28525E-05	5.53402E-07	1.24033E-05	1.68249E-05	1.16125E-05	8.12513E-06	5.82721E-06	4.28696E-06
0.000524117	7.06651E-05	3.57965E-06	3.24172E-05	1.16913E-05	9.63514E-08	5.04304E-29	1.91835E-29	7.94404E-30	3.53341E-30
0.000444045	8.63195E-07	5.48701E-05	1.28012E-05	2.22092E-05	2.48325E-05	1.81981E-05	1.33214E-05	9.82213E-06	7.29148E-06
0.000466654	6.23439E-05	2.76337E-06	2.49637E-05	1.05975E-05	4.20338E-07	2.37332E-23	1.13359E-23	5.83408E-24	3.19708E-24
0.000351402	4.56284E-05	9.12811E-05	5.34367E-05	5.31129E-05	5.05466E-05	4.04411E-05	3.19953E-05	2.52945E-05	1.99871E-05

ka = 1.50	ka = 1.60	ka = 1.70	ka = 1.80	ka = 1.90	ka = 2.00
1.80171E-36	2.07805E-36	5.65956E-37	0	0	6.13618E-38
3.20908E-06	2.41486E-06	1.80599E-06	1.33109E-06	9.62003E-07	6.80171E-07
1.65991E-30	8.10389E-31	4.05819E-31	2.06462E-31	1.06017E-31	5.47129E-32
5.42898E-06	4.03333E-06	2.97554E-06	2.17205E-06	1.56534E-06	1.11241E-06
1.83798E-24	1.09265E-24	6.63815E-25	4.08572E-25	2.53259E-25	1.57492E-25
1.57721E-05	1.24154E-05	9.73965E-06	7.60957E-06	5.91935E-06	4.58393E-06

Table 7.11 Accuracy check of non-dimensionalized second order vertical forces on submerged twin cylinders for different inclinations (d/a = 2.0, c/a = 4.0, Fn = 0.20, in head waves)

Second order Y forces	ka = 0.02	ka = 0.04	ka = 0.06	ka = 0.08	ka = 0.10	ka = 0.20	ka = 0.30	ka = 0.40
0 degree tilt (L.-N. App.)	0.0261039	0.0675612	0.121589	0.184181	0.249939	0.484663	0.648626	0.811922
0 degree tilt (Press. Int.)	0.0254976	0.0720815	0.137235	0.217239	0.307504	0.752575	0.988649	1.04635
5 degree tilt (L.-N. App.)	0.0262113	0.0678417	0.122127	0.185067	0.251231	0.486214	0.649812	0.811701
5 degree tilt (Press. Int.)	0.0267281	0.0746639	0.141361	0.223112	0.315322	0.771544	1.01723	1.08123
10 degree tilt (L.-N. App.)	0.0265596	0.0687559	0.123889	0.187979	0.255484	0.491037	0.653107	0.809831
10 degree tilt (Press. Int.)	0.0309064	0.0834251	0.155351	0.243047	0.341886	0.836204	1.11427	1.19886

ka = 0.50	ka = 0.60	ka = 0.70	ka = 0.80	ka = 0.90	ka = 1.00	ka = 1.10	ka = 1.20	ka = 1.30	ka = 1.40
0.834661	0.744938	0.667384	0.607461	0.522523	0.434073	0.351789	0.279825	0.219437	0.170166
1.02121	0.962774	0.890938	0.813786	0.735314	0.657962	0.583428	0.513031	0.447735	0.388169
0.831021	0.740901	0.664734	0.605003	0.520587	0.432631	0.350711	0.279016	0.218836	0.169723
1.05989	1.00366	0.933035	0.856482	0.778241	0.700882	0.626181	0.555487	0.489764	0.429624
0.818238	0.727661	0.656451	0.597651	0.514786	0.428268	0.347415	0.276536	0.216992	0.168365
1.18936	1.13965	1.07233	0.997169	0.919171	0.841381	0.765853	0.694051	0.626943	0.565093

ka = 1.50	ka = 1.60	ka = 1.70	ka = 1.80	ka = 1.90	ka = 2.00
0.130756	0.0996906	0.0754792	0.0567851	0.0424688	0.0315869
0.334644	0.287194	0.245612	0.209517	0.178411	0.151733
0.130431	0.0994526	0.0753046	0.0566571	0.0423751	0.0315185
0.375356	0.326973	0.284261	0.246839	0.214225	0.185887
0.129435	0.0987234	0.0747706	0.0562661	0.0420893	0.0313104
0.508721	0.457771	0.411993	0.371001	0.334333	0.301512

Table 7.12 Comparison of non-dimensionalized steady tilt moments on submerged twin cylinders for different inclinations (d/a = 2.0, c/a = 4.0, Fn = 0.20 in head waves)

Steady tilt moments	ka = 0.02	ka = 0.04	ka = 0.06	ka = 0.08	ka = 0.10	ka = 0.20	ka = 0.30	ka = 0.40
0 degree tilt	-1.72793E-05	-0.000149551	-0.000525498	-0.00124608	-0.00232267	-0.00711193	-0.00516482	-0.00237286
5 degree tilt	0.00638901	0.0135611	0.0219239	0.0315543	0.0423917	0.109704	0.175096	0.218231
10 degree tilt	0.0141452	0.0300501	0.0487222	0.0704171	0.0950054	0.244497	0.382185	0.470966

ka = 0.50	ka = 0.60	ka = 0.70	ka = 0.80	ka = 0.90	ka = 1.00	ka = 1.10	ka = 1.20	ka = 1.30	ka = 1.40
-0.000782968	-0.000215034	-0.000145105	-0.000147516	-9.83841E-05	-6.89873E-05	-4.91556E-05	-3.35706E-05	-2.20865E-05	-1.40779E-05
0.241566	0.251475	0.252753	0.248587	0.240947	0.231031	0.219693	0.207491	0.194793	0.181854
0.518472	0.538489	0.540932	0.532278	0.516671	0.496755	0.474283	0.450361	0.425681	0.400693

ka = 1.50	ka = 1.60	ka = 1.70	ka = 1.80	ka = 1.90	ka = 2.00
-8.74961E-06	-5.34225E-06	-3.23167E-06	-1.95425E-06	-1.19107E-06	-7.35891E-07
0.168869	0.155998	0.143382	0.131145	0.119397	0.108227
0.375713	0.350988	0.326729	0.303123	0.280331	0.258485

Table 7.13 Accuracy check of non-dimensionalized second order horizontal forces on submerged twin cylinders for different Froude numbers (d/a = 2.0, c/a = 4.0, no tilt in following waves)

Second order X forces	ka = 0.02	ka = 0.04	ka = 0.06	ka = 0.08	ka = 0.10	ka = 0.20	ka = 0.30	ka = 0.40
Fn=0.0 (Approx.)	4.86455E-07	7.32327E-06	3.46182E-05	0.000100645	0.000221684	0.00154954	0.00249562	0.00245487
Fn=0.0 (Press. Integ.)	4.00291E-07	6.65518E-06	3.24409E-05	9.56976E-05	0.000212511	0.00150117	0.00240648	0.00234725
Fn=0.2 (Approx.)	3.57466E-07	4.79436E-06	2.09523E-05	5.75711E-05	0.000121793	0.000798502	0.00130315	0.00128688
Fn=0.2 (Press. Integ.)	2.45338E-07	3.84417E-06	1.76235E-05	4.95184E-05	0.000106021	0.000701475	0.00112186	0.00107109
Fn=0.4 (Approx.)	2.76789E-07	2.30899E-06	4.83636E-06	5.16843E-06	7.11278E-06	0.000467223	0.00382126	0.00851672
Fn=0.4 (Press. Integ.)	1.04519E-07	6.96375E-07	1.32242E-06	1.09652E-05	2.69127E-05	0.000200954	0.00434923	0.00915026

ka = 0.50	ka = 0.60	ka = 0.70	ka = 0.80	ka = 0.90	ka = 1.00	ka = 1.10	ka = 1.20	ka = 1.30	ka = 1.40
0.00204398	0.00159851	0.00121032	0.000893148	0.000642084	0.000448717	0.000304176	0.000199671	0.000126793	7.78743E-05
0.00193833	0.00150659	0.00113658	0.000837299	0.000601437	0.000419812	0.000283762	0.000185146	0.000116286	7.01309E-05
0.00104138	0.000765932	0.000531721	0.000353474	0.000225917	0.000138455	8.06451E-05	4.38885E-05	2.16382E-05	9.09468E-06
0.000829661	0.000578671	0.000376844	0.000231253	0.000132519	6.84581E-05	2.86176E-05	5.19173E-06	7.32768E-06	1.27661E-05
0.000465552	0.0135529	0.0579297	0.0717787	0.0390475	0.000118933	0.0365951	0.0352893	0.0179829	0.00630302
0.00107442	0.0141956	0.0586831	0.0724571	0.0394552	0.000303351	0.0369548	0.0355681	0.0181275	0.00636059

ka = 1.50	ka = 1.60	ka = 1.70	ka = 1.80	ka = 1.90	ka = 2.00
4.63036E-05	2.67155E-05	1.50162E-05	8.26981E-06	4.49566E-06	2.43321E-06
4.05178E-05	2.23702E-05	1.17655E-05	5.86528E-06	2.74549E-06	1.18301E-06
2.81371E-06	3.62661E-07	5.78161E-08	7.71657E-07	1.79037E-06	2.70414E-06
1.37933E-05	1.22862E-05	9.55593E-06	6.48777E-06	3.63709E-06	1.30441E-06
0.000845986	0.000276705	0.00338317	0.00915278	0.0164604	0.0228065
0.000858135	0.000274274	0.00338871	0.00918227	0.0165233	0.0228985

Table 7.14 Accuracy check of non-dimensionalized second order vertical forces on submerged twin cylinders for different Froude numbers (d/a = 2.0, c/a = 4.0, no tilt in following waves)

Second order Y forces	ka = 0.02	ka = 0.04	ka = 0.06	ka = 0.08	ka = 0.10	ka = 0.20	ka = 0.30	ka = 0.40
Fn=0.0 (Lee-Newman)	0.0101411	0.0381831	0.0805503	0.133423	0.192755	0.467475	0.605668	0.674928
Fn=0.0 (Press. Integ.)	0.0266781	0.0770267	0.148679	0.238071	0.340356	0.849721	1.08971	1.11542
Fn=0.2 (Lee-Newman)	0.0279683	0.0722354	0.129216	0.195345	0.266863	0.584726	0.730185	0.786752
Fn=0.2 (Press. Integ.)	0.0302769	0.0881427	0.172091	0.279352	0.405052	1.04472	1.28729	1.24928
Fn=0.4 (Lee-Newman)	0.0865602	0.188549	0.300825	0.419627	0.540764	1.00267	1.12501	1.21384
Fn=0.4 (Press. Integ.)	0.0390193	0.114262	0.227449	0.379669	0.568613	1.63014	1.88958	1.68743

ka = 0.50	ka = 0.60	ka = 0.70	ka = 0.80	ka = 0.90	ka = 1.00	ka = 1.10	ka = 1.20	ka = 1.30	ka = 1.40
0.717595	0.725966	0.692291	0.623101	0.533615	0.439335	0.351317	0.275303	0.212911	0.163317
1.05937	0.978842	0.892389	0.805959	0.721943	0.641723	0.566292	0.496362	0.432389	0.374594
0.809491	0.796828	0.744085	0.659055	0.557299	0.454102	0.359975	0.280008	0.215219	0.164295
1.13808	1.01955	0.906954	0.802181	0.705556	0.617316	0.537571	0.466196	0.402845	0.347013
1.33003	1.37096	1.25251	1.05384	0.880649	0.635377	0.212343	0.145794	0.133981	0.113365
1.49134	1.34889	1.11386	0.817757	0.660712	0.778877	0.574101	0.214732	0.0837673	0.0326511

ka = 1.50	ka = 1.60	ka = 1.70	ka = 1.80	ka = 1.90	ka = 2.00
0.124632	0.0947519	0.0717786	0.0541582	0.0406752	0.0303931
0.322984	0.277385	0.237478	0.202831	0.172941	0.147273
0.124967	0.0948496	0.0718474	0.0542783	0.0408547	0.0306084
0.298112	0.255513	0.218585	0.186709	0.159292	0.135777
0.0903895	0.0691866	0.0511101	0.0362976	0.0245132	0.0159971
0.0128378	0.00963664	0.0181191	0.0376919	0.0715207	0.127214

Table 7.15 Comparison of non-dimensionalized steady tilt moments on submerged twin cylinders for different Froude numbers (d/a = 2.0, c/a = 4.0, no tilt in following waves)

Steady tilt moments	ka = 0.02	ka = 0.04	ka = 0.06	ka = 0.08	ka = 0.10	ka = 0.20	ka = 0.30	ka = 0.40
Fn = 0.00	1.26934E-05	9.62735E-05	0.000306072	0.000674099	0.00120137	0.00453393	0.00541708	0.00452499
Fn = 0.20	9.88908E-06	6.83218E-05	0.000204174	0.000430852	0.000746184	0.00275371	0.00343207	0.00297597
Fn = 0.40	8.15522E-06	5.48524E-05	0.000159782	0.000325168	0.000534906	0.00226137	0.00556879	0.00487957

ka = 0.50	ka = 0.60	ka = 0.70	ka = 0.80	ka = 0.90	ka = 1.00	ka = 1.10	ka = 1.20	ka = 1.30	ka = 1.40
0.00341656	0.00249515	0.00178249	0.00124285	0.000842683	0.000554185	0.000353107	0.000218037	0.000130696	7.63126E-05
0.00230198	0.00171421	0.00125515	0.000907367	0.000646977	0.000454061	0.000313185	0.000212282	0.000141697	9.36151E-05
0.00481651	0.0464284	0.0770667	0.0148345	0.0724438	0.0104979	0.220127	0.134802	0.0564911	0.0179551

ka = 1.50	ka = 1.60	ka = 1.70	ka = 1.80	ka = 1.90	ka = 2.00
4.36431E-05	2.46362E-05	1.38592E-05	7.85027E-06	4.51827E-06	2.65779E-06
6.17605E-05	4.12058E-05	2.82142E-05	2.00701E-05	1.48961E-05	1.14655E-05
-0.00231157	-0.000745565	-0.00943203	-0.0273039	-0.0551118	-0.0925726

Table 7.16 Accuracy check of non-dimensionalized second order horizontal forces on submerged twin cylinders for different submerged depths (c/a = 4.0, Fn = 0.2, no tilt in following waves)

Second order X forces	ka = 0.02	ka = 0.04	ka = 0.06	ka = 0.08	ka = 0.10	ka = 0.20	ka = 0.30	ka = 0.40
d/a=2.0 (Approx.)	3.57466E-07	4.79436E-06	2.09523E-05	5.75711E-05	0.000121793	0.000798502	0.00130315	0.00128688
d/a=2.0 (Press. Integ.)	2.45338E-07	3.84417E-06	1.76235E-05	4.95184E-05	0.000106021	0.000701475	0.00112186	0.00107109
d/a=4.0 (Approx.)	2.43846E-07	2.66846E-06	9.47581E-06	2.11538E-05	3.65275E-05	0.000104683	0.000103698	7.20227E-05
d/a=4.0 (Press. Integ.)	2.29099E-07	2.56642E-06	9.18521E-06	2.05842E-05	3.56238E-05	0.000102558	0.000101899	7.10391E-05

ka = 0.50	ka = 0.60	ka = 0.70	ka = 0.80	ka = 0.90	ka = 1.00	ka = 1.10	ka = 1.20	ka = 1.30	ka = 1.40
0.00104138	0.000765932	0.000531721	0.000353474	0.000225917	0.000138455	8.06451E-05	4.38885E-05	2.16382E-05	9.09468E-06
0.000829661	0.000578671	0.000376844	0.000231253	0.000132519	6.84581E-05	2.86176E-05	5.19173E-06	7.32768E-06	1.27661E-05
4.23183E-05	2.23984E-05	1.09345E-05	4.96631E-06	2.10095E-06	8.24011E-07	2.96145E-07	9.52617E-08	2.61334E-08	5.45019E-09
4.19141E-05	2.22721E-05	1.09087E-05	4.96681E-06	2.10467E-06	8.26283E-07	2.97098E-07	9.55701E-08	2.62037E-08	5.45288E-09

ka = 1.50	ka = 1.60	ka = 1.70	ka = 1.80	ka = 1.90	ka = 2.00
2.81371E-06	3.62661E-07	5.78161E-08	7.71657E-07	1.79037E-06	2.70414E-06
1.37933E-05	1.22862E-05	9.55593E-06	6.48777E-06	3.63709E-06	1.30441E-06
5.83346E-10	3.23641E-12	1.85599E-10	3.05636E-10	2.95547E-10	2.25461E-10
5.83375E-10	3.45254E-12	1.82291E-10	3.04446E-10	2.95341E-10	2.25602E-10

Table 7.17 Accuracy check of non-dimensionalized second order vertical forces on submerged twin cylinders for different submerged depths (c/a = 4.0, Fn = 0.2, no tilt in following waves)

Second order Y forces	ka = 0.02	ka = 0.04	ka = 0.06	ka = 0.08	ka = 0.10	ka = 0.20	ka = 0.30	ka = 0.40
d/a=2.0 (Lee-Newman)	0.0279683	0.0722354	0.129216	0.195345	0.266863	0.584726	0.730185	0.786752
d/a=2.0 (Press. Integ.)	0.0302769	0.0881427	0.172091	0.279352	0.405052	1.04472	1.28729	1.24928
d/a=4.0 (Lee-Newman)	0.0249254	0.0586093	0.0954621	0.131518	0.164108	0.246126	0.226589	0.172692
d/a=4.0 (Press. Integ.)	0.0123223	0.0391335	0.0737489	0.110629	0.145596	0.236965	0.219381	0.169914

ka = 0.50	ka = 0.60	ka = 0.70	ka = 0.80	ka = 0.90	ka = 1.00	ka = 1.10	ka = 1.20	ka = 1.30	ka = 1.40
0.809491	0.796828	0.744085	0.659055	0.557299	0.454102	0.359975	0.280008	0.215219	0.164295
1.13808	1.01955	0.906954	0.802181	0.705556	0.617316	0.537571	0.466196	0.402845	0.347013
0.118772	0.0762161	0.0464372	0.0271809	0.0154189	0.00853324	0.00463003	0.00247185	0.00130188	0.000677779
0.121654	0.0830906	0.0547884	0.0350833	0.0219052	0.0133837	0.00802951	0.00474624	0.00277295	0.00160589

ka = 1.50	ka = 1.60	ka = 1.70	ka = 1.80	ka = 1.90	ka = 2.00
0.124967	0.0948496	0.0718474	0.0542783	0.0408547	0.0306084
0.298112	0.255513	0.218585	0.186709	0.159292	0.135777
0.000349339	0.000178481	9.04818E-05	4.55555E-05	2.27954E-05	1.13437E-05
0.000925141	0.000529482	0.000302464	0.000172424	9.81374E-05	5.57764E-05

Table 7.18 Comparison of non-dimensionalized steady tilt moments on submerged twin cylinders for different submerged depths (c/a = 4.0, Fn = 0.20, no tilt in following waves)

Steady tilt moments	ka = 0.02	ka = 0.04	ka = 0.06	ka = 0.08	ka = 0.10	ka = 0.20	ka = 0.30	ka = 0.40
d/a = 2.0	9.88908E-06	6.83218E-05	0.000204174	0.000430852	0.000746184	0.00275371	0.00343207	0.00297597
d/a = 4.0	6.49426E-06	3.63463E-05	8.75486E-05	0.000148751	0.000208175	0.000314103	0.000215399	0.000115081

ka = 0.50	ka = 0.60	ka = 0.70	ka = 0.80	ka = 0.90	ka = 1.00	ka = 1.10	ka = 1.20	ka = 1.30	ka = 1.40
0.00230198	0.00171421	0.00125515	0.000907367	0.000646977	0.000454061	0.000313185	0.000212282	0.000141697	9.36151E-05
5.47069E-05	2.39945E-05	9.77481E-06	3.67488E-06	1.25155E-06	3.70308E-07	8.49512E-08	8.06679E-09	5.44393E-09	4.06905E-09

ka = 1.50	ka = 1.60	ka = 1.70	ka = 1.80	ka = 1.90	ka = 2.00
6.17605E-05	4.12058E-05	2.82142E-05	2.00701E-05	1.48961E-05	1.14655E-05
5.31696E-10	8.58006E-11	5.47769E-10	5.36526E-10	3.85307E-10	2.37213E-10

Table 7.19 Accuracy check of non-dimensionalized second order horizontal forces on submerged twin cylinders for different separation distances (d/a = 2.0, Fn = 0.20, no tilt in following waves)

Second order X forces	ka = 0.02	ka = 0.04	ka = 0.06	ka = 0.08	ka = 0.10	ka = 0.20	ka = 0.30	ka = 0.40
c/a=4.0 (Approx.)	3.57466E-07	4.79436E-06	2.09523E-05	5.75711E-05	0.000121793	0.000798502	0.00130315	0.00128688
c/a=4.0 (Press. Integ.)	2.45338E-07	3.84417E-06	1.76235E-05	4.95184E-05	0.000106021	0.000701475	0.00112186	0.00107109
c/a=6.0 (Approx.)	6.61994E-08	8.76425E-07	3.78064E-06	1.02565E-05	2.14365E-05	0.000134768	0.000214766	0.000201995
c/a=6.0 (Press. Integ.)	5.29209E-08	1.07872E-07	4.12833E-07	2.28272E-06	6.11264E-06	4.52149E-05	4.73415E-05	1.33692E-06

ka = 0.50	ka = 0.60	ka = 0.70	ka = 0.80	ka = 0.90	ka = 1.00	ka = 1.10	ka = 1.20	ka = 1.30	ka = 1.40
0.00104138	0.000765932	0.000531721	0.000353474	0.000225917	0.000138455	8.06451E-05	4.38885E-05	2.16382E-05	9.09468E-06
0.000829661	0.000578671	0.000376844	0.000231253	0.000132519	6.84581E-05	2.86176E-05	5.19173E-06	7.32768E-06	1.27661E-05
0.000147875	9.19939E-05	4.93376E-05	2.19148E-05	6.97591E-06	8.46647E-07	2.35975E-07	2.51148E-06	5.69805E-06	8.45455E-06
4.79714E-05	7.89511E-05	9.10423E-05	9.03817E-05	8.24671E-05	7.06622E-05	5.69674E-05	4.28826E-05	2.97349E-05	1.86021E-05

ka = 1.50	ka = 1.60	ka = 1.70	ka = 1.80	ka = 1.90	ka = 2.00
2.81371E-06	3.62661E-07	5.78161E-08	7.71657E-07	1.79037E-06	2.70414E-06
1.37933E-05	1.22862E-05	9.55593E-06	6.48777E-06	3.63709E-06	1.30441E-06
1.00489E-05	1.02861E-05	9.36813E-06	7.71053E-06	5.76891E-06	3.91665E-06
1.01279E-05	4.43395E-06	1.18738E-06	2.20821E-07	4.72036E-07	1.60656E-07

Table 7.20 Accuracy check of non-dimensionalized second order vertical forces on submerged twin cylinders for different separation distances (d/a = 2.0, Fn = 0.20, no tilt in following waves)

Second order Y forces	ka = 0.02	ka = 0.04	ka = 0.06	ka = 0.08	ka = 0.10	ka = 0.20	ka = 0.30	ka = 0.40
c/a=4.0 (Lee-Newman)	0.0279683	0.0722354	0.129216	0.195345	0.266863	0.584726	0.730185	0.786752
c/a=4.0 (Press. Integ.)	0.0302769	0.0881427	0.172091	0.279352	0.405052	1.04472	1.28729	1.24928
c/a=6.0 (Lee-Newman)	0.0290879	0.0739382	0.130765	0.195822	0.265235	0.569768	0.750161	0.891753
c/a=6.0 (Press. Integ.)	0.0303691	0.0858474	0.164295	0.262634	0.376216	0.952594	1.21571	1.23821

ka = 0.50	ka = 0.60	ka = 0.70	ka = 0.80	ka = 0.90	ka = 1.00	ka = 1.10	ka = 1.20	ka = 1.30	ka = 1.40
0.809491	0.796828	0.744085	0.659055	0.557299	0.454102	0.359975	0.280008	0.215219	0.164295
1.13808	1.01955	0.906954	0.802181	0.705556	0.617316	0.537571	0.466196	0.402845	0.347013
0.975105	0.952698	0.838751	0.685202	0.537182	0.416355	0.325489	0.258327	0.207007	0.165628
1.17015	1.06685	0.949809	0.831928	0.721164	0.621456	0.534011	0.458488	0.393799	0.338555

ka = 1.50	ka = 1.60	ka = 1.70	ka = 1.80	ka = 1.90	ka = 2.00
0.124967	0.0948496	0.0718474	0.0542783	0.0408547	0.0306084
0.298112	0.255513	0.218585	0.186709	0.159292	0.135777
0.130972	0.101768	0.0776282	0.0582824	0.0432568	0.0318784
0.291329	0.250797	0.215829	0.185516	0.159161	0.136234

Table 7.21 Comparison of non-dimensionalized steady tilt moments on submerged twin cylinders for different separation distances (d/a = 2.0, Fn = 0.20, no tilt in following waves)

Steady tilt moments	ka = 0.02	ka = 0.04	ka = 0.06	ka = 0.08	ka = 0.10	ka = 0.20	ka = 0.30	ka = 0.40
c/a = 4.0	9.88908E-06	6.83218E-05	0.000204174	0.000430852	0.000746184	0.00275371	0.00343207	0.00297597
c/a = 6.0	1.22773E-06	8.46401E-06	2.53435E-05	5.38315E-05	9.43264E-05	0.000403241	0.000655766	0.000766194

ka = 0.50	ka = 0.60	ka = 0.70	ka = 0.80	ka = 0.90	ka = 1.00	ka = 1.10	ka = 1.20	ka = 1.30	ka = 1.40
0.00230198	0.00171421	0.00125515	0.000907367	0.000646977	0.000454061	0.000313185	0.000212282	0.000141697	9.36151E-05
0.000773947	0.000711423	0.000607457	0.000489237	0.000377226	0.000282706	0.000208984	0.000154274	0.000114544	8.55427E-05

ka = 1.50	ka = 1.60	ka = 1.70	ka = 1.80	ka = 1.90	ka = 2.00
6.17605E-05	4.12058E-05	2.82142E-05	2.00701E-05	1.48961E-05	1.14655E-05
6.38576E-05	4.71915E-05	3.41901E-05	2.40983E-05	1.64492E-05	1.08626E-05

Table 7.22 Accuracy check of non-dimensionalized second order horizontal forces on submerged twin cylinders for different inclinations (d/a = 2.0, c/a = 4.0, Fn = 0.20 in following waves)

Second order X forces	ka = 0.02	ka = 0.04	ka = 0.06	ka = 0.08	ka = 0.10	ka = 0.20	ka = 0.30	ka = 0.40
0 degree tilt (Approx.)	3.57466E-07	4.79436E-06	2.09523E-05	5.75711E-05	0.000121793	0.000798502	0.00130315	0.00128688
0 degree tilt (Press. Int.)	2.45338E-07	3.84417E-06	1.76235E-05	4.95184E-05	0.000106021	0.000701475	0.00112186	0.00107109
5 degree tilt (Approx.)	3.60368E-07	4.83834E-06	2.11696E-05	5.82445E-05	0.000123391	0.000813557	0.00132684	0.00130287
5 degree tilt (Press. Int.)	3.54941E-07	4.11509E-06	1.81324E-05	5.04164E-05	0.000107567	0.000710917	0.00113213	0.00106943
10 degree tilt (Approx.)	3.69741E-07	4.98092E-06	2.18772E-05	6.04469E-05	0.000128635	0.000863814	0.00140471	0.00135221
10 degree tilt (Press. Int.)	4.87477E-07	4.39293E-06	1.86152E-05	5.13601E-05	0.000109535	0.000728671	0.00113644	0.00101849

ka = 0.50	ka = 0.60	ka = 0.70	ka = 0.80	ka = 0.90	ka = 1.00	ka = 1.10	ka = 1.20	ka = 1.30	ka = 1.40
0.00104138	0.000765932	0.000531721	0.000353474	0.000225917	0.000138455	8.06451E-05	4.38885E-05	2.16382E-05	9.09468E-06
0.000829661	0.000578671	0.000376844	0.000231253	0.000132519	6.84581E-05	2.86176E-05	5.19173E-06	7.32768E-06	1.27661E-05
0.00104598	0.000762658	0.000524953	0.000346271	0.000219836	0.000133997	7.77328E-05	4.22034E-05	2.08105E-05	8.79484E-06
0.000815564	0.000557391	0.000353531	0.000209191	0.000113211	5.22301E-05	1.51963E-05	5.91267E-06	1.66112E-05	2.06404E-05
0.00105629	0.000747741	0.000500197	0.000321619	0.000199851	0.000119772	6.86439E-05	3.70184E-05	1.82626E-05	7.82281E-06
0.000713177	0.000426572	0.000215323	7.69119E-05	6.70581E-06	5.33454E-05	7.64206E-05	8.49632E-05	8.47599E-05	7.94741E-05

ka = 1.50	ka = 1.60	ka = 1.70	ka = 1.80	ka = 1.90	ka = 2.00
2.81371E-06	3.62661E-07	5.78161E-08	7.71657E-07	1.79037E-06	2.70414E-06
1.37933E-05	1.22862E-05	9.55593E-06	6.48777E-06	3.63709E-06	1.30441E-06
2.78538E-06	4.27262E-07	1.05841E-07	7.48922E-07	1.68297E-06	2.52405E-06
2.05634E-05	1.81608E-05	1.46704E-05	1.09292E-05	7.46532E-06	4.56716E-06
2.60034E-06	4.99779E-07	1.22758E-07	5.62141E-07	1.25969E-06	1.90281E-06
7.14552E-05	6.22432E-05	5.28575E-05	4.39577E-05	3.59391E-05	2.89971E-05

Table 7.23 Accuracy check of non-dimensionalized second order vertical forces on submerged twin cylinders for different inclinations (d/a = 2.0, c/a = 4.0, Fn = 0.20 in following waves)

Second order Y forces	ka = 0.02	ka = 0.04	ka = 0.06	ka = 0.08	ka = 0.10	ka = 0.20	ka = 0.30	ka = 0.40
0 degree tilt (L.-N. App.)	0.0279683	0.0722354	0.129216	0.195345	0.266863	0.584726	0.730185	0.786752
0 degree tilt (Press. Int.)	0.0302769	0.0881427	0.172091	0.279352	0.405052	1.04472	1.28729	1.24928
5 degree tilt (L.-N. App.)	0.0280839	0.0725323	0.129767	0.196226	0.268111	0.587707	0.732511	0.788347
5 degree tilt (Press. Int.)	0.0320011	0.0923354	0.179621	0.291209	0.422269	1.09683	1.36056	1.32606
10 degree tilt (L.-N. App.)	0.0284585	0.0734985	0.131567	0.199112	0.272305	0.597484	0.739743	0.792937
10 degree tilt (Press. Int.)	0.0379444	0.106873	0.205874	0.332771	0.482937	1.28479	1.62704	1.60434

ka = 0.50	ka = 0.60	ka = 0.70	ka = 0.80	ka = 0.90	ka = 1.00	ka = 1.10	ka = 1.20	ka = 1.30	ka = 1.40
0.809491	0.796828	0.744085	0.659055	0.557299	0.454102	0.359975	0.280008	0.215219	0.164295
1.13808	1.01955	0.906954	0.802181	0.705556	0.617316	0.537571	0.466196	0.402845	0.347013
0.810972	0.797942	0.744318	0.658264	0.555755	0.452241	0.358167	0.278471	0.214026	0.163424
1.21169	1.08802	0.969806	0.859617	0.758104	0.665636	0.582317	0.507947	0.442073	0.384082
0.815091	0.800701	0.744074	0.654715	0.549944	0.445642	0.351965	0.273311	0.210082	0.160582
1.47626	1.33161	1.19127	1.06032	0.940549	0.832613	0.736442	0.651434	0.576681	0.511138

ka = 1.50	ka = 1.60	ka = 1.70	ka = 1.80	ka = 1.90	ka = 2.00
0.124967	0.0948496	0.0718474	0.0542783	0.0408547	0.0306084
0.298112	0.255513	0.218585	0.186709	0.159292	0.135777
0.124355	0.0944248	0.0715501	0.0540654	0.0406979	0.0304904
0.333284	0.288971	0.250439	0.217024	0.188098	0.163082
0.122378	0.0930688	0.0706126	0.0534021	0.0402153	0.0301315
0.453751	0.403514	0.359504	0.320891	0.286937	0.257004

Table 7.24 Comparison of non-dimensionalized steady tilt moments on submerged twin cylinders for different inclinations (d/a = 2.0, c/a = 4.0, Fn = 0.20 in following waves)

Steady tilt moments	ka = 0.02	ka = 0.04	ka = 0.06	ka = 0.08	ka = 0.10	ka = 0.20	ka = 0.30	ka = 0.40
0 degree tilt	9.88908E-06	6.83218E-05	0.000204174	0.000430852	0.000746184	0.00275371	0.00343207	0.00297597
5 degree tilt	0.00860192	0.0207074	0.0368664	0.0574098	0.0822058	0.232912	0.327475	0.352121
10 degree tilt	0.0192397	0.0464173	0.0827766	0.129153	0.185398	0.533781	0.755399	0.809842

ka = 0.50	ka = 0.60	ka = 0.70	ka = 0.80	ka = 0.90	ka = 1.00	ka = 1.10	ka = 1.20	ka = 1.30	ka = 1.40
0.00230198	0.00171421	0.00125515	0.000907367	0.000646977	0.000454061	0.000313185	0.000212282	0.000141697	9.36151E-05
0.344741	0.324945	0.300685	0.275611	0.251542	0.229301	0.209125	0.190937	0.174517	0.159604
0.787784	0.737284	0.677875	0.618289	0.562546	0.512165	0.467311	0.427497	0.391998	0.360082

ka = 1.50	ka = 1.60	ka = 1.70	ka = 1.80	ka = 1.90	ka = 2.00
6.17605E-05	4.12058E-05	2.82142E-05	2.00701E-05	1.48961E-05	1.14655E-05
0.145956	0.133372	0.121701	0.110831	0.100696	0.0912499
0.331104	0.304552	0.280043	0.257303	0.236146	0.216446

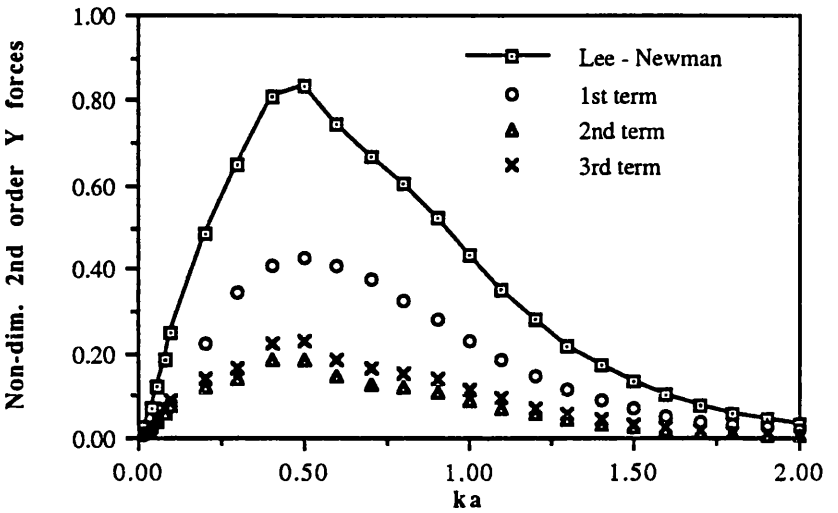

Fig.7.1 Summary of non-dimensionalized 2nd order Y forces(d/a=2.0,c/a=4.0,Fn=0.2, no tilt in head waves)

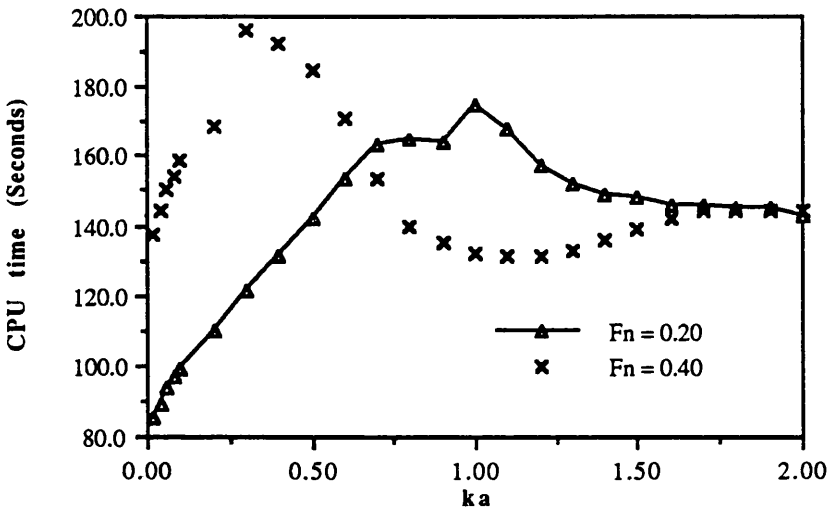

Fig.7.2 Comparison of CPU time against wave numbers for Froude numbers (d/a=2.0, c/a=4.0, no tilt in head waves)

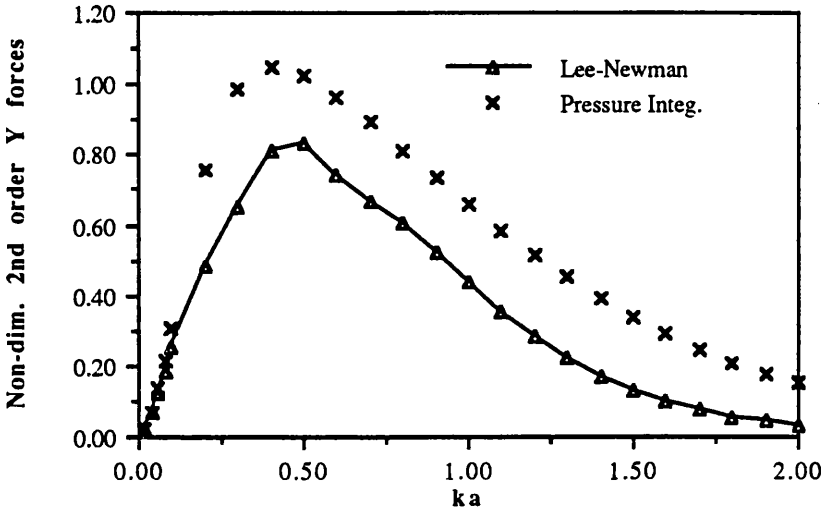

Fig.7.3 Comparison of non-dimensionalized 2nd order Y forces (d/a=2.0,c/a=4.0,Fn=0.2 no tilt in head waves)

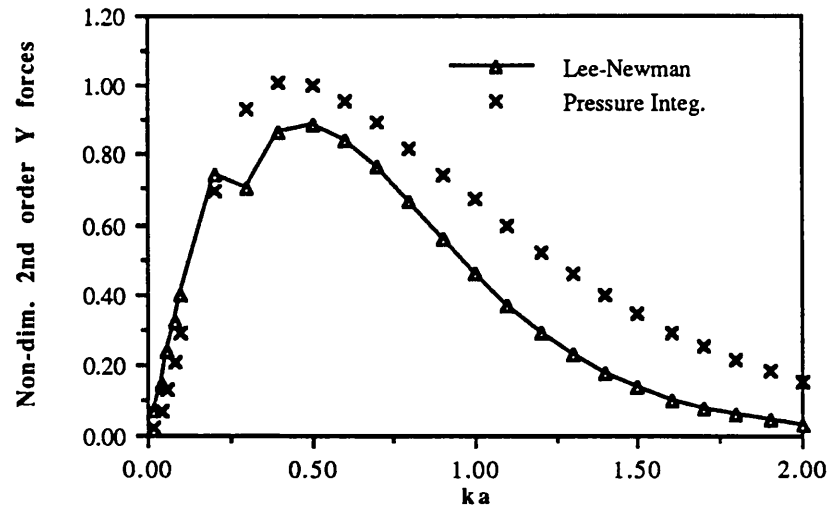

Fig.7.4 Comparison of non-dimensionalized 2nd order Y forces (d/a=2.0,c/a=4.0,Fn=0.4 no tilt in head waves)

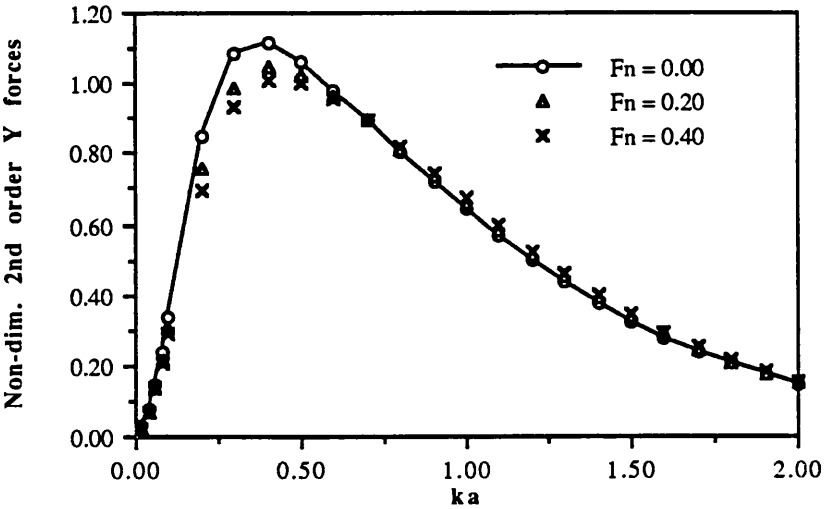

Fig.7.5 Non-dimensionalized 2nd order Y force for different Froude numbers(d/a=2, c/a=4, no tilt in head waves)

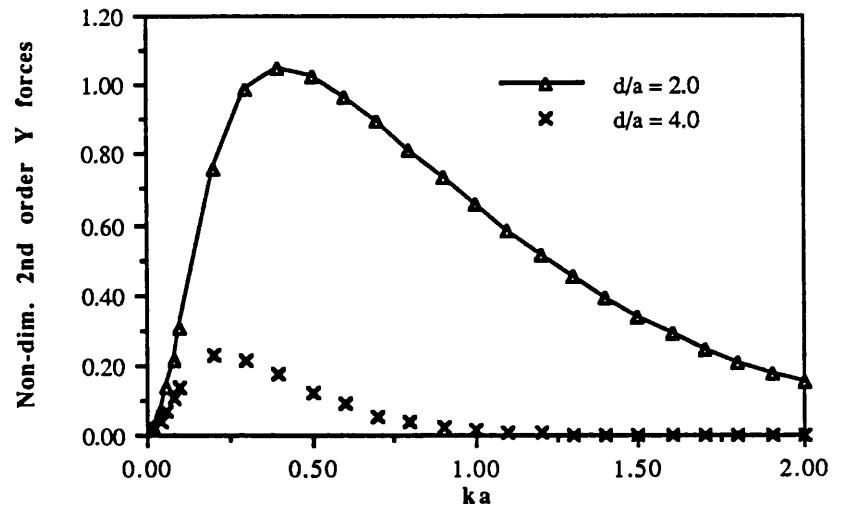

Fig.7.6 Non-dimensionalized 2nd order Y forces for different depths (c/a=4.0,Fn=0.2, no tilt in head waves)

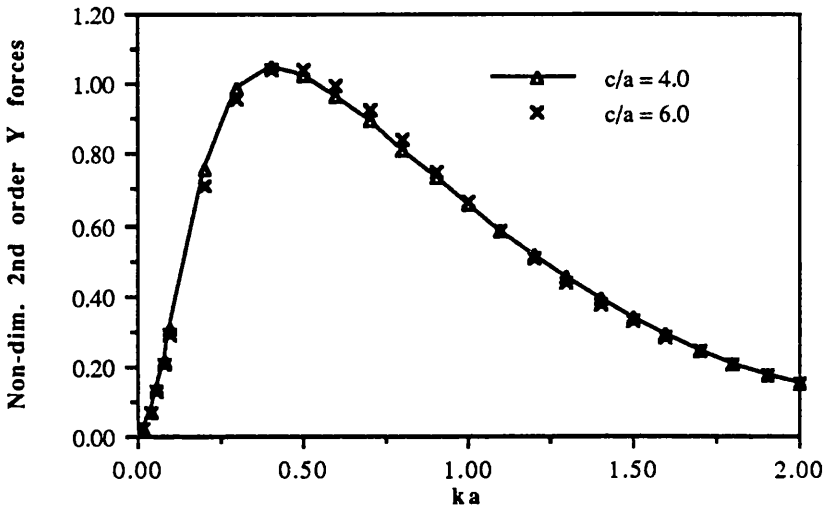

Fig.7.7 Non-dimensionalized 2nd order Y forces for different separation distances (d/a=2.0, Fn=0.20, no tilt in head waves)

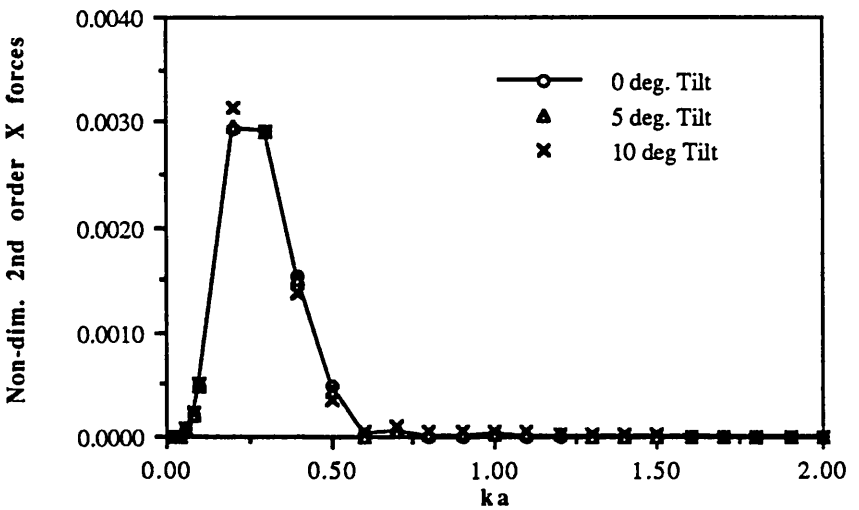

Fig.7.8 Non-dimensionalized 2nd order X forces for different inclinations(d/a=2.0, c/a=4.0, Fn=0.20 in head waves)

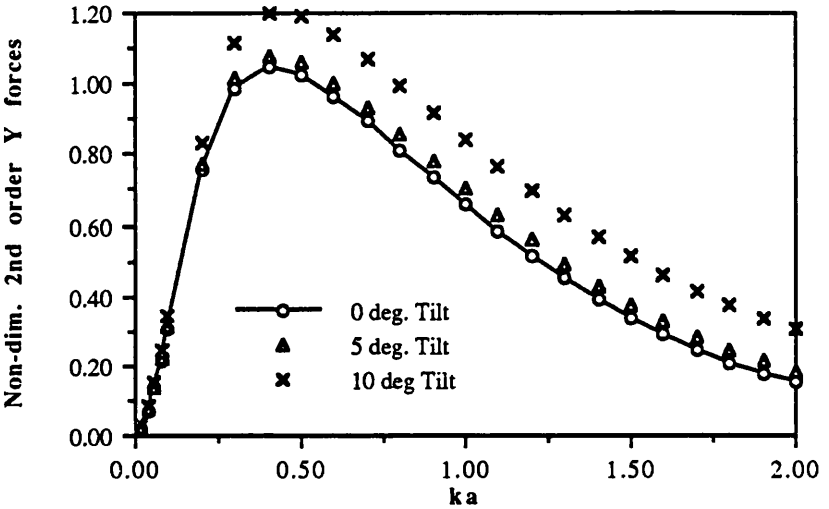

Fig.7.9 Non-dimensionalized 2nd order Y forces for different inclinations(d/a=2.0, c/a=4.0, Fn=0.20 in head waves)

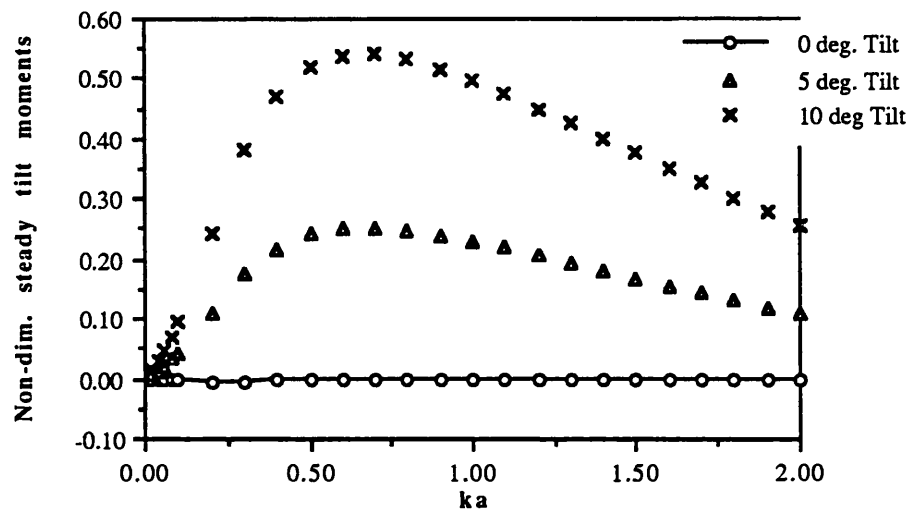

Fig.7.10 Non-dimensionalized steady tilt moments for different inclinations(d/a=2.0, c/a=4.0, Fn=0.20 in head waves)

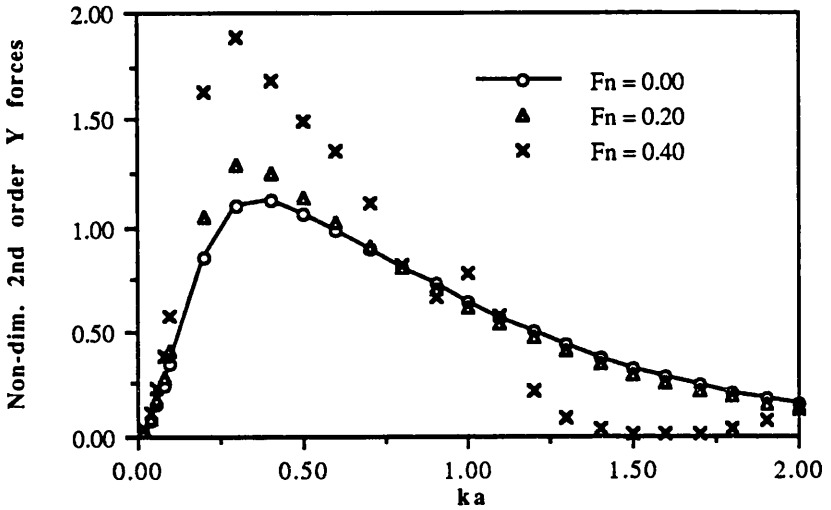

Fig.7.11 Non-dimensionalized 2nd order Y forces for different Froude numbers (d/a=2, c/a=4, no tilt in following waves)

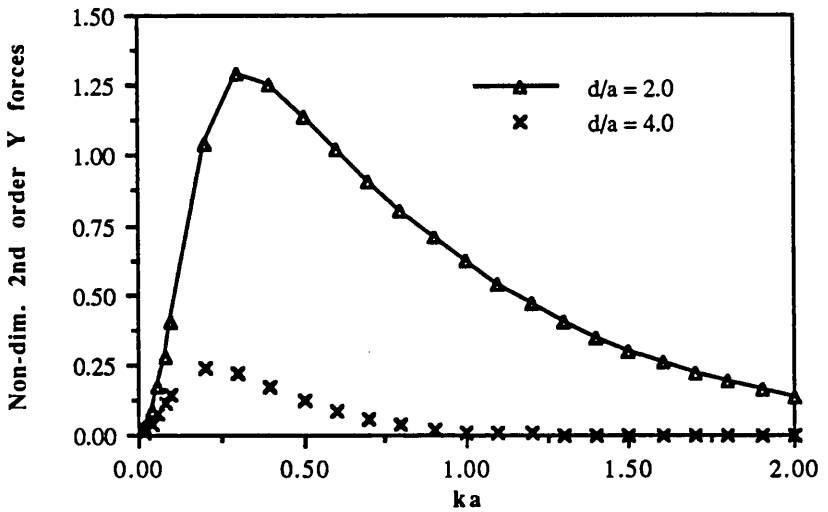

Fig.7.12 Non-dimensionalized 2nd order Y forces for different depths(c/a=4.0,Fn=0.2, no tilt in following waves)

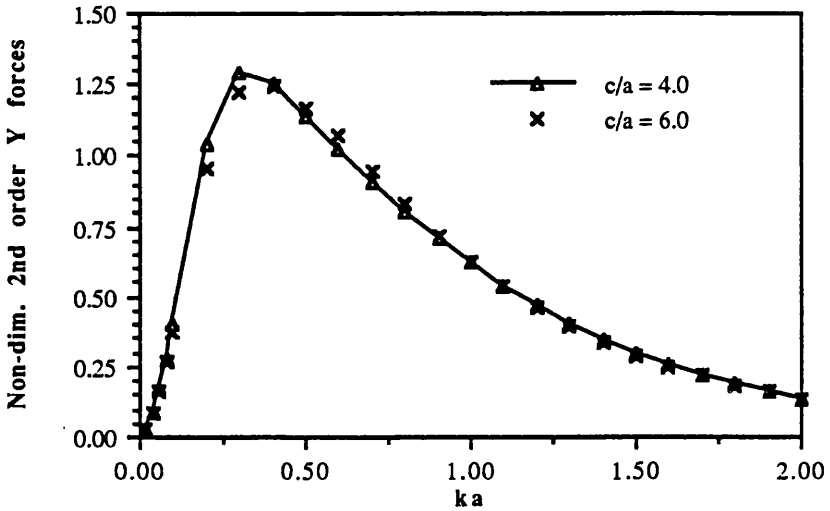

Fig.7.13 Non-dimensionalized 2nd order Y forces for different separation distances (d/a=2.0,Fn=0.2, no tilt in following waves)

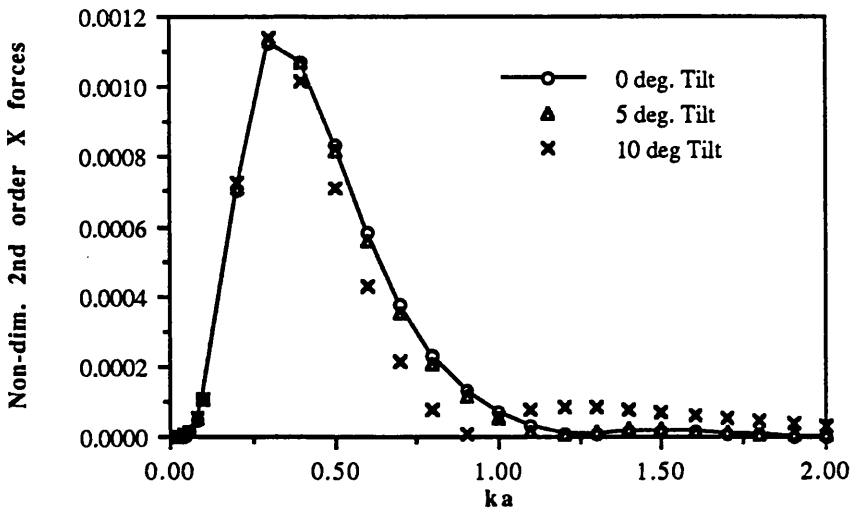

Fig.7.14 Non-dimensionalized 2nd order X forces for different inclinations(d/a=2.0, c/a=4.0, Fn=0.20 in following waves)

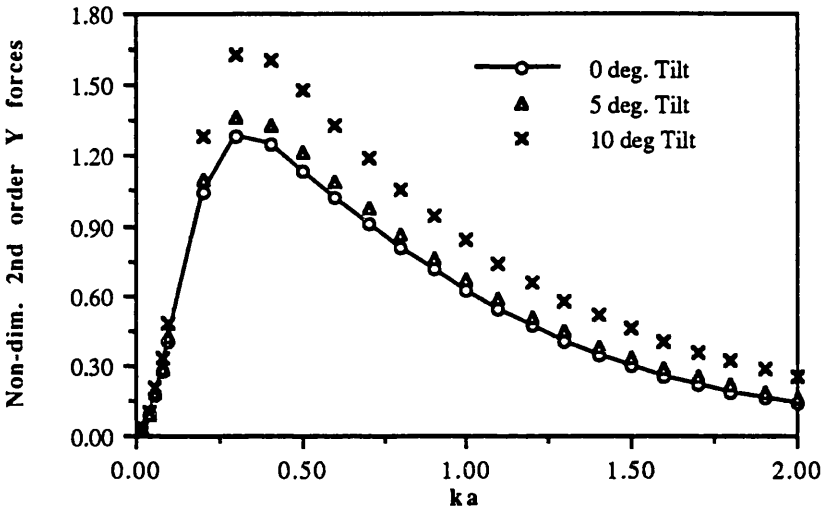

Fig.7.15 Non-dimensionalized 2nd order Y forces for different inclinations (d/a=2.0, c/a=4.0, Fn=0.20 in following waves)

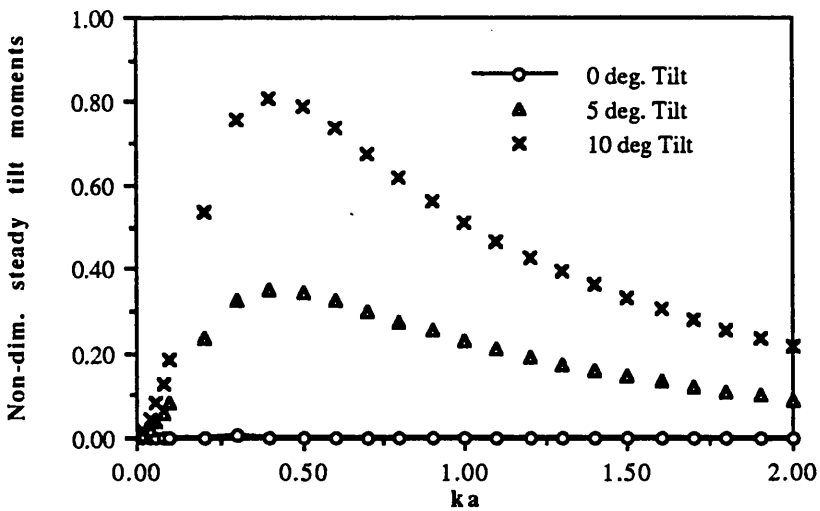

Fig.7.16 Non-dimensionalized steady tilt moments for different inclinations(d/a=2.0, c/a=4.0, Fn=0.20 in following waves)

Table 8.1 Results between CPU time and discrete element numbers for different submerged depths (c/a = 4.0, Fn = 0.20, no tilt in head waves ; NI = 10)

CPU time (Seconds)	NE = 10.0	NE = 20.0	NE = 30.0	NE = 40.0	NE = 50.0	NE = 60.0	NE = 70.0	NE = 80.0
d/a = 1.0	16	58	130	231	363	528	723	952
d/a = 2.0	16	61	137	244	383	556	762	1003
d/a = 3.0	15	58	129	231	363	526	722	950

Table 8.2 Results between CPU time and image numbers for different submerged depths (c/a = 4.0, Fn = 0.20, no tilt in head waves ; NE = 50)

CPU time (Seconds)	NI = 8.0	NI = 10.0	NI = 12.0	NI = 14.0	NI = 16.0	NI = 18.0	NI = 20.0	NI = 22.0
d/a = 1.0	365	364	364	365	365	365	364	365
d/a = 2.0	384	384	384	384	384	384	384	385
d/a = 3.0	363	363	364	363	364	364	364	364

Table 8.3 Results between error of surge damping coefficients and element numbers for different submerged depths (c/a = 4.0, Fn = 0.20, no tilt in head waves ; NI = 10)

Error of surge coef. (%)	NE = 10.0	NE = 20.0	NE = 30.0	NE = 40.0	NE = 50.0	NE = 60.0	NE = 70.0	NE = 80.0
d/a = 1.0	9.44	36.7	3.52	63.4	16.7	63.2	68.2	65.9
d/a = 2.0	2.77	1.11	0.69	0.5	0.39	0.32	0.27	0.23
d/a = 3.0	2.72	1.11	0.69	0.5	0.39	0.32	0.27	0.24

Table 8.4 Results between error of heave damping coefficients and element numbers for different submerged depths (c/a = 4.0, Fn = 0.20, no tilt in head waves ; NI = 10)

Error of heave coef. (%)	NE = 10.0	NE = 20.0	NE = 30.0	NE = 40.0	NE = 50.0	NE = 60.0	NE = 70.0	NE = 80.0
d/a = 1.0	207	80.3	6.83	26.8	282	48	55.8	55.3
d/a = 2.0	2.66	1.13	0.71	0.51	0.4	0.33	0.26	0.24
d/a = 3.0	2.72	1.14	0.71	0.52	0.41	0.33	0.28	0.246

Table 8.5 Results between error of pitch damping coefficients and element numbers for different submerged depths (c/a = 4.0, Fn = 0.20, no tilt in head waves ; NI = 10)

Error of pitch coef. (%)	NE = 10.0	NE = 20.0	NE = 30.0	NE = 40.0	NE = 50.0	NE = 60.0	NE = 70.0	NE = 80.0
d/a = 1.0	14.9	241	3.76	42.2	110	367	273	388
d/a = 2.0	2.65	1.12	0.69	0.5	0.39	0.32	0.27	0.24
d/a = 3.0	2.71	1.12	0.69	0.51	0.4	0.33	0.276	0.239

Table 8.6 Results between error of surge damping coefficients and image numbers for different submerged depths (c/a = 4.0, Fn = 0.20, no tilt in head waves ; NE = 50)

Error of surge coef. (%)	NI = 8.0	NI = 10.0	NI = 12.0	NI = 14.0	NI = 16.0	NI = 18.0	NI = 20.0	NI = 22.0
d/a = 1.0	16.7	16.7	16.7	16.7	16.7	16.7	16.7	16.7
d/a = 2.0	0.39	0.39	0.39	0.39	0.39	0.39	0.39	0.39
d/a = 3.0	0.39	0.39	0.39	0.39	0.39	0.39	0.39	0.39

Table 8.7 Results between error of heave damping coefficients and image numbers for different submerged depths (c/a = 4.0, Fn = 0.20, no tilt in head waves ; NE = 50)

Error of heave coef. (%)	NI = 8.0	NI = 10.0	NI = 12.0	NI = 14.0	NI = 16.0	NI = 18.0	NI = 20.0	NI = 22.0
d/a = 1.0	282	282	282	282	282	282	282	282
d/a = 2.0	0.4	0.4	0.4	0.4	0.4	0.4	0.4	0.4
d/a = 3.0	0.41	0.41	0.41	0.41	0.41	0.41	0.41	0.41

Table 8.8 Results between error of pitch damping coefficients and image numbers for different submerged depths (c/a = 4.0, Fn = 0.20, no tilt in head waves ; NE = 50)

Error of pitch coef. (%)	NI = 8.0	NI = 10.0	NI = 12.0	NI = 14.0	NI = 16.0	NI = 18.0	NI = 20.0	NI = 22.0
d/a = 1.0	110	110	110	110	110	110	110	110
d/a = 2.0	0.39	0.39	0.39	0.39	0.39	0.39	0.39	0.39
d/a = 3.0	0.4	0.4	0.4	0.4	0.4	0.4	0.4	0.4

Table 8.9 Accuracy check of surge damping coefficients for different submerged depths (c/a = 4.0, Fn = 0.20, no tilt in head waves ; NE = 50, NI = 10)

Check of surge damp. coef.	NE = 10.0	NE = 20.0	NE = 30.0	NE = 40.0	NE = 50.0	NE = 60.0	NE = 70.0	NE = 80.0
d/a = 1 (Pressure integration)	0.165	0.0889	0.309	0.119	-0.0377	1.554	1.291	1.051
d/a = 1 (Energy flux check)	0.199	0.0411	0.332	0.0266	-0.0527	6.886	6.818	5.112
d/a = 2 (Pressure integration)	0.0228	0.0238	0.0241	0.0242	0.0243	0.0243	0.0244	0.0244
d/a = 2 (Energy flux check)	0.0241	0.0244	0.0245	0.0245	0.0245	0.0245	0.0245	0.0245
d/a = 3 (Pressure integration)	0.0025	0.00261	0.00264	0.00265	0.00266	0.00266	0.00266	0.00267
d/a = 3 (Energy flux check)	0.00264	0.00267	0.00267	0.00268	0.00268	0.00268	0.00268	0.00268

Table 8.10 Accuracy check of heave damping coefficients for different submerged depths (c/a = 4.0, Fn = 0.20, no tilt in head waves ; NE = 50, NI = 10)

Check of heave damp. coef.	NE = 10.0	NE = 20.0	NE = 30.0	NE = 40.0	NE = 50.0	NE = 60.0	NE = 70.0	NE = 80.0
d/a = 1 (Pressure integration)	-0.195	0.0778	0.452	0.119	0.0216	2.332	1.897	1.492
d/a = 1 (Energy flux check)	0.199	0.0411	0.332	0.0266	-0.0454	6.641	6.694	5.189
d/a = 2 (Pressure integration)	0.0266	0.0279	0.0283	0.0284	0.0285	0.0285	0.0286	0.0286
d/a = 2 (Energy flux check)	0.0281	0.0286	0.0287	0.0287	0.0287	0.0287	0.0287	0.0287
d/a = 3 (Pressure integration)	0.00934	0.00969	0.00978	0.00982	0.00984	0.00986	0.00987	0.00988
d/a = 3 (Energy flux check)	0.00986	0.00991	0.00992	0.00992	0.00992	0.00992	0.00992	0.00992

Table 8.11 Accuracy check of pitch damping coefficients for different submerged depths (c/a = 4.0, Fn = 0.20, no tilt in head waves ; NE = 50, NI = 10)

Check of pitch damp. coef.	NE = 10.0	NE = 20.0	NE = 30.0	NE = 40.0	NE = 50.0	NE = 60.0	NE = 70.0	NE = 80.0
d/a = 1 (Pressure integration)	1.329	-0.0675	0.019	0.0128	0.16	-1.205	-1.03	-0.836
d/a = 1 (Energy flux check)	1.795	0.0279	0.0204	0.0314	-0.00747	2.107	2.22	1.417
d/a = 2 (Pressure integration)	0.0504	0.0519	0.0523	0.0524	0.0526	0.0526	0.0527	0.0527
d/a = 2 (Energy flux check)	0.0531	0.053	0.053	0.053	0.053	0.053	0.053	0.053
d/a = 3 (Pressure integration)	0.00934	0.00969	0.00978	0.00982	0.00984	0.00986	0.00987	0.00988
d/a = 3 (Energy flux check)	0.00986	0.00991	0.00992	0.00992	0.00992	0.00992	0.00992	0.00992

Table 8.12 Accuracy check of surge Kochin functions for different submerged depths (c/a = 4.0, Fn = 0.20, no tilt in head waves ; NE = 50, NI = 10)

Check of surge Kochin fun.	NE = 10.0	NE = 20.0	NE = 30.0	NE = 40.0	NE = 50.0	NE = 60.0	NE = 70.0	NE = 80.0
d/a = 1 (Radiation problem)	1.299	0.799	2.335	0.605	0.184	17.709	13.826	10.59
d/a = 1 (Haskind-Newman)	1.189	0.614	2.238	0.573	0.319	16.779	13.203	10.259
d/a = 2 (Radiation problem)	0.634	0.637	0.638	0.638	0.638	0.638	0.638	0.638
d/a = 2 (Haskind-Newman)	0.599	0.623	0.629	0.632	0.633	0.634	0.635	0.635
d/a = 3 (Radiation problem)	0.215	0.217	0.217	0.217	0.217	0.217	0.217	0.217
d/a = 3 (Haskind-Newman)	0.204	0.212	0.214	0.215	0.215	0.216	0.216	0.216

Table 8.13 Accuracy check of heave Kochin functions for different submerged depths (c/a = 4.0, Fn = 0.20, no tilt in head waves ; NE = 50, NI = 10)

Check of heave Kochin fun.	NE = 10.0	NE = 20.0	NE = 30.0	NE = 40.0	NE = 50.0	NE = 60.0	NE = 70.0	NE = 80.0
d/a = 1 (Radiation problem)	1.252	0.253	2.548	0.929	2.001	17.56	14.057	11.105
d/a = 1 (Haskind-Newman)	1.959	1.362	3.007	1.371	2.111	24.62	18.818	13.789
d/a = 2 (Radiation problem)	0.684	0.689	0.691	0.691	0.691	0.691	0.691	0.691
d/a = 2 (Haskind-Newman)	0.649	0.674	0.681	0.684	0.685	0.687	0.687	0.688
d/a = 3 (Radiation problem)	0.232	0.233	0.233	0.233	0.233	0.233	0.233	0.233
d/a = 3 (Haskind-Newman)	0.219	0.228	0.231	0.231	0.231	0.232	0.232	0.232

Table 8.14 Accuracy check of pitch Kochin functions for different submerged depths (c/a = 4.0, Fn = 0.20, no tilt in head waves ; NE = 50, NI = 10)

Check of pitch Kochin fun.	NE = 10.0	NE = 20.0	NE = 30.0	NE = 40.0	NE = 50.0	NE = 60.0	NE = 70.0	NE = 80.0
d/a = 1 (Radiation problem)	1.356	0.659	0.526	0.395	0.795	11.284	8.927	7.021
d/a = 1 (Haskind-Newman)	3.271	1.243	0.699	0.517	2.481	18.799	15.043	11.342
d/a = 2 (Radiation problem)	0.941	0.938	0.938	0.937	0.937	0.937	0.937	0.937
d/a = 2 (Haskind-Newman)	0.892	0.918	0.925	0.928	0.931	0.931	0.932	0.933
d/a = 3 (Radiation problem)	0.416	0.417	0.417	0.418	0.418	0.418	0.418	0.418
d/a = 3 (Haskind-Newman)	0.394	0.408	0.412	0.413	0.414	0.415	0.415	0.416

Table 8.15 Comparison of CPU time between two approaches (d/a = 2.0, c/a = 4.0, Fn = 0.20, 5 degree tilt in head waves ; NE = 50, NI = 10)

CPU time (Seconds)	ka = 0.02	ka = 0.04	ka = 0.06	ka = 0.08	ka = 0.10	ka = 0.20	ka = 0.30	ka = 0.40	ka = 0.50	ka = 0.60	ka = 0.70
Discrete source method	172	184	197	204	208	235	262	288	315	343	368
Direct Green function method	85	90	94	98	100	110	121	131	141	152	163

ka = 0.80	ka = 0.90	ka = 1.00	ka = 1.10	ka = 1.20	ka = 1.30	ka = 1.40	ka = 1.50	ka = 1.60	ka = 1.70	ka = 1.80	ka = 1.90	ka = 2.00
374	368	384	356	333	324	320	319	319	320	319	317	315
165	163	171	165	152	148	146	145	145	144	143	142	142

Table 8.16 Relative error of surge damping coefficients between two approaches (d/a = 2.0, c/a = 4.0, Fn = 0.20, 5 degree tilt in head waves ; NE = 50, NI = 10)

Error of surge damp coef. (%)	Ka = 0.0212	Ka = 0.0433	Ka = 0.0661	Ka = 0.0893	Ka = 0.113	Ka = 0.237	Ka = 0.369	Ka = 0.508	Ka = 0.651	Ka = 0.801	Ka = 0.954
Discrete source method	0.388	0.464	0.477	0.483	0.487	0.492	0.467	0.464	0.533	0.561	0.579
Direct Green function method	0.016	0.049	0.06	0.065	0.067	0.07	0.057	0.068	0.096	0.11	0.12

Ka = 1.112	Ka = 1.274	Ka = 1.441	Ka = 1.609	Ka = 1.783	Ka = 1.961	Ka = 2.141	Ka = 2.325	Ka =2.512	Ka = 2.702	Ka =2.896	Ka =3.092	Ka = 3.291
0.472	0.429	0.395	0.389	0.384	0.38	0.376	0.373	0.37	0.369	0.37	0.374	0.389
0.07	0.049	0.026	0.022	0.019	0.016	0.014	0.012	0.01	0.008	0.007	0.007	0.011

Table 8.17 Relative error of heave damping coefficients between two approaches (d/a = 2.0, c/a = 4.0, Fn = 0.20, 5 degree tilt in head waves ; NE = 50, NI = 10)

Error of heave damp coef. (%)	Ka = 0.0212	Ka = 0.0433	Ka = 0.0661	Ka = 0.0893	Ka = 0.113	Ka = 0.237	Ka = 0.369	Ka = 0.508	Ka = 0.651	Ka = 0.801	Ka = 0.954
Discrete source method	0.454	0.476	0.482	0.486	0.488	0.493	0.467	0.445	0.516	0.548	0.567
Direct Green function method	0.07	0.074	0.075	0.077	0.078	0.08	0.065	0.061	0.092	0.11	0.11

Ka = 1.112	Ka = 1.274	Ka = 1.441	Ka = 1.609	Ka = 1.783	Ka = 1.961	Ka = 2.141	Ka = 2.325	Ka =2.512	Ka = 2.702	Ka =2.896	Ka = 3.092	Ka = 3.291
0.461	0.429	0.401	0.396	0.392	0.389	0.385	0.382	0.38	0.377	0.376	0.375	0.376
0.052	0.048	0.032	0.03	0.029	0.028	0.027	0.025	0.025	0.024	0.023	0.023	0.024

Table 8.18 Relative error of pitch damping coefficients between two approaches (d/a = 2.0, c/a = 4.0, Fn = 0.20, 5 degree tilt in head waves ; NE = 50, NI = 10)

Error of pitch damp coef. (%)	Ka = 0.0212	Ka = 0.0433	Ka = 0.0661	Ka = 0.0893	Ka = 0.113	Ka = 0.237	Ka = 0.369	Ka = 0.508	Ka = 0.651	Ka = 0.801	Ka = 0.954
Discrete source method	0.441	0.435	0.509	0.518	0.518	0.518	0.52	0.516	0.488	0.422	0.42
Direct Green function method	0.01	0.014	0.077	0.089	0.089	0.086	0.086	0.082	0.066	0.035	0.039

Ka = 1.112	Ka = 1.274	Ka = 1.441	Ka = 1.609	Ka = 1.783	Ka = 1.961	Ka = 2.141	Ka = 2.325	Ka =2.512	Ka = 2.702	Ka =2.896	Ka =3.092	Ka = 3.291
0.421	0.398	0.395	0.395	0.398	0.408	0.439	0.522	0.557	0.465	0.417	0.398	0.391
0.04	0.025	0.023	0.023	0.025	0.032	0.052	0.108	0.12	0.061	0.035	0.025	0.02

Table 8.19 Accuracy check of surge damping coefficients between two approaches (d/a = 2.0, c/a = 4.0, Fn = 0.20, 5 degree tilt in head waves; NE = 50, NI = 10)

Check of surge damp coef.	Ka = 0.0212	Ka = 0.0433	Ka = 0.0661	Ka = 0.0893	Ka = 0.113	Ka = 0.237	Ka = 0.369	Ka = 0.508	Ka = 0.651	Ka = 0.801	Ka = 0.954
.S. Method (Pressure integration)	0.0112	0.0464	0.105	0.182	0.267	0.41	0.173	0.0893	0.141	0.123	0.0364
.S. Method (Energy flux check)	0.0113	0.0468	0.106	0.184	0.27	0.414	0.175	0.0902	0.142	0.125	0.0368
ect G.F.M.(Pressure integration)	0.0117	0.0492	0.113	0.2	0.299	0.467	0.1845	0.1218	0.2099	0.1807	0.05487
rect G.F.M. (Energy flux check)	0.0117	0.0491	0.113	0.1997	0.298	0.467	0.1843	0.1217	0.2095	0.1804	0.05473

Ka = 1.112	Ka = 1.274	Ka = 1.441	Ka = 1.609	Ka = 1.783	Ka = 1.961	Ka = 2.141	Ka = 2.325	Ka =2.512	Ka = 2.702	Ka = 2.896	Ka =3.092	Ka = 3.291
0.00606	0.0127	0.0172	0.0207	0.0213	0.0196	0.0164	0.0126	0.009	0.00593	0.0036	0.00199	0.000999
0.00611	0.0129	0.0174	0.0208	0.0215	0.0197	0.0165	0.0127	0.00907	0.00598	0.00363	0.00201	0.00101
0.00992	0.02093	0.02617	0.03113	0.03218	0.02988	0.0254	0.01993	0.0145	0.009766	0.006059	0.00343	0.00175
0.0099	0.02091	0.02616	0.03111	0.03217	0.02987	0.02539	0.01993	0.0145	0.009765	0.006058	0.00343	0.00175

Table 8.20 Accuracy check of heave damping coefficients between two approaches (d/a = 2.0, c/a = 4.0, Fn = 0.20, 5 degree tilt in head waves; NE = 50, NI = 10)

Check of heave damp coef.	Ka = 0.0212	Ka = 0.0433	Ka = 0.0661	Ka = 0.0893	Ka = 0.113	Ka = 0.237	Ka = 0.369	Ka = 0.508	Ka = 0.651	Ka = 0.801	Ka = 0.954
.S. Method (Pressure integration)	0.0146	0.0605	0.137	0.238	0.349	0.522	0.213	0.108	0.167	0.145	0.0435
.S. Method (Energy flux check)	0.0147	0.0611	0.139	0.241	0.353	0.527	0.215	0.109	0.168	0.147	0.044
ect G.F.M.(Pressure integration)	0.01527	0.06427	0.1485	0.2628	0.3921	0.5951	0.2235	0.1443	0.2474	0.2128	0.06529
rect G.F.M. (Energy flux check)	0.01525	0.06418	0.1483	0.2624	0.3915	0.5941	0.2232	0.1441	0.2469	0.2123	0.06514

Ka = 1.112	Ka = 1.274	Ka = 1.441	Ka = 1.609	Ka = 1.783	Ka = 1.961	Ka = 2.141	Ka = 2.325	Ka =2.512	Ka = 2.702	Ka =2.896	Ka = 3.092	Ka =3.291
0.00646	0.0142	0.0201	0.0248	0.0261	0.0244	0.0207	0.0162	0.0118	0.00792	0.00492	0.00281	0.00146
0.00652	0.0144	0.0203	0.025	0.0263	0.0245	0.0209	0.0164	0.0119	0.00798	0.00496	0.00283	0.00147
0.01057	0.02334	0.03061	0.03733	0.03933	0.03714	0.03207	0.0256	0.01897	0.01305	0.008305	0.004849	0.002566
0.01056	0.02332	0.03059	0.03731	0.03931	0.03711	0.03205	0.02558	0.01896	0.01304	0.008301	0.004847	0.002565

Table 8.21 Accuracy check of pitch damping coefficients between two approaches (d/a = 2.0, c/a = 4.0, Fn = 0.20, 5 degree tilt in head waves ; NE = 50, NI = 10)

Check of pitch damp coef.	Ka = 0.0212	Ka = 0.0433	Ka = 0.0661	Ka = 0.0893	Ka = 0.113	Ka = 0.237	Ka = 0.369	Ka = 0.508	Ka = 0.651	Ka = 0.801	Ka = 0.954
.S. Method (Pressure integration)	0.000278	0.0016	0.00599	0.0167	0.0374	0.31	0.551	0.498	0.279	0.141	0.122
.S. Method (Energy flux check)	0.000276	0.00161	0.00606	0.0169	0.0378	0.313	0.557	0.504	0.281	0.143	0.123
ect G.F.M.(Pressure integration)	0.0003036	0.001852	0.007091	0.02013	0.04611	0.4036	0.7095	0.6224	0.3365	0.1734	0.1595
rect G.F.M. (Energy flux check)	0.0003099	0.001852	0.00708	0.0201	0.04602	0.4029	0.7082	0.6214	0.3361	0.1733	0.1593

Ka = 1.112	Ka = 1.274	Ka = 1.441	Ka = 1.609	Ka = 1.783	Ka = 1.961	Ka = 2.141	Ka = 2.325	Ka =2.512	Ka = 2.702	Ka = 2.896	Ka = 3.092	Ka =3.291
0.0978	0.0636	0.0418	0.0249	0.0133	0.00613	0.00234	0.000792	0.000488	0.00072	0.00105	0.00126	0.0013
0.0986	0.0641	0.0421	0.0251	0.0134	0.00618	0.00237	0.0008	0.000494	0.000727	0.00106	0.00127	0.00131
0.1302	0.08198	0.05422	0.0326	0.01748	0.008058	0.003045	0.001026	0.0007325	0.001202	0.001808	0.002225	0.002347
0.1301	0.08194	0.05419	0.03258	0.01748	0.008052	0.003042	0.001024	0.0007307	0.0012	0.001807	0.002224	0.002346

Table 8.22 Accuracy check of surge Kochin functions between two approaches (d/a = 2.0, c/a = 4.0, Fn = 0.20, 5 degree tilt in head waves ; NE = 50, NI = 10)

Check of surge Kochin fun.	ka = 0.02	ka = 0.04	ka = 0.06	ka = 0.08	ka = 0.10	ka = 0.20	ka = 0.30	ka = 0.40	ka = 0.50	ka = 0.60	ka = 0.70
D.S. Method (Radiation problem)	0.226	0.436	0.626	0.795	0.941	1.331	1.25	0.943	0.587	0.251	0.161
D.S. Method (Haskind-Newman)	0.228	0.44	0.634	0.807	0.959	1.381	1.31	1.017	0.668	0.339	0.158
Direct G.F.M.(Radiation problem)	0.2285	0.4433	0.6403	0.8234	0.984	1.454	1.385	1.0571	0.6792	0.327	0.1955
Direct G.F.M. (Haskind-Newman)	0.2283	0.4442	0.6431	0.8171	0.9772	1.405	1.318	0.9739	0.5764	0.2683	0.1632

ka = 0.80	ka = 0.90	ka = 1.00	ka = 1.10	ka = 1.20	ka = 1.30	ka = 1.40	ka = 1.50	ka = 1.60	ka = 1.70	ka = 1.80	ka = 1.90	ka = 2.00
0.265	0.435	0.546	0.605	0.618	0.596	0.549	0.484	0.411	0.332	0.257	0.188	0.128
0.191	0.375	0.501	0.574	0.599	0.587	0.546	0.486	0.414	0.338	0.263	0.193	0.132
0.2788	0.4515	0.596	0.683	0.7191	0.7116	0.6701	0.6038	0.5218	0.432	0.3416	0.255	0.1681
0.3615	0.5516	0.677	0.744	0.7609	0.7372	0.6827	0.6071	0.5188	0.4254	0.3328	0.246	0.1764

Table 8.23 Accuracy check of heave Kochin functions between two approaches (d/a = 2.0, c/a = 4.0, Fn = 0.20, 5 degree tilt in head waves ; NE = 50, NI = 10)

Check of heave Kochin fun.	ka = 0.02	ka = 0.04	ka = 0.06	ka = 0.08	ka = 0.10	ka = 0.20	ka = 0.30	ka = 0.40	ka = 0.50	ka = 0.60	ka = 0.70
D.S. Method (Radiation problem)	0.262	0.509	0.735	0.938	1.112	1.512	1.387	1.071	0.698	0.331	0.188
D.S. Method (Haskind-Newman)	0.265	0.512	0.74	0.942	1.114	1.507	1.409	1.131	0.784	0.425	0.162
Direct G.F.M.(Radiation problem)	0.266	0.5191	0.754	0.9656	1.148	1.567	1.467	1.1766	0.8097	0.4239	0.1984
Direct G.F.M. (Haskind-Newman)	0.266	0.5196	0.7561	0.9707	1.158	1.591	1.451	1.1048	0.7775	0.3713	0.1982

ka = 0.80	ka = 0.90	ka = 1.00	ka = 1.10	ka = 1.20	ka = 1.30	ka = 1.40	ka = 1.50	ka = 1.60	ka = 1.70	ka = 1.80	ka = 1.90	ka = 2.00
0.262	0.458	0.589	0.661	0.683	0.665	0.617	0.549	0.471	0.386	0.304	0.227	0.159
0.177	0.387	0.534	0.622	0.657	0.651	0.611	0.549	0.473	0.391	0.309	0.232	0.164
0.3343	0.5353	0.7536	0.8368	0.8766	0.8064	0.7675	0.6903	0.5944	0.4986	0.4003	0.3056	0.2188
0.3642	0.5838	0.7322	0.8153	0.8421	0.8231	0.7688	0.6899	0.5959	0.4949	0.3938	0.2979	0.2111

Table 8.24 Accuracy check of pitch Kochin functions between two approaches (d/a = 2.0, c/a = 4.0, Fn = 0.20, 5 degree tilt in head waves ; NE = 50, NI = 10)

Check of pitch Kochin fun.	ka = 0.02	ka = 0.04	ka = 0.06	ka = 0.08	ka = 0.10	ka = 0.20	ka = 0.30	ka = 0.40	ka = 0.50	ka = 0.60	ka = 0.70
D.S. Method (Radiation problem)	0.00971	0.0137	0.0555	0.113	0.183	0.644	1.073	1.336	1.443	1.435	1.349
D.S. Method (Haskind-Newman)	0.0099	0.0135	0.0548	0.11	0.177	0.601	0.983	1.217	1.321	1.327	1.268
Direct G.F.M.(Radiation problem)	0.009725	0.01433	0.05694	0.1145	0.1844	0.6909	1.063	1.414	1.618	1.621	1.536
Direct G.F.M. (Haskind-Newman)	0.009816	0.01441	0.05801	0.1181	0.1924	0.7007	1.188	1.483	1.602	1.596	1.504

ka = 0.80	ka = 0.90	ka = 1.00	ka = 1.10	ka = 1.20	ka = 1.30	ka = 1.40	ka = 1.50	ka = 1.60	ka = 1.70	ka = 1.80	ka = 1.90	ka = 2.00
1.209	1.035	0.845	0.656	0.477	0.317	0.181	0.0995	0.0946	0.0871	0.119	0.142	0.151
1.157	1.009	0.839	0.663	0.492	0.335	0.198	0.0883	0.0966	0.0955	0.113	0.138	0.148
1.359	1.128	0.932	0.7438	0.558	0.3837	0.2282	0.1096	0.1171	0.1212	0.1569	0.1912	0.1979
1.354	1.164	0.955	0.7432	0.5413	0.3582	0.2094	0.1205	0.1121	0.1121	0.1634	0.1935	0.2056

Table 8.25 Accuracy check of second order horizontal forces between two approaches (d/a = 2.0, c/a = 4.0, Fn = 0.20, 5 degree tilt in head waves; NE = 50, NI = 10)

Check of 2nd order forces	ka = 0.02	ka = 0.04	ka = 0.06	ka = 0.08	ka = 0.10	ka = 0.20	ka = 0.30	ka = 0.40	ka = 0.50	ka = 0.60	ka = 0.70
D.S. Method (Pressure integration)	0.0021534	0.002752	0.0019942	0.000069327	0.0028129	0.022914	0.037944	0.045138	0.047453	0.046621	0.04375
D.S. Method(Momentum flux check)	6.702E-07	0.000011515	0.000059601	0.00018379	0.00041609	0.0022455	0.0021909	0.0011628	0.00037933	0.000049034	2.5922E-06
Direct G.F.M. (Pressure integration)	5.853E-07	0.000011875	0.000065069	0.0002097	0.00049375	0.0029648	0.0029047	0.001501	0.00044405	8.432E-07	0.00005487
Direct G.F.M. (Momentum check)	7.0799E-07	0.000012508	0.000066826	0.00021325	0.00049974	0.0029929	0.0029639	0.001579	0.00052412	0.000070665	3.5797E-06

ka = 0.80	ka = 0.90	ka = 1.00	ka = 1.10	ka = 1.20	ka = 1.30	ka = 1.40	ka = 1.50	ka = 1.60	ka = 1.70	ka = 1.80	ka = 1.90	ka = 2.00
0.039695	0.035118	0.030584	0.026334	0.022484	0.019072	0.016091	0.013513	0.011303	0.0094126	0.007831	0.006494	0.0053756
0.000015657	3.9394E-06	2.8656E-08	3.2374E-36	1.4238E-36	6.224E-37	2.7069E-37	1.1731E-37	0	0	0	0	0
0.000012801	0.000022209	0.000024833	0.000018198	0.000013321	9.8221E-06	7.2915E-06	0.000005429	4.0333E-06	2.9755E-06	0.000021721	1.5653E-06	1.1124E-06
0.000032417	0.000011691	9.6351E-08	5.043E-29	1.9184E-29	7.944E-30	3.5334E-30	1.6599E-30	8.1039E-31	4.0582E-31	2.0646E-31	1.0602E-31	5.4713E-32

Table 8.26 Comparison of surge amplitudes between both approaches (d/a = 2.0, c/a = 4.0, Fn = 0.20, 5 degree tilt in head waves ; NE = 50, NI = 10)

Surge amplitude (M/M)	ka = 0.02	ka = 0.04	ka = 0.06	ka = 0.08	ka = 0.10	ka = 0.20	ka = 0.30	ka = 0.40	ka = 0.50	ka = 0.60	ka = 0.70
Discrete source method	0.34	0.473	0.528	0.546	0.544	0.437	0.329	0.226	0.123	0.049	0.015
Direct Green function method	0.336	0.473	0.531	0.552	0.553	0.451	0.351	0.246	0.132	0.048	0.014

ka = 0.80	ka = 0.90	ka = 1.00	ka = 1.10	ka = 1.20	ka = 1.30	ka = 1.40	ka = 1.50	ka = 1.60	ka = 1.70	ka = 1.80	ka = 1.90	ka = 2.00
0.029	0.032	0.039	0.039	0.037	0.033	0.029	0.023	0.019	0.014	0.01	0.007	0.005
0.026	0.04	0.046	0.047	0.045	0.041	0.035	0.029	0.024	0.018	0.014	0.01	0.007

Table 8.27 Comparison of heave amplitudes between both approaches (d/a = 2.0, c/a = 4.0, Fn = 0.20, 5 degree tilt in head waves ; NE = 50, NI = 10)

Heave amplitude (M/M)	ka = 0.02	ka = 0.04	ka = 0.06	ka = 0.08	ka = 0.10	ka = 0.20	ka = 0.30	ka = 0.40	ka = 0.50	ka = 0.60	ka = 0.70
Discrete source method	0.371	0.507	0.562	0.58	0.581	0.499	0.325	0.187	0.114	0.063	0.026
Direct Green function method	0.367	0.507	0.565	0.588	0.592	0.512	0.339	0.191	0.121	0.07	0.031

ka = 0.80	ka = 0.90	ka = 1.00	ka = 1.10	ka = 1.20	ka = 1.30	ka = 1.40	ka = 1.50	ka = 1.60	ka = 1.70	ka = 1.80	ka = 1.90	ka = 2.00
0.023	0.033	0.038	0.039	0.037	0.033	0.029	0.024	0.019	0.015	0.011	0.008	0.005
0.03	0.041	0.047	0.048	0.046	0.041	0.036	0.03	0.024	0.019	0.014	0.01	0.007

Table 8.28 Comparison of pitch amplitudes between both approaches (d/a = 2.0, c/a = 4.0, Fn = 0.20, 5 degree tilt in head waves ; NE = 50, NI = 10)

Pitch amplitude (Radian)	ka = 0.02	ka = 0.04	ka = 0.06	ka = 0.08	ka = 0.10	ka = 0.20	ka = 0.30	ka = 0.40	ka = 0.50	ka = 0.60	ka = 0.70
Discrete source method	0.002	0.029	0.055	0.079	0.1	0.164	0.217	0.254	0.236	0.19	0.145
Direct Green function method	0.002	0.029	0.055	0.079	0.101	0.164	0.233	0.288	0.271	0.219	0.166

ka = 0.80	ka = 0.90	ka = 1.00	ka = 1.10	ka = 1.20	ka = 1.30	ka = 1.40	ka = 1.50	ka = 1.60	ka = 1.70	ka = 1.80	ka = 1.90	ka = 2.00
0.112	0.083	0.06	0.042	0.028	0.017	0.01	0.006	0.004	0.005	0.005	0.006	0.005
0.129	0.096	0.07	0.049	0.033	0.02	0.012	0.007	0.006	0.007	0.007	0.008	0.007

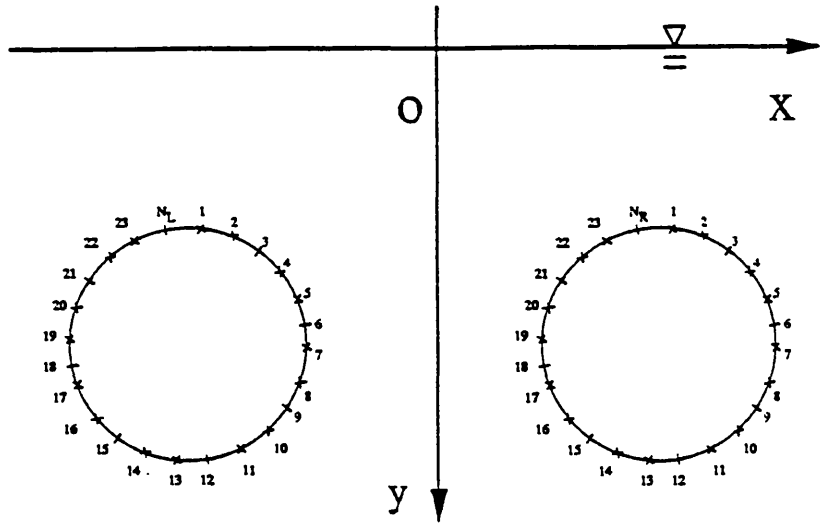

Fig.8.1 The schematic illustration of the simplified model in numerical computations

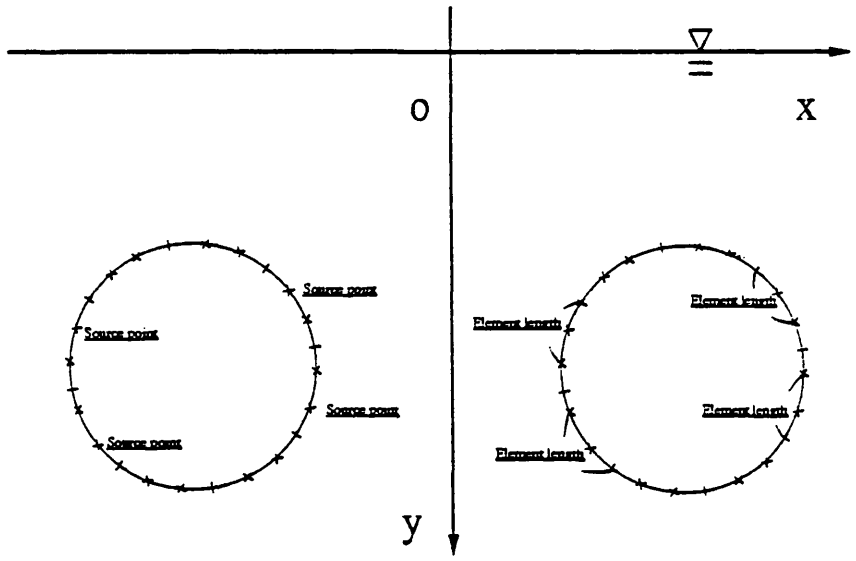

Fig.8.2 The description of discretized elements in numerical computations

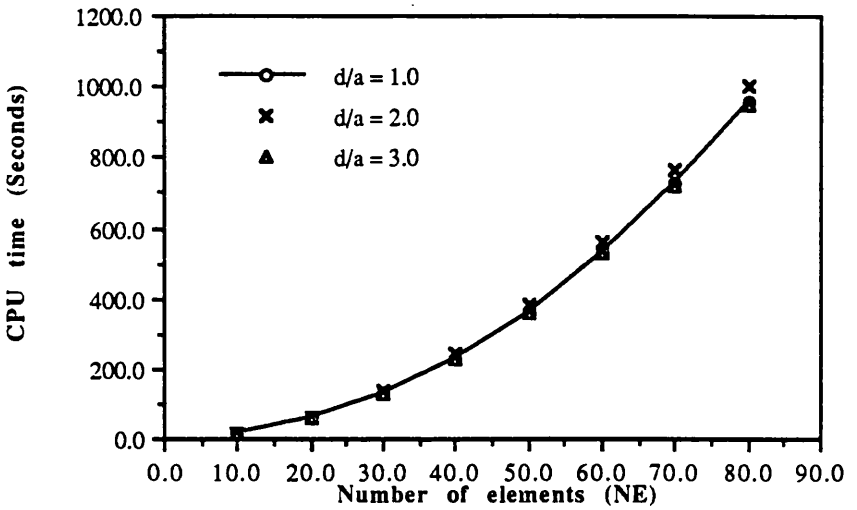

Fig.8.3 Relation between CPU time and element numbers for different depths (c/a=4,Fn=0.2,no tilt in head waves;NI=10)

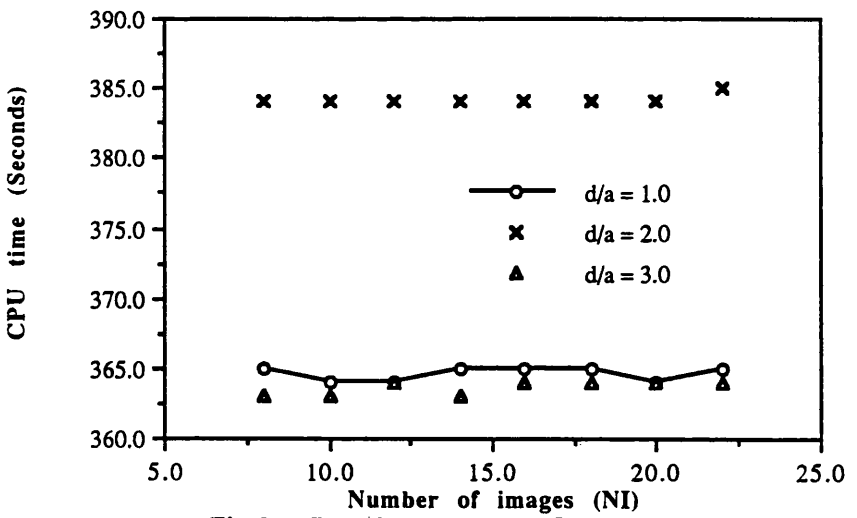

Fig.8.4 Relation between CPU time and image numbers for different depths(c/a=4, Fn=0.2,0 deg. tilt in head waves;NE=50)

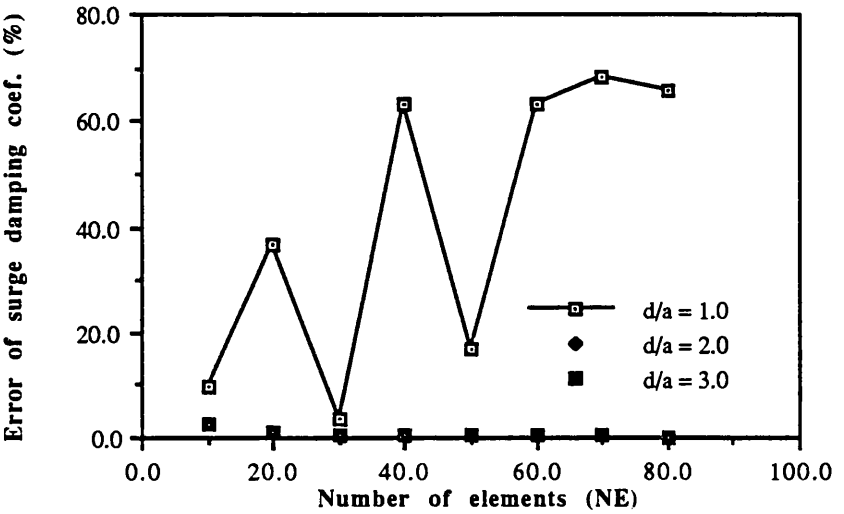

Fig.8.5 Relative error of surge damp. coef. for different submerged depths (c/a=4.0, Fn=0.20, no tilt in head waves ; NI=10)

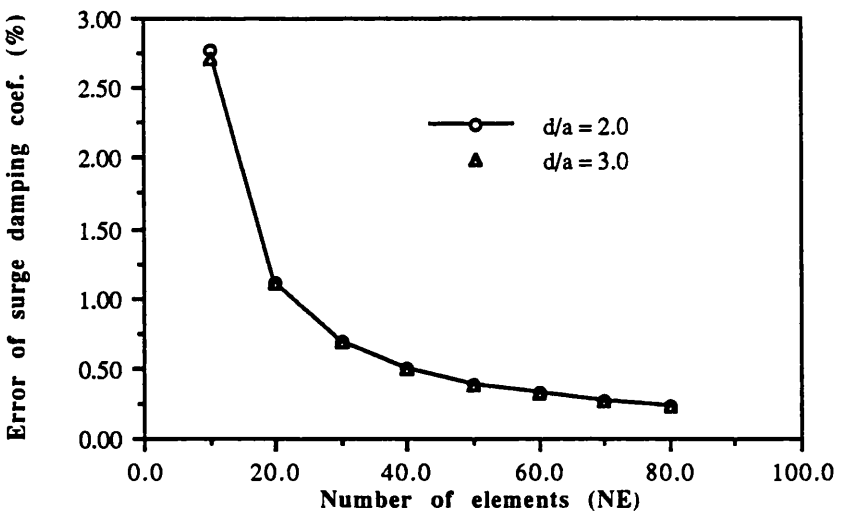

Fig.8.6 Relative error of surge damp. coef. for different submerged depths (c/a=4.0, Fn=0.20, no tilt in head waves ; NI=10)

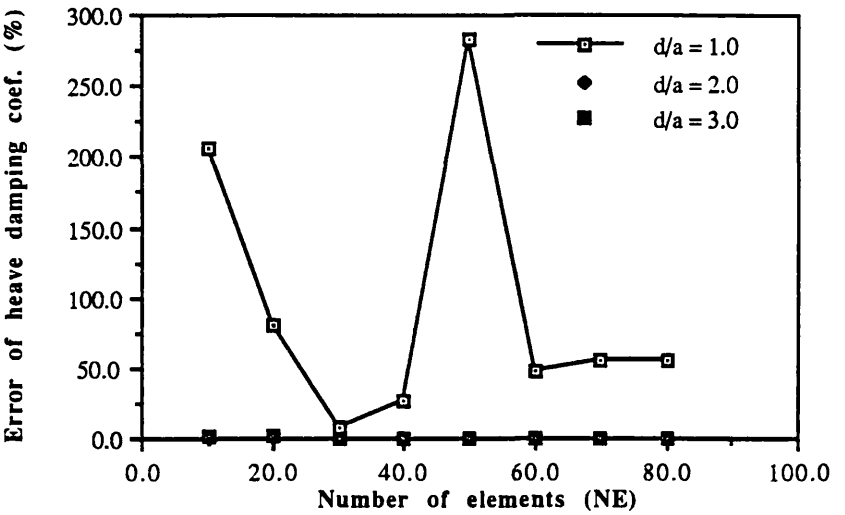

Fig.8.7 Relative error of heave damp. coef. for different submerged depths (c/a=4.0, Fn=0.20, no tilt in head waves ; NI=10)

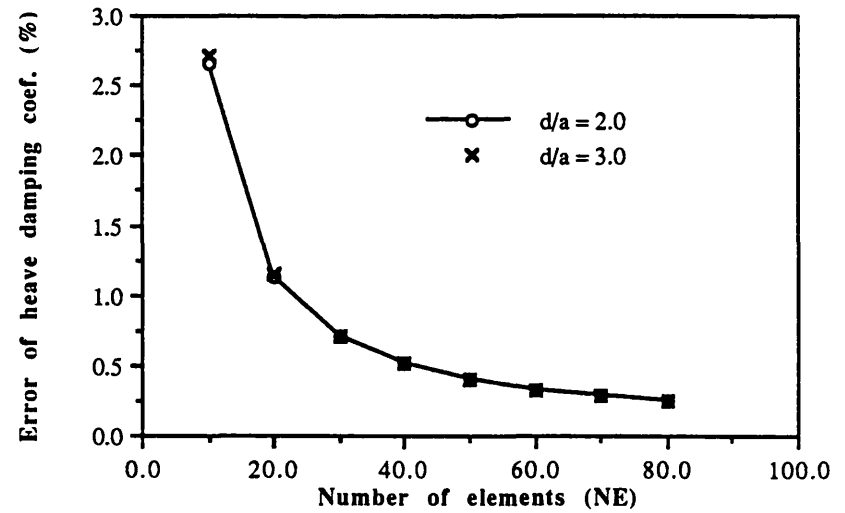

Fig.8.8 Relative error of heave damp. coef. for different submerged depths (c/a=4.0, Fn=0.20, no tilt in head waves ; NI=10)

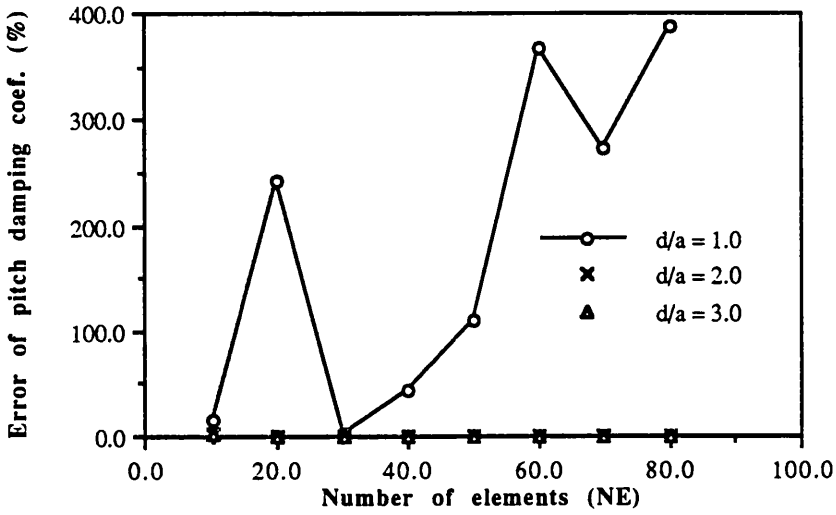

Fig.8.9 Relative error of pitch damp. coef. for different submerged depths (c/a=4.0, Fn=0.20, no tilt in head waves ; NI=10)

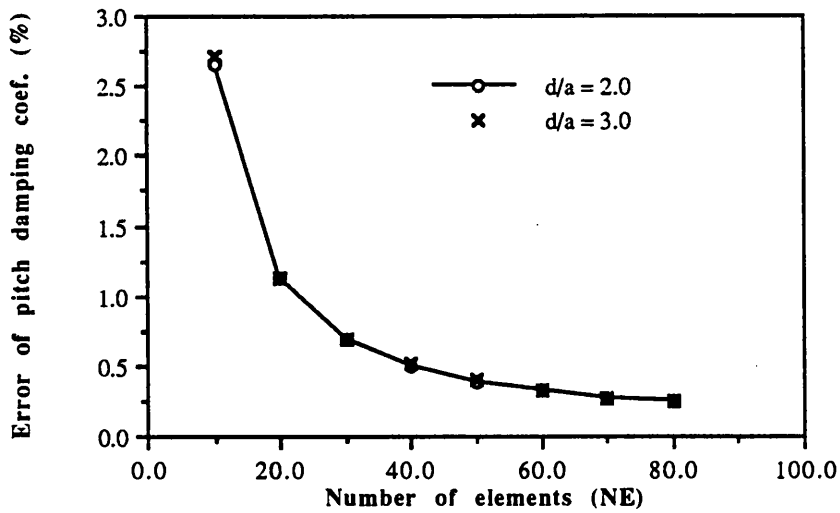

Fig.8.10 Relative error of pitch damp. coef. for different submerged depths (c/a=4.0, Fn=0.20, no tilt in head waves ; NI=10)

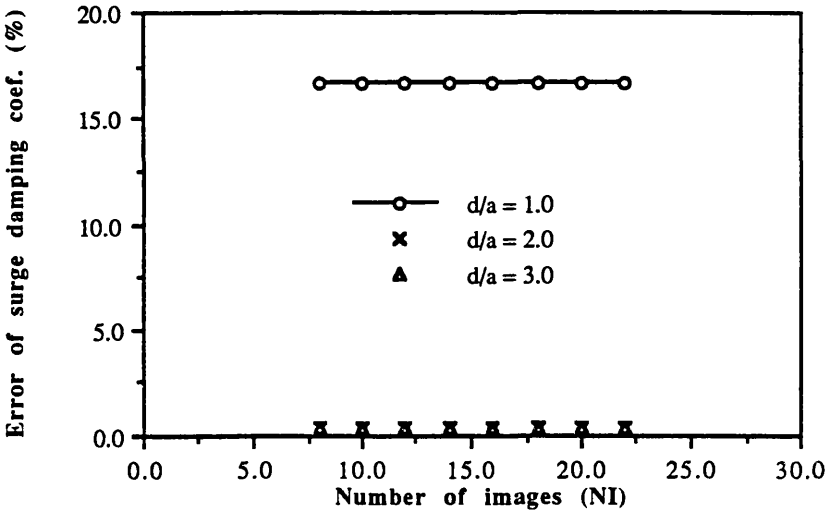

Fig.8.11 Relative error of surge damp. coef. for different submerged depths (c/a=4.0, Fn=0.20, no tilt in head waves ; NE=50)

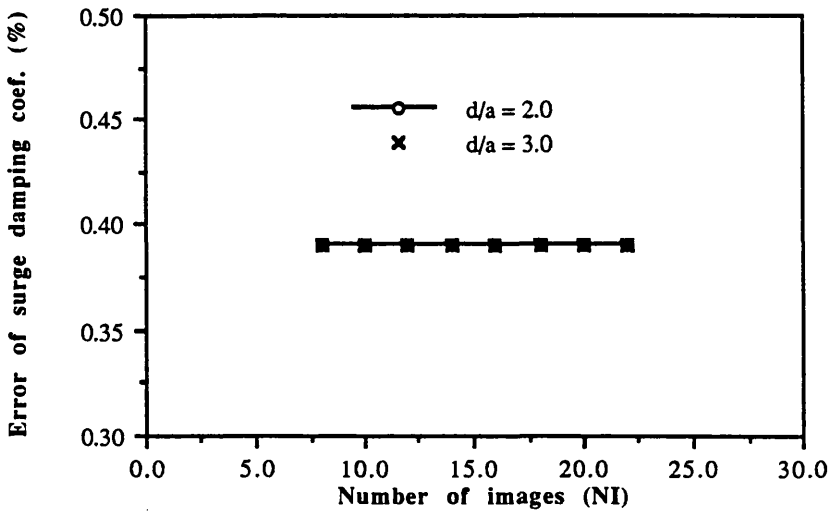

Fig.8.12 Relative error of surge damp. coef. for different submerged depths (c/a=4.0, Fn=0.20, no tilt in head waves ; NE=50)

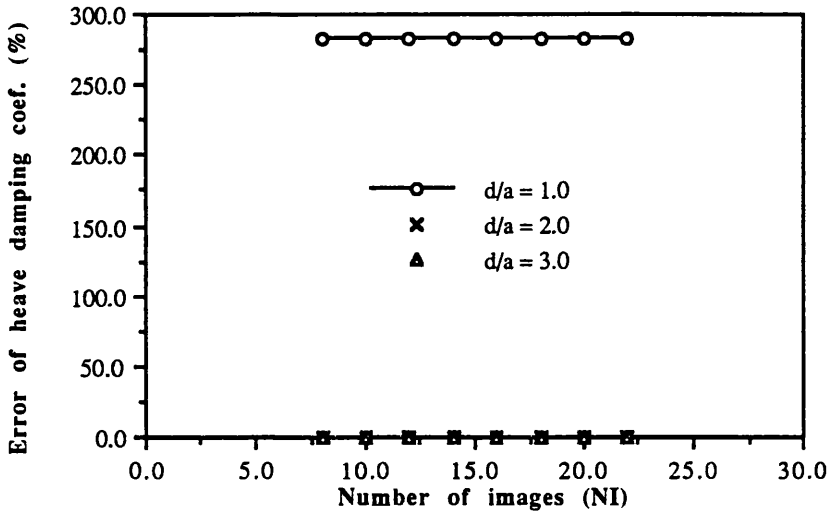

Fig.8.13 Relative error of heave damping coefficient for different submerged depths (c/a=4,Fn=0.2, no tilt in head waves;NE=50)

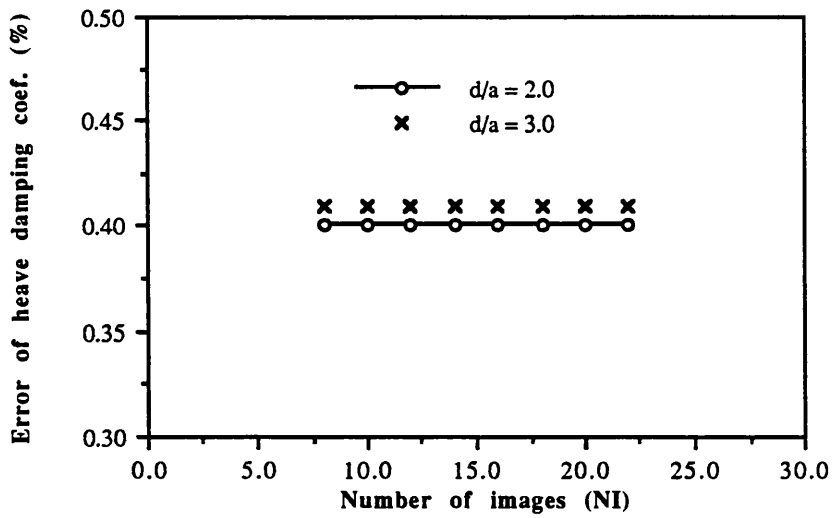

Fig.8.14 Relative error of heave damping coefficient for different submerged depths (c/a=4,Fn=0.2, no tilt in head waves;NE=50)

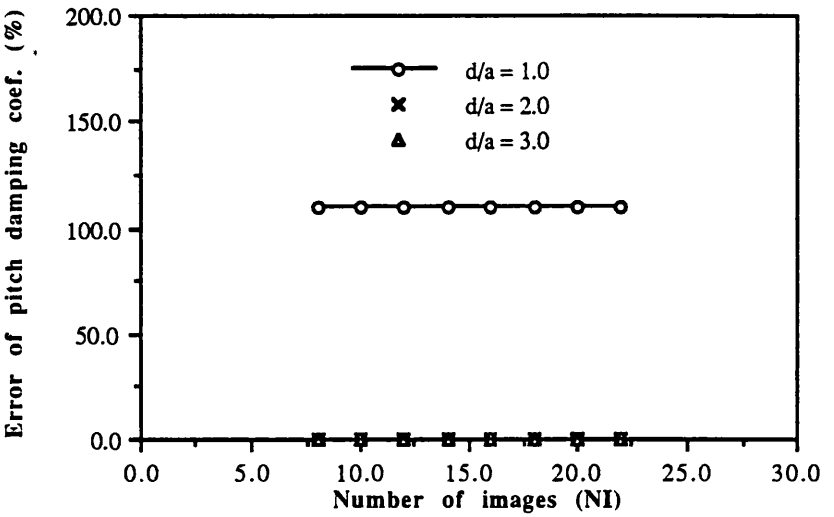

Fig.8.15 Relative error of pitch damp. coef. for different submerged depths (c/a=4.0, Fn=0.20, no tilt in head waves ; NE=50)

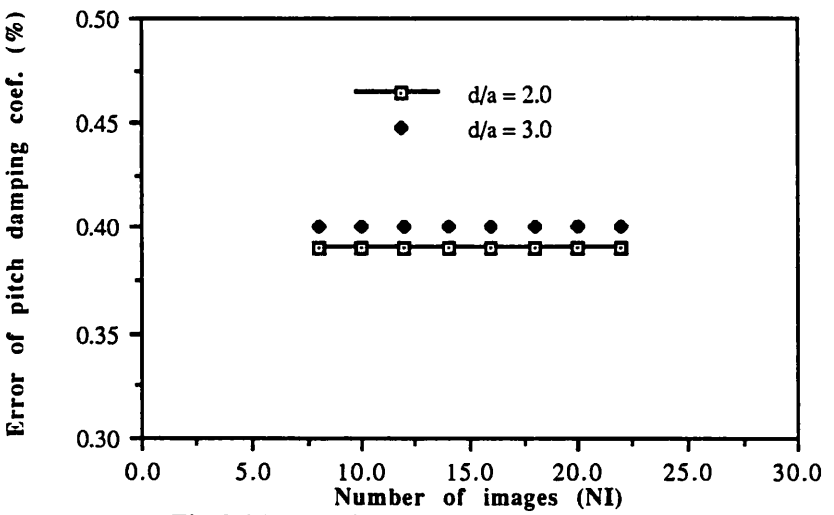

Fig.8.16 Relative error of pitch damp. coef. for different submerged depths (c/a=4.0, Fn=0.20, no tilt in head waves ; NE=50)

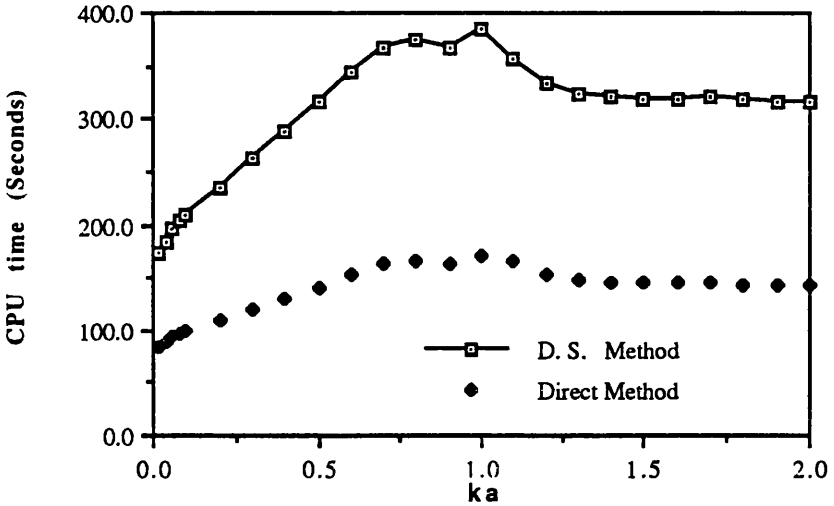

Fig.8.17 Comparison of CPU time between two numerical approaches(d/a=2.0,c/a=4.0, Fn=0.20, 5 degree tilt in head waves)

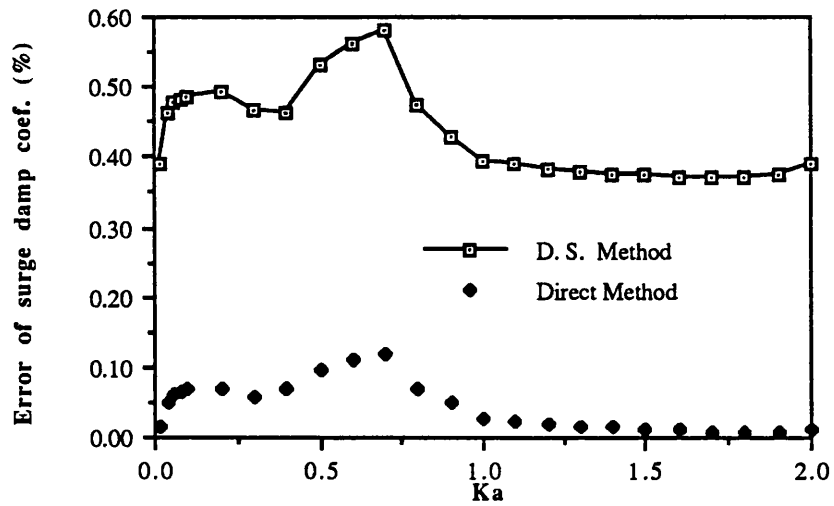

Fig.8.18 Comparison of surge damp. coef. between two approaches(d/a=2.0,c/a=4.0, Fn=0.20, 5 degree tilt in head waves)

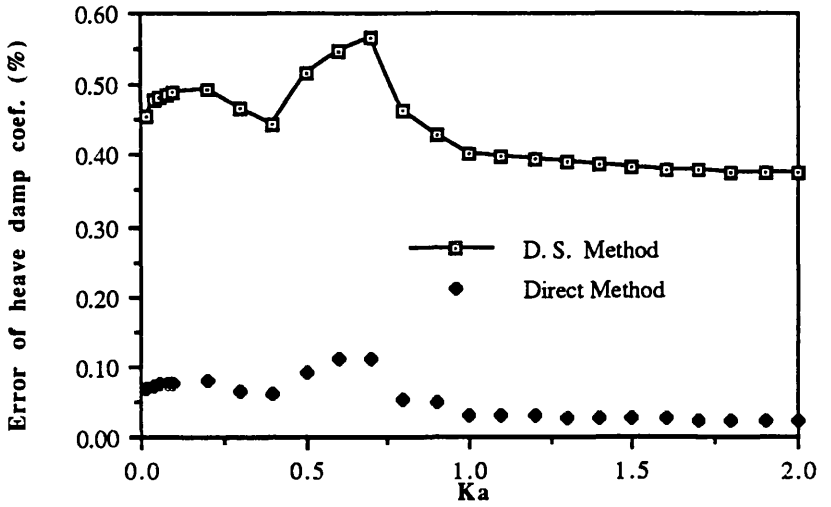

Fig.8.19 Comparison of heave damp. coef. between two approaches(d/a=2.0,c/a=4.0, Fn=0.20, 5 degree tilt in head waves)

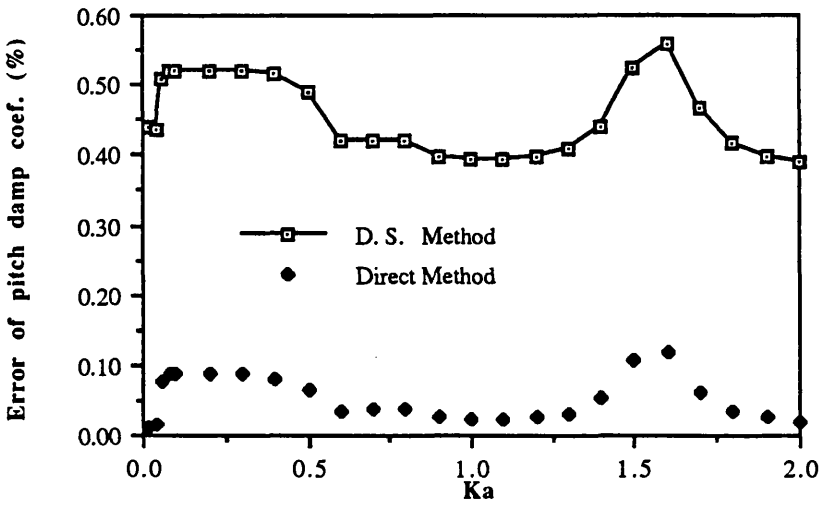

Fig.8.20 Comparison of pitch damp. coef. between two approaches(d/a=2.0,c/a=4.0, Fn=0.20, 5 degree tilt in head waves)

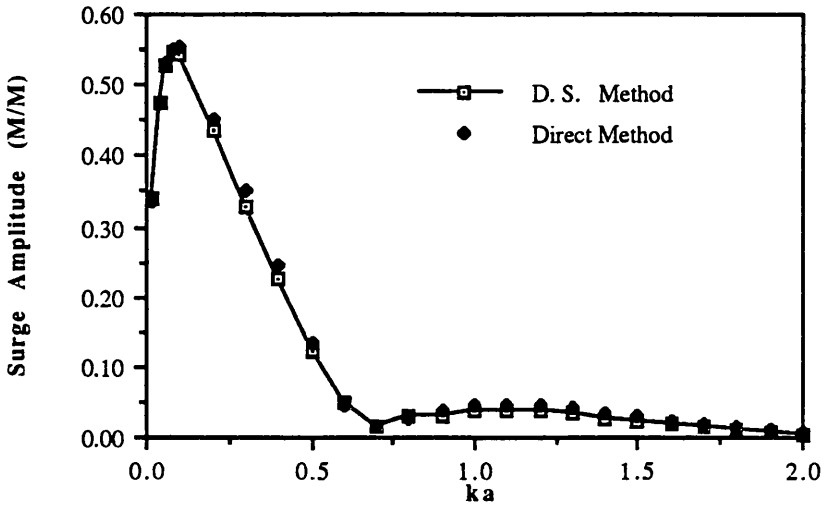

Fig.8.21 Comparsion of surge amplitudes between two approaches (d/a=2.0,c/a=4.0, Fn=0.20, 5 degree tilt in head waves)

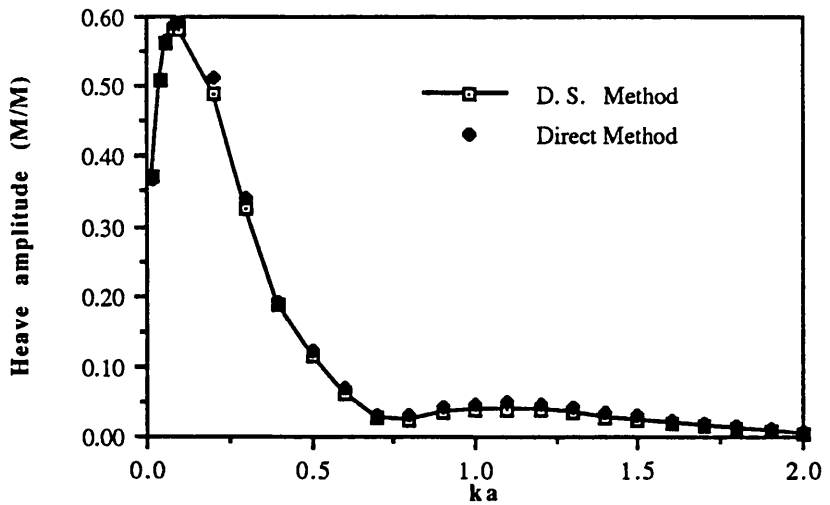

Fig.8.22 Comparison of heave amplitudes between two approaches(d/a=2.0,c/a=4.0, Fn=0.20, 5 degree tilt in head waves)

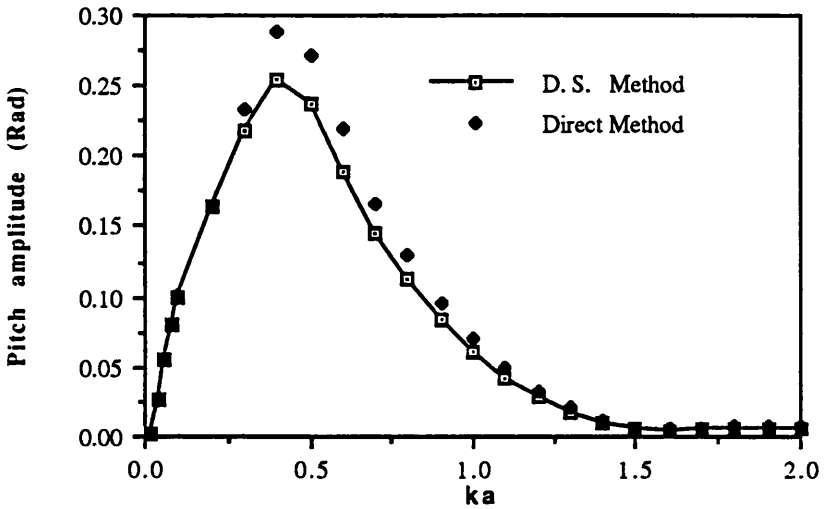

Fig.8.23 Comparison of pitch amplitudes between two approaches(d/a=2.0,c/a=4.0, Fn=0.20, 5 degree tilt in head waves)

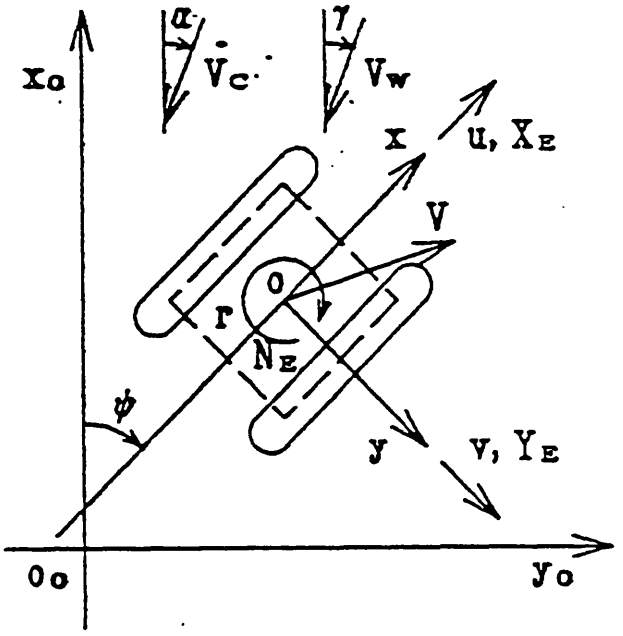

Fig.9.1 Coordinate system of twin hulled marine vehicles in dynamic positioning aspects

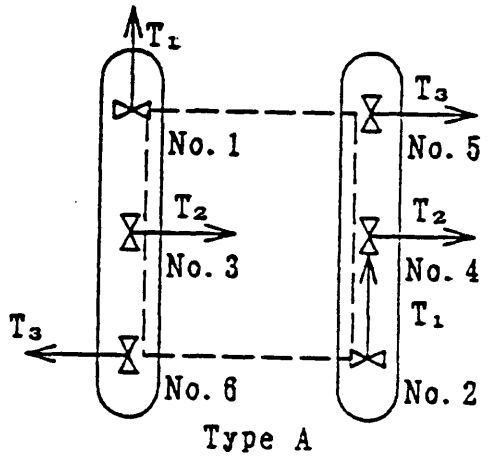

Fig.9.2 The arrangement of type A thruster system

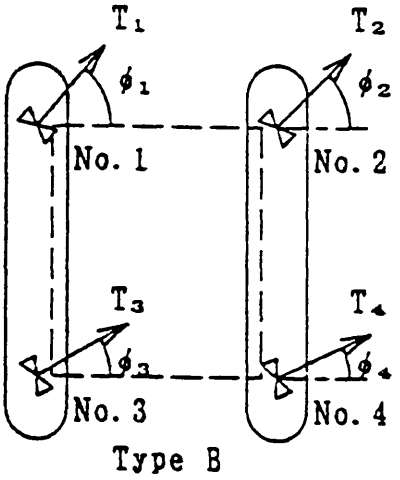

Fig.9.3 The arrangement of type B thruster system

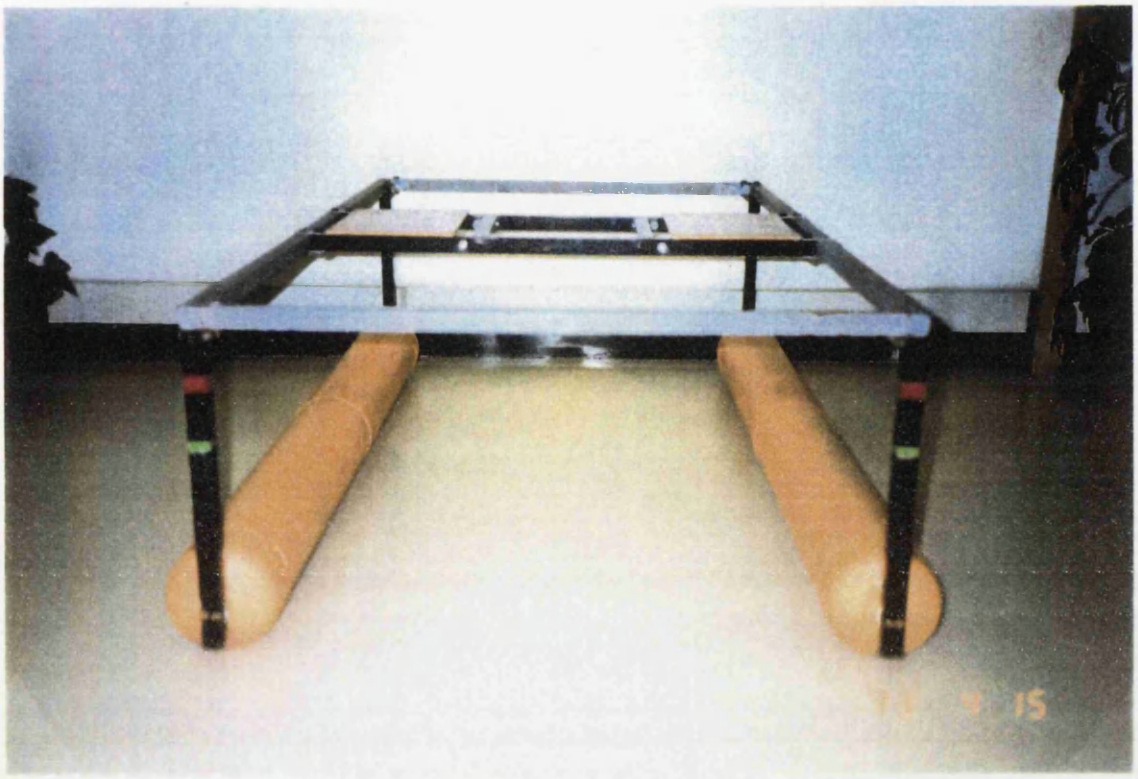

Fig.9.4 Front view of the twin hulled circular cylinder model

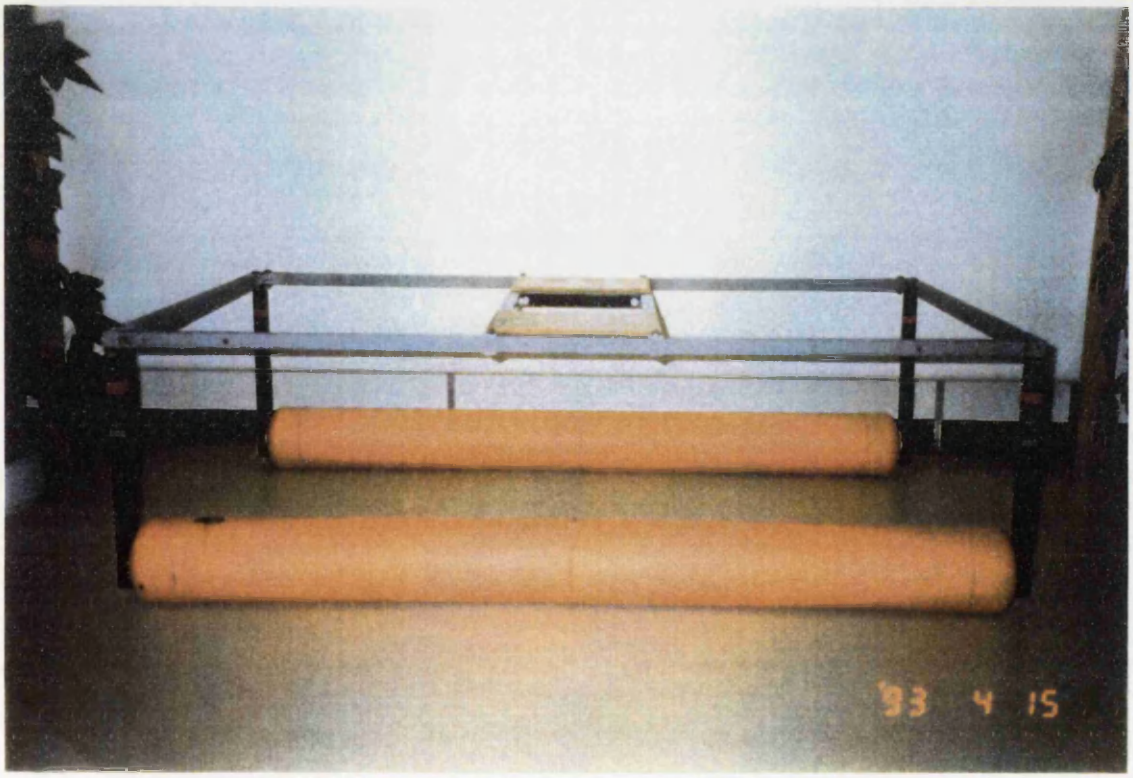

Fig.9.5 Side view of the twin hulled circular cylinder model

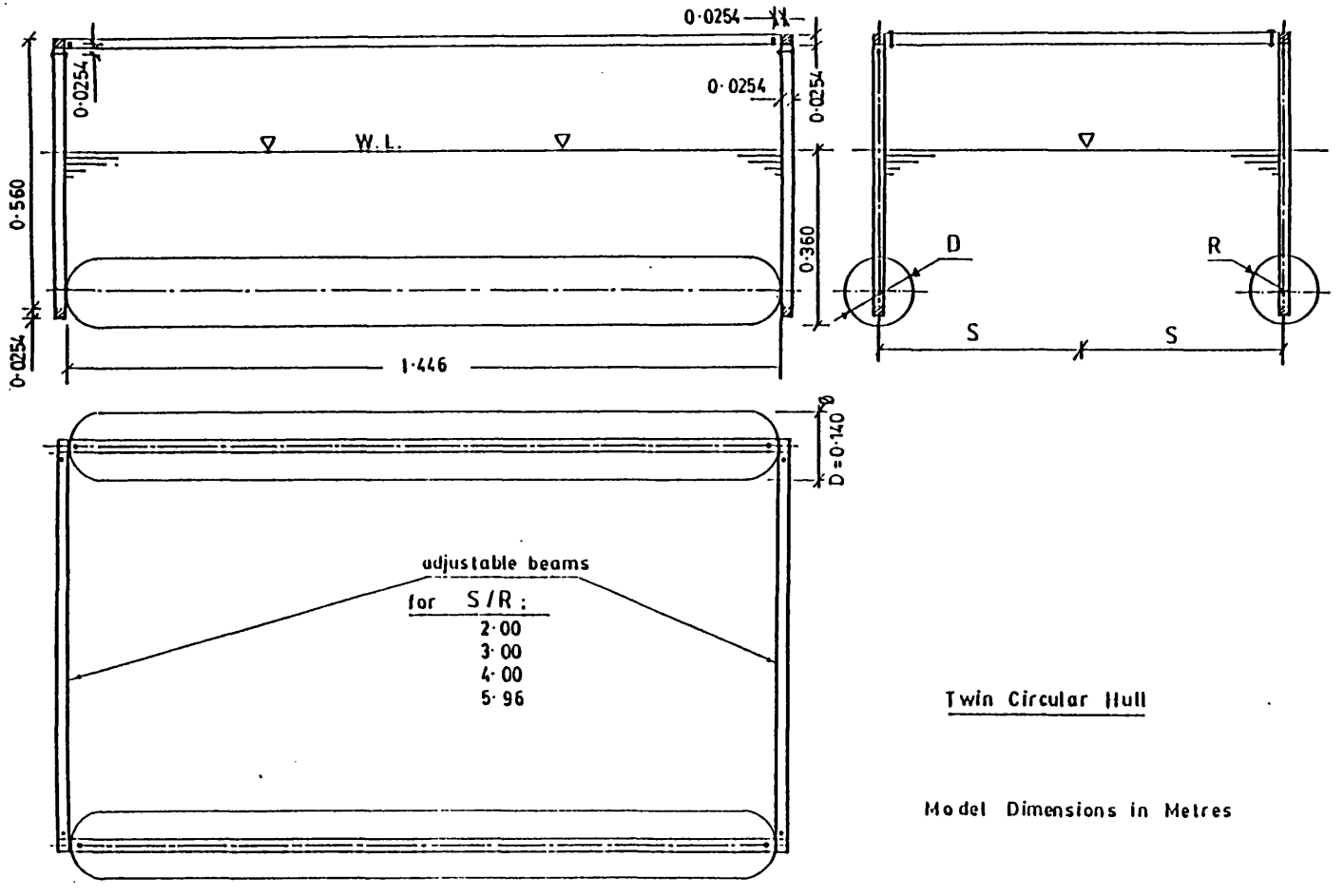

Fig.9.6 General arrangement of the twin hulled circular cylinder model

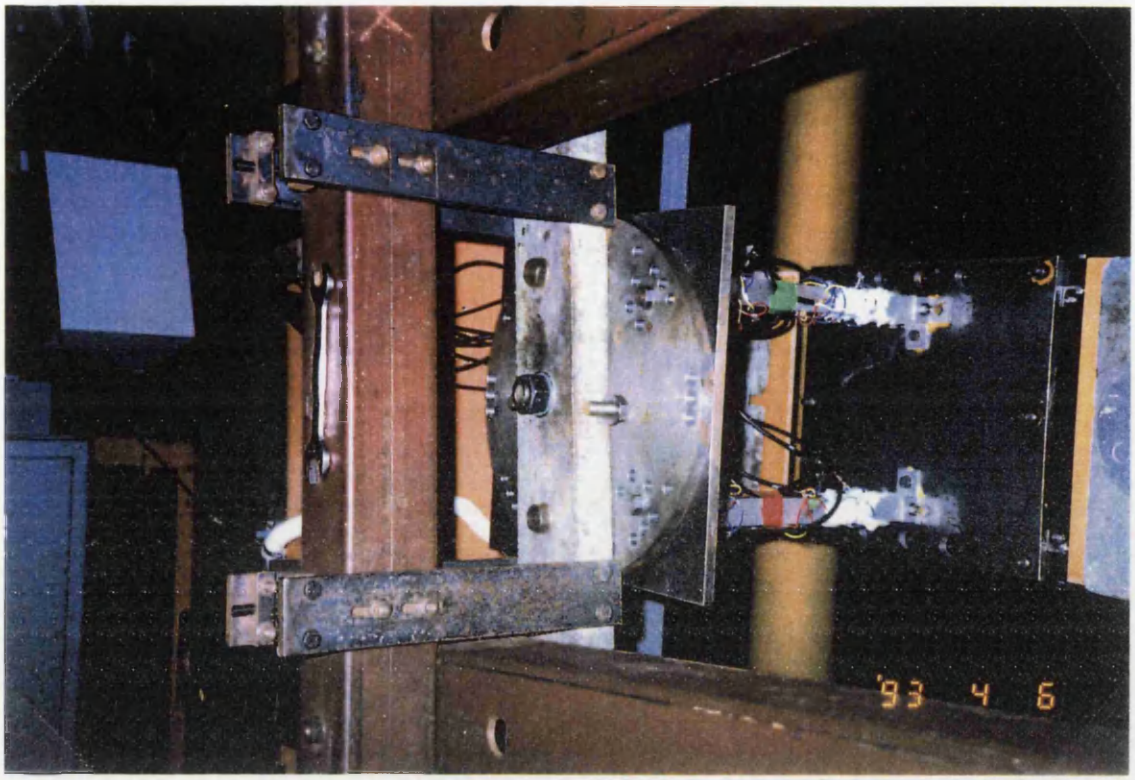

Fig.9.7 Two straight bar device for experimental data measurement

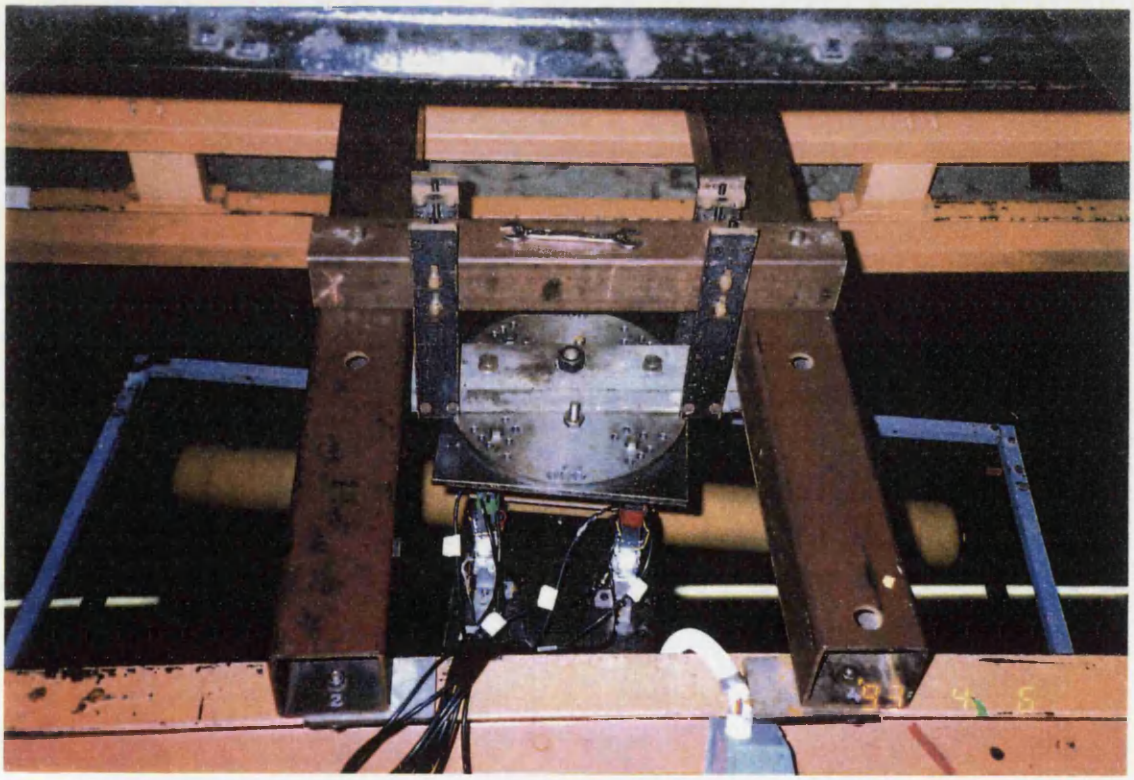

Fig.9.8 Turnplate facility for specific drift angles

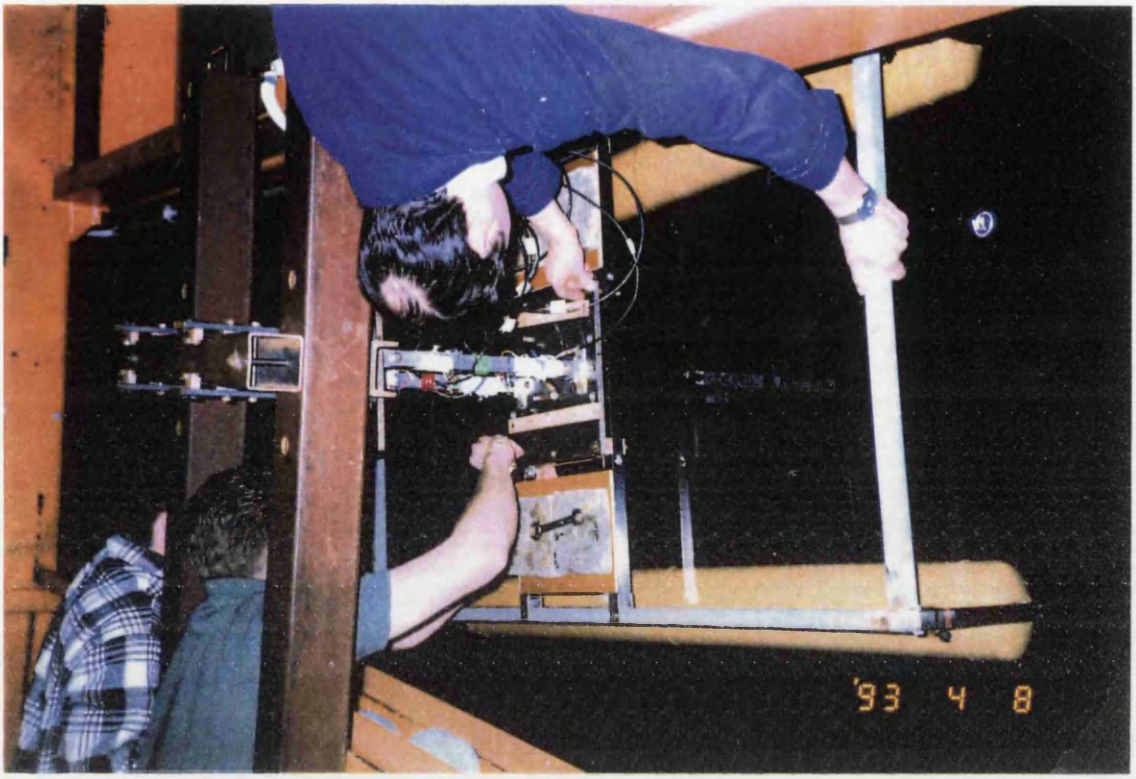

Fig.9.9 Adjustment of wooden wedge for specific trim angles

Fig.9.11 Main carriage and speed control system

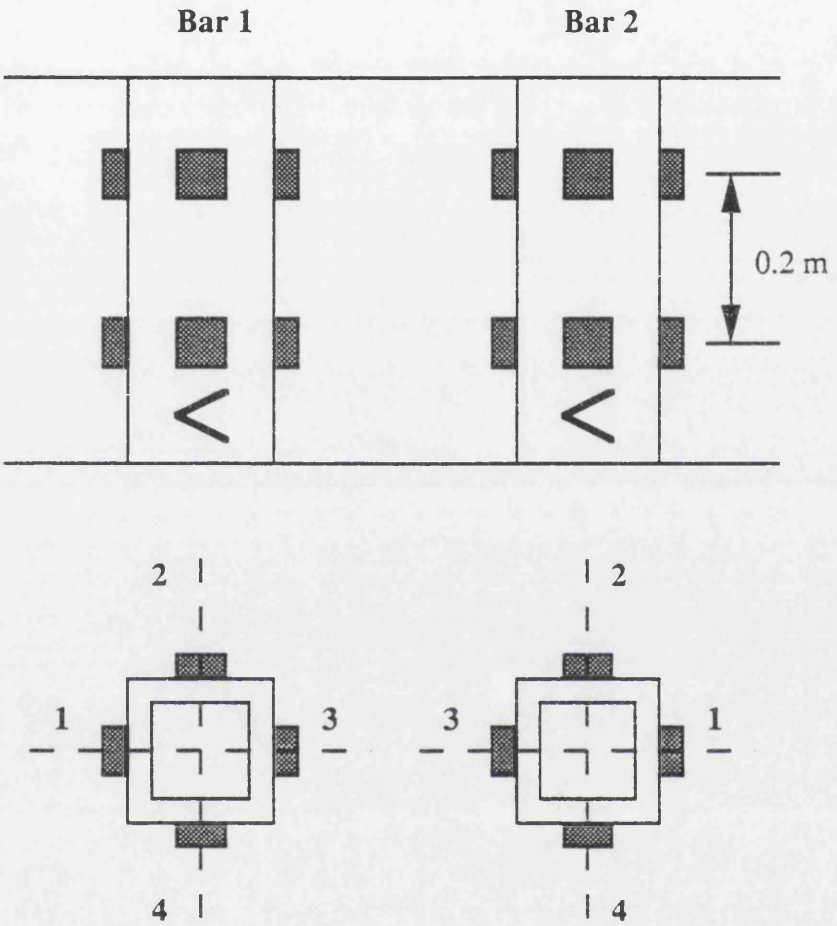

Fig.9.10 Arrangement of load cell transducers on two straight bar device

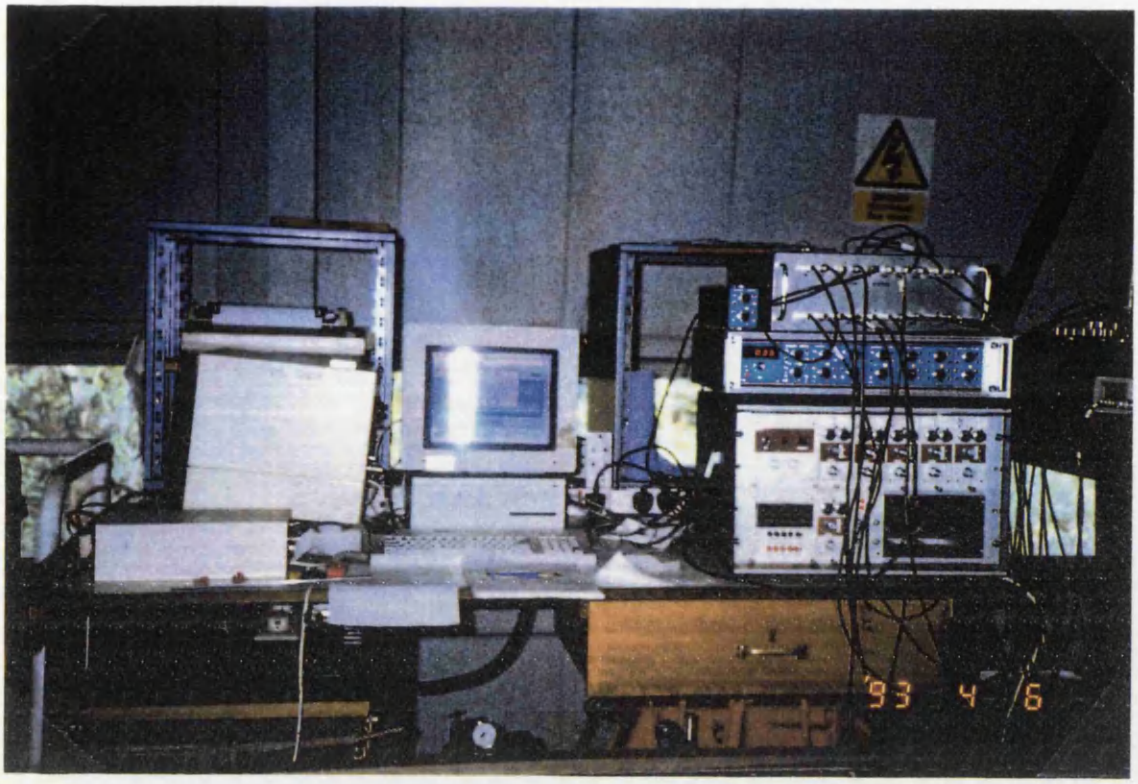

Fig.9.12 Data acquisition system

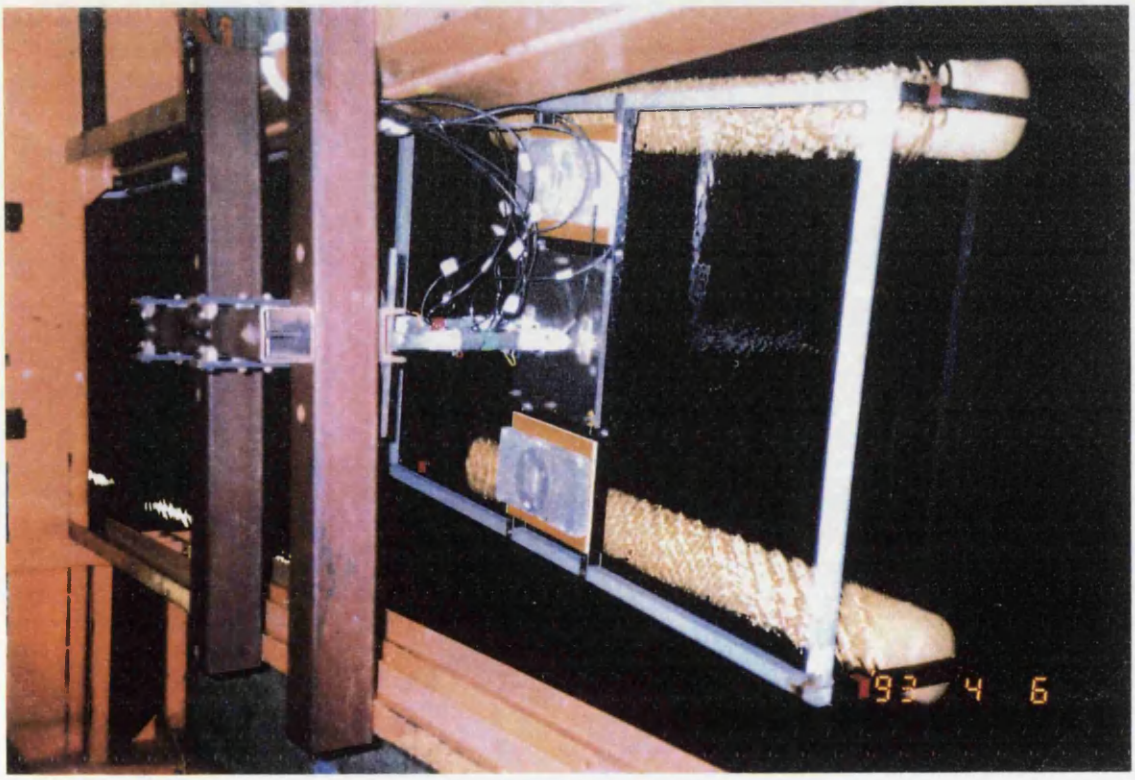

Fig.9.34 The twin hulled model in +6 degree drift and no trim condition (d/a = 4.0, c/a = 10.0)

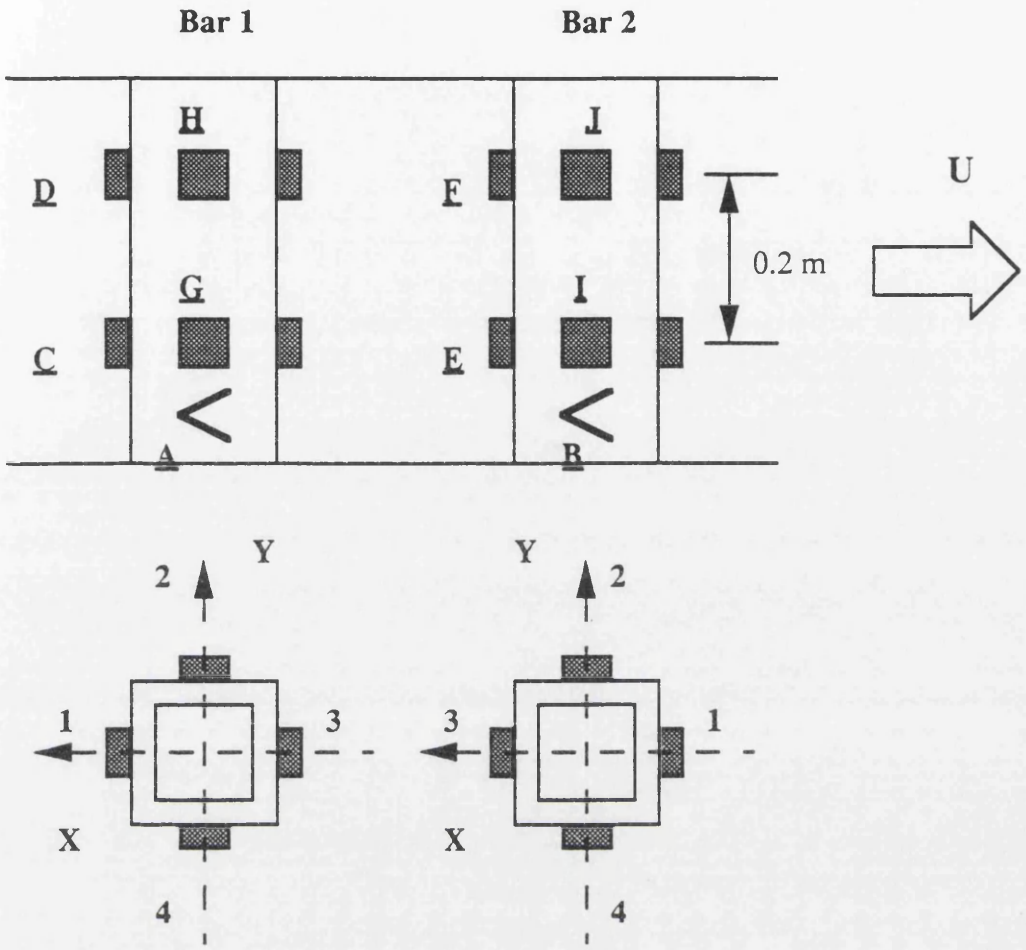

Where :

Symbol A denotes the position of data channel 1
Symbol B denotes the position of data channel 2
Symbol C denotes the position of data channel 3
Symbol D denotes the position of data channel 4
Symbol E denotes the position of data channel 5
Symbol F denotes the position of data channel 6
Symbol G denotes the position of data channel 7
Symbol H denotes the position of data channel 8
Symbol I denotes the position of data channel 9
Symbol J denotes the position of data channel 10

Fig.9.13 Channel arrangement for data acquisition in two straight bar system

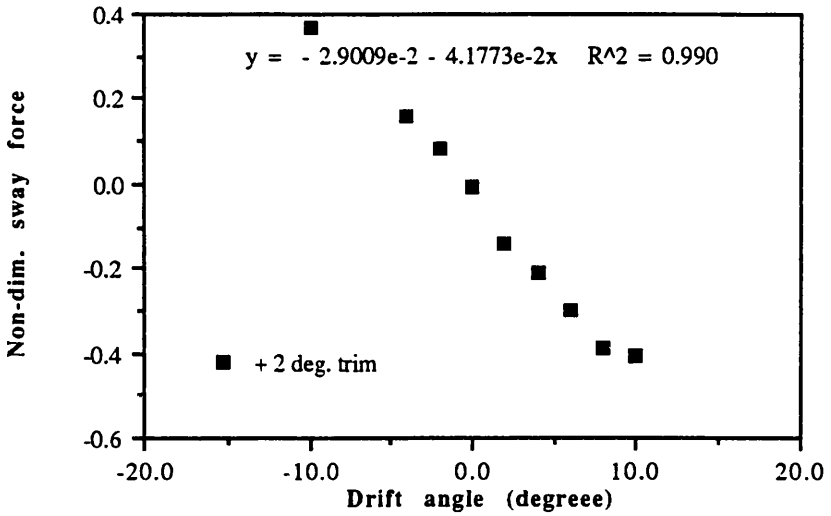

Fig.9.14 Non-dimensionalized sway force on twin hulled model in 2 degree trim by stern condition (d/a=4.0,c/a=10.0)

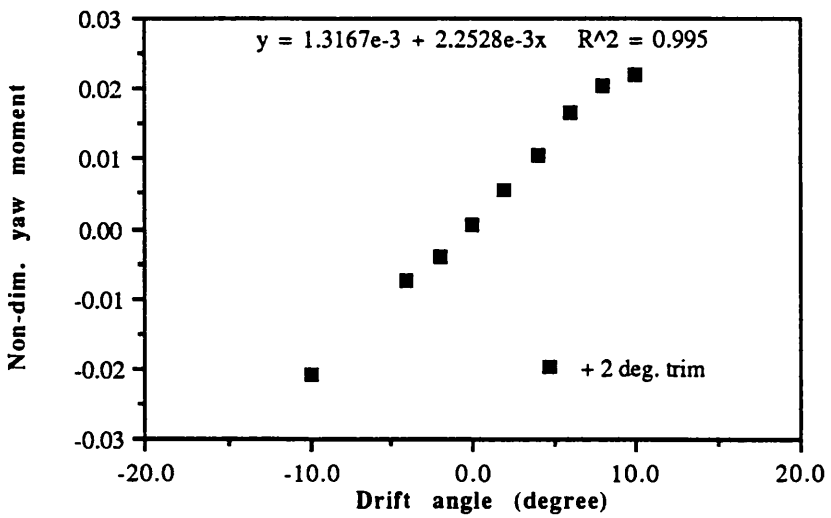

Fig.9.15 Non-dimensionalized yaw moment on twin hulled model in 2 degree trim by stern condition (d/a=4.0,c/a=10.0)

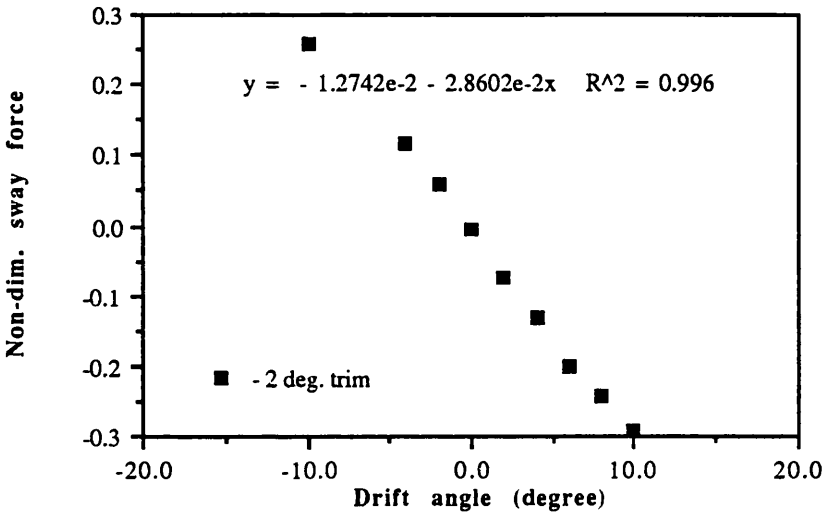

Fig.9.16 Non-dimensionalized sway force on twin hulled model in 2 degree trim by bow condition (d/a=4.0,c/a=10.0)

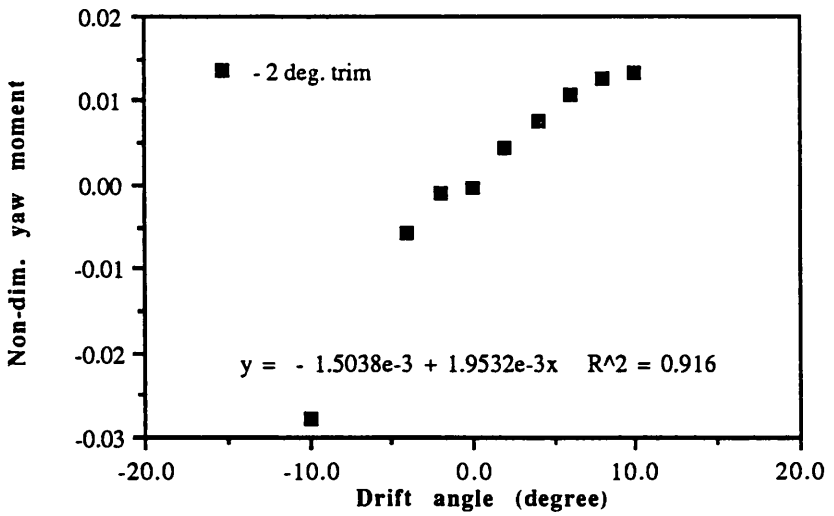

Fig.9.17 Non-dimensionalized yaw moment on twin hulled model in 2 degree trim by bow condition (d/a=4.0,c/a=10.0)

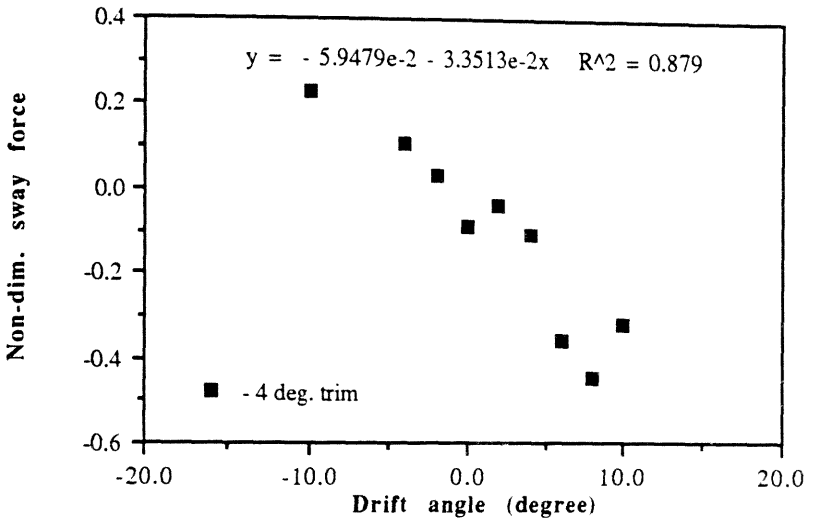

Fig.9.18 Non-dimensionalized sway force on twin hulled model in 4 degree trim by bow condition (d/a=4.0,c/a=10.0)

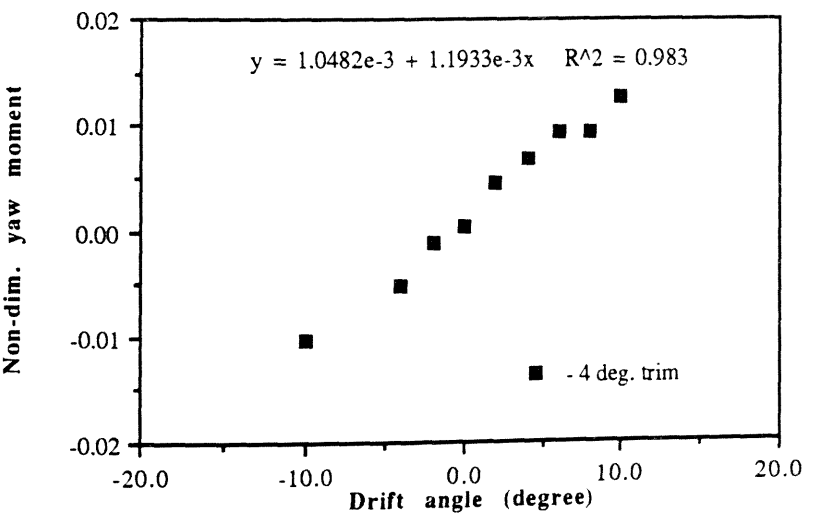

Fig.9.19 Non-dimensionalized yaw moment on twin hulled model in 4 degree trim by bow condition (d/a=4.0,c/a=10.0)

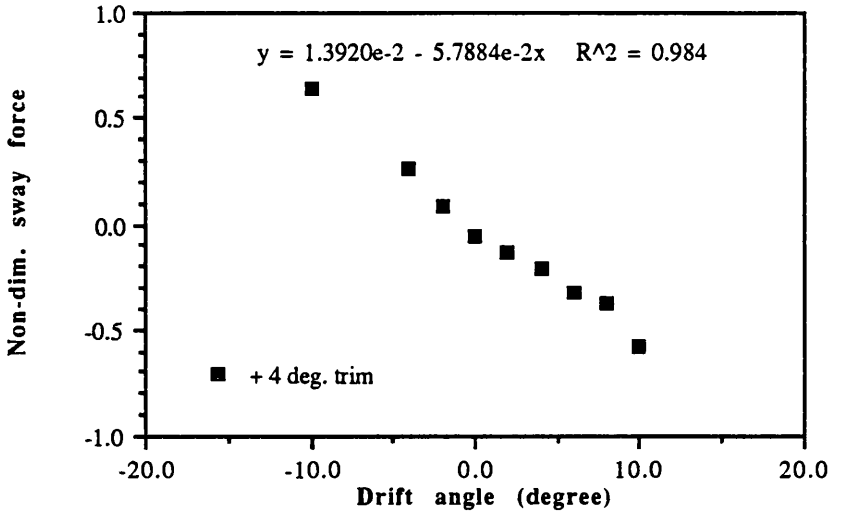

Fig.9.20 Non-dimensionalized sway force on twin hulled model in 4 degree trim by stern condition (d/a=4.0,c/a=10.0)

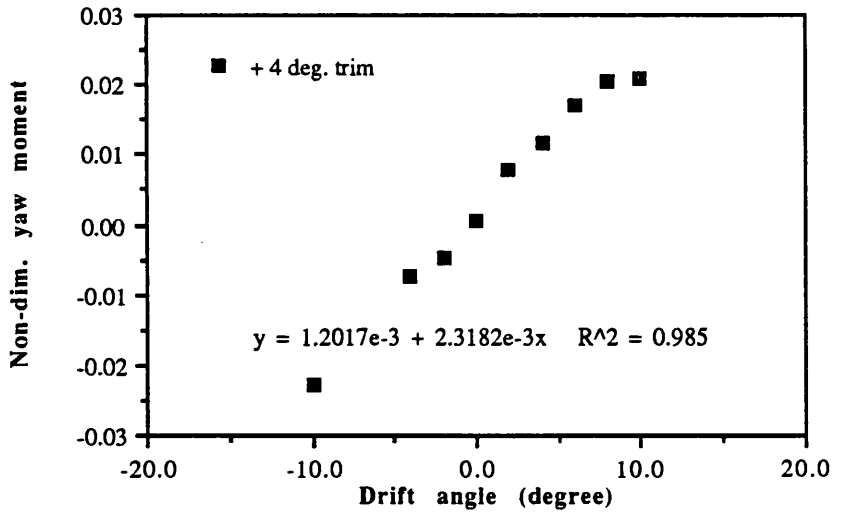

Fig.9.21 Non-dimensionalized yaw moment on twin hulled model in 4 degree trim by stern condition (d/a=4.0,c/a=10.0)

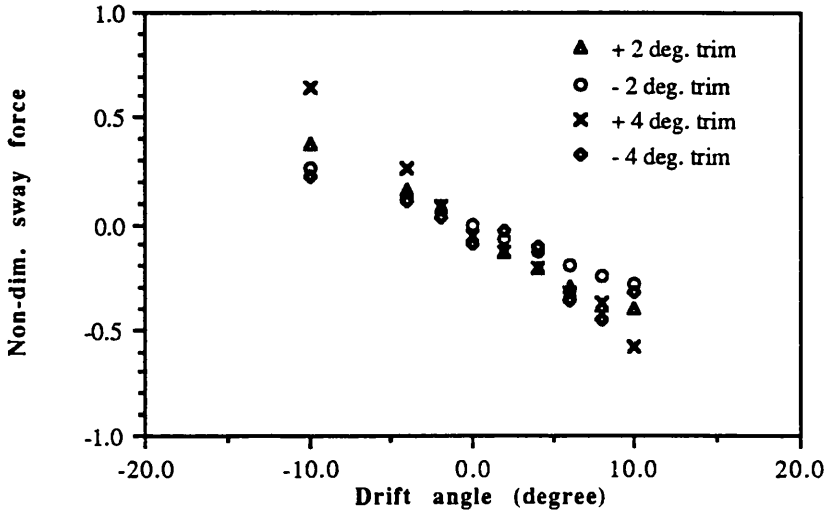

Fig.9.22 Comparison of non-dim. sway force on twin hulled model in trim conditions (d/a=4.0,c/a=10.0)

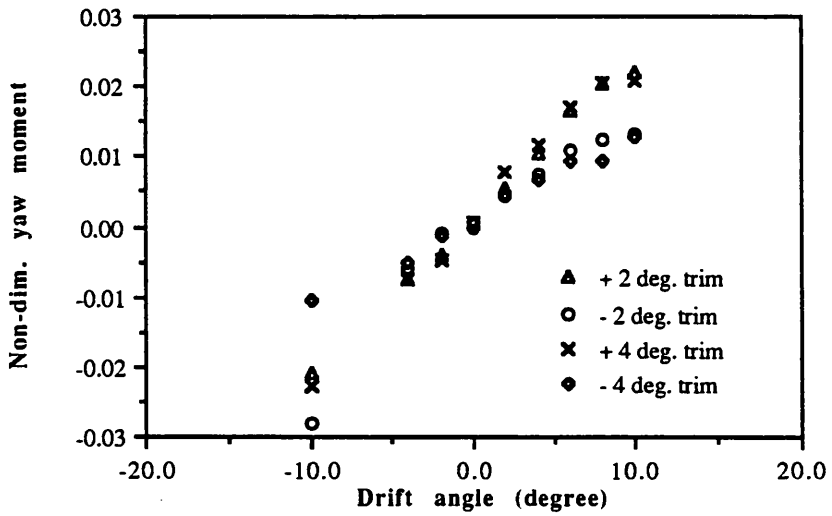

Fig.9.23 Comparison of non-dim. yaw moment on twin hulled model in trim conditions (d/a=4.0,c/a=10.0)

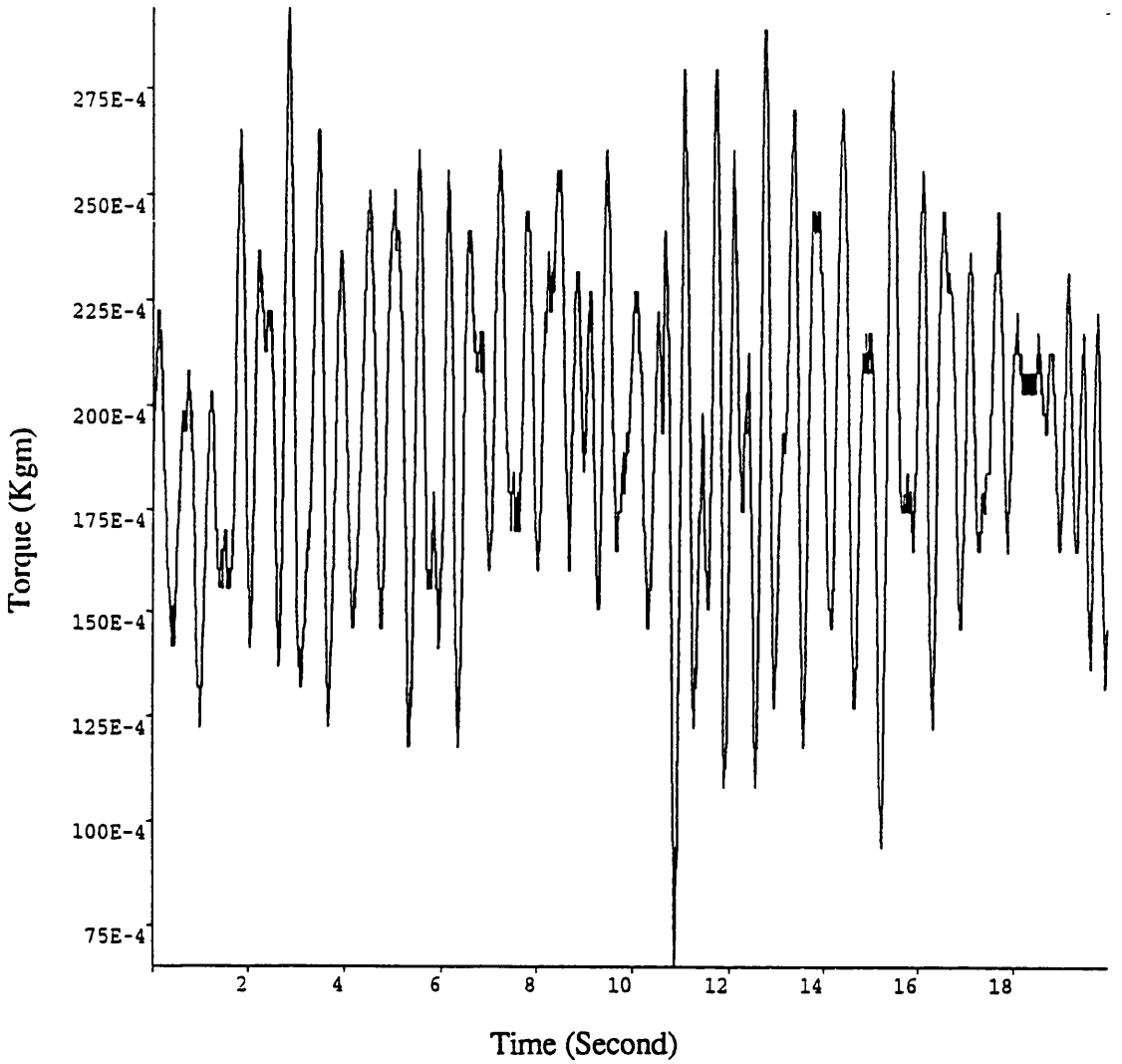

Fig.9.24 Measuring signals of Channel 1 (M1) (d/a = 4.0, c/a = 10.0)

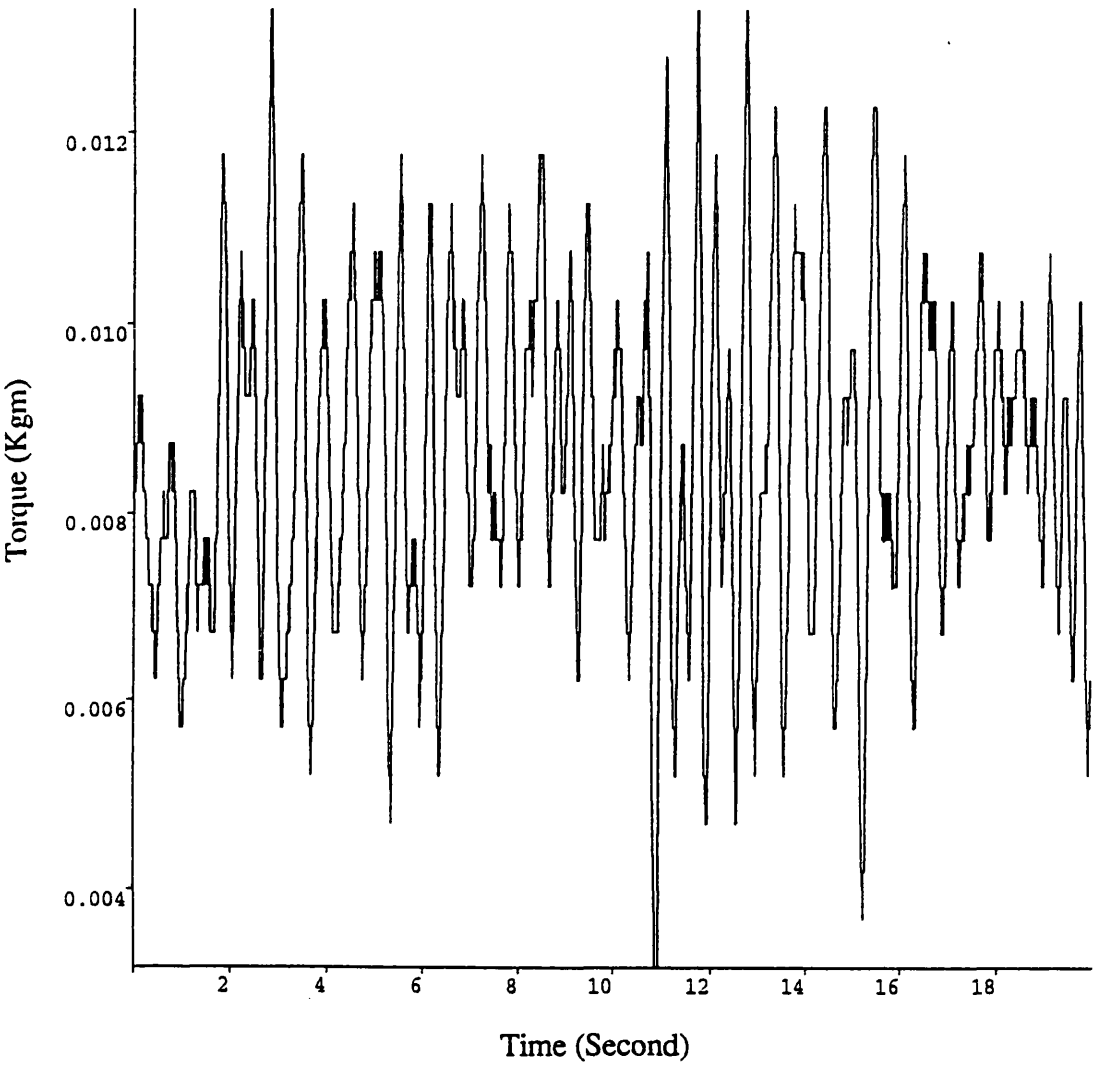

Fig.9.25 Measuring signals of Channel 2 (M2) (d/a = 4.0, c/a = 10.0)

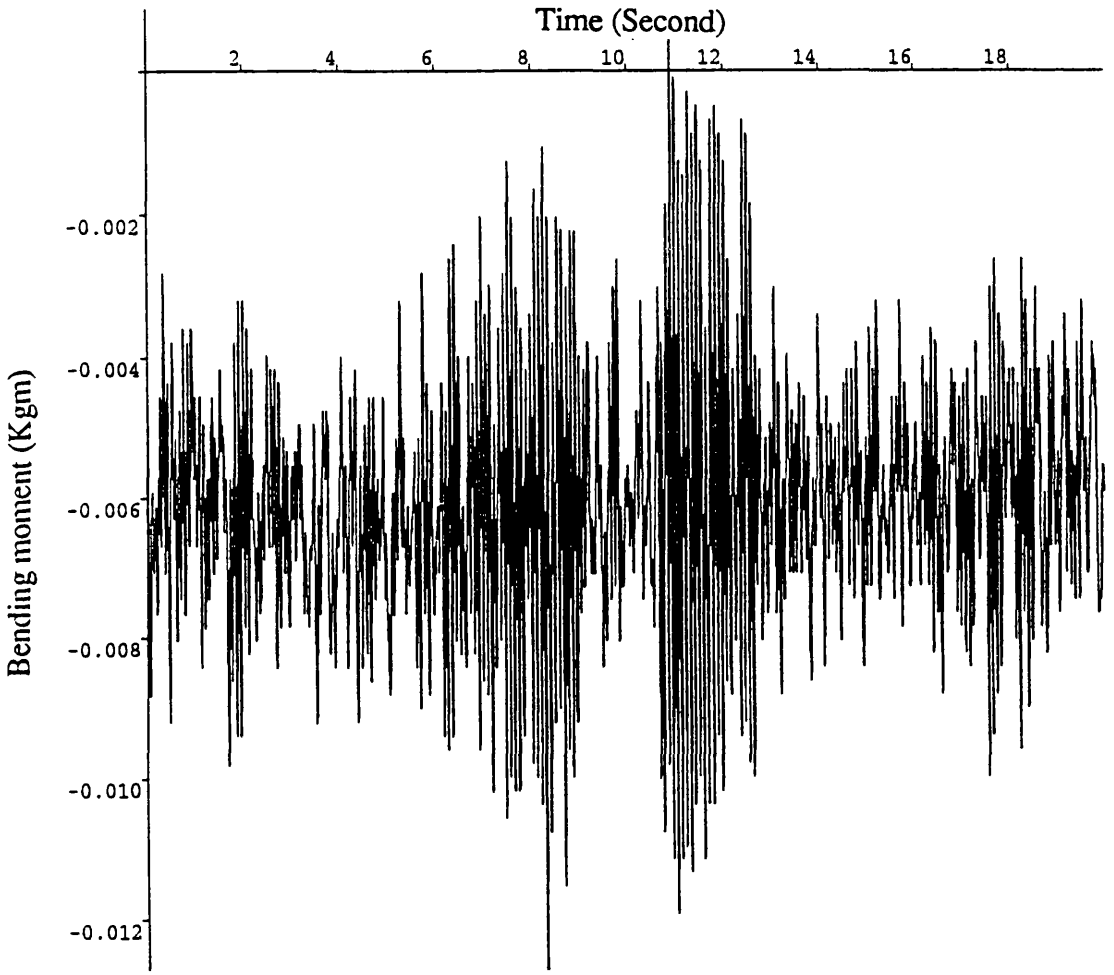

Fig.9.26 Measuring signals of Channel 3 (M3) (d/a = 4.0, c/a = 10.0)

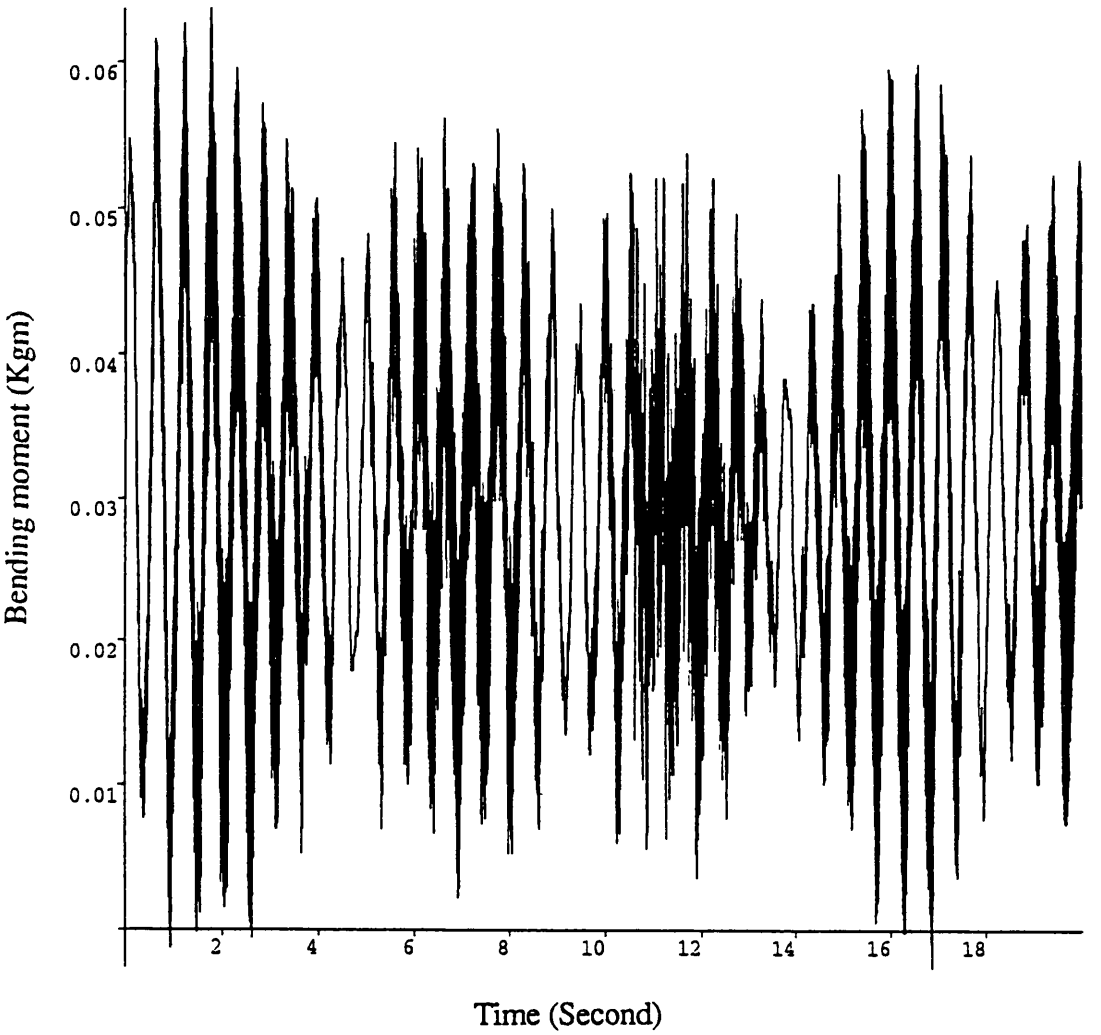

Fig.9.27 Measuring signals of Channel 4 (M4) (d/a = 4.0, c/a = 10.0)

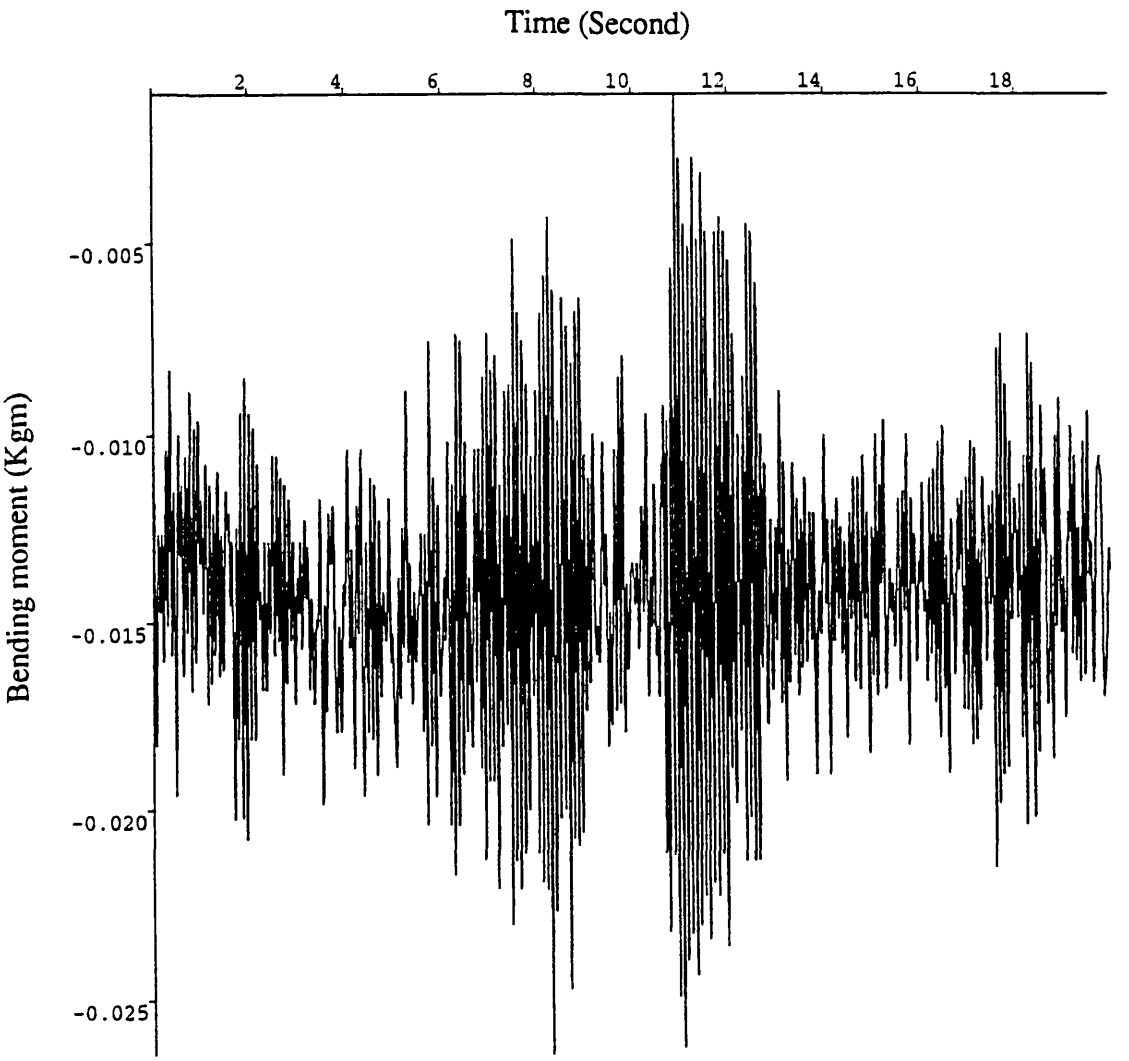

Fig.9.28 Measuring signals of Channel 5 (M5) (d/a = 4.0, c/a = 10.0)

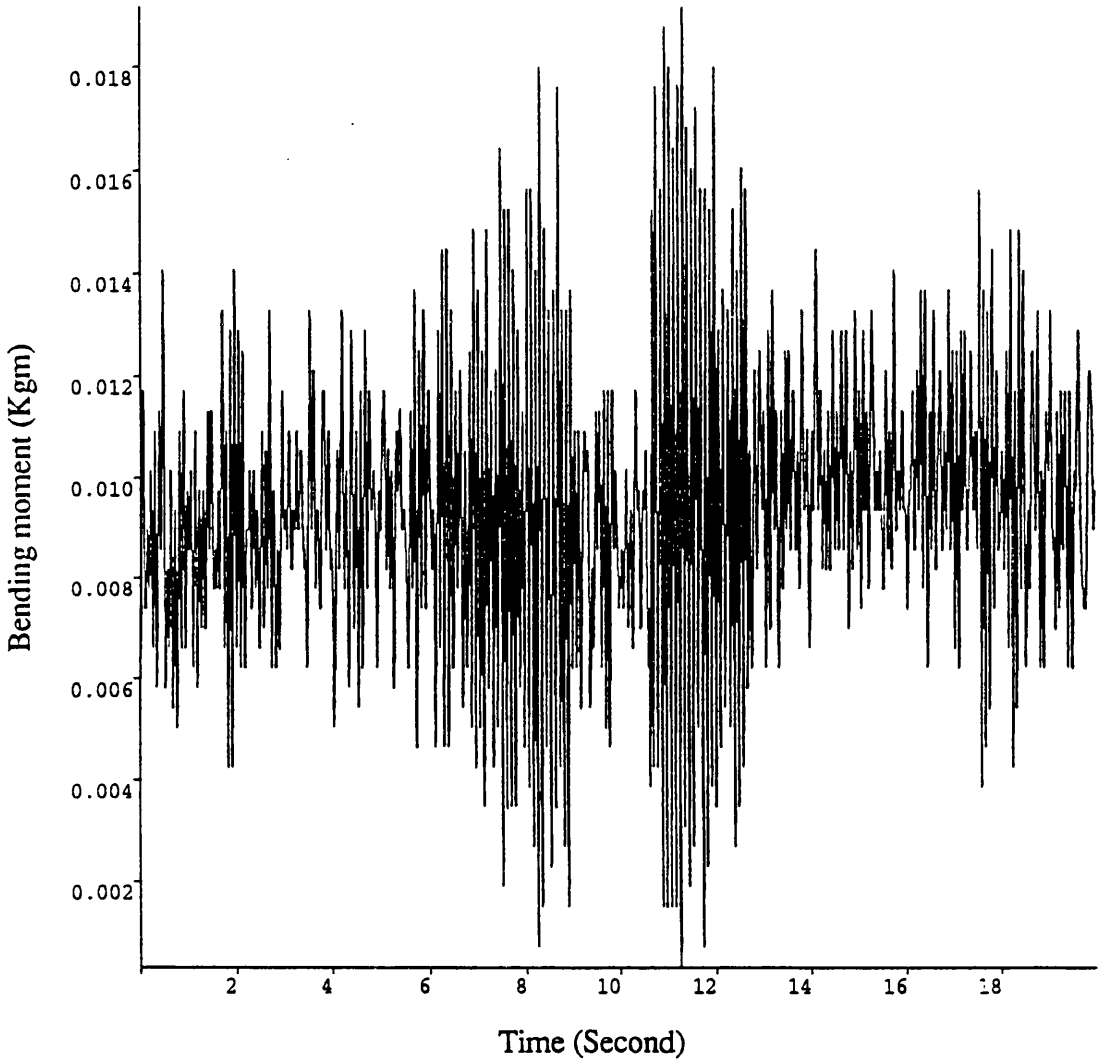

Fig.9.29 Measuring signals of Channel 6 (M6) (d/a = 4.0, c/a = 10.0)

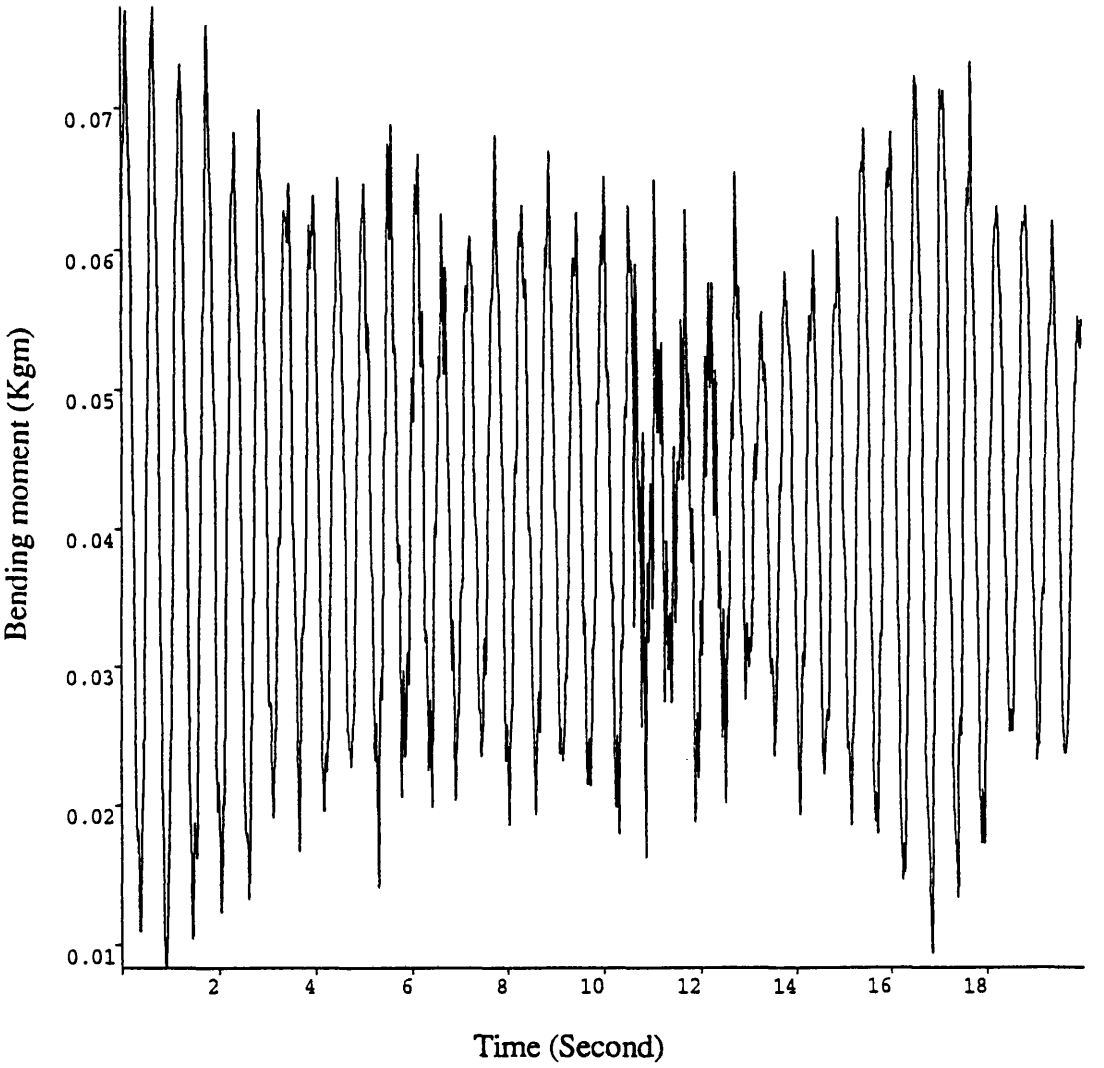

Fig.9.30 Measuring signals of Channel 7 (M7) (d/a = 4.0, c/a = 10.0)

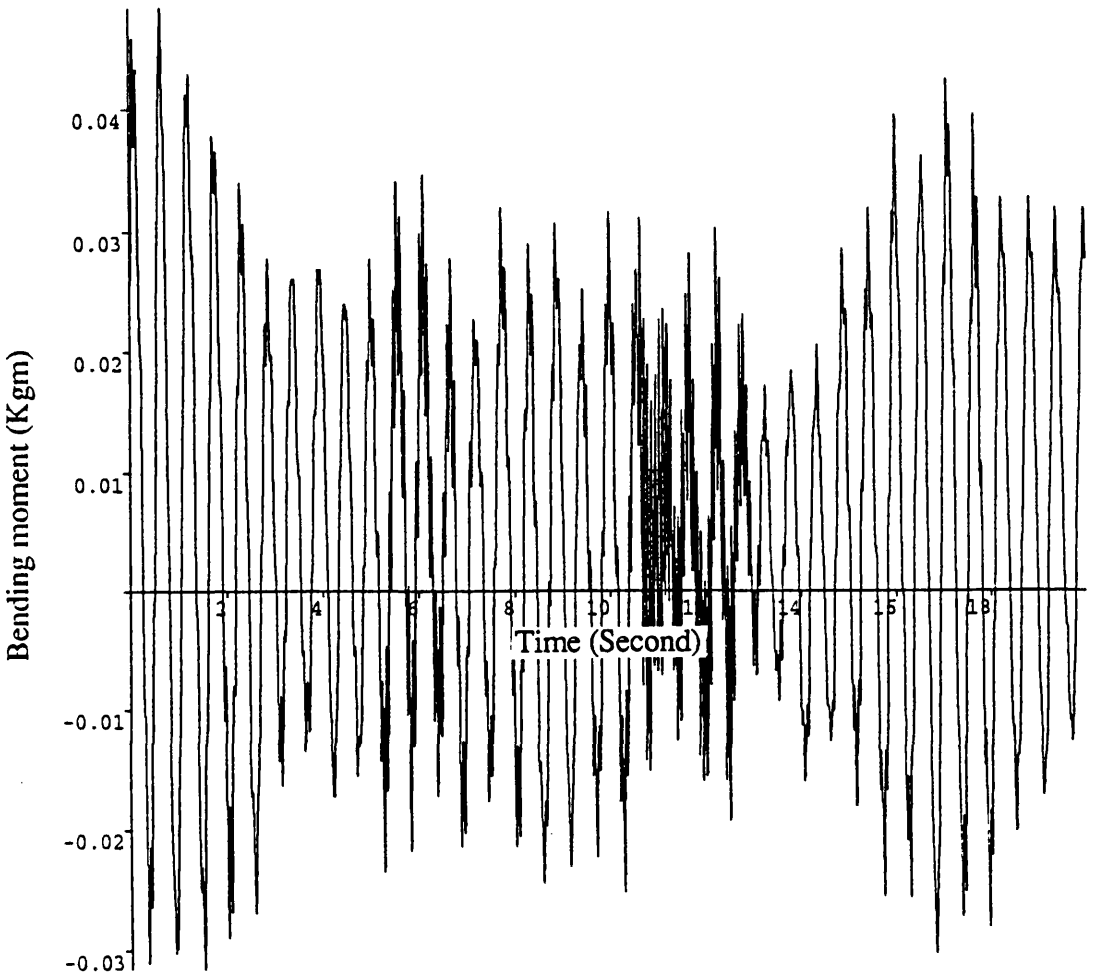

Fig.9.31 Measuring signals of Channel 8 (M8) (d/a = 4.0, c/a = 10.0)

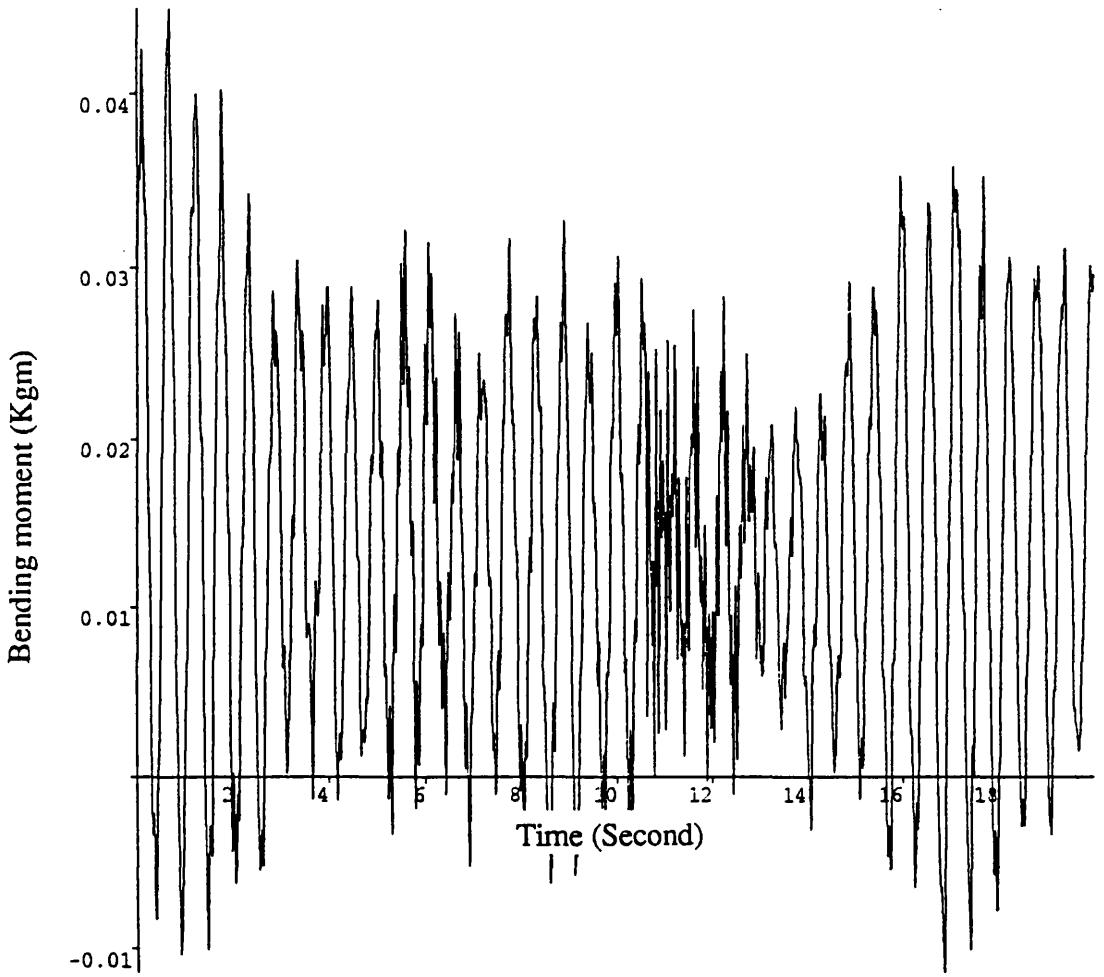

Fig.9.32 Measuring signals of Channel 9 (M9) (d/a = 4.0, c/a = 10.0)

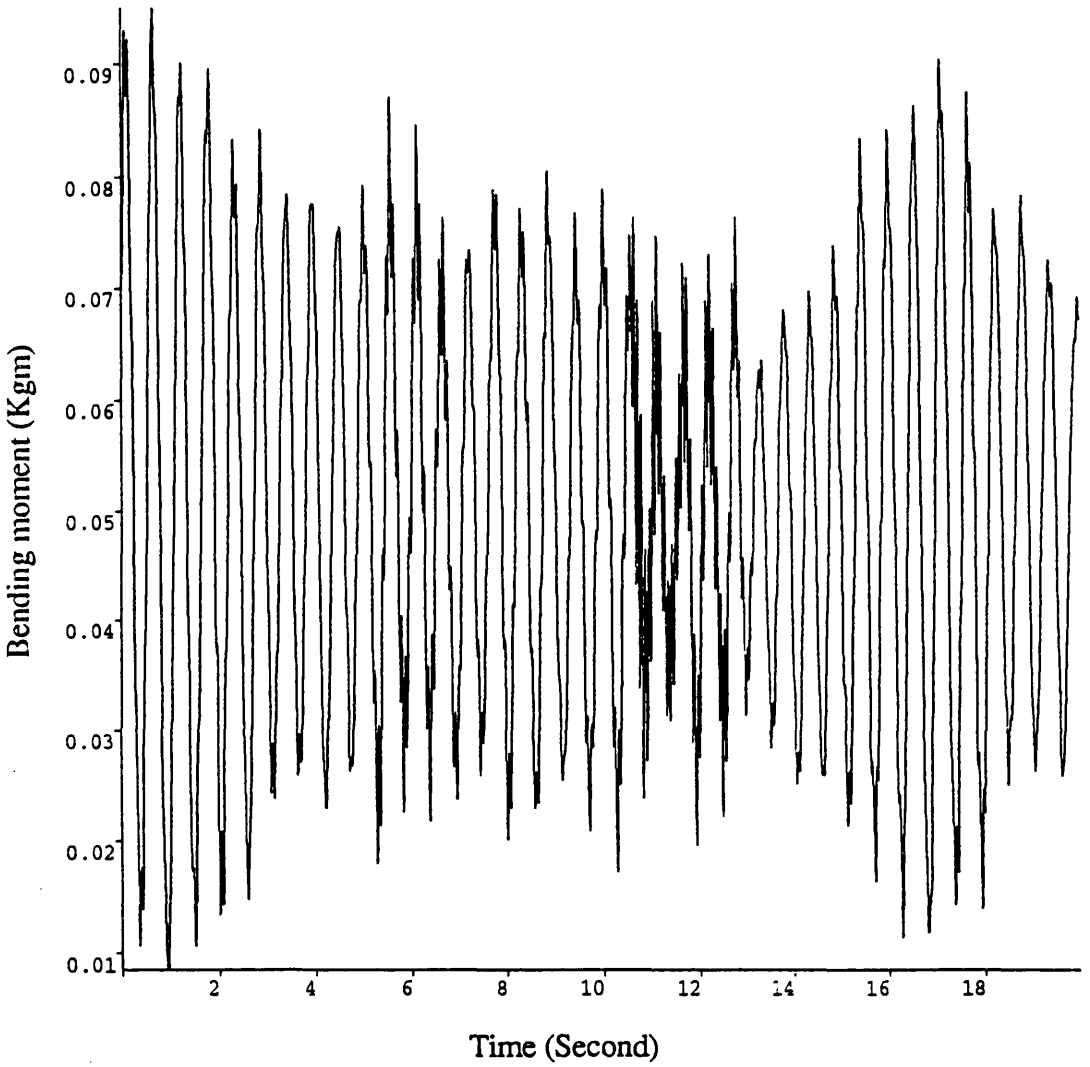

Fig.9.33 Measuring signals of Channel 10 (M10) (d/a = 4.0, c/a = 10.0)

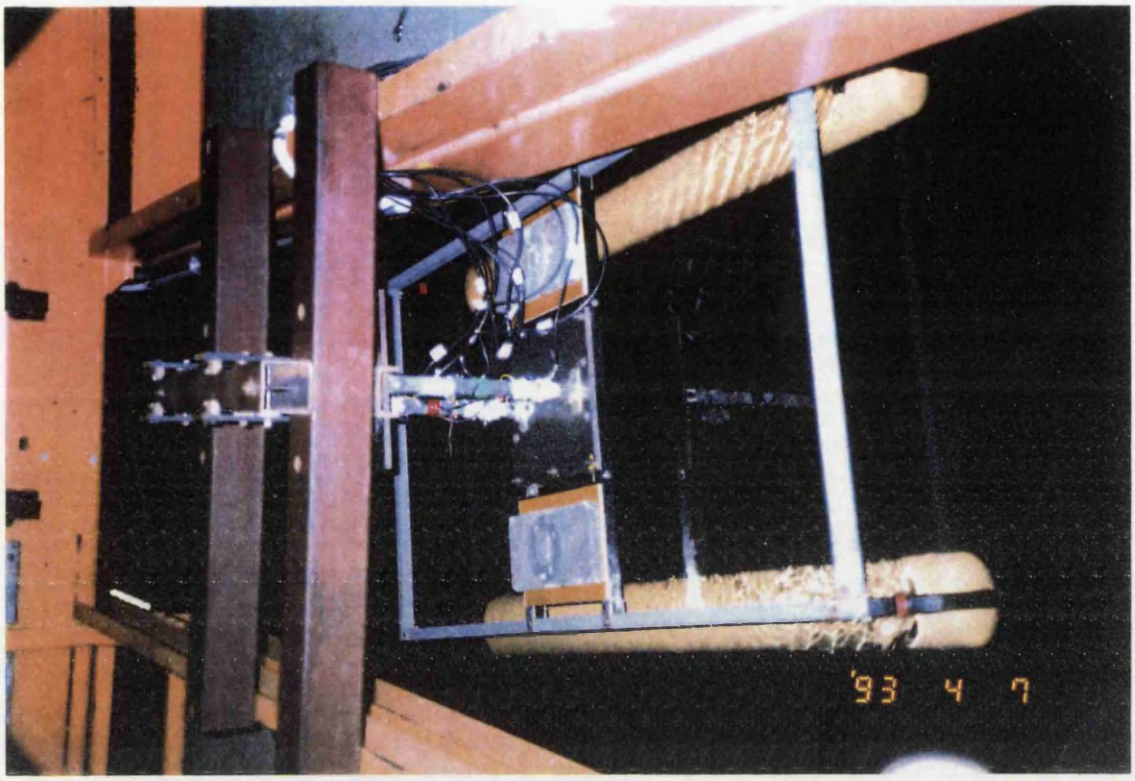

Fig.9.35 The twin hulled model in -10 degree drift and no trim condition
(d/a = 4.0, c/a = 10.0)

Fig.9.36 The twin hulled model in no drift and trim condition
(d/a = 4.0, c/a = 10.0)

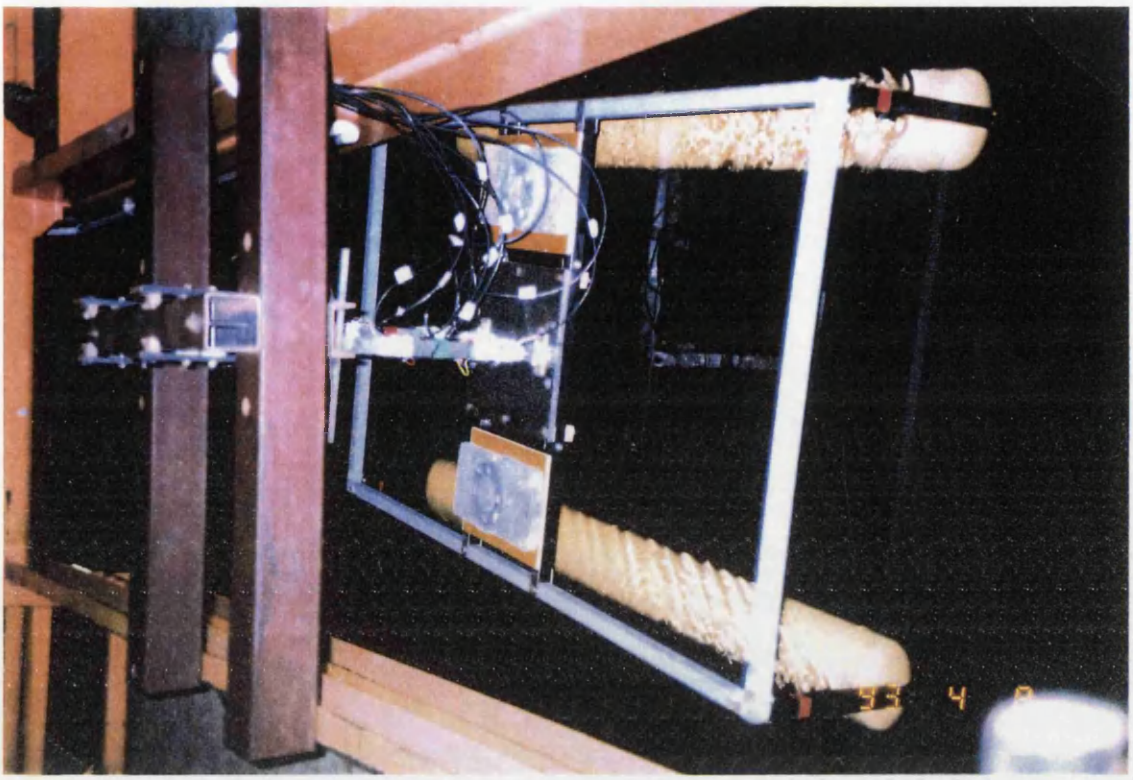

Fig.9.37 The twin hulled model in +8 degree drift and 2 degree trim by stern condition (d/a = 4.0, c/a = 10.0)

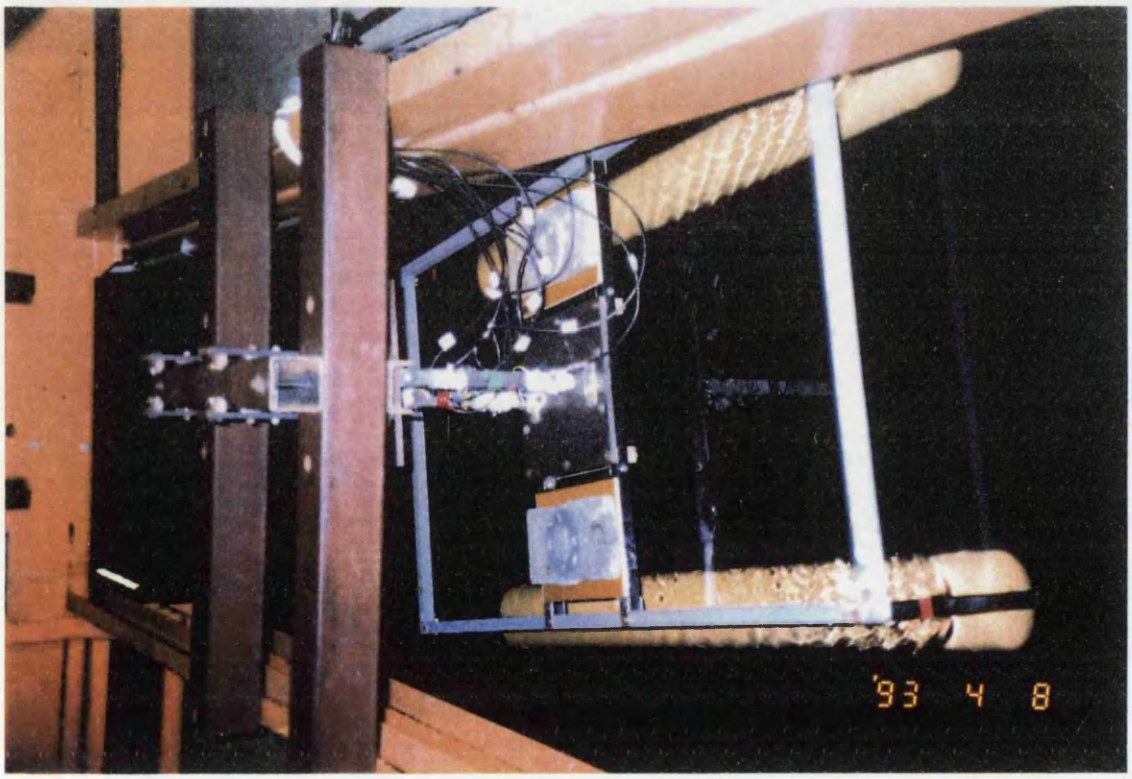

Fig.9.38 The twin hulled model in -10 degree drift and 2 degree trim by stern condition (d/a = 4.0, c/a = 10.0)

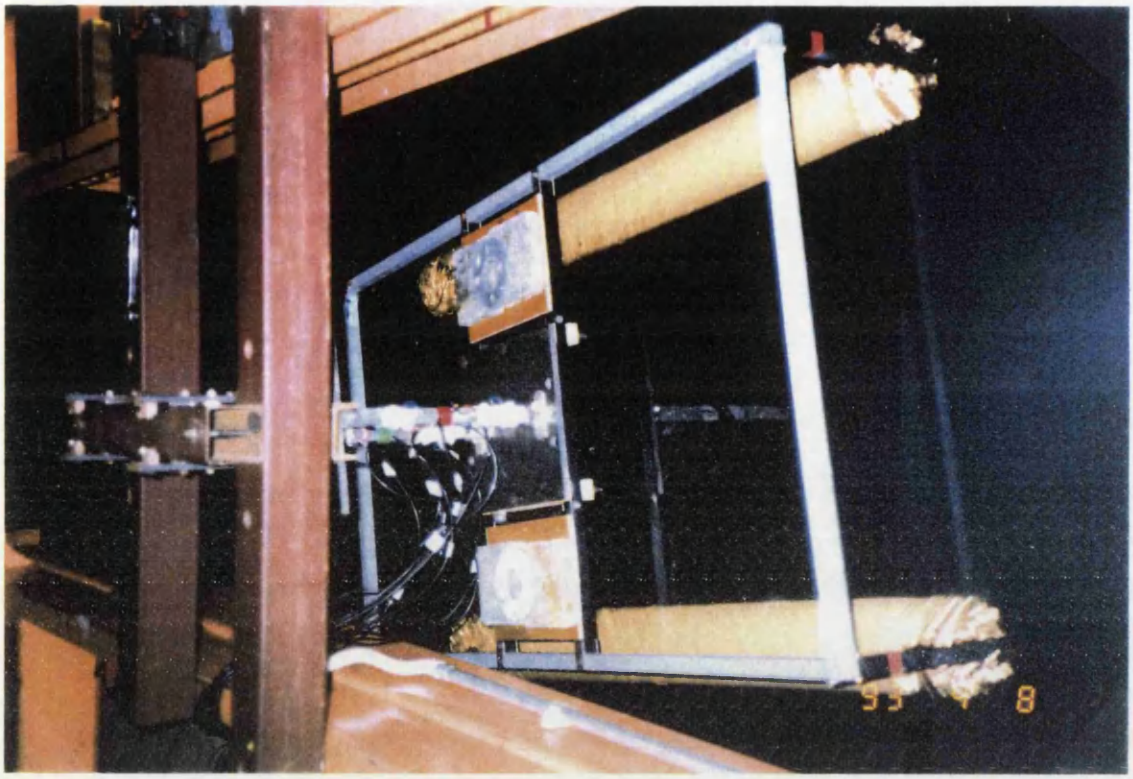

Fig.9.39 The twin hulled model in -10 degree drift and 4 degree trim by bow condition (d/a = 4.0, c/a = 10.0)

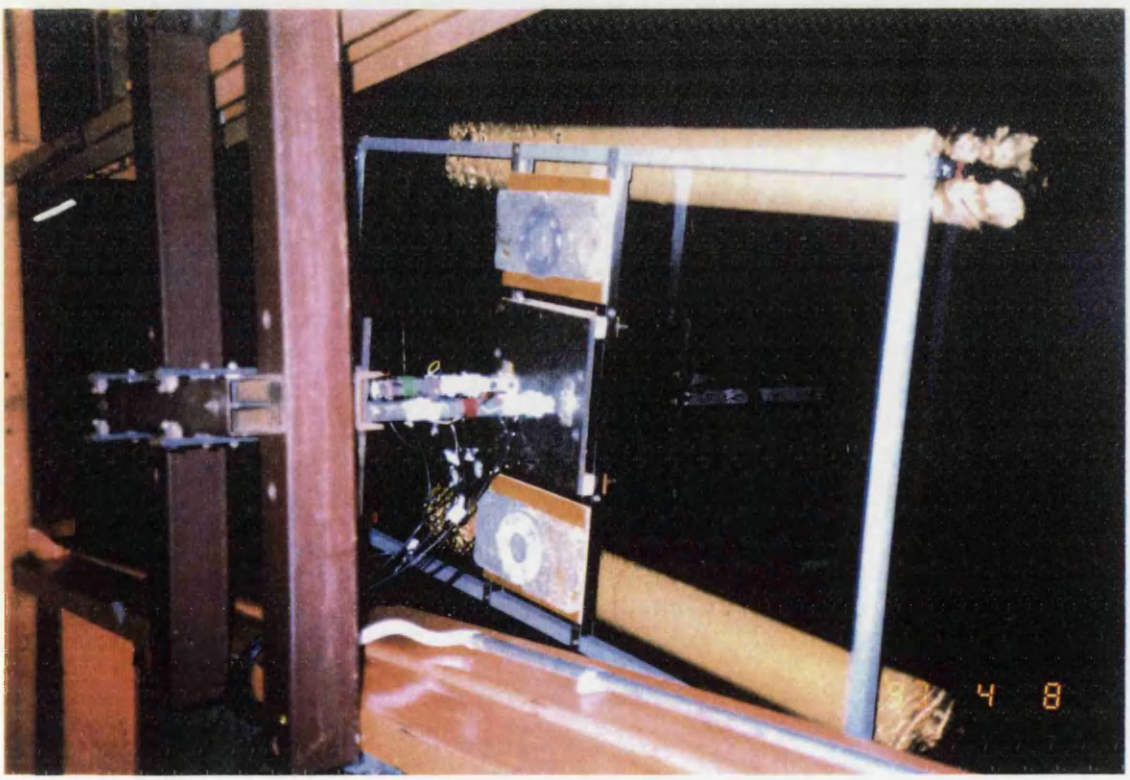

Fig.9.40 The twin hulled model in +6 degree drift and 4 degree trim by stern condition (d/a = 4.0, c/a = 10.0)

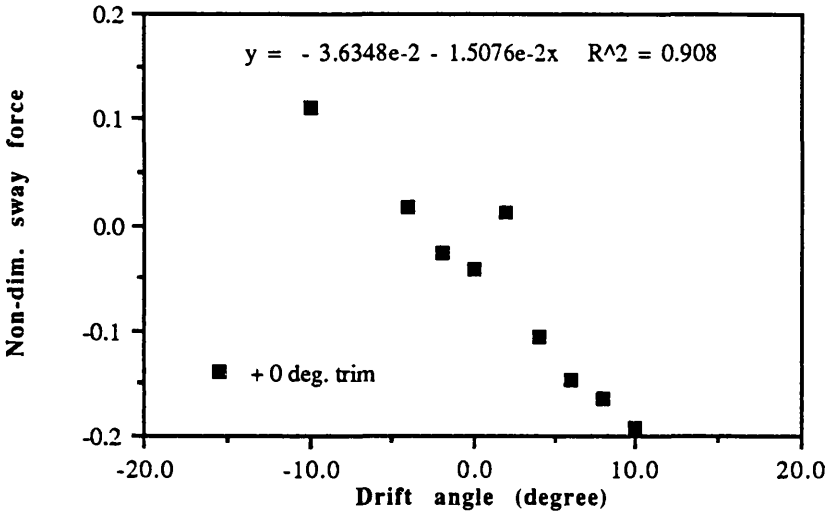

Fig.9.41 Non-dimensionalized sway force on twin hulled model in no trim condition (d/a=3.0,c/a=10.0)

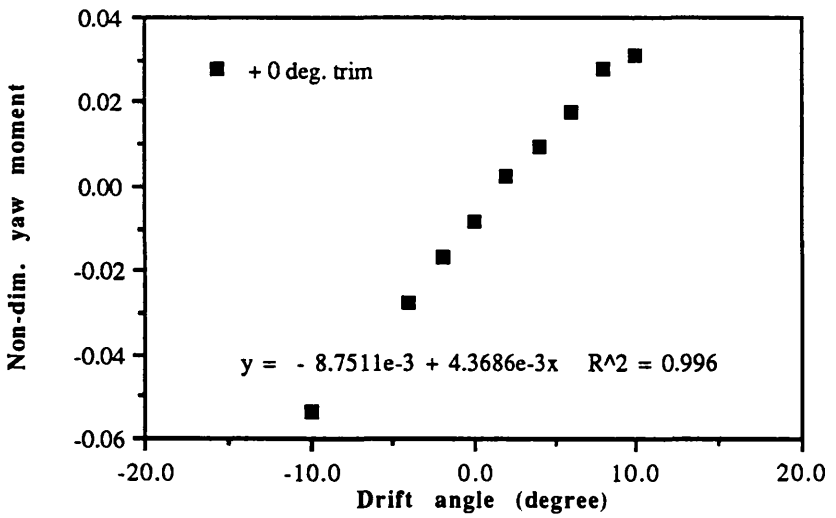

Fig.9.42 Non-dimensionalized yaw moment on twin hulled model in no trim condition (d/a=3.0,c/a=10.0)

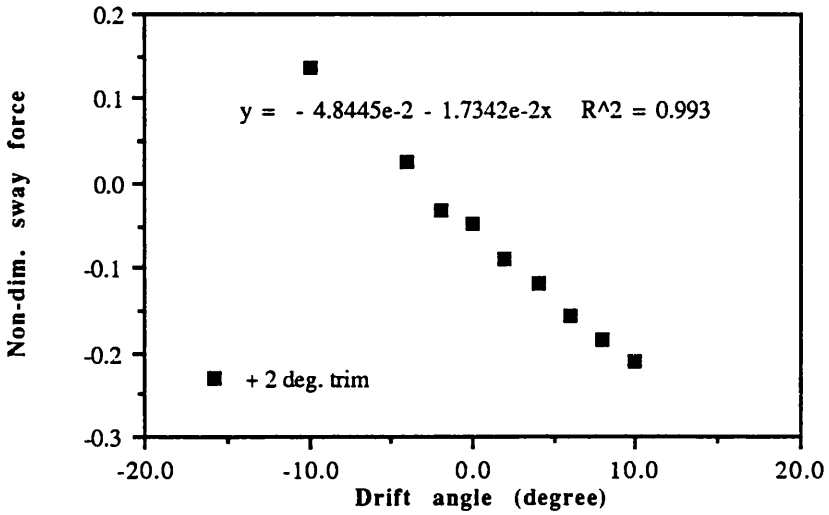

Fig.9.43 Non-dimensionalized sway force on twin hulled model in 2 degree trim by stern condition (d/a=3.0,c/a=10.0)

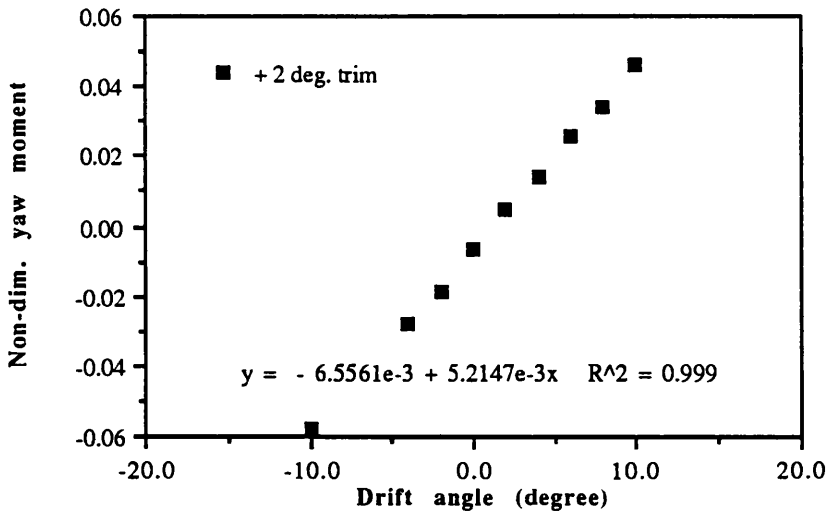

Fig.9.44 Non-dimensionalized yaw moment on twin hulled model in 2 degree trim by stern condition (d/a=3.0,c/a=10.0)

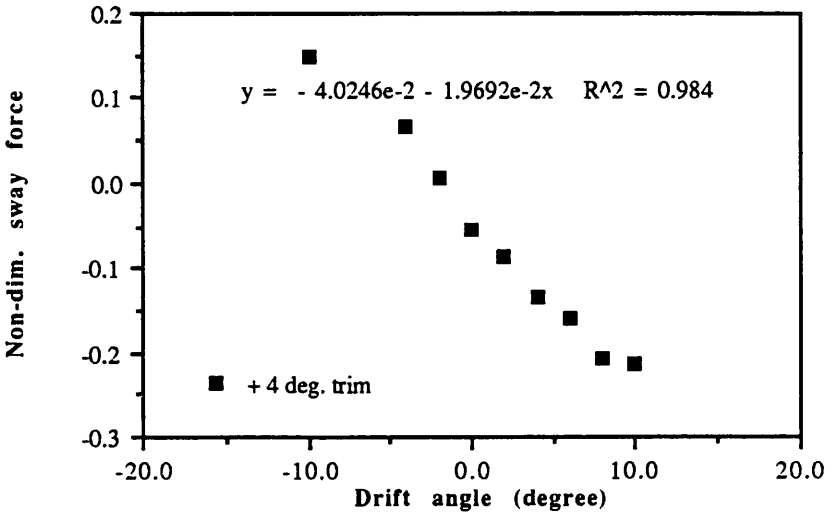

Fig.9.45 Non-dimensionalized sway force on twin hulled model in 4 degree trim by stern condition (d/a=3.0,c/a=10.0)

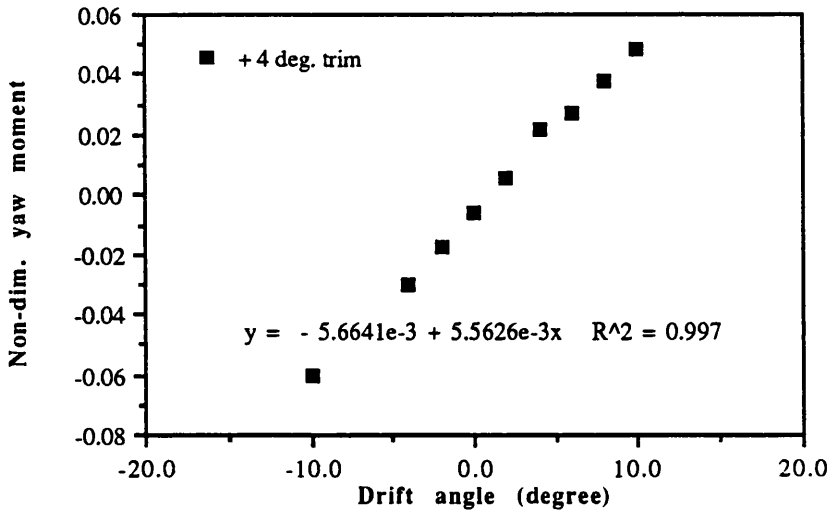

Fig.9.46 Non-dimensionalized yaw moment on twin hulled model in 4 degree trim by stern condition (d/a=3.0,c/a=10.0)

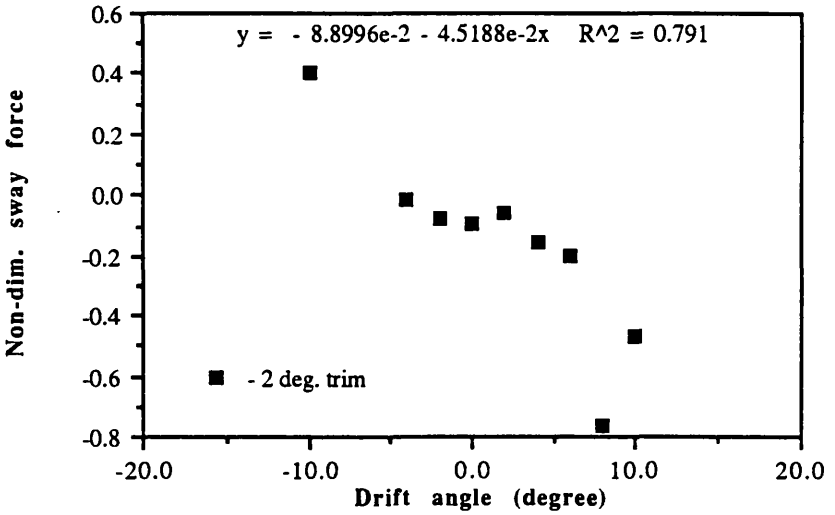

Fig.9.47 Non-dimensionalized sway force on twin hulled model in 2 degree trim by bow condition (d/a=3.0,c/a=10.0)

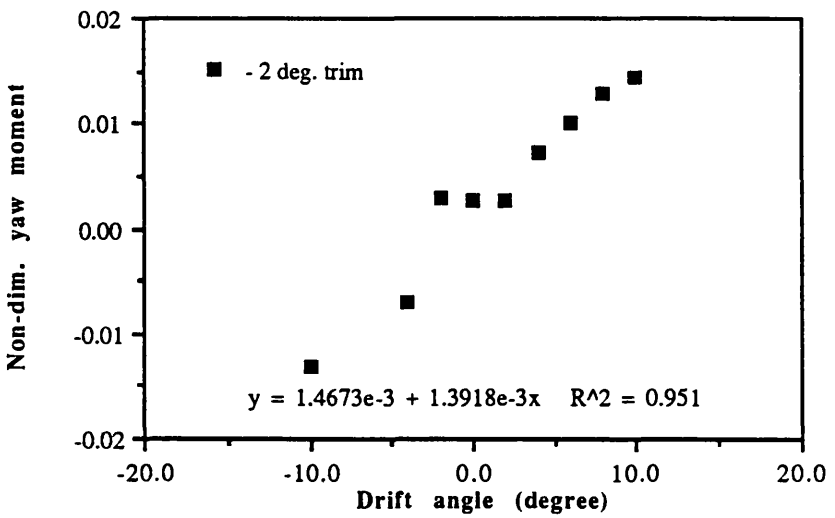

Fig.9.48 Non-dimensionalized yaw moment on twin hulled model in 2 degree trim by bow condition (d/a=3.0,c/a=10.0)

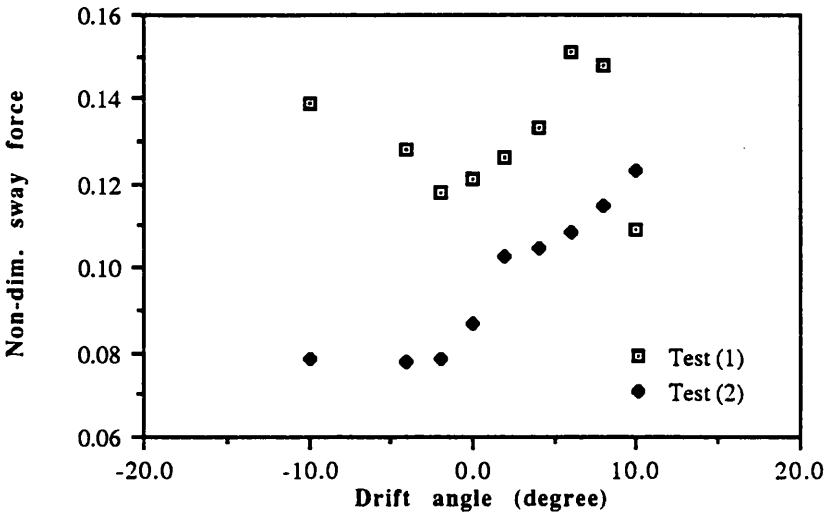

Fig.9.49 Comparison of non-dim. sway force on twin hulled model in 4 degree trim by bow condition (d/a=3.0,c/a=10.0)

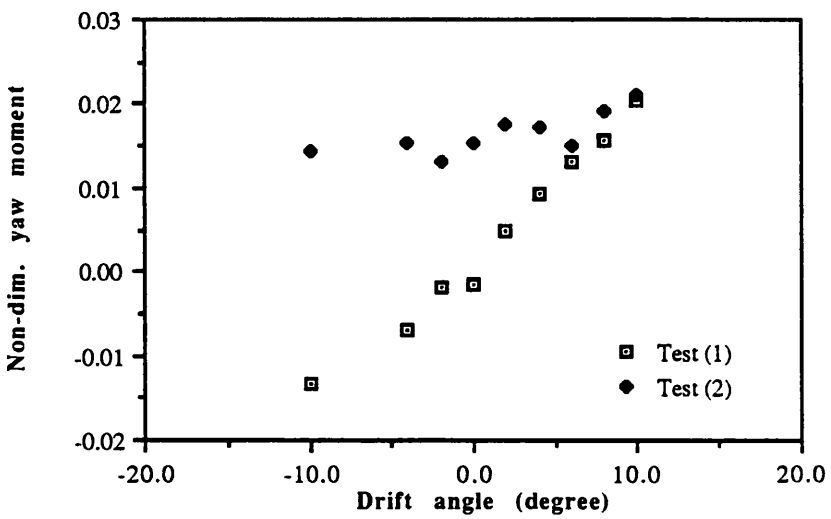

Fig.9.50 Comparison of non-dim. yaw moment on twin hulled model in 4 degree trim by bow condition (d/a=3.0,c/a=10.0)

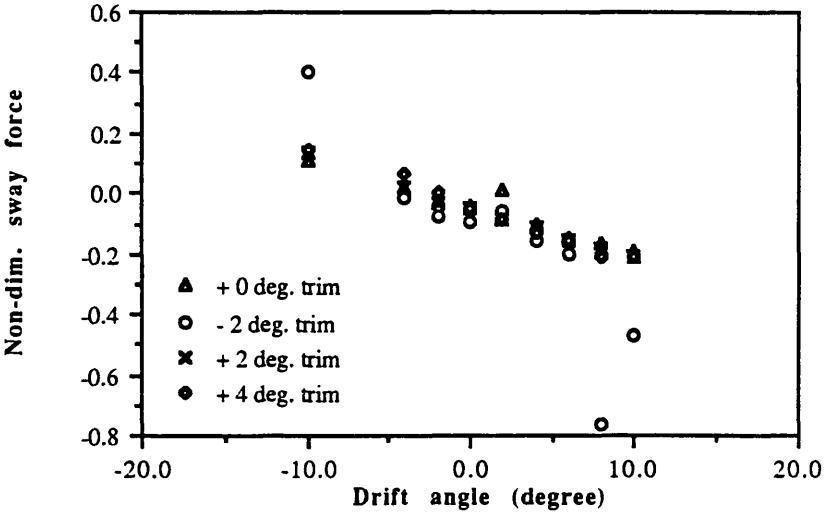

Fig.9.51 Comparison of non-dim. sway force on twin hulled model in trim conditions (d/a=3.0,c/a=10.0)

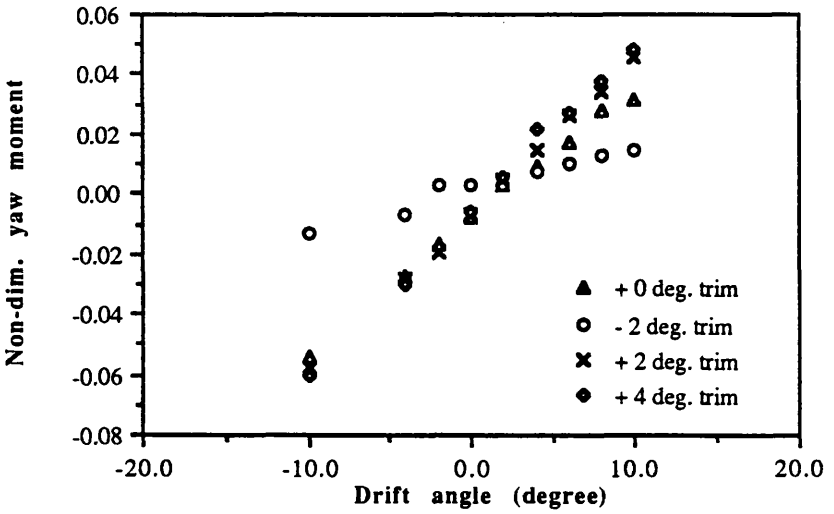

Fig.9.52 Comparison of non-dim. yaw moment on twin hulled model in trim conditions (d/a=3.0,c/a=10.0)

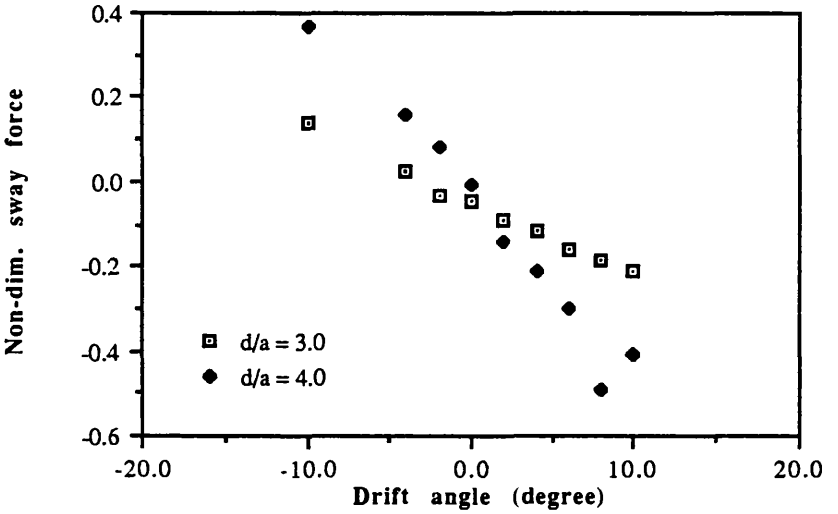

Fig.9.53 Comparison of non-dim. sway force for different depths in 2 degree trim by stern condition

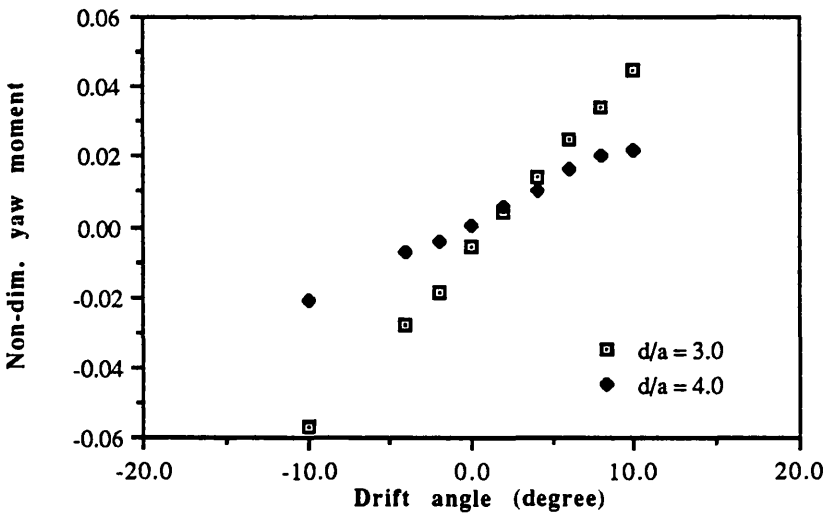

Fig.9.54 Comparison of non-dim. yaw moment for different depths in 2 degree trim by stern condition

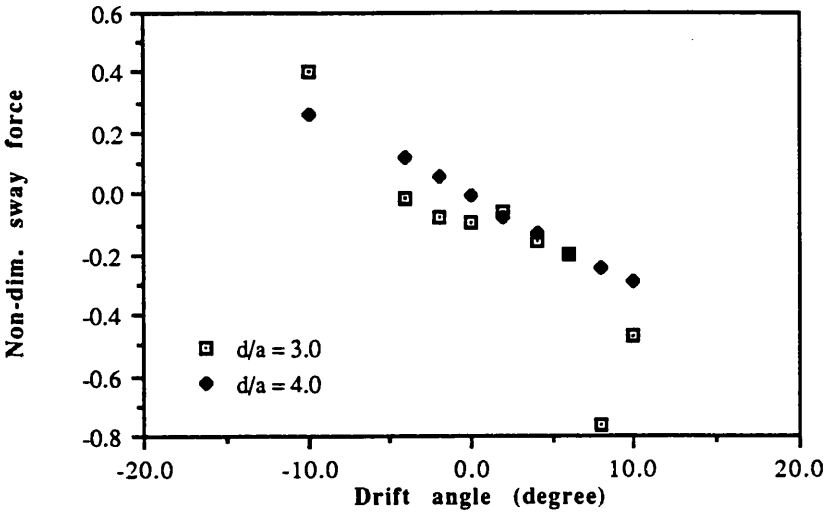

Fig.9.55 Comparison of non-dim. sway force for different depths in 2 degree trim by bow condition

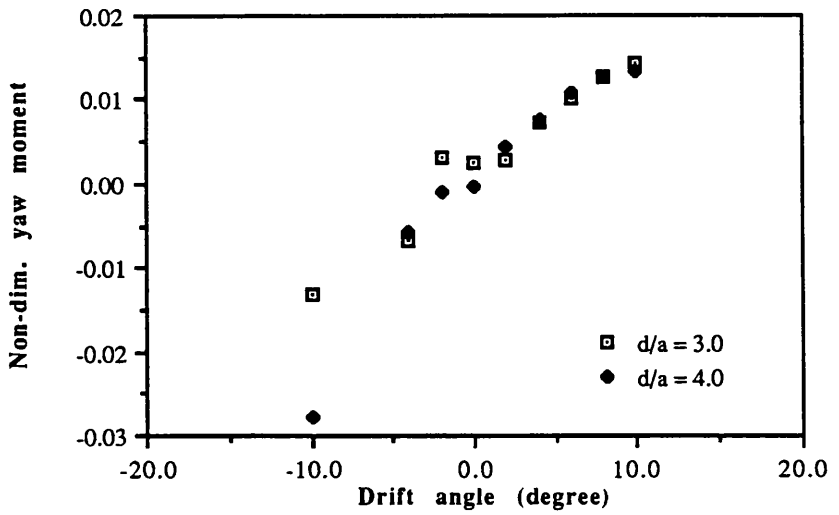

Fig.9.56 Comparison of non-dim. yaw moment for different depths in 2 degree trim by bow condition

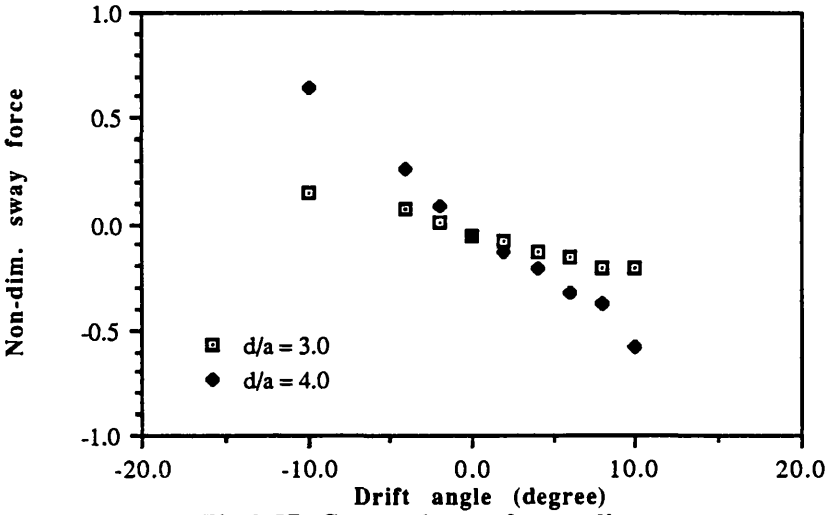

Fig.9.57 Comparison of non-dim. sway force for different depths in 4 degree trim by stern condition

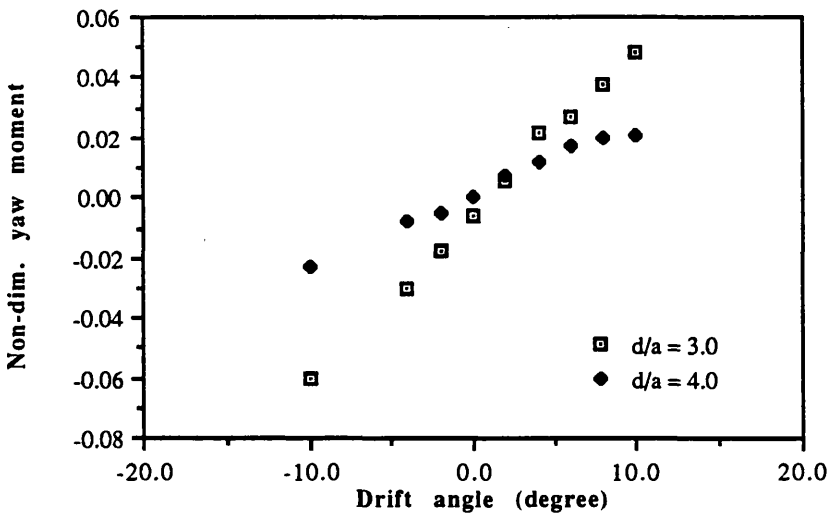

Fig.9.58 Comparison of non-dim. yaw moment for different depths in 4 degree trim by stern condition

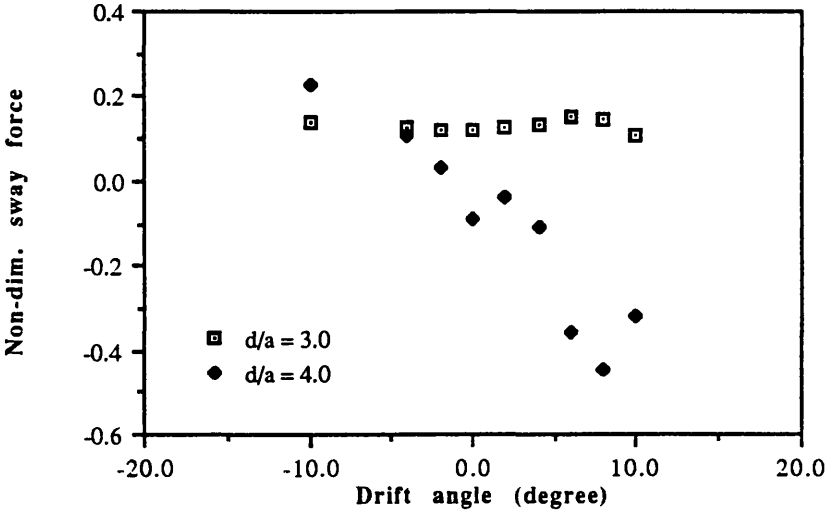

Fig.9.59 Comparison of non-dim. sway force for different depths in 4 degree trim by bow condition

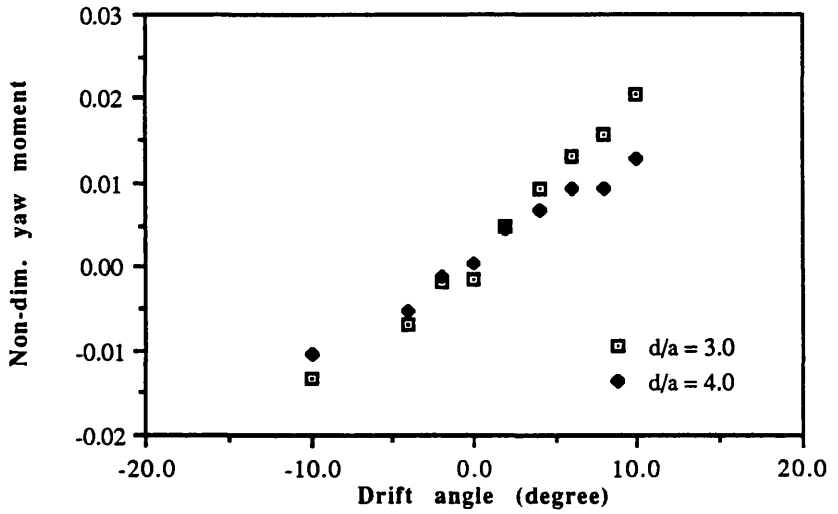

Fig.9.60 Comparison of non-dim. yaw moment for different depths in 4 degree trim by bow condition

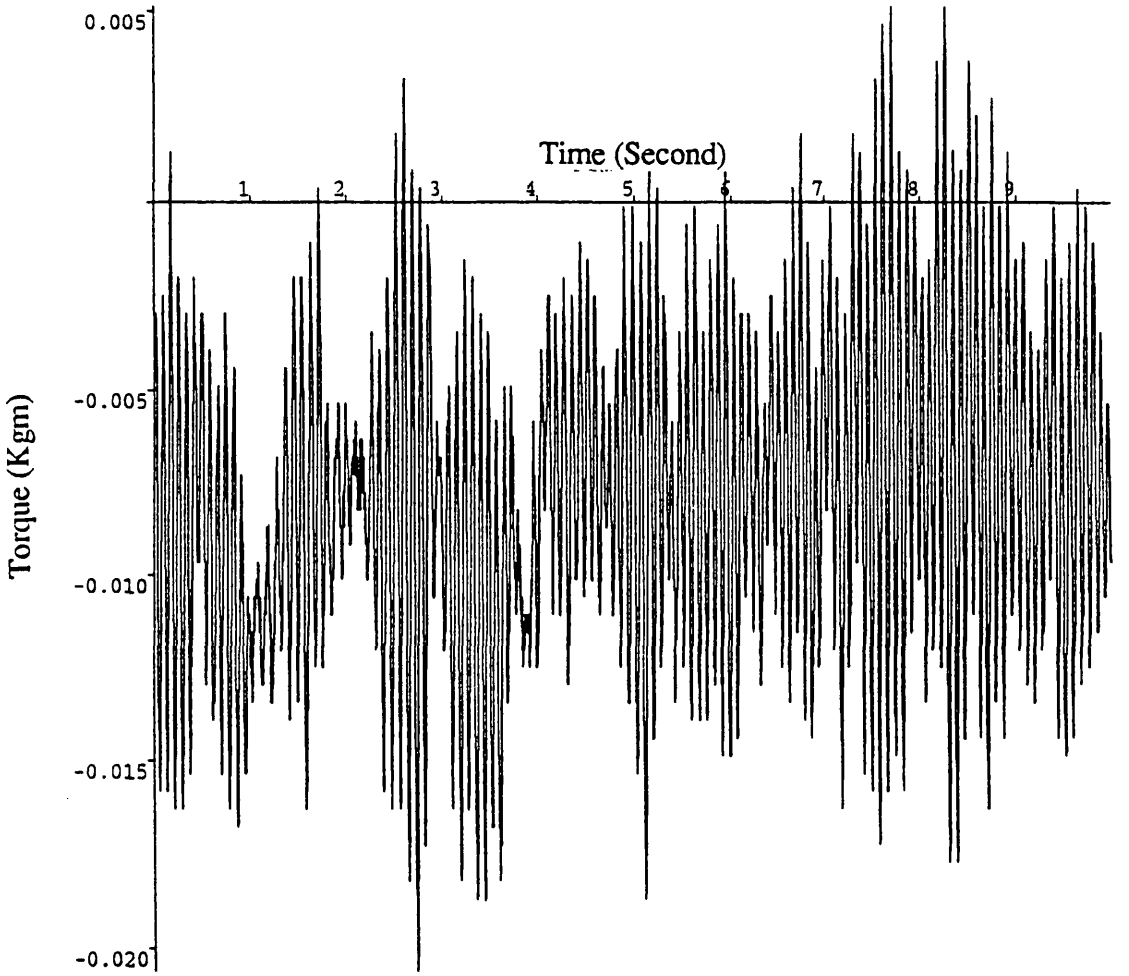

Fig.9.61 Measuring signals of Channel 1 (M1) (d/a = 3.0, c/a = 10.0)

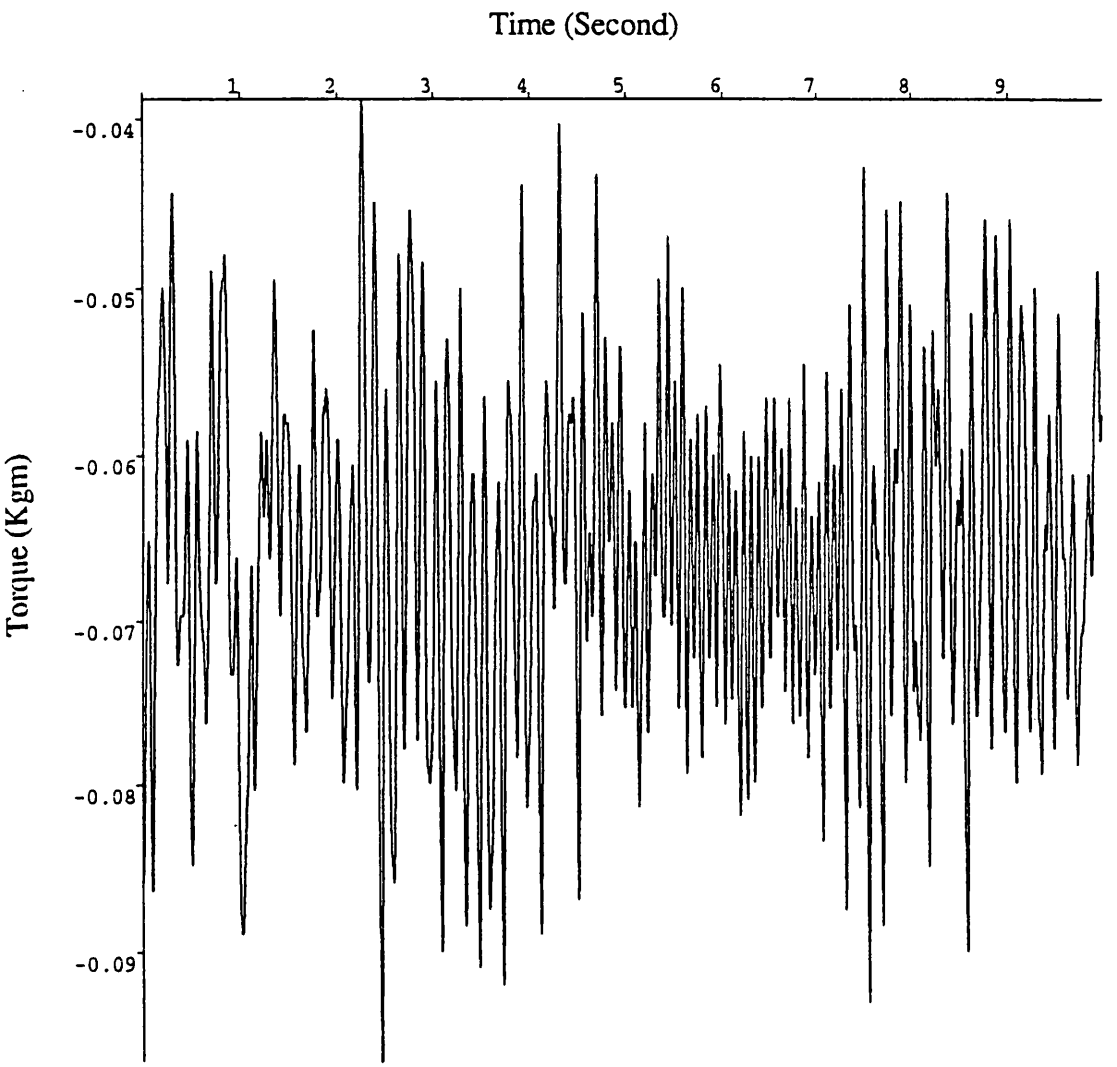

Fig.9.62 Measuring signals of Channel 2 (M2) (d/a = 3.0, c/a = 10.0)

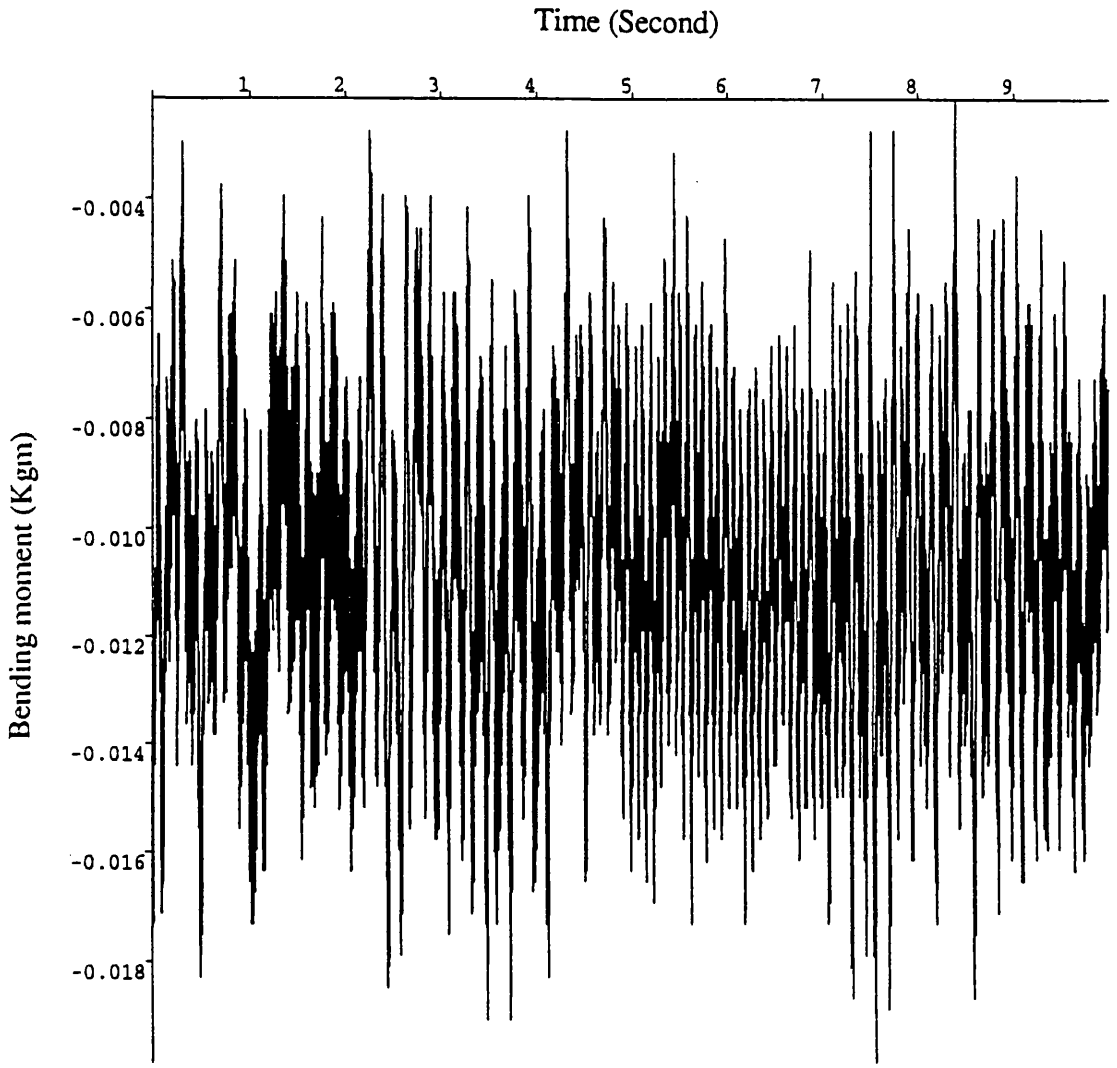

Fig.9.63 Measuring signals of Channel 3 (M3) (d/a = 3.0, c/a = 10.0)

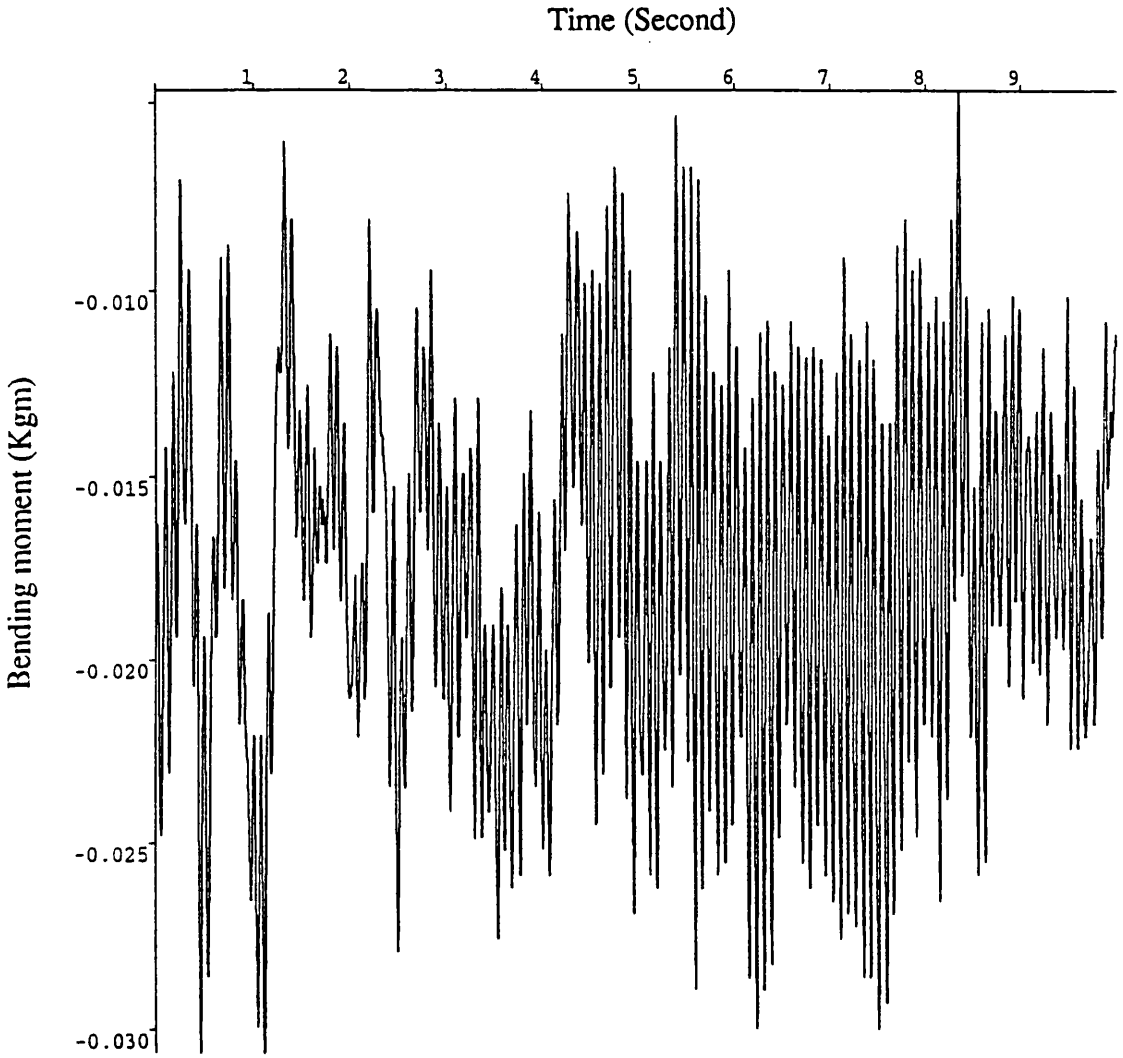

Fig.9.64 Measuring signals of Channel 4 (M4) (d/a = 3.0, c/a = 10.0)

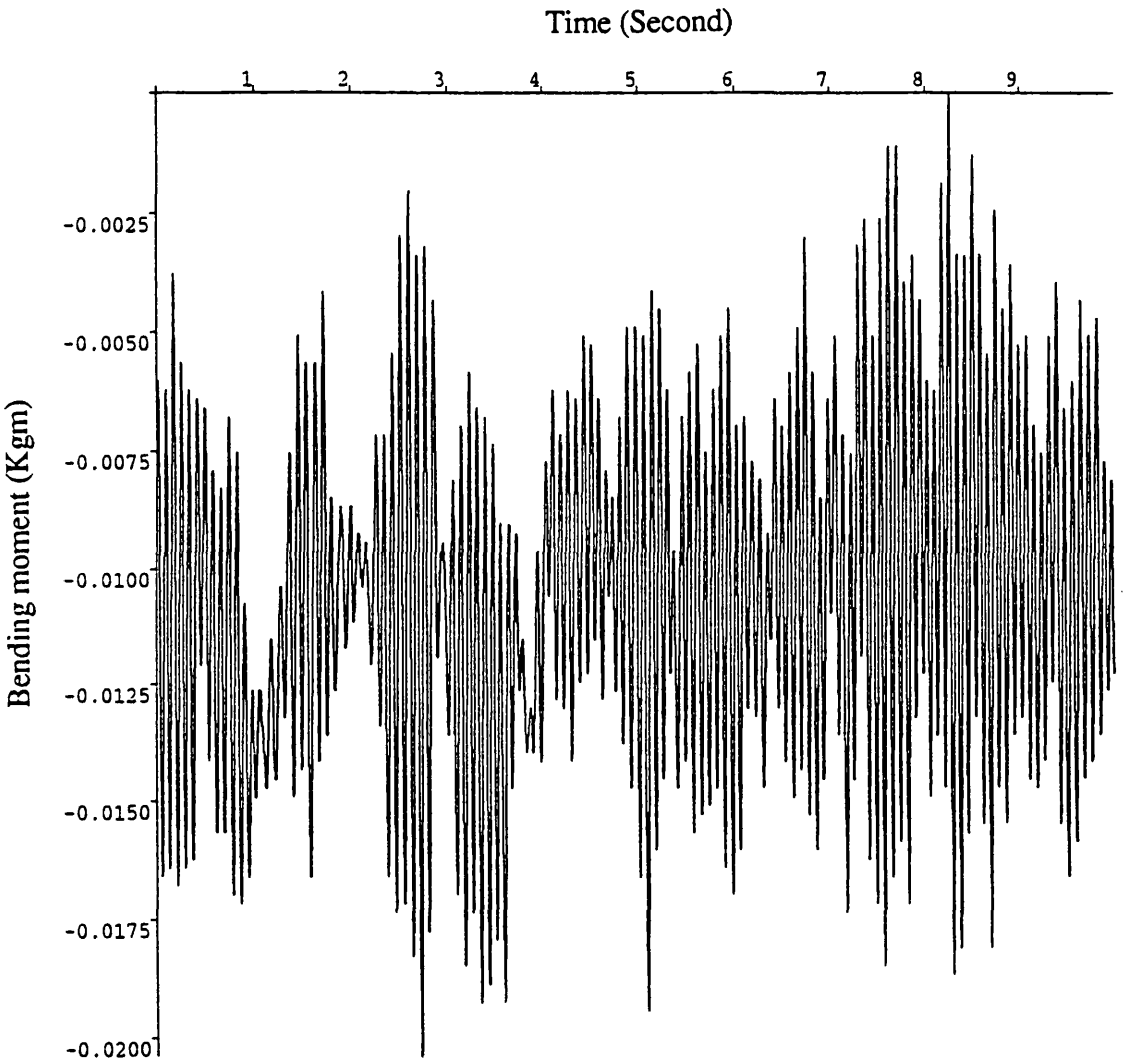

Fig.9.65 Measuring signals of Channel 5 (M5) (d/a = 3.0, c/a = 10.0)

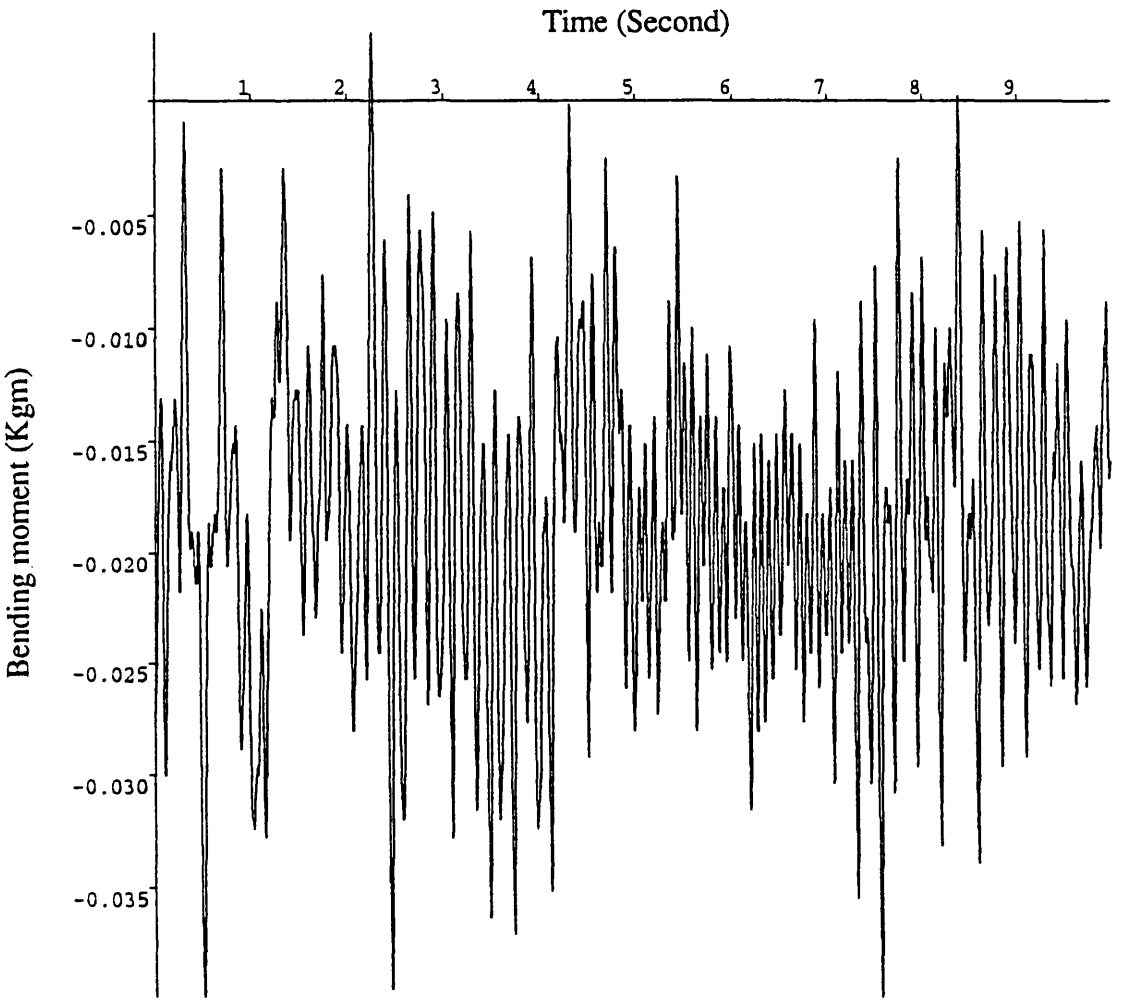

Fig.9.66 Measuring signals of Channel 6 (M6) (d/a = 3.0, c/a = 10.0)

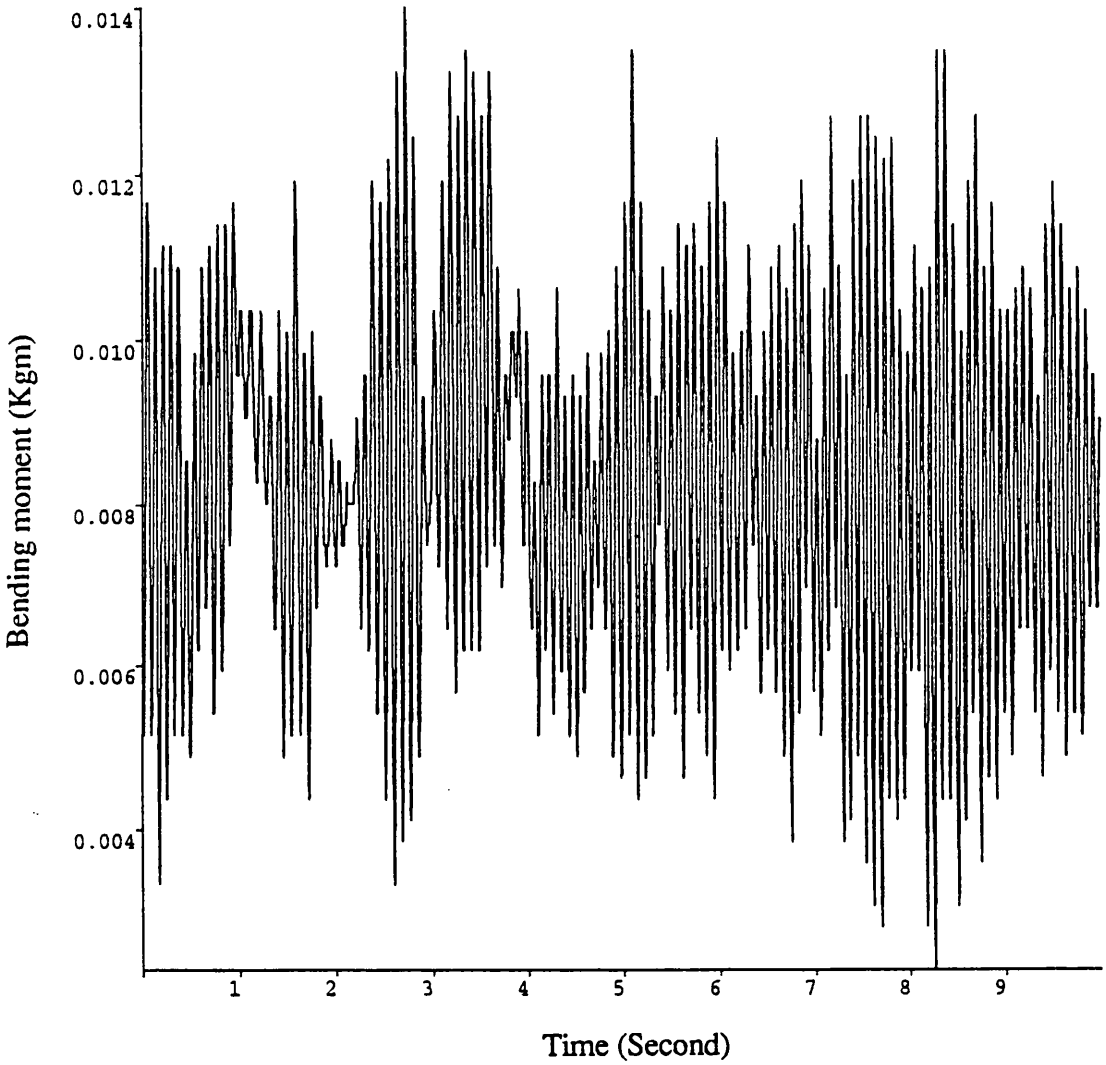

Fig.9.67 Measuring signals of Channel 7 (M7) (d/a = 3.0, c/a = 10.0)

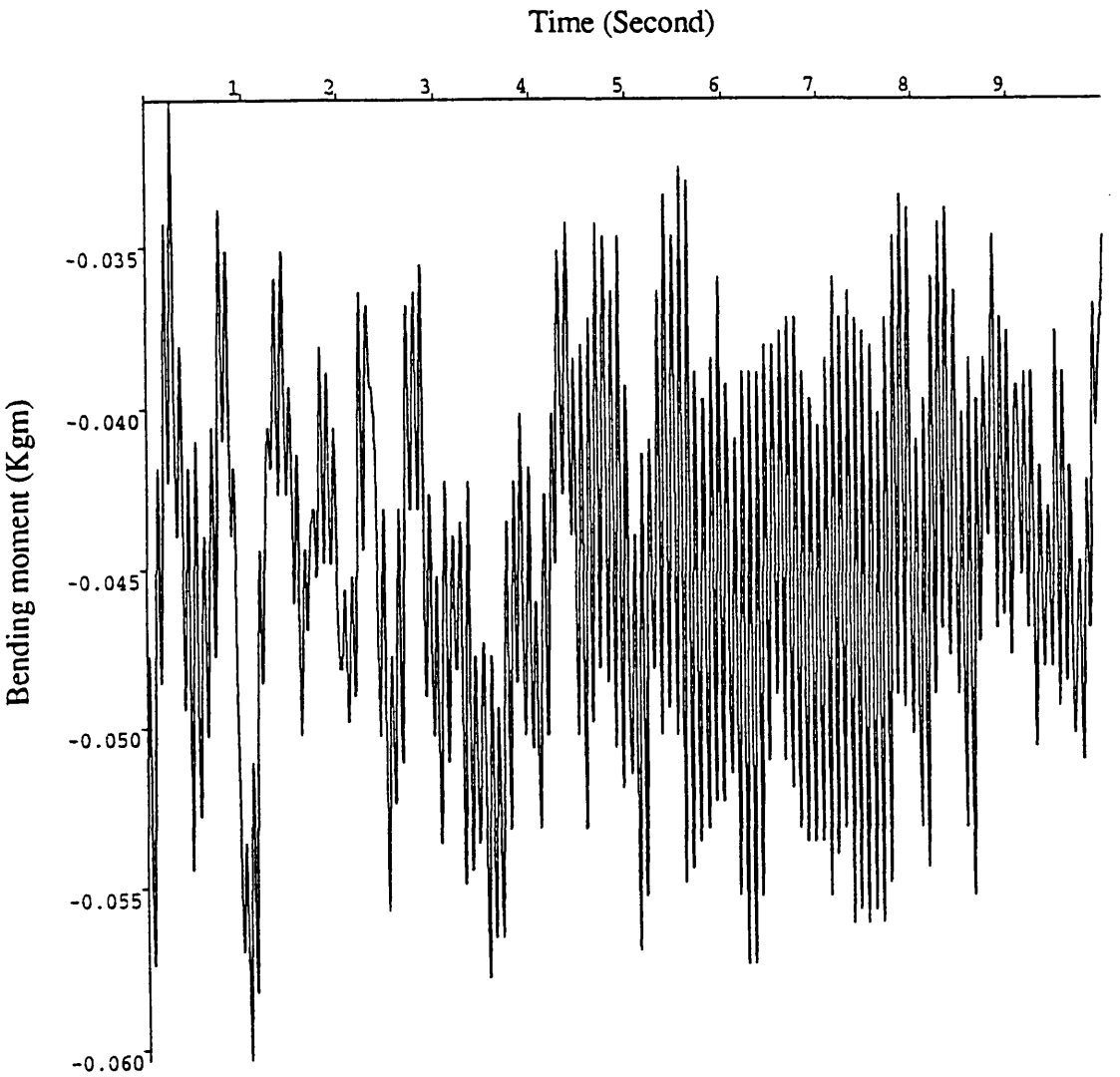

Fig.9.68 Measuring signals of Channel 8 (M8) (d/a = 3.0, c/a = 10.0)

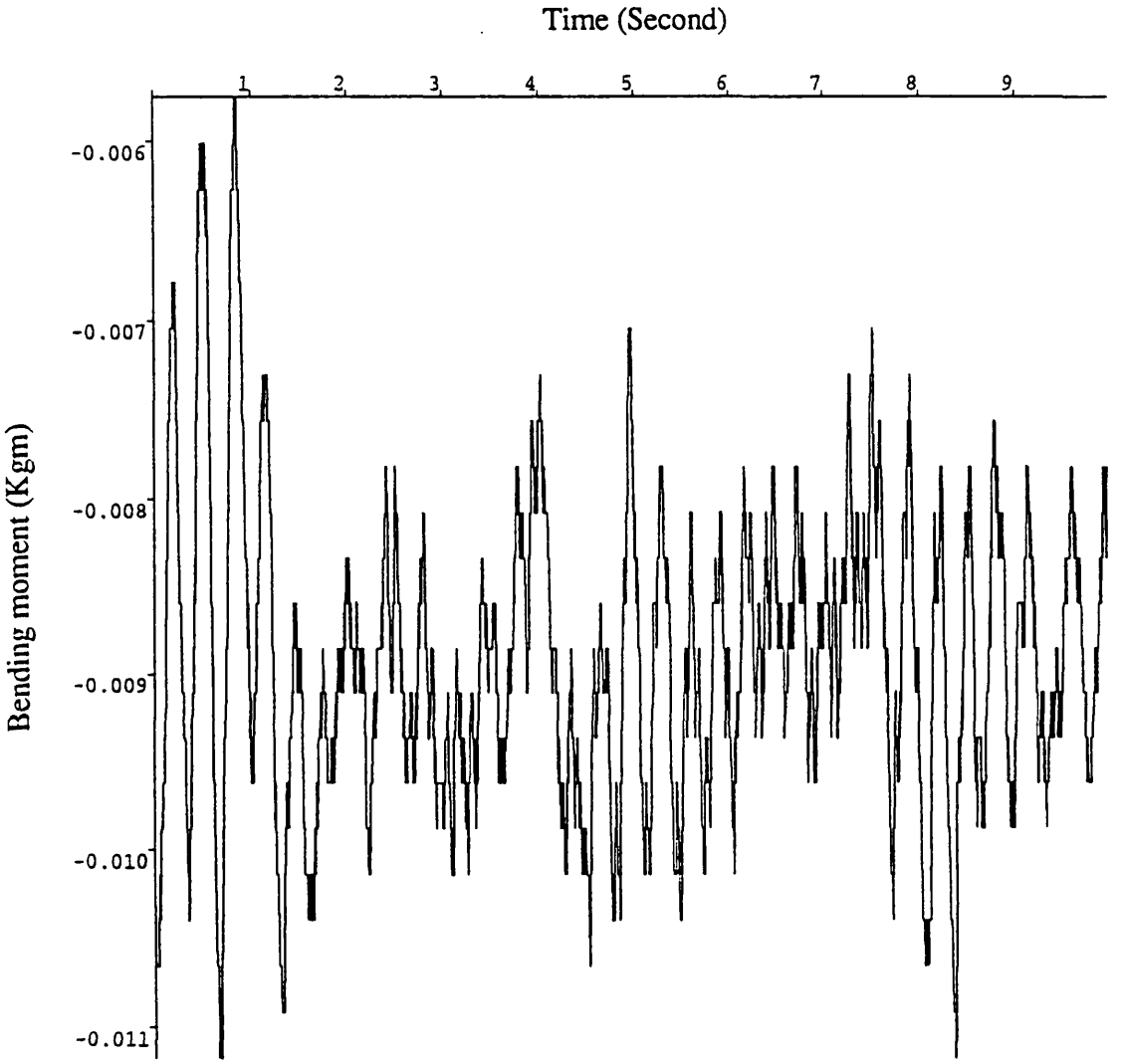

Fig.9.69 Measuring signals of Channel 9 (M9) (d/a = 3.0, c/a = 10.0)

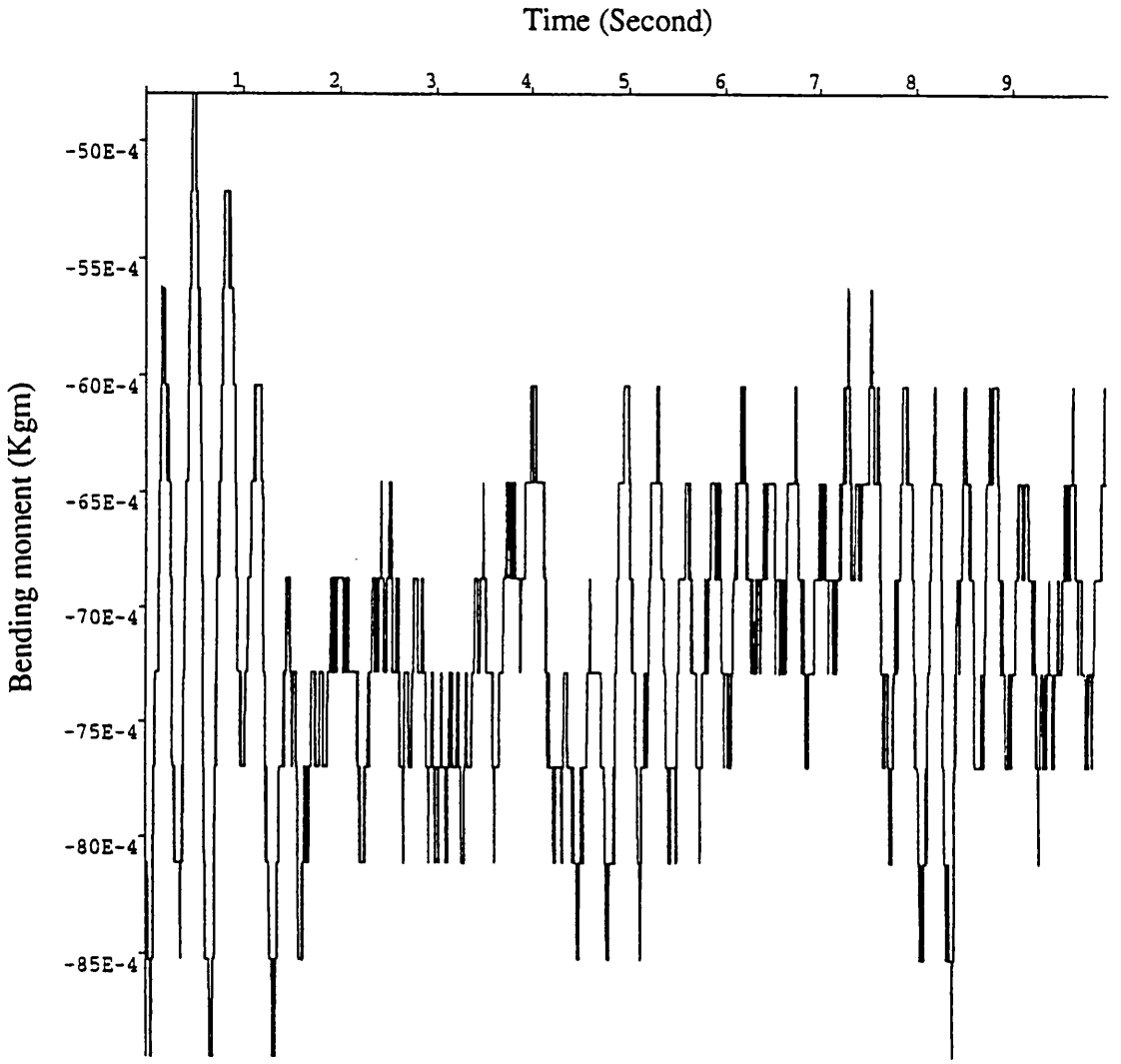

Fig.9.70 Measuring signals of Channel 10 (M10) (d/a = 3.0, c/a = 10.0)

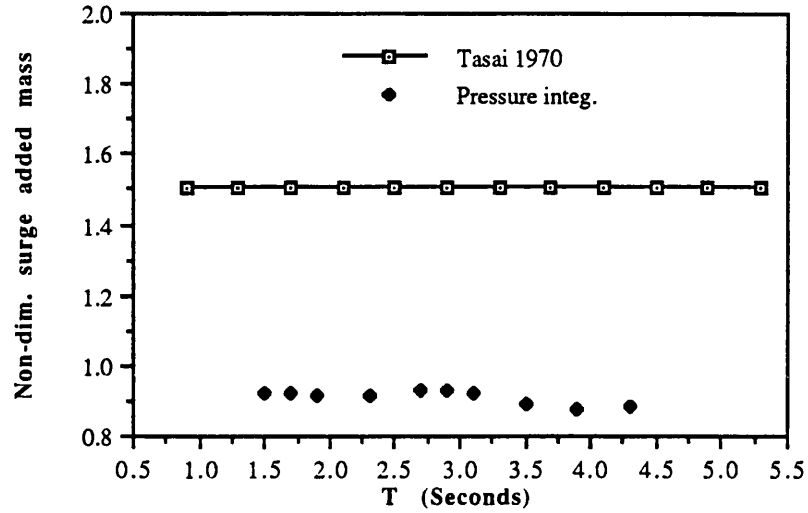

Fig.10.1 Comparison of non-dim. surge added mass coefficients (d/a=4.18, c/a=7.73, Fn=0.0 in no tilt condition)

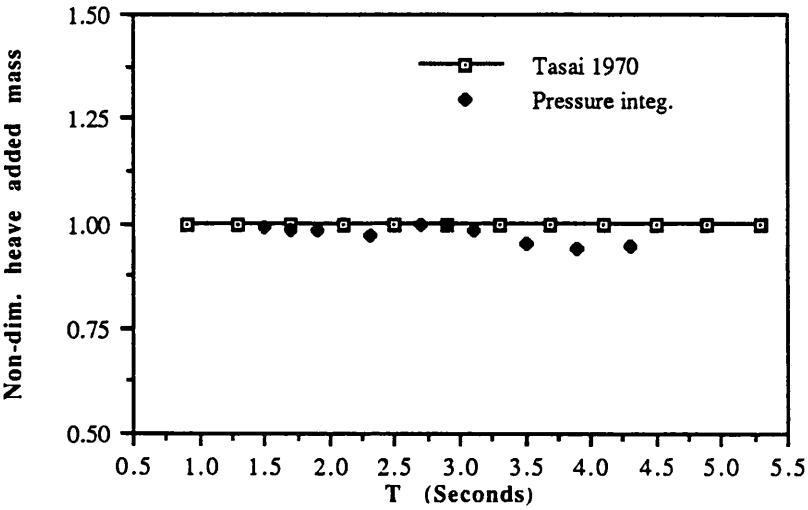

Fig.10.2 Comparison of non-dim. heave added mass coefficients (d/a=4.18, c/a=7.73, Fn=0.0 in no tilt condition)

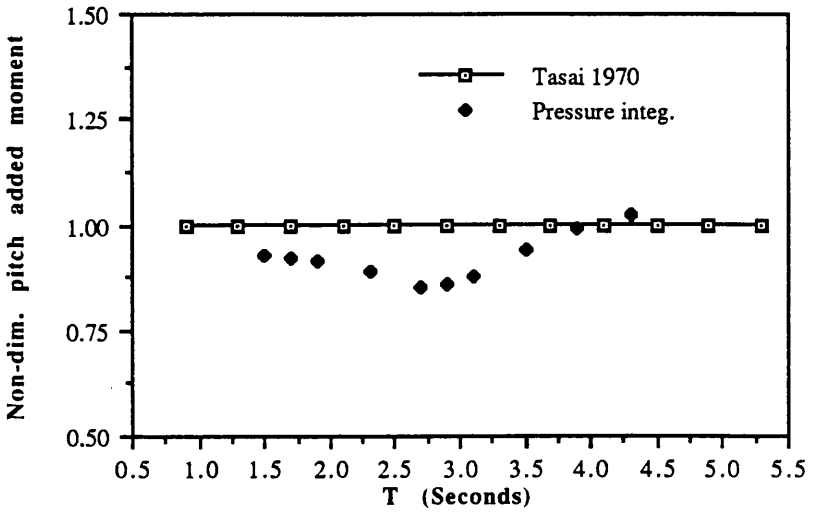

Fig.10.3 Comparison of non-dim. pitch added moment of inertia (d/a=4.18, c/a=7.73, Fn=0.0 in no tilt condition)

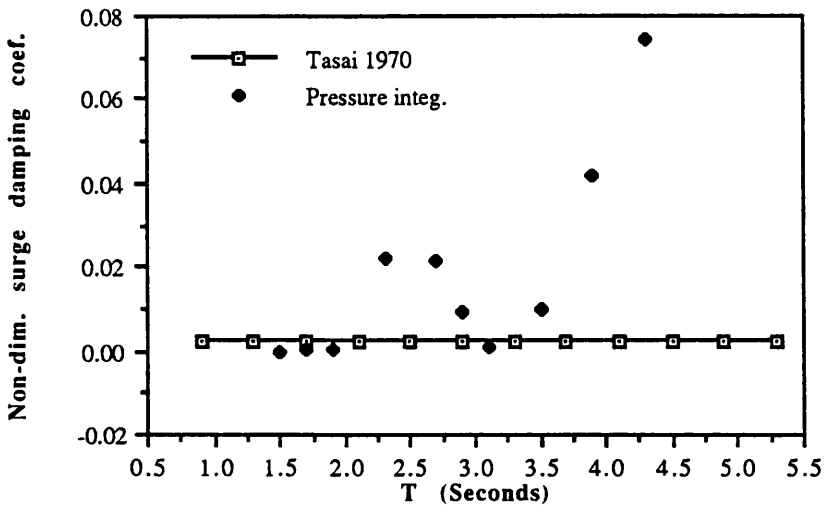

Fig.10.4 Comparison of non-dim. surge damping coefficients(d/a=4.18,c/a=7.73, Fn=0.0 in no tilt condition)

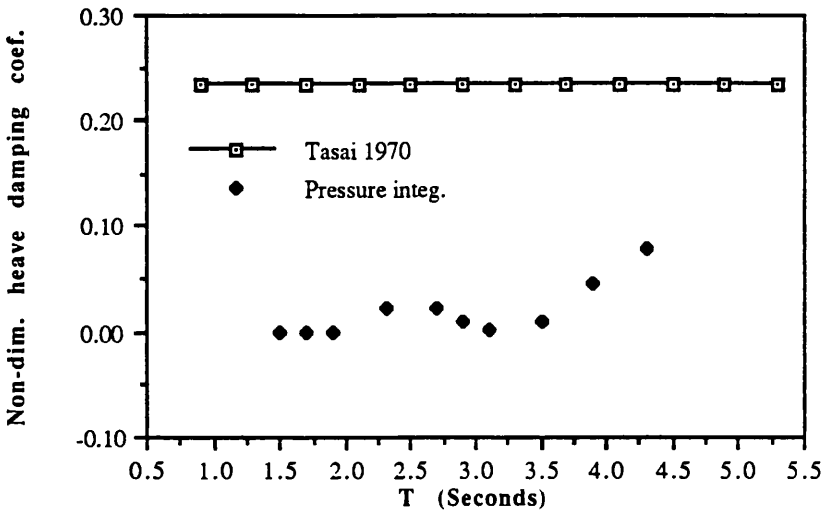

Fig.10.5 Comparison of non-dim. heave damping coefficients(d/a=4.18,c/a=7.73, Fn=0.0 in no tilt condition)

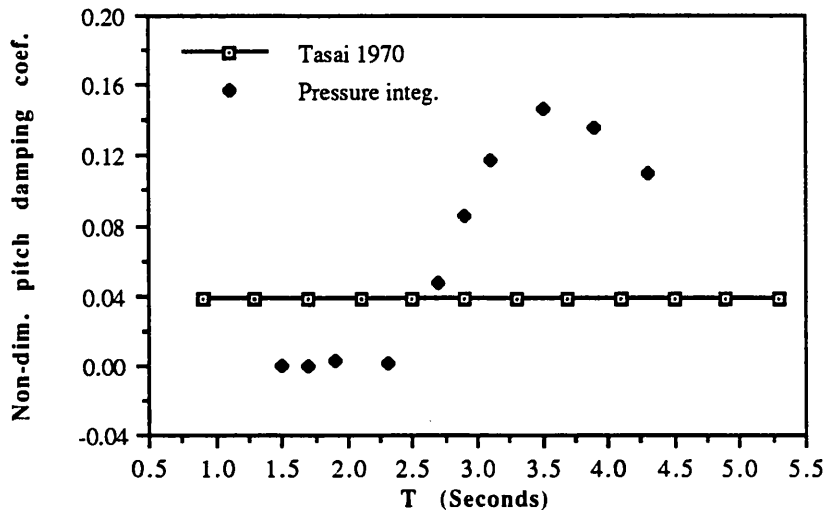

Fig.10.6 Comparison of non-dim. pitch damping coefficients(d/a=4.18,c/a=7.73, Fn=0.0 in no tilt condition)

PRINCIPAL DIMENSIONS

ITEM	MODEL 1/64	SHIP
Length (m)	1.797	115.0
Breadth (m)	1.172	75.0
Depth (m) (to Main Deck)	0.594	38.0
Draught (m)	0.313	20.0
Displacement (in fresh water)	131.8 kg	34551 ton
KG (m)	0.273	17.5
GM$_T$ (m)	0.045	2.87
GM$_L$ (m)	0.037	2.37

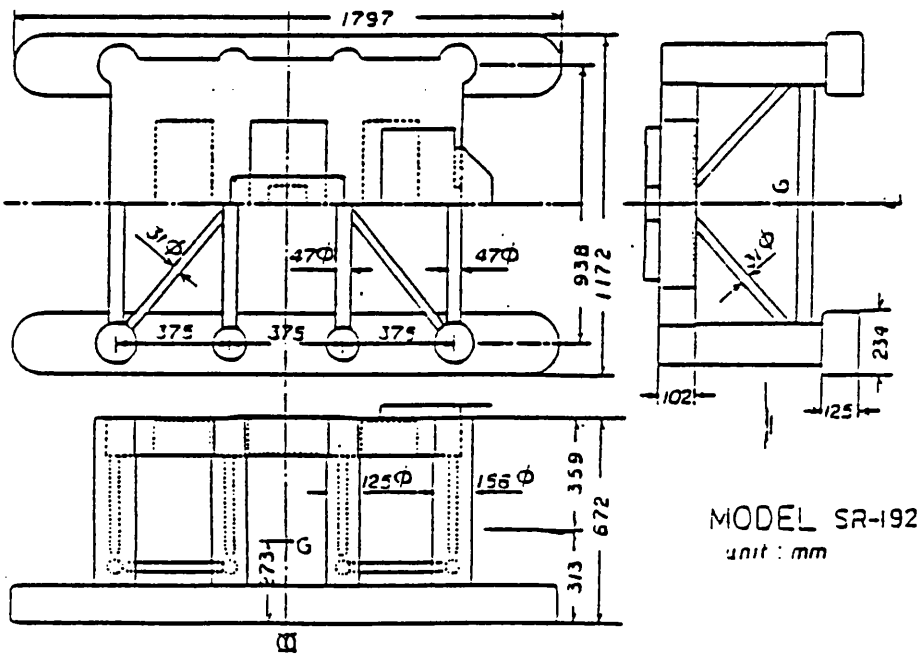

Fig.10.7 Basic configuration of the Japan SR-192 semi-submersible model

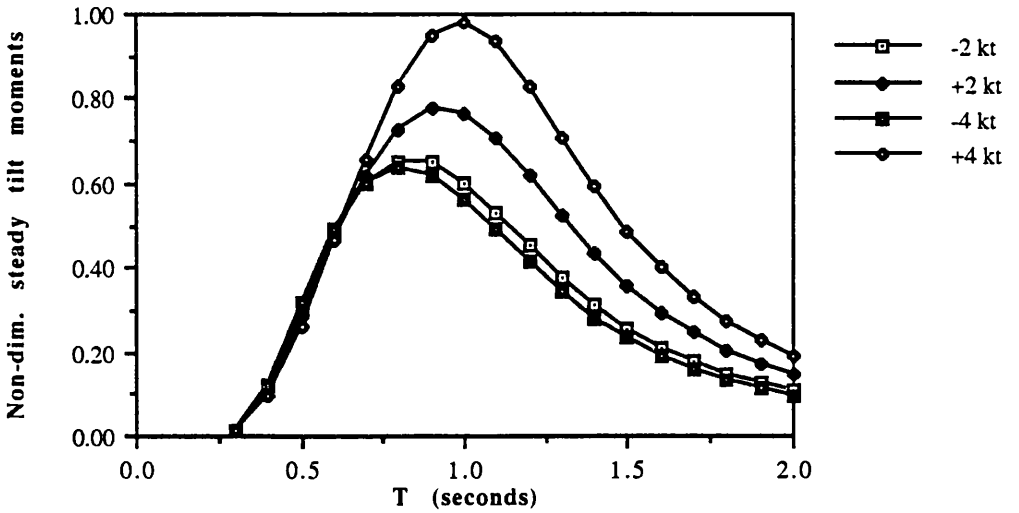

Fig.10.8 Comparison of non-dim. steady tilt moments for different current speeds in +10 degree tilt condition

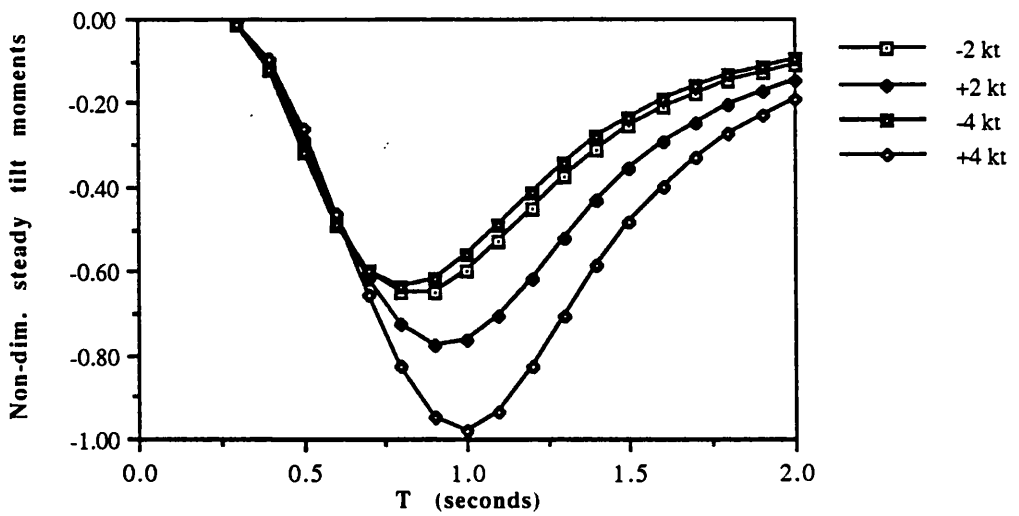

Fig.10.9 Comparison of non-dim. steady tilt moments for different current speeds in -10 degree tilt condition

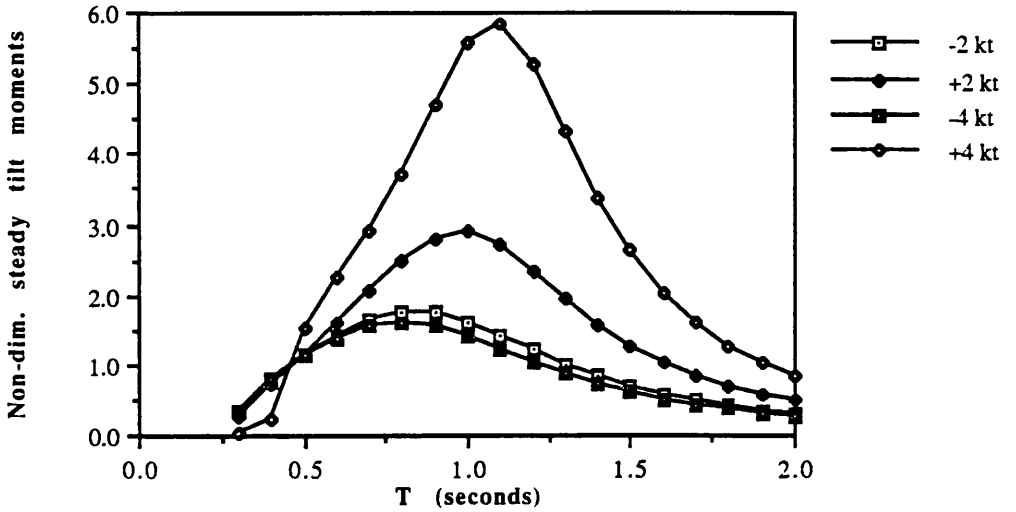

Fig.10.10 Comparison of non-dim. steady tilt moments for different current speeds in +15 degree tilt condition

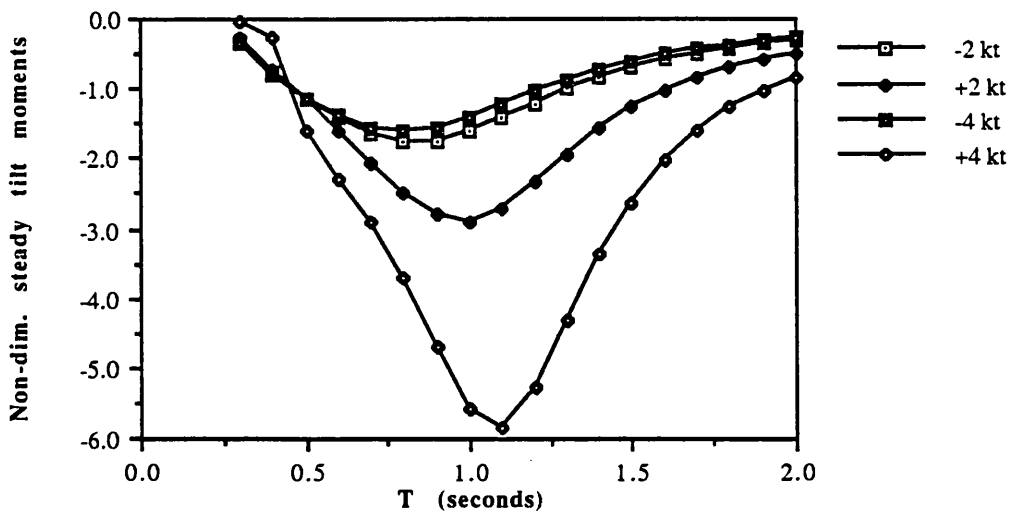

Fig.10.11 Comparison of non-dim. steady tilt moments for different current speeds in -15 degree tilt condition

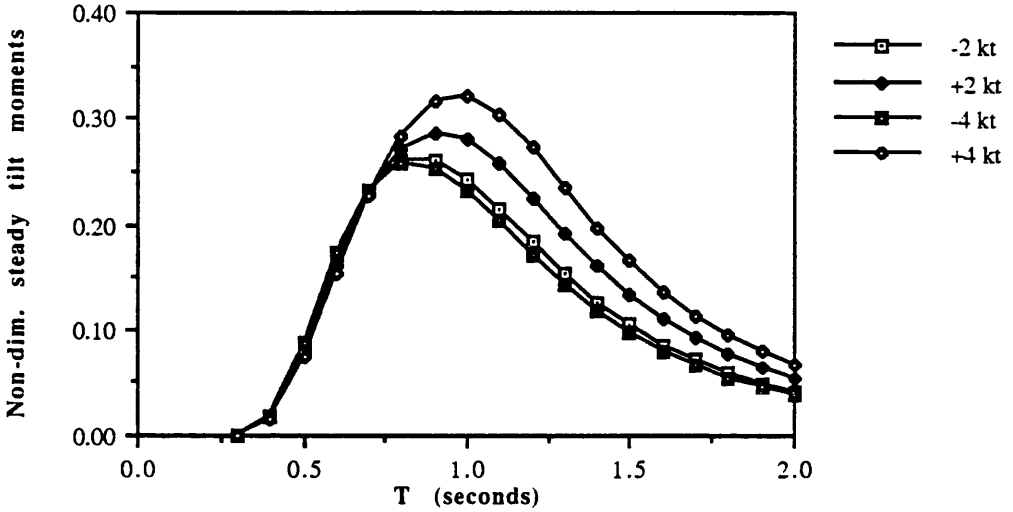

Fig.10.12 Comparison of non-dim. steady tilt moments for different current speeds in +5 degree tilt condition

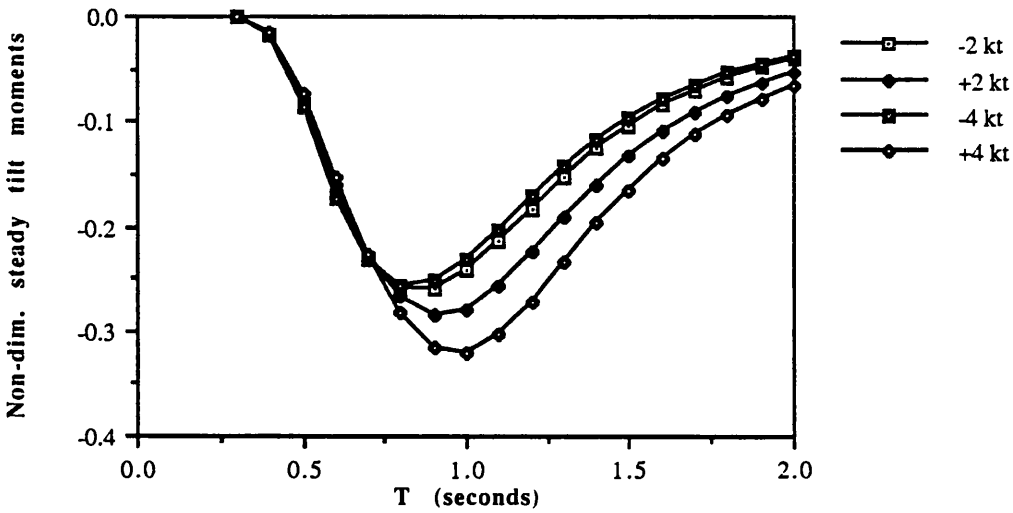

Fig.10.13 Comparison of non-dim. steady tilt moments for different current speeds in -5 degree tilt condition

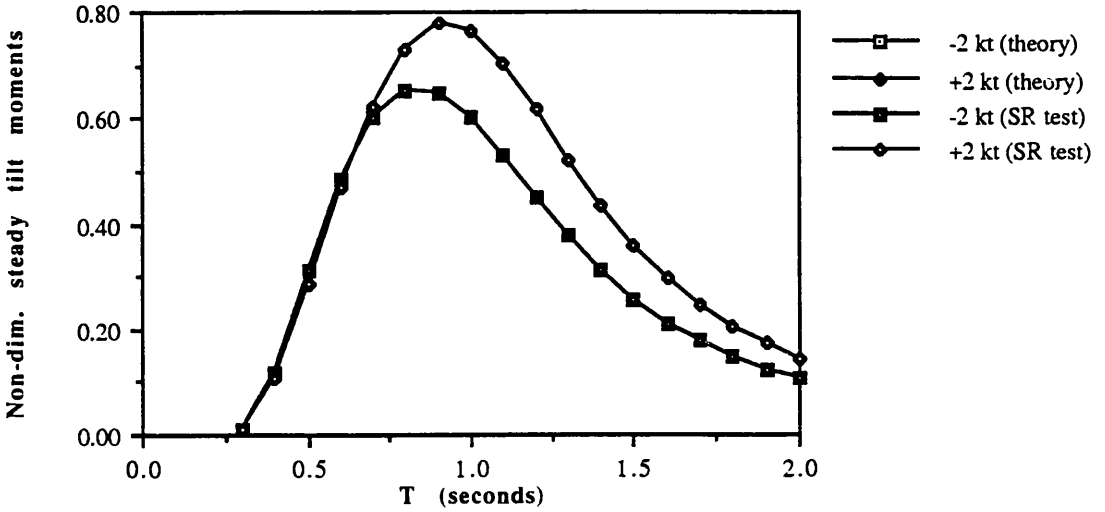

Fig.10.14 Comparison of non-dim. steady tilt moments for different current speeds in +10 degree tilt condition

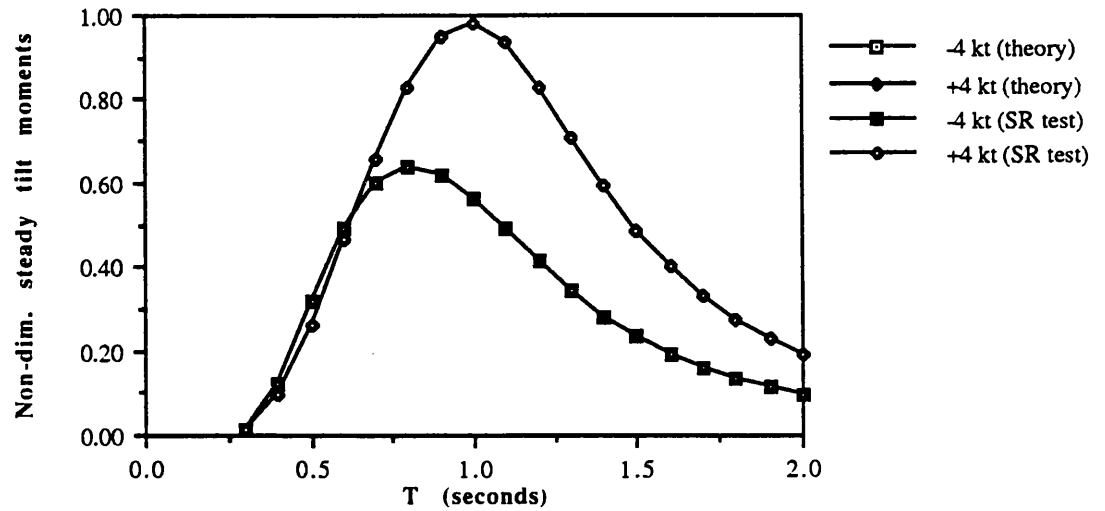

Fig.10.15 Comparison of non-dim. steady tilt moments for different current speeds in +10 degree tilt condition

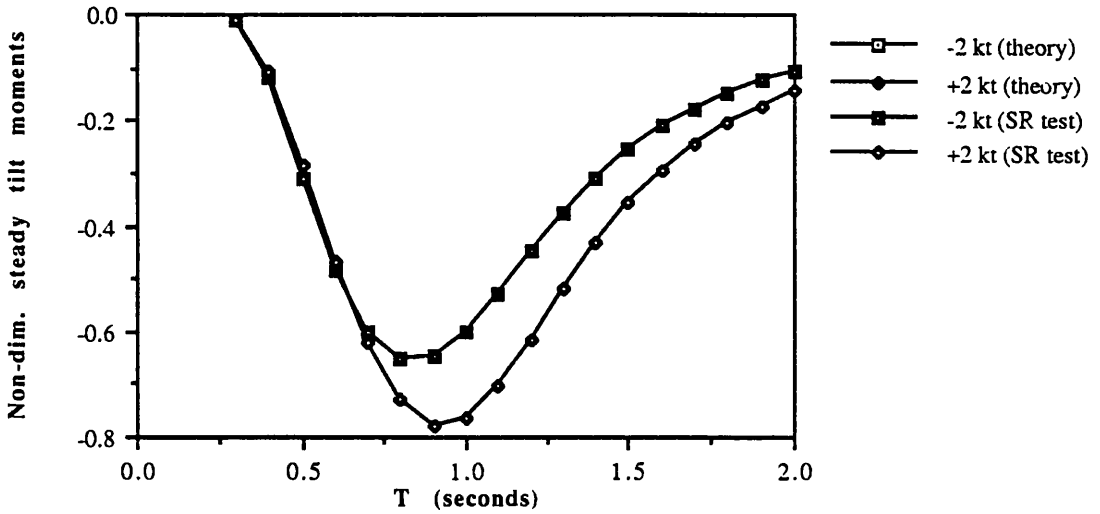

Fig.10.16 Comparison of non-dim. steady tilt moments for different current speeds in -10 degree tilt condition

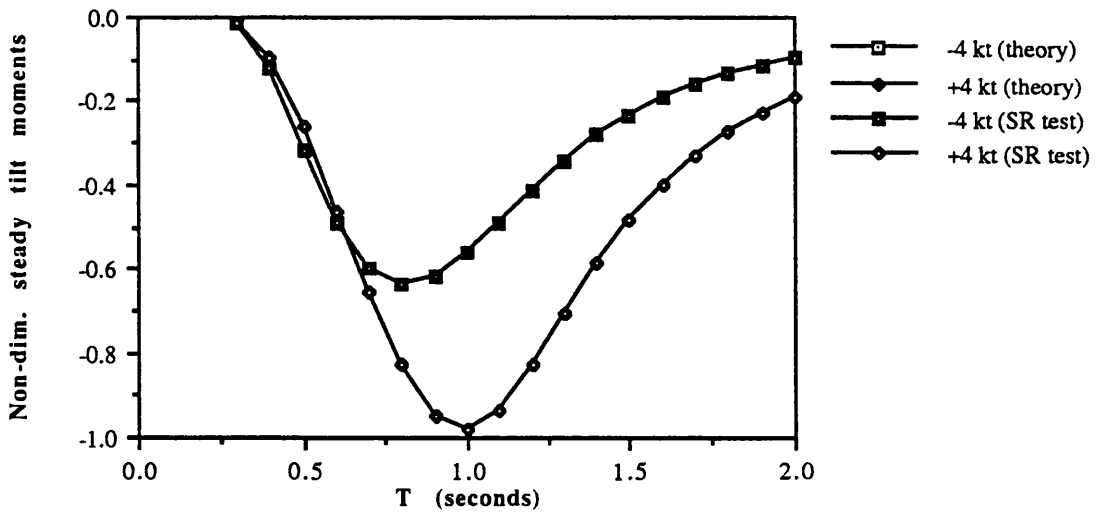

Fig.10.17 Comparison of non-dim. steady tilt moments for different current speeds in -10 degree tilt condition

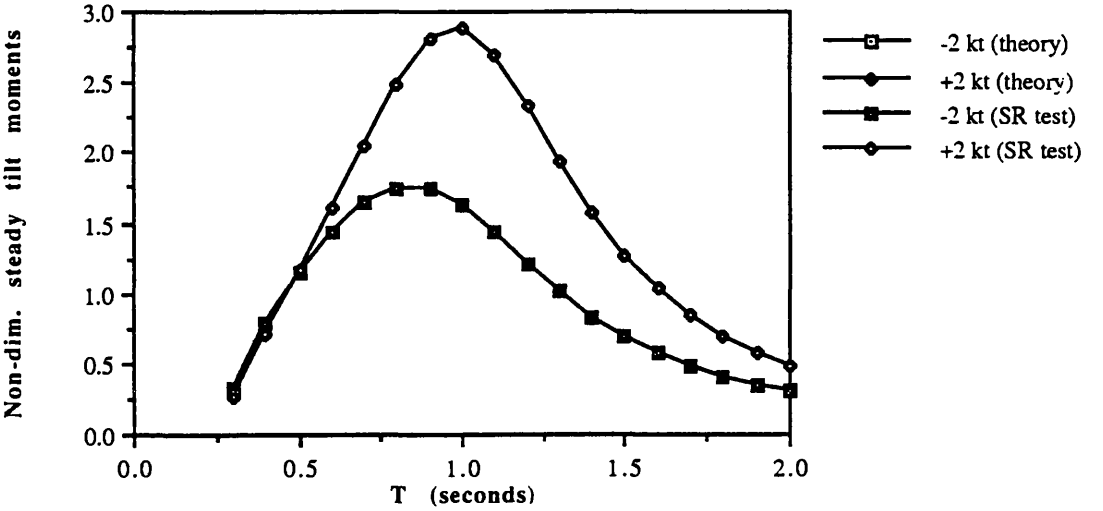

Fig.10.18 Comparison of non-dim. steady tilt moments for different current speeds in +15 degree tilt condition

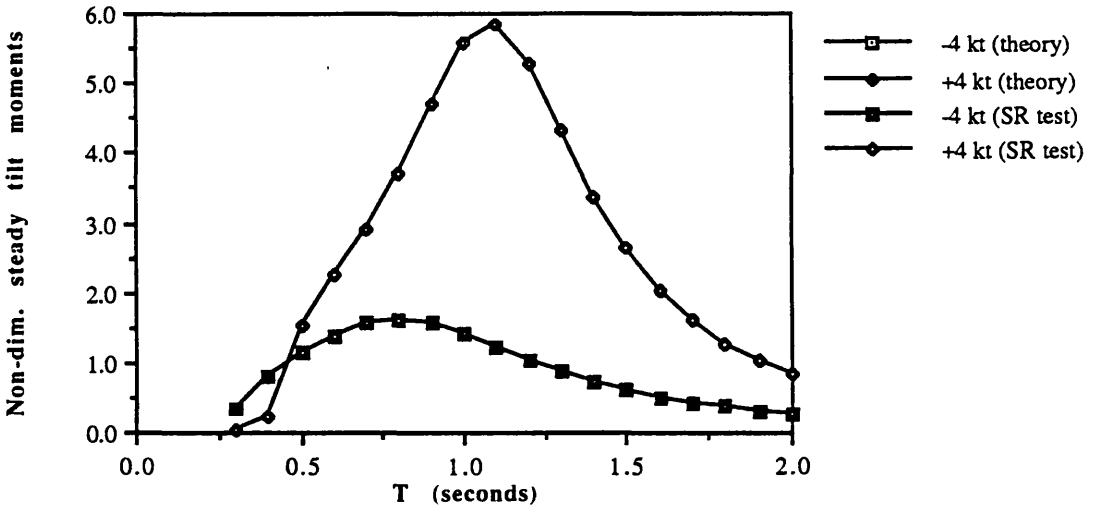

Fig.10.19 Comparison of non-dim. steady tilt moments for different current speeds in +15 degree tilt condition

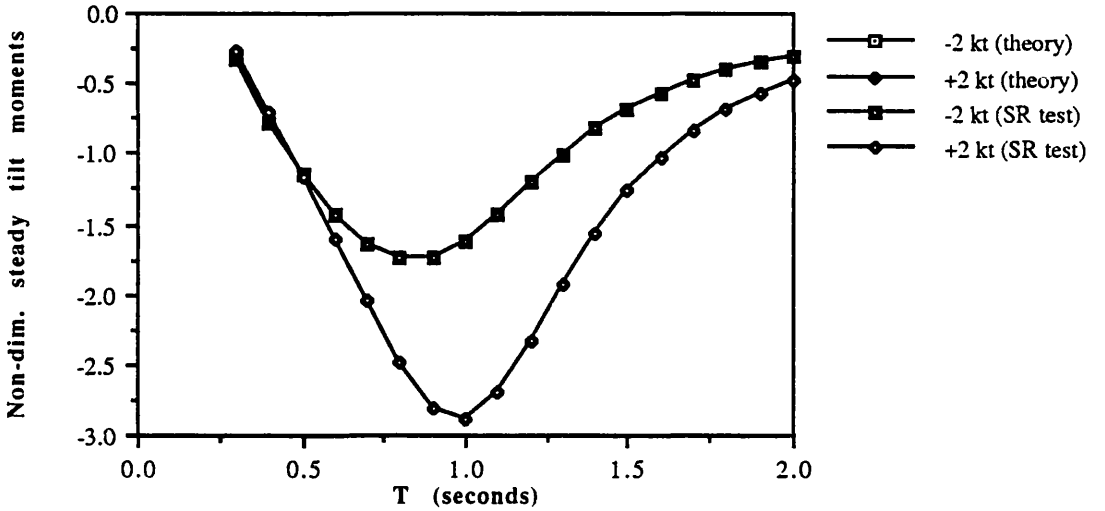

Fig.10.20 Comparison of non-dim. steady tilt moments for different current speeds in -15 degree tilt condition

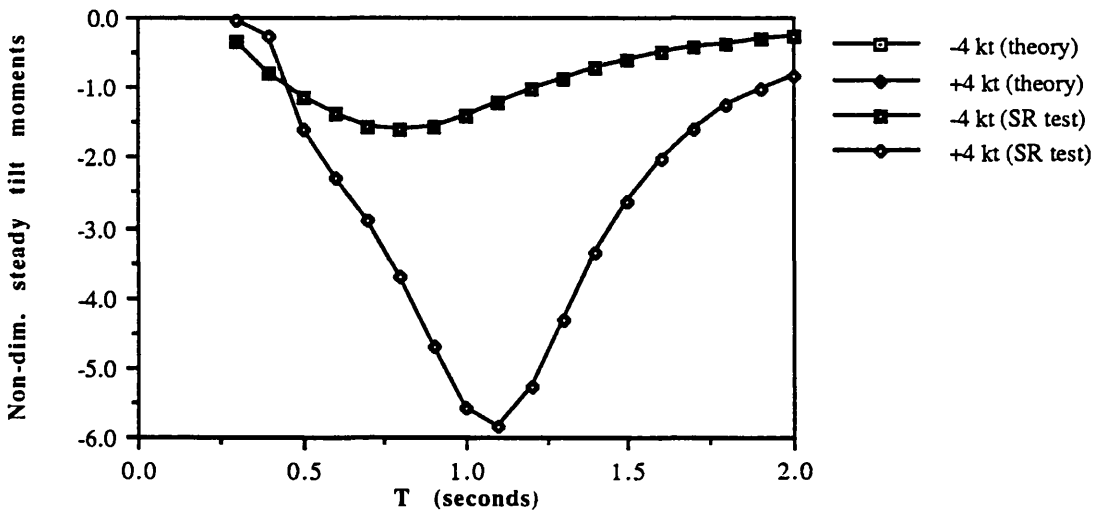

Fig.10.21 Comparison of non-dim. steady tilt moments for different current speeds in -15 degree tilt condition

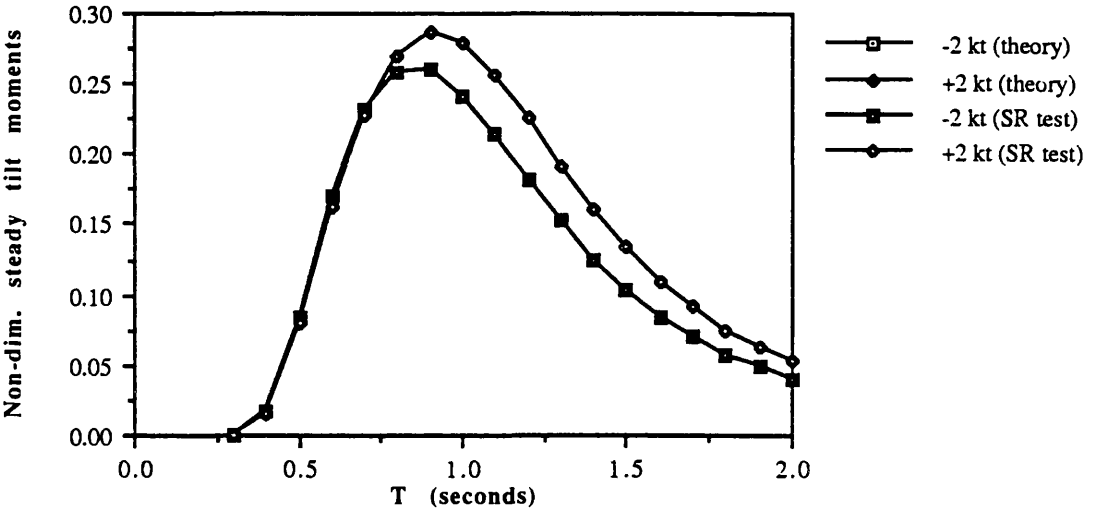

Fig.10.22 Comparison of non-dim. steady tilt moments for different current speeds in +5 degree tilt condition

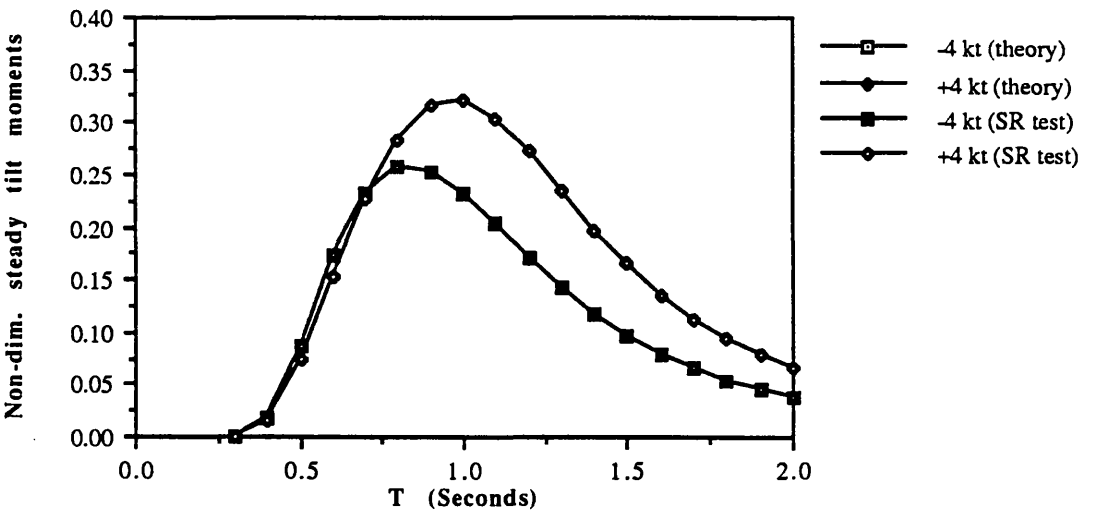

Fig.10.23 Comparison of non-dim. steady tilt moments for different current speeds in +5 degree tilt condition

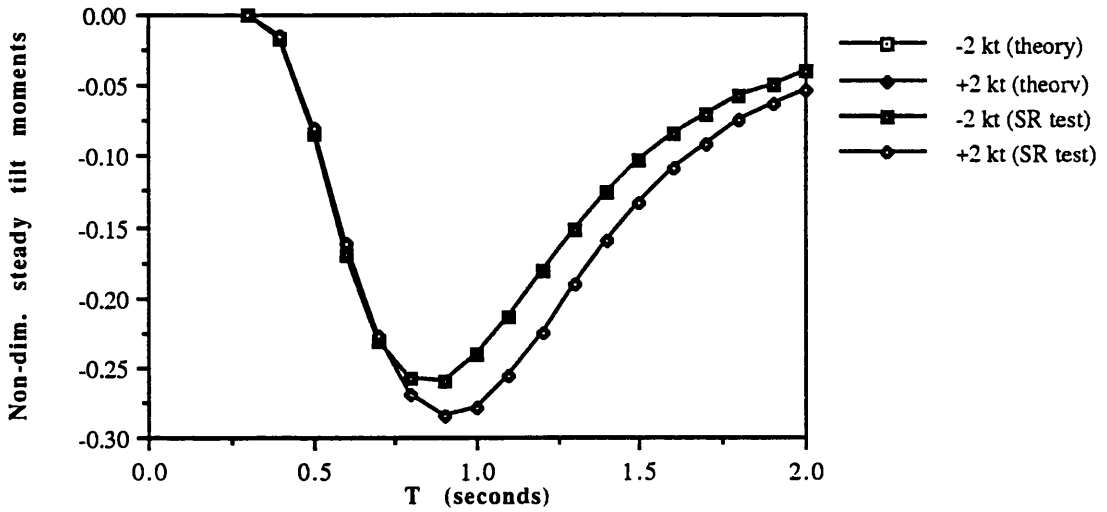

Fig.10.24 Comparison of non-dim. steady tilt moments for different current speeds in -5 degree tilt condition

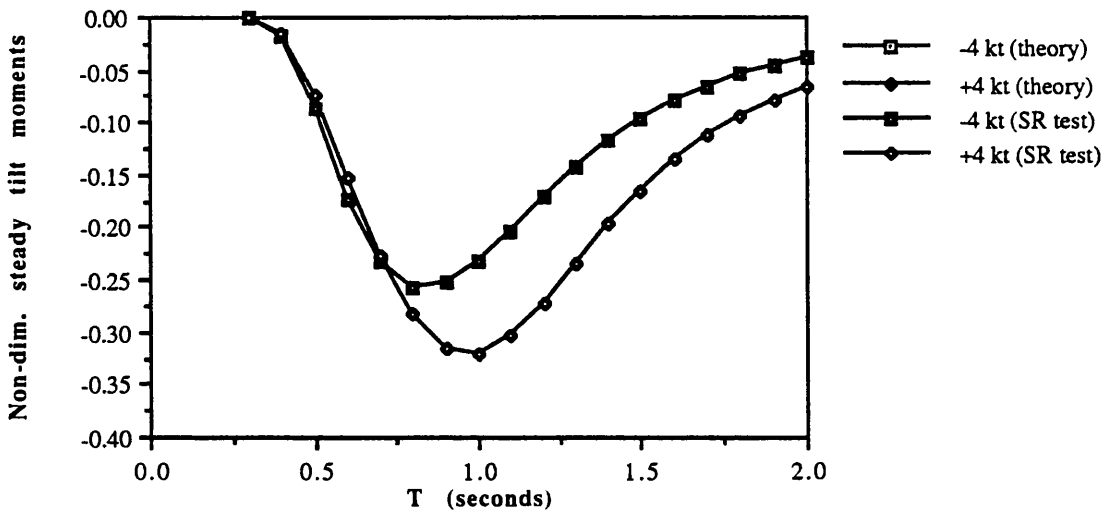

Fig.10.25 Comparison of non-dim. steady tilt moments for different current speeds in -5 degree tilt condition

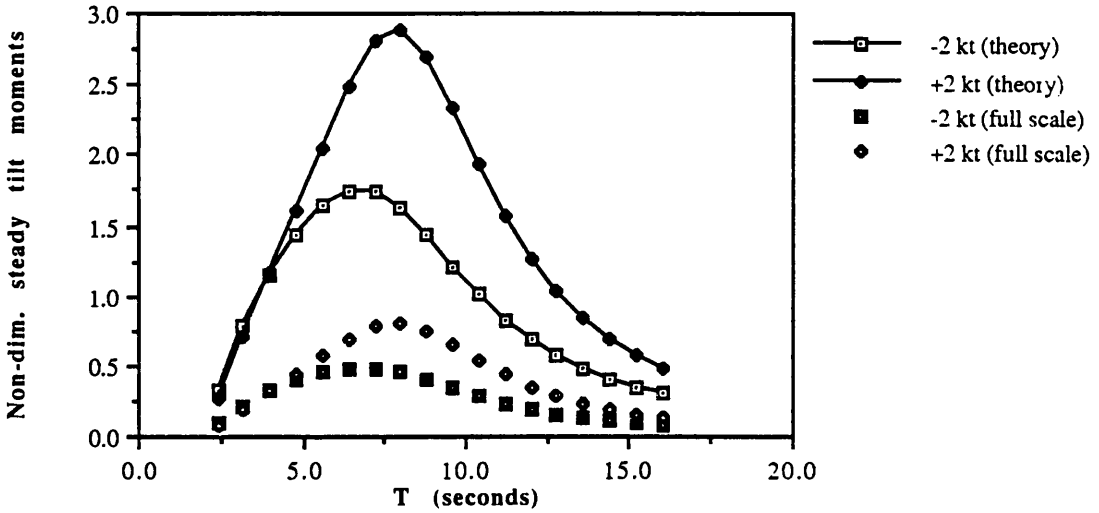

Fig.10.26 Comparison of non-dim. steady tilt moments for different current speeds in +15 degree tilt condition

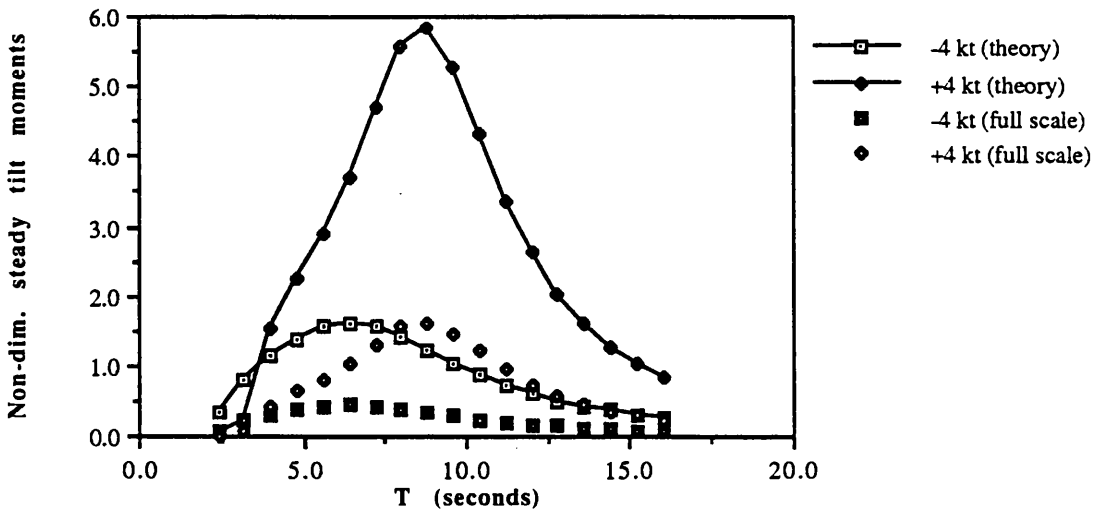

Fig.10.27 Comparison of non-dim. steady tilt moments for different current speeds in +15 degree tilt condition

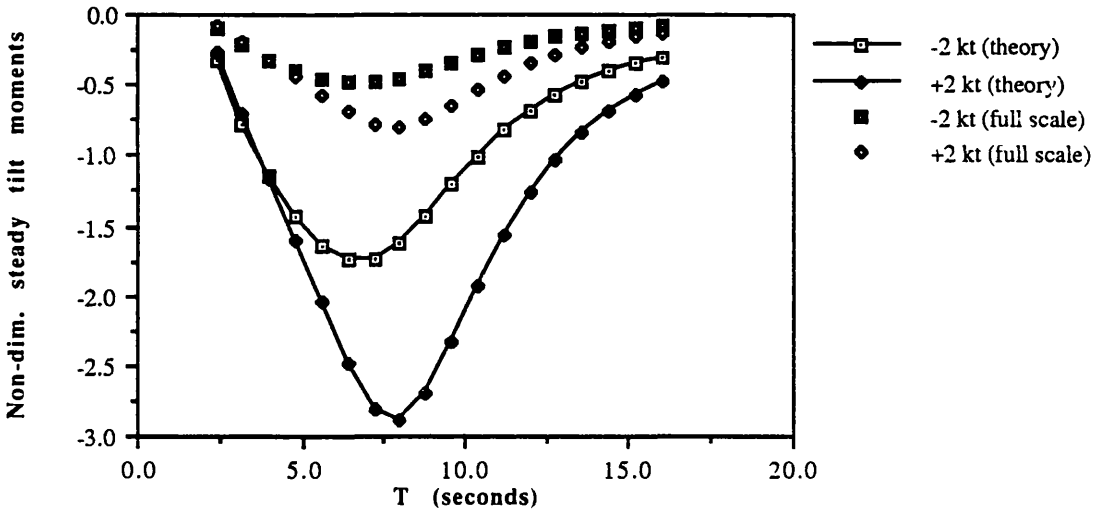

Fig.10.28 Comparison of non-dim. steady tilt moments for different current speeds in -15 degree tilt condition

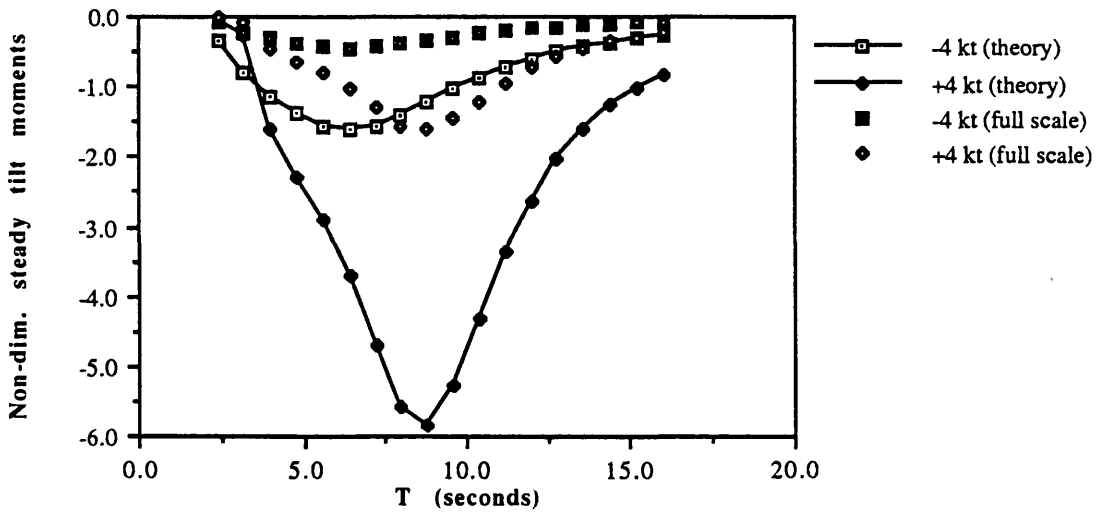

Fig.10.29 Comparison of non-dim. steady tilt moments for different current speeds in -15 degree tilt condition

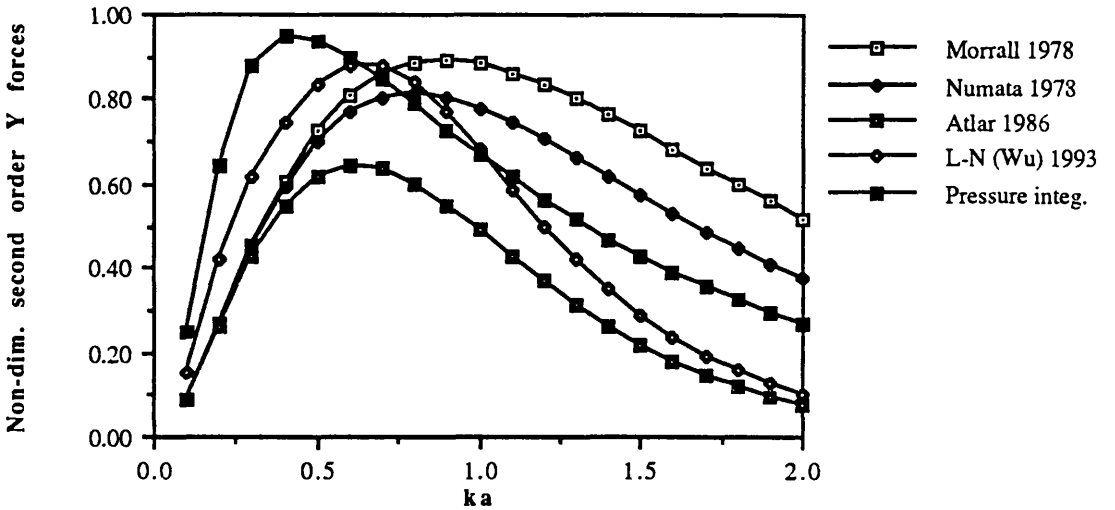

Fig.10.30 Comparison of non-dim. second order vertical forces on left cylinder (d/a=2, c/a=4, 10 degree tilt condition)

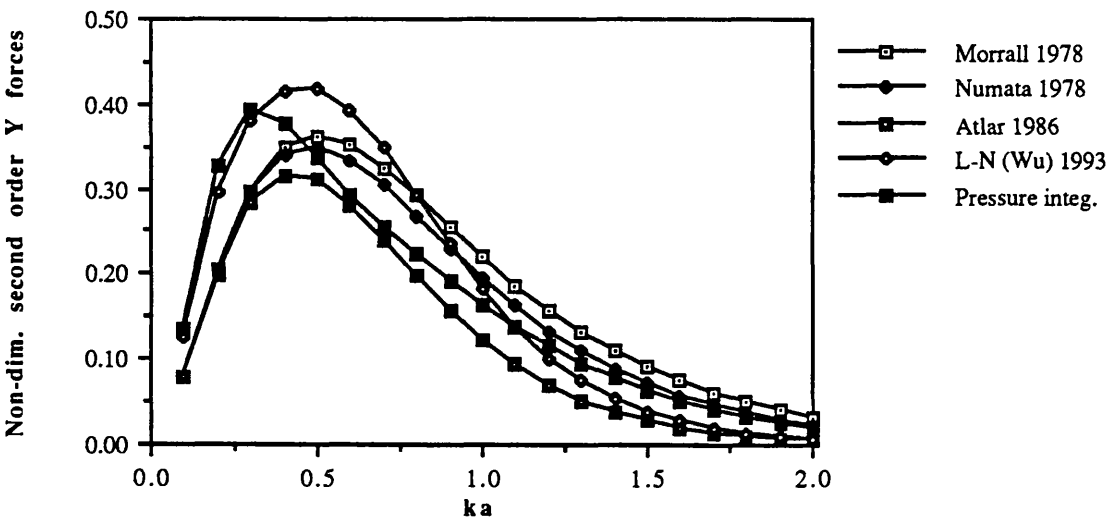

Fig.10.31 Comparison of non-dim. second order vertical forces on right cylinder (d/a=2, c/a=4, 10 degree tilt condition)

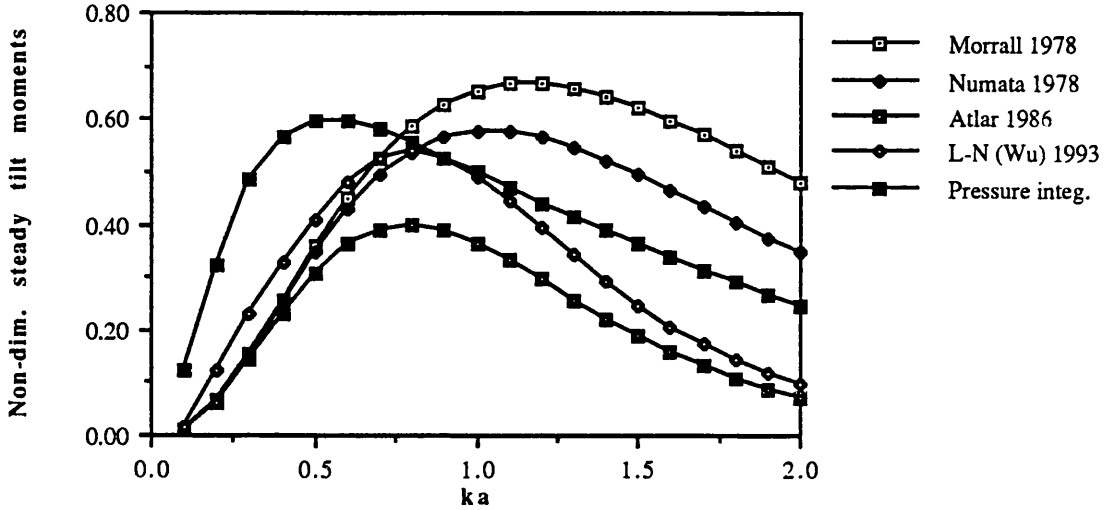

Fig.10.32 Comparison of non-dim. steady tilt moments on twin cylinder model (d/a=2, c/a=4, 10 degree tilt condition)

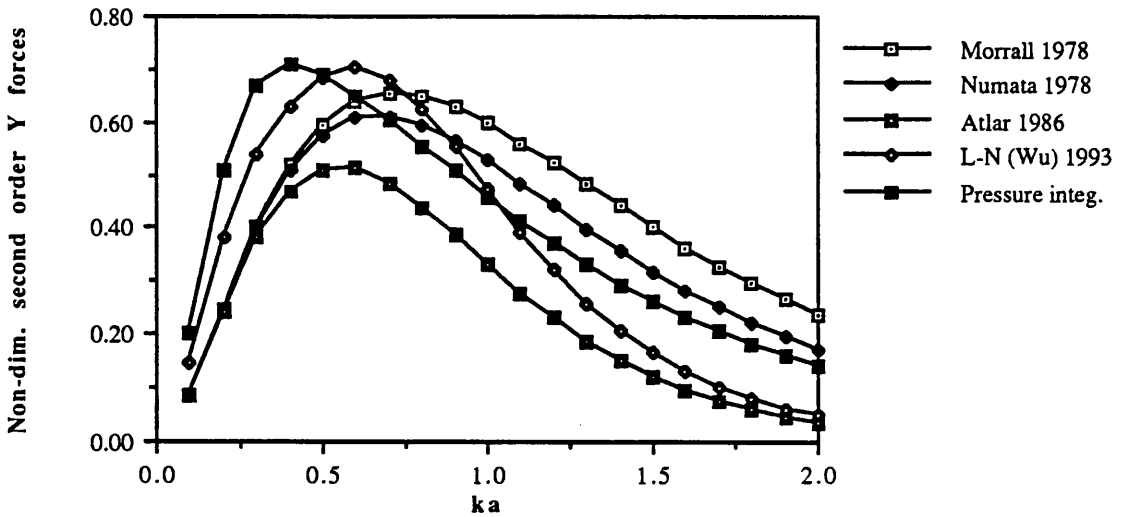

Fig.10.33 Comparison of non-dim. second order vertical forces on left cylinder (d/a=2, c/a=4, 5 degree tilt condition)

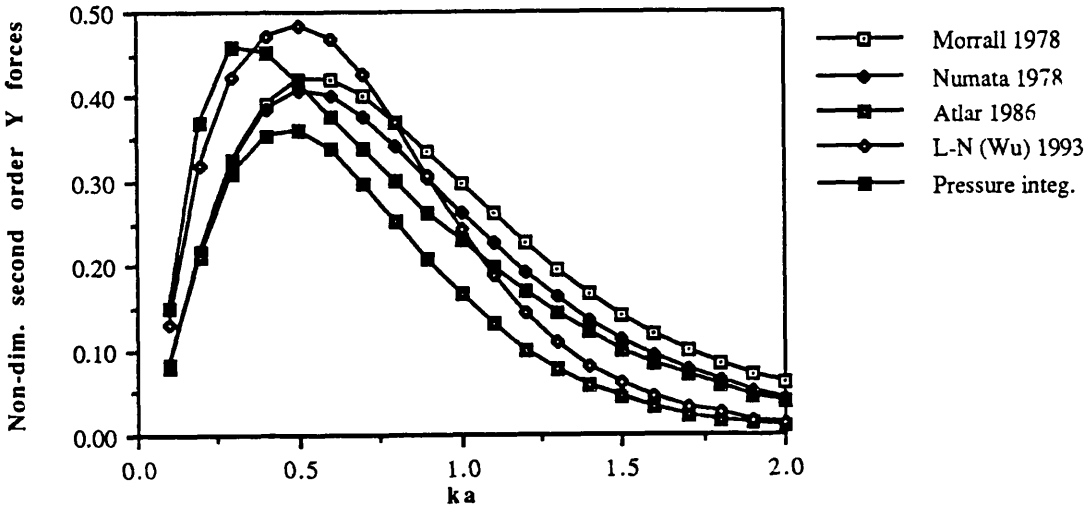

Fig.10.34 Comparison of non-dim. second order vertical forces on right cylinder (d/a=2, c/a=4, 5 degree tilt condition)

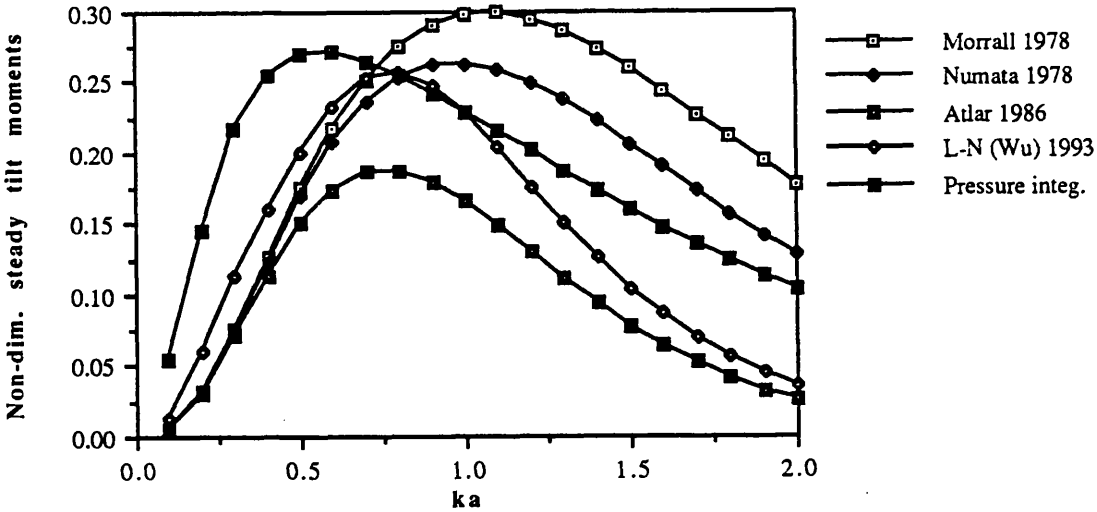

Fig.10.35 Comparison of non-dim. steady tilt moments on twin cylinder model (d/a=2, c/a=4, 5 degree tilt condition)

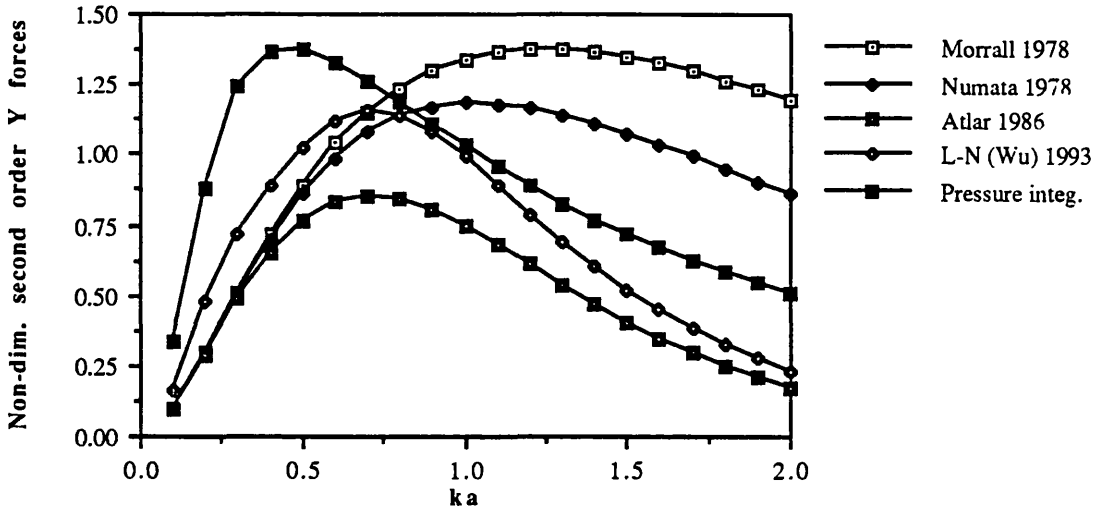

Fig.10.36 Comparison of non-dim. second order vertical forces on left cylinder (d/a=2, c/a=4, 15 degree tilt condition)

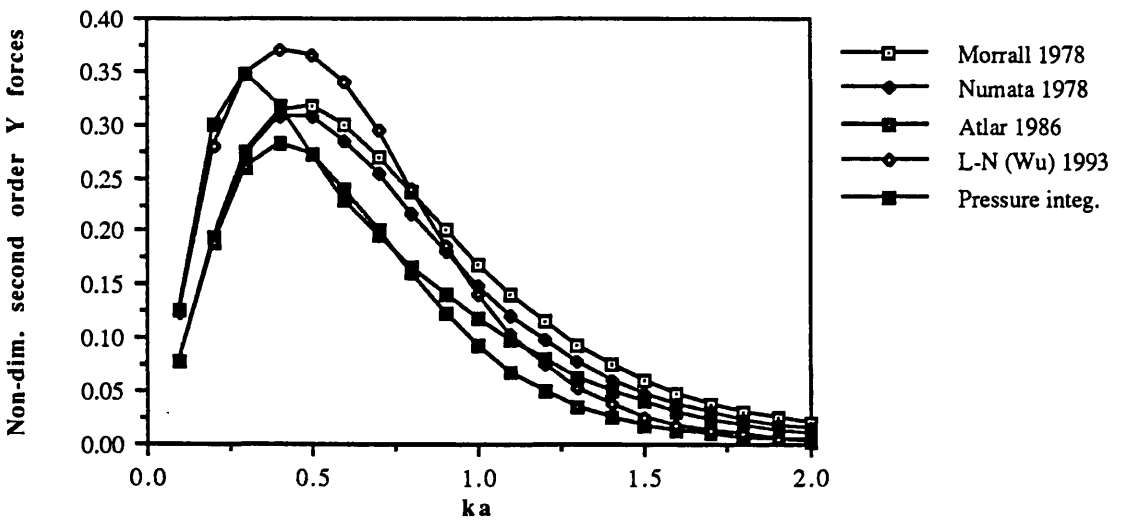

Fig.10.37 Comparison of non-dim. second order vertical forces on right cylinder (d/a=2, c/a=4, 15 degree tilt condition)

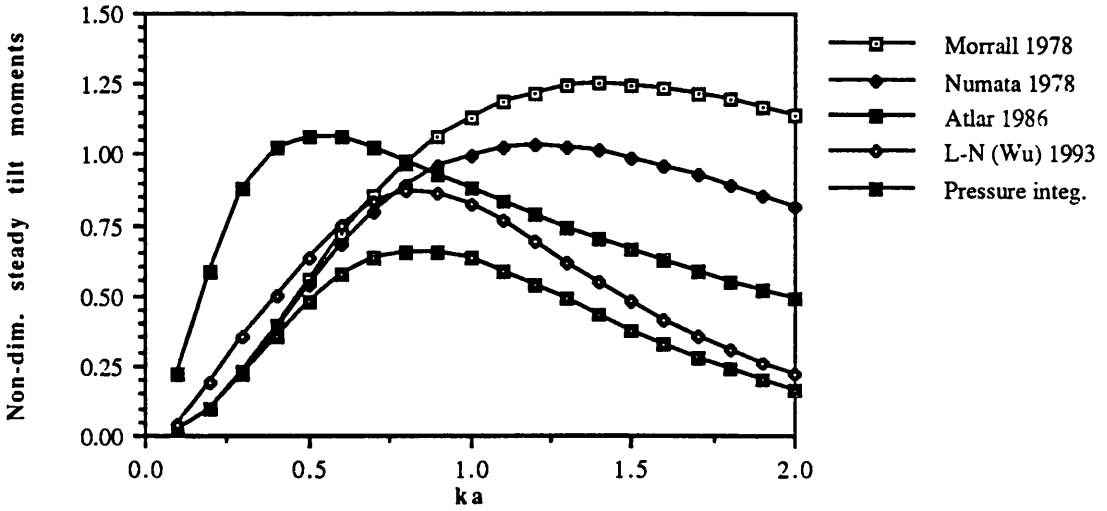

Fig.10.38 Comparison of non-dim. steady tilt moments on twin cylinder model (d/a=2, c/a=4, 15 degree tilt condition)

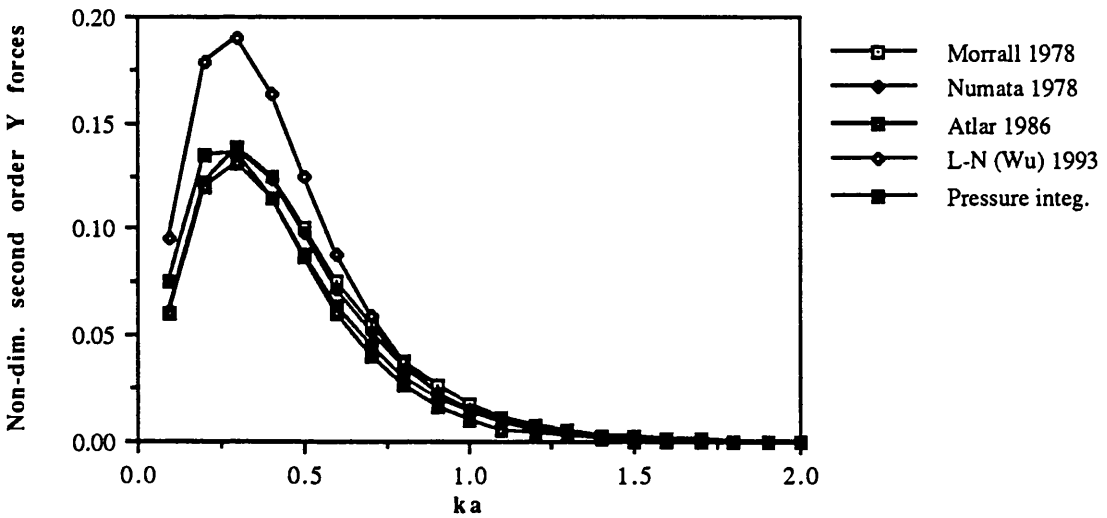

Fig.10.39 Comparison of non-dim. second order vertical forces on left cylinder (d/a=4, c/a=4, 10 degree tilt condition)

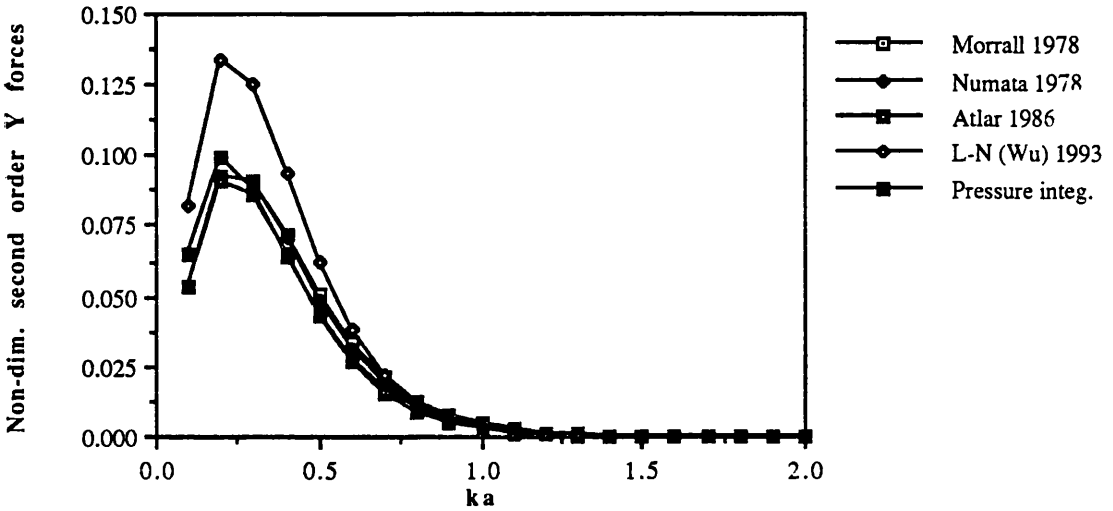

Fig.10.40 Comparison of non-dim. second order vertical forces on right cylinder (d/a=4, c/a=4, 10 degree tilt condition)

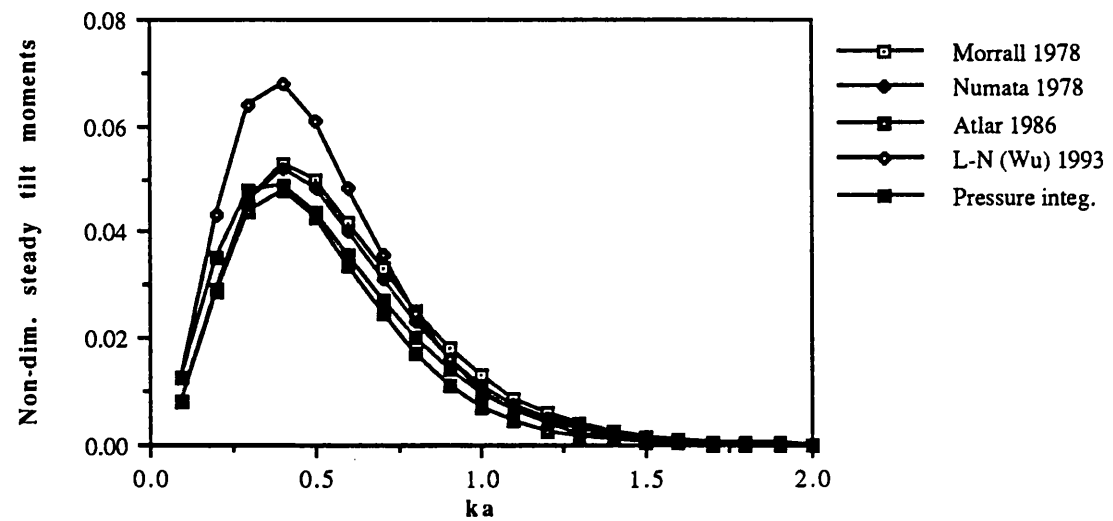

Fig.10.41 Comparison of non-dim. steady tilt moments on twin cylinder model (d/a=4, c/a=4, 10 degree tilt condition)

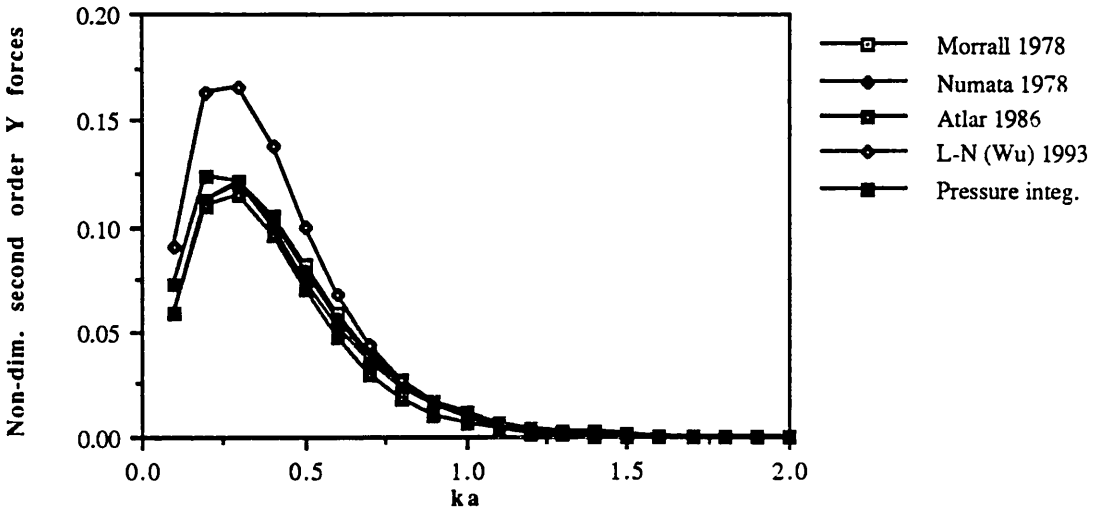

Fig.10.42 Comparison of non-dim. second order vertical forces on left cylinder (d/a=4, c/a=4, 5 degree tilt condition)

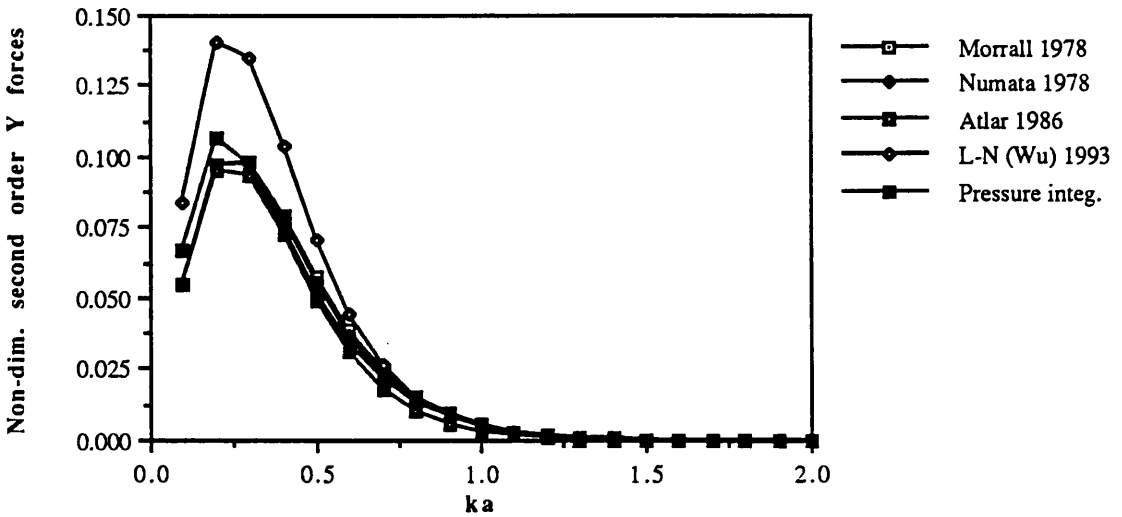

Fig.10.43 Comparison of non-dim. second order vertical forces on right cylinder (d/a=4, c/a=4, 5 degree tilt condition)

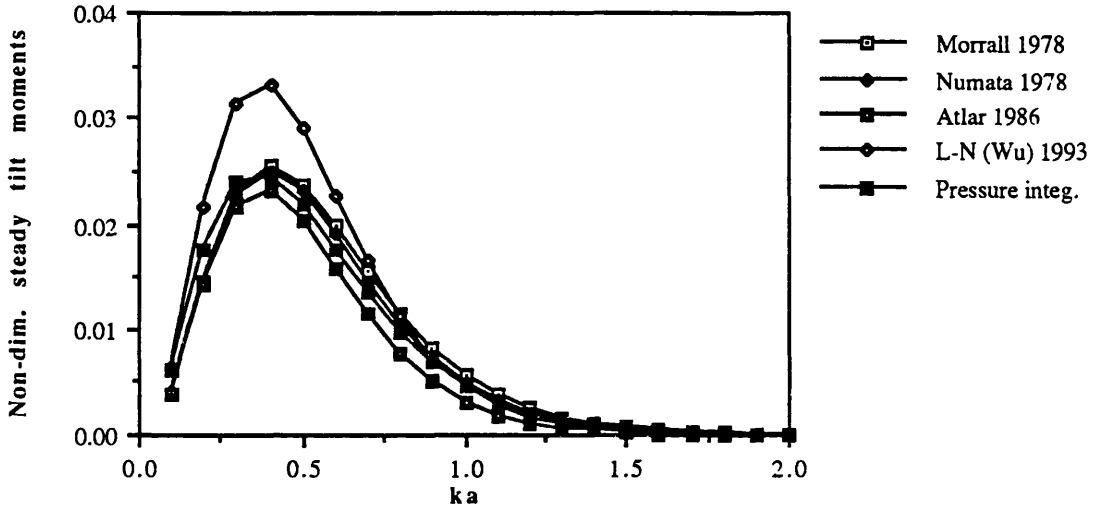

Fig.10.44 Comparison of non-dim. steady tilt moments on twin cylinder model (d/a=4, c/a=4, 5 degree tilt condition)

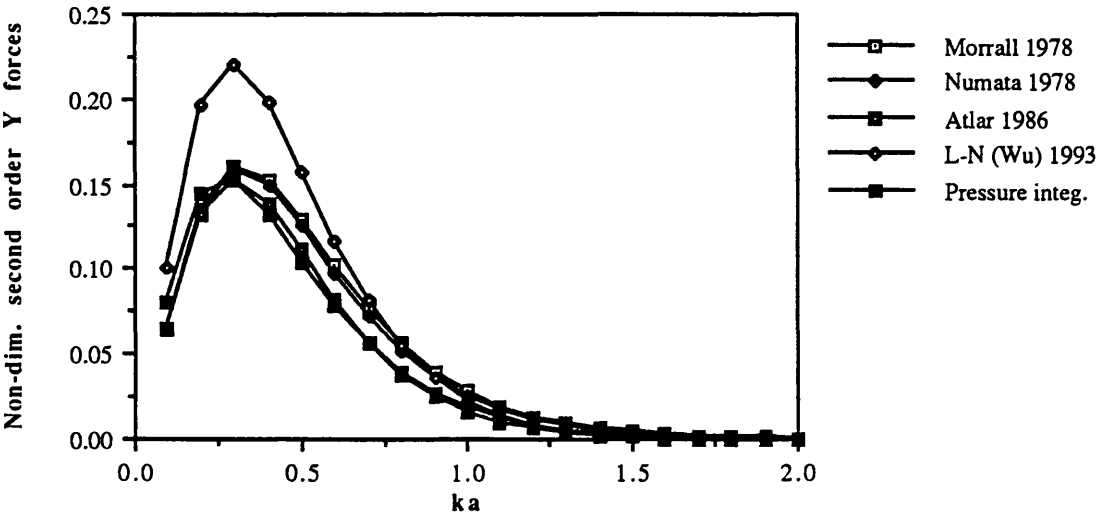

Fig.10.45 Comparison of non-dim. second order vertical forces on left cylinder (d/a=4, c/a=4, 15 degree tilt condition)

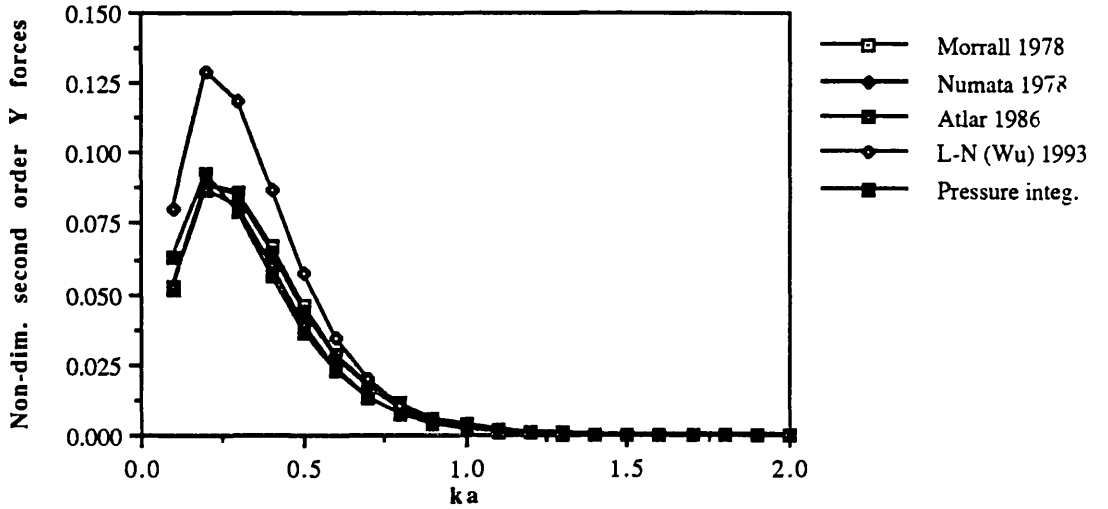

Fig.10.46 Comparison of non-dim. second order vertical forces on right cylinder (d/a=4, c/a=4, 15 degree tilt condition)

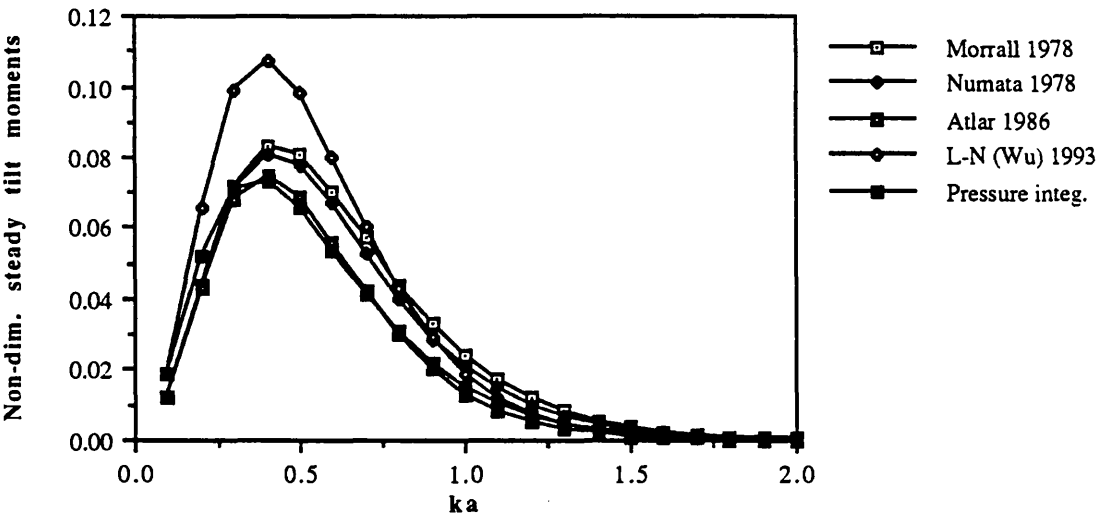

Fig.10.47 Comparison of non-dim. steady tilt moments on twin cylinder model (d/a=4, c/a=4, 15 degree tilt condition)

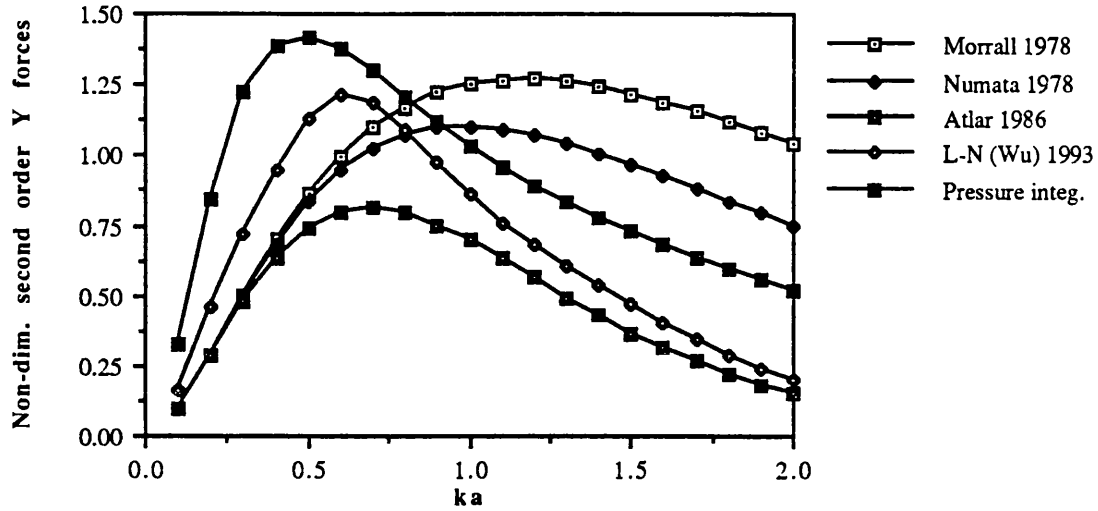

Fig.10.48 Comparison of non-dim. second order vertical forces on left cylinder (d/a=2, c/a=6, 10 degree tilt condition)

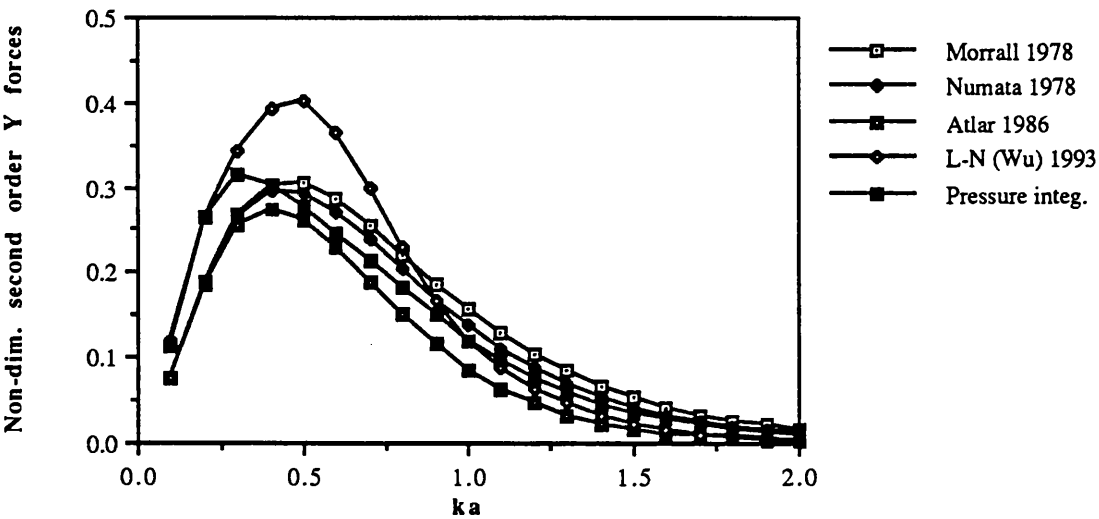

Fig.10.49 Comparison of non-dim. second order vertical forces on right cylinder (d/a=2, c/a=6, 10 degree tilt condition)

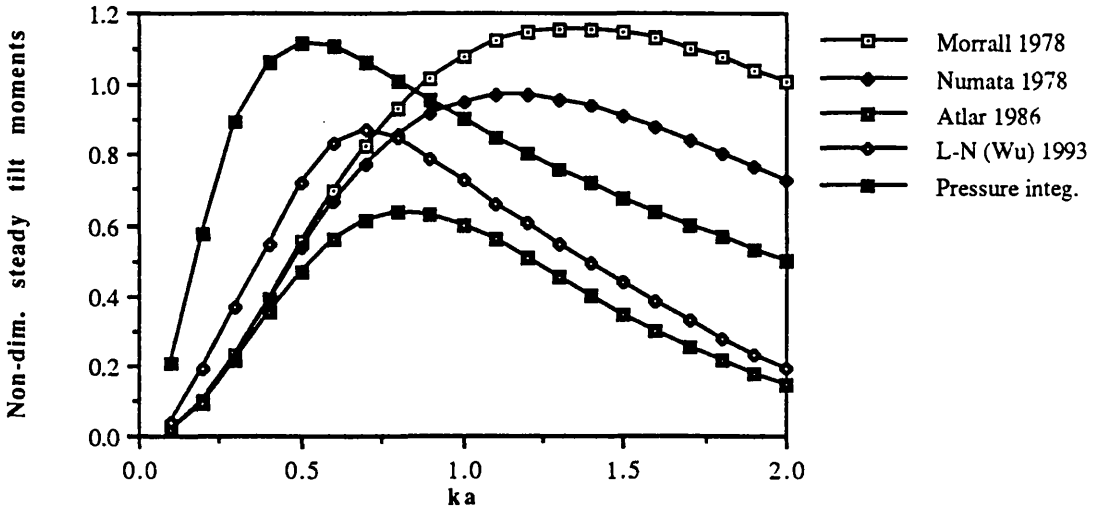

Fig.10.50 Comparison of non-dim. steady tilt moments on twin cylinder model (d/a=2, c/a=6, 10 degree tilt condition)

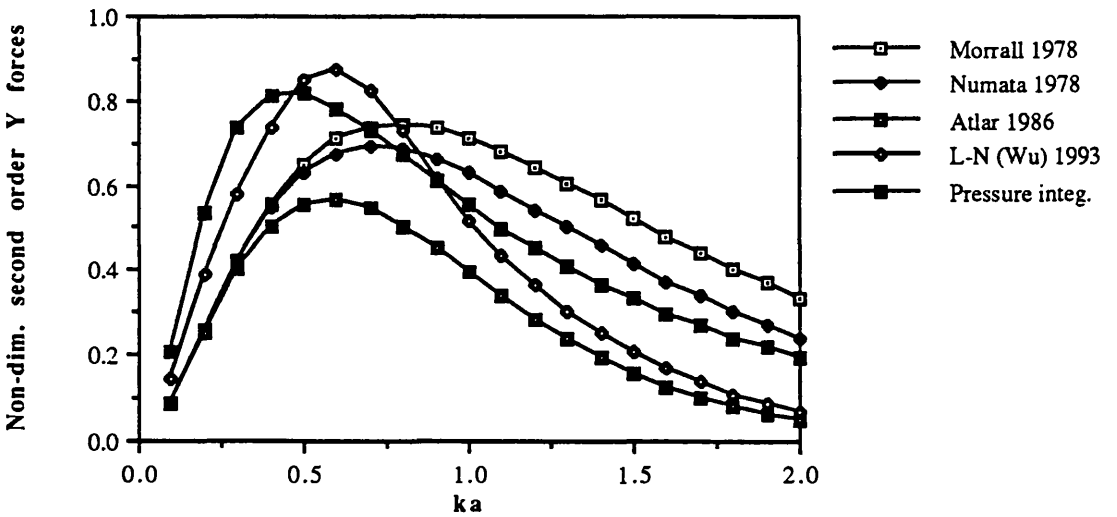

Fig.10.51 Comparison of non-dim. second order vertical forces on left cylinder (d/a=2, c/a=6, 5 degree tilt condition)

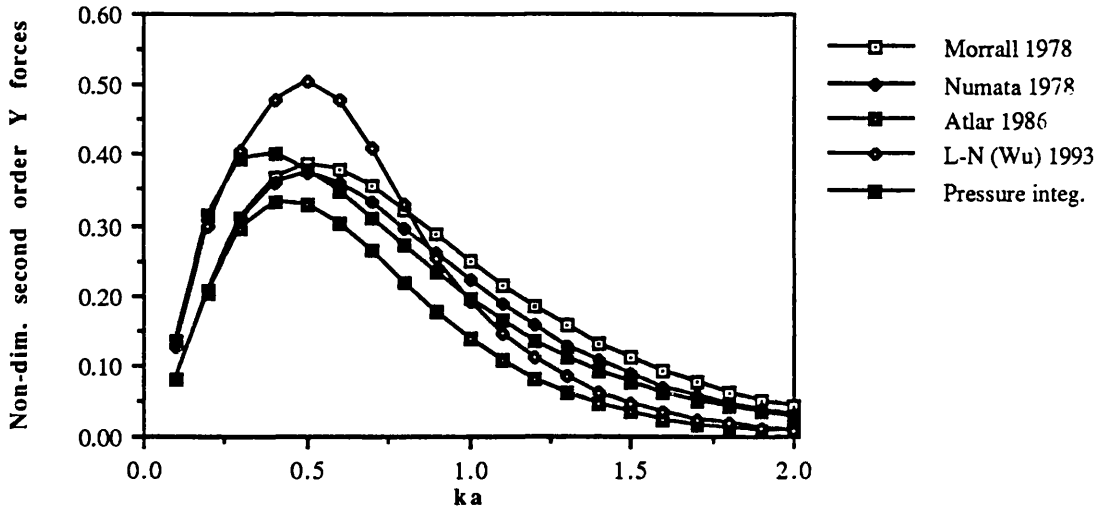

Fig.10.52 Comparison of non-dim. second order vertical forces on right cylinder (d/a=2, c/a=6, 5 degree tilt condition)

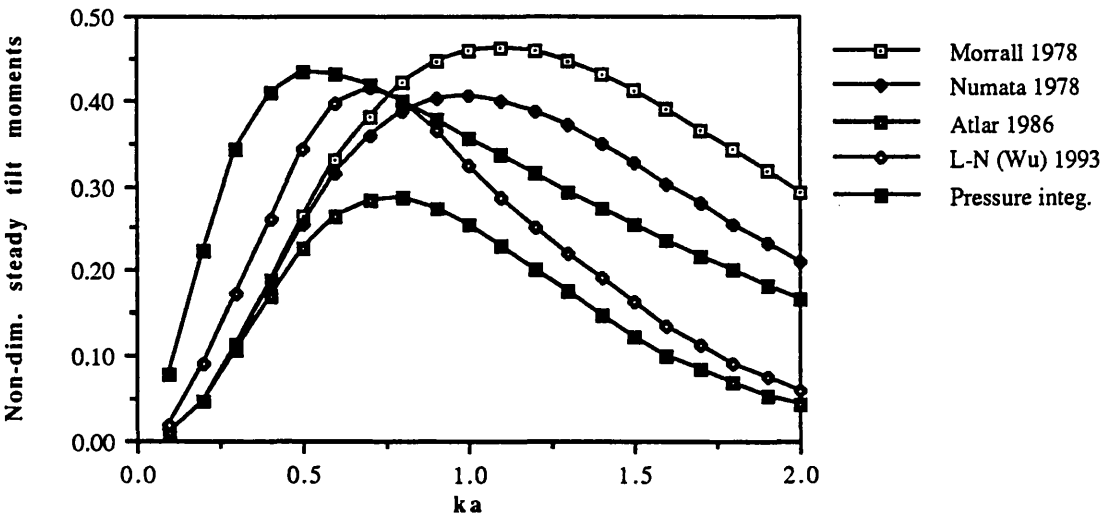

Fig.10.53 Comparison of non-dim. steady tilt moments on twin cylinder model (d/a=2, c/a=6, 5 degree tilt condition)

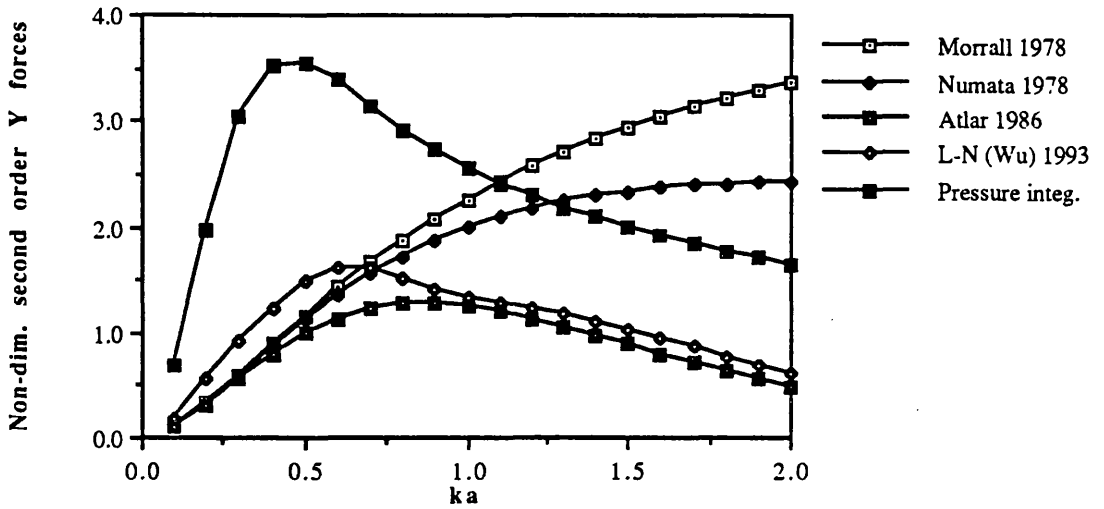

Fig.10.54 Comparison of non-dim. second order vertical forces on left cylinder (d/a=2, c/a=6, 15 degree tilt condition)

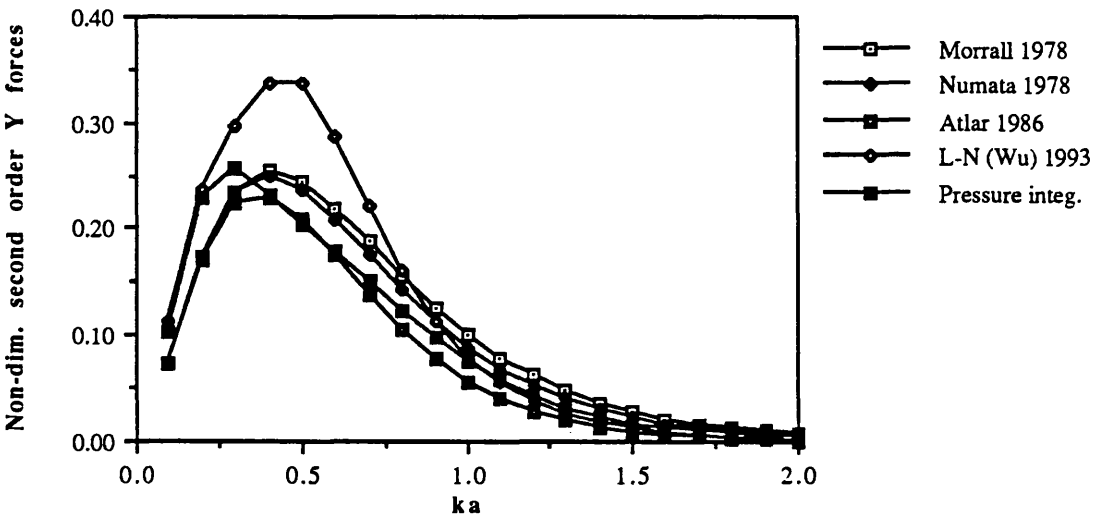

Fig.10.55 Comparison of non-dim. second order vertical forces on right cylinder (d/a=2, c/a=6, 15 degree tilt condition)

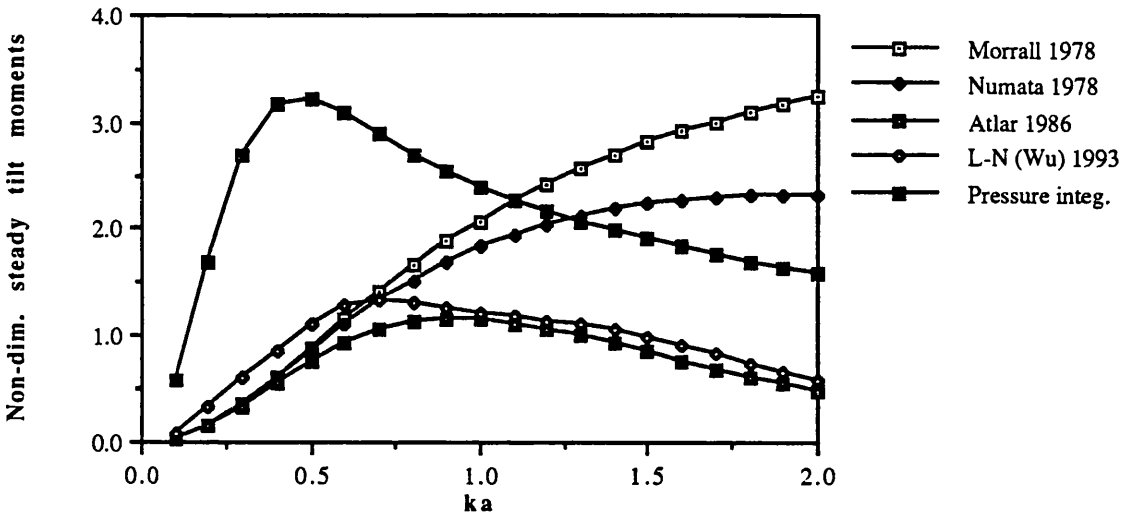

Fig.10.56 Comparison of non-dim. steady tilt moments on twin cylinder model (d/a=2, c/a=6, 15 degree tilt condition)

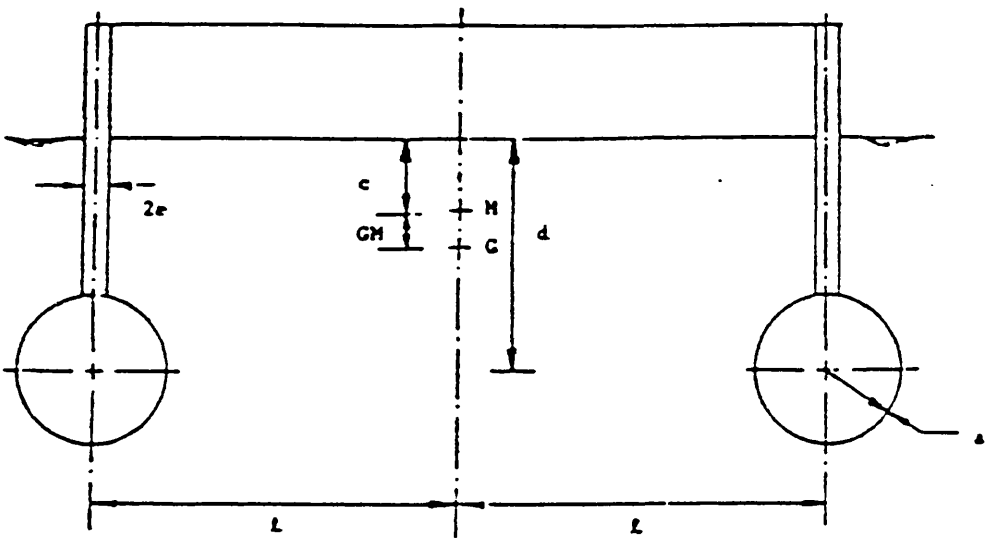

Geometry of the semi-submersible in its equilibrium position for still water. G is the centre of gravity and M is the metacentre. For the standard test configuration:

a = 6m, c = 3·72m, d = 19m, e = 1m, ℓ = 30m,

the radius of gyration about G is 20m.

Fig.10.57 Basic configuration of the semi-submersible model designed by Martin (1978)

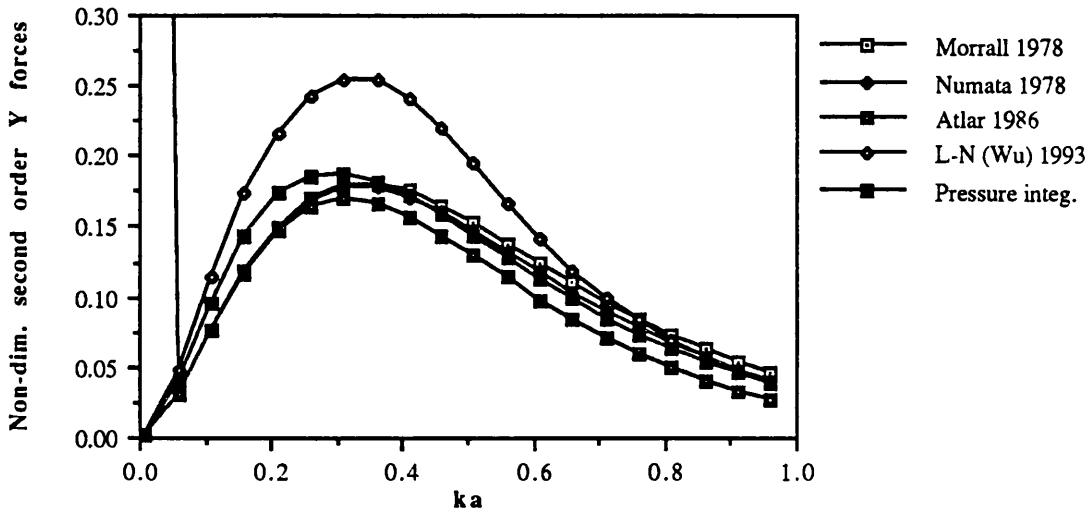

Fig.10.58 Comparison of non-dim. second order vertical forces on left cylinder (d/a=3.17, c/a=10.0 in no tilt condition)

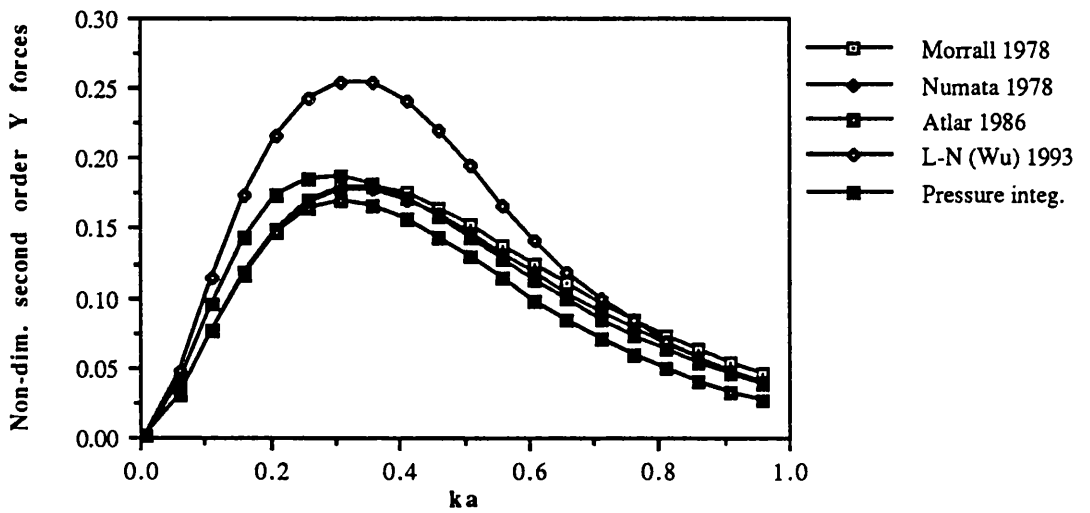

Fig.10.59 Comparison of non-dim. second order vertical forces on right cylinder (d/a=3.17, c/a=10.0 in no tilt condition)

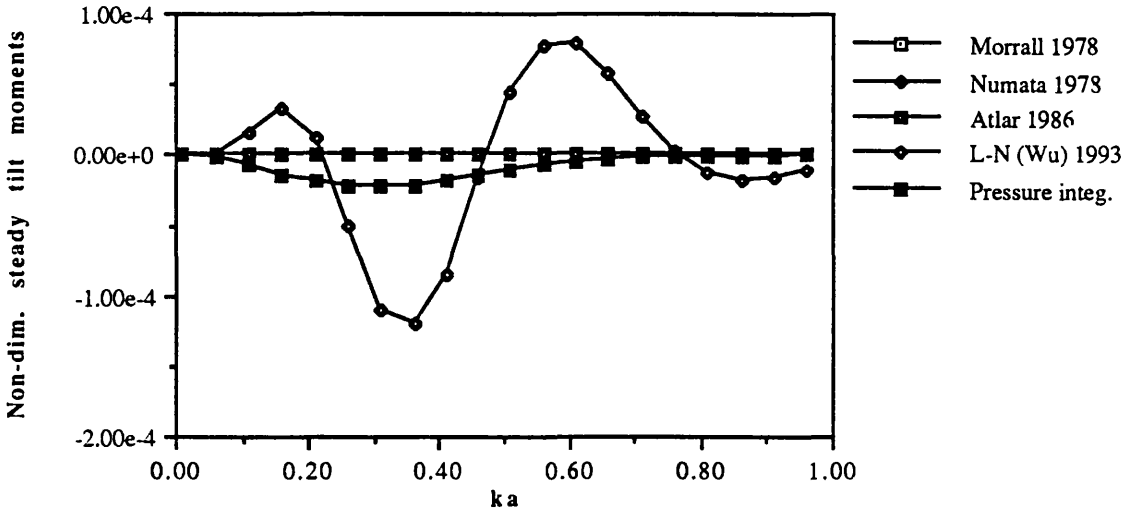

Fig.10.60 Comparison of non-dim. steady tilt moments for twin cylinders model (d/a=3.17,c/a=10.0 in no tilt condition)

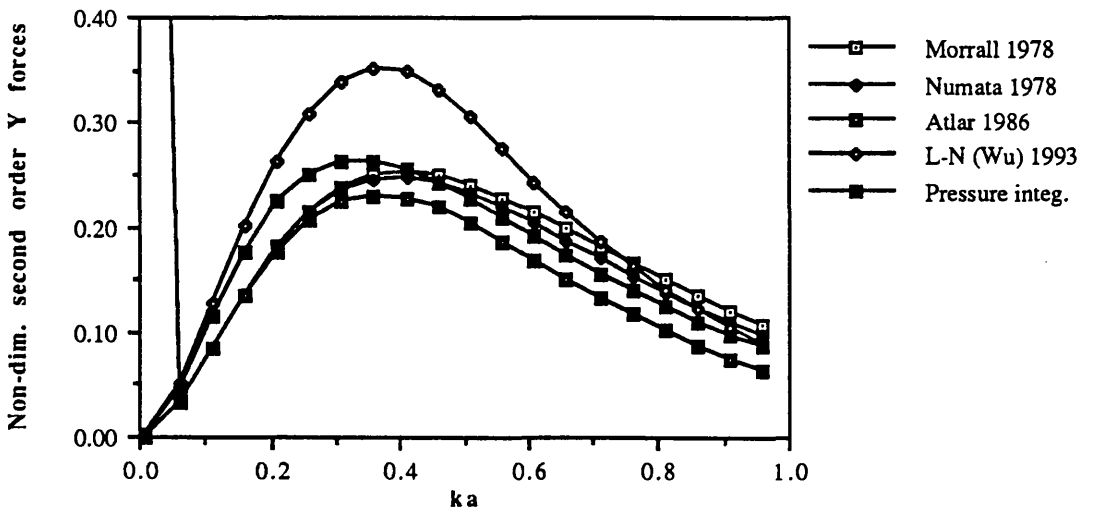

Fig.10.61 Comparison of non-dim. second order vertical forces on left cylinder (d/a=3.17, c/a=10.0 in 5 degree tilt)

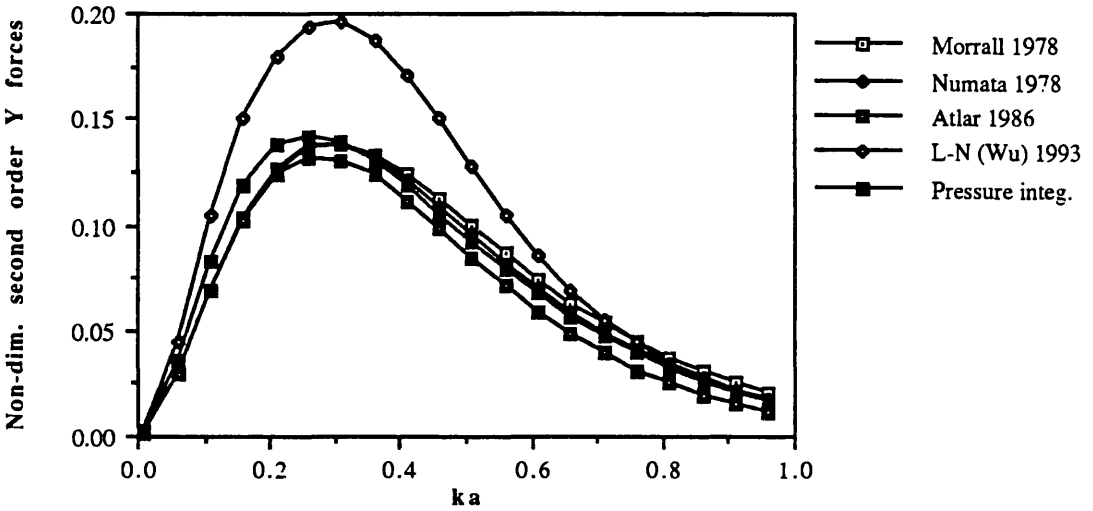

Fig.10.62 Comparison of non-dim. second order vertical forces on right cylinder (d/a=3.17, c/a=10.0 in 5 degree tilt)

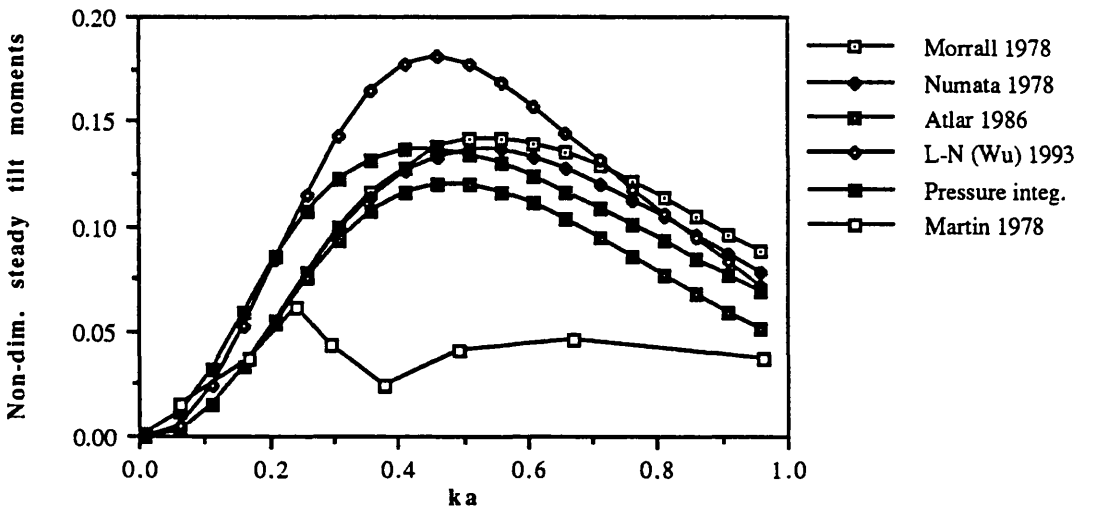

Fig.10.63 Comparison of non-dim. steady tilt moments on twin cylinder model (d/a=3.17, c/a=10.0 in 5 degree tilt)

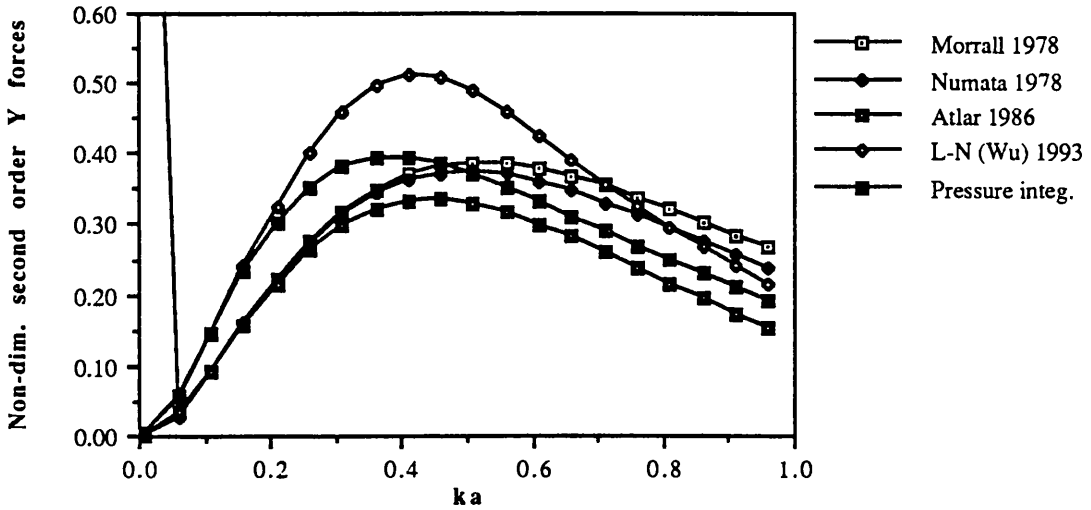

Fig.10.64 Comparison of non-dim. second order vertical forces on left cylinder (d/a=3.17, c/a=10.0 in 10 degree tilt)

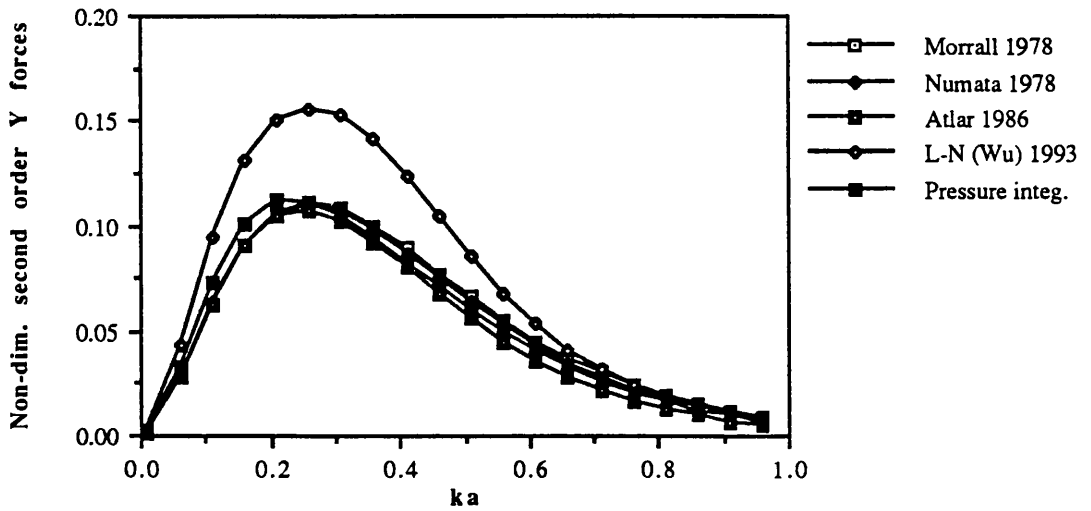

Fig.10.65 Comparison of non-dim. second order vertical forces on right cylinder (d/a=3.17, c/a=10.0 in 10 degree tilt)

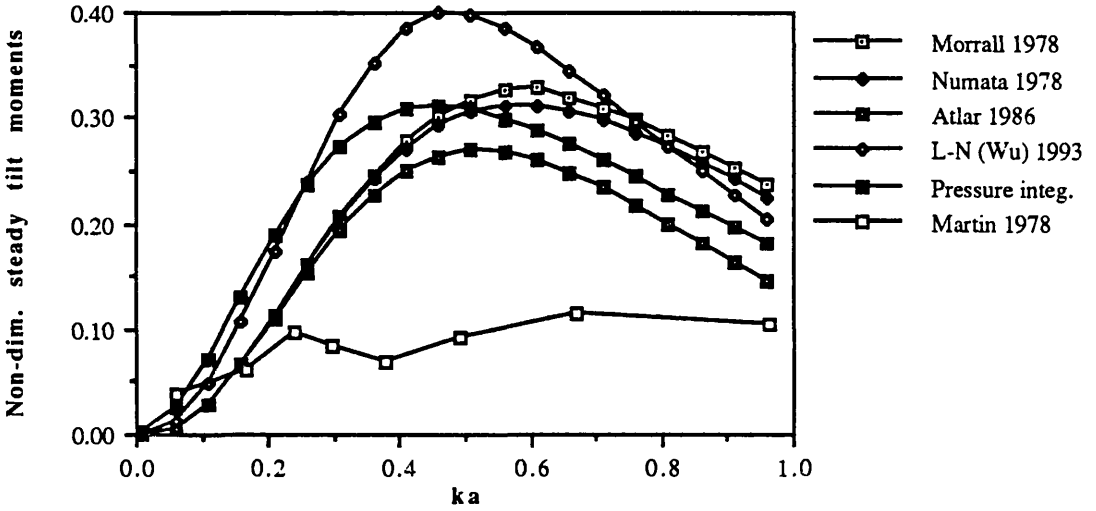

Fig.10.66 Comparison of non-dim. steady tilt moments on twin cylinder model (d/a=3.17, c/a=10.0 in 10 degree tilt)

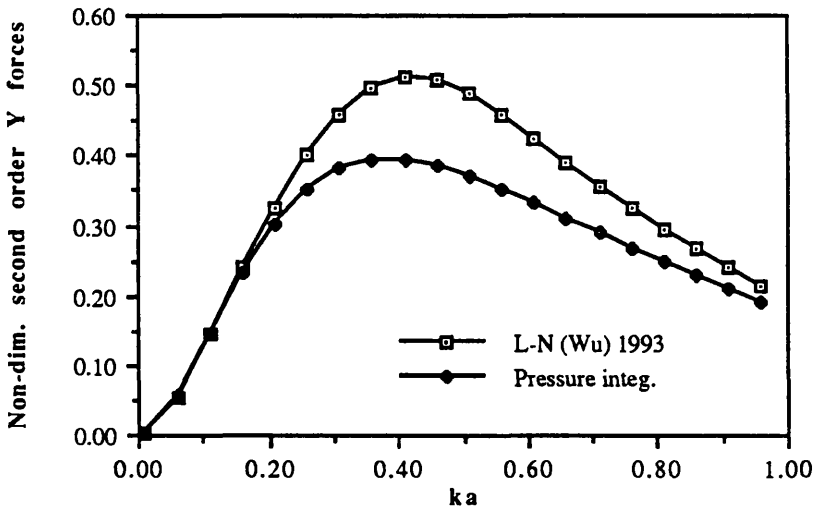

Fig.10.67 Comparison of non-dim. second order vertical forces on left cylinder (d/a=3.17,c/a=10,Fn=0.0 in 10 degree tilt)

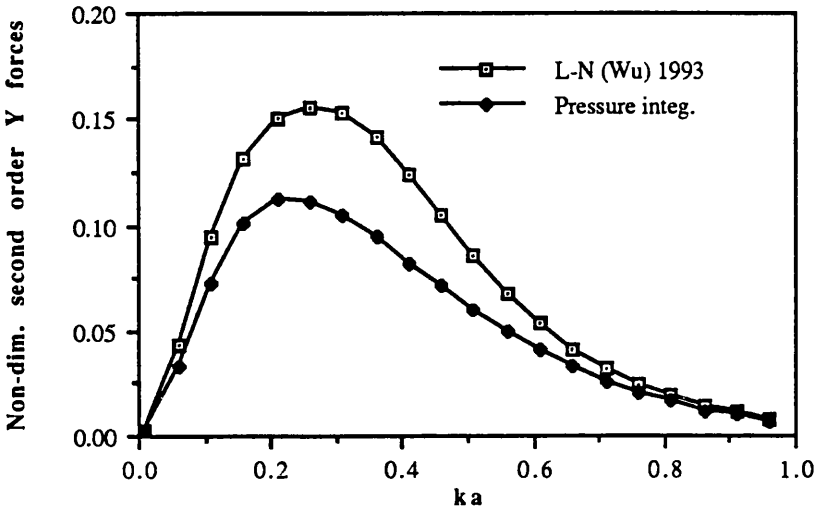

Fig.10.68 Comparison of non-dim. second order vertical forces on right cylinder (d/a=3.17,c/a=10.0,Fn=0.0 in 10 degree tilt)

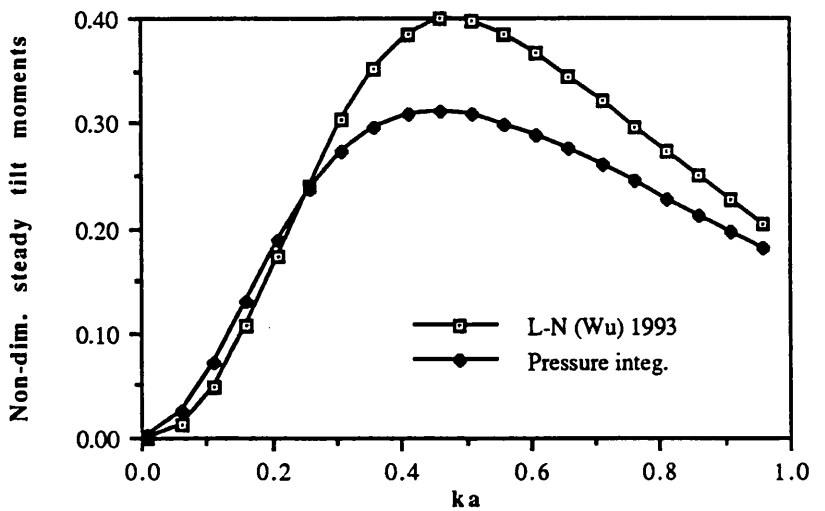

Fig.10.69 Comparison of non-dim. steady tilt moments on twin cylinder model (d/a=3.17,c/a=10.0,Fn=0.0 in 10 degree tilt)

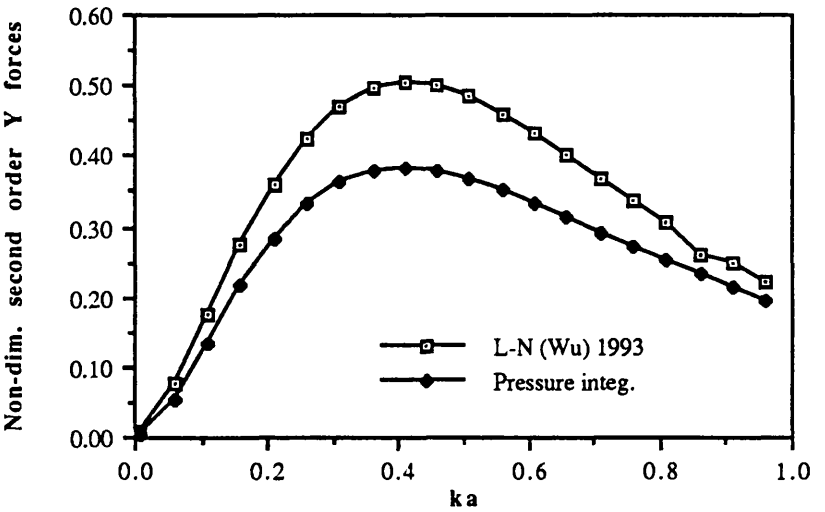

Fig.10.70 Comparison of non-dim. second order vertical forces on left cylinder (d/a=3.17,c/a=10.,Fn=0.20 in 10 degree tilt)

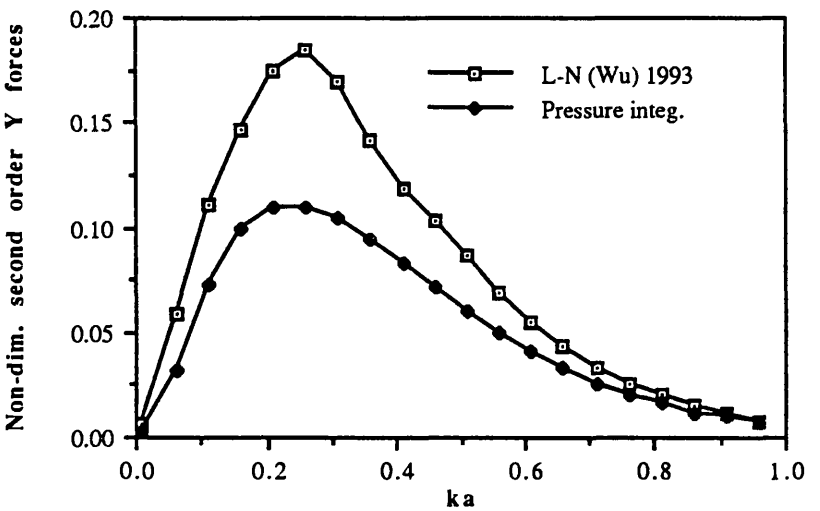

Fig.10.71 Comparison of non-dim. second order vertical forces on right cylinder (d/a=3.17,c/a=10.,Fn=0.20 in 10 degree tilt)

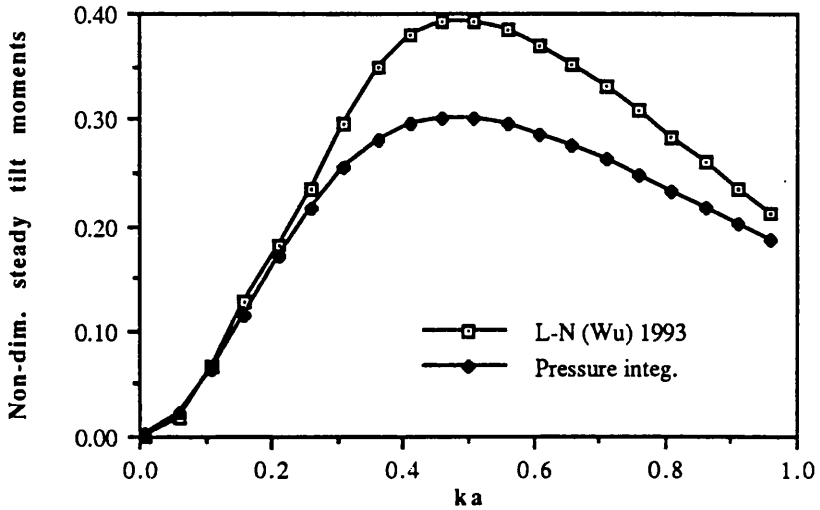

Fig.10.72 Comparison of non-dim. steady tilt moments on twin cylinder model (d/a=3.17,c/a=10.,Fn=0.20 in 10 degree tilt)

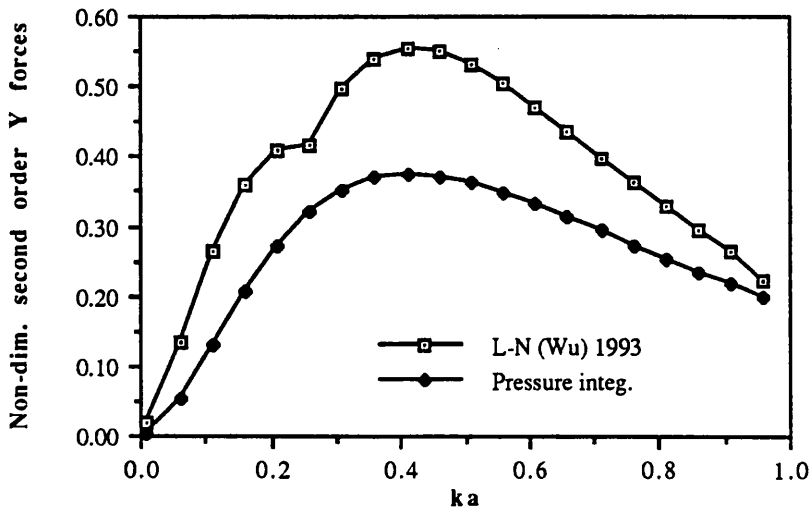

Fig.10.73 Comparison of non-dim. second order vertical forces on left cylinder (d/a=3.17,c/a=10.,Fn=0.40 in 10 degree tilt)

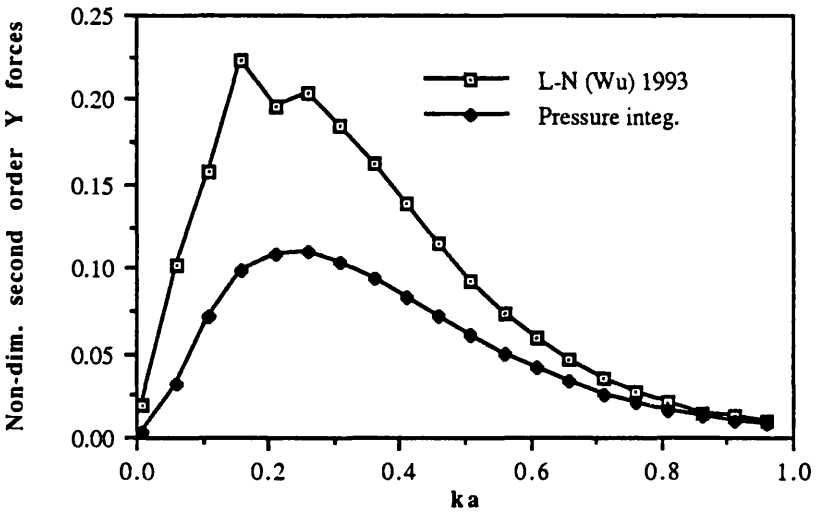

Fig.10.74 Comparison of non-dim. second order vertical forces on right cylinder (d/a=3.17,c/a=10.,Fn=0.40 in 10 degree tilt)

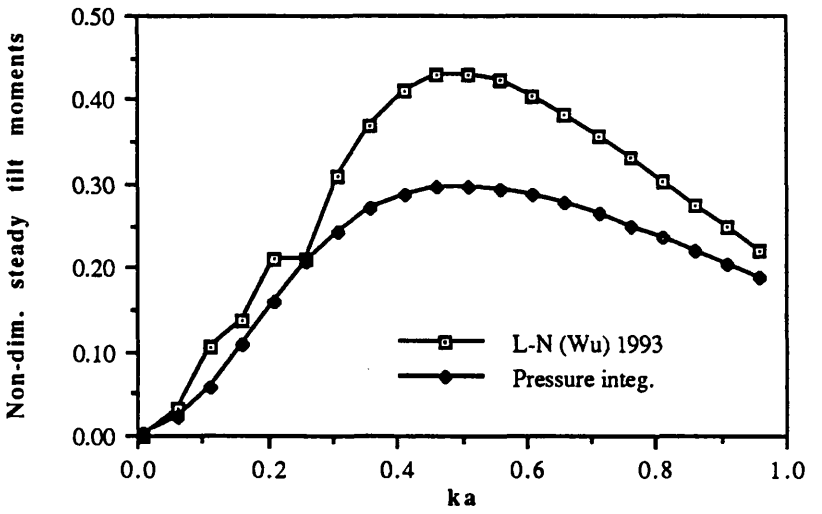

Fig.10.75 Comparison of non-dim. steady tilt moments on twin cylinder model (d/a=3.17,c/a=10.,Fn=0.40 in 10 degree tilt)

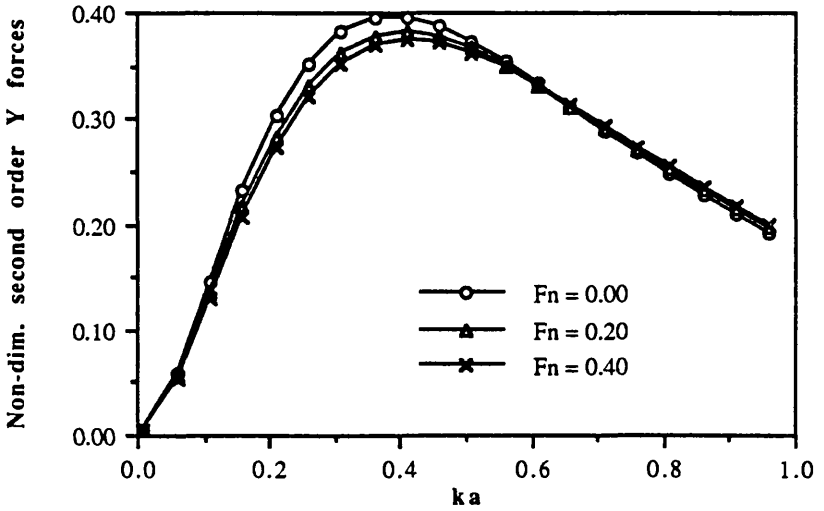

Fig.10.76 Comparison of non-dim. second order vertical forces on left cylinder for different current speeds in 10 degree tilt

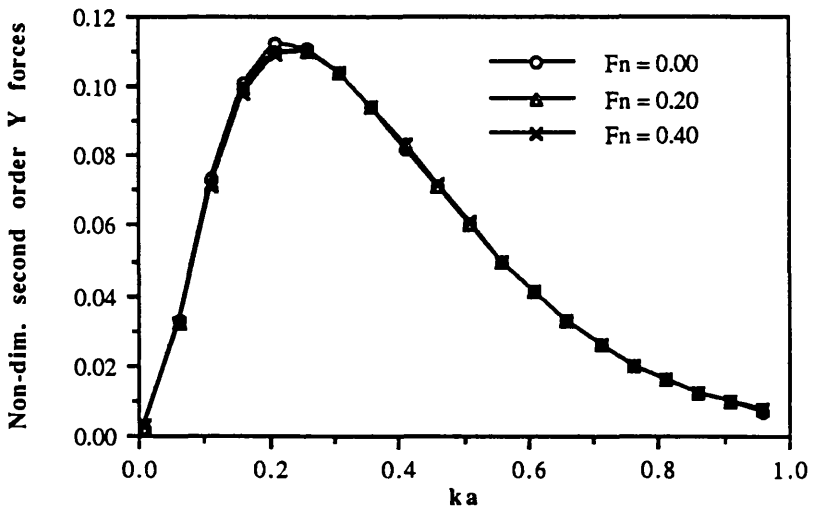

Fig.10.77 Comparison of non-dim. second order vertical forces on right cylinder for different current speeds in 10 degree tilt

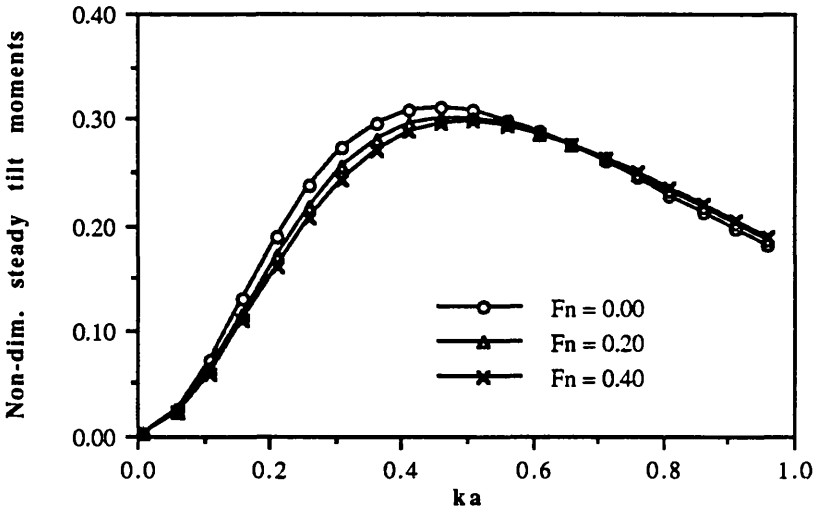

Fig.10.78 Comparison of non-dim. steady tilt moments on twin cylinder model for different current speeds in 10 degree tilt

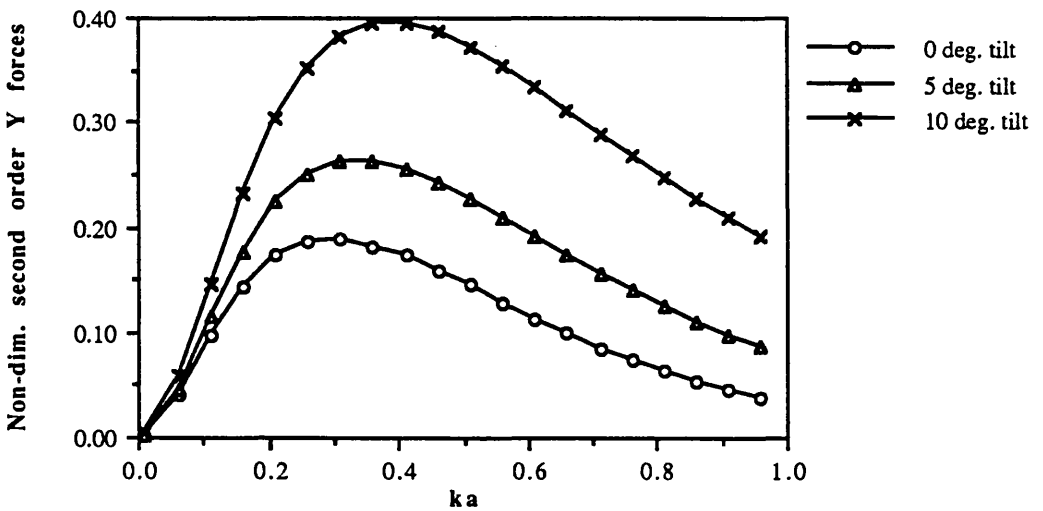

Fig.10.79 Comparison of non-dim. second order vertical forces on left cylinder for different inclinations(d/a=3.17,c/a=10.0)

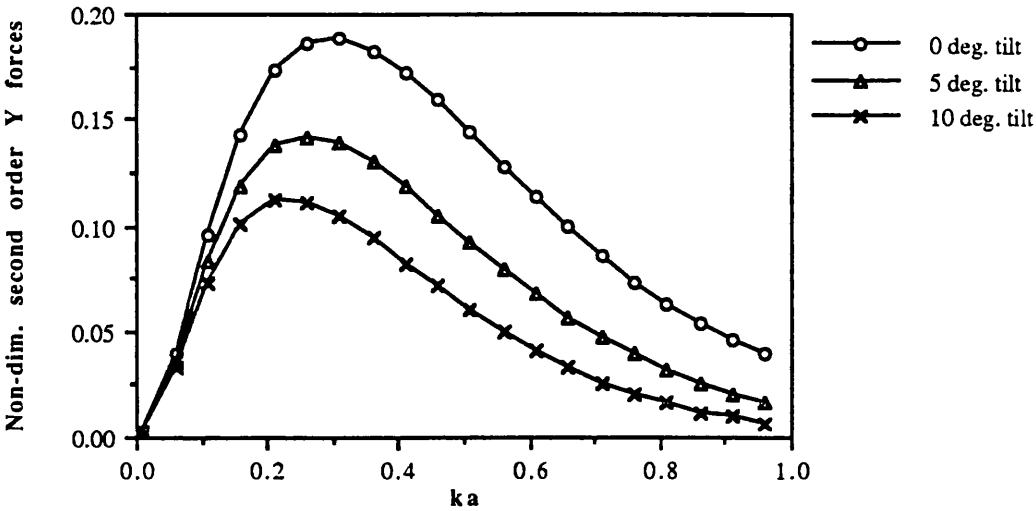

Fig.10.80 Comparison of non-dim. second order vertical forces on right cylinder for different inclinations(d/a=3.17,c/a=10.0)

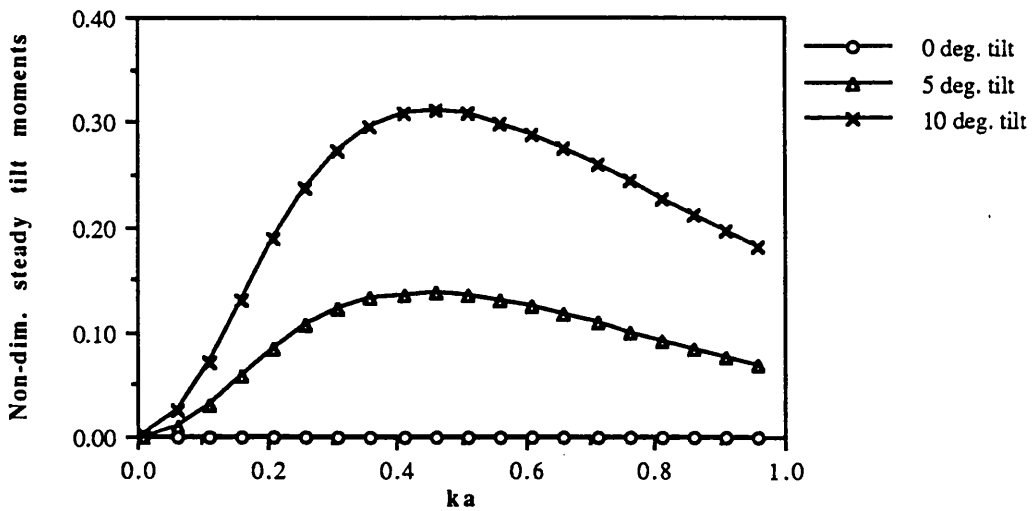

Fig.10.81 Comparison of non-dim. steady tilt moments on twin cylinder model for different inclinations(d/a=3.17,c/a=10.0)

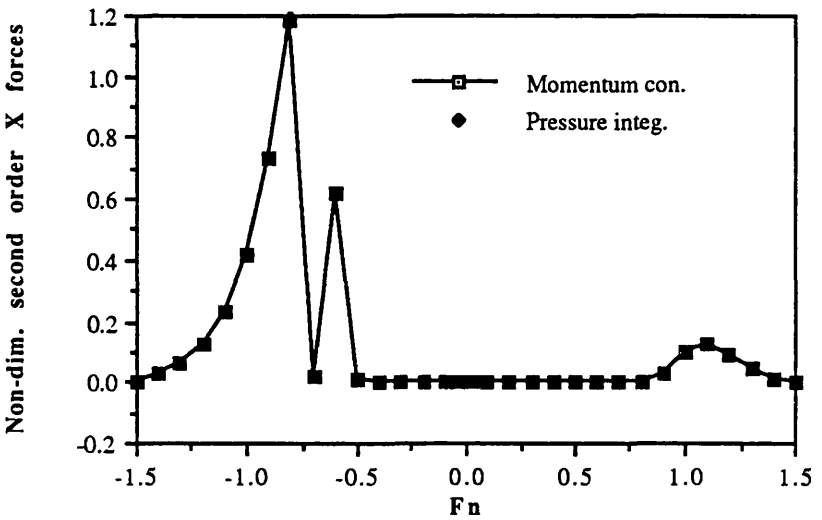

Fig.10.82 Non-dimensionalized second order X forces against Froude numbers (d/a=2,c/a=4,k=0.10 in no tilt condition)

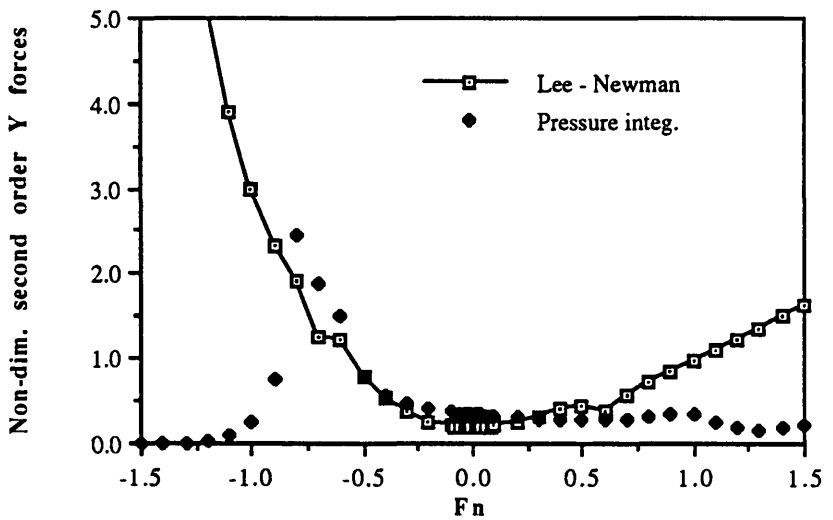

Fig.10.83 Non-dimensionalized second order Y forces against Froude numbers (d/a=2,c/a=4,k=0.10 in no tilt condition)

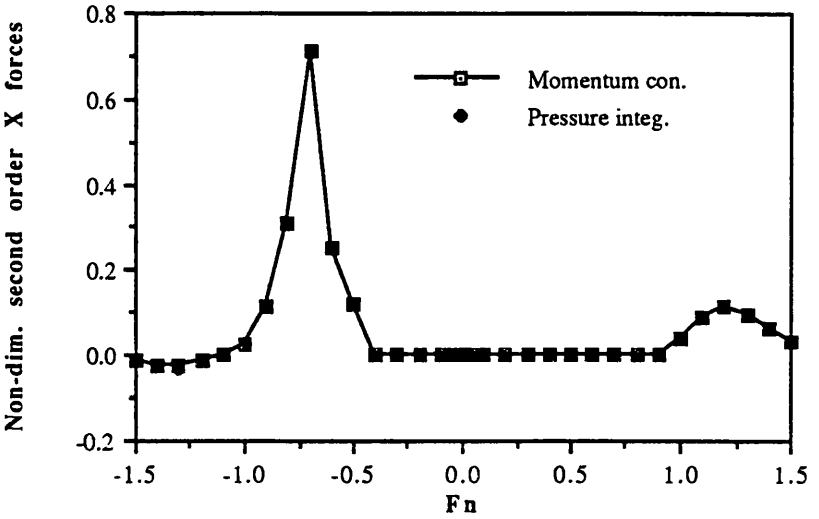

Fig.10.84 Non-dimensionalized second order X forces against Froude numbers (d/a=2,c/a=4,k=0.20 in no tilt condition)

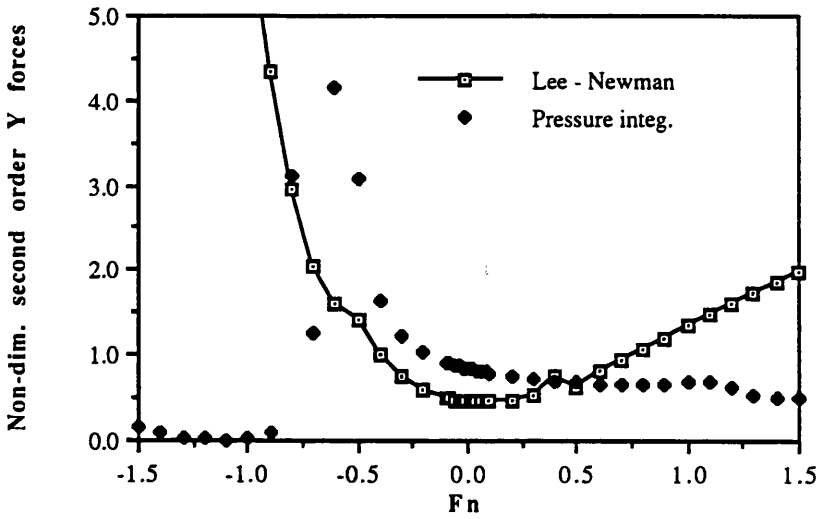

Fig.10.85 Non-dimensionalized second order Y forces against Froude numbers (d/a=2,c/a=4,k=0.20 in no tilt condition)

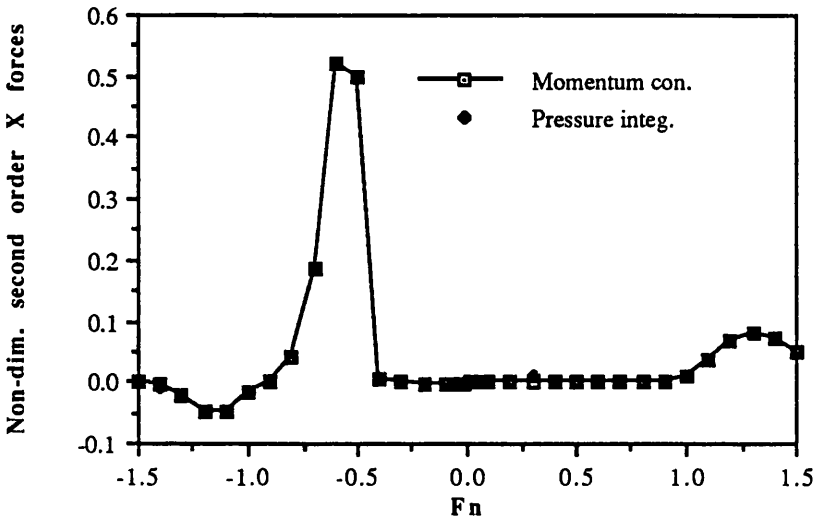

Fig.10.86 Non-dimensionalized second order X forces against Froude numbers (d/a=2,c/a=4,k=0.30 in no tilt condition)

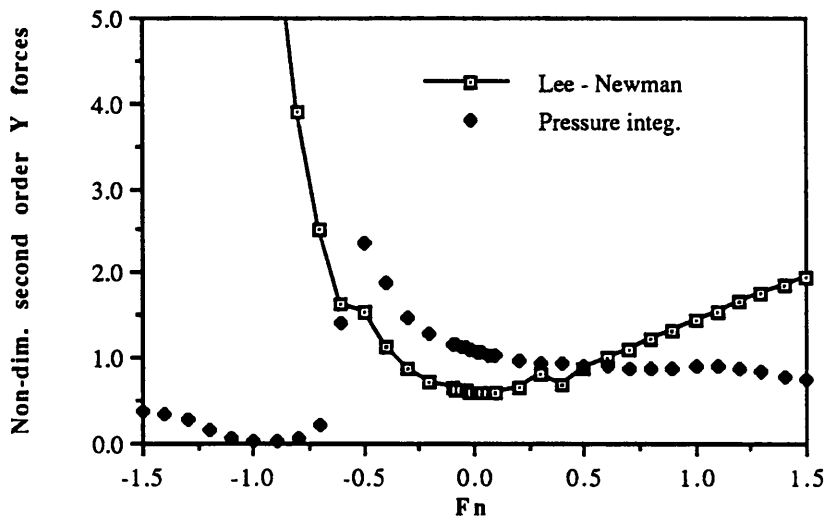

Fig.10.87 Non-dimensionalized second oder Y forces against Froude numbers (d/a=2,c/a=4,k=0.30 in no tilt condition)

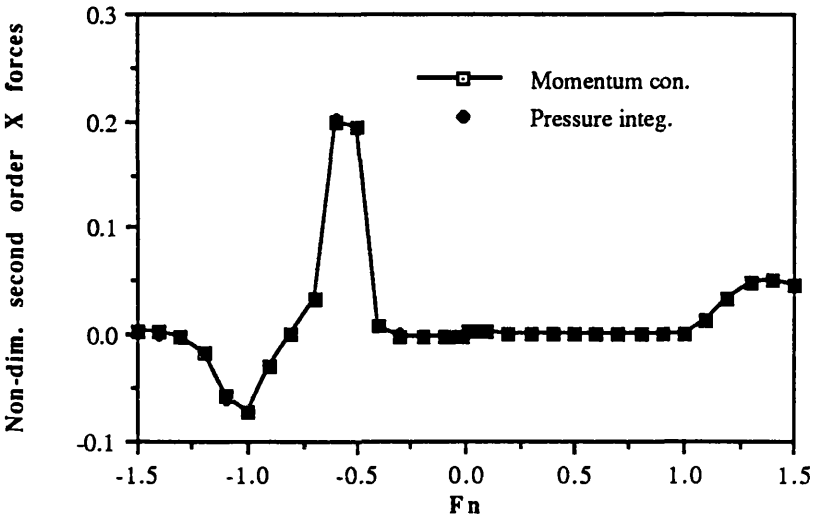

Fig.10.88 Non-dimensionalized second order X forces against Froude numbers (d/a=2,c/a=4,k=0.40 in no tilt condition)

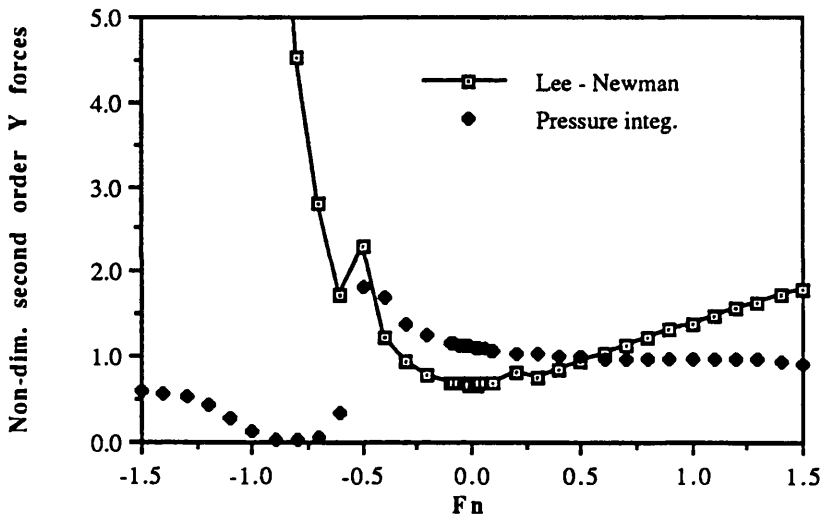

Fig.10.89 Non-dimensionalized second order Y forces against Froude numbers (d/a=2,c/a=4,k=0.40 in no tilt condition)

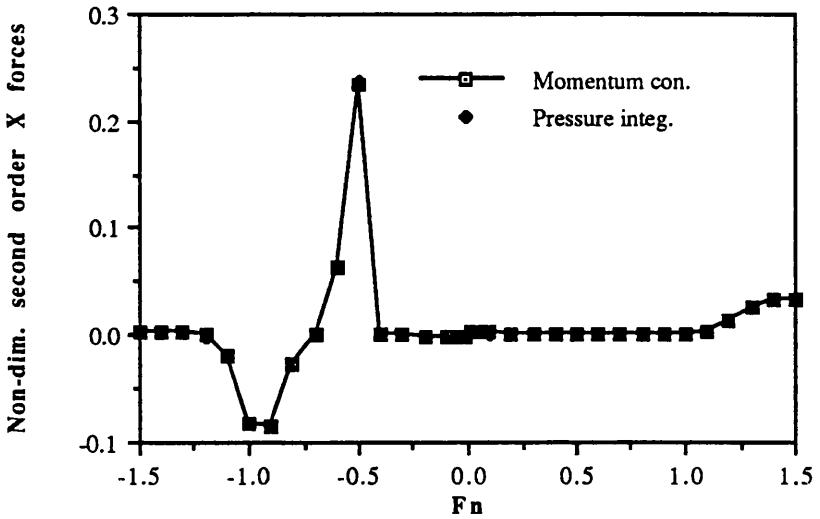

Fig.10.90 Non-dimensionalized second order X forces aginst Froude numbers (d/a=2,c/a=4,k=0.50 in no tilt condition)

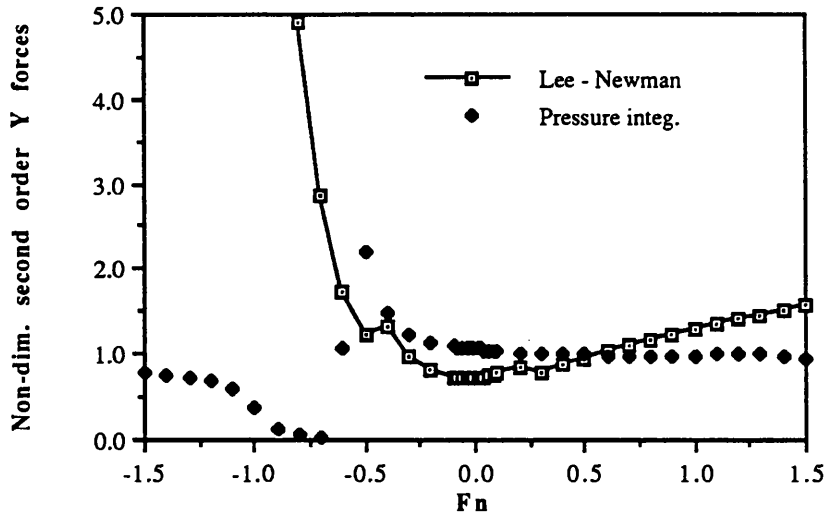

Fig.10.91 Non-dimensionalized second order Y forces against Froude numbers (d/a=2,c/a=4,k=0.50 in no tilt condition)

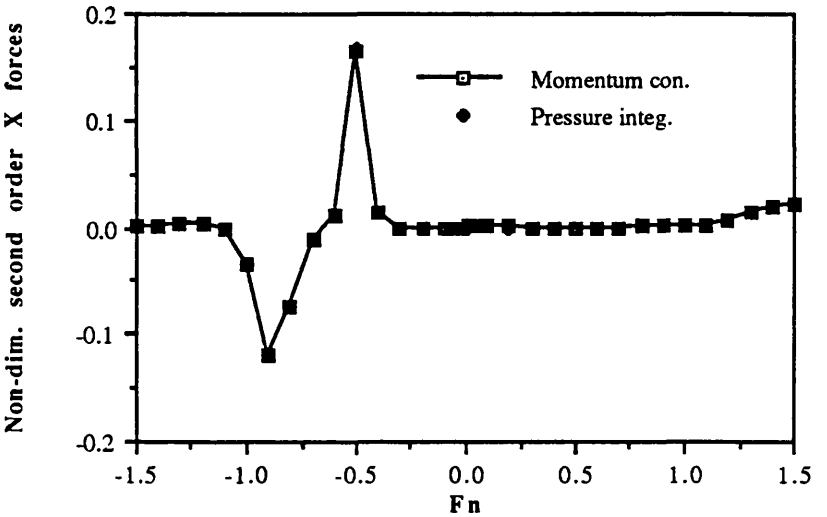

Fig.10.92 Non-dimensionalized second order X forces against Froude numbers (d/a=2,c/a=4,k=0.60 in no tilt condition)

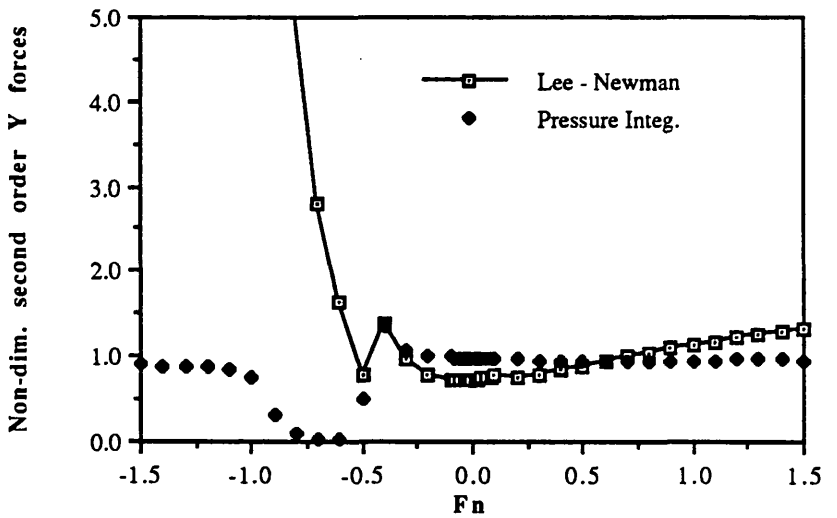

Fig.10.93 Non-dimensionalized second order Y forces against Froude numbers (d/a=2,c/a=4,k=0.60 in no tilt condition)

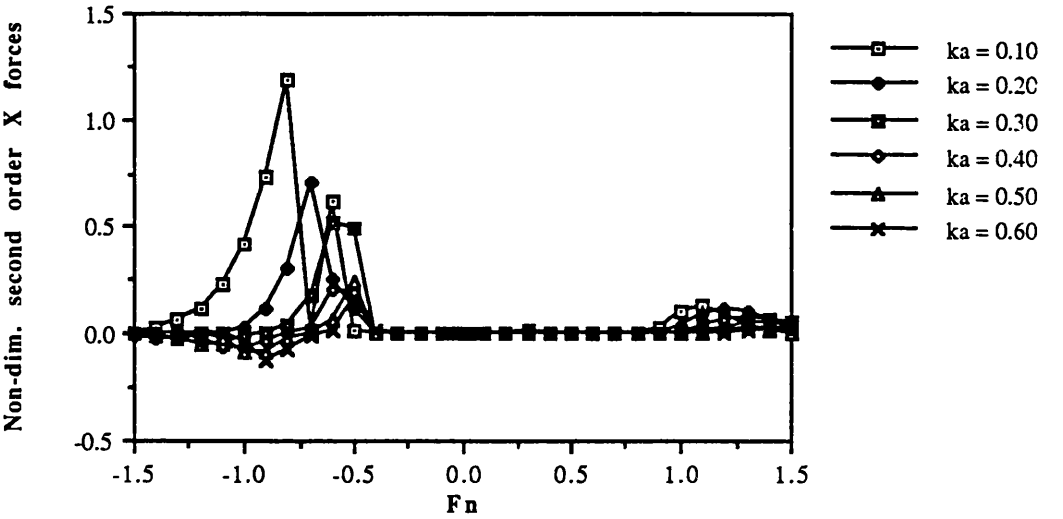

Fig.10.94 Non-dimensionalized second order X forces for different wave numbers (d/a=2, c/a=4 in no tilt condition)

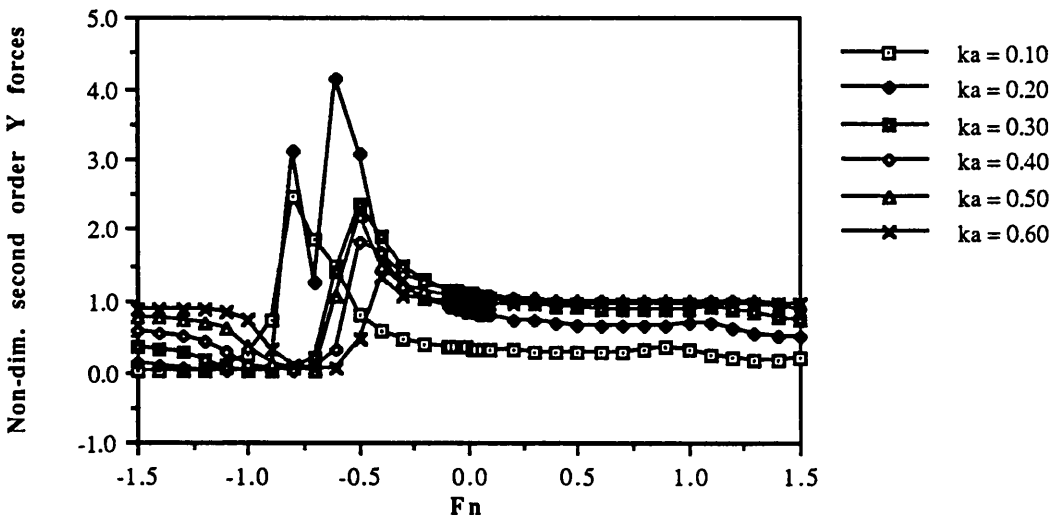

Fig.10.95 Non-dimensionalized second order Y forces for different wave numbers (d/a=2, c/a=4 in no tilt condition)

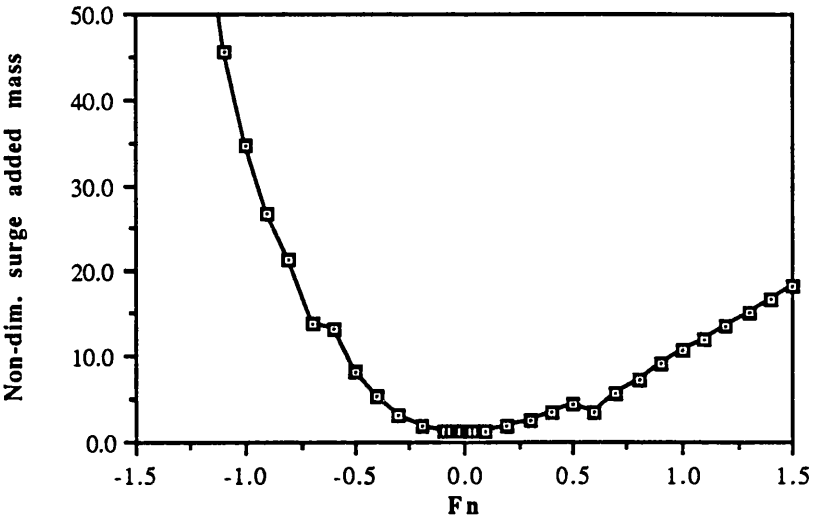

Fig.10.96 Non-dimensionalized surge added mass against Froude numbers(d/a=2,c/a=4, Ka=0.10 in no tilt condition)

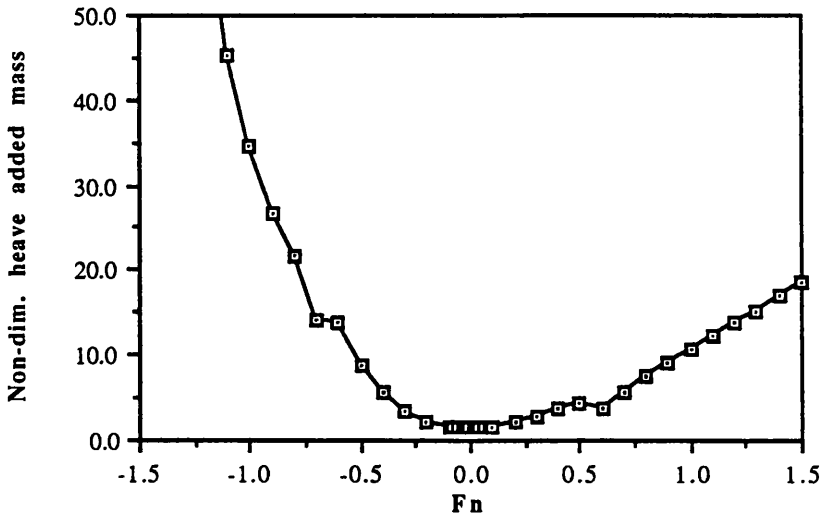

Fig.10.97 Non-dimensionalized heave added mass against Froude numbers (d/a=2,c/a=4,Ka=0.10 in no tilt condition)

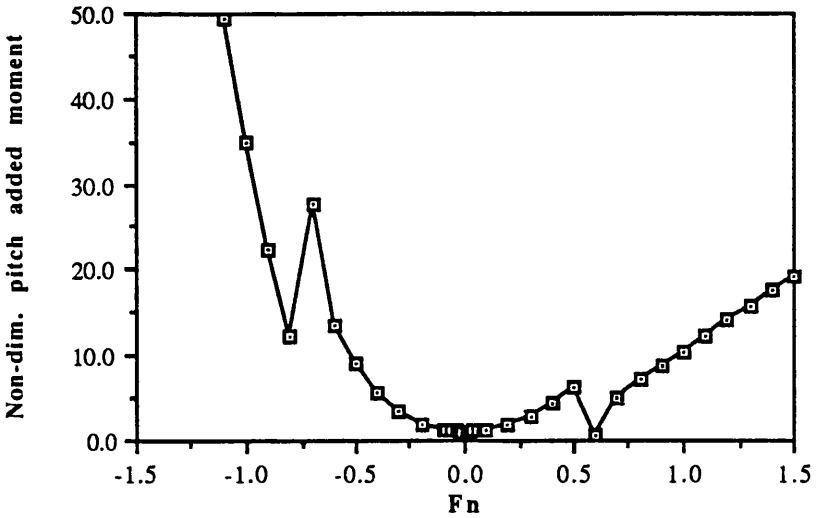

Fig.10.98 Non-dimensionalized pitch added moment against Froude numbers (d/a=2, c/a=4, Ka=0.10 in no tilt condition)

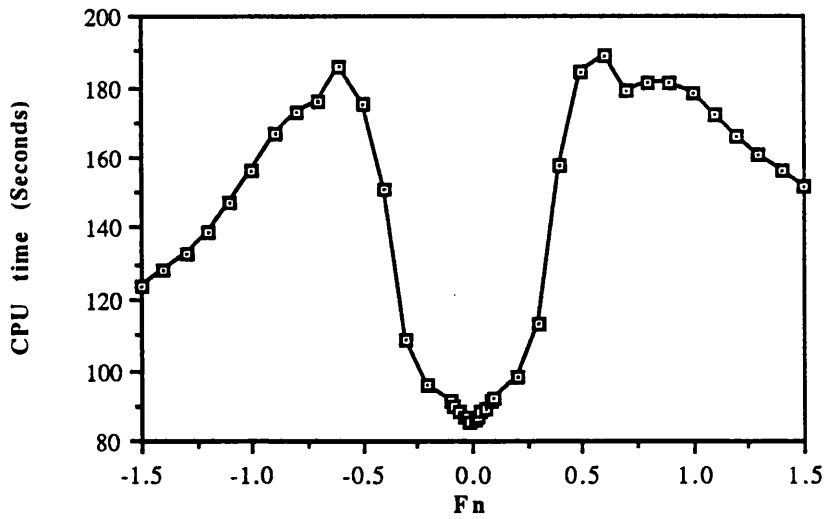

Fig.10.99 Relation between CPU time and Froude numbers (d/a=2, c/a=4, Ka=0.10 in no tilt condition)

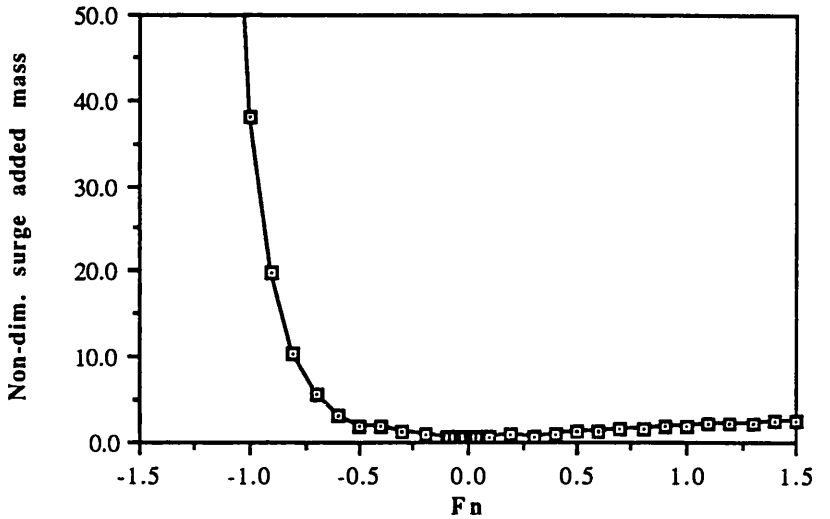

Fig.10.100 Non-dimensionalized surge added mass against Froude numbers (d/a=2,c/a=4,ka=0.50 in no tilt condition)

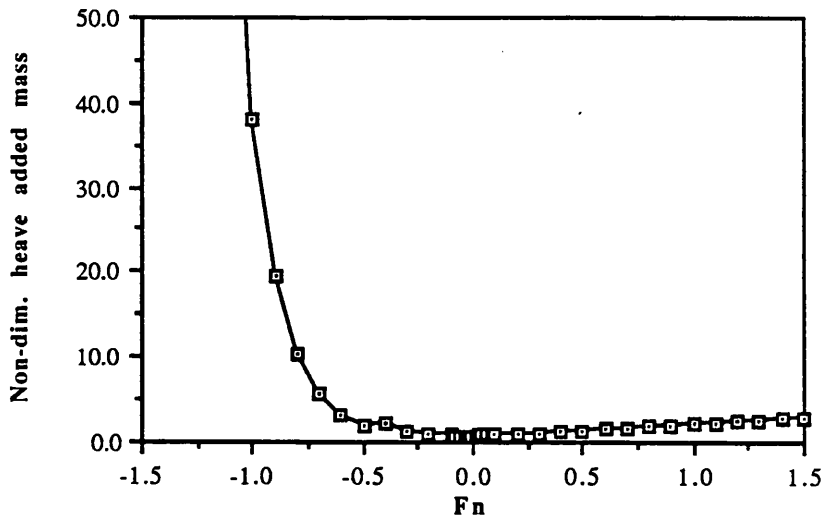

Fig.10.101 Non-dimensionalized heave added mass against Froude numbers (d/a=2,c/a=4,ka=0.50 in no tilt condition)

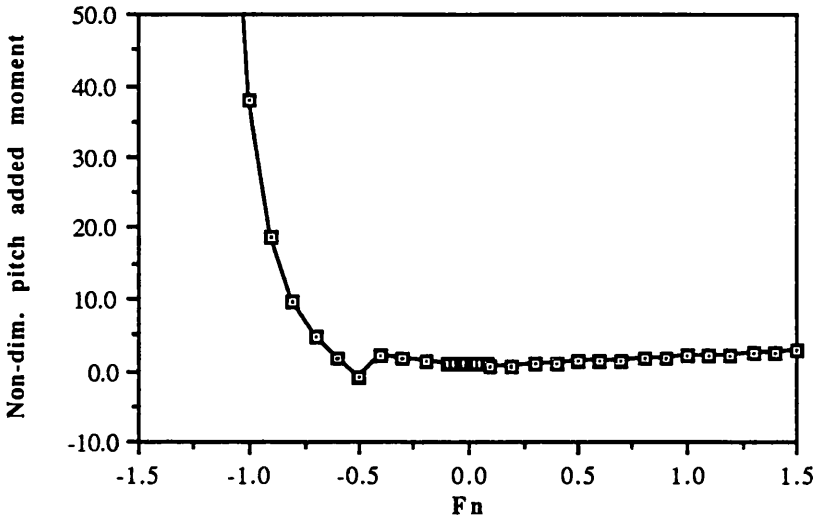

Fig.10.102 Non-dimensionalized pitch added moment against Froude numbers (d/a=2,c/a=4, ka=0.50 in no tilt condition)

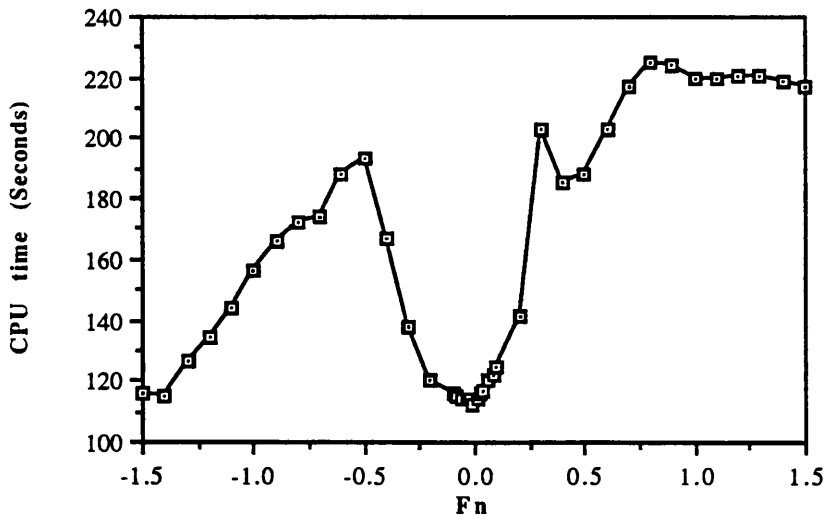

Fig.10.103 Relation between CPU time and Froude numbers (d/a=2, c/a=4, ka=0.50 in no tilt condition)

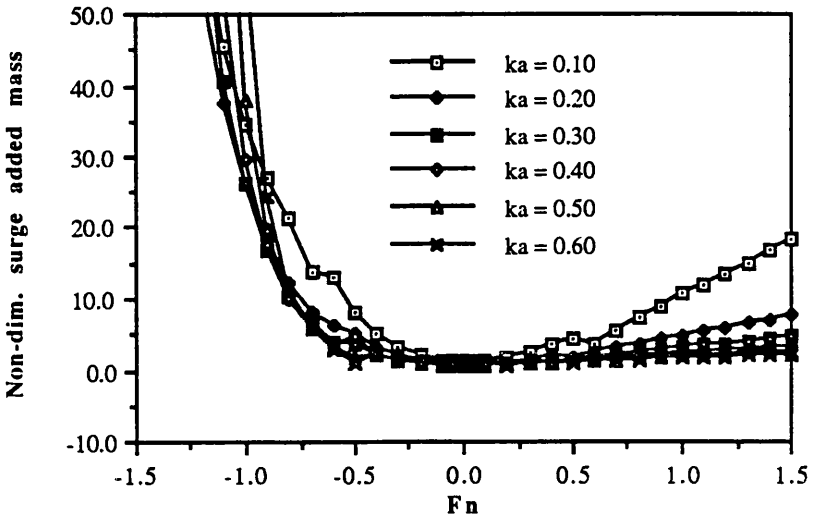

Fig.10.104 Non-dimensionalized surge added mass for different wave numbers (d/a=2, c/a=4 in no tilt condition)

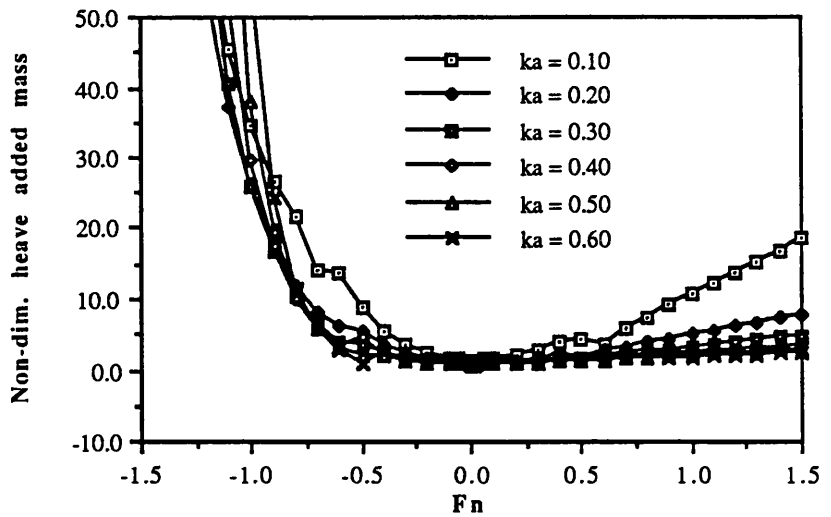

Fig.10.105 Non-dimensionalized heave added mass for different wave numbers (d/a=2, c/a=4 in no tilt condition)

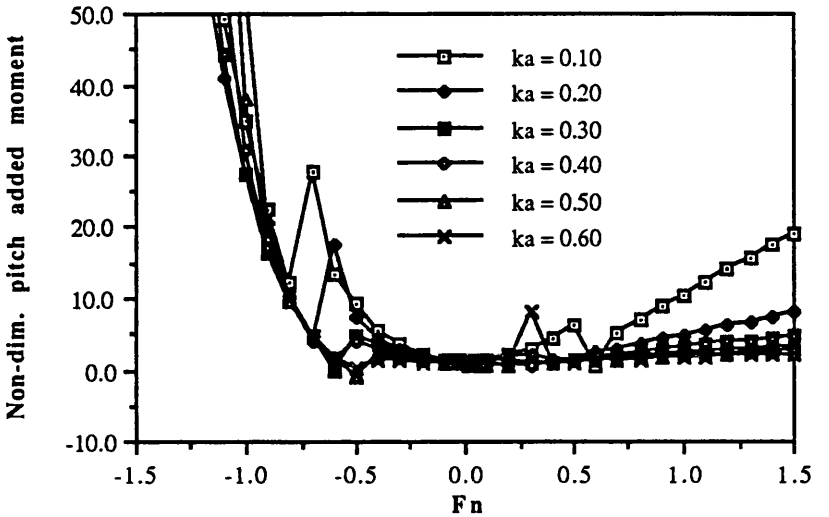

Fig.10.106 Non-dimensionalized pitch added moment for different wave numbers (d/a=2, c/a=4 in no tilt condition)

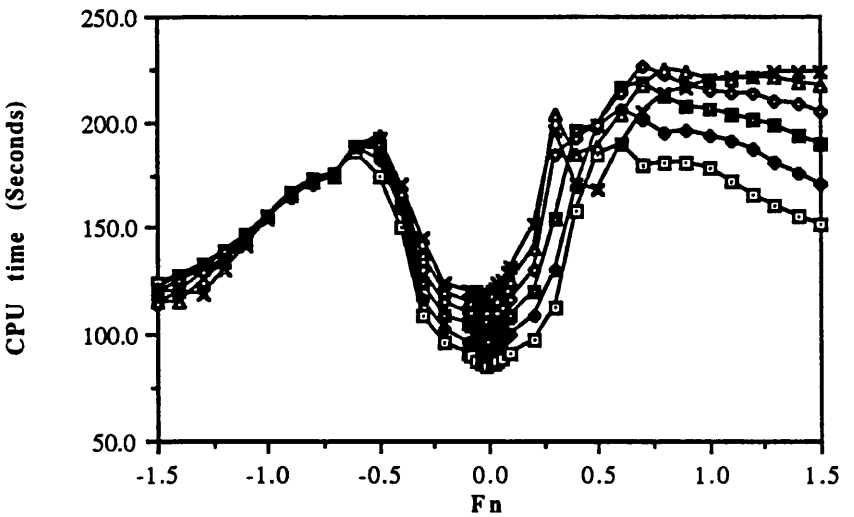

Fig.10.107 Relation of CPU time and Froude numbers for different wave numbers (d/a=2, c/a=4 in no tilt condition)

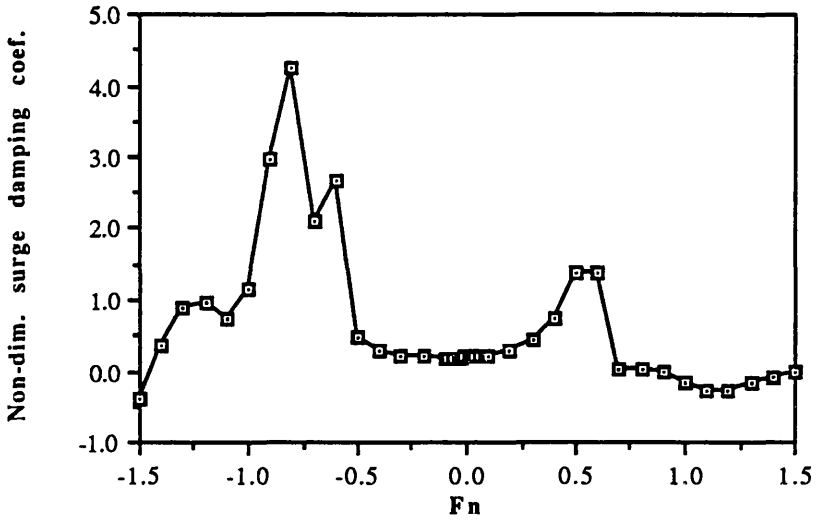

Fig.10.108 Non-dim. surge damping coefficient against Froude numbers (d/a=2,c/a=4,Ka=0.10 in no tilt condition)

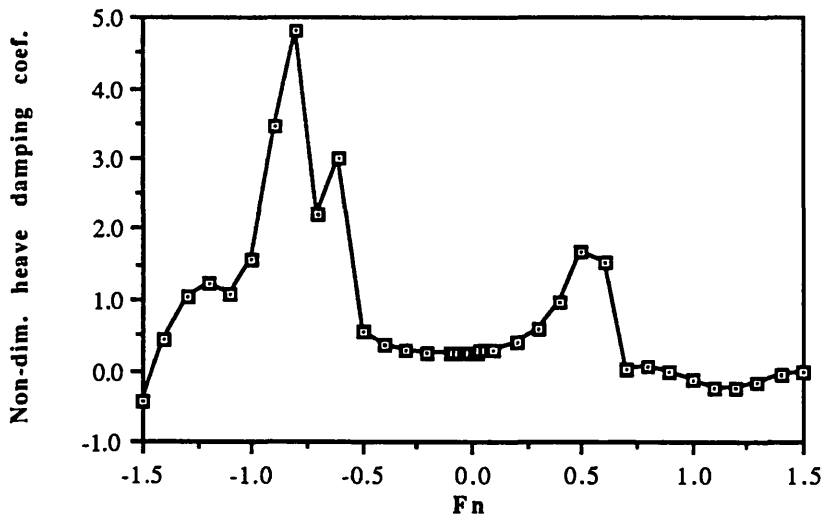

Fig.10.109 Non-dim. heave damping coefficient against Froude numbers (d/a=2,c/a=4,Ka=0.10 in no tilt condition)

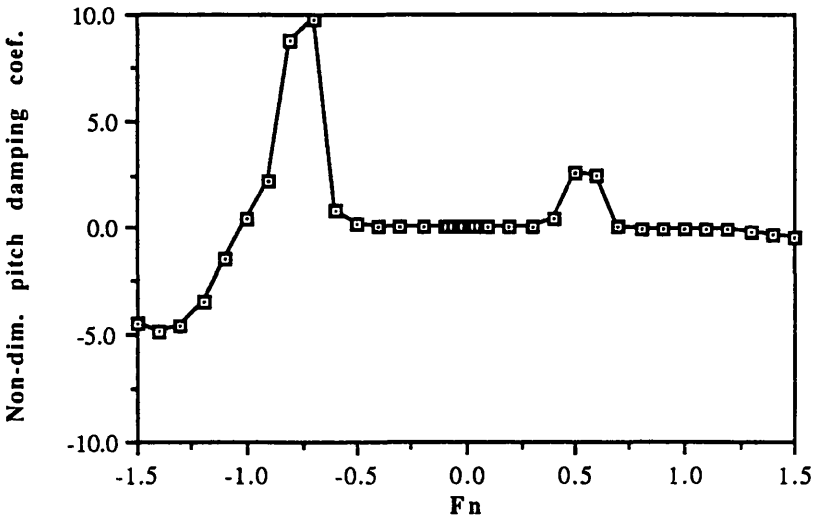

Fig.10.110 Non-dim. pitch damping coefficient against Froude numbers (d/a=2,c/a=4,Ka=0.10 in no tilt condition)

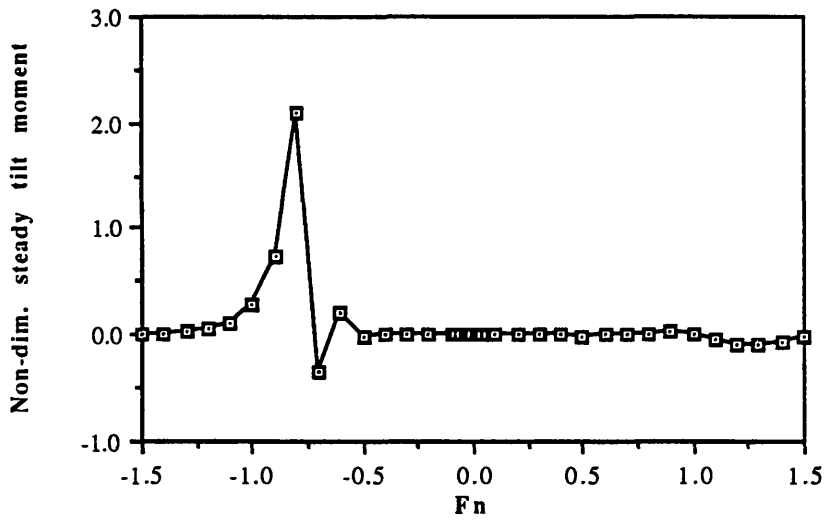

Fig.10.111 Non-dim. steady tilt moment against Froude numbers (d/a=2, c/a=4, ka=0.10 in no tilt condition)

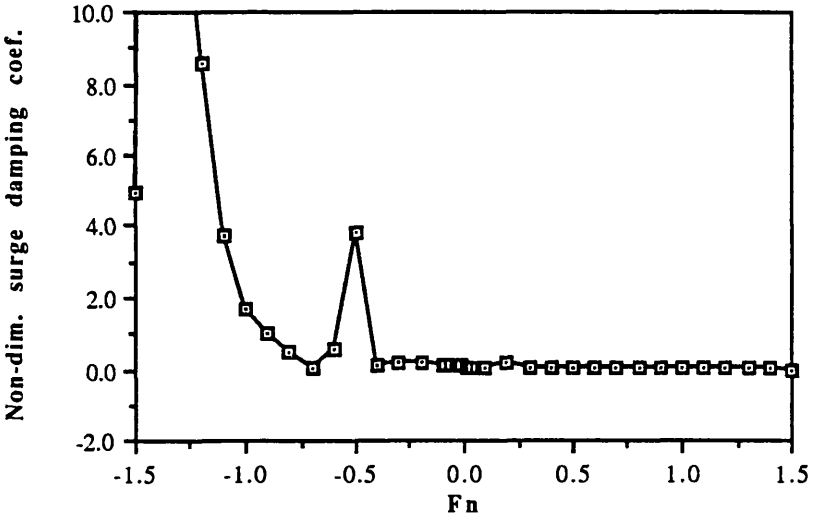

Fig.10.112 Non-dim. surge damping coefficient against Froude numbers (d/a=2,c/a=4,Ka=0.50 in no tilt condition)

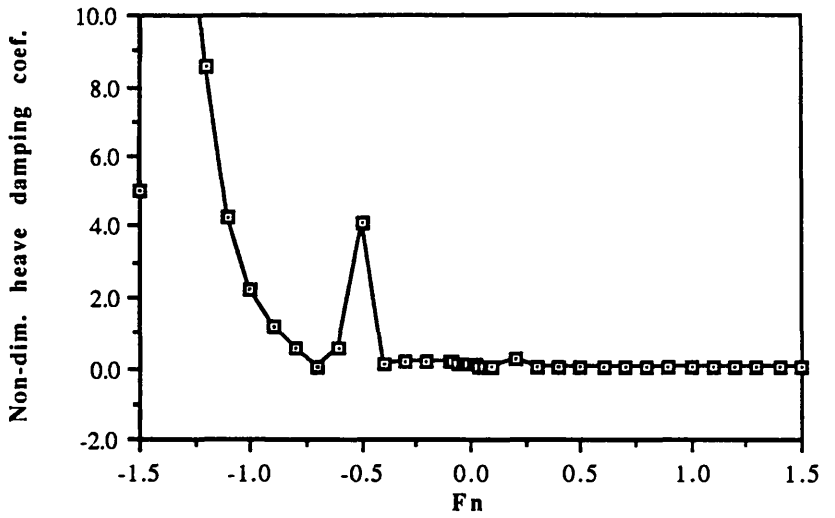

Fig.10.113 Non-dim. heave damping coefficient against Froude numbers (d/a=2,c/a=4,Ka=0.50 in no tilt condition)

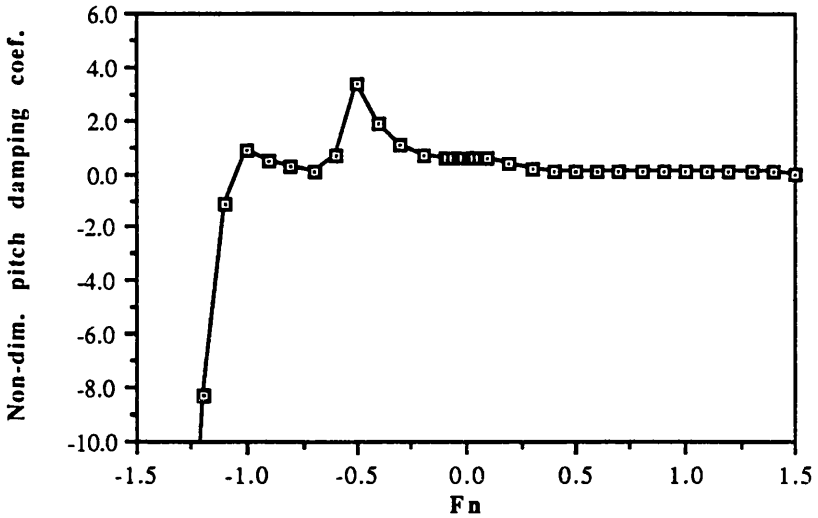

Fig.10.114 Non-dim. pitch damping coefficient against Froude numbers (d/a=2,c/a=4,Ka=0.50 in no tilt condition)

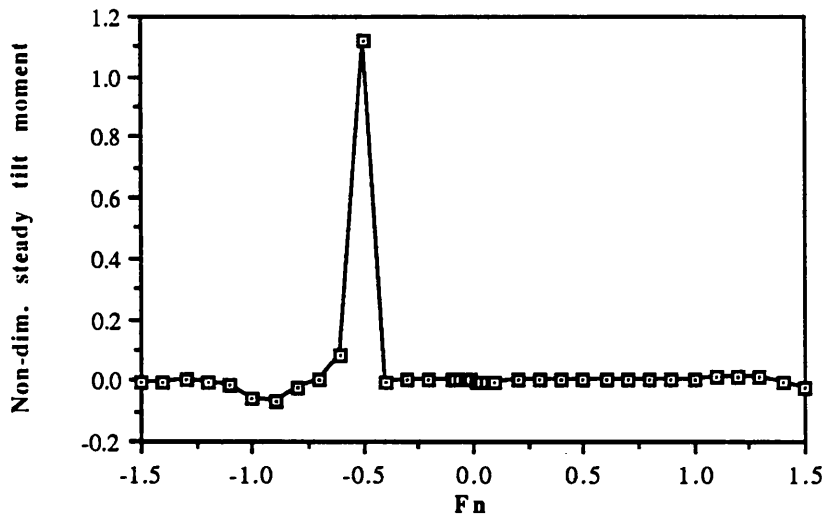

Fig.10.115 Non-dim. steady tilt moment against Froude numbers (d/a=2, c/a=4, ka=0.50 in no tilt condition)

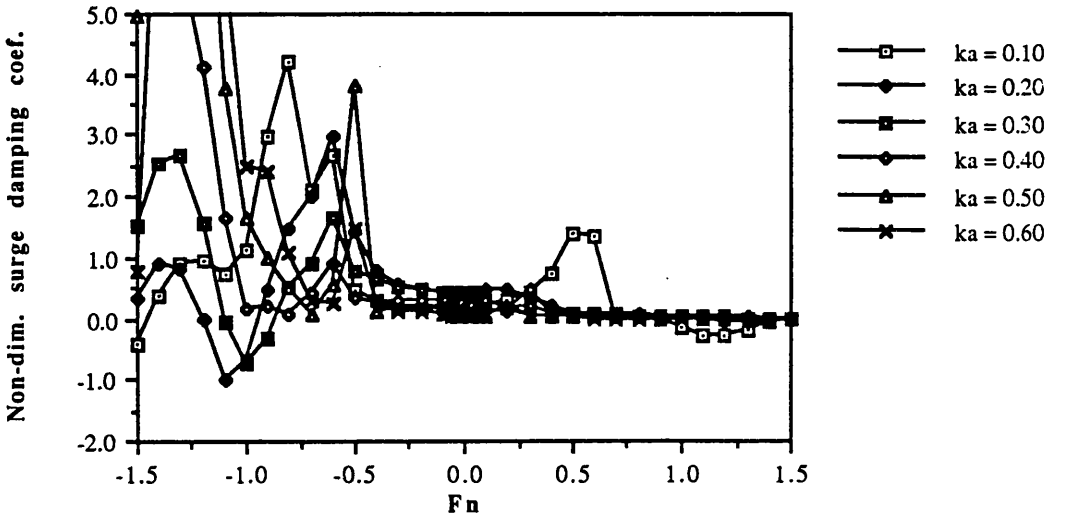

Fig.10.116 Non-dim. surge damping coefficients for different wave numbers (d/a=2,c/a=4 in no tilt condition)

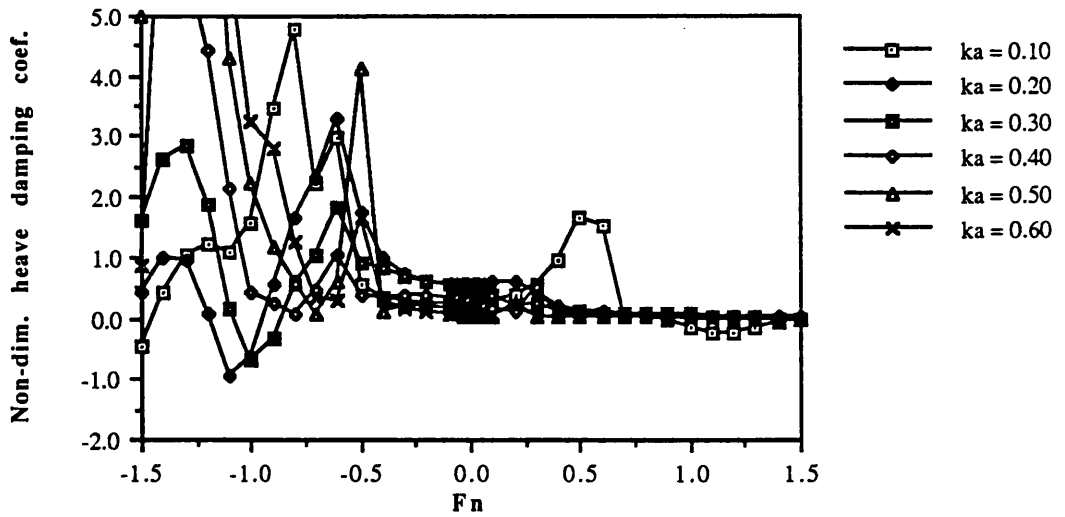

Fig.10.117 Non-dim. heave damping coefficients for different wave numbers (d/a=2,c/a=4 in no tilt condition)

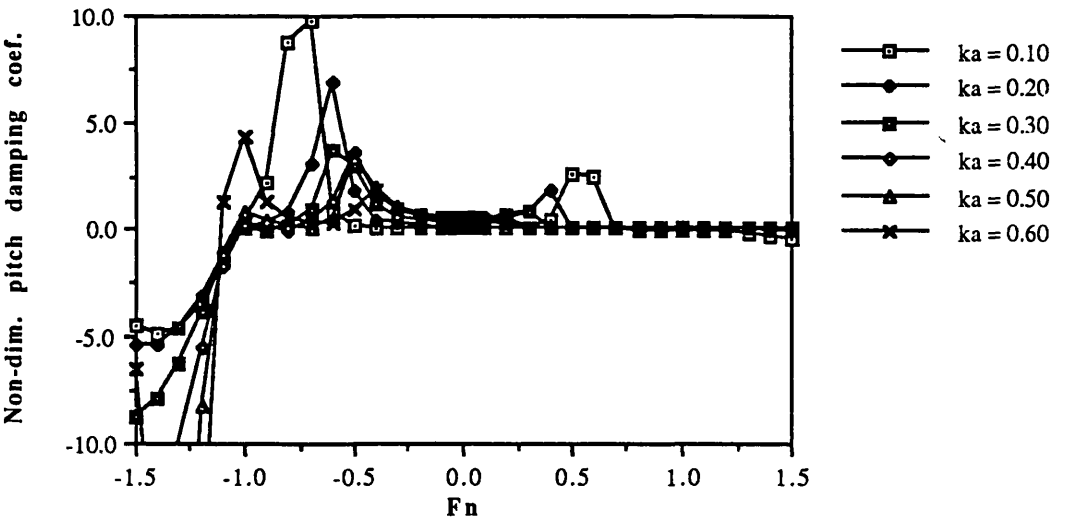

Fig.10.118 Non-dim. pitch damping coefficients for different wave numbers (d/a=2,c/a=4 in no tilt condition)

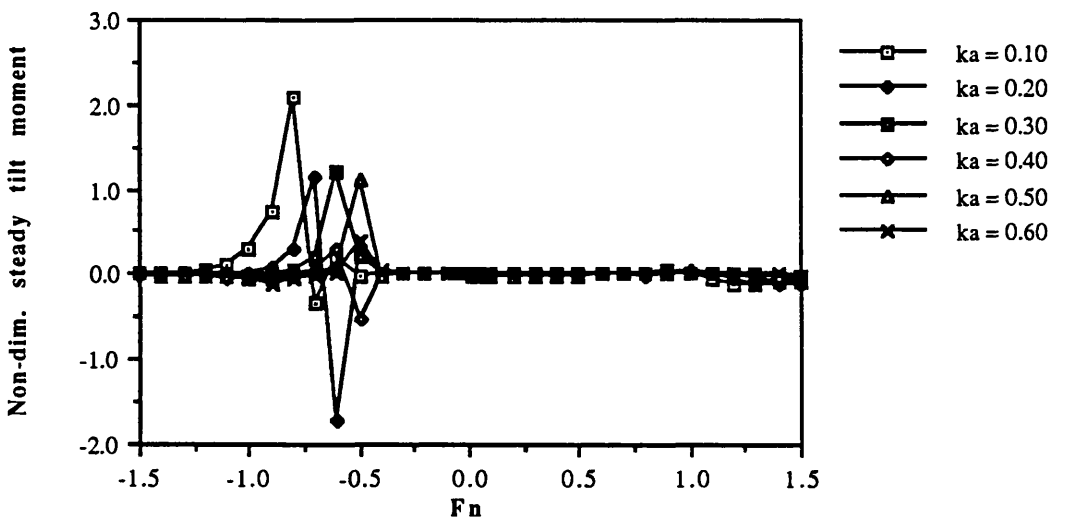

Fig.10.119 Non-dim. steady tilt moments for different wave numbers (d/a=2,c/a=4 in no tilt condition)

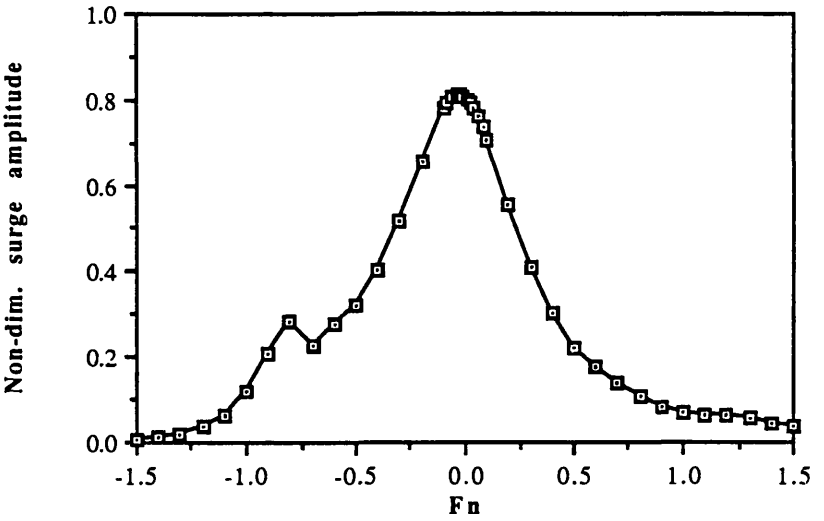

Fig.10.120 Non-dimensionalized surge amplitude against Froude numbers (d/a=2,c/a=4,ka=0.10 in no tilt condition)

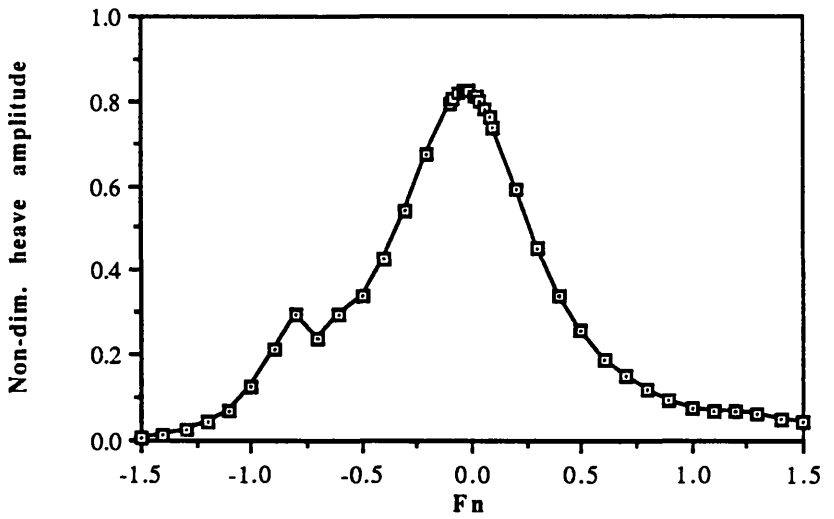

Fig.10.121 Non-dimensionalized heave amplitude against Froude numbers (d/a=2,c/a=4,ka=0.10 in no tilt condition)

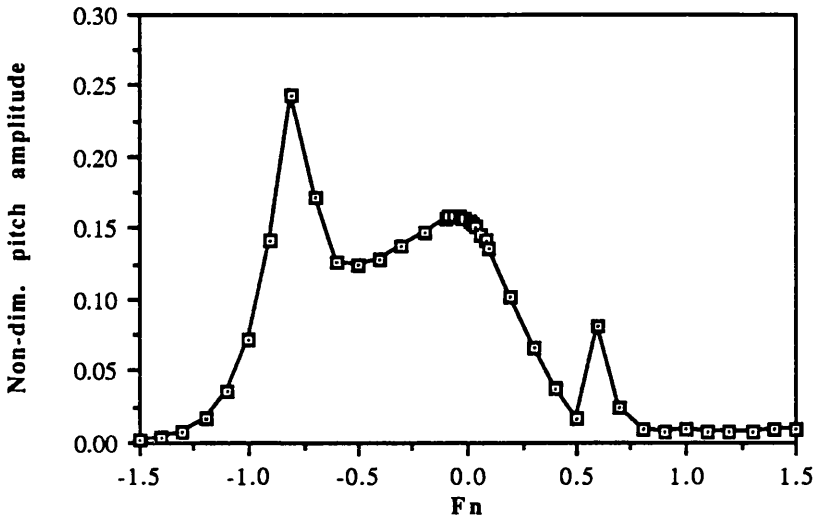

Fig.10.122 Non-dimensionalized pitch amplitude against Froude numbers (d/a=2,c/a=4,ka=0.10 in no tilt condition)

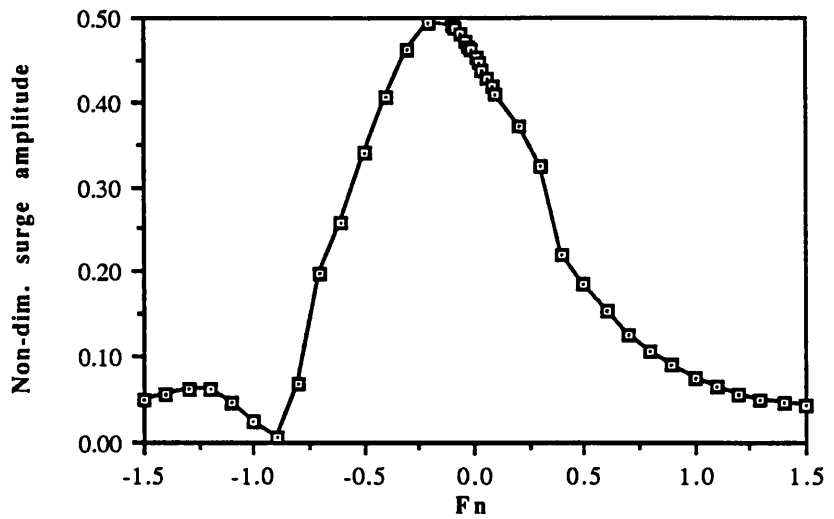

Fig.10.123 Non-dimensionalized surge amplitude against Froude numbers (d/a=2,c/a=4,ka=0.30 in no tilt condition)

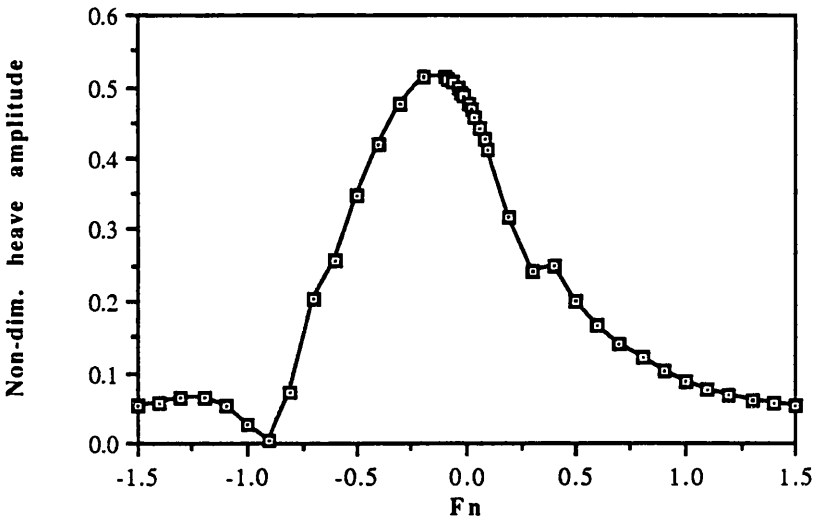

Fig.10.124 Non-dimensionalized heave amplitude against Froude numbers (d/a=2,c/a=4,ka=0.30 in no tilt condition)

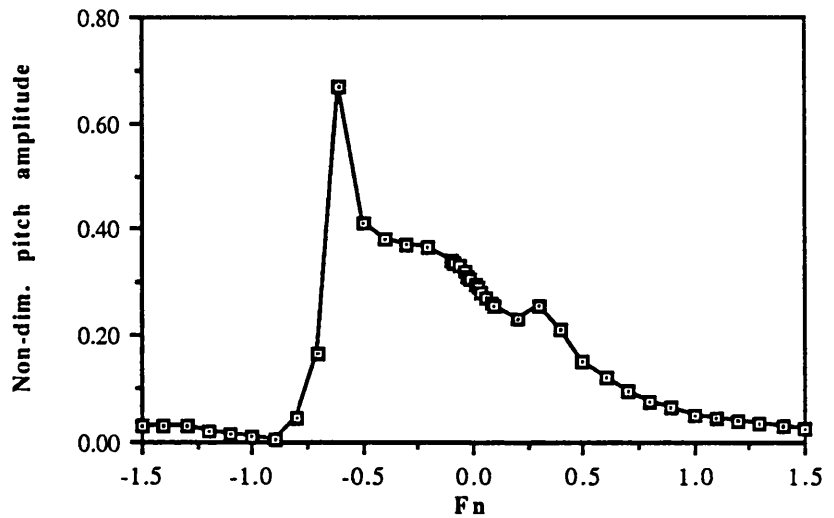

Fig.10.125 Non-dimensionalized pitch amplitude against Froude numbers (d/a=2,c/a=4,ka=0.30 in no tilt condition)

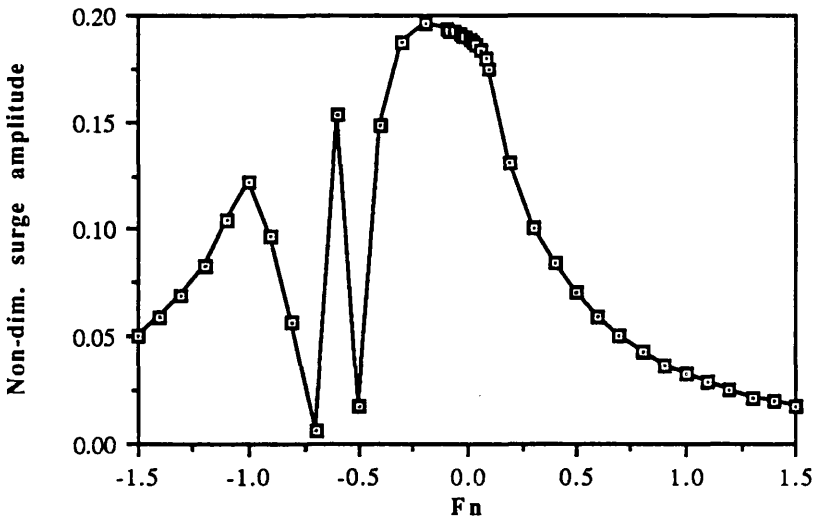

Fig.10.126 Non-dimensionalized surge amplitude against Froude numbers (d/a=2,c/a=4,ka=0.50 in no tilt condition)

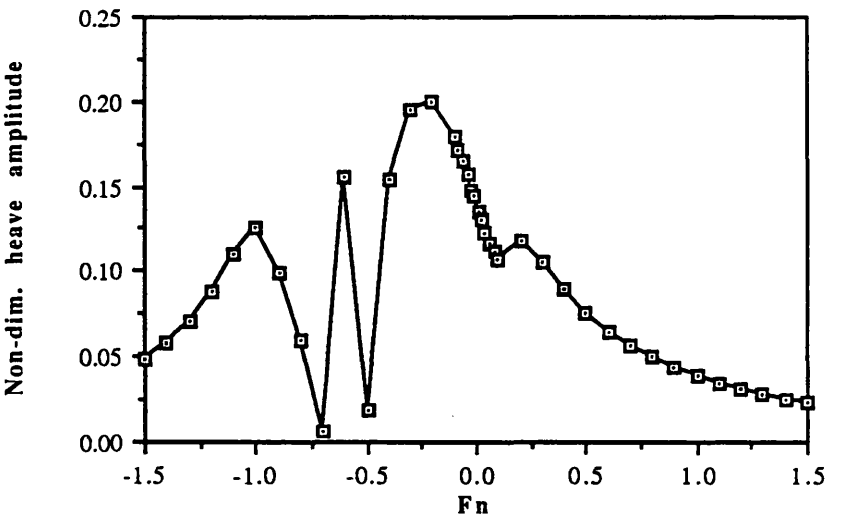

Fig.10.127 Non-dimensionalized heave amplitude against Froude numbers (d/a=2,c/a=4,ka=0.50 in no tilt condition)

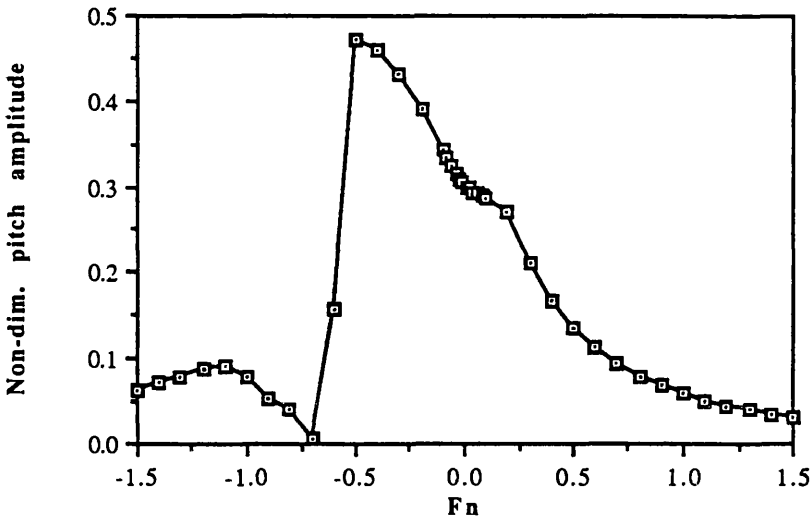

Fig.10.128 Non-dimensionalized pitch amplitude against Froude numbers (d/a=2,c/a=4,ka=0.50 in no tilt condition)

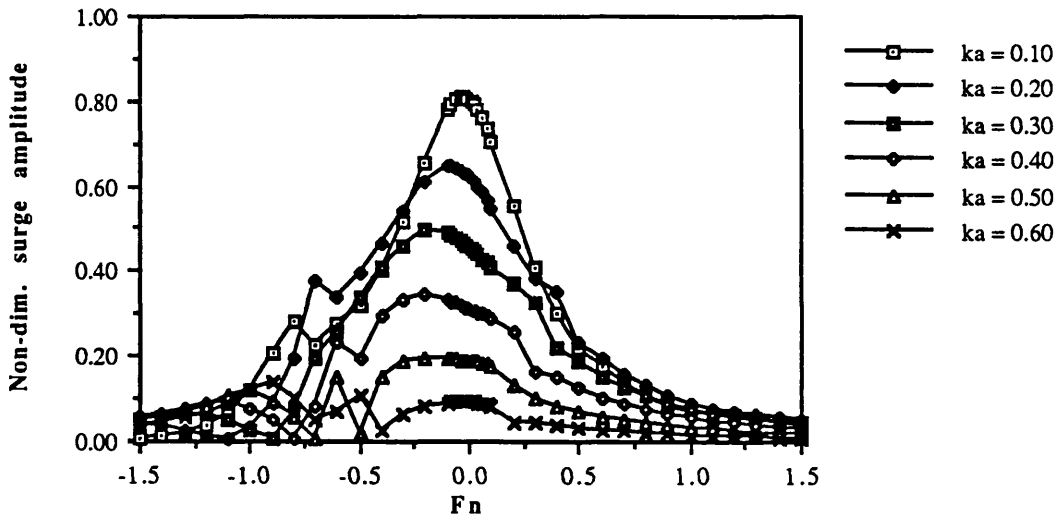

Fig.10.129 Non-dimensionalized surge amplitudes for different wave numbers (d/a=2, c/a=4 in no tilt condition)

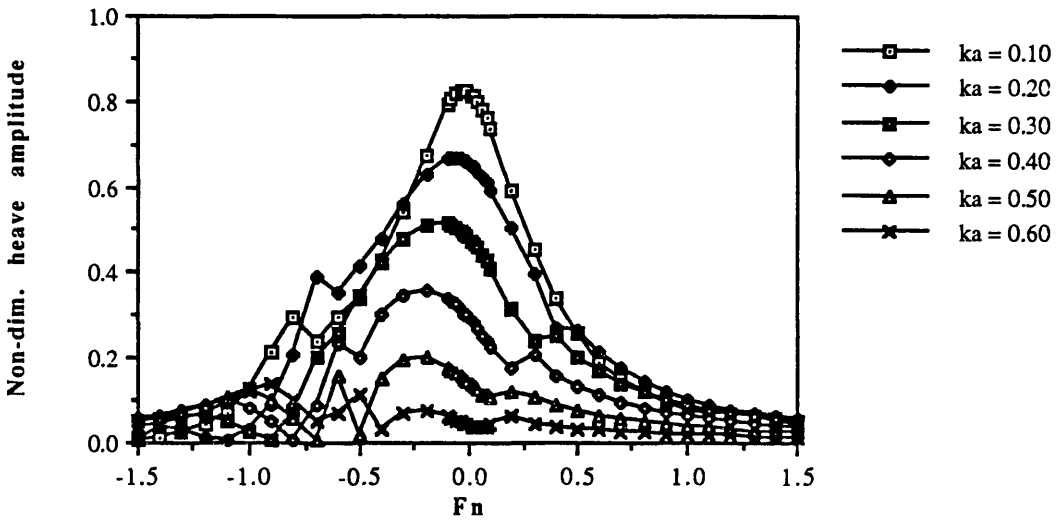

Fig.10.130 Non-dimensionalized heave amplitude for different wave numbers (d/a=2, c/a=4 in no tilt condition)

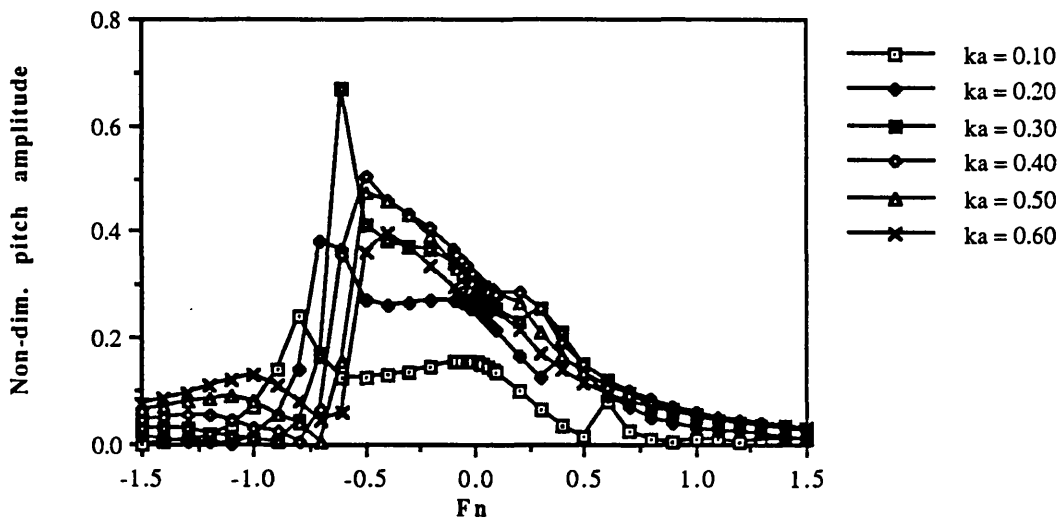

Fig.10.131 Non-dimensionalized pitch amplitudes for different wave numbers (d/a=2, c/a=4 in no tilt condition)

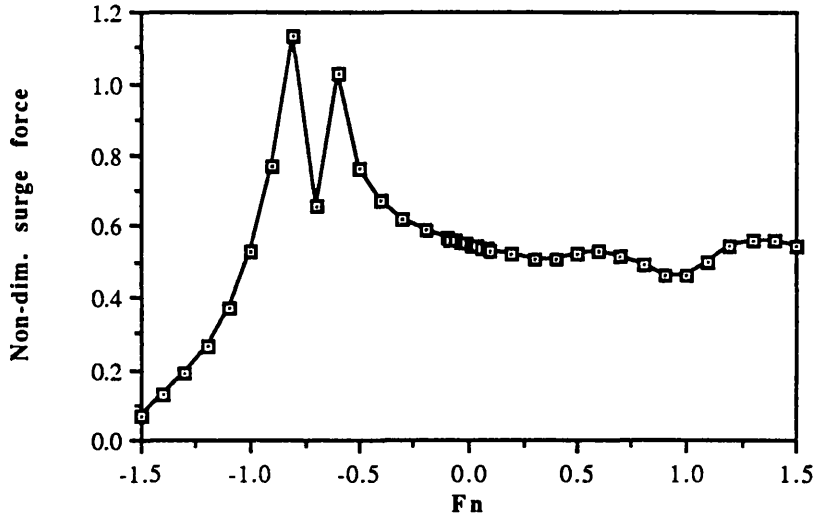

Fig.10.132 Non-dimensionalized surge force against Froude numbers (d/a=2,c/a=4,ka=0.10 in no tilt condition)

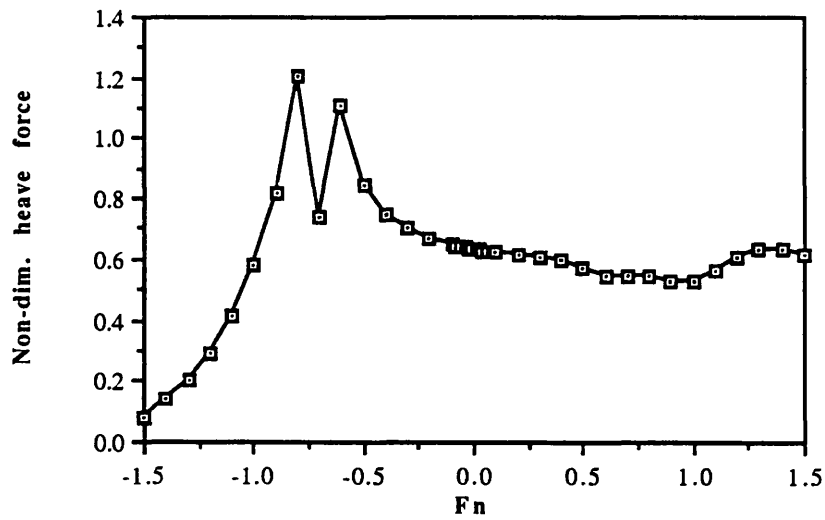

Fig.10.133 Non-dimensionalized heave force against Froude numbers (d/a=2,c/a=4,ka=0.10 in no tilt condition)

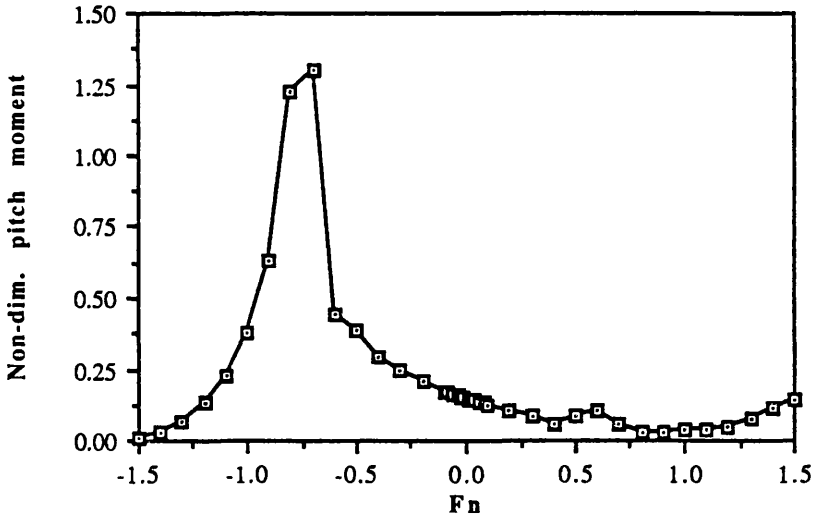

Fig.10.134 Non-dimensionalized pitch moment against Froude numbers (d/a=2,c/a=4,ka=0.10 in no tilt condition)

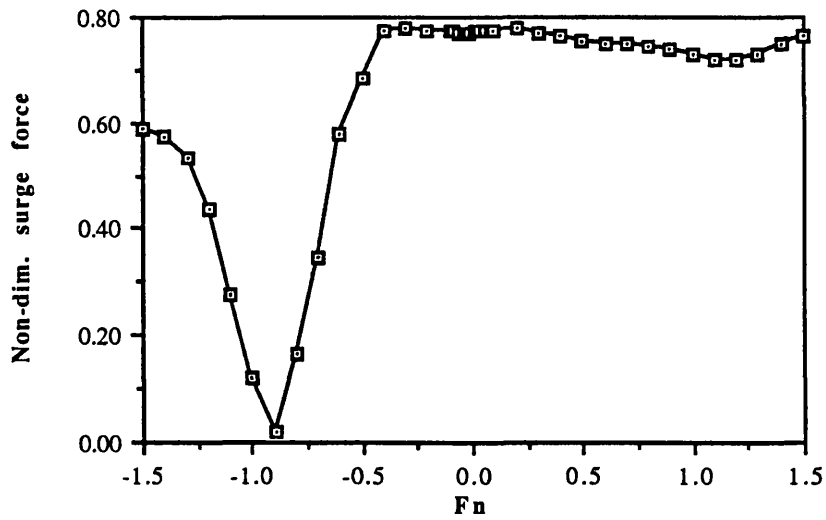

Fig.10.135 Non-dimensionalized surge force against Froude numbers (d/a=2,c/a=4,ka=0.30 in no tilt condition)

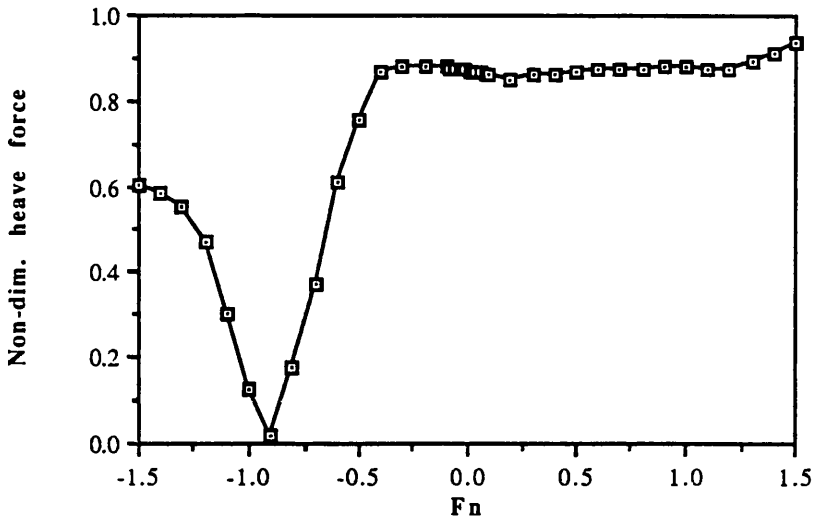

Fig.10.136 Non-dimensionalized heave force against Froude numbers (d/a=2,c/a=4,ka=0.30 in no tilt condition)

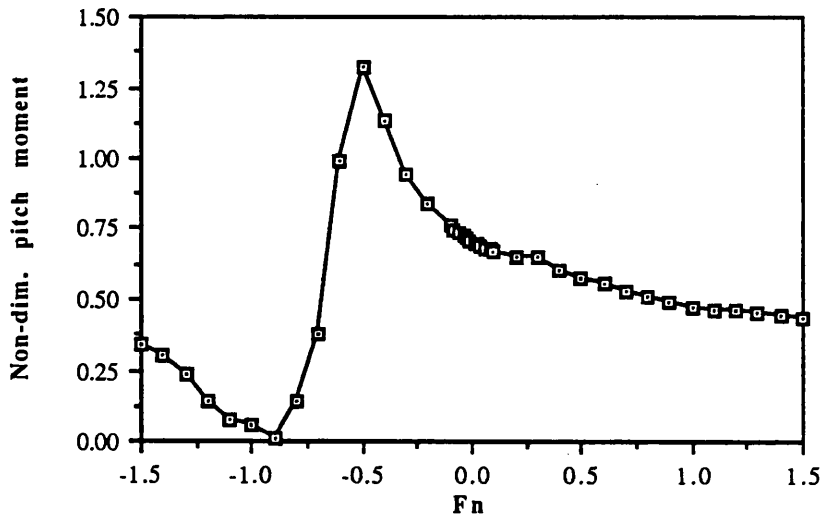

Fig.10.137 Non-dimensionalized pitch moment against Froude numbers (d/a=2,c/a=4,ka=0.30 in no tilt condition)

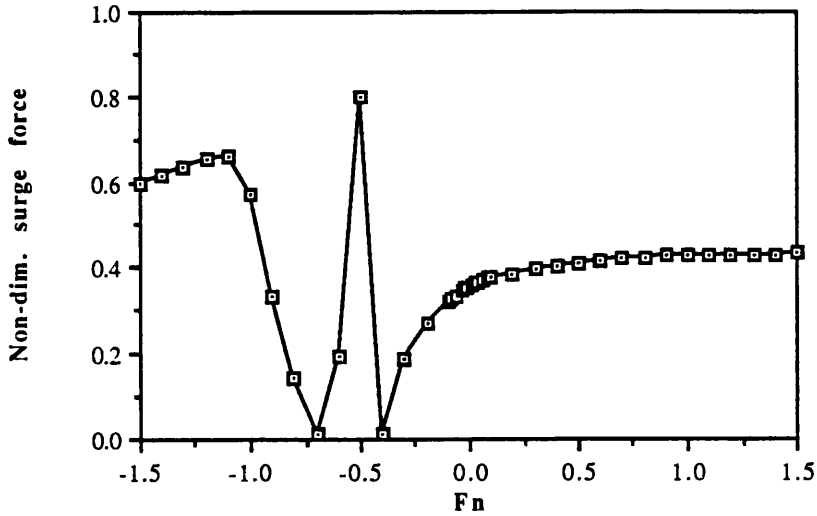

Fig.10.138 Non-dimensionalized surge force against Froude numbers (d/a=2,c/a=4,ka=0.50 in no tilt condition)

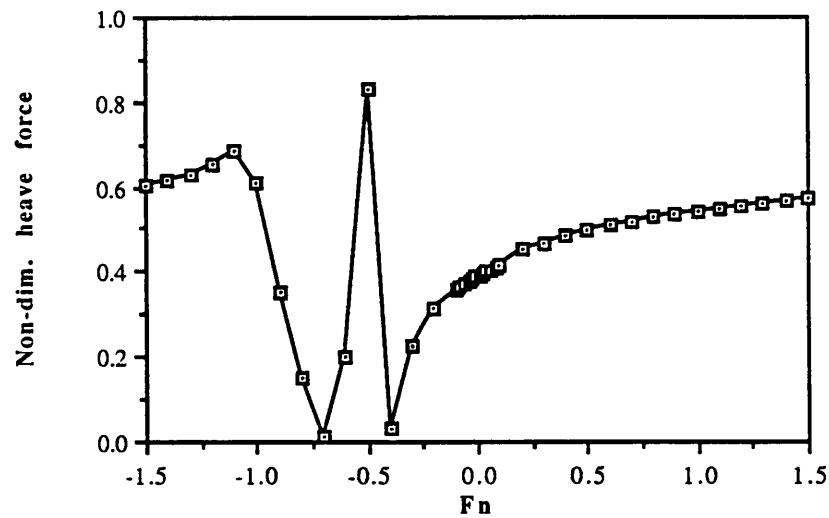

Fig.10.139 Non-dimensionalized heave force against Froude numbers (d/a=2,c/a=4,ka=0.50 in no tilt condition)

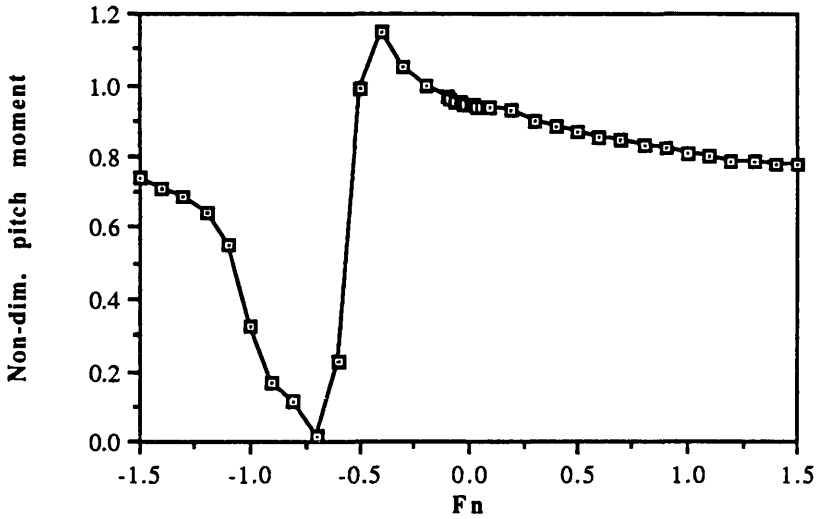

Fig.10.140 Non-dimensionalized pitch moment against Froude numbers (d/a=2,c/a=4,ka=0.50 in no tilt condition)

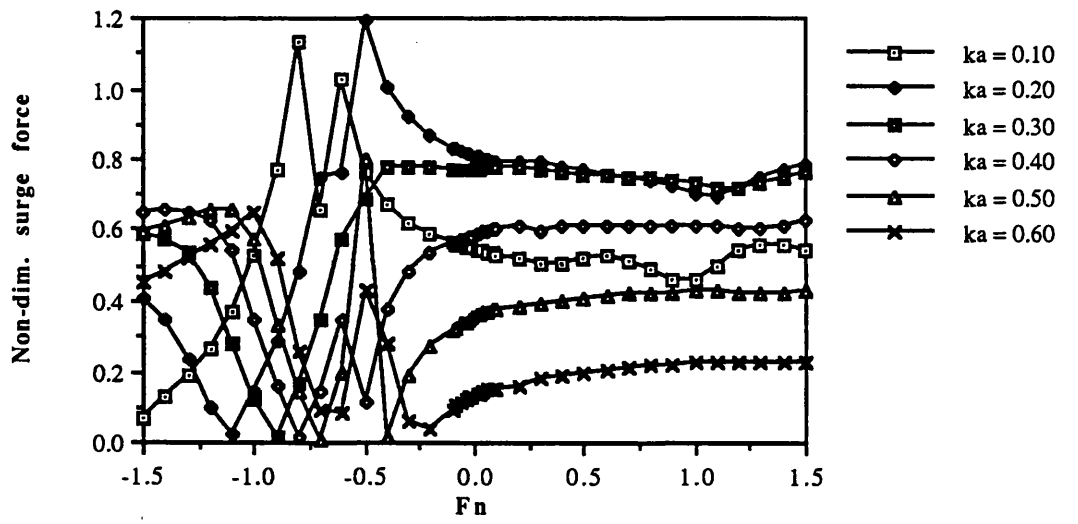

Fig.10.141 Non-dimensionalized surge forces for different wave numbers (d/a=2, c/a=4 in no tilt condition)

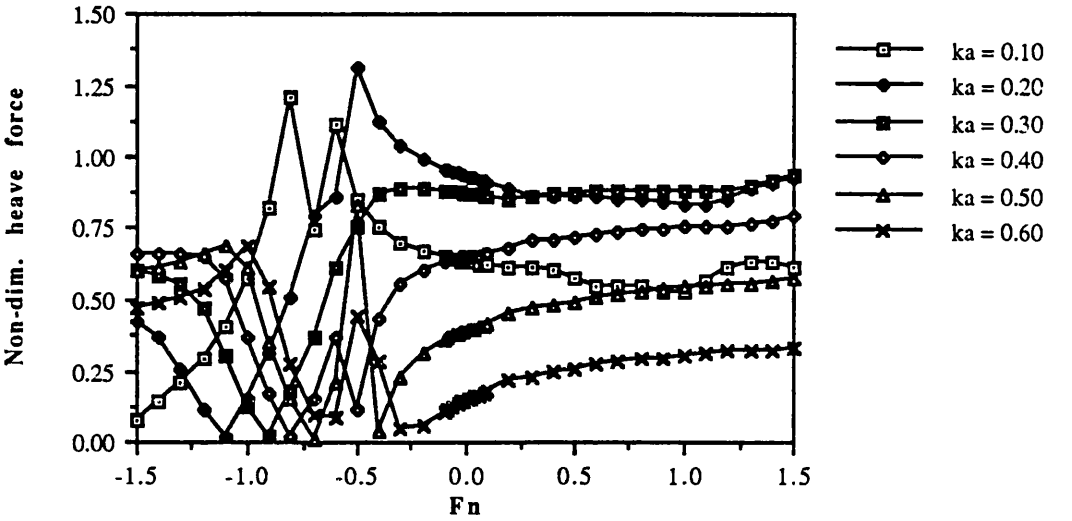

Fig.10.142 Non-dimensionalized heave forces for different wave numbers (d/a=2, c/a=4 in no tilt condition)

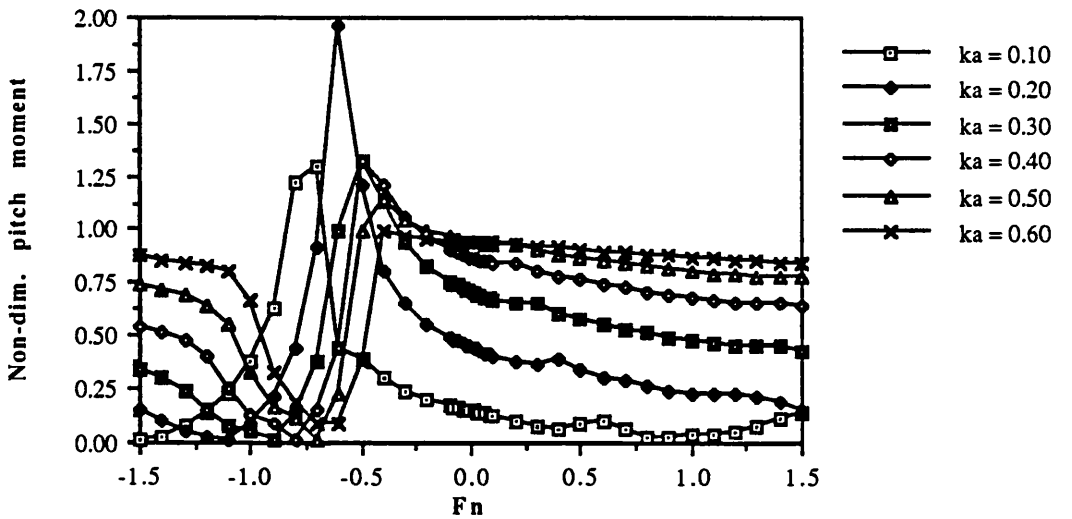

Fig.10.143 Non-dimensionalized pitch moments for different wave numbers (d/a=2, c/a=4 in no tilt condition)

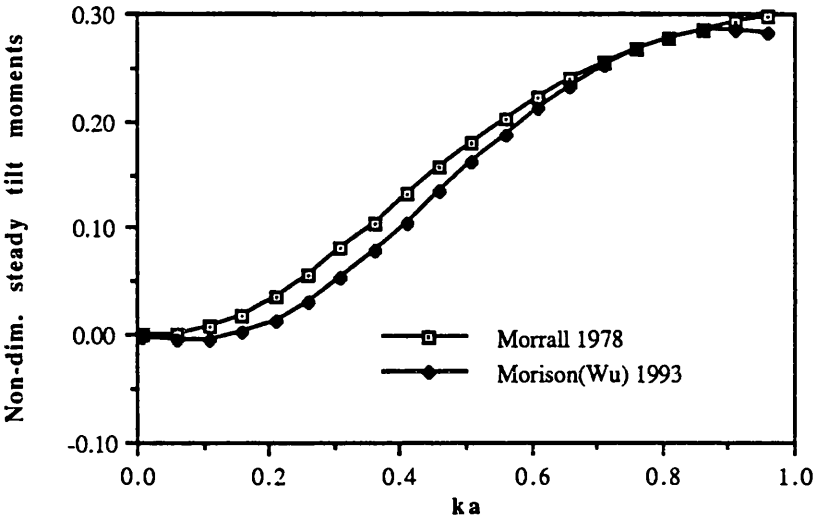

Fig.10.144 Comparison of non-dim. steady tilt moment with viscous effects on vertical columns(d/a=2, c/a=4, GM=0.3)

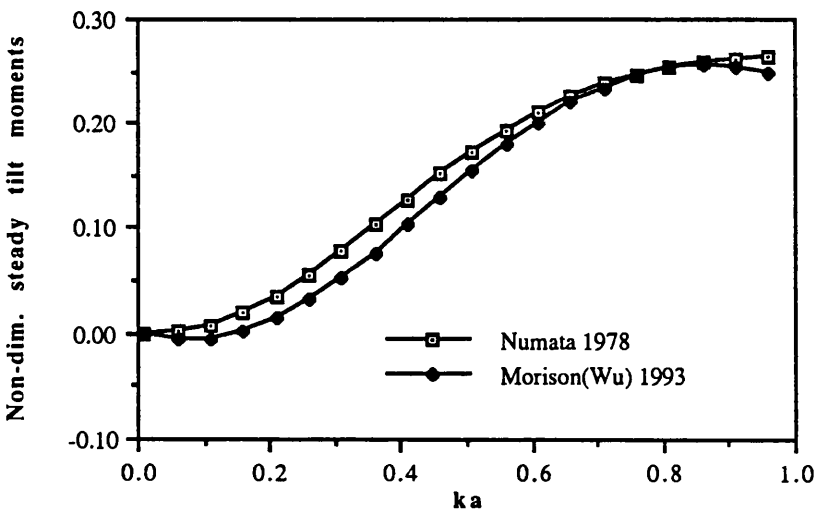

Fig.10.145 Comparison of non-dim. steady tilt moments with viscous effects on vertical columns(d/a=2, c/a=4, GM=0.3)

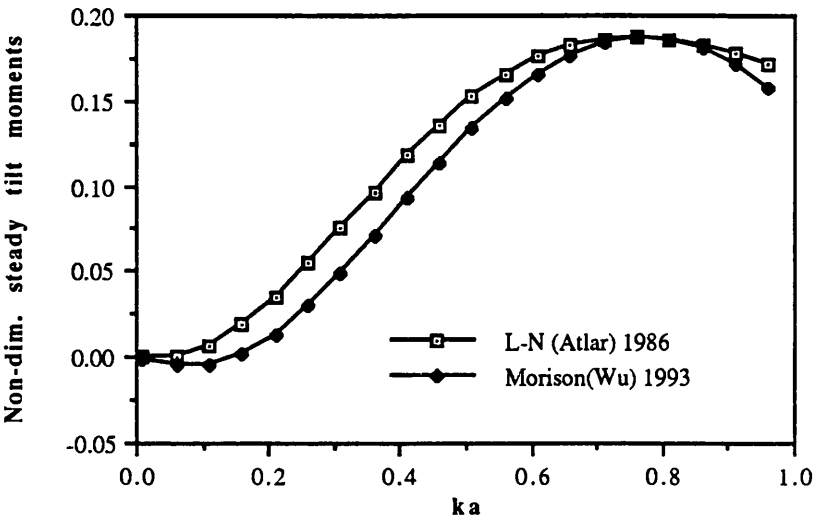

Fig.10.146 Comparison of non-dim. steady tilt moments with viscous effects on vertical columns(d/a=2, c/a=4, GM=0.3)

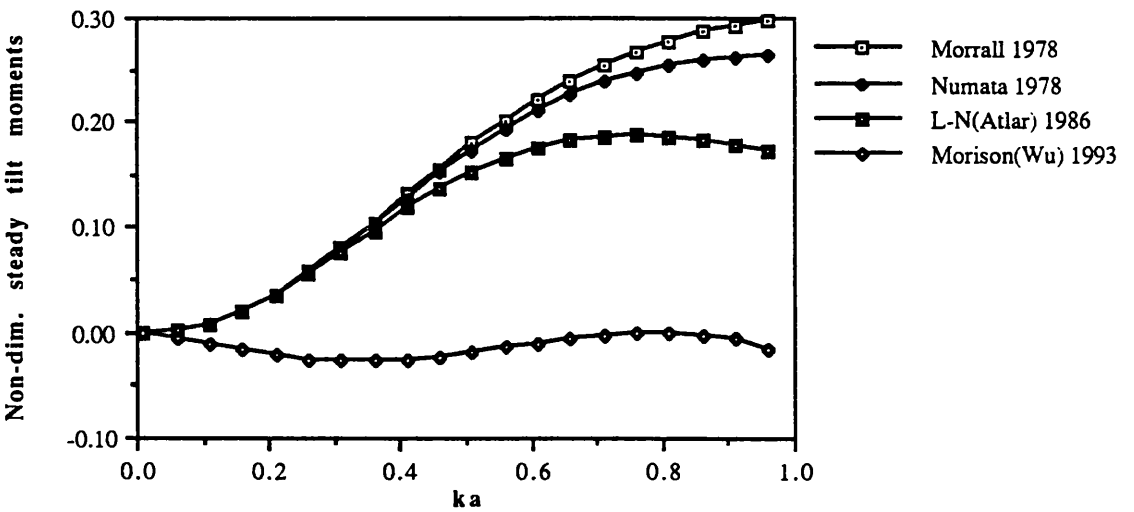

Fig.10.147 Comparison of non-dim. steady tilt moments with viscous effects on vertical columns(d/a=2, c/a=4, GM=0.3)

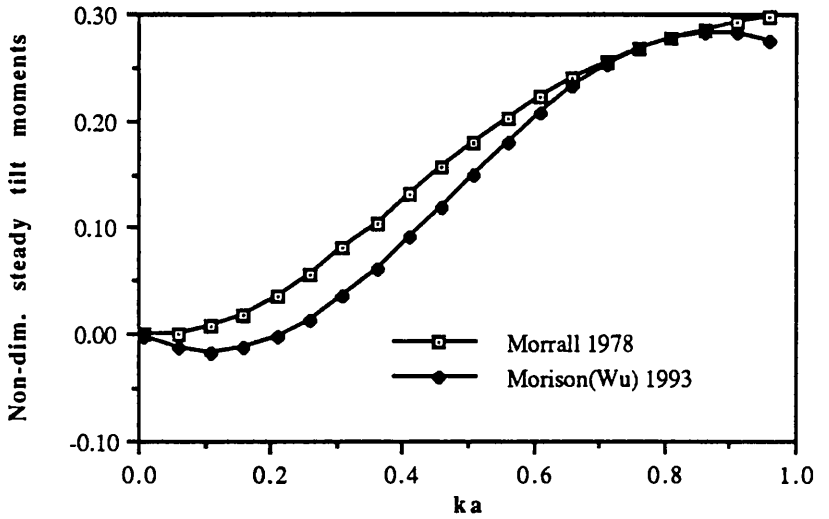

Fig.10.148 Comparison of non-dim. steady tilt moments with viscous effects on vertical columns(d/a=2, c/a=4, GM=0.4)

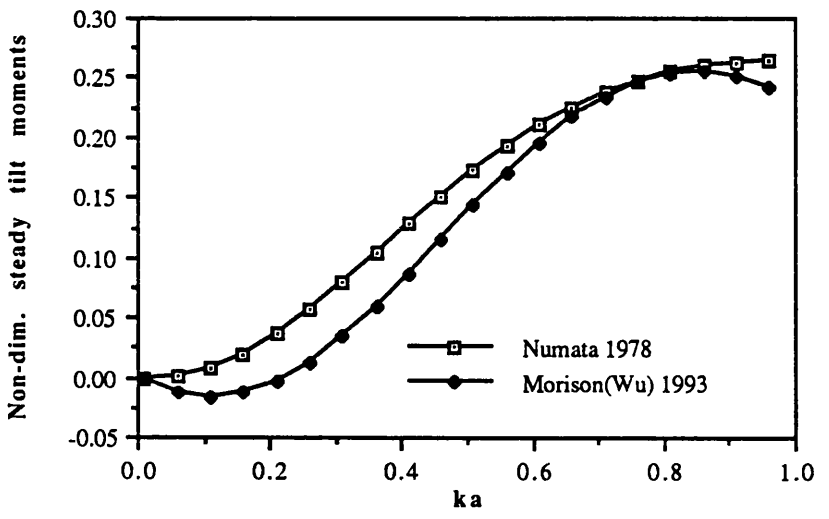

Fig.10.149 Comparison of non-dim. steady tilt moments with viscous effects on vertical columns(d/a=2, c/a=4, GM=0.4)

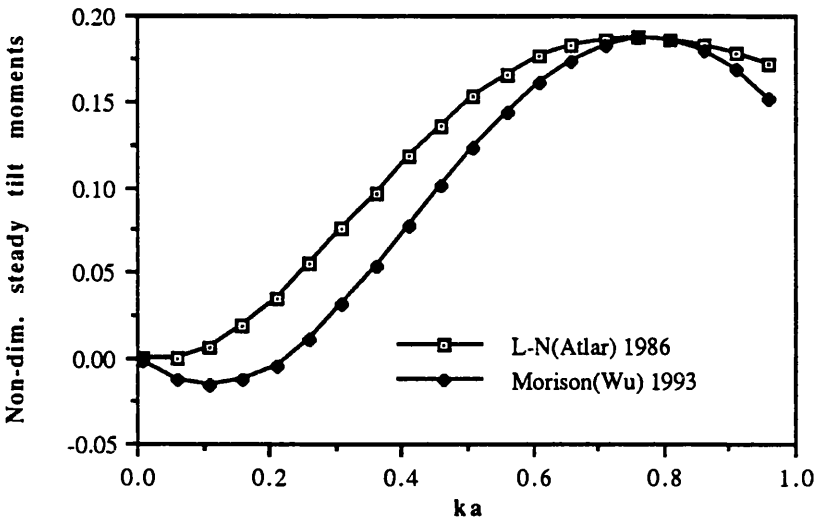

Fig.10.150 Comparison of non-dim. steady tilt moments with viscous effects on vertical columns(d/a=2, c/a=4, GM=0.4)

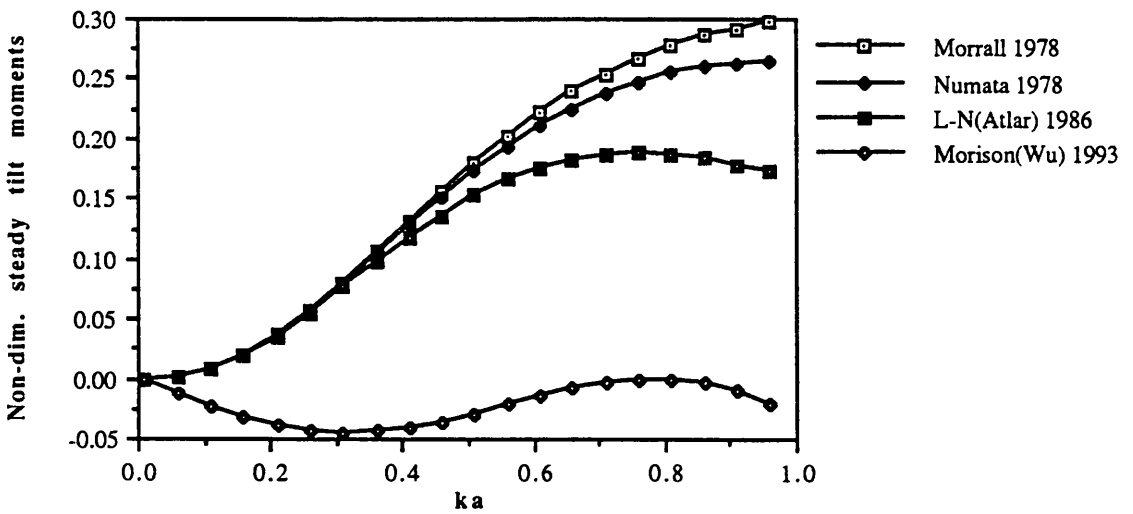

Fig.10.151 Comparison of non-dim. steady tilt moments with viscous effects on vertical columns(d/a=2, c/a=4, GM=0.4)

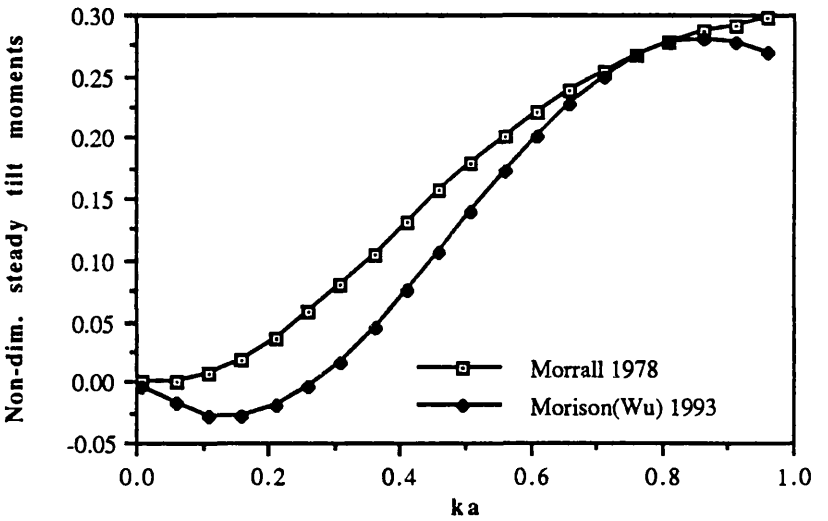

Fig.10.152 Comparison of non-dim. steady tilt moments with viscous effects on vertical columns(d/a=2, c/a=4, GM=0.5)

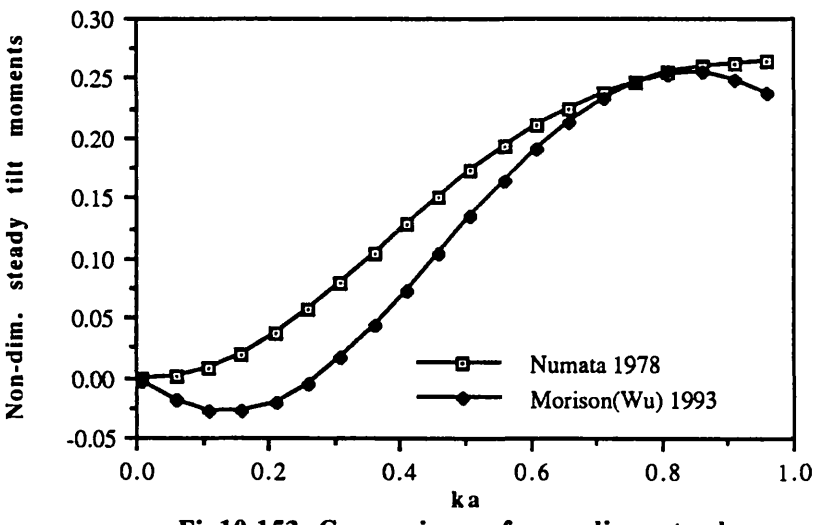

Fig10.153 Comparison of non-dim. steady tilt moments with viscous effects on vertical columns(d/a=2, c/a=4, GM=0.5)

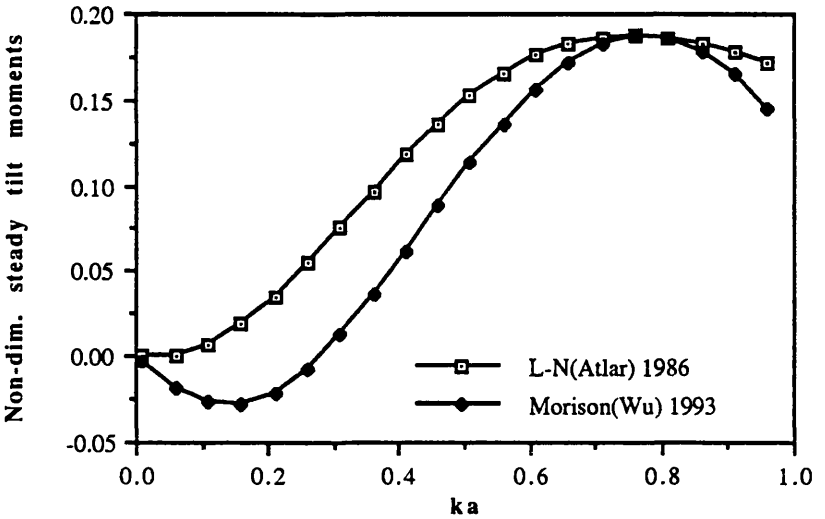

Fig.10.154 Comparison of non-dim. steady tilt moments with viscous effects on vertical columns(d/a=2, c/a=4, GM=0.5)

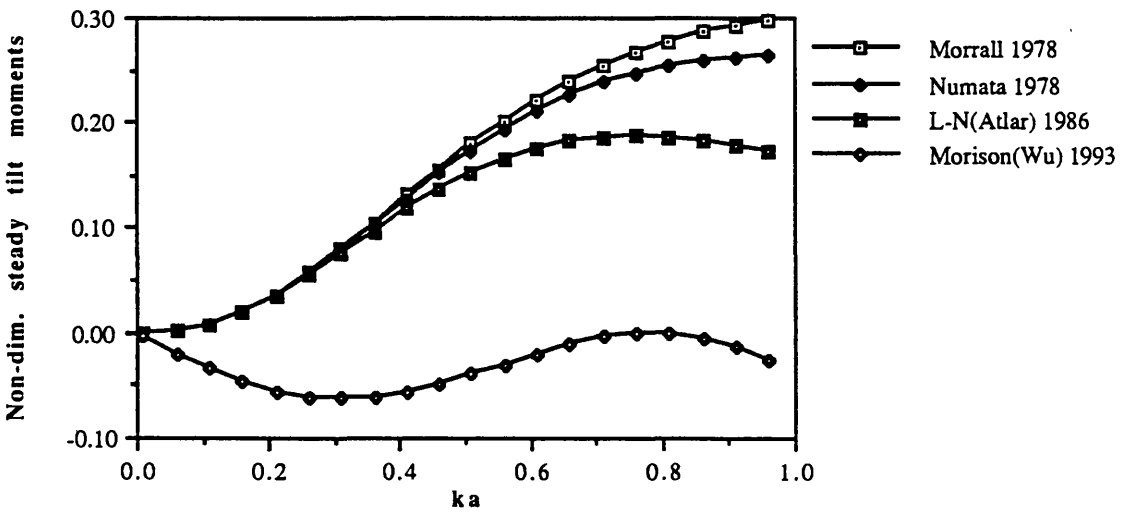

Fig.10.155 Comparison of non-dim. steady tilt moments with viscous effects on vertical columns(d/a=2, c/a=4, GM=0.5)

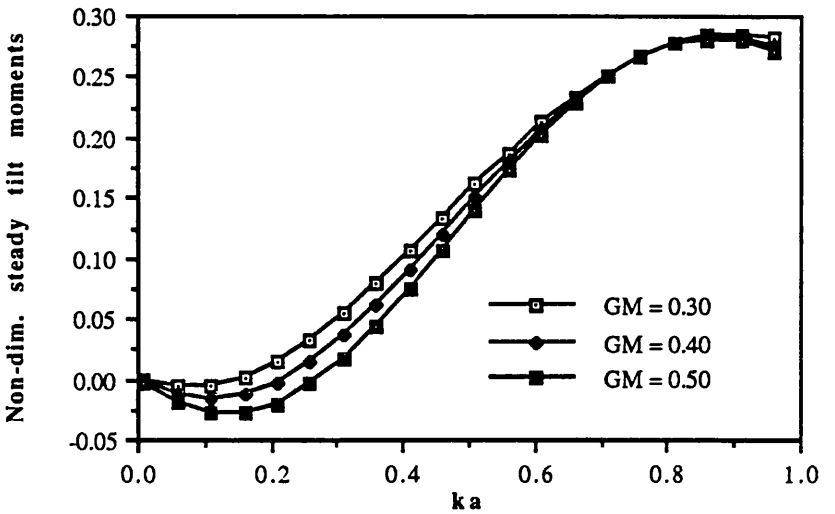

Fig.10.156 Comparison of non-dim. steady tilt moments with viscous effects for different GM heights(d/a=2, c/a=4)

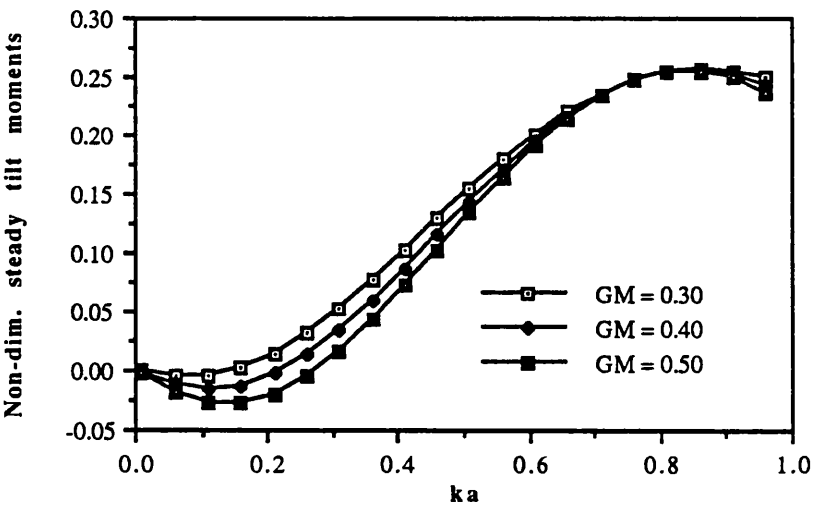

Fig.10.157 Comparison of non-dim. steady tilt moments with viscous effects for different GM heights (d/a=2, c/a=4)

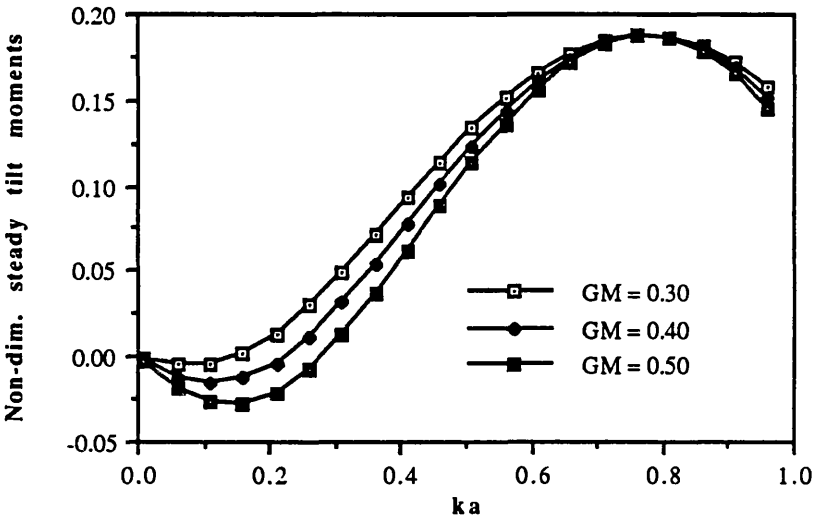

Fig.10.158 Comparison of non-dim. steady tilt moments with viscous effects for different GM heights (d/a=2, c/a=4)

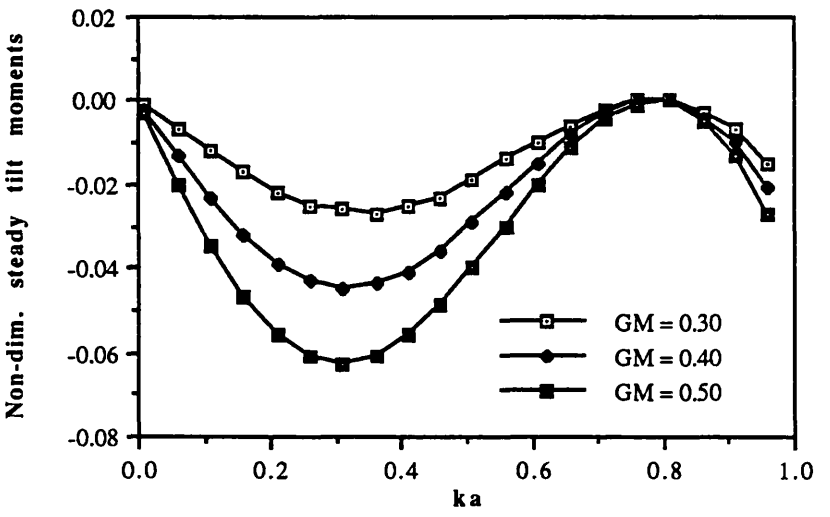

Fig.10.159 Comparison of non-dim. steady tilt moments due to viscous effects for different GM heights (d/a=2, c/a=4)

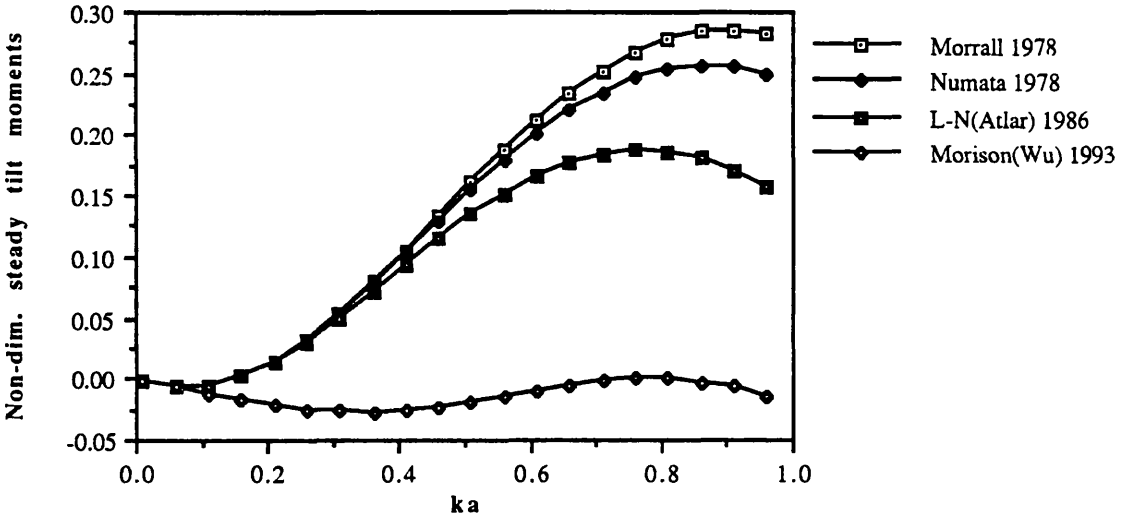

Fig.10.160 Comparison of non-dim. steady tilt moments with viscous effects on vertical columns(d/a=2, c/a=4, GM=0.3)

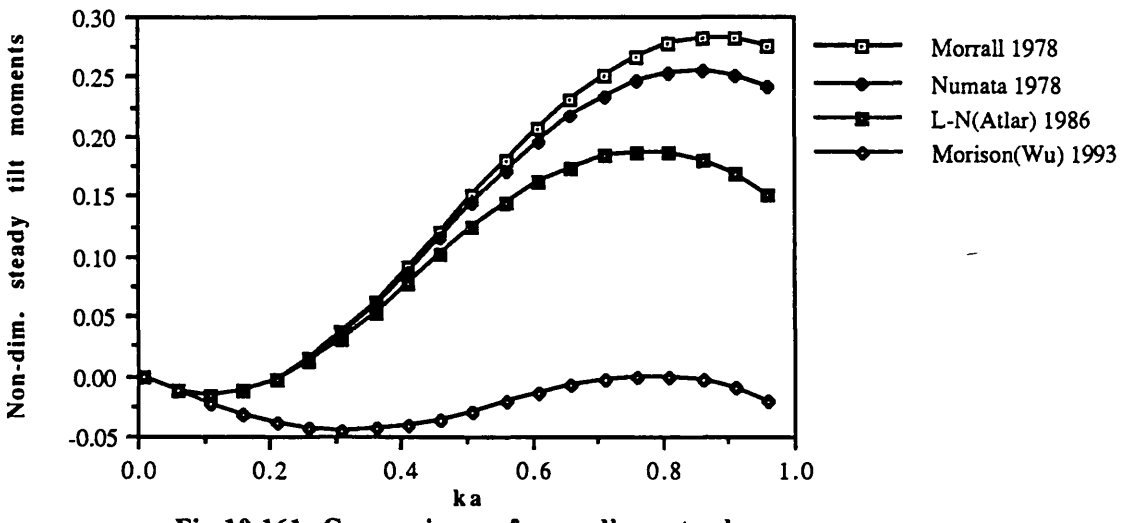

Fig.10.161 Comparison of non-dim. steady tilt moments with viscous effects on vertical columns(d/a=2, c/a=4, GM=0.4)

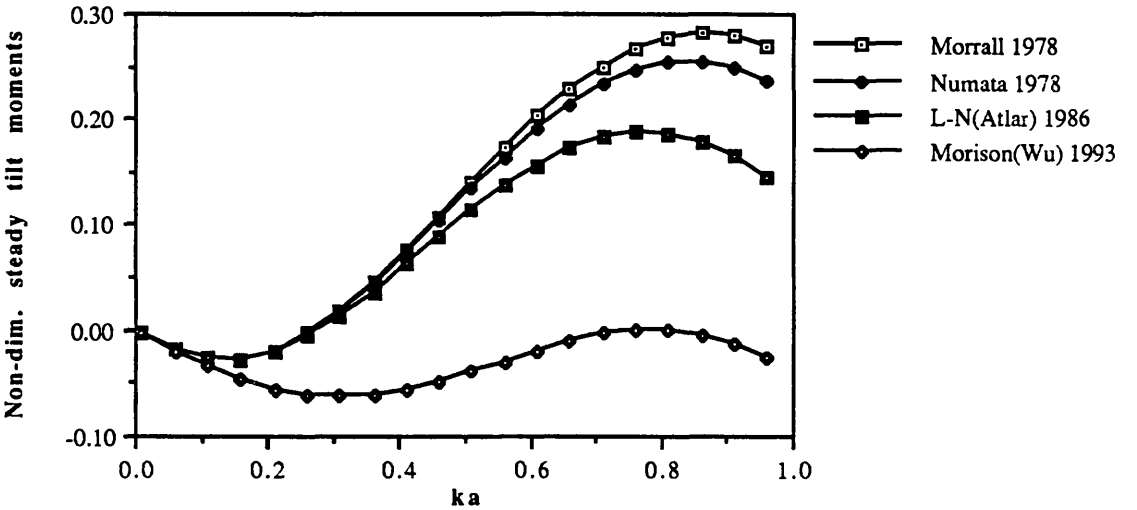

Fig.10.162 Comparison of non-dim. steady tilt moments with viscous effects on vertical columns(d/a=2, c/a=4, GM=0.5)

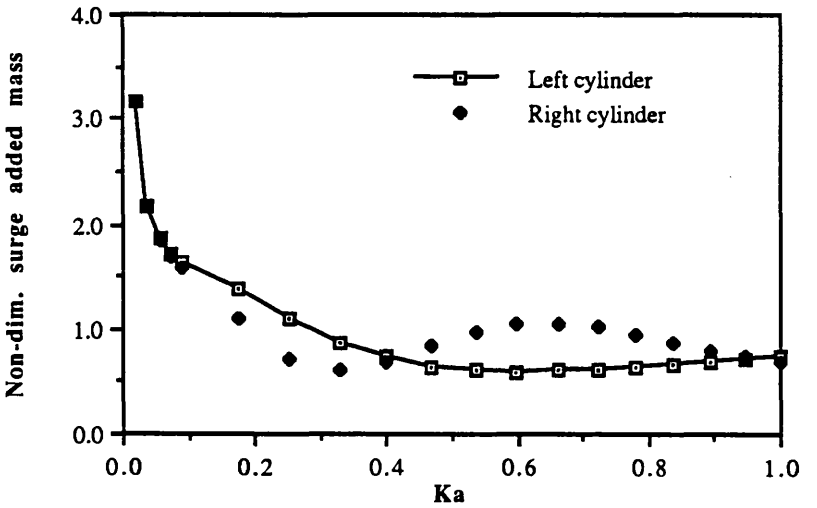

Fig.10.163 Comparison of non-dim. surge added mass between two cylinders (d/a=2,Fn=0.15, no tilt in following waves)

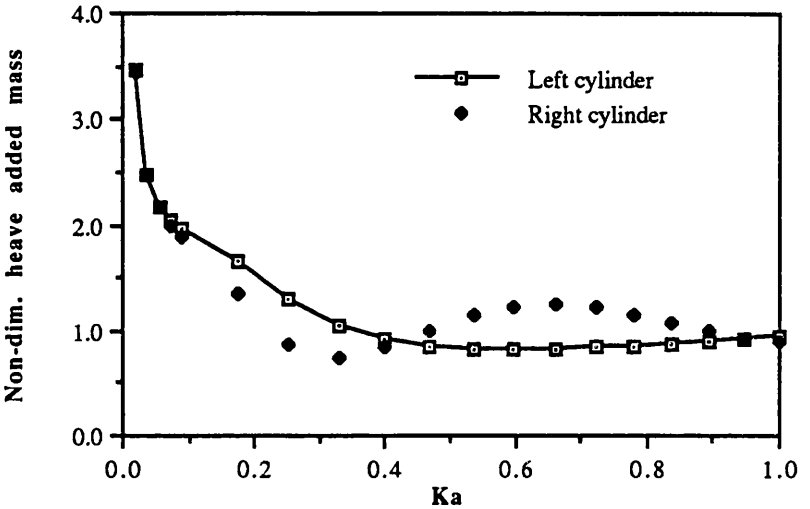

Fig.10.164 Comparison of non-dim. heave added mass between two cylinders (d/a=2,Fn=0.15, no tilt in following waves)

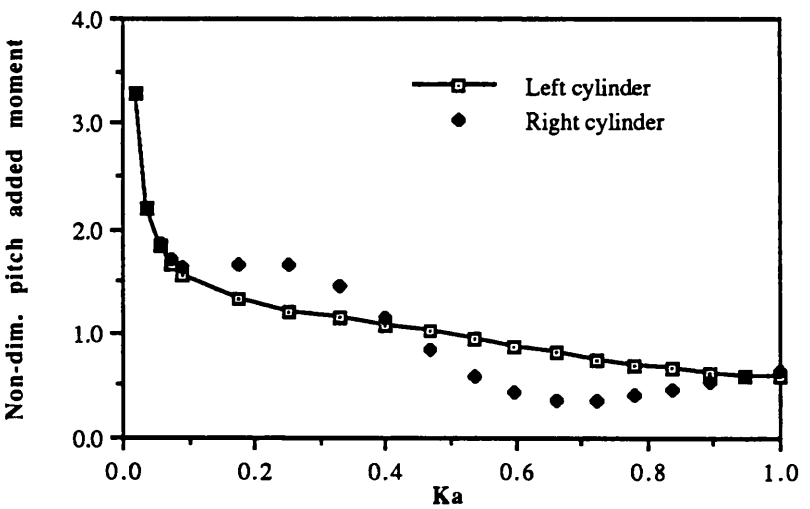

Fig.10.165 Comparison of non-dim. pitch added moment between two cylinders (d/a=2,Fn=0.15, no tilt in following waves)

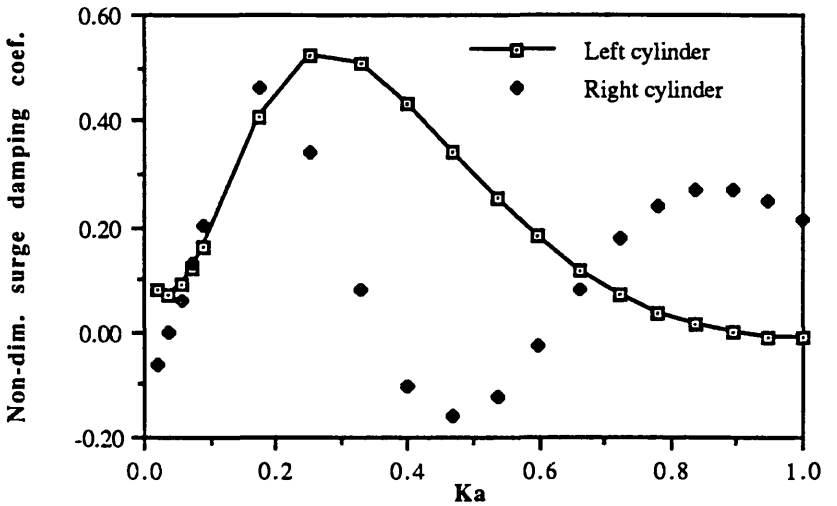

Fig.10.166 Comparison of non-dim. surge damping coefficients btwn two cylinders (d/a=2,Fn=0.15, no tilt in following waves)

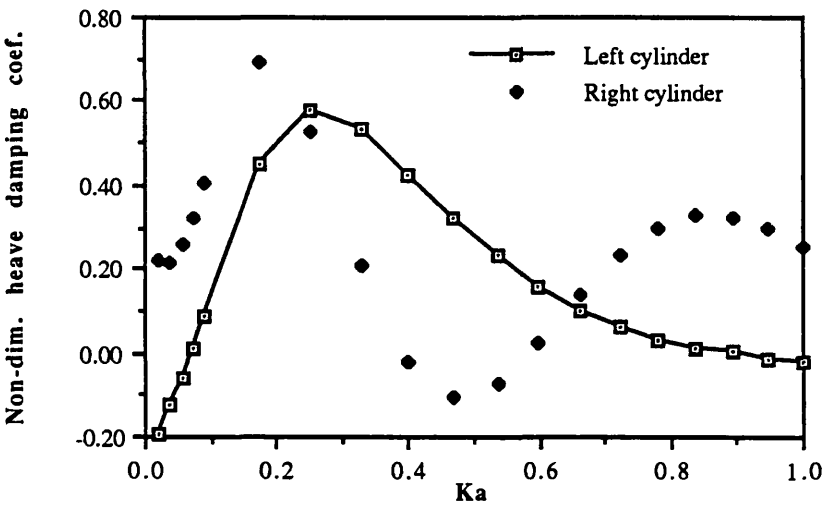

Fig.10.167 Comparison of non-dim. heave damping coefficients btwn two cylinders (d/a=2,Fn=0.15, no tilt in following waves)

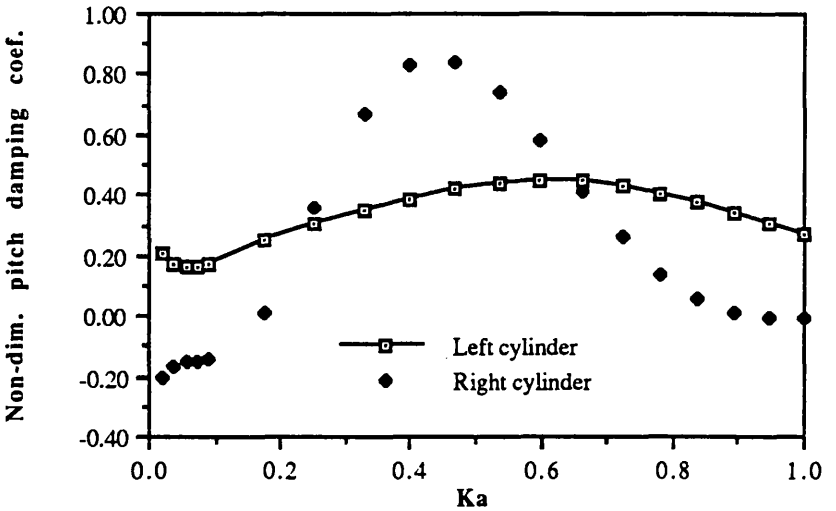

Fig.10.168 Comparison of non-dim. pitch damping coefficients btwn two cylinders (d/a=2,Fn=0.15, no tilt in following waves)

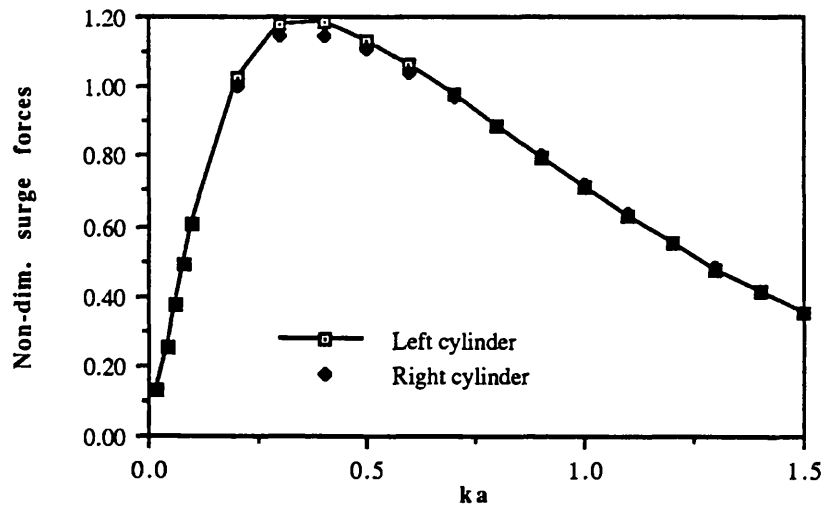

Fig.10.169 Comparison of non-dim. surge forces between two cylinders (d/a=2, c/a=4,Fn=0.15, no tilt in following waves)

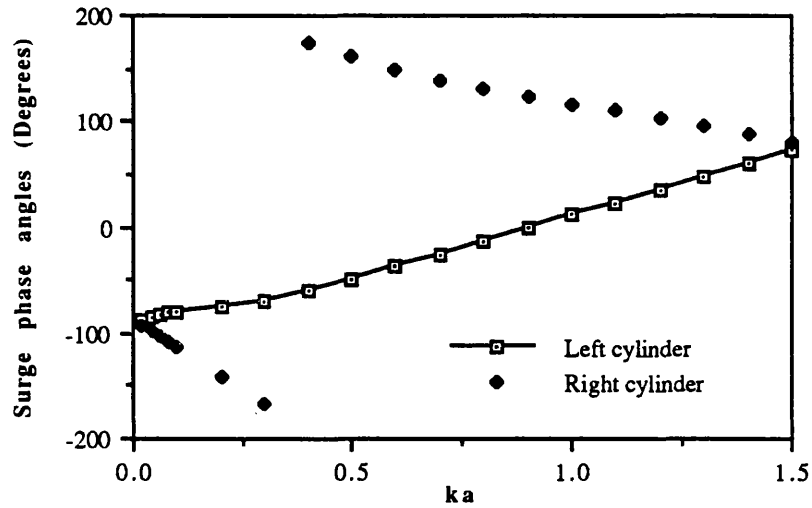

Fig.10.170 Comparison of surge phase angles between two cylinders (d/a=2.0, c/a=4.0,Fn=0.15,no tilt in following waves)

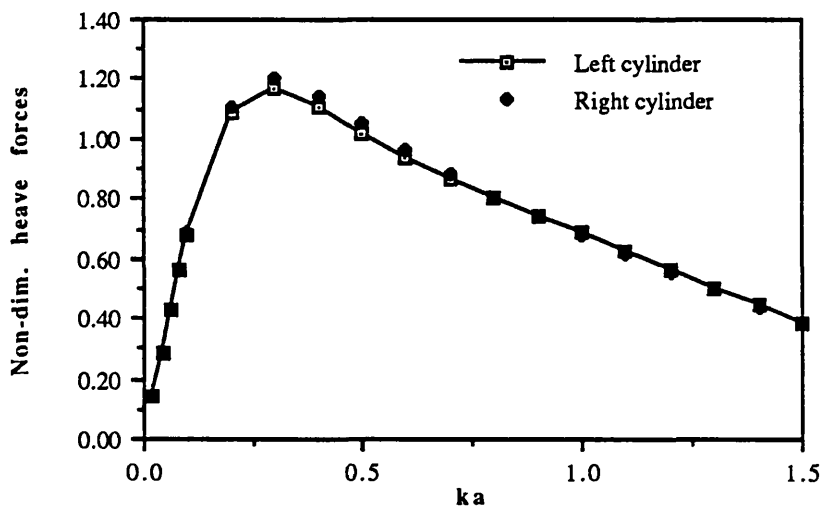

Fig.10.171 Comparison of non-dim. heave forces between two cylinders (d/a=2, c/a=4,Fn=0.15, no tilt in following waves)

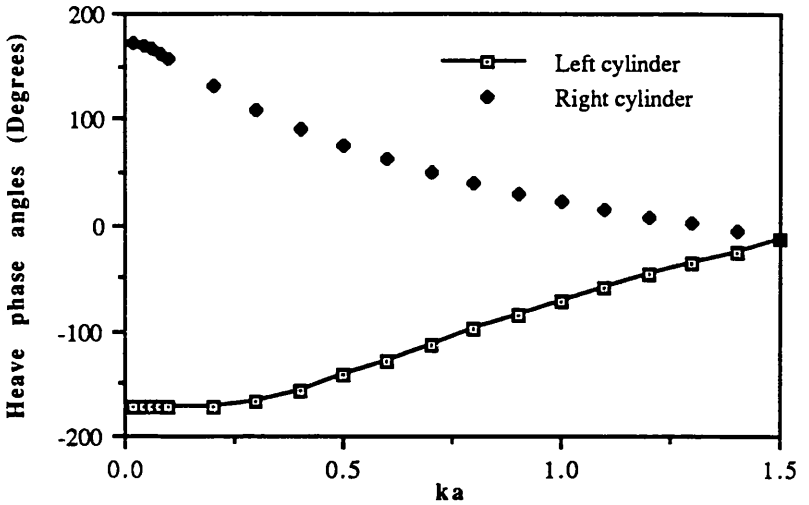

Fig.10.172 Comparison of heave phase angles between two cylinders (d/a=2.0, c/a=4.0,Fn=0.15, no tilt in following waves)

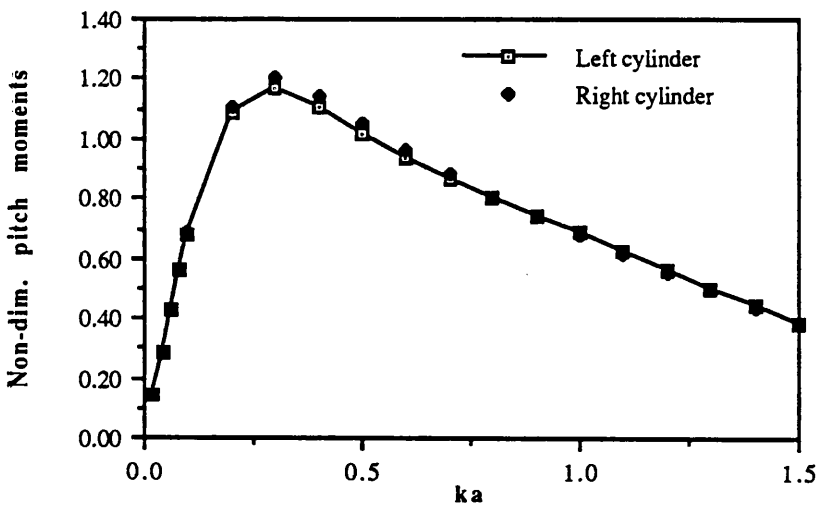

Fig.10.173 Comparison of non-dim. pitch moments betweenn two cylinders(d/a=2, c/a=4,Fn=0.15, no tilt in following waves)

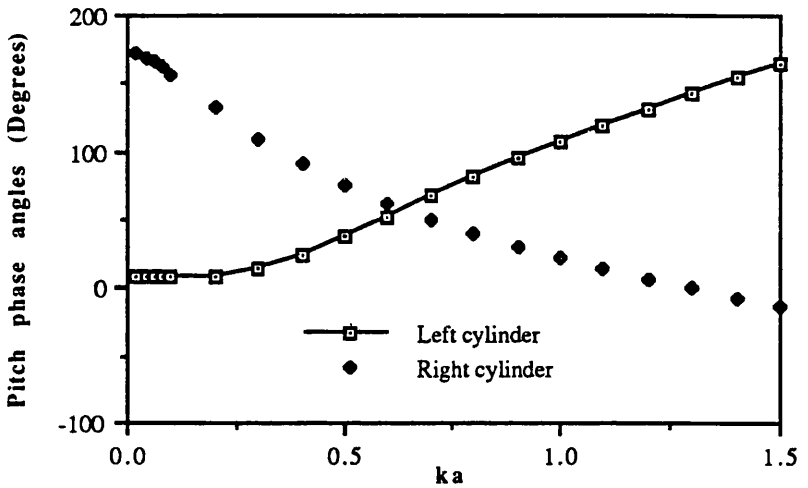

Fig.10.174 Comparison of pitch phase angles between two cylinders (d/a=2.0, c/a=4.0,Fn=0.15, no tilt in following waves)